



Electrochemically Enabled Synthesis of Substituted Isoxazolines

A thesis submitted to the University of Strathclyde
for the degree of Doctor of Philosophy (PhD) in
the Faculty of Pure and Applied Chemistry

2020

Samuel David Lee Holman

Declaration of Authenticity and Author's Rights

This thesis is the result of the author's original research. It has been composed by the author and has not been previously submitted for examination which has led to the award of a degree.

The copyright of this thesis belongs to GlaxoSmithKline (GSK) in accordance with the authors contract of engagement with GSK under the terms of the United Kingdom Copyright Acts. Due acknowledgement must always be made of the use of any material contained in, or derived from, this thesis.

Signed: 

Date: 27/03/2020

Acknowledgements

Firstly, I would like to thank my wife, Natalia, for her unwavering support and patience throughout my PhD; she has kept me sane (somewhat) and is always a breath of fresh air whenever returning home from the lab. I'd also like to thank my parents for also supporting and encouraging me throughout my life – especially when I needed it the most. Further thanks go to Daniel and Sam who have both made my time inside and outside GSK very enjoyable.

Huge thanks must go to my academic supervisor, Dr Marc Reid (University of Strathclyde) and my industrial supervisor, Dr Neal Fazakerley (GlaxoSmithKline), without who I would not have made it this far. Their enthusiasm and encouragement inspired me to be the best I can be. Both their guidance and their willingness to let me chase my own ideas (whether for better or worse), has been incredible. It has been an amazing privilege to have worked with both of them. I would like to thank the team at GSK for welcoming with open arms and putting up with my incessant optimistic approach to life! I'd also like to thank the Reid group and the Kerr group for taking good care of me on my placement in the labs at Strathclyde – the karaoke night is a night I will never forget!

I owe my place on the program to both Dr Harry Kelly (GSK) and Dr William Kerr (University of Strathclyde); I thank them for their belief in me and for giving me this chance to take on and accomplish the science throughout my three and a half years. I thank them also for their support and encouragement to attend the fantastic conferences.

Finally, I'd like to thank both the University of Strathclyde and GlaxoSmithKline for the opportunity to undertake this research and the people behind the scenes who have helped me along the way, in particular, Kerry and Hannah, for their amazing work keeping the labs running smoothly; Alfie, Darren and Catherine, for their helpful discussions about my work; Sean, for his help with NMR acquisition; and the people in Bay 0 and Bay 1, for their conversation at much needed tea breaks.

Contents

Declaration of Authenticity and Author's Rights	i
Acknowledgements.....	ii
Abbreviations.....	vii
Abstract	xi
1. Introduction.....	1
1.1. Electroorganic Synthesis	4
1.1.1. Background	4
1.1.2. Electrochemical Reactor Design.....	5
1.1.3. Electrical Double Layer.....	7
1.1.4. Cyclic Voltammetry.....	9
1.1.5. Direct Electroorganic Synthesis.....	13
1.1.6. Mediated Electroorganic Synthesis.....	20
1.2. 1,3-Dipolar Cycloadditions.....	29
1.2.1. Mechanism	31
1.2.2. Frontier Molecular Orbital Interactions	35
1.2.3. Regioselectivity.....	39
1.2.4. Stereospecificity	41
1.2.5. Diastereoselectivity.....	43
1.3. Synthesis of Isoxazolines	44
1.3.1. Synthesis of Isoxazolines <i>via</i> 1,3-Dipolar Cycloadditions.....	49
1.3.2. Asymmetric Isoxazoline Synthesis.....	64
1.4. Introduction Summary.....	71
2. Aim of Investigation	72
3. Results and Discussion	74
3.1. Initial Scoping.....	74
3.1.1. Observed Diastereoselectivity	77

3.1.2.	External Electrolyte Screen	87
3.2.	Optimisation of Electrochemical Reaction.....	89
3.2.1.	Electrode Material Screen	89
3.2.2.	Mediator/Electrolyte Screen.....	91
3.2.3.	Reproducibility of Carousel	93
3.2.4.	Charge Transferred Screen	98
3.2.5.	Solvent Screen	100
3.2.6.	Additive Screen	103
3.2.7.	Reproducibility of Electrodes	106
3.2.8.	Further Screening of Conditions	107
3.2.9.	Initial Proposed Reaction Pathway	110
3.3.	Design of Experiments.....	112
3.4.	Substrate Scope	118
3.5.	Reaction Kinetic Analysis	123
3.5.1.	<i>In-situ</i> IR Monitoring	123
3.5.2.	¹ H NMR Monitoring.....	126
3.6.	Cyclic Voltammetry Experiments	141
3.7.	Revised Proposed Reaction Pathway	161
3.8.	Flow Electrochemistry.....	166
3.9.	Pyrazoline Synthesis and One-Pot Chemistry.....	175
3.10.1.	Attempted Pyrazoline Synthesis.....	175
3.10.2.	One-Pot Synthesis from Aldehydes.....	177
4.	Conclusion.....	179
5.	Future Work.....	181
6.	Experimental.....	184
6.1.	General Experimental Data Methods	184
6.2.	General Experimental Procedures	191

6.2.1.	General Procedure 1 for Oxime Synthesis (GP1)	191
6.2.2.	General Procedure 2 for Chemical Isoxazoline Synthesis (GP2)	222
6.2.3.	General Procedure 3 for Electrochemical Synthesis (GP3).....	226
6.2.4.	Substrates Not Tolerated Under Electrochemical Conditions.....	251
6.2.5.	Pyrazoline Synthesis Attempts	252
6.3.	Electrochemical Synthesis of 221a on 5 mmol Scale.....	254
6.4.	Derivatisation of 221a	255
6.5.	Initial Scoping	259
6.5.1.	Initial Scoping Reactions	259
6.5.2.	Additional Electrolyte Screen.....	261
6.6.	Optimisation of Electrochemical Isoxazoline Procedure.....	262
6.6.1.	Electrode Material Screen	262
6.6.2.	Mediator Screen	264
6.6.3.	Solvent Screen	266
6.6.4.	Charge Transferred Screen	268
6.6.5.	Additive Screen	270
6.6.6.	Concentration Screen.....	272
6.7.	Design of Experiments.....	273
6.8.	Control Experiments	275
6.8.1.	No HFIP Control	275
6.8.2.	No Chloride Control	276
6.8.3.	(<i>Z</i>)-Benzaldehyde oxime studies	277
6.9.	Flow Electrochemical Optimisation	279
6.9.1.	General Procedure for Optimisation using Matrices.....	279
6.9.2.	Isolation of Flow Experiments	288
6.10.	ReactIR Experiments	291
6.10.1.	Monitoring of Chemical Reaction.....	291

6.10.2.	Monitoring of Electrochemical Reaction	295
6.11.	Hammett Analysis	298
6.11.1.	Maximum Rate Kinetic Analysis:	298
6.11.2.	Swain-Lupton Analysis	304
6.11.3.	Well-Mixed Regime Kinetic Analysis	306
6.11.4.	Stir Speed Analysis	311
6.11.5.	Kinetic Isotope Effect Study	313
6.11.6.	Alternative Hammett Analyses	315
6.12.	Cyclic Voltammetry	317
6.12.1.	General Procedure for Cyclic Voltammetry	317
6.12.2.	Cyclic Voltammograms	319
7.	References	340

Abbreviations

ABNO – 9-azabicyclo[3.3.1]nonane *N*-oxyl

Ac – acetate

amu – atomic mass unit

Ar – aromatic

Bn – benzyl

Boc – *tert*-butyloxycarbonyl

Bu – butyl

Bz – benzoyl

Cbz – carboxybenzyl

CCE – Constant Current Electrolysis

CDC – Cross-Dehydrogenative Coupling

CPE – Constant Potential Electrolysis

CV – Cyclic Voltammetry

Cy – cyclohexyl

DBU – 1,8-diazabicyclo[5.4.0]undec-7-ene

DCE – dichloroethane

DCM – dichloromethane

de – diastereomeric excess

DFT – Density Functional Theory

DHEA – dehydroepiandrosterone

(*R,R*)-DIPT – *R,R*-diisopropyl tartrate

DMF – *N,N*-dimethylformamide

DMSO – dimethyl sulfoxide

DoE – Design of Experiments

dr – diastereomeric ratio

EC₅₀ – half-maximal effectiveness concentration

EDG – Electron-donating Group

ee – enantiomeric excess

Et – ethyl

EWG – Electron-withdrawing Group

Fc – ferrocene

Fmoc – fluorenylmethoxycarbonyl

G – graphite

GC – glassy carbon

GSK – GlaxoSmithKline

HeLa – cell line derived from a patient in the 1950s

Hex – hexyl

HFIP – 1,1,1,3,3,3-hexafluoroisopropanol

HOMO – Highest Occupied Molecular Orbital

HpH – High pH

HPLC – High-Performance Liquid Chromatography

HRMS – High Resolution Mass Spectrometry

hr – hour(s)

IBX – 2-iodoxybenzoic acid

IR – Infrared Radiation

LCMS – Liquid Chromatography-Mass Spectrometry

LUMO – Lowest Unoccupied Molecular Orbital

Me – methyl

Mes – mesityl

min – minute(s)

mM – millimolar

MOM – methoxymethyl

NBS – *N*-bromosuccinimide

NCS – *N*-chlorosuccinimide

NHPI – *N*-hydroxyphthalimide

NMR – Nuclear Magnetic Resonance

Ns – nosyl

OVAT – One Variable at a Time

Ph – phenyl

Piv – pivaloyl

PPS – Polyphenylene sulfide

PVDF – poly(vinylidene fluoride)

Py – pyridine

rr – regioisomeric ratio

rt – room temperature

RVC – Reticulated Vitreous Carbon

SCE – Saturated Calomel Electrode

SET – Single Electron Transfer

SEM – 2-(trimethylsilyl) ethoxymethyl

SHE – Standard Hydrogen Electrode

SS – Stainless-steel

TBHP – *tert*-butylhydroperoxide

TBS – *tert*-butyldimethylsilyl

TCNHPI – tetrachloro-*N*-hydroxyphthalimide

Teoc – trimethylsilylethoxycarbonyl

Tf – triflyl

TEMPO – 2,2,6,6-tetramethylpiperidine *N*-oxyl

THF – tetrahydrofuran

TIPS – triisopropylsilyl

TLC – Thin-Layer Chromatography

t_R – retention time

Ts – tosyl

Abstract

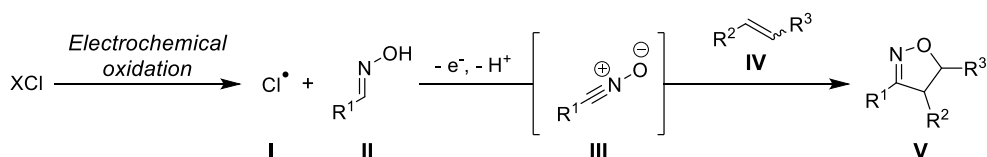
Synthetic electroorganic chemistry has recently become an attractive method for the preparation of many organic molecules.¹ With the introduction of enabling technologies, such as IKA's ElectraSyn 2.0, synthetic electrochemistry can be applied in a standardised way, allowing reproducible procedures.

The study presented herein explores the electrochemical synthesis of substituted isoxazolines, using an inexpensive, environmentally benign mediator. Isoxazolines can be found in many natural products, as well as pharmaceutical and agricultural compounds. Traditionally, isoxazolines have been prepared using 1,3-dipolar cycloaddition reactions between nitrile oxides and dipolarophiles; other methods, such as transition metal-catalysed ring closures, have also been reported. However, nitrile oxides, with the exception of sterically encumbered aromatic nitrile oxides, are reactive and rapidly form dimers. *In-situ* preparations of these highly reactive species have been developed, though these often require toxic and/or expensive reagents, such as electrophilic halogenating agents and strong oxidants. There have been very few reports of more benign and environmentally friendly procedures, with alternative approaches which address these issues desirable.

The electrochemically enabled synthesis of substituted isoxazolines has been realised, with a substrates scope of 45 examples that were isolated in up to 86% yield. Of particular note, previously elusive alkyl derived aldoximes have been successfully electrolysed under the optimised conditions, furnishing the desired products in moderate to good yields. Furthermore, green metrics were obtained that showed that this electrochemical procedure has a smaller impact on the environment when compared with other non-electrochemical methods.

Building on previous work by Shono, it is envisioned that an electrochemical oxidation of a halide anion and subsequent combination with an aldoxime, followed by further oxidation and deprotonation by conjugate base, could generate a nitrile oxide. This nitrile oxide could participate in a 1,3-dipolar cycloaddition reaction with a dipolarophile to fashion a substituted isoxazoline. The reaction pathway was probed using both *in-situ* IR monitoring (using the commercially available ReactIR experimental set up) and ¹H NMR. IR reaction profiling revealed pseudo-zero order reaction kinetics, as expected of a surface-mediated reaction. ¹H NMR profiling of the electrochemical reaction between *para*-substituted benzaldehyde oximes and *tert*-

butyl acrylate allowed Hammett and Swain-Lupton analyses to be performed. These analyses gave an inverted V-shaped plot that is indicative of change in rate-limiting step, consistent with a 1,3-dipolar cycloaddition reaction of ambiphilic nitrile oxide dipoles, as the change in rate-limiting step is attributed to the change in interacting frontier molecular orbitals. These NMR profiles may suggest that underlying physical phenomena may be responsible for the inverted V-shape of the Hammett and Swain-Lupton analyses.



Additionally, the batch electrochemical reaction was successfully adapted into a flow procedure. These early results have allowed the isolation of the desired isoxazoline in 49% yield, showing great promise. Further work needs to be conducted as full consumption of starting material after a first-pass through the electrochemical cell has not been achieved to date.

patients with autism; iv) Fluranaler (**7**) is an oral insecticide and acaricide for use in flea removal in dogs; v) Topramezone (**8**) is a pesticide that is currently used and marketed in the UK.

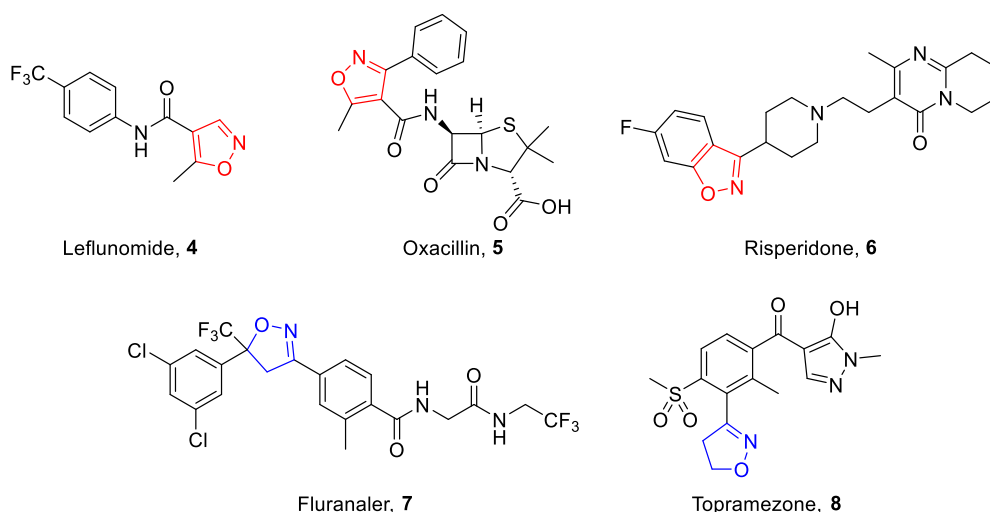
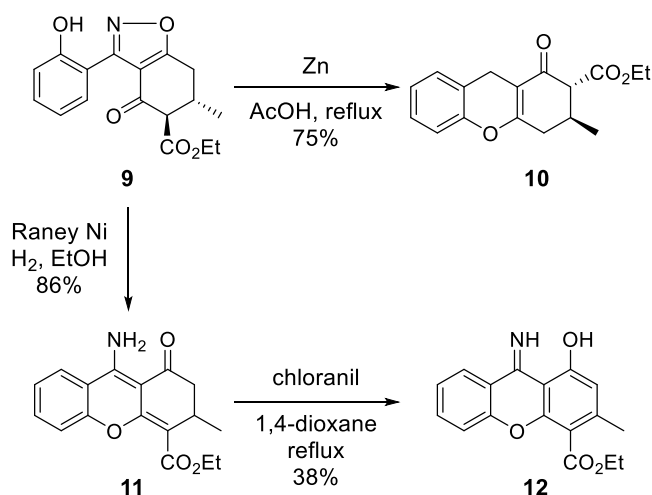


Figure 2: Current pharmaceuticals and agricultural products containing isoxazoles or isoxazolines.

Due to its high value as a pharmacophore in medicines, there has been much attention given to the synthesis of substituted isoxazoles and the semi-saturated derivative isoxazolines. However, it is not only their biological properties that make isoxazolines interesting to the chemical community, but also their use as masked 1,3-dicarbonyls (**Scheme 1**).⁸



Scheme 1: Bode *et al.* showed that isoxazoles can be used as masked carbonyls or amino ketones.

Bode *et al.* demonstrated that reduction by different metals can give either enamines (**11** with Raney Nickel) or cyclic enones (**10** with zinc). Further derivatisation of **10** showed the versatility of these isoxazole/isoxazoline structural motifs.^{8b, 9}

1.1. Electroorganic Synthesis

Electroorganic synthesis has recently re-emerged as a growing field of synthetic chemistry due to the drive for reactions with better environmental profiles.^{1, 10} Treating electrons as reagents and the electrodes as materials that are not consumed during the course of a reaction, electrochemistry complies well with the 12 principles of green chemistry.¹¹ Electrochemistry can also negate the need for strong oxidising or reducing agents and hence toxic waste is not generated. Additionally, in some cases, the use of electrons as “catalysts” can reduce the energy consumption of a given electrochemical reaction, compared with that of a heated reaction with alternative catalysts/reagents.^{10d, 12}

Electrochemistry on an industrial scale has been used for many years, particularly in the refining of ores. Aluminium metal is refined by electrolysis of its molten ore at a carbon electrode, and produces metric tons each year.¹³ Chlorine gas and sodium hydroxide are produced from the electrolysis of brine. In terms of synthetic organic reactions, adiponitrile is produced on a large scale from the electrochemically enabled dimerisation of acrylonitrile; adiponitrile is used in the production of nylon-6,6. Other large scale electrolyses also include preparation of *p*-methoxybenzaldehyde and acetoin from BASF.¹⁴ However, in the pharmaceutical industry, electrochemistry is in the early stages of adoption.

1.1.1. Background

Electroorganic chemistry, has not been widely adopted until recently, which may have been due to the lack of enabling technology.¹ Prior to IKA's release of the ElectraSyn 2.0, many examples of electrochemistry required bespoke glassware which represented a barrier to use of this powerful tool, although other commercial electrochemical cells were available.

There are several essential aspects to an electrolytic cell. A typical electrolysis cell contains an anode, a cathode, an electrolyte solution, and a potentiostat to control the current or potential of the cell. The anode and cathode must both be immersed in a solution that is of sufficient conductivity to allow migration of ions between the cathode and the anode. This solution is called the electrolyte solution and is usually an organic solvent with a salt dissolved into it to increase conductivity. In an electrolytic cell, the cathode has a negative polarity, at which reductions occur, and the anode, at which

oxidations occur, is positive. In some experiments, especially in analytical electrochemical cells, a reference electrode is necessary. The reference electrode is used to accurately measure the potential that is applied across the anode and cathode. The potential or current of an electrochemical reaction is controlled by a potentiostat, which can be thought of as a variable battery.

During an electrolysis experiment, a potential is applied across the anode and cathode in solution to effect either an oxidation or reduction of a substrate. The working electrode, which can be either the anode or the cathode, is the electrode at which the desired reaction is occurring. For instance, if the desired reaction is an oxidation, the working electrode is the anode. The second electrode in the cell then becomes the counter, or auxiliary, electrode and is simply used to complete the circuit. Secondary (or even 'sacrificial') reactions occur at this electrode. The anode and the cathode material can vary between experiments, but the most common materials include carbon (graphite, reticulated vitreous carbon), platinum, magic diamond (boron-doped carbon) and stainless steel. The reference electrode is typically a silver wire electrode in an aqueous solution of KCl; this electrode is usually encased in a porous material that allows ions to pass through so that the electrode can be used in organic solvents.

1.1.2. Electrochemical Reactor Design

There are two types of electrochemical reactor: (a) a divided and (b) an undivided cell (**Figure 3**). A divided cell is one in which the anode and cathode are in separate compartments. In this case, a reference electrode may be necessary which is placed in the same compartment as the working electrode. The compartments are usually separated by a porous frit or membrane, but a salt bridge can also be used. This salt bridge allows electrons and ions, but not organic molecules, to flow freely between the compartments. Sometimes, the electrolyte solution, which is placed in the anodic compartment of the cell, is called the anolyte, while the electrolyte solution in the cathodic compartment is referred to as the catholyte. A divided cell is required if the product of the electrochemical reaction is also redox active, and the reverse reaction is observed at the opposite electrode. One such reaction would be the electrochemical oxidation of an alcohol to a carbonyl. The carbonyl can be reduced back to the alcohol at the cathode, and therefore the experimental set up could benefit from a divided cell. Electrolysis substrates that contain acid-sensitive or electro-active substituents that are not the desired group to be electrolysed, may also benefit from a divided cell set

up. Large potentials/lower currents are often observed due to the increase in resistance from the membrane or salt bridge when using a divided cell.

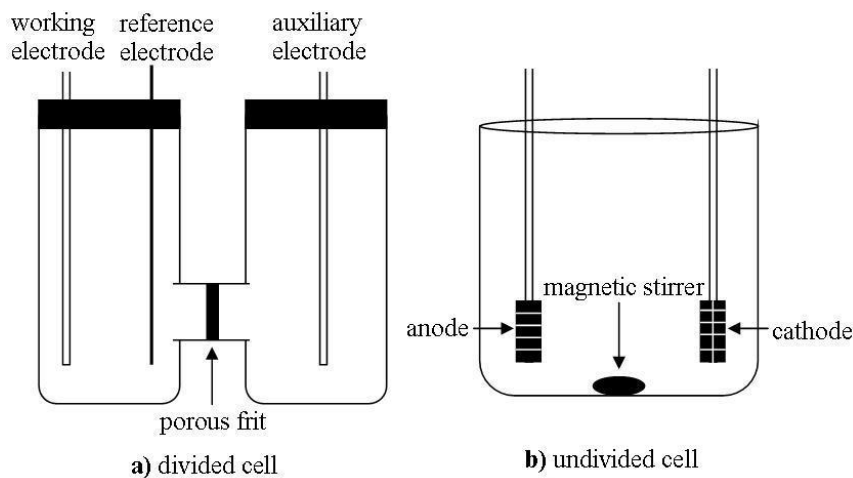


Figure 3: The two main types of electrochemical reactor designs: a) divided cell; b) undivided cell.

An undivided cell is the easier of the two cell types to set up and to use; it is simply a vessel into which an electrolyte solution is placed along with submerged electrodes. This type of electrolytic cell is used when the products are not susceptible to reaction at the opposite electrode. Undivided cells are most commonly used for constant current electrolysis (CCE), while divided cells are better suited for constant potential electrolysis (CPE). A constant current experiment is one in which the current is kept constant while the potential is allowed to vary. The converse is true for a constant potential experiment, where the potential is kept constant while the current is allowed to vary. Both cell types will benefit from being stirred as this will improve the mass transfer of substrate to the electrode surface.

A constant potential experiment allows for greater control and selectivity over which substrates are oxidised or reduced. This derives from the fact that each substrate will have a different oxidation or reduction potential. A common belief is that if the potential across the electrodes in an electrochemical reactor is set to a given value, only those electroactive species whose oxidation or reduction potentials are below the set value will be oxidised or reduced. However, this is not always as simple as an “on/off” switch with applied potentials and redox potentials of substrates. The potential that is selected and applied across the electrodes is set relative to a reference electrode and therefore constant potential reactions require a third electrode to be placed in the electrolyte solution. One disadvantage of a constant potential experiment is that as the electroactive species is consumed during the reaction, the observed current in the

solution will decrease. This means that constant potential experiments are hard to drive to completion, with complete conversion achieved only after extended reaction times.

Constant current experiments, by contrast, may not be as selective as constant potential experiments. A current is maintained by the potentiostat and the potential is allowed to vary, either positively or negatively, until the oxidation or reduction potential of the electroactive species is achieved. In an ideal situation, the potential is then stabilised until all the electroactive species is consumed, at which point the potential is allowed to vary again until it reaches the oxidation or reduction potential of the next electroactive species. However, this may not be the case in reality due to other factors such as mass transfer to and from the electrode as the potential can vary according to the electrical double layer. It is assumed that the oxidation or reduction potential of the substrate is known as this can be used to determine when the reaction is complete, which is shown by the potential increasing or decreasing further. Oxidations occur at the anode where electrons are transferred from molecule to electrode, while reductions occur at the cathode, where electrons are transferred from electrode to molecule. This transfer of electrons between molecule and electrode can be viewed as an overall flow of current from the cathode to the anode and therefore an electrical circuit is completed.

1.1.3. Electrical Double Layer

Electrochemical reactions are dependent on the choice of electrode material. This is because the transfer of electrons between the substrate and electrode occurs solely on the surface of the electrode. Helmholtz described an electrical double layer in solution at the electrode surface when a potential is applied.¹⁵ For instance, at the anode, a positive charge is applied. This positive charge generates a strong electrical field which attracts negative ions from the solution to form what is known as the compact inner layer that is only a few Ångstroms wide. As shown in **Figure 4**, the compact inner layer is illustrated as the distance from the electrode to d_1 . These negative ions can in turn attract positive ions, but with less of an effect than the anode attracts the negative ions. The diffuse layer is the plane described by Helmholtz as the distance from d_1 to d_2 in **Figure 4**, and is thought to be tens to hundreds of Ångstroms wide. The potential in the compact inner layer decreases linearly with increasing distance from the electrode until d_1 is reached, at which point the potential

decreases exponentially. It is generally accepted that all reductions and oxidations take place within the compact layer, which is why highly reactive radical species can be generated in the presence of nucleophilic and protic solvents. This compatibility can be explained by the fact that the radical species formed at the electrode needs to diffuse away from the surface of the electrodes before reacting with other organic molecules. Furthermore, these electrogenerated radicals are formed in very small quantities; the concentration of these species is limited by the surface area of the electrodes. However, in some cases (such as Kolbe electrolysis) the local concentration (when compared to the bulk solution) of radical species can be generated which may be of benefit to the desired reaction.

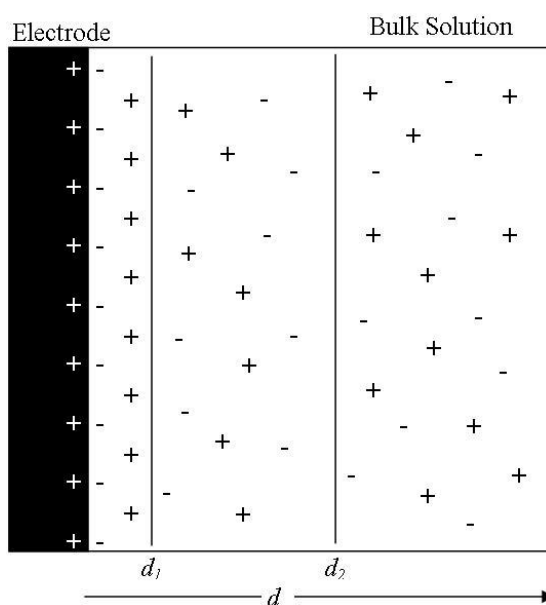


Figure 4: Illustration of the electrical double layer produced when a potential is applied to an electrode.

1.1.4. Cyclic Voltammetry

To determine the potential at which an electroactive species either oxidises or reduces, voltammetry can be performed. There are two types of voltammetry, namely linear sweep voltammetry and cyclic voltammetry. Linear sweep voltammetry is the procedure in which the potential during the analysis is swept between two potentials in one direction. Cyclic voltammetry, on the other hand, is the analytical method in which the potential is swept from one potential to another and then back to the original potential. In both cases, the potential is controlled and the current is measured. The rate at which the potential is swept between the two desired points is called the scan rate and typically has units of $\text{mV}\cdot\text{s}^{-1}$. Electric potential, or simply potential, is defined as the amount of work needed to move a unit of positive charge from a reference location to a specific point inside an electric field without producing acceleration; potential has units volts, V (or $\text{J}\cdot\text{C}^{-1}$), with potential also be denoted by V . Electric current (or current) is defined as the flow of electric charge, i.e. the movement of electrons inside a wire, and has units of amperes, A, and is denoted by i ; ampere is the flow of electric charge across a surface at a rate of one coulomb of charge per second ($\text{C}\cdot\text{s}^{-1}$) It can also be defined as the movement of ions in an electrolyte solution.

Cyclic voltammetry (CV) is the most common and preferred method of electrochemical analysis of substrates. CV allows for the calculation of several useful parameters that can help to determine the reaction conditions. For instance, from CV, the oxidation or reduction potential of an electroactive species can be calculated and therefore establish at what potential the electrolysis is to be conducted. A further useful parameter that can be calculated from CV experiments is the diffusion coefficient, which is calculated by performing a CV experiment at several scan rates and plotting the peak current against the square root of the scan rate; this plot should produce a straight line as the current is directly proportional to the square root of the scan rate (at room temperature), as shown by the Randles-Sevcik equation (**Equation 1**):¹⁶

$$i_p = 268,600n^{\frac{3}{2}}AD^{\frac{1}{2}}C\nu^{\frac{1}{2}}$$

Equation 1: The Randles-Sevcik equation used to determine the diffusion co-efficient of an electrochemical species; where i_p is the peak potential, n is the number of electrons in the oxidation/reduction that are transferred, A is the area of the electrode surface, D is the diffusion coefficient, C is the concentration of solution and ν is the scan rate.

One benefit from performing cyclic voltammetry on the constituent parts of the electrochemical experiment, or just the species of interest, is that the CV can give an insight into the nature of the oxidation or reduction. For example, a CV can show whether the oxidation or reduction is reversible or irreversible. A reversible cyclic voltammogram is shown in **Figure 5**; the potential has been swept from 0 V to 1 V and back to 0 V. As can be seen in the CV, there is an oxidative peak at 0.53 V, followed by a reductive peak at 0.45 V. In this case, ferrocene is the electroactive species and is oxidised to the ferrocenium ion, which is subsequently reduced back to ferrocene in a classic one electron process. The stability and reliability of the ferrocene/ferrocenium electrochemical redox couple has led to its adoption as an external standard for calibrating CV experiments. A decrease in current is observed in all cyclic voltammograms after the peak current is achieved as mass transport to the electrode surface is limited by the diffusion of the electroactive species. However, the current does not reach zero because the electron transfer process is still occurring but at a higher rate and is limited by the diffusion of the electroactive species to and from the surface, and therefore a current can still pass through the solution. This phenomenon is only observed in a CV experiment in which the solution is not stirred. Stirring the solution will assist the diffusion of the electroactive species and the current would plateau at the peak current.

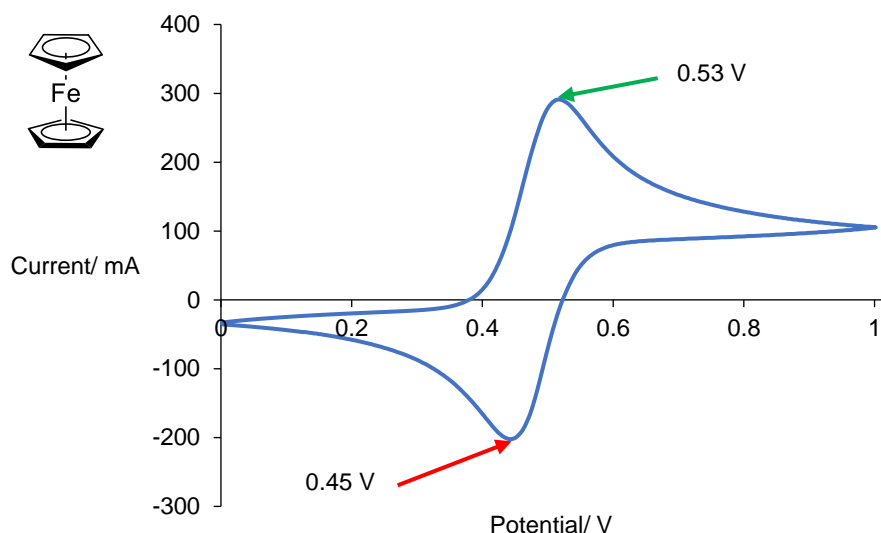


Figure 5: The cyclic voltammogram of ferrocene vs. Ag/AgCl reference electrode; an example of a reversible oxidation of an electroactive species. Conditions: 10 mM Ferrocene, 0.1 M Et₄NBF₄-MeCN, GC anode, Pt cathode, 50 mV.s⁻¹.

For many organic molecules in a CV experiment, an irreversible cyclic voltammogram is observed. This is due to the instability and high reactivity of the oxidised or reduced molecule, which is assumed to irreversibly react with another component in the electrolyte solution. **Figure 6** shows an example of an irreversible cyclic voltammogram of an organic molecule; as illustrated in the CV of *N*-Boc-pyrrolidine, only an oxidative peak is observed at 1.61 V when the potential is swept from 0 V to 2 V and back.

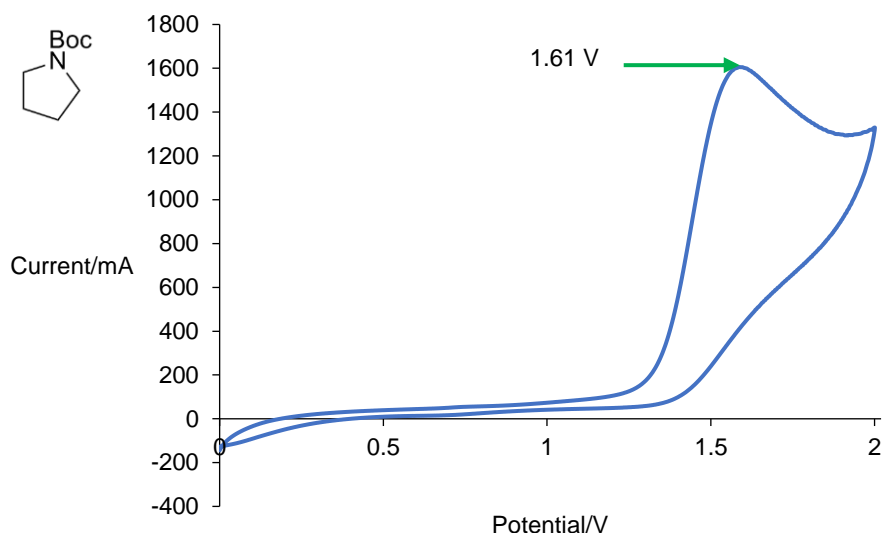
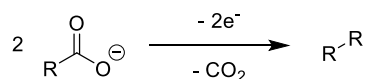


Figure 6: An example of the irreversible oxidation of *N*-Boc-pyrrolidine vs. Ag/AgCl reference electrode. Conditions: 10 mM *N*-Boc-pyrrolidine, 0.1 M Et₄NBF₄-MeCN, GC anode, Pt cathode, 50 mV.s⁻¹.

Cyclic voltammetry experiments can also provide useful information on the conditions of the electroorganic reaction. For instance, solvents can play a significant role in electrochemical reactions and different solvents have varying potential windows. A suitable solvent can be chosen using CV, to avoid oxidation of the solvent. Furthermore, the choice of electrolyte can affect the potential window of the solvent;¹⁷ using acetonitrile as the solvent and lithium perchlorate as the electrolyte, a potential window of -3.0 V to +2.5 V can be achieved. If tetraethylammonium tetrafluoroborate (Et₄NBF₄) is used as the electrolyte in acetonitrile, a potential window of -1.8 V to +3.2 V can be achieved. Outside of the potential windows, the solvents may be oxidised or reduced preferentially over the substrate.

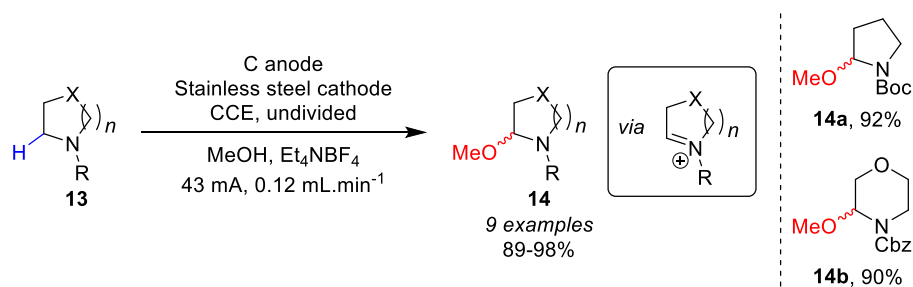
1.1.5. Direct Electroorganic Synthesis

Direct, or non-mediated, electrochemical reactions involve the electroactive species being directly oxidised or reduced at the electrode. Synthetic electrochemistry has been around since the 19th century when Kolbe published the electrochemical homo-coupling of carboxylate anions.¹⁸ This reaction, known as the Kolbe electrolysis, has been used extensively over many years, and is a powerful method for C–C bond formation (**Scheme 2**).¹⁹



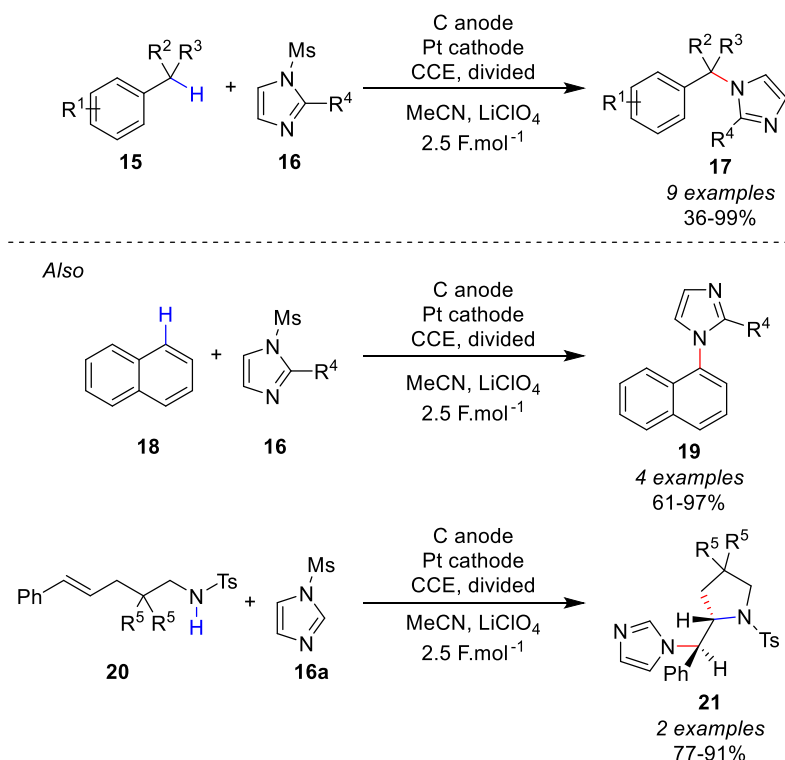
Scheme 2: Homo-coupling of radicals derived from carboxylate anions using Kolbe electrolysis.

A revival of electroorganic chemistry took place in the 1970s and 1980s. A notable direct electrolysis reaction was from Shono *et al.* and involved the anodic oxidation of carbamates as a key step in the carbon-carbon bond forming reaction of amines.²⁰ The anodic oxidation of amines gave an acyliminium ion *in-situ* which was trapped by the methanolic solvent, to give α -methoxylated carbamates. This reaction is now known as the Shono oxidation and is often employed for the synthesis of intermediates that are suitable for the Lewis or Brønsted acid mediated C–C bond formation. The Shono oxidation has recently been adapted for use in an undivided microfluidic electrochemical flow system by the group of Brown.²¹ They passed a solution of *N*-formylpyrrolidine in Et₄NBF₄-MeOH through the electrochemical flow cell at a constant current of 44 mA to give a conversion to the α -methoxylated amides of greater than 90%. Two years later, the Ley group used flow chemistry as an enabling technology for the Shono oxidation; the methodology was used to prepare α -methoxylated cyclic amines as key intermediates in the synthesis of nazlinine and other alkaloid derivatives (**Scheme 3**).²² The cyclic substrates required *N*-protection, with protecting groups including *tert*-butyloxycarbonyl (Boc), acetyl (Ac) and trimethylsilylethoxycarbonyl (Teoc). All reported α -methoxylations gave high yields of 89 - 98%, with the Cbz-protected morpholine giving the α -methoxylated morpholinyl product **14b** in 90% isolated yield. It is also noted that this system was shown to work with a 20 mol% electrolyte solution, while most electrolysis reactions are typically carried out with an electrolyte solution of at least 100 mol%.



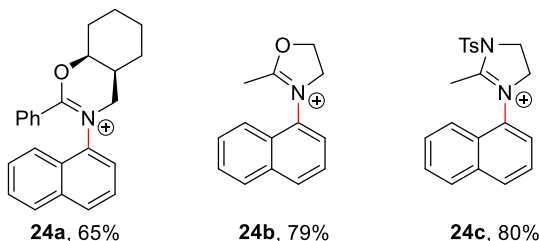
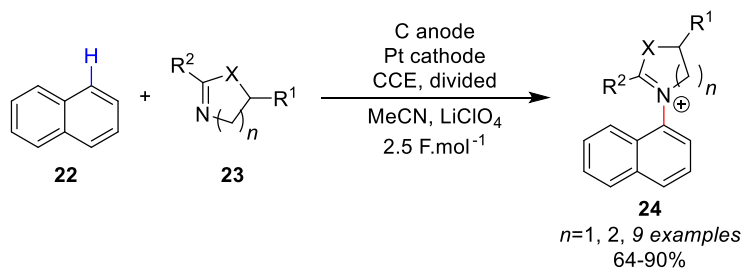
Scheme 3: The Shono oxidation of carbamates in a flow electrochemical cell by the Ley group.

The synthesis of biologically active imidazole-substituted aromatic compounds was achieved electrochemically by the Yoshida group (**Scheme 4**).²³ Using a divided cell to avoid over-oxidation, a one-electron oxidation to form the *N*-arylimidazolium ions, followed by a non-oxidative removal of the imidazole protecting group, gave the corresponding imidazole-substituted aromatic and benzylic compounds **17** in 36 to 99% isolated yields. Electron-donating groups, such as methoxy, on the aromatic rings helped to facilitate the electrochemical reaction by stabilising the resulting cation that was formed. Furthermore, the methoxy group could also be used as a handle for subsequent chemistry. A robustness screen was also carried out and showed that halide substituents were compatible with the oxidative electrochemistry, providing further chemical handles for a variety of downstream chemistry.

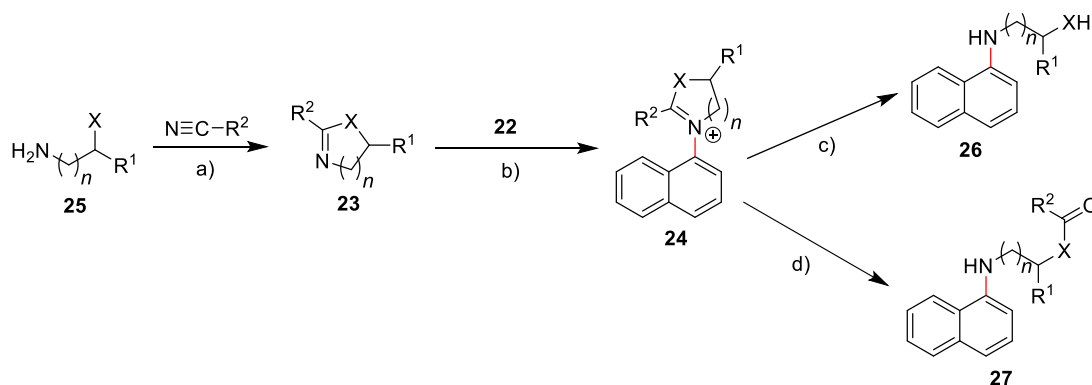


Scheme 4: The electrooxidative C–H functionalisation of aromatic and benzylic compounds in a direct C–N coupling with imidazoles.

Yoshida and co-workers went on to develop an approach to achieving the same coupling but for functional alkylamines (**Scheme 5**).²⁴ Their approach consisted of preparing masked functional alkylamines **23** and oxidatively coupling them with the aromatic compounds **22**. This heterocyclisation (**Scheme 6**) gave several key benefits: i) over-oxidation of the heterocycles was not observed due to the increased stability of the cationic intermediates; ii) there were no protons in either of the groups after the cyclisation which could disturb the electrochemical reaction; iii) the oxidation potential of the heterocycles was much higher than the oxidation potential of the aromatic compounds due to the hybridisation of the nitrogen centre; iv) the heterocycles are sufficiently nucleophilic to trap the radical cation intermediate of the aromatic compound. **Scheme 6** shows the cationic intermediate **24** that was formed and the functionalised alkylamine groups could be unmasked; during work up with aqueous sodium carbonate **27** was obtained, while work up with ethylenediamine gave the free alcohol **26** (when X = O).



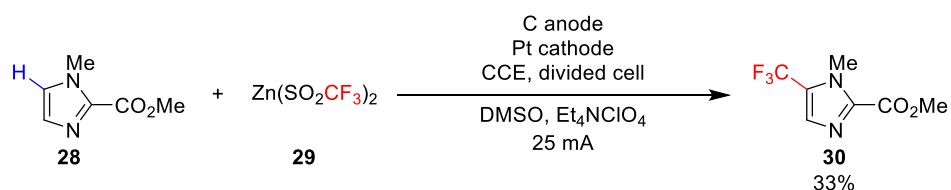
Scheme 5: The direct electrolysis of masked functional alkylamines in the C–H functionalisation of aromatic compounds.



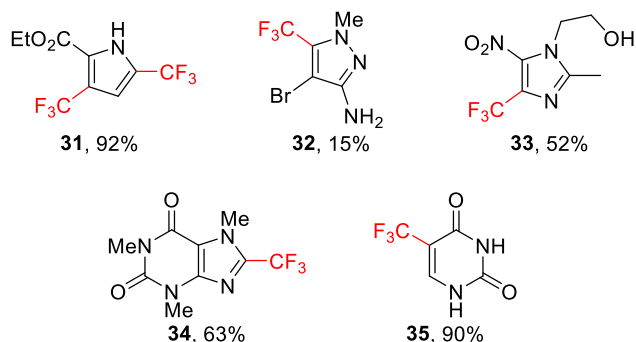
Scheme 6: The direct electrolysis of masked functional alkylamines in the C–H functionalisation of aromatic compounds. a) condensation with nitriles; b) electrochemical coupling; c) ethylenediamine work up; d) aqueous sodium carbonate work up.

An example of electrochemistry providing a greener and safer approach is the work of Baran which used electrochemistry as an alternative radical initiator to *tert*-butylhydroperoxide (TBHP) in the trifluoromethylation of heterocyclic substrates.²⁵ In this methodology, zinc trifluoromethanesulfinate salts were used as the CF₃ radical source. In the original approach, TBHP oxidised the sulfinate which eliminated SO₂ gas to form CF₃ radicals.²⁶ However, this procedure had several limitations including low yields for some substrates, and these limitations were not well understood. Calorimetry provided valuable insight into the initiation, with an unproductive heat observed when the sulfinate salt was mixed with TBHP. It was suggested that this, combined with high loadings (up to 4 equivalents) of the salt and TBHP, led to side-reactions of the CF₃ radicals that were formed. Electrochemistry provided greater

control over the formation of the trifluoromethyl radicals which led to improved yields over the traditional chemical approach. Heterocyclic substrate **28** could be converted into the corresponding trifluoromethylated heterocycle **30** with lower loadings (decreased from 4 eq. to 1.4 eq.) of the sulfinate salt **29**. Substrates that were previously found to possess poor reactivity towards the TBHP-initiated methodology could now be employed in the electrochemical route. One such substrate is compound **31** shown in **Scheme 7** that was synthesised in an excellent 92% isolated yield. This investigation demonstrates the capability of electrochemistry, even on gram scale, as an alternative to other approaches.

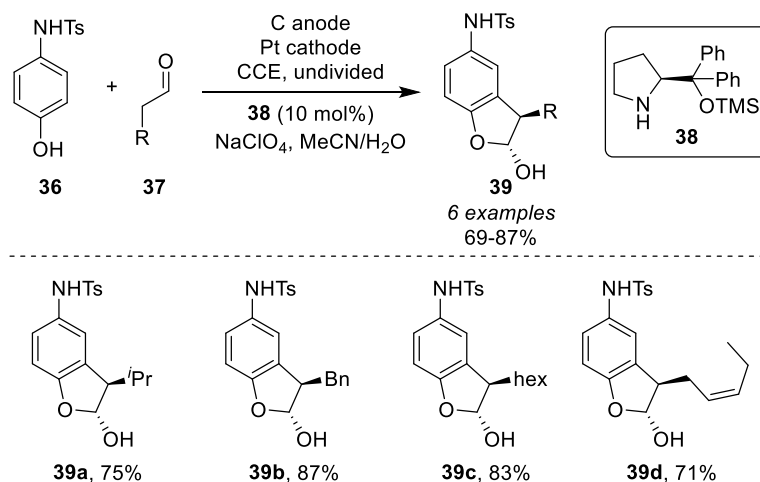


Further derivatisations include other N-heterocycles:



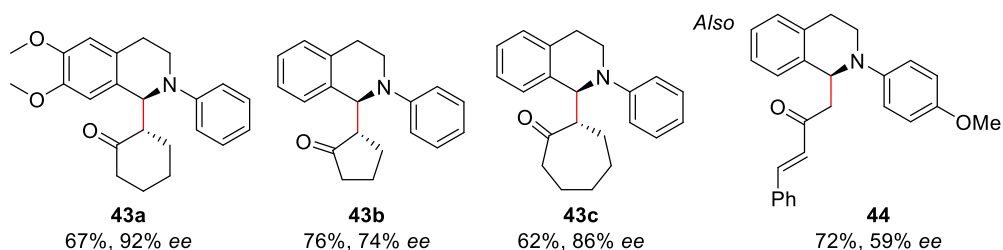
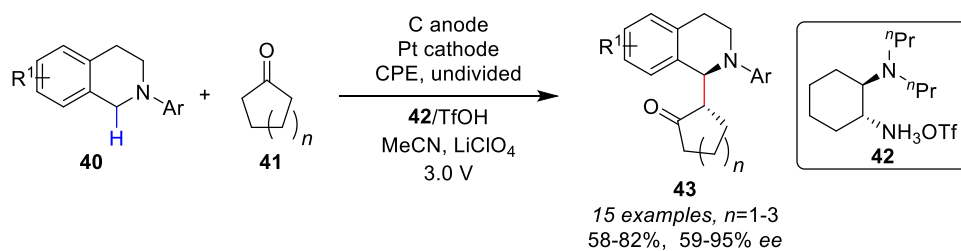
Scheme 7: An alternative to a radical initiation by peroxide; trifluoromethyl C–H functionalisation under electrochemical control.

Enantioselective C–H functionalisation has previously proved to be a difficult transformation, but recent success has involved a synergistic coupling of C–H activation and C–H functionalisation. The use of anodic oxidation paired with organocatalysis was demonstrated by Jørgensen and co-workers when they stereoselectively coupled electron-rich phenols with aldehydes (**Scheme 8**).²⁷ However, this method only worked for electron-rich phenols.

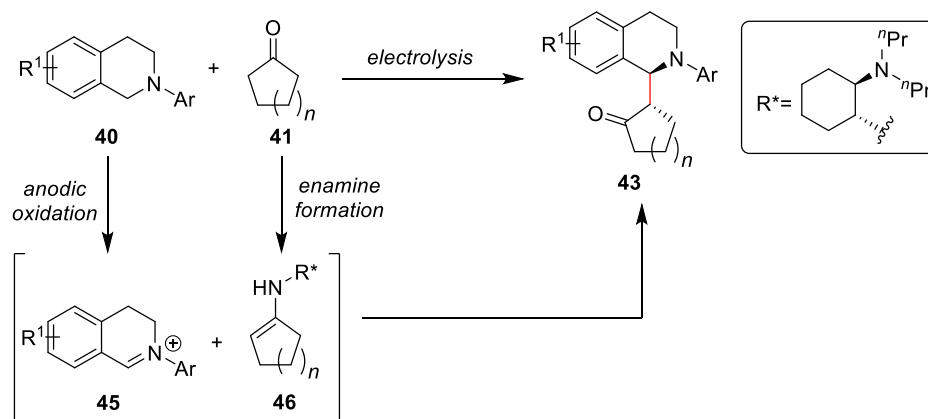


Scheme 8: The combined electrocatalytic and organocatalytic coupling of electron-rich phenols with aldehydes by the Jørgensen group.

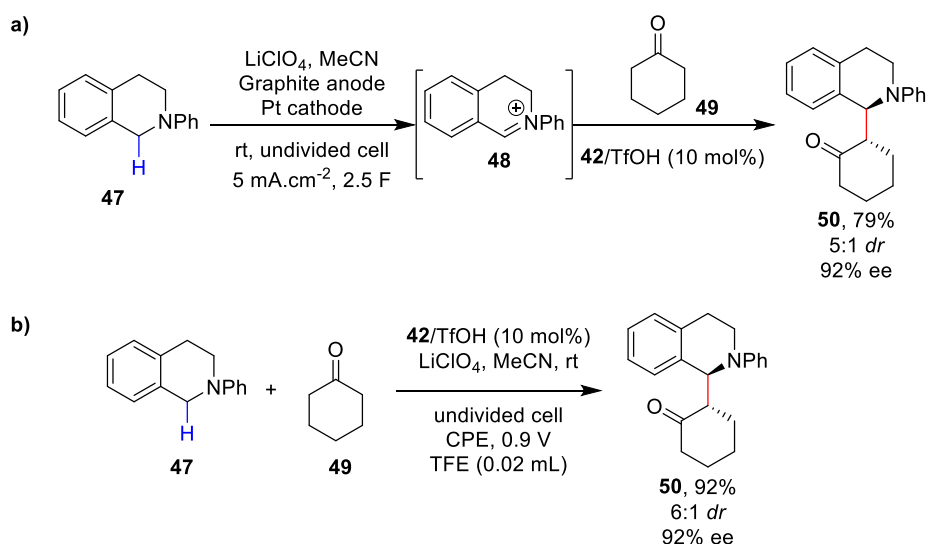
Moreover, a catalytic asymmetric cross-dehydrogenative coupling (CDC) of simple ketones with secondary amines under electrochemical conditions was developed by Luo (**Scheme 9**).²⁸ The Luo group expanded the scope to include the coupling of simple ketones with secondary amines using a chiral primary amine as an organocatalyst. The catalyst reacts to form an enamine (**46**, **Scheme 10**) *in-situ*, which subsequently combines with iminium ion **45** generated by the electrochemical oxidation of secondary amine **40**. It was demonstrated that substituents at all positions of the *N*-aryl ring were tolerated. Cyclopentanone and cycloheptanone, which had previously proved to be difficult substrates in CDC reactions, were shown to be effective partners with **43b** and **43c** prepared in 76% and 62% yield, respectively. Furthermore, the utility of this electrochemical reaction was demonstrated by the synthesis of **44** showing that acyclic ketones could also be coupled. Good to excellent enantiomeric excesses were achieved and moderate to good diastereomeric ratios were observed. Control experiments demonstrated that controlled potential electrolysis was much more selective than controlled current experiments. By electrolyzing **47** under constant current conditions first and then introducing the ketone/organocatalyst mixture, a yield of 79% was achieved (**Scheme 11a**). However, electrolyzing the whole mixture of components under constant potential conditions, a yield of 92% was achieved (**Scheme 11b**). Neither the enantiomeric excess nor the diastereomeric ratio was affected by the mode of electrolysis.



Scheme 9: Catalytic asymmetric electrochemical oxidative CDC of tertiary amines with ketones.



Scheme 10: The *in situ* generated enamine nucleophile is used to trap the iminium that is formed by anodic oxidation.



Scheme 11: a) Two-step constant current electrolysis control experiment; b) Constant potential electrolysis (CPE) control experiment.

1.1.6. Mediated Electroorganic Synthesis

The use of a mediator during electrochemical reactions has advantages over direct electrolysis. One such advantage is that the mediator usually exhibits a lower potential than the substrate and as such, a lower potential (or current) can be applied to the reaction mixture to affect an electrochemical reaction. However, one must be aware of the subtle differences in reaction mechanisms between using a mediator and not using a mediator. These subtle differences manifest themselves in the type of electron transfer that occurs, whether this is by an outer-sphere electron transfer or inner-sphere. One further point is that in both mediated and non-mediated electrochemical reactions, the initial electron transfer is a heterogeneous electron transfer to the electrode from the species that is being oxidised (or from the electrode to the species, in the case of a reduction).

An outer-sphere heterogeneous electron transfer reaction is one in which the reactants, products and intermediates do not react directly with the electrode surface; instead the electron that is transferred is believed to tunnel through a monolayer of solvent molecules.²⁹ Outer-sphere electron transfer reactions are usually unaffected by the electrode material, i.e. changing electrode material has negligible effect on the efficiency of the process.

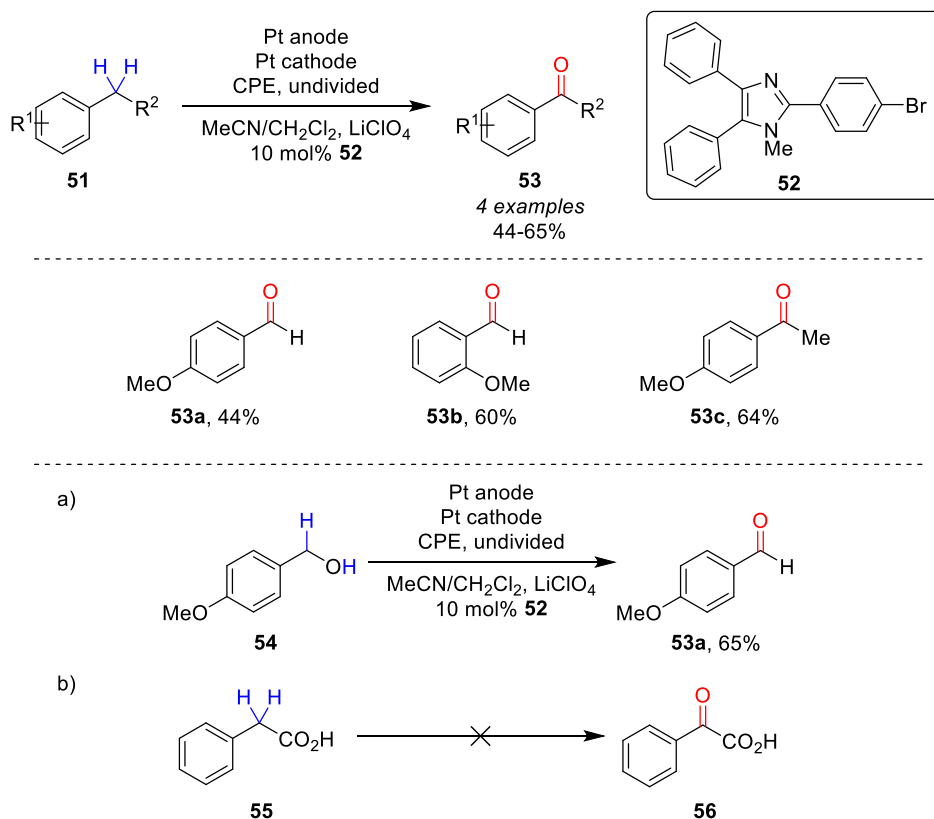
On the other hand, inner-sphere heterogeneous electron transfer reactions are those in which the reactant or product forms a strong interaction with the electrode surface, which facilitates the electron transfer; such interactions can include adsorption to the surface. Inner-sphere electron transfer reactions are heavily dependent on the electrode material as this will govern the interaction between the electrode surface and the reactants.

In some cases, the potential of a direct oxidation/reduction of a reactant at an electrode is greater than that of the solvent. In this situation, there is either a poor matching of the redox potential of the reactant with the Fermi level of the electrode material or there is poor surface chemistry, i.e. the interaction between the reactant and the electrode is not sufficient to allow an electron to transfer between them. A simple solution to the first problem is switching electrode materials. However, if the reaction still does not proceed, then use of a mediator may be necessary.

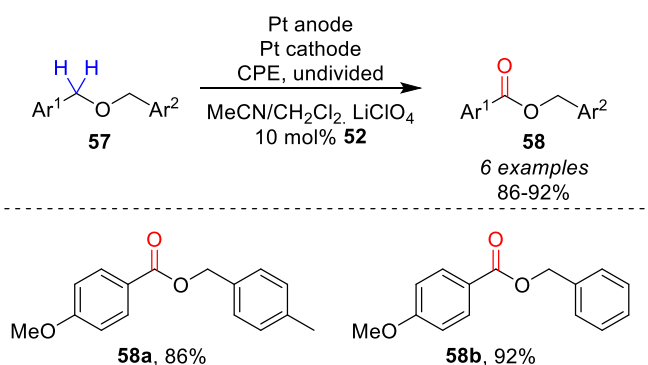
A mediator can be particularly useful when the potential of the substrate is beyond the potential of the solvent. Electrochemical reactions involving the functionalisation

of unactivated C–H bonds, which typically have oxidation potentials >3 V, are often carried out using mediators such as (2,2,6,6-tetramethylpiperidin-1-yl)oxyloroxidanyl (TEMPO).^{10d}

Triarylaminines have found use as redox mediators but have several shortcomings including complex synthesis and poor chromatographic separation after reactions.³⁰ However, a recent development from the Little group has shown that triarylimidazole scaffolds can act as redox catalysts, with these issues addressed.³¹ Little and co-workers showed that redox catalyst **52**, under constant potential conditions, effectively catalysed the oxidation of aromatic compounds **51**, with examples of benzylic C–H oxidation demonstrated (**Scheme 12**). They showed three examples bearing only *ortho* or *para*-methoxy substituted benzenes. Utilising the same conditions, it was demonstrated that 4-methoxybenzyl alcohol **54** could be oxidised to the corresponding aldehyde **53a**. However, no reaction was observed when an analogous acid was subject to electrolysis (**Scheme 12b**). It was suspected that these observations were a result of a large potential difference between the mediator and substrate. In the oxidation of unsymmetrically substituted aryl ethers **57**, it was observed that the benzylic position of the most electron-rich aromatic group was preferentially oxidised (**Scheme 13**). Furthermore, as with the previous benzylic oxidations, if the difference in redox potentials between the mediator and the substrate was too large, no conversion was observed. It was also demonstrated that, in the absence of mediator, no reaction was observed, evidencing the advantages of mediated electrolysis over non-mediated electrolysis.



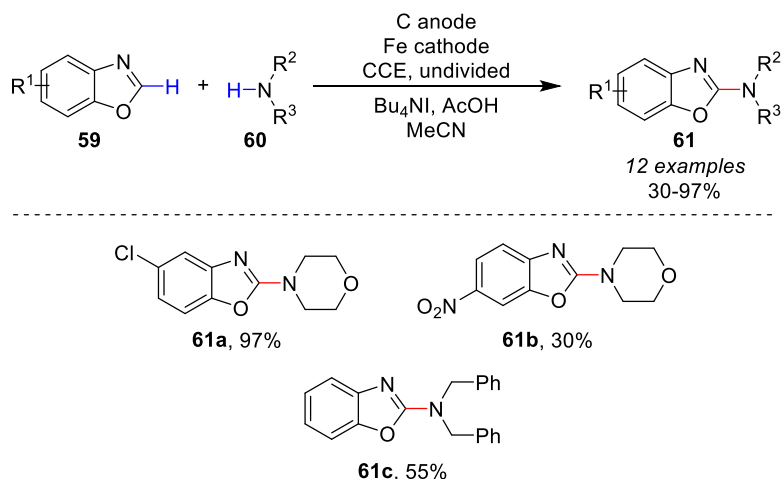
Scheme 12: The benzylic oxidation mediated by a triarylimidazole redox catalyst from the group of Little.



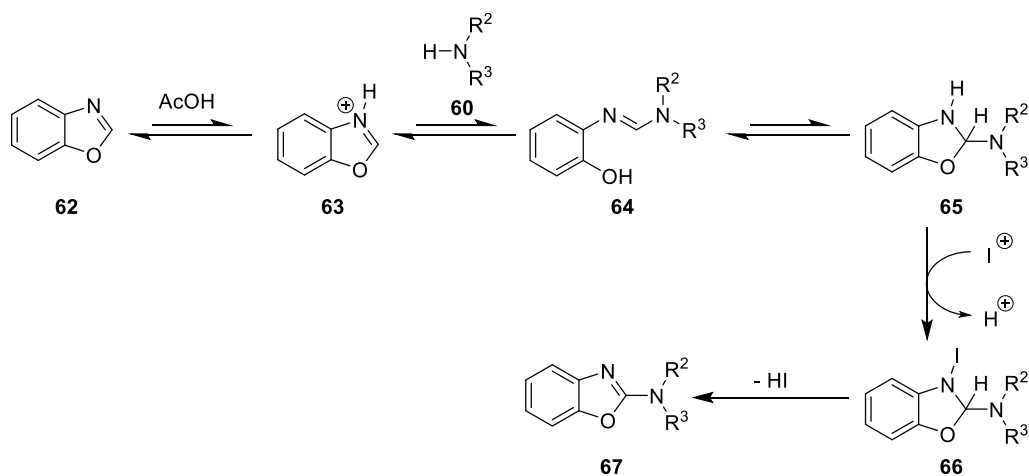
Scheme 13: The mediated oxidation of unsymmetrical biaryl ethers using a triarylimidazole mediator.

Among the multitude of redox catalysts available to the synthetic electrochemist, sources of halide ions have emerged as very versatile mediators in cooperation with other redox catalysts.³² The Little group have demonstrated that tetrabutylammonium iodide can effectively catalyse the electrochemical oxidative amination of benzoxazoles **59** in poor to excellent yields (**Scheme 14**).³³ The mechanism that was proposed (**Scheme 15**) showed that the acetic acid additive protonated the

benzoxazole **62** to give **63**, which was then ring-opened by nucleophilic attack of amine **60** to give **64**. An equilibrium between the imine **64** and the closed ring form **65** was then established. The substituted benzoxazoline **66** underwent a substitution of the acidic proton for the electrophilic iodine species, which was formed from the anodic oxidation of the iodide anion; base-facilitated elimination of HI from **66** yielded the product **67**.



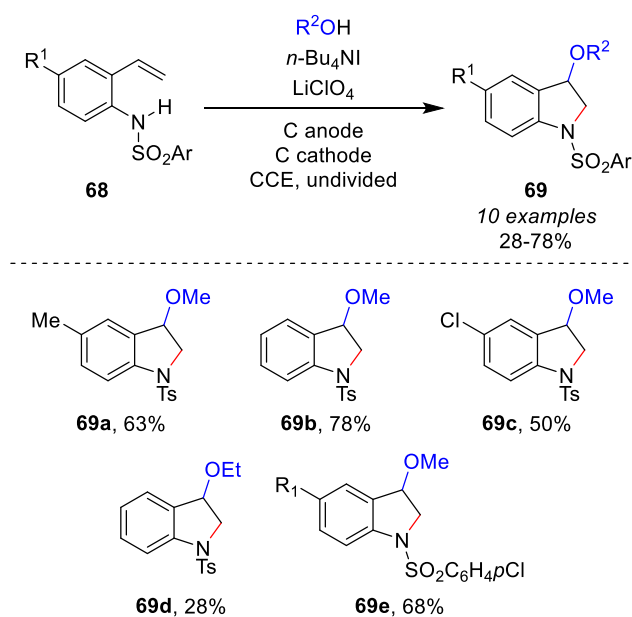
Scheme 14: The iodide-mediated electrochemical oxidative amination of benzoxazoles developed by Little and co-workers.



Scheme 15: The proposed mechanism from the Little group for the oxidative amination of benzoxazoles.

Tetrabutylammonium iodide has been demonstrated to be an effective redox catalyst for the formation of indolines through a C–N/C–O cascade bond formation sequence.³⁴ Application of constant current electrolysis to *N*-(2-vinylphenyl)-sulfonamide derivatives **68** with tetrabutylammonium iodide in methanol afforded the

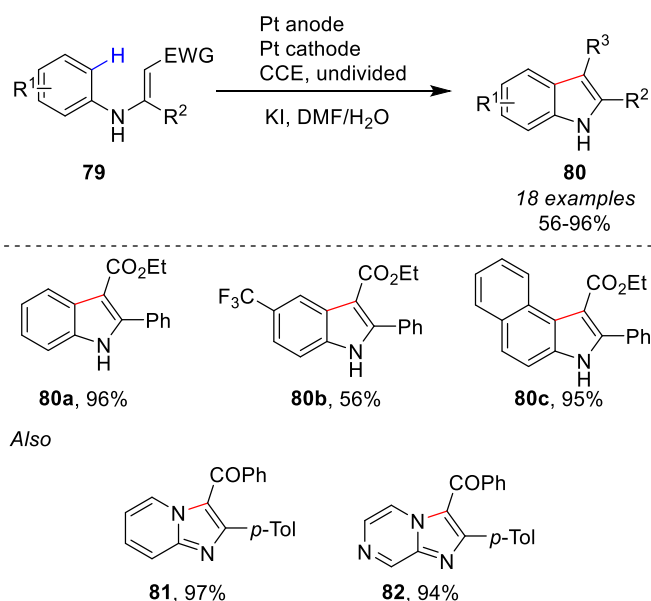
corresponding products **69** (**Scheme 16**). The yield of the reaction was influenced by the properties of the substituents on the phenyl ring, with higher yields observed with electron-withdrawing groups. Moreover, a gram-scale reaction was carried out resulting in 68% isolated yield of **69b**, demonstrating the practicality and facile scalability of such an electrochemical transformation. Furthermore, the electrochemical reaction could be performed under conditions in which no additional electrolyte was necessary. This represented a sustainable process that produces much less waste.



Scheme 16: The intramolecular oxidative annulation of N-aryl enamines to give substituted indole derivatives.

3-Amino-2-thiocyanato- α,β -unsaturated carboxyl compounds have found use in the synthesis of thiazole derivatives which show herbicidal and other biologically relevant activities. However, synthesis of compounds such as **72** often require strong oxidising agents, harsh conditions and several steps. It was envisioned by the Little group that C–H functionalisation of β -dicarbonyl compounds **70** could be achieved under electrochemical conditions with the use of bromide ions as redox catalysts (**Scheme 17**).³⁵ Under constant current electrolysis, dicarbonyl compounds **70**, in the presence of an NH_2 and SCN source, underwent a C–N/C–S bond forming sequence, and subsequent C–H functionalisation, to give the corresponding 3-amino-2-thiocyanato- α,β -unsaturated carboxyl derivatives **72** in moderate to good yields (**Scheme 17**). The NH_2 and SCN source was ammonium carbamodithioate **71**, although other sources

Intramolecular CDC reactions to form indoles have been known for many years, however, these often require strong oxidising agents in vast excesses. A more atom-economical route to substituted indoles would be direct annulation, with hydrogen gas as the primary by-product. The Lei group developed such a reaction in which *N*-aryl enamines were electrolysed under constant current conditions with an iodide redox catalyst (**Scheme 19**).³⁶ The yields for this transformation were moderate to excellent and demonstrated the utility of electrochemical redox reactions. Both electron-withdrawing and electron-donating groups were well tolerated. Furthermore, *N*-pyridyl enamines were shown to give imidazo[1,2-*a*]-pyridines **81** and **82** in excellent yields. In the proposed reaction pathway, the iodide anion was oxidised at the anode to produce the electrophilic iodine species, which was substituted for the proton on the nitrogen of enamine **79**. The N–I bond was homolytically cleaved to give a nitrogen-centred radical, which rearranged to give a carbon-centred radical in the β -position of the imine. This carbon radical then cyclised onto the ring and the resulting species was oxidised further, with subsequent tautomerisation giving the corresponding product **80**.

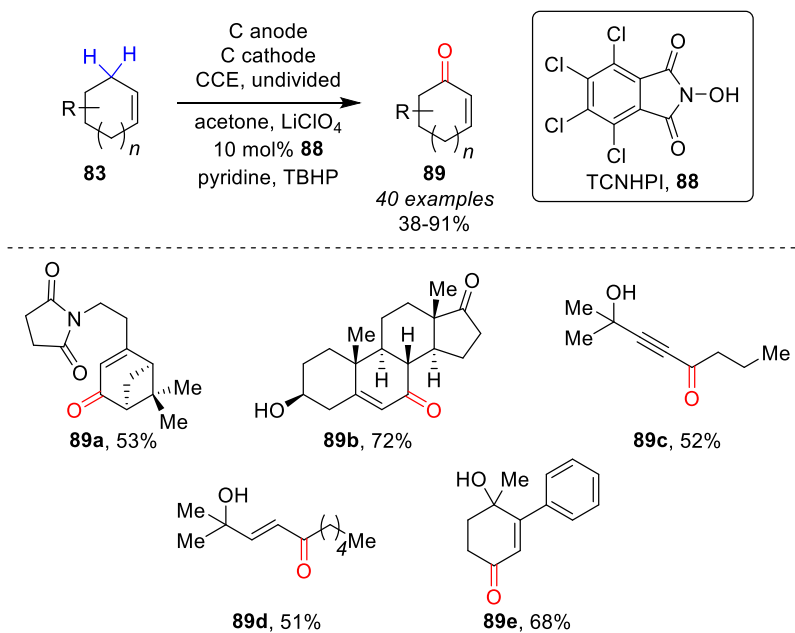


Scheme 19: The iodide-mediated electrolysis of *N*-aryl enamines to give substituted indole derivatives

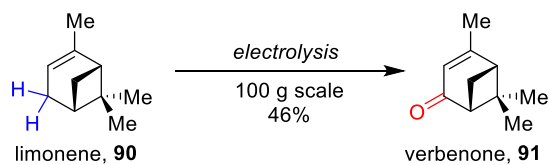
C–H functionalisation has recently become an intensely researched area due to the atom economical aspects of the transformation. The combined use of C–H functionalisation of unactivated bonds and synthetic organic electrochemistry not only

represents a very green process but may also allow access to much more reactive intermediates. These highly reactive intermediates could participate in a variety of pathways, some of which may be novel. Synthetic electrochemistry can also remove the necessity for the use of strong oxidising reagents, as well as expensive transition metal catalysts such as palladium, rhodium and iridium. Retrosynthetic analyses of molecules, particularly in the pharmaceutical industry, could be heavily impacted by the emergence of direct C–H functionalisation transformations and lead to more efficient routes to desired compounds.

Oxidation of allylic systems is an important application in the synthesis of many compounds by virtue of the versatility of enones and allylic alcohols. These oxidations are sometimes carried out using superstoichiometric amounts of reagents, toxic oxidants or expensive catalysts, some of which include rhodium,³⁷ palladium,³⁸ and chromium.³⁹ However, the Baran group recently developed an electrochemical allylic oxidation procedure that is scalable and sustainable (**Scheme 20**).⁴⁰ With a combination of tetrachloro-*N*-hydroxyphthalimide (TCNHPI) **88** as the redox catalyst and TBHP as a co-oxidant, oxidation of allylic systems can be achieved with yields that are similar to, or better than, those observed when using transition metal catalysis or strong oxidants. The versatility of the procedure was demonstrated with oxidation of allylic systems of steroids and other steroidal derivatives. Protection of alcohols was shown to be unnecessary with the oxidised dehydroepiandrosterone (DHEA) **89b** synthesised in 72% isolated yield. In addition, glycosylated DHEA, with unprotected alcohols, was oxidised in 38% isolated yield. Acyclic substrates were well tolerated with **89c** synthesised in 52% and an acyclic alkenyl alcohol **89d** isolated in 51% yield. A reaction conducted on a hundred-gram scale demonstrated the ease of scalability, with verbenone **91** isolated in 46% yield (**Scheme 21**). Traditional oxidations on this scale using chromium oxidants would require at least 81 g of chromium reagent and the need for special waste treatment. It is noted that not all acyclic alkenes gave the ketone product in high conversion, as some showed conversion to the allylic alcohol. However, longer reaction times converted the allylic alcohols to the desired ketones.



Scheme 20: Electrochemical allylic C–H oxidation mediated by Cl₄NHPI and using TBHP as a co-oxidant from the Baran group.

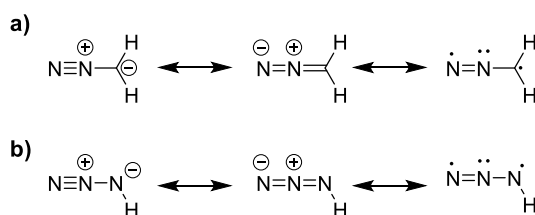


Scheme 21: The allylic C–H oxidation of limonene to verbenone, conducted on a 100 g scale.

1.2. 1,3-Dipolar Cycloadditions

1,3-Dipolar cycloadditions are a class of reaction that involve the coupling of a 1,3-dipole and a dipolarophile, the product of which is a five-membered ring. Although 1,3-dipolar cycloadditions had been known since the late 19th century,⁴¹ with a review published by Smith in the late 1930s,⁴² it was the pioneering work of Rolf Huisgen in the 1960s that demonstrated the extent of the utility of these reactions. His group conducted ground-breaking work on elucidating the mechanism and synthetic applications. Due to this seminal work, 1,3-dipolar cycloadditions are often referred to as Huisgen cycloadditions, although this is used primarily for the reaction between azides and alkynes to give 1,2,3-triazoles. Synthetic utility of 1,3-dipolar cycloadditions can be found in the regioselective and stereospecific formation of five-membered heterocycles and their acyclic derivatives.

A 1,3-dipole is a zwitterionic species whose structure can be represented as either a propargyl/allenyl-type or allyl-type octet/sextet. These structures share 4π electrons over three atoms and they can be shown using resonance structures that delocalise the charges over an extended π -system (**Scheme 22**). The allyl-type dipoles have a bent ground state geometry while the propargyl/allenyl-type dipoles have a linear geometry. As a consequence of the resonance structures that can be drawn for 1,3-dipoles, each terminus can be both nucleophilic and electrophilic in nature. The true nature of each terminus can be determined by calculating the co-efficient of the highest occupied molecular orbital (HOMO) on each atom; the atom bearing the largest co-efficient of HOMO is nucleophilic and conversely, the atom bearing the largest co-efficient of the lowest unoccupied molecular orbital (LUMO) is electrophilic.



Scheme 22: a) The suggested resonance structures of diazomethane;
b) The proposed resonance structures of an azide.

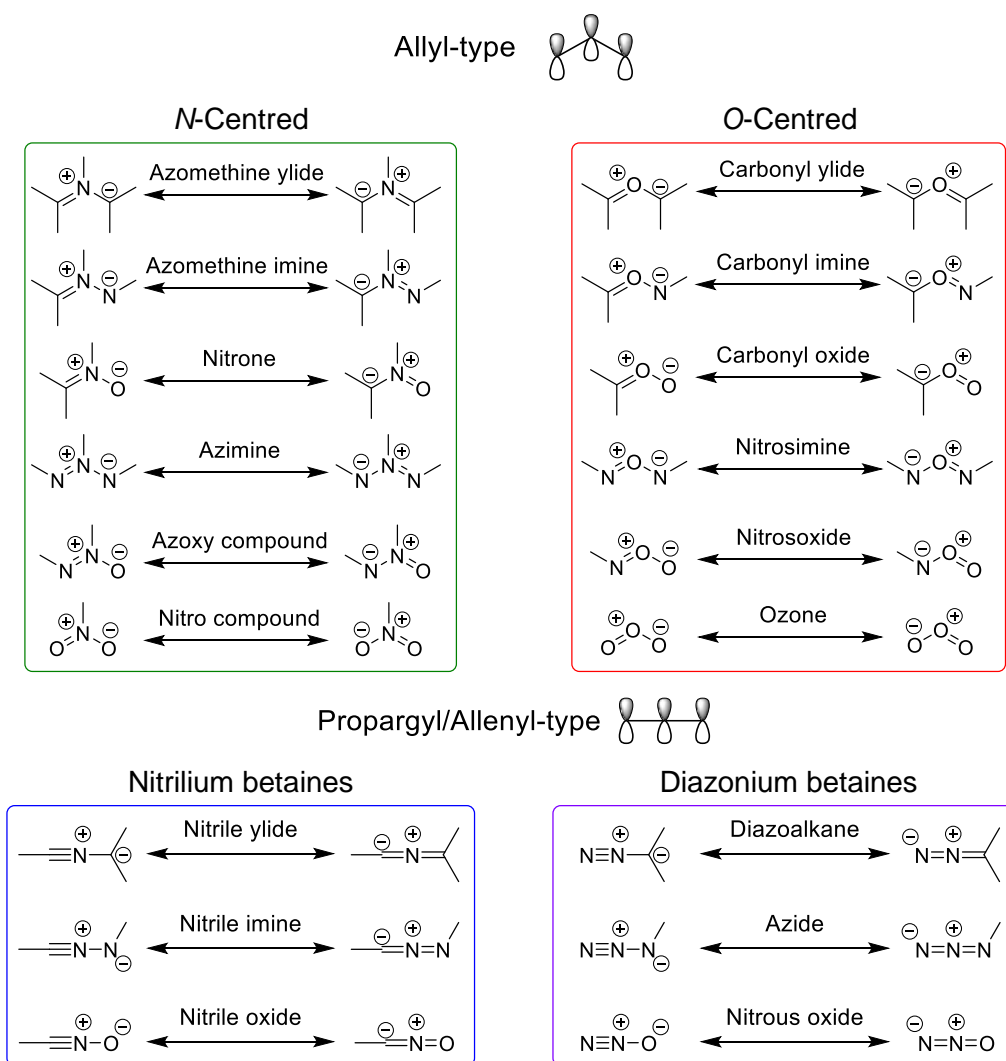


Figure 7: Types of 1,3-dipoles that can participate in 1,3-dipolar cycloaddition reactions

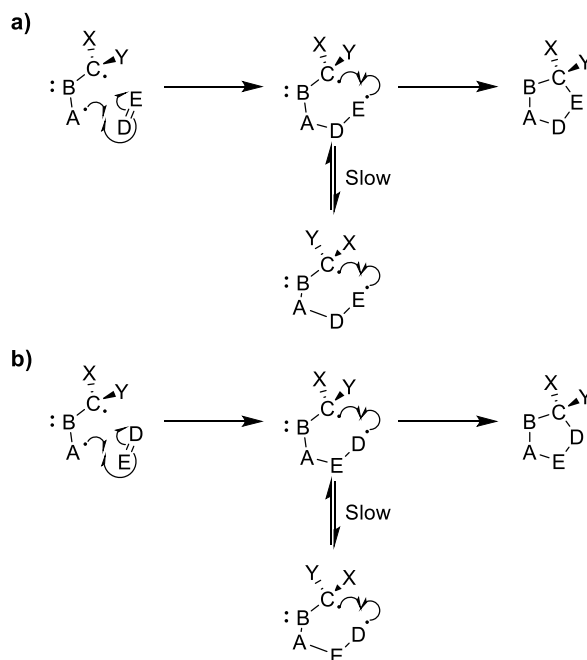
This suggests that the most electron-rich atom is the nucleophile, but this is not always the case. Examples of 1,3-dipoles are shown in **Figure 7**: these are classified by the central atom (for allyl-type 1,3-dipoles) and the type of betaine (for propargyl/allenyl 1,3-dipoles).

A dipolarophile is an organic species that contains a multiple bond system and can participate in 1,3-dipolar cycloadditions. These molecules are often alkenes and alkynes, but dipolarophiles containing heteroatoms, such as aldehydes/ketones and imines/nitriles, have also found use in this reaction.

1.2.1.Mechanism

There was much debate regarding the mechanism of 1,3-dipolar cycloadditions in the late 1960s. This culminated in a publication from Raymond Firestone,⁴³ and its reply from Rolf Huisgen.⁴⁴

Firestone suggested that the reaction progressed in an asynchronous fashion through a spin-paired biradical intermediate (**Scheme 23**). He proposed that the stereospecificity of the reaction could be explained by the high barrier of bond rotation of the biradical species and so no stereochemical information was lost. Furthermore, Firestone proposed that, although it is supposedly still allowed by the Woodward-Hoffmann rules, the reacting partners may not need to avoid a co-planar transition state; these reactions could proceed through either a co-planar transition state or a transition state in which the dipolarophile approached from above or below the plane of the 1,3-dipole. Firestone also offered an explanation for the regioselectivity of the addition of unsymmetrical dipolarophiles to unsymmetrical 1,3-dipoles, stating that, if all other factors including sterics are controlled, the regiochemistry was solely governed by the electronics of the cycloaddition. This means that the more electrophilic end of the dipolarophile would react with the more nucleophilic end of the 1,3-dipole. Although Firestone was an advocate for a two-step process, he did concede that the same regiochemical hypothesis also applied to a concerted cycloaddition mechanism. Firestone also admitted that understanding of radicals and their behaviour was very limited at the time and not all outcomes could be explained thoroughly due to lack of experimental data.

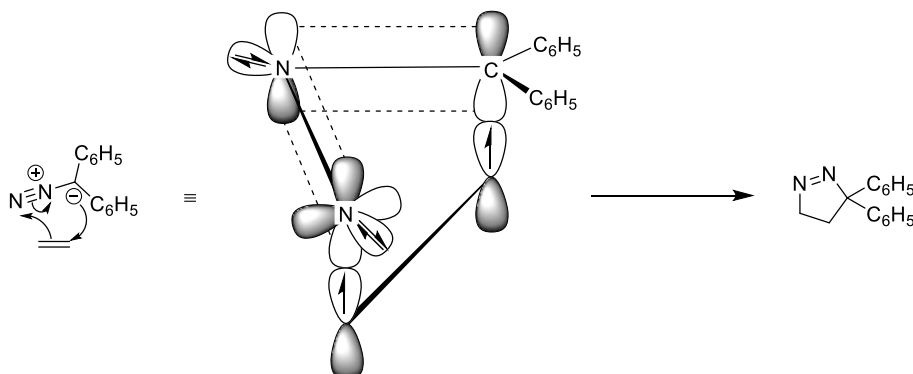


Scheme 23: Firestone's proposed mechanistic pathway, involving the a spin-paired biradical intermediate species.

On the other hand, Huisgen proposed a concerted pathway for dipolar cycloaddition reactions. Huisgen argued that due to resonance theory and molecular orbital (MO) theory, the diradical resonance form that Firestone proposed could not exist. According to resonance theory put forward by Wheland,⁴⁵ diradical resonance forms could be neglected as they contain less σ -bonds than the zwitterionic resonance forms. Additionally, Huisgen pointed out that the spin-paired bi-radical intermediate put forward by Firestone could not obey the Woodward-Hoffmann rules as the electrons participating in the reaction, on the part of the 1,3-dipole, are not arranged in an appropriate molecular orbital. These electrons do not contribute to any π -bonding system because they occupy lone pair orbitals and so the conjugation throughout the biradical system was impaired.

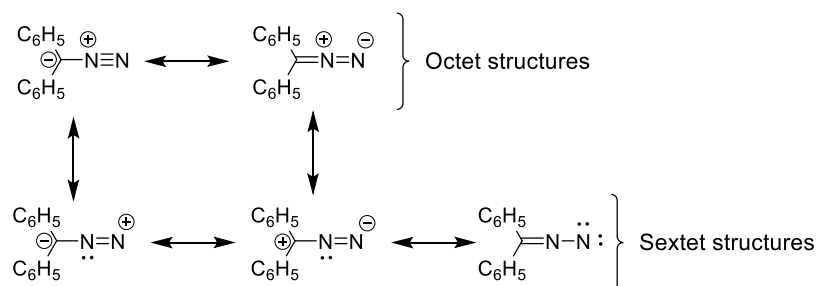
Huisgen went on to point out that a transition state in which the dipolarophile reacts from above or below the plane of the 1,3-dipole must occur for all 1,3-dipolar cycloaddition reactions (**Scheme 24**). This is supported by the Woodward-Hoffmann rules⁴⁶ and by the fact that this orientation preserved the resemblance of the 1,3-dipoles to allyl anions (or propargyl/allenyl structures). Huisgen also likened the transition state of these cycloadditions to that of the Diels-Alder reaction which he

claimed further strengthened his hypothesis that the cycloaddition proceeded in a concerted fashion.



Scheme 24: An example of a 1,3-dipolar cycloaddition transition state: the 1,3-dipole LUMO and dipolarophile HOMO react in such a way that the dipolarophile approaches from above or below the plane of the dipole.

With regards to Firestone's assumption that a 1,3-dipole has a nucleophilic end and an electrophilic end, Huisgen argued that that hypothesis was unlikely to be true. This is because resonance theory suggests that there is no full formal charge on either end of the dipole, but rather there are several contributing structures in which full charges are placed on the termini of the molecule (**Scheme 25**). This breeds confusion as it could be interpreted as separate isomers of the dipole, rather than canonical structures. Furthermore, as a consequence of these resonance structures, relatively small dipole moments are observed for many 1,3-dipoles. Huisgen further added that these resonance structures were also responsible for the small observed solvent effects, with 1,3-dipolar cycloadditions not affected by solvent polarity to any significant extent. It is often observed that the dipole moment of the product from cycloadditions is larger than that of the starting 1,3-dipole, another fact that Huisgen insisted bolstered the idea that 1,3-dipoles reacted *via* a zwitterionic form.



Scheme 25: A small dipole moment is observed for many 1,3-dipoles since the resonance hybrid (or true chemical form) of these molecules does not have full formal charges on either terminus of the dipole, and so electronically are almost symmetrical.

To counter Firestone's suggestion on the orientation of dipolarophile addition, Huisgen stated that, through numerous experiments from within his group, the regioselectivity was kinetically driven rather than thermodynamically driven. Huisgen also noted that this orientation phenomenon was not well known at the time, a similar problem observed for the Diels-Alder reaction, and that more detailed empirical data was still lacking.

The mechanism that is generally accepted today is that of the concerted pathway and all stereochemical and regiochemical outcomes can be predicted *via* the same rules that allow predictions of the outcomes of all concerted cycloaddition reactions (such as Diels-Alder reactions). However, it has been known that 1,3-dipolar cycloadditions can occur in a step-wise fashion,⁴⁷ although these are few and far between. In addition to this, further experimental data has shown that the concerted mechanism is asynchronous; although the reaction is concerted, the two σ -bonds in the transition state are formed at different rates.

1.2.2. Frontier Molecular Orbital Interactions

1,3-Dipolar cycloadditions are pericyclic reactions which obey, the Dewar-Zimmerman rules⁴⁸ as well as the Woodward-Hoffmann rules.⁴⁶ Applying the Dewar-Zimmerman rules, the dipolar cycloadditions proceed through a five-membered, aromatic six-electron Hückel transition state that has zero nodes (**Figure 8a**). Furthermore, application of the Woodward-Hoffmann rules state that the 1,3-dipole and the dipolarophile will interact in a $4\pi_s+2\pi_s$ fashion, which is a thermally, and symmetry, allowed suprafacial-suprafacial interaction (**Figure 8b** and **Figure 8c**). This interaction can be achieved in one of three ways: Type I, Type II or Type III. The dominant interaction in the transition state is the one in which the HOMO-LUMO energy gap is the smallest.

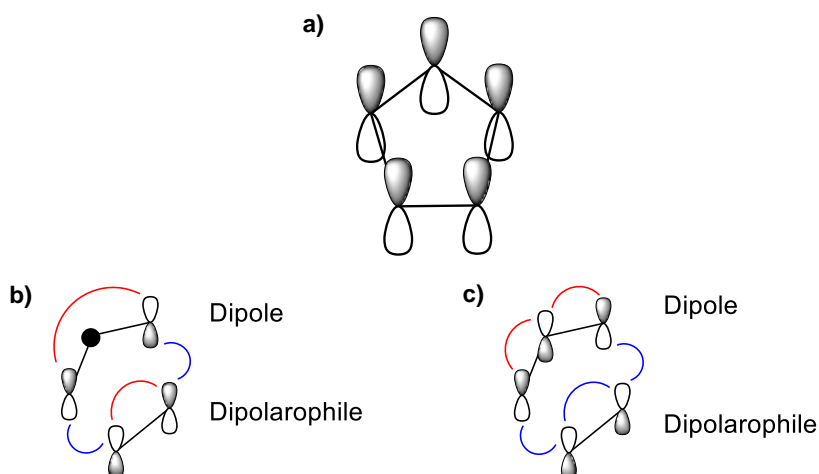


Figure 8: a) Zimmerman-Dewar treatment gives a five-centre, six electron Hückel transition state which is an allowed transformation; b) $\text{HOMO}_{\text{dipole}}\text{-LUMO}_{\text{dipolarophile}}$ interaction is symmetry allowed as there are two phase changes; c) $\text{LUMO}_{\text{dipole}}\text{-HOMO}_{\text{dipolarophile}}$ interaction is also symmetry allowed as it possesses two phase changes.

Type I interactions (**Figure 9**, red path) are those in which the high-lying HOMO of the dipole interacts with the dipolarophile LUMO. Dipoles that interact in this way are often termed as HOMO-controlled or nucleophilic dipoles, of which examples include the nitrile ylide, carbonyl imine and diazoalkane. Rates of reaction in which Type I dipoles are involved can be accelerated with electron-withdrawing groups (EWGs) on the dipolarophile, lowering the energy of the dipolarophile LUMO, or electron-donating groups (EDGs) on the dipole, raising the energy of the dipole HOMO. This type of reactivity and interaction is most commonly observed during normal-electron-demand Diels-Alder reactions, in which the diene HOMO reacts with the dienophile LUMO.

Rate accelerations by tempering the electronics of the substrate in this way is exemplified by the reaction of diazomethane with ethyl acrylate, whose rate is a million times faster than the corresponding reaction with butyl vinyl ether (**Scheme 26**).⁴⁹

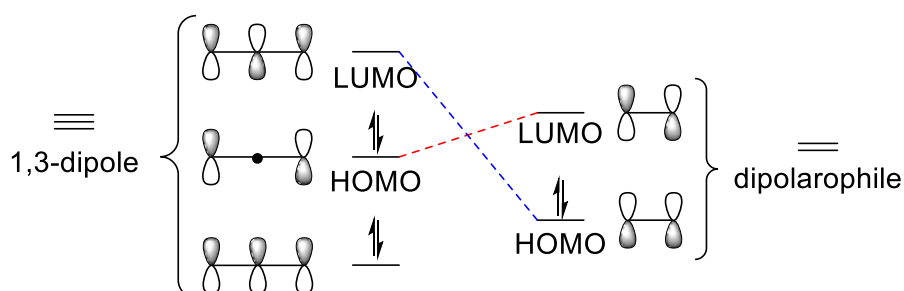
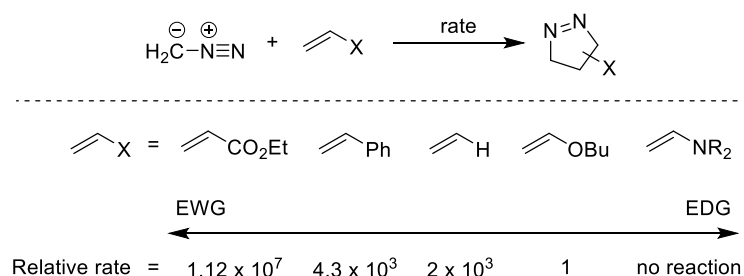
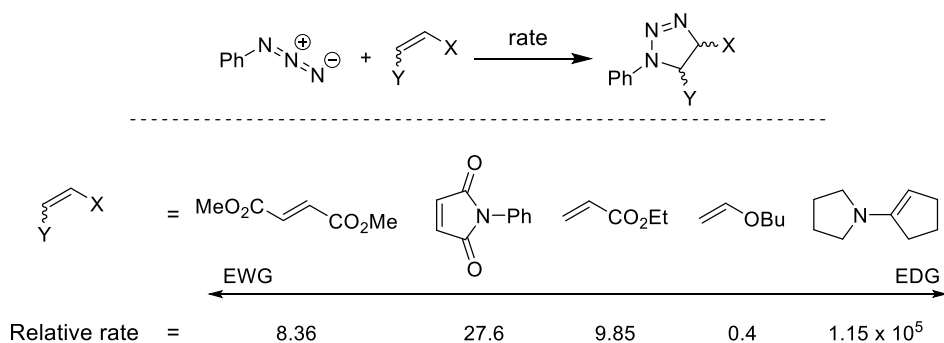


Figure 9: Molecular orbital diagram showing the possible interactions between 1,3-dipoles and dipolarophiles in 1,3-dipolar cycloaddition reactions.



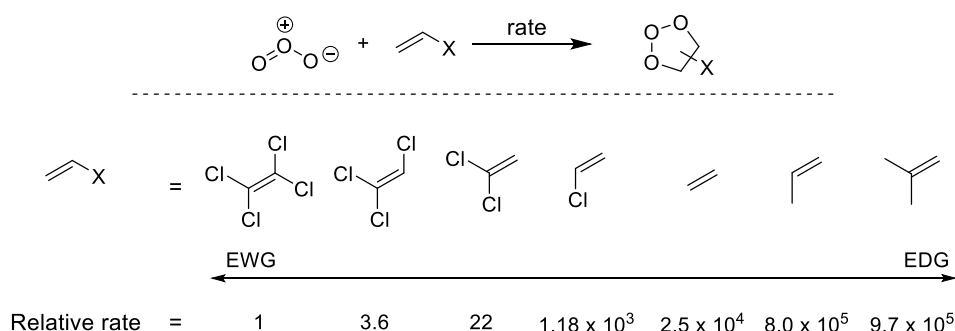
Scheme 26: The rate of reaction of dipolar cycloadditions with Type I interactions can be increased by using an electron-poor dipolarophile.

Type II interactions (**Figure 9**, either path) are interactions in which the HOMO or LUMO of the dipole can interact with the LUMO or HOMO of the dipolarophile as the energy gaps between the orbitals are relatively small and are similar in either direction. 1,3-Dipoles that react in this manner are often termed HOMO-LUMO-controlled dipoles or ambiphilic dipoles; nitrile imines, nitrile oxides and azides are among those dipoles that fall into this category. Any substitution on either partner of the reaction can increase the rate of reaction either by raising the HOMO with EDGs or lowering the LUMO with EWGs; these substituents serve to decrease the energy gap between the interacting orbitals and therefore increase the rate of reaction (**Scheme 27**).⁵⁰



Scheme 27: The rate of reaction for Type II interactions can be increased with any substitution on either reaction partner as the energy levels are very similar.

Finally, dipoles that possess a low-lying LUMO interact with the HOMO of the dipolarophile in Type III interactions (**Figure 9**, blue path). These dipoles are referred to as electrophilic or LUMO-controlled dipoles and include the likes of ozone and nitrous oxide. As is expected by this type of interaction, substitution on the dipole with EWGs serves to increase the rate of reaction by lowering the LUMO. Conversely, substitution with EDGs gives rise to a decreased rate as this raises the LUMO, increasing the energy gap between the two interacting orbitals. Inverse-electron demand Diels-Alder reactions are often characterised by this type of interaction in which the diene LUMO interacts with the dienophile HOMO. The effect of these substitutions on the rate of reaction is illustrated in **Scheme 28**, in which ozone is observed to react with the more-electron rich dimethylpropene approximately 100,000 times faster than with the electron-poor tetrachloroethene.⁵¹



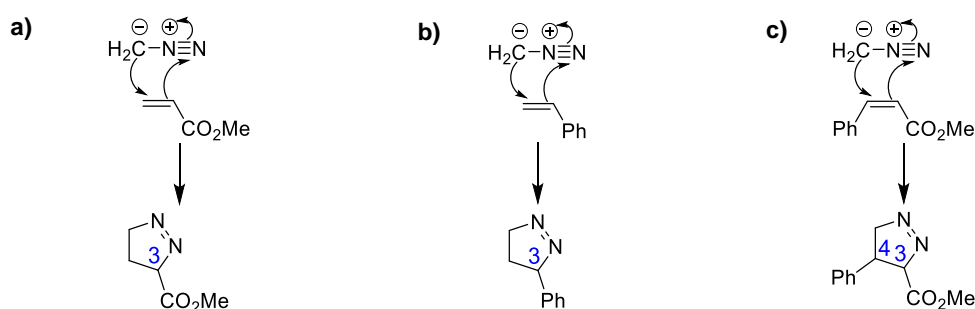
Scheme 28: Rate acceleration of dipolar cycloadditions in which Type III interactions occur can be achieved with EDGs on the dipolarophile, raising the HOMO.

Apart from being able to vary the rate of reaction by altering the energies of the interacting frontier molecular orbitals, many other factors contribute to the reactivity of 1,3-dipoles with dipolarophiles. Concerted pericyclic reactions, such as 1,3-dipolar

cycloadditions, require relatively low enthalpies of activation but, because they proceed through a highly ordered transition state, these reactions display very large, negative entropies of activation. Some general observations based on empirical evidence has offered some insight into the factors that govern reactivity. For example, hetero-dipolarophiles will combine with 1,3-dipoles more slowly than their C–C counterparts as there is less net gain in energy when forming C–heteroatom σ -bonds and breaking C–heteroatom π -bonds in the transition state. Furthermore, the geometric isomeric form of the dipolarophile can greatly influence the rate of a 1,3-dipolar cycloaddition reaction. For instance, *cis*-stilbenes add to nitrile imines 27 times slower than *trans*-stilbenes due to the phenyl groups in the *cis*-stilbene eclipsing each other in the transition states as the bond angles decrease from 120° to 109°.

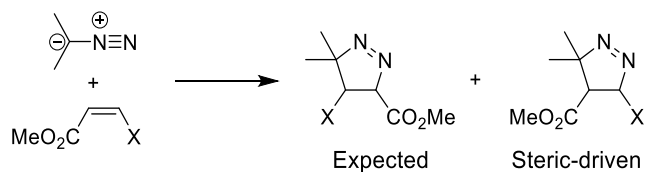
1.2.3. Regioselectivity

The largest factor that governs regioselectivity of 1,3-dipolar cycloadditions is electronics. As mentioned above (Section 1.2.2), the more nucleophilic end of the 1,3-dipole will interact with the more electrophilic end of the dipolarophile. The atom bearing the largest HOMO coefficient on the 1,3-dipole (and therefore the most nucleophilic) will interact with the atom bearing the largest LUMO coefficient on the dipolarophile (which is by comparison, the most electrophilic atom).⁵² The pairing of the orbitals in this particular way is only true for Type I interactions where the HOMO of the dipole is interacting with the LUMO of the dipolarophile. However, the principle still holds for the other types of interactions as the atoms bearing the largest coefficients of the interacting frontier molecular orbitals, be it the HOMO or LUMO of either partner, will still combine in this regioselective manner. For example, **Scheme 29** shows the reaction of diazomethane with different dipolarophiles and in all cases the diazomethane carbon bears the largest HOMO coefficient:⁴⁹ i) C3 substitution is observed during the reaction with methyl acrylate as the terminal alkene carbon possesses the largest LUMO coefficient (**Scheme 29a**); ii) C3 substitution is also observed for the reaction with styrene as the largest LUMO coefficient is also on the terminal alkene carbon (**Scheme 29b**); iii) reaction with methyl cinnamate yields the 2-pyrazoline in which the methyl ester is in the C3 position as the largest LUMO coefficient is on the β -carbon from the ester group due to the ester being the most electron-withdrawing substituent on the dipolarophile (**Scheme 29c**).



Scheme 29: a) The terminal carbon has the largest LUMO coefficient resulting a 3-substituted pyrazoline; b) The terminal carbon has the largest LUMO coefficient resulting in a 3-substituted pyrazoline; c) The β -carbon to the ester bears the largest LUMO coefficient and gives the observed 3,4-substituted pyrazoline.

However, sterics can overcome the electronic effects when the substituent is large enough. As shown in **Figure 10**, the cycloaddition of 2-diazopropane on methyl acrylate gives the expected 3-carboxyl-substituted pyrazoline; as the steric bulk is increased, more steric demands are placed on the transition state and the alternative regioisomer was observed.⁵³ When X = *t*-butyl, the regioselectivity is completely reversed and sterics out-compete the electronics to give the 4-carboxyl-substituted pyrazoline as the sole product. This reactivity is also observed for analogous reactions with alkynes as the dipolarophile.



X	A-Value	Expected/%	Steric-Driven/%
H	0	100	0
Me	1.74	91	9
Et	1.75	80	20
ⁱ Pr	2.15	47	53
^t Bu	5	0	100

Figure 10: Increasing steric bulk can overcome electronic effects to govern regioselectivity.

1.2.4. Stereospecificity

1,3-Dipolar cycloadditions are, by their very nature, often pericyclic reactions and therefore usually proceed in a stereospecific manner. This is true with respect to both the 1,3-dipole and the dipolarophile. **Figure 11a** illustrates how *cis*-substituted alkenyl dipolarophiles will react with a 1,3-dipole such that the substituents will end up in the *syn*-configuration in the product; correspondingly, *trans*-substituted alkenyl dipolarophiles will give the *anti*-configuration in the product (**Figure 11b**).⁵⁴

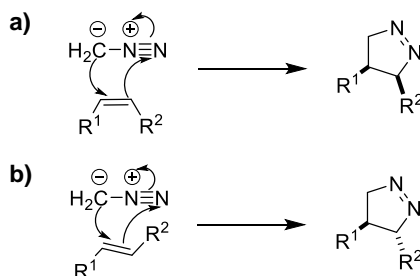


Figure 11: a) *cis*-alkenes stereospecifically give *syn*-products; b) *trans*-alkenes stereospecifically give *anti*-products.

Stereospecificity of this kind gives further evidence that the 1,3-dipolar cycloaddition is a concerted reaction in which all bonds are broken and formed in a process that has no long lived intermediate.

Due to facile bond rotation and the relatively small dipole, because of the structure of the resonance hybrid, stereochemistry with respect to the dipolarophile is not usually a concern. However, Huisgen showed that 1,3-dipolar cycloadditions are stereospecific with respect to the dipole (**Figure 12**).⁵⁵ By preparing diastereopure azomethine ylides *via* electrocyclic ring opening, Huisgen demonstrated that fast trapping of the resulting 1,3-dipole with a strongly activated dipolarophile, can result in a stereospecific cycloaddition that can occur before bond rotation. Dipolarophiles that react slower result in a degradation of the stereospecificity, as the azomethine ylide bonds can rotate, destroying any stereochemical information.

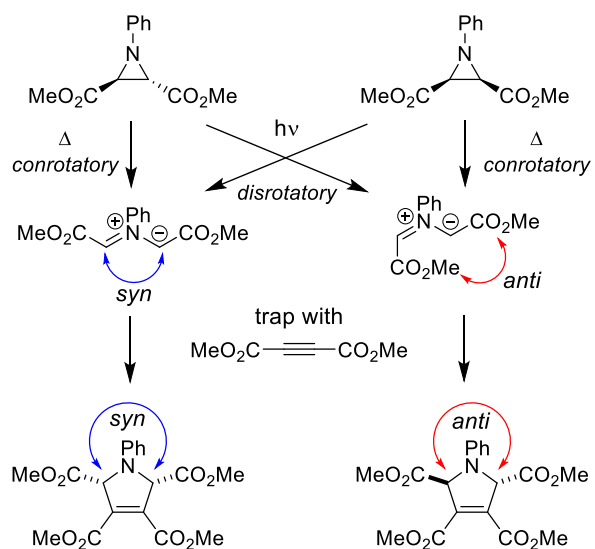


Figure 12: Huisgen and co-workers showed that 1,3-dipolar cycloadditions also proceed with retention of stereochemistry from the 1,3-dipole.

1.2.5. Diastereoselectivity

As secondary orbital overlap can govern diastereoselectivity in the Diels-Alder reactions, similar interactions can influence the diastereochemical outcome of 1,3-dipolar cycloadditions, in which two stereocenters are formed in the product. One factor that impacts the diastereoselectivity (and/or regioselectivity) is the attractive π -interactions between the 1,3-dipole and the dipolarophile.⁵⁶ This interaction is comparable to the secondary orbital overlap interactions that favour *endo*-selectivity in Diels-Alder reactions. π -Stacking of the phenyl ring and the methyl ester outweighs the steric clash between these two groups, resulting in the observed regioselectivity (**Figure 13a**). A second factor is the repulsive steric interactions in the transition state.⁵⁷ Avoiding steric clashes in the transition state can greatly impact the diastereoselectivity such that this becomes the dominant force (**Figure 13b**). *Exo*-selectivity is achieved in the reaction between dihydrofuran and nitrene as this minimises steric repulsion. A further factor that governs diastereoselectivity is the avoidance of ring strain in the final product; this is exemplified by the short synthesis of isoretronecanol in which the intramolecular azomethine ylide cycloaddition gives rise to a *cis*-fused ring system that possesses less ring strain than the corresponding *trans*-fused system (**Figure 13c**).⁵⁸

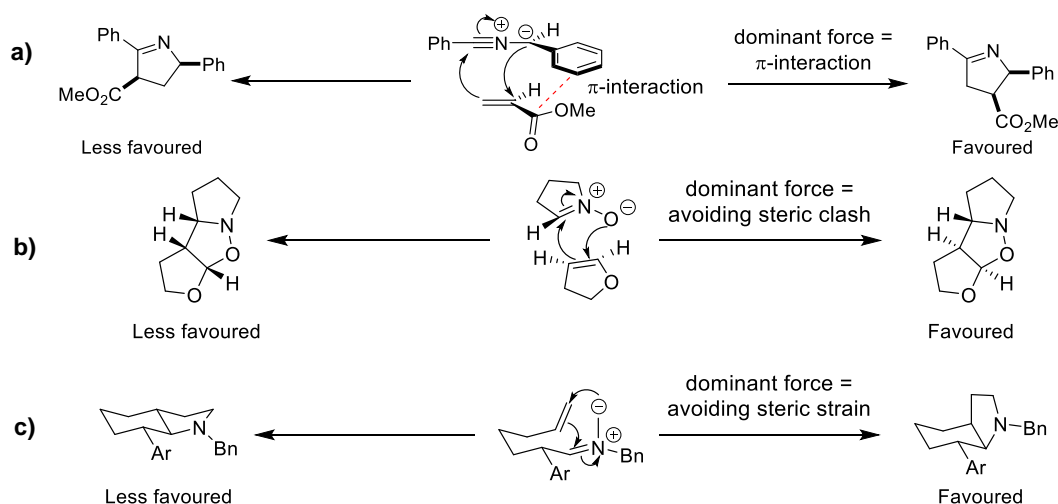
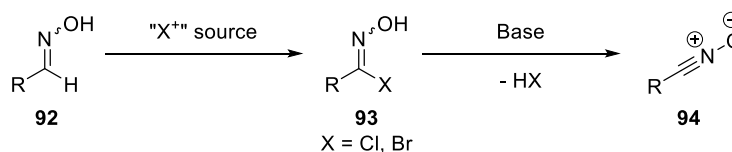


Figure 13: a) An example where regioselectivity is governed by secondary orbital interactions in the form of π -stacking; b) Avoidance of steric clash in the transition state provides diastereoselectivity; c) Avoiding steric strain in the product drives diastereoselectivity.

1.3. Synthesis of Isoxazolines

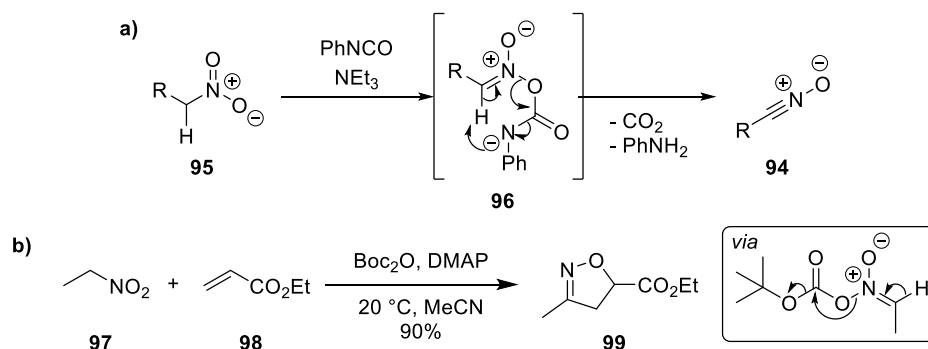
Isoxazolines can be prepared from the corresponding oximes *via* several methods, the most common of which is cyclisation by 1,3-dipolar cycloaddition. This can be achieved in two ways: i) electrophilic addition of hypohalites to oximes and elimination of HX to give nitrile oxides, which can undergo 1,3-dipolar cycloadditions with dipolarophiles; ii) dehydration of nitroalkanes to give nitrile oxides, which can directly participate in dipolar cycloaddition reactions.

Electrophilic chlorination has been the most explored method of preparing hydroxyimoyl chlorides **93** (X = Cl), which are the precursors to nitrile oxides **94** (**Scheme 30**); such chlorinating agents include *N*-chlorosuccinimide (NCS),⁵⁹ hypochlorite salts,⁶⁰ and other chlorite sources.⁶¹ Alternative halogenating sources can be used, including *N*-bromosuccinimide (NBS)⁶² and hypobromite salts.⁶³ Base-promoted elimination of hydroxyimoyl halides gives the nitrile oxide that undergoes facile cycloaddition to dipolarophiles to furnish the desired isoxazoline (when using an alkene as the dipolarophile) or isoxazole (when using an alkyne as the dipolarophile).



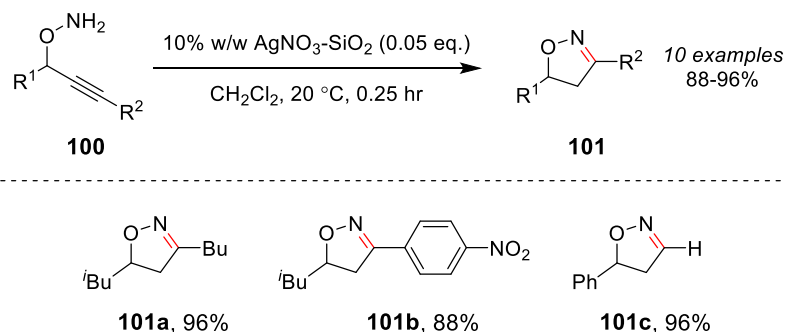
Scheme 30: Nitrile oxides are most commonly formed *via* the addition of an electrophilic halide species, followed by the base-promoted elimination of HX.

Dehydration of nitroalkanes **95**, with dehydrating reagents such as isocyanates⁶⁴ and acid anhydrides, directly gives nitrile oxides **94** which can add to dipolarophiles in 1,3-dipolar cycloadditions (**Scheme 31**). The proposed mechanism for this is shown in **Scheme 31a** in which addition of an isocyanate to a nitroalkane, and subsequent base-promoted loss of carbamic acid, gives the nitrile oxide that is used directly in the next reaction to give isoxazolines or isoxazoles. Furthermore, dehydration of nitroalkanes using di-*tert*-butyl dicarbonate (Boc₂O) has been demonstrated to be a facile *in-situ* entry into substituted isoxazoline derivatives (**Scheme 31b**).⁶⁵

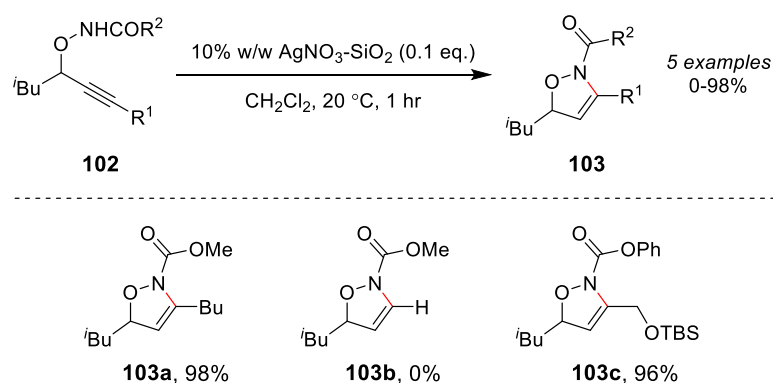


Scheme 31: a) Nitrile oxide formation *via* dehydration of nitroalkanes using isocyanates; b) example of using dehydration of nitroalkanes to provide access to nitrile oxides that can participate in 1,3-dipolar cycloadditions.

Alternative methods of synthesising isoxazolines have been explored. For example, the Knight group have reported a regioselective silver-catalysed ring-closing approach to the synthesis of substituted isoxazolines (**Scheme 32**).⁶⁶ The authors showed that 0.05 equivalents of a 10% w/w silver nitrate-silica gel catalyst allowed the preparation of 5-substituted isoxazolines **101** in excellent yields from propargylic hydroxylamines **100**. Notably, terminal alkynes were tolerated under the reaction conditions and gave **101c** in 96% isolated yield. Furthermore, carbamate protected propargylic hydroxylamine derivatives **102** were also subjected to the cyclisation conditions, albeit using 0.1 eq. of catalyst, and gave isomeric isoxazoline products **103** in excellent yields (**Scheme 33**). However, Knight *et al.* did note that terminal alkynes of this kind did not cyclise under these conditions, as exemplified by **103b**. Additionally, the authors mentioned that the use of sulfonamide protecting groups resulted in alternative products being formed, including isoxazoline derivatives in which the protecting group was eliminated. This could be avoided by using tosyl protecting groups and bulkier substituents on the alkyne, such as the phenyl group.

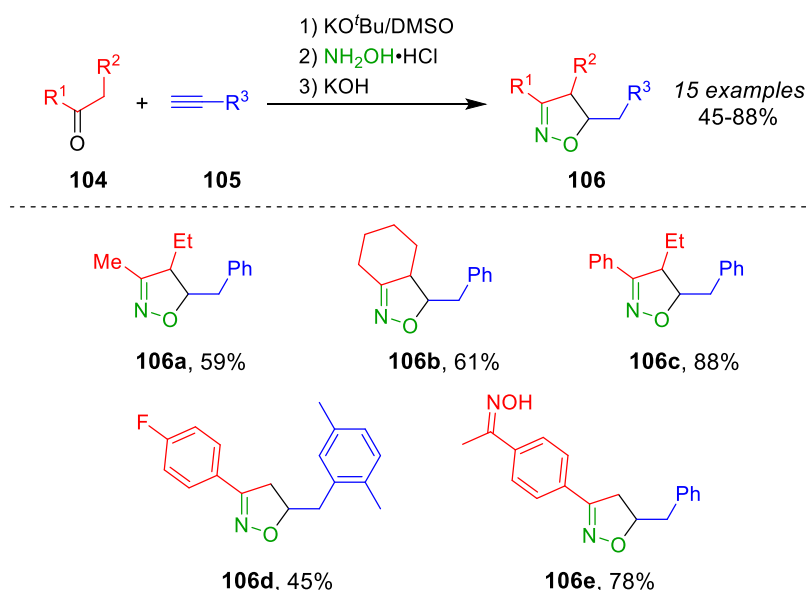


Scheme 32: Knight *et al.* demonstrated the use of a solid phase silver catalyst for the regioselective cyclisation of propargylic hydroxylamines.

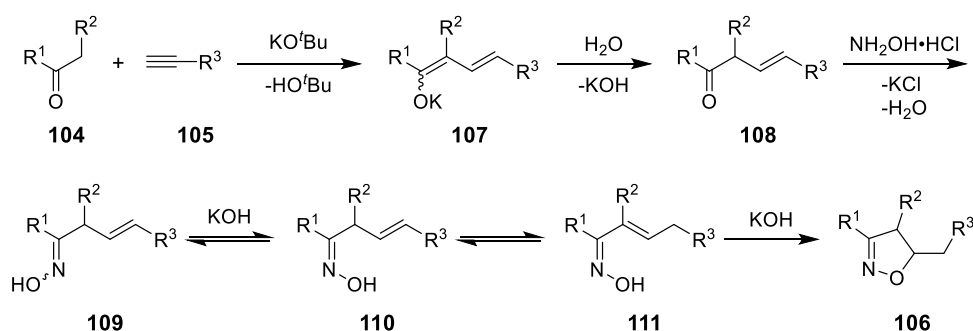


Scheme 33: The Knight group expanded further their substrate scope to include carbamate-protected propargylic hydroxylamines.

A one-pot approach to the synthesis of 3,4,5-substituted isoxazolines from ketones and arylacetylenes has been developed by Trofimov *et al.* (**Scheme 34**).⁶⁷ They demonstrated that using sequential additions of reagents, substituted isoxazolines could be prepared in moderate to excellent yields. This reaction procedure was well tolerated with dialkyl (**106a**, 59%), cycloalkyl (**106b**, 61%) and alkylaryl (**106c**, 88%) ketones demonstrating good reactivity. However, lower yields were exhibited for aryl ketones bearing a fluoro substituent (**106d**, 45%). The authors attributed the decreased yields to the fact that there are several steps in the overall process; the proposed reaction pathway is shown in **Scheme 35**. It was suggested that the first step was a base-promoted enolate addition to the alkyne to give dienolate **107**. Protonation gave β,γ -unsaturated ketone **108**, which underwent condensation with hydroxylamine to form ketoxime **109**. Upon addition of KOH, an equilibrium between **109** and **110** would be set up, with **110** isomerised further to **111** from which cyclisation could occur to give substituted isoxazoline **106**. Naturally the electronics play a significant role on the rate of reaction of most of these steps, and particularly on where the equilibria will lie. For instance, when using the more electron-poor *para*-fluoroacetophenone, those steps that involve nucleophilic addition to the ketone will be accelerated due to the increased electrophilicity of the carbonyl carbon. This increase in electrophilicity is a result of the inductive effects of the *para*-fluoro substituent on the aryl ring. However, this same effect will render the oxime portion of the molecule less nucleophilic and therefore decrease the rate of reaction, resulting in a poorer yield over the reaction time specified. Conversely, more electron-rich ketones would demonstrate slower reaction rates in the addition steps, but vastly accelerated rates during the cyclisation.



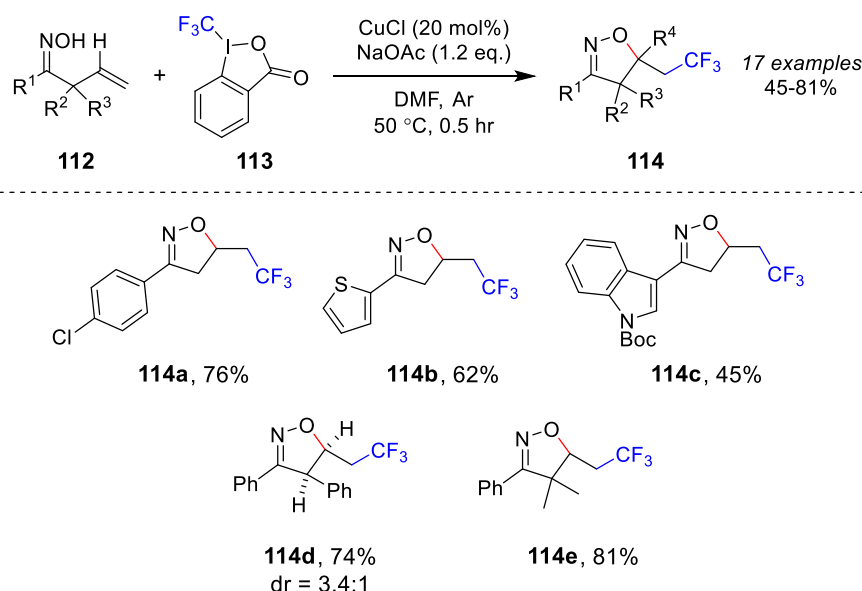
Scheme 34: The Trofimov group developed a one-pot approach to the synthesis of substituted isoxazolines without the need for transition metals.



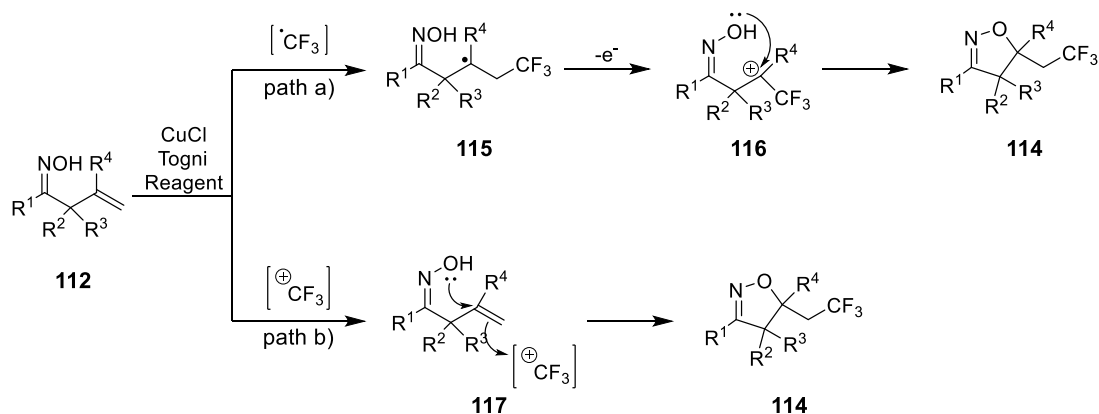
Scheme 35: The proposed base-promoted mechanism from Trofimov *et al.* for the conversion of ketones and alkynes to isoxazolines.

Employing copper catalysis, the Liang group demonstrated the synthesis of trifluoromethyl-substituted isoxazolines (**Scheme 36**).⁶⁸ A combination of Togni's reagent (**113**) and CuCl gave trifluoromethylated isoxazolines **114**. Moderate to good yields were achieved when applied to a substrate scope that included substituents such as aryl (**114a**, 76%) and heteroaryl (**114b**, 62%); both electron-withdrawing and electron-donating substituents were well tolerated on the aryl substituted oximes. An *N*-Boc protected indole oxime gave the desired isoxazoline **114c** with a decreased 45% yield when compared with other heteroaryl isoxazolines. Isoxazoline **114d** was obtained in 74% with a diastereomeric ratio of 3.4:1, in favour of the *syn*-configuration. Furthermore, the tetra-substituted isoxazoline **114e** was obtained in a good yield of 81%, demonstrating that steric bulk in the α -position to the oxime may aid the

cyclisation. The authors proposed two possible pathways for the cyclisation of the unsaturated oximes (**Scheme 37**): path a) employs a radical mechanism in which a CF_3 radical adds to the terminal alkene carbon, while path b) invokes a pathway in which a CF_3 cation is trapped by the terminal alkene carbon. Whether the cyclisation in path b) is concerted or stepwise was not alluded to in the report.



Scheme 36: The group of Liang used copper catalysis and Togni's reagent to develop a cyclisation process with which CF_3 -substituted isoxazolines can be prepared.

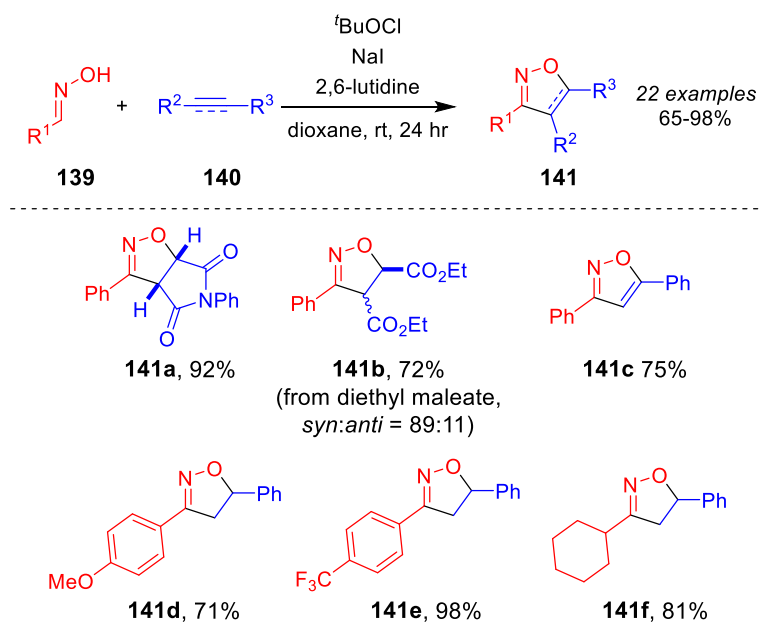


Scheme 37: The two possible pathways proposed by Liang *et al.* for the copper catalysed cyclisation of unsaturated oximes to give substituted isoxazolines.

1.3.1. Synthesis of Isoxazolines *via* 1,3-Dipolar Cycloadditions

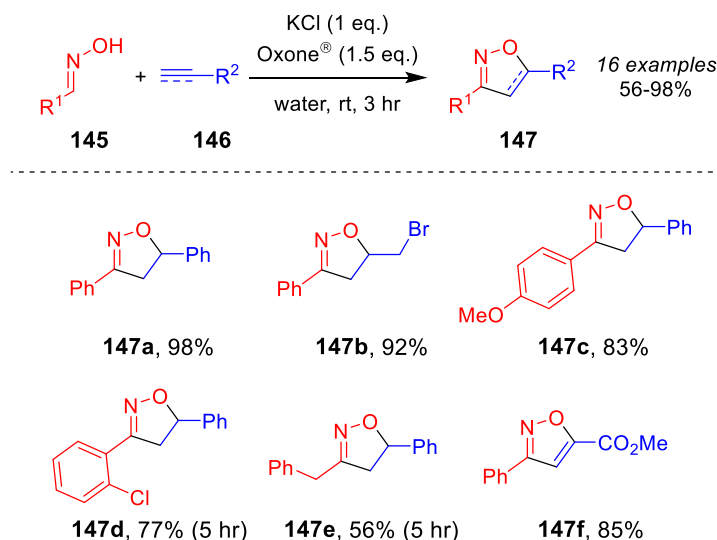
Most commonly, nitrile oxides are formed from the elimination of HCl from hydroxyimoyl chlorides; these chlorinated species are synthesised by halogenation of aldoximes using electrophilic chlorine sources such as NCS, NaClO, Cl₂ and many others (see Section 1.3). Electrophilic bromine sources have also found a use in halogenating aldoximes as pre-cursors to nitrile oxides (see Section 1.3). However, only recently have hypervalent iodine and electrophilic iodine reagents found utility in forming pre-cursors for nitrile oxides in the context of 1,3-dipolar cycloadditions. Prior to this, they have been used for CO₂ fixation by allyl alcohols⁶⁹ and the synthesis of nitrogen-containing heterocycles from simple amides and alkenes.⁷⁰

Use of an electrophilic iodine reagent for the generation of nitrile oxides from aldoximes was reported by the group of Minakata (**Scheme 38**).⁷¹ *t*-BuOCl was converted to the desired *t*-BuOI by halogen exchange with sodium iodide; this exchange occurred *in-situ* during the reaction. Both electron-donating (**141d**) and electron-withdrawing (**141e**) substituents on the aryl aldoxime were well tolerated; electron-rich aldoximes were obtained in slightly lower yields than electron-poor aldoximes. Isoxazolines derived from alkyl oximes were obtained in good yields (**141f**, 81%), as were isoxazolines from 1,2-disubstituted alkenes (**141b**, 72%), though disubstituted alkenes, such as dimethyl maleate, gave rise to diastereoisomers. Furthermore, isoxazoles, synthesised by the 1,3-dipolar cycloaddition of nitrile oxides and alkynes, were also exemplified with isoxazole **141c** isolated in a good 75% yield. The bicyclic isoxazoline **141a**, derived from the dipolar cycloaddition of *N*-phenyl maleimide and benzonitrile oxide, was obtained in an excellent 92% yield, demonstrating the versatility of this reaction.



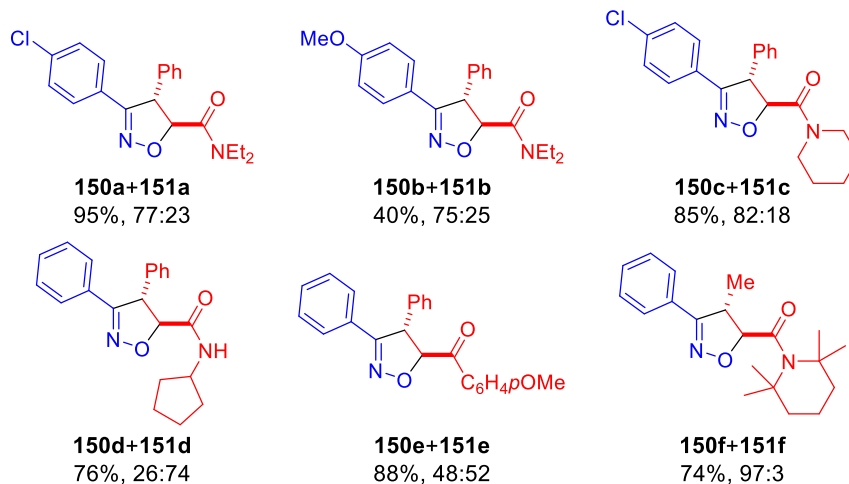
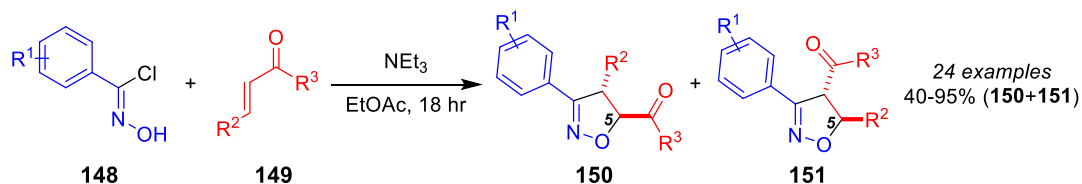
Scheme 38: Minakata and co-workers developed a process in which the electrophilic iodine reagent, *t*BuOI, promoted the 1,3-dipolar cycloaddition between nitrile oxides and suitable dipolarophiles.

Hypervalent iodine reagents have also found use for promoting 1,3-dipolar cycloaddition reactions. An example of this is reported by the Zhdankin group in which they demonstrated the use of Oxone[®] as a terminal oxidant to form the hypervalent iodine species which allowed the oxidation of aldoximes to nitrile oxides.⁷² Moreover, Zhdankin demonstrated that this process could be conducted using catalytic amounts of aryl iodide. Applying the reaction conditions detailed in **Scheme 39**, substituted isoxazolines and isoxazoles were obtained in poor to excellent yields. Styrenyl dipolarophiles bearing both electron-withdrawing and electron-donating groups proceeded smoothly, furnishing the desired isoxazolines in good yields (**144b** and **144a**). Similarly, 3,5-diphenylisoxazole **144e** was obtained in 75% yield from the 1,3-dipolar cycloaddition between phenylacetylene and the *in-situ* generated benzonitrile oxide. The limitation of this catalytic process was evident by the poor yield achieved when employing norbornene as dipolarophile, giving the corresponding tricyclic isoxazoline **144c** in 30% yield. Likewise, alkyl aldoximes were also poor substrates for this procedure, providing **144d** in just 17% yield. The authors noted that a small amount of water was needed and is most likely to be necessary due to the insolubility of Oxone[®] in purely organic solvents.



Scheme 40: The environmentally benign 1,3-dipolar cycloaddition reaction, promoted by Oxone[®] and KCl in water, was developed by the group of Yan.

During their investigations of 1,3-dipolar cycloadditions between nitrile oxides and tertiary cinnamides or crotonamides, Turchi *et al.* observed unusual regioselectivity in their isoxazoline products.⁷⁴ They found that when tertiary crotonamides or cinnamides were used, preferential formation of the isoxazoline with the amide group in the 5-position was observed (**Scheme 41**); this unusual regioselectivity is in contrast to the expected product in which the amide group would be in the 4-position. This could be predicted by the frontier molecular orbital interactions in which the atom bearing the largest coefficients of the relevant orbitals interact. Firstly, they assumed that the electronic difference between the ester and amide functionalities was responsible for the unexpected regioselectivity. However, when employing a secondary amide, the Turchi group saw that the expected product was formed in high regioselectivity; these results ruled out electronic differences driving regioselectivity. They then suggested that it was steric bulk influencing the regioselectivity and this was supported by the reaction of hydroxyimoyl chloride **148** with *N,N*-dimethyl cinnamide **149** ($\text{R}^2 = \text{Ph}$, $\text{R}^3 = \text{NMe}_2$), which gave a ratio of 31:69 in favour of the product with the amide group in the 5-position (**Figure 14**). Further evidence that the unusual regioselectivity is governed by sterics, a screen of bulkier amide functionalities on the cinnamide showed that the larger the group, the better the regioselectivity for substitution of the amide group in the 5-position (**Figure 14**).



Scheme 41: Unusual regioselectivity was observed by Turchi *et al.* during their investigation into 1,3-dipolar cycloadditions of nitrile oxides and crotonamides or cinnamides.

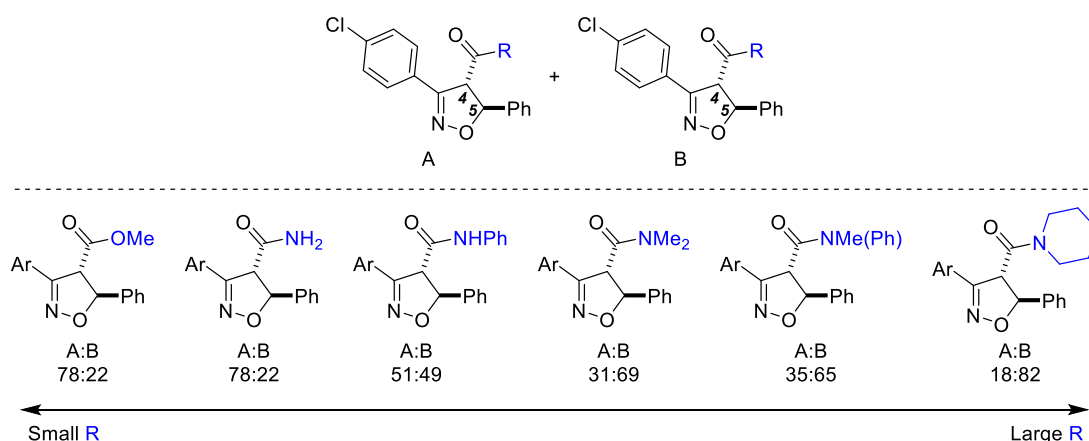


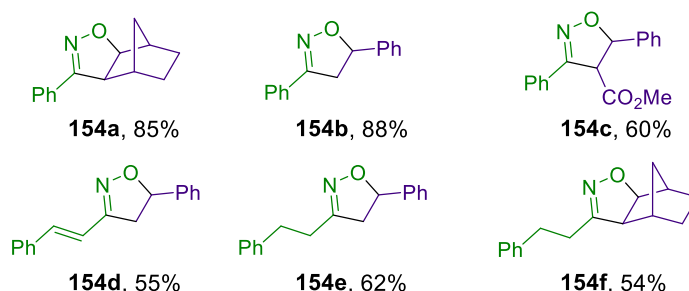
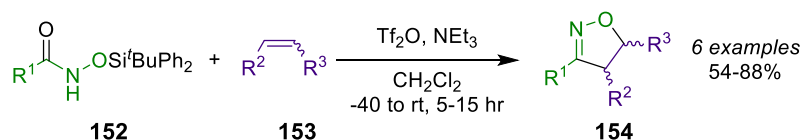
Figure 14: The larger the groups on the amide/ester functionality, the more regioselective for the 4-phenyl regioisomer (**B**).

Semi-empirical and *ab initio* calculations of several crotonamide and cinnamides revealed that the β -substituent of each species was most likely responsible for the regioselectivities observed. Turchi *et al.* found that the transition state towards the 4-carbonyl isomers was slightly asynchronous while the transition state towards the 5-carbonyl isomers was much more synchronous; by more synchronous, the authors suggested that the transition state lifetime, going from starting materials to products, was smaller (from DFT calculations). These results suggested that it was the steric repulsion between the phenyl group of the nitrile oxide and the substituents on either

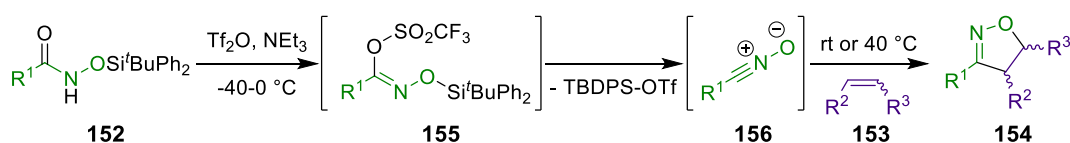
end of the double bond of the crotonamides/cinnamides that gave the observed regioselectivities. Nevertheless, they maintained that it was not only the β -substituent that was responsible for the regiochemical outcome, but that the amide functionality also plays a role.

Throughout this investigation, Turchi's group found that the electronics of the phenyl ring of the cinnamides or the nitrile oxide made trivial difference to the observed reactivity and regioselectivity. However, use of 4-nitrobenzotrile oxide was omitted as dimerisation to form the furoxane was faster than the rate of the desired reaction.

Although use of hydroxyimoyl chlorides provide an easy and efficient entry into nitrile oxides, these species are known to be poorly stable at ambient temperatures over an extended period. The Carreira group addressed this issue and developed *O*-silylated hydroxamic acids as stable, readily accessible and crystalline alternatives; using dehydrating conditions, nitrile oxide formation was facile and was achieved by the addition of Tf_2O and NEt_3 (**Scheme 42**).⁷⁵ The isoxazole products were prepared in moderate to good yields and the scope included aryl and alkyl chain silyl-protected hydroxamic acids. The hydroxamates **152** were easily prepared either from the corresponding hydroxamic acid or by coupling of the carboxylic acid with *O*- Si^tBuPh_2 hydroxylamine (which itself has a facile preparation and was a stable, crystalline solid). Furthermore, the authors stated that intramolecular nitrile oxide 1,3-dipolar cycloadditions were also possible through this method. As illustrated in **Scheme 43**, the *O*-silylated hydroxamic acid **152** was cooled to $-40\text{ }^\circ\text{C}$ and triflic anhydride was added; this produced the postulated intermediate **155** which, after elimination of TBDPS-OTf , underwent 1,3-dipolar cycloaddition with dipolarophile **153** to yield the corresponding isoxazoline products **154**.



Scheme 42: The Carreira group developed a procedure in which dehydration of silyl-protected hydroxamic acids provides a facile entry into nitrile oxides for use in 1,3-dipolar cycloaddition reactions.

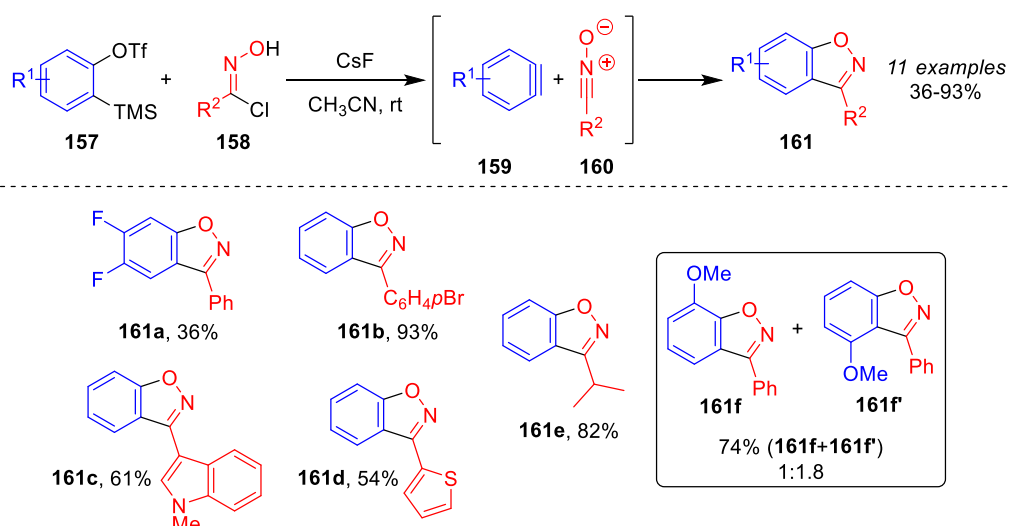


Scheme 43: Postulated reaction pathway for the 1,3-dipolar cycloaddition reaction between silyl-protected hydroxamic acids and alkene dipolarophiles.

It is noteworthy that with the use of triflic anhydride, no additional deprotecting agent was needed to remove the silyl-protecting group; other silyl-protected derivatives required this extra deprotecting agent to furnish the final isoxazoline. The authors did not mention any reasoning for this observation, but perhaps the reactivity and stability of the chosen silyl protecting group were in a fine balance and allowed this transformation to occur, in addition to the fact that the nitrile oxide formed is a good leaving group. Alternative *O*-protecting groups were investigated but it was found that *O*-Boc or *O*-*tert*-butyl derivatives tended to give preferential formation of isocyanates *via* the Lössen rearrangement. Furthermore, smaller silyl-protecting groups on the acid functionality were observed to be too labile for their use in a general procedure.

Syntheses of benzisoxazoles have previously been achieved *via* three to four step processes. However, Larock showed that this fused heterocycle can be prepared through a 1,3-dipolar cycloaddition of a benzyne and hydroxyimoyl chloride (**Scheme 44**).⁷⁶ *o*-(Trimethylsilyl)aryl triflate **157** could be converted to the corresponding benzyne **159** with the use of CsF, which also facilitated the formation of nitrile oxide **160** from hydroxyimoyl chloride **158**; subsequent 1,3-dipolar cycloaddition yielded benzisoxazole products **161**. All bar one (**161f/161f'**, **Scheme 44**) of the substrates

gave a single regioisomer in moderate to excellent yields. The regioselectivity observed was suggested to arise from a combination of steric and electronic effects but in the case of **161f/161f'**, electronic effects dominated and gave the unexpected regioisomeric ratio. **Figure 15** shows the postulated orientations that results in the two regioisomers of **161f/161f'**; the dipole moments of the two reacting partners were either aligned to give the minor regioisomer (**162**) or anti-parallel to give the major regioisomer (**163**). Having the dipoles anti-parallel to each other is a much more favourable orientation to reduce electrostatic repulsion in the transition state. In the remaining cases, the steric effects dominated, and the observed products were those in which the largest groups on both reacting partners were positioned away from each other so as to reduce steric clashes in the transition state. However, this explanation of the observed regioselectivity is only part of the story. Garg and Houk showed, both experimentally and computationally, that it was the distortion of the aryne bond angles that are responsible for regioselectivity.⁷⁷ They demonstrated that, although there is polarisation of the aryne triple bond, the magnitude of the charge difference between the arynyl carbons is not sufficient to give the observed high regioselectivities, and can only provide qualitative predictions of regioselectivities. Instead, Garg and Houk suggested an alternative model, termed the Aryne Distortion Model, which quantitatively gave accurate predictions of the regioselectivities of 3-halobenzenes, in both methyl azide cycloaddition reactions and reactions with methyl aniline. This alternative model may provide a much more accurate explanation for the observed benzisoxazole regioselectivities from the Larock group.



Scheme 44: Larock demonstrated the synthesis of benzisoxazoles by using benzyne as the dipolarophile in a 1,3-dipolar cycloaddition with nitrile oxides.

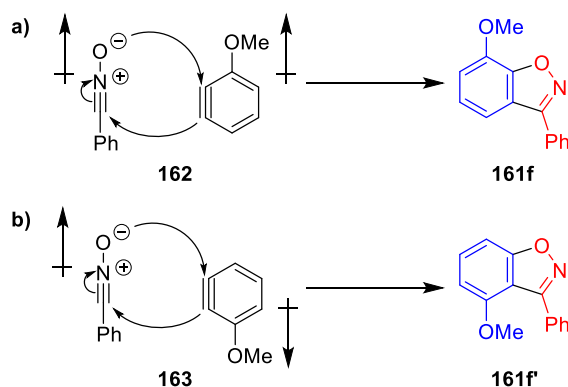
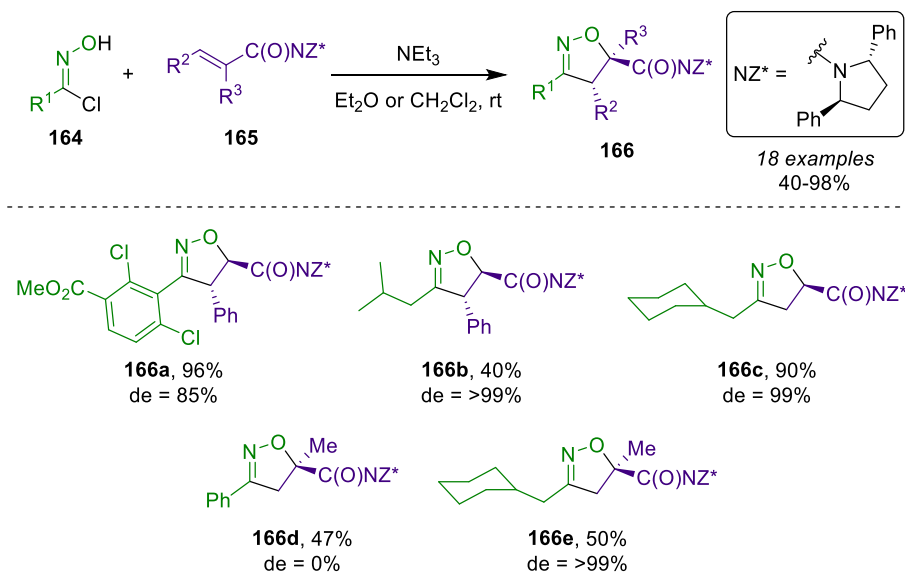


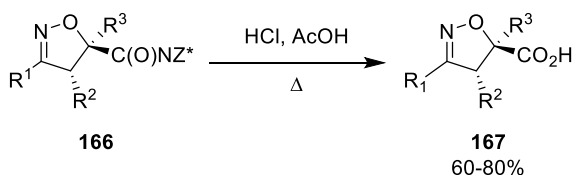
Figure 15: Postulated orientations of the transition states of the unsymmetrical benzyne, resulting in regioisomeric products.

Throughout their optimisation, the Larock group found that the rate of dimerisation of the nitrile oxide formed was similar to the rate of cycloaddition and so poor conversion to desired benzisoxazole was observed. To accommodate this fast rate of dimerisation, an excess of the *o*-(trimethylsilyl)aryl triflate was employed in the reaction.

1,3-Dipolar cycloadditions are stereospecific reactions in which the stereochemistry of the dipolarophile is retained in the product. However, dipolar cycloadditions are only diastereoselective and control of the diastereochemical outcome is usually achieved by using a chiral auxiliary; this quite often comes with poor atom economy and some chiral auxiliaries are not suitable for certain chemistries. The Lassaletta group have reported the use of 2,5-*trans*-diphenylpyrrolidine as a suitable chiral auxiliary for the synthesis of enantiopure 4,5-dihydroisoxazole-5-carboxylic acid derivatives.⁷⁸ They showed that nitrile oxides, formed from the base-promoted dehydrochlorination of hydroxyimoyl chlorides **164**, could participate in 1,3-dipolar cycloaddition with α,β -unsaturated amides containing a chiral auxiliary (**165**) to give stereo- and regioselective isoxazolines **166** (**Scheme 45**). The cycloaddition reaction proceeded well in most cases, fashioning the desired isoxazolines in moderate to good yields; diastereoselectivity, in all but three examples, was excellent. Deprotection of the substituted isoxazolines **166** with HCl in acetic acid gave enantiopure carboxylic acid derivatives **167** (**Scheme 46**). Poor stereoselectivity is observed with the use of methyl acrylamides as cycloaddition partners and the stereochemical outcome was shown to be substrate-dependent and only gave high stereoselectivity for aliphatic substrates.

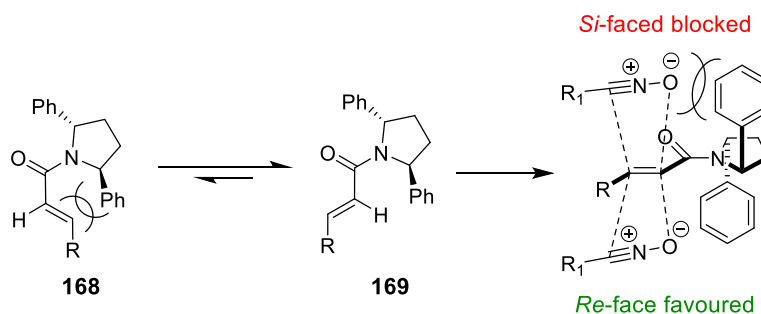


Scheme 45: Synthesis of enantiopure isoxazoline carboxylic acid derivatives by Lassaletta *et al.*



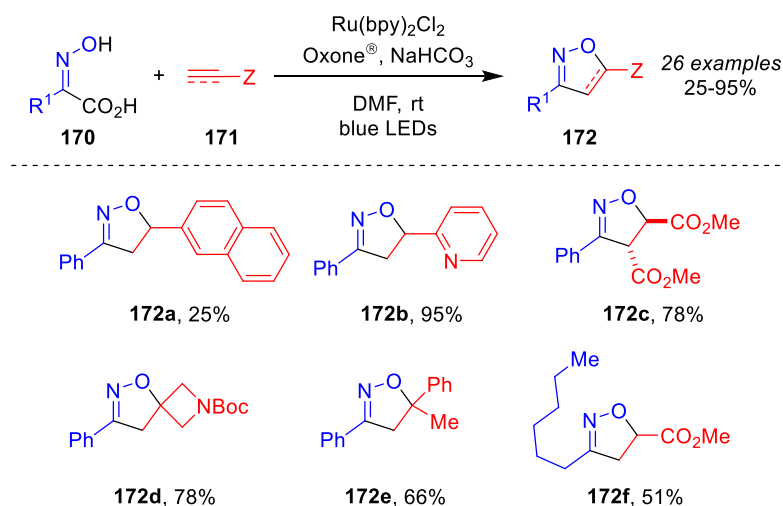
Scheme 46: Acid-promoted removal of the chiral auxiliary gives the enantiopure isoxazoline carboxylic acid derivatives.

The authors suggested that the high stereochemical inductions observed could be explained by the fact that one of the faces of the alkene (the *Si*-face) would be blocked to the approach of the nitrile oxide and so the *Re*-face was the preferred face of approach. This transition state orientation is illustrated in **Scheme 47**, where the preferred conformation of the alkene bond geometry is *s-cis* (**169**), as this lowers steric clash between the β -substituent of the alkene with the phenyl groups of the pyrrolidine moiety. The nitrile oxide can now only approach from the *Re*-face as the *Si*-face is blocked by one of the phenyl rings, giving the observed stereoselectivity.



Scheme 47: Stereochemical induction is achieved as the approach to the *Si*-face is blocked and so the nitrile oxide must add across the alkene *via* the *Re*-face.

The Leonori group developed a photochemical process in which hydroxyimino acids **170** underwent a radical decarboxylation and subsequent single electron transfer (SET) to give nitrile oxides that could then participate in 1,3-dipolar cycloaddition reactions to provide substituted isoxazolines **172** (**Scheme 48**).⁷⁹ From the very beginning of their investigation, the Leonori group set out to provide a method for isoxazoline synthesis that used nitrile oxide precursors that were easy-to-make, bench-stable and offer high structural modularity. These were provided by hydroxyimino acids that could be made efficiently from the condensation of α -ketoacids with hydroxylamine. The hydroxyimino acids were then suitable reagents for photochemical decarboxylation to give α -imino acyl radicals **179**, which could participate in the photochemical redox cycle illustrated in **Figure 16**.



Scheme 48: The Leonori group used photocatalysis to provide *in situ* access to nitrile oxides to participate in 1,3-dipolar cycloaddition to a range of dipolarophiles.

Through detailed computational and experimental considerations, it was found that the photocatalyst **173** did not have the required redox potential to oxidise the

hydroxyimino acids directly [$E_{1/2}^{red} = 1.31$ V (vs. SCE), **Figure 16**]. Rather the more potent oxidising agent **175**, which is formed from the oxidation of the excited state photocatalyst by Oxone[®], was responsible for the SET [$E_{1/2}^{red} = 1.29$ V (vs. SCE)]. Leonori then suggested three alternative pathways that the α -imino acyl radical could take: Path A) a second SET gives the nitrile oxide **180** and subsequent dipolar cycloaddition fashions the desired isoxazoline **172**; Path B) radical addition to the dipolarophile to gives species **182** followed by SET and intramolecular trapping by the hydroxyl group to furnish the desired product **172**; Path C) radical addition to methyl acrylate gives intermediate **183** which then undergoes rearrangement and subsequent SET to provide the isoxazoline product. Path B was discounted as the Hammett plot derived from *para*-substituted styrenes did not support this mechanism, instead it gave a V-shape which suggested a change in mechanism on going from electron-rich systems to electron-poor systems. The Hammett analysis thus gave a strong indication for Path A as the switch of mechanism aligns well with the change of the frontier molecular orbital interactions during the cycloaddition step. Path C cannot be ruled out as the barrier for the radical addition is relatively low ($\Delta G^\ddagger = 1.3$ kcal.mol⁻¹ from DFT calculations) and the subsequent cyclisation has an activation barrier of $\Delta G^\ddagger = 11.8$ kcal.mol⁻¹ (from DFT calculations), which is not an unreasonable barrier to overcome under the reaction conditions.

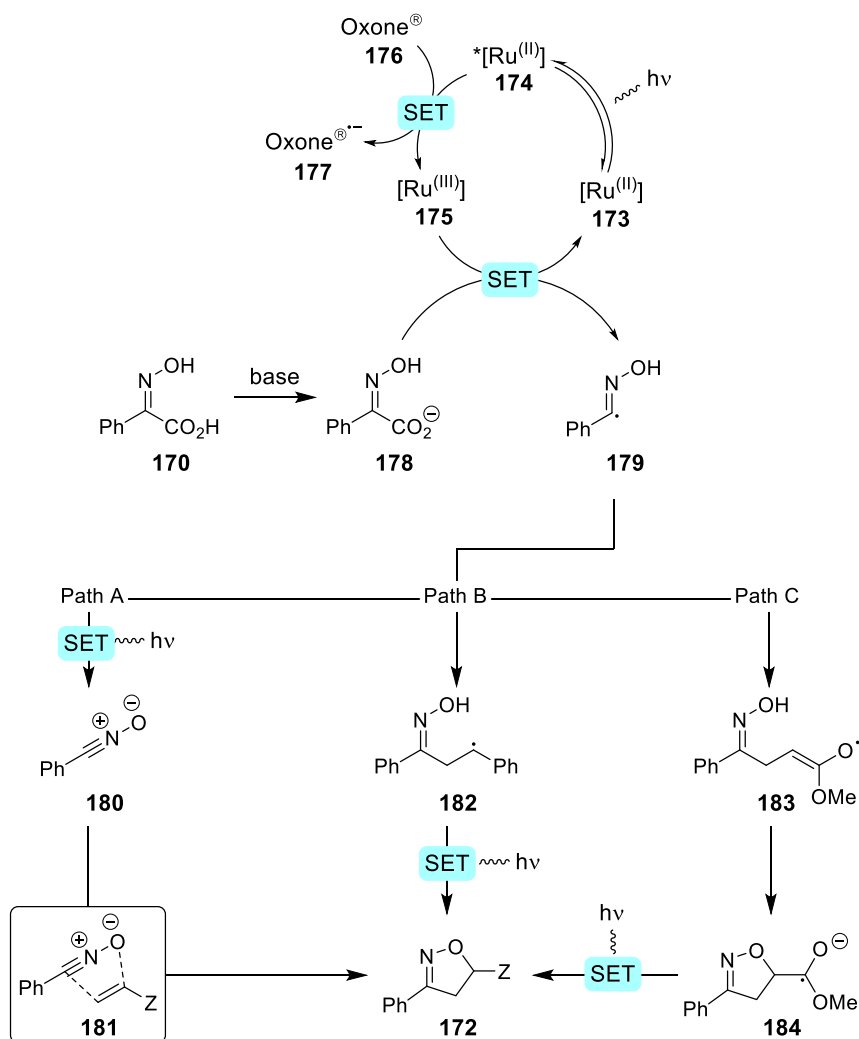
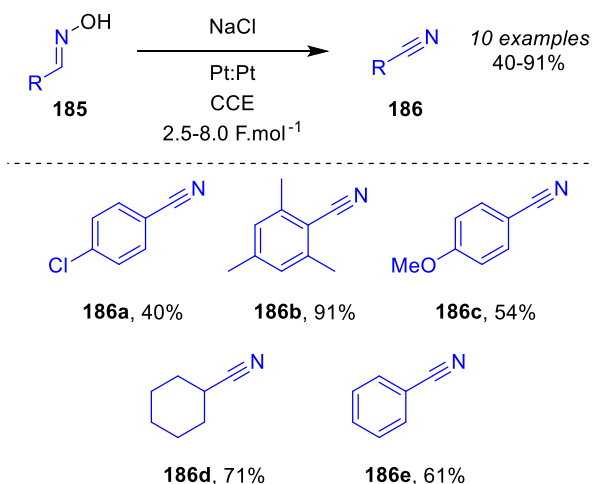


Figure 16: The proposed photocatalytic cycle for the 1,3-dipolar cycloaddition reaction developed by the Leonori group; several reaction pathways were investigated.

The Shono group demonstrated that NaCl could mediate the formation of a nitrile oxide from an oxime using electrochemistry.⁸⁰ The publication showed that aldoximes **185** could be converted to nitriles **186** via an electrochemically-assisted formal dehydration reaction (**Scheme 49**). The chloride anion **187** (from the NaCl, used as both the mediator and electrolyte) was suggested to be oxidised to the corresponding electrophilic species **188** (**Figure 17**), which was then trapped by oxime **185**, forming hydroxyimoyl chloride **189**. Elimination of HCl from **189** gave nitrile oxide **190** that was converted to nitrile **186** by reduction at the cathode. They showed that the reaction worked independently to the choice of electrolyte, however a halide mediator gave the best results, with NaCl the most reactive. Furthermore, it was demonstrated that the reaction could be performed with only 10 mol% NaCl, although a poorer yield

(12%) was achieved. Similar work was carried out by the group of Waldvogel, who demonstrated that this reaction can proceed in the absence of chloride mediator at carbon-based electrodes.⁸¹



Scheme 49: Electrocatalytic conversion of oximes to nitriles using a halide mediator was demonstrated by Shono.

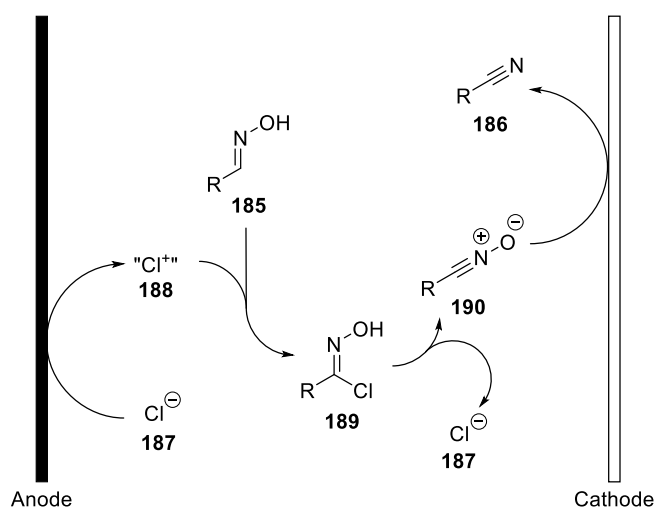
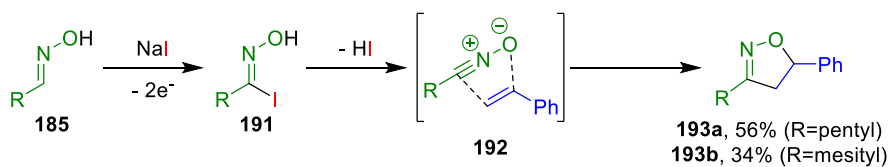


Figure 17: The proposed electrocatalytic cycle from Shono for the conversion of aldoximes to nitrile *via* nitrile oxides.

To provide evidence for their suggested reaction pathway, the Shono group electrolysed aldoxime **185** in the presence of NaI and a dipolarophile (**Scheme 50**). The products formed were those expected from a 1,3-dipolar cycloaddition reaction between a nitrile oxide and a dipolarophile (**193**) and provided the evidence for the transient nitrile oxide intermediate.

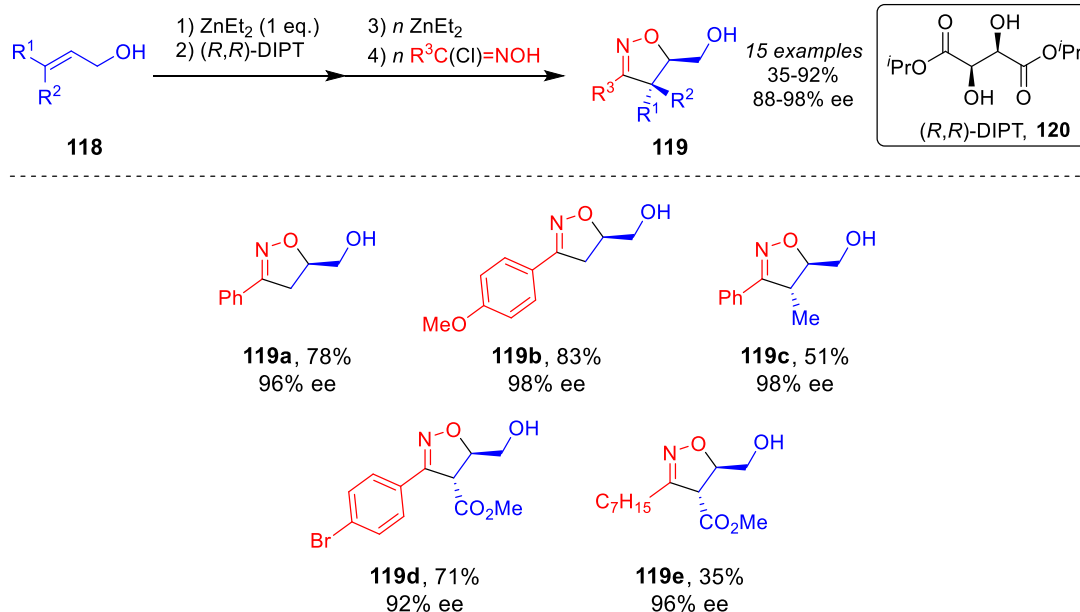


Scheme 50: Evidence of the formation of nitrile oxide during the electrocatalytic conversion of oximes to nitriles was provided by the trapping of the intermediate with a dipolarophile in a 1,3-dipolar cycloaddition.

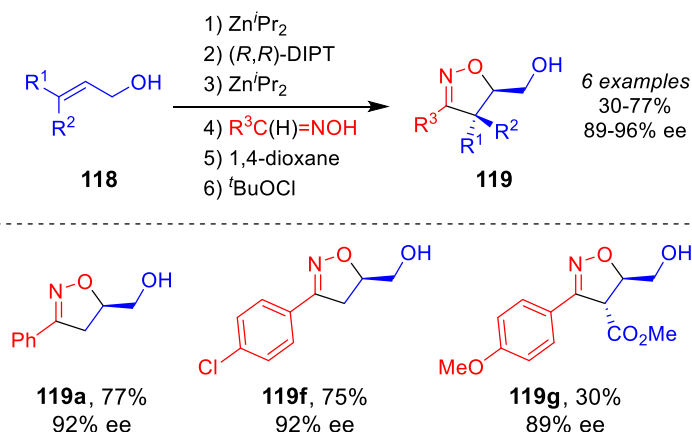
1.3.2. Asymmetric Isoxazoline Synthesis

Functionalised isoxazolines are of great interest to the medicinal chemist as they are present in both natural products and drug molecules (see Section 1). The majority of the methods to synthesise isoxazolines involve a 1,3-dipolar cycloaddition reaction between a nitrile oxide, generated *in-situ*, and a suitable dipolarophile. Although 1,3-dipolar cycloadditions are inherently stereospecific and diastereoselective (see Section 1.2.4 and 1.2.5, respectively), these factors are controlled by sterics and electronics and may not produce the desired chirality in the target molecule. To this end, considerable attention has been given to developing asymmetric 1,3-dipolar cycloadditions in which chiral auxiliaries are coordinated to metal centres. A recent review by Hashimoto and Maruoka provides a comprehensive summary of recent advances of asymmetric 1,3-dipolar cycloadditions, including use of dipoles other than nitrile oxide.⁸² Further reviews detail asymmetric variants of 1,3-dipolar cycloaddition reactions with acrylamides⁸³ and asymmetric 1,3-dipolar cycloadditions up to the end of the last century.⁸⁴

Inomata and Ukaji developed an asymmetric 1,3-dipolar cycloaddition between allyl alcohols and hydroxyimoyl chlorides using zinc metal centres coordinated by tartaric ester derivatives.⁸⁵ The authors demonstrated that this 1,3-dipolar cycloaddition proceeds smoothly, in good yields and high stereoselectivities (**Scheme 51**). Unsubstituted allyl alcohols gave the desired optically active isoxazolines in good to excellent yields and high enantiomeric excesses (**119a** and **119b**). However, when using 2-buten-1-ol, a decreased yield of 51% was obtained, although high stereoselectivity was maintained (**119c**, 98% ee). Aryl hydroxyimoyl chlorides were generally well tolerated, with *para*-bromo substituted hydroxyimoyl chloride furnishing the isoxazoline **119d** in 71% and 92% ee. Unfortunately, alkyl chains were not well tolerated with isoxazoline **119e** obtained in a poor 35% yield but an excellent 96% ee. Additionally, the authors adapted this procedure to provide a one-pot protocol, which included forming the nitrile oxide *in-situ* from the oxime (**Scheme 52**).^{85a, 86} Unsubstituted allyl alcohols gave the corresponding isoxazolines in good yield and excellent enantiomeric excess (**119a** and **119f**). On the other hand, substituted allyl alcohols seem to hinder the reaction, giving isoxazoline **119g** in a poor 30% yield but still maintaining a high enantiomeric excess.

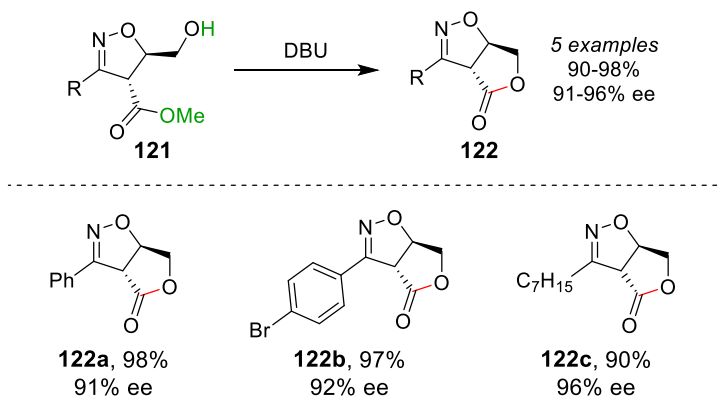


Scheme 51: Inomata and Ukaji developed an asymmetric 1,3-dipolar cycloaddition reaction between achiral propenyl alcohols and nitrile oxides, using (*R,R*)-DIPT as chiral auxiliary.



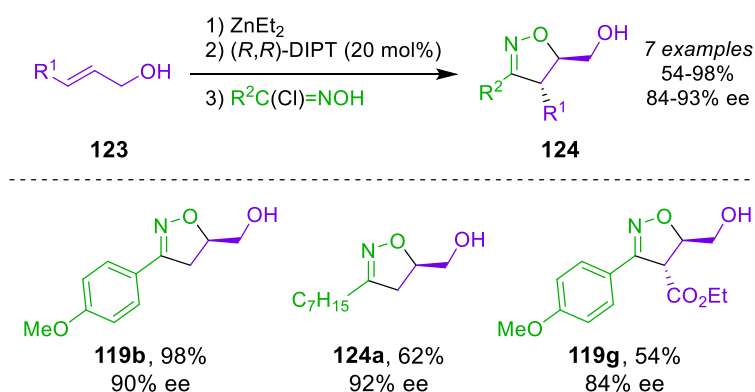
Scheme 52: Further development for the Inomata group provided a one-pot approach to the asymmetric 1,3-dipolar cycloaddition between achiral propenyl alcohols and oximes.

During this investigation, following preparative TLC of isoxazoline **119g**, a cyclic lactone was observed. Further exploration allowed the development of a cyclisation procedure that can be used as a subsequent step to the dipolar cycloaddition, when using ester substituted allyl alcohols. The base-promoted lactonisation is illustrated in **Scheme 53**: all reactions proceeded smoothly through to the bicyclic *trans*-lactone in excellent yields and enantioselectivity. Both aryl (**122a** and **122b**) and alkyl groups (**122c**) were well tolerated.



Scheme 53: Lactonisation of the optically active isoxazolines from the asymmetric 1,3-dipolar cycloaddition was achieved by addition of DBU base, proceeding without loss of optical purity.

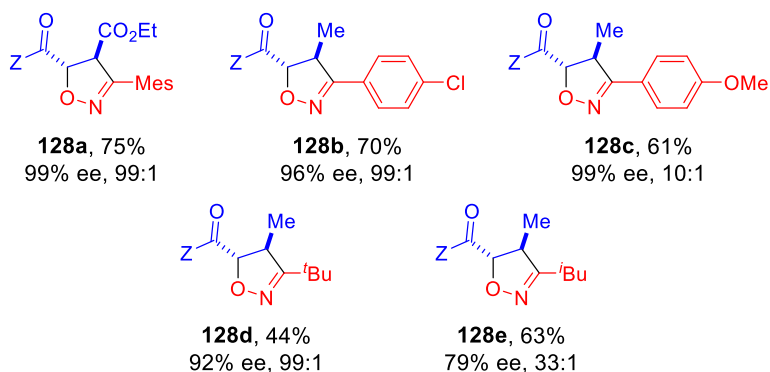
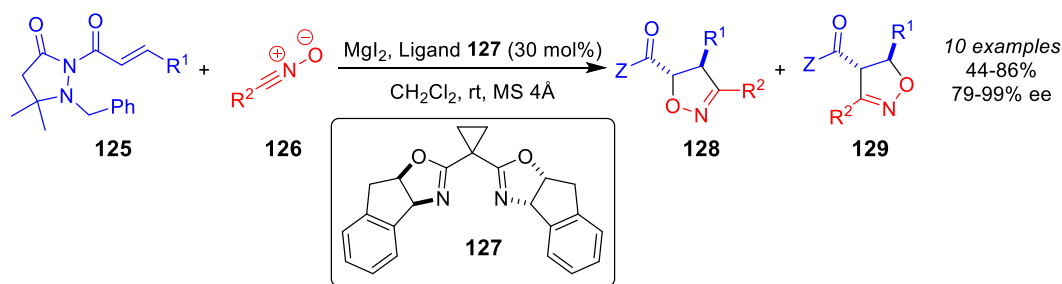
Moreover, Inomata and Ukaji elaborated their previous asymmetric work and demonstrated that the *R,R*-diisopropyl tartrate ((*R,R*)-DIPT) chiral auxiliary can be used in catalytic amounts, providing a succinct and facile protocol for catalytic asymmetric 1,3-dipolar cycloadditions between achiral allyl alcohols and nitrile oxides (**Scheme 54**).^{85a, 87} The isolated yields and enantiomeric excesses achieved with the catalytic variant of the reaction is very similar to the non-catalytic, with **119b** being synthesised in 98% yield and 90% ee. Improvement in isolated yield when using alkyl hydroxyimoyl chlorides was exemplified by **124a**, which was obtained in a 62% yield (vs. 35%, **Scheme 51**). However, this catalytic asymmetric cycloaddition reaction gave **119g** in a lower yield and ee than for the non-catalytic method (54% vs. 82%; 84% ee vs. 92% ee).



Scheme 54: The catalytic variant of the asymmetric 1,3-dipolar cycloaddition of propenyl alcohols and nitrile oxides, developed by the group of Inomata.

Chiral Lewis acid catalysis in 1,3-dipolar cycloadditions of nitrile oxides has previously been hampered by amine bases that coordinate to the Lewis acid; the amine base is

required for the *in-situ* formation of the nitrile oxide from hydroxyimoyl chlorides. However, Sibi *et al.* had developed a protocol in which a magnesium Lewis acid, with a chiral ligand, is employed to confer stereo- and regioselectivity to 1,3-dipolar cycloadditions between nitrile oxides and variously substituted crotonates (**Scheme 55**).⁸⁸ Notably, it was necessary to have steric bulk, in the form of an achiral pyrazolidinone amide, on the dipolarophile to influence the regioselectivity. Furthermore, all nitrile oxides employed in this protocol were prepared either prior to introduction to the reaction mixture (if stability allowed) or formed *in-situ* using Amberlyst® 21 to promote the elimination of HCl. In general, aryl nitrile oxides were tolerated better than alkyl nitrile oxides, with *tert*-butyl nitrile oxide providing isoxazoline **128d** in a modest 44% yield. However, although a lower yield was achieved, the reaction did proceed with high regioselectivity (99:1) and high stereoselectivity (92% ee). Both electron-withdrawing (**128b**, 70%) and electron-donating (**128c**, 61%) aryl nitrile oxides gave the corresponding isoxazolines in good yields, yet *para*-methoxybenzotrile oxide delivered poorer regioselectivity with a ratio of 10:1 in favour of the desired diastereomer. The authors tentatively proposed a stereochemical model, which is shown in **Figure 18**: they suggest that a five- or six-coordinate magnesium cation is bound by the chiral ligand. The dipolarophile is also bound in a bidentate manner through the carbonyl oxygens. This coordination sphere is in the *s-cis* conformation with one of the faces of the dipolarophile blocked by one of the bisoxazoline fragments and this is thought to provide the observed high stereoselectivity. Moreover, Sibi *et al.* suggest that the bulky pyrazolidinone delivers the regioselectivity by increasing the steric bulk at that end of the dipolarophile and it is believed that the nitrile oxide carbon prefers to approach from the front of the molecule.



Scheme 55: Sibi *et al.* exploited a magnesium chiral Lewis acid to provide an asymmetric 1,3-dipolar cycloaddition reaction between crotonates and nitrile oxides.

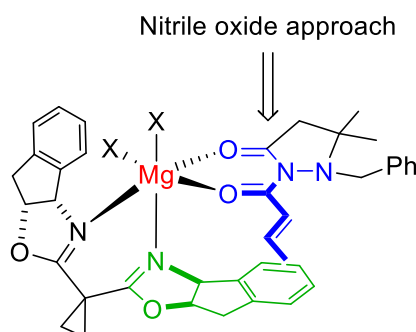
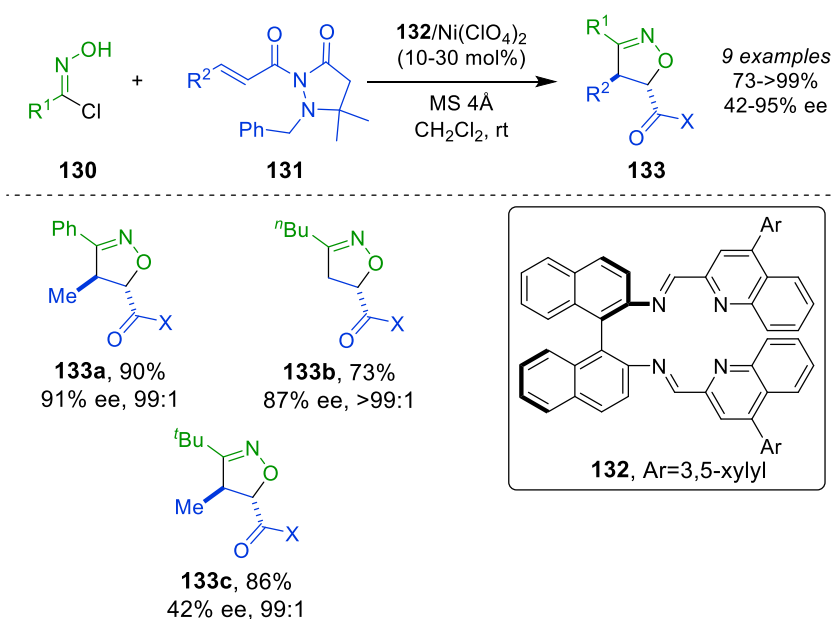


Figure 18: The proposed stereochemical model for the chiral Lewis acid catalyzed 1,3-dipolar cycloaddition developed by the group of Sibi.

Although there have been several reports showing that Lewis acid catalysis can be used to impart asymmetry in 1,3-dipolar cycloadditions, these have typically suffered from either limited substrate scope (i.e. poor/low reactivity of alkyl oximes) or less than ideal enantioselectivity. In an attempt to combat this problem, the group of Suga turned to employing a nickel catalyst bound with a large chiral ligand (**Scheme 56**).^{82, 89} Similar to that seen in the work by Sibi *et al.*, the Suga group opted to use the pyrazolidinone template to encourage regio- and enantioselectivity. Employing ligand **132** (**Scheme 56**) and a $\text{Ni}(\text{ClO}_4)_2$ catalyst, good to excellent yields were achieved with all substrates subjected to this reaction system. Furthermore, very high

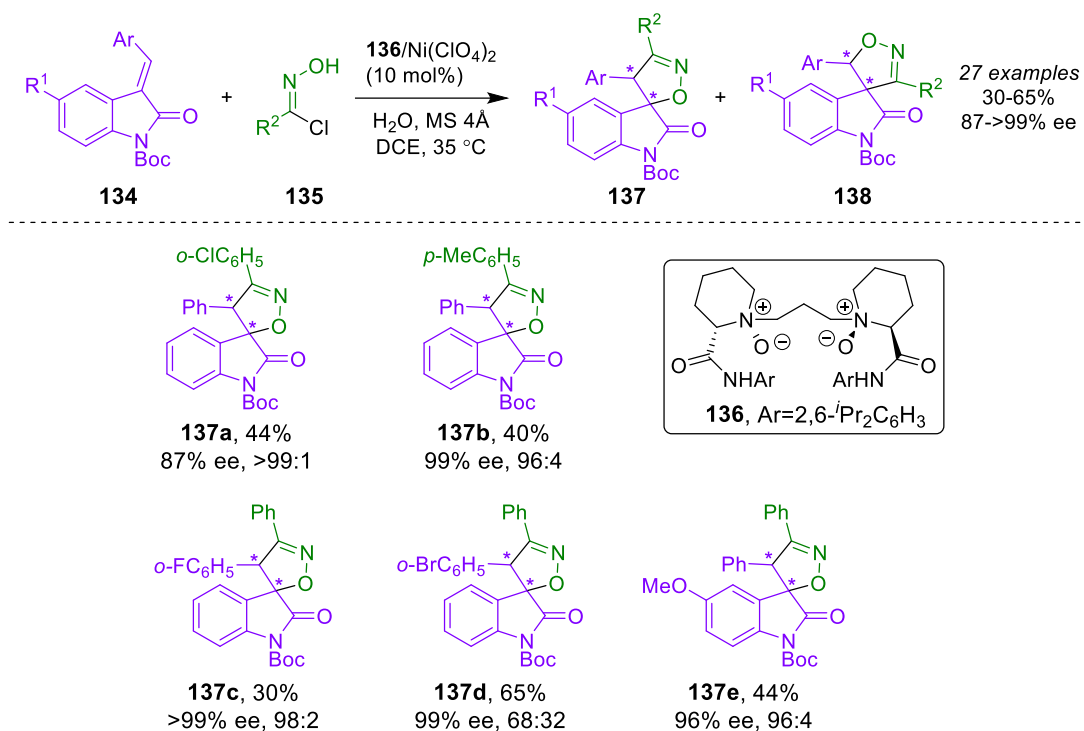
regioselectivities were observed and the authors attributed this to the pyrazolidinone template. Additionally, Suga *et al.* demonstrated that this catalyst system can achieve high yields, regio- and enantioselectivities, even at 10 mol% catalyst loading, with aliphatic, straight-chain hydroxyimoyl chlorides (**133b**); this has previously proven to be elusive due to the high propensity for these moieties to dimerise rapidly. The authors also note that when using bulkier aliphatic hydroxyimoyl chlorides, i.e. *t*-butyl vs. *n*-butyl, a decrease in enantioselectivity was observed, but they gave no indication as to a cause.



Scheme 56: Nickel catalysis with a bulky chiral ligand allowed Suga *et al.* to develop an asymmetric 1,3-dipolar cycloaddition that proceeded with high yields, regio- and enantioselectivities.

Employing a nickel catalyst bound with a chiral ligand was further explored by the group of Feng.⁹⁰ Using an *N*-oxide ligand (**136**, **Scheme 57**), high regioselectivities and excellent enantioselectivities were observed for the intermolecular 1,3-dipolar cycloaddition reaction to furnish spiro[isoxazolin-3,3'-oxindoles] **137**. It is noteworthy that, although high regio- and enantioselectivities were observed, the isolated yields of the products were much lower than those observed in previous reports. Feng *et al.* demonstrated that the enantioselectivity observed was insensitive to electronic and steric properties of the substituents on the phenyl ring of **135**. Both electron-withdrawing (**137a**) and electron-donating (**137b**) substituents gave high enantioselectivity (87% and 99% ee) as well as excellent regioselectivity (>99:1 and 96:4), furnishing the desired spiro compounds in moderate yields (44% and 40%).

Furthermore, the electronics of the 3-arylidene-oxindoles **134**, either by substitution directly on the ring system or in the aryl group, had negligible effect on the enantioselectivity. However, when Ar = *o*-BrC₆H₅ the regioselectivity of the corresponding spirooxindole was much lower, with a ratio of 68:32 in favour of the desired regioisomer (**137d**, **Scheme 57**). The authors also noted that no reaction of alkylideneoxindoles under their current conditions was observed, which is a significant limitation of this method when compared to previous protocols.



Scheme 57: Spirooxindoles can be fashioned from the Ni-catalysed asymmetric 1,3-dipolar cycloaddition between 3-arylidene-oxindoles and aryl hydroxymoyl chlorides, developed by the group of Feng.

1.4. Introduction Summary

In summary, a brief introduction to synthetic organic electrochemistry was discussed, with the field finding renewed interest from many groups. Many reports of mediated and non-mediated processes were reviewed, including examples of C–H bond functionalisation at a late stage.^{40, 91} It was demonstrated that electrochemistry can provide a tool which is synthetically useful, can negate the need for strong and toxic oxidants/reductants, and can be environmentally benign.

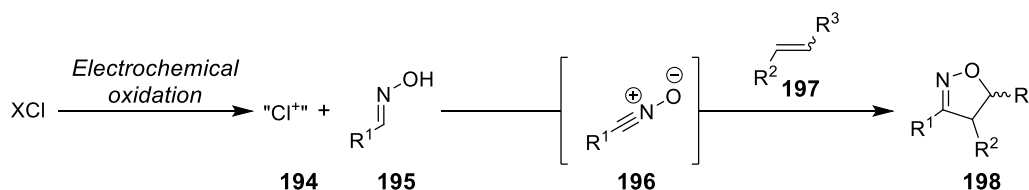
Additionally, a review of recent publications in the field of 1,3-dipolar cycloaddition reactions involving nitrile oxides was undertaken. It was illustrated that there were several methods in which nitrile oxides can be formed, including dehydration of nitroalkanes and dehydrohalogenation of hydroxyimoyl halides. The mechanistic aspects of 1,3-dipolar cycloadditions were also discussed, with in depth analysis of the frontier molecular orbital interactions as well as the stereospecificity and regio- and diastereoselectivity of these reactions.

The work detailed in this report brings together these two fields of research, with the intention of developing an electrochemical protocol for the synthesis of substituted isoxazolines *via* nitrile oxide 1,3-dipolar cycloaddition reactions. An additional objective is to develop a process which is a greener alternative to the current methods; this will advance the field of both synthetic organic electrochemistry and isoxazoline synthesis significantly. Furthermore, it is also the hope that this work will encourage more synthetic organic chemists to contemplate the use of electrochemistry, especially since the commercial availability of technology such as IKA's ElectraSyn 2.0 has allowed standardisation of the equipment that is being used.

2. Aim of Investigation

1. Optimisation of Reaction

The investigation herein builds on the work by Shono (**Scheme 50**, Section 1.3.1), aiming to optimise for electrode material, electrolyte/mediator, solvent and charge transferred. This is proposed to provide an electrochemical alternative to established nitrile oxide formations using an inexpensive source of chloride. From previous reports, the mechanistic hypothesis was thus: a chloride anion undergoes an electrochemical two-electron oxidation forming electrophilic species **194** (**Scheme 58**), which was suggested to be trapped by aldoxime **195** to give a hydroxyimoyl chloride. *In-situ* elimination of HCl could furnish nitrile oxide **196**, that could be intercepted by a suitable dipolarophile **197**, fashioning substituted isoxazolines **198**. It is proposed that optimisation of the electrochemically enabled synthesis of isoxazolines be realised *via* a Design of Experiments (DoE)⁹² approach to optimise for mediator/electrolyte equivalents, dipolarophile equivalents, and stir speed, enabling insights into the effect of these factors on the reaction.



Scheme 58: This work focuses on developing an electrochemical protocol for the conversion of aldoximes to substituted isoxazolines *via* a 1,3-dipolar cycloaddition reaction.

2. Application of Electrochemical Reaction

With optimised conditions in hand, an investigation into the substrate scope in both aldoxime and dipolarophile is proposed, which will demonstrate the promise and limitations of this electrochemical method towards isoxazoline synthesis. Derivatisation of a substituted isoxazoline, made *via* the developed method, is proposed to, in turn, show the use of the newly accessed isoxazoline cores as masked motifs. Finally, adaptation of batch-optimised processes into a flow electrochemical procedure is also proposed.

3. Mechanistic Investigation

To complement methodological efforts, ¹H NMR and IR analysis of the reaction profile are proposed in order to gain insight into the operative reaction mechanism(s). These

experiments should provide sufficient information on a plausible reaction pathway (or pathways) that are involved in the formation of a nitrile oxide and its participation in the designed 1,3-dipolar cycloaddition with a dipolarophile. Overall, it is envisaged that this approach will provide ready information for future expansion and adaption of the methods pioneered herein.

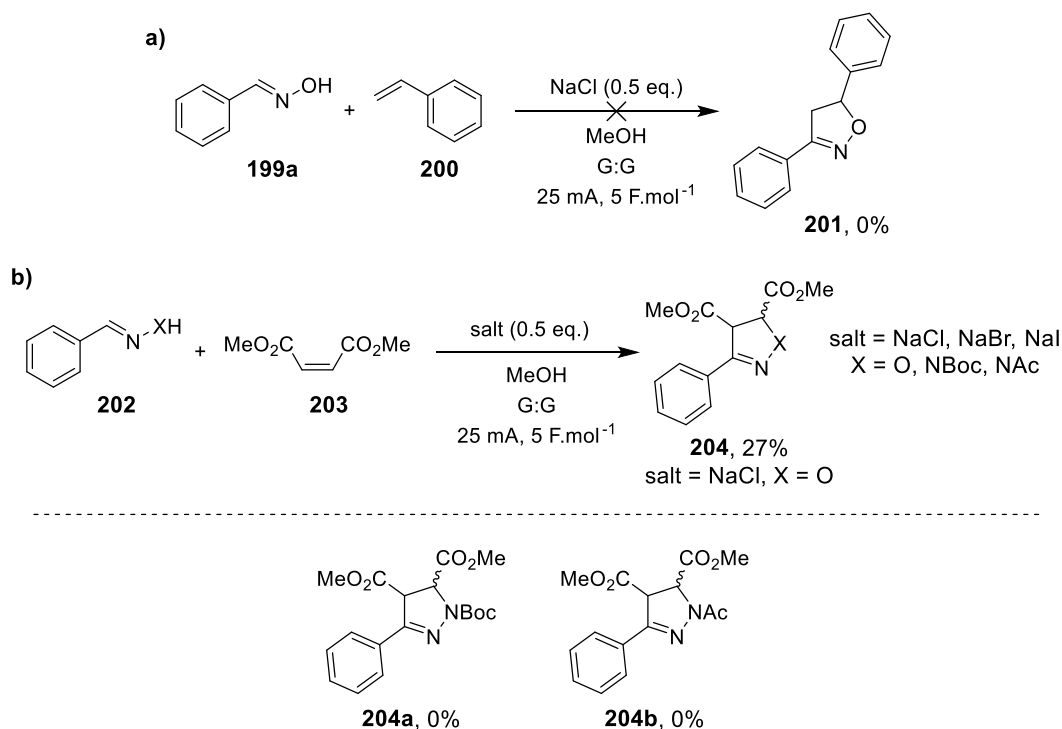
Through the proposed investigation, the overall aim is to provide expedient access to a wide range of isoxazoline cores that are inaccessible by established means and can be accessed by means boasting green and sustainability profiles competitive with what is known in the literature.

3. Results and Discussion

Similar to Shono's work with the electrochemical conversion of oximes to nitriles *via* nitrile oxides (see Section 1.3.1),⁸⁰ this work began with adapting the conditions to encourage 1,3-dipolar cycloaddition between the nitrile oxide formed and an external dipolarophile. Initially, scoping reactions were performed to determine the effects of the major reaction components, such as charge transferred, current and electrode material. A small screen to establish the need for an supporting electrolyte was devised and carried out. A formal optimisation was completed based on initial results, including a statistical Design of Experiments (DoE) screen. All aldoximes used in this work were synthesised from the corresponding aldehydes by condensation with hydroxylamine; the geometric isomers were separated by column chromatography and the isomer shown in schemes was the isomer used. All details of oxime synthesis are in the Experimental section.

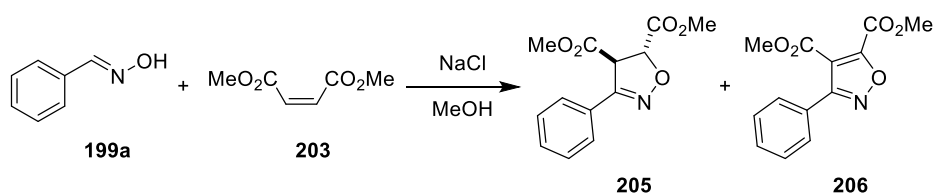
3.1. Initial Scoping

Previous unpublished work in this area conducted at GSK, showed that the use of graphite electrodes (for both anode and cathode) in combination with styrene, under otherwise analogous conditions to the Shono work (including the amount of charge passed), gave no reaction (**Scheme 59a**).⁹³ However, switching dipolarophile to dimethyl maleate and using NaCl as mediator gave the desired isoxazoline **204** (X = O) in 27% yield (**Scheme 59b**). Employing dimethyl acetylenedicarboxylate as dipolarophile also provided no observed reaction, as did switching the mediator to either NaBr or NaI. Attempts to prepare 2-pyrazolines **204a** and **204b** from **202** (X = NBoc, NAc) also resulted in no observed reaction.



Scheme 59: Initial scoping reactions provided an insight into the reaction: a) no reaction was observed using graphite electrodes in the IKA ElectroSyn 2.0; b) switching dipolarophile gave conversion to desired isoxazoline product but changing halide salt was detrimental as was employing hydrazones.

This work has built upon these previous experiments. Firstly, the electrode materials, current and charge transferred were explored, and the results are shown in **Table 1**. Graphite electrodes exclusively gave the over-oxidised isoxazole **206** but switching to RVC electrodes gave only the desired isoxazoline **205** (Entries 1 and 5, **Table 1**). Lowering the current was detrimental to the isolated yield (Entry 2), as was increasing the mediator loading (Entry 4). However, reducing the current and increasing the charge transferred gave a comparable yield (Entry 3). When the polarity of the RVC electrodes was switched every 15 mins, an increase in yield was observed (Entry 6 vs. Entry 5). Changing the dipolarophile to dimethyl fumarate furnished the desired isoxazoline in 76% (Entry 7), in line with the theory that *trans*-alkenes react faster compared to their analogous *cis*-alkenes.



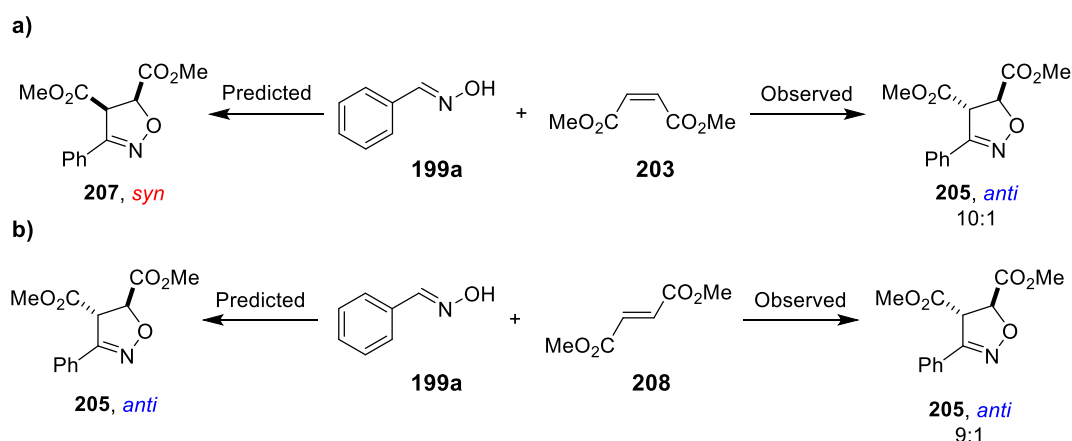
Entry	Anode	Cathode	Current/ mA	Charge transferred/F.mol ⁻¹	dr (<i>anti:syn</i>)	Yield 205 (206)/%
1 ^a	G	G	25	5	-	0 (27)
2 ^a	RVC	RVC	16.8	2	17:1	14 (0)
3	RVC	RVC	11.4	2.6	9:1	28 (0)
4 ^{a,b}	RVC	RVC	25	3	9:1	15 (0)
5	RVC	RVC	25	4.5	17:1	27 (0)
6 ^c	RVC	RVC	25	4.5	33:1	36 (0)
7 ^d	RVC	RVC	25	4.5	9:1	76 (0)

Table 1: Conditions: Oxime (0.5 mmol), dimethyl maleate (5 eq.), NaCl (0.5 eq.), MeOH (0.07 M), [anode], [cathode], [current] mA, [charge transferred] F.mol⁻¹, dr determined by ¹H NMR; ^aReaction conducted at 0.1 M concentration; ^b1 eq. NaCl used; ^cPolarity of the electrodes was switched every 15 mins; ^dDimethyl fumarate used instead of dimethyl maleate; G = graphite; RVC = reticulated vitreous carbon.

Interestingly, the diastereoselectivity observed did not match the diastereoselectivity that would be predicted by theory (see Section 1.2.5): employing a *cis*-alkene should furnish the desired isoxazoline as the *syn*-diastereoisomer. However, throughout this investigation, a diastereomeric ratio was observed that favoured the *anti*-configuration.

3.1.1. Observed Diastereoselectivity

The predicted diastereoselectivity (assuming a pericyclic 1,3-dipolar cycloaddition) is that the *cis*-alkene (dimethyl maleate) would give the *syn*-diastereomer **207**, while the *trans*-alkene (dimethyl fumarate) would give the *anti*-diastereomer **205**. That is, the reaction was hypothesised to be stereospecific in the dipolarophile. However, both alkenes, under electrochemical conditions, gave the same product with similar diastereomeric ratios (**Scheme 60**); even under chemical (non-electrolysing) conditions, mixtures of diastereomers were observed. Predicted H–CC–H dihedral angles for the lowest energy product conformations were 29.6° (*syn*) and 99.2° (*anti*), resulting in predicted (from Karplus curve) $^3J_{\text{H-H}}$ -couplings of 10 - 12 Hz and 2 - 4 Hz, respectively. The angles were calculated using MOE software and energy minimisation of the conformations. The major diastereomer had a measured coupling of 4.4 Hz and the minor 11.5 Hz, which are both in strong agreement with the predicted values for *anti* and *syn*, respectively (**Figure 19**).



Scheme 60: The observed vs. predicted diastereoselectivities of the electrochemically enabled 1,3-dipolar cycloaddition between (*E*)-benzaldehyde oxime and *cis*- and *trans*-alkenes.

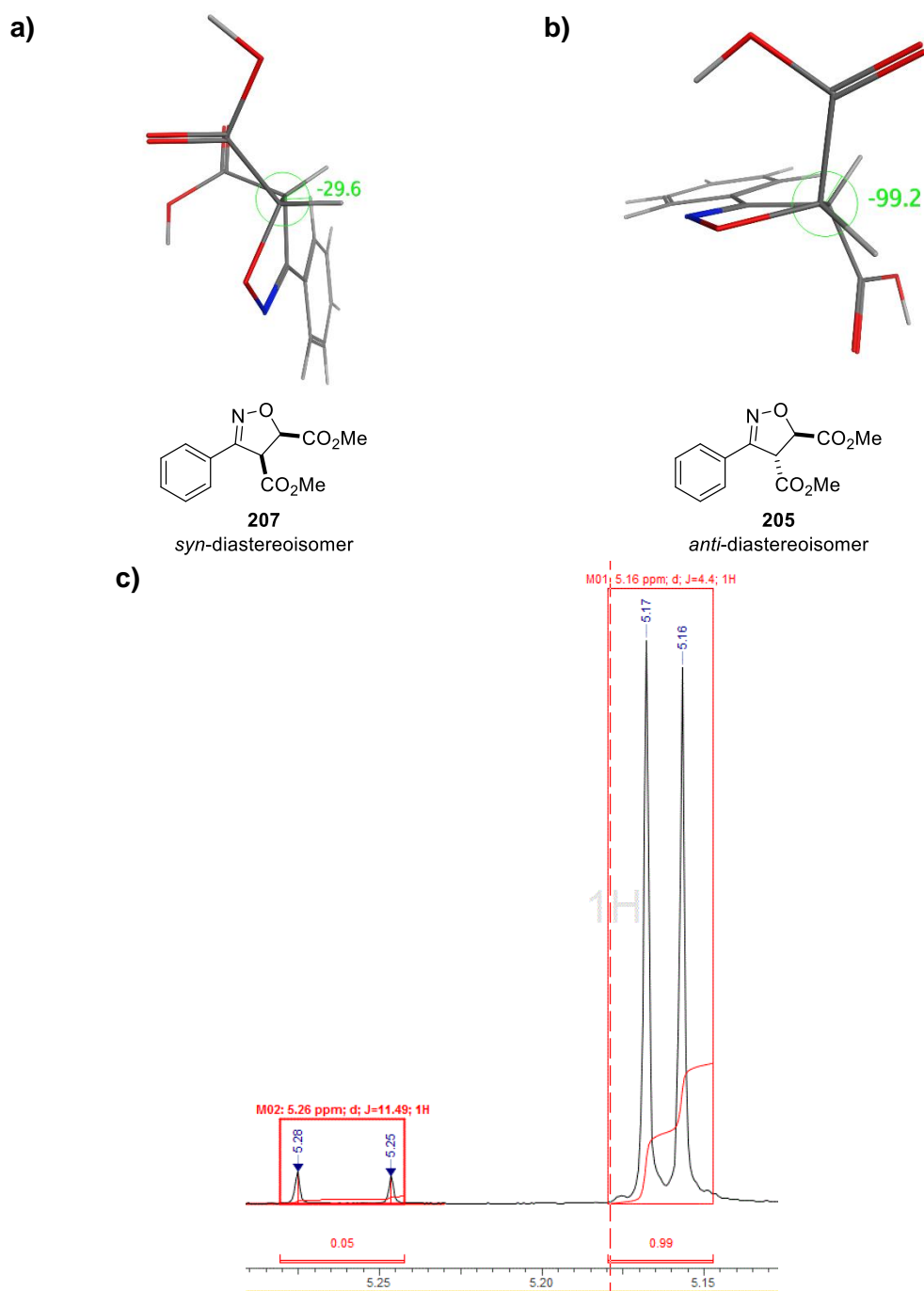
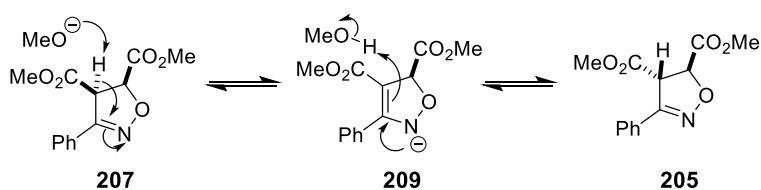


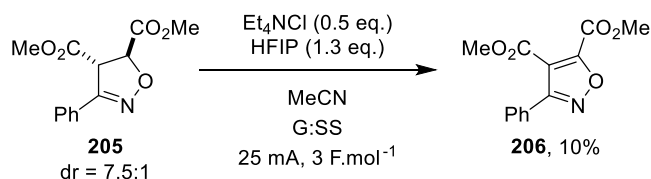
Figure 19: a) The predicted conformation of the *syn*-diastereomer **207**, with a dihedral angle of 29.6° ; b) The predicted conformation of the *anti*-diastereomer **205**, with a calculated dihedral angle of 99.2° ; c) The ^1H NMR extract showing the measured $^3J_{\text{H-H}}$ -couplings for the mixture of major and minor diastereoisomers of **205** obtained from the electrochemical reaction between (*E*)-benzaldehyde oxime and dimethyl maleate.

Several theories could explain the observed diastereoselectivity. Firstly, the conjugate base of the alcoholic solvent could epimerise one of the stereocentres in the expected product (**Scheme 61**). This would mean that the predicted *syn*-diastereomer **207** (when using dimethyl maleate as dipolarophile) is formed initially and epimerisation

to the thermodynamically more favourable *anti*-configuration **205** occurs. As this epimerisation is under thermodynamic control, a mixture of diastereoisomers would be expected. This is shown throughout by observed diastereomeric ratios that favour the *anti*-configured isoxazoline. A related explanation would be H-atom abstraction from the predicted product **207** that would also epimerise a stereocentre and give the same diastereochemical outcome. To determine whether this would be a likely pathway to the unexpected diastereomeric ratio of products, an experiment in which the major diastereoisomer was subjected to the reaction conditions could be conducted. If the *syn*-diastereoisomer was observed in the ^1H NMR after the reaction, it would suggest that epimerisation of one of the stereocentres had occurred. Alternatively, if the major diastereoisomer was subjected to basic conditions, and the minor diastereoisomer was observed, this would give evidence for epimerisation of the stereocentres by conjugate base. Subjecting **205** (synthesised from dimethyl maleate) to the optimised electrochemical conditions only resulted in oxidation to the fully unsaturated substituted oxazole **206**, with no scrambling of stereochemistry (**Scheme 62**).



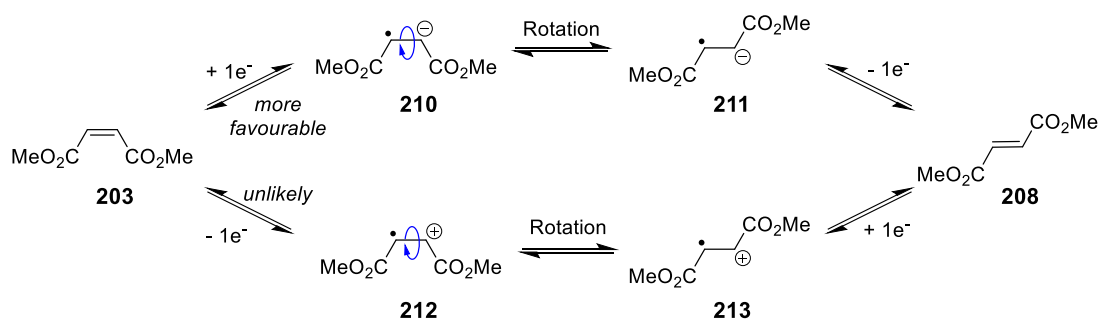
Scheme 61: Epimerisation of the predicted *syn*-diastereoisomer could occur *in situ* and explain the observed diastereomeric ratio which is likely be under thermodynamic control.



Scheme 62: Scrambling of stereochemistry is not observed when subjecting the disubstituted isoxazoline to the optimised electrochemical conditions; only oxidation to the isoxazole was observed. Used optimised conditions (*vide infra*).

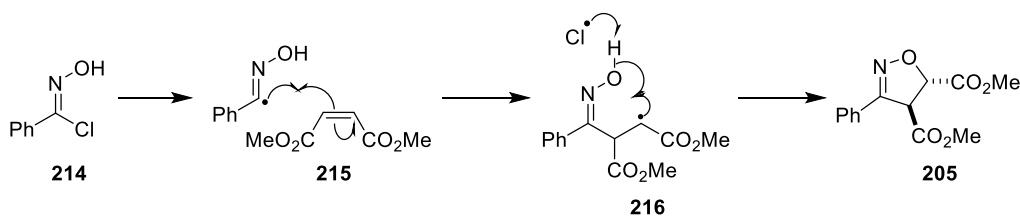
Secondly, isomerisation of the *cis*-alkene could occur *via* single electron transfer (SET) at either electrode (**Scheme 63**). A single electron reduction or single electron oxidation of **203** would give the radical cation **212** or radical anion **210**, which could undergo rotation about the single bond. Thermodynamically, the *trans*-alkene would be the more favourable configuration and would react faster than the *cis*-alkene as

there would be fewer eclipsing interactions in the transition. The equilibrium between the two geometric isomers of the alkene could explain the observed diastereomeric ratio. As both alkenes are highly electron-deficient, it is more likely that reduction would occur preferentially over oxidation. Subjecting dimethyl maleate to the electrochemical conditions, in the absence of oxime, would allow the exploration of this theory: should SET be responsible for isomerisation, dimethyl fumarate would be formed and could be observed by ^1H NMR. Electrolysing both dimethyl fumarate and dimethyl maleate separately under the optimised electrochemical conditions (in the absence of aldoxime), it was found that isomerisation was not observed. Consumption of both disubstituted alkenes occurred, with no identifiable species in either ^1H NMR or LCMS spectra. It is recognised that this experiment does not entirely rule out the pathway proposed in **Scheme 63** as, in the absence of aldoxime, any SET intermediates (see below) may react with each other and attenuate presumed polymerisation reactions.



Scheme 63: Isomerisation of the alkene could lead to the observed diastereoselectivity; SET to form a radical cationic or radical anionic species would allow rotation around a single bond and a second SET would give the thermodynamically more favourable *trans*-alkene. Not observed.

Lastly, it is possible that the reaction with dimethyl maleate or dimethyl fumarate proceeds *via* a non-concerted, step-wise mechanism (**Scheme 64**). In this scenario, the hydroxyimoyl radical **215** (formed from the homolytic cleavage of the C–Cl bond of **214**), could add to one end of the alkene to give species **216**. As this species possesses rotational freedom, the more thermodynamically favourable *anti*-diastereoisomer **205** will be formed. It is also possible that the hydroxyimoyl radical **215** can be formed directly at the electrode and this is evidenced by isolation of desired isoxazoline in the absence of a halide source (Entry 2, **Table 2**).



Scheme 64: If a step-wise mechanism is invoked for the electrochemical reaction between (*E*)-benzaldehyde oxime and dimethyl maleate, this could be an explanation for the observed unexpected diastereoselectivity.

Through reaction monitoring by ^1H NMR and attempted non-electrochemical generation of the *syn*-diastereoisomer, it is likely that the observed diastereoselectivity of the electrochemical reaction is due to an alternative mechanism occurring when employing dimethyl fumarate or dimethyl maleate, in combination with chemical instability of any *syn*-diastereoisomer formed. During isolation, following a non-electrochemical method for the isoxazoline synthesis, it was found that the ratio of *syn*- and *anti*-diastereoisomers changed, with the conversion of the *syn*-diastereoisomer to the *anti*-diastereoisomer observed. This is illustrated by **Figure 20** in which ^1H NMR extracts of the crude mixture prior to work-up (**Figure 20a**), the crude mixture after work up (**Figure 20b**), and the products from column chromatography are shown (**Figure 20c**). As shown, the ratio of diastereoisomers changes after each manipulation, but with the *syn*-diastereoisomer observed in a reasonable ratio of 1:2 *syn:anti* at the start, which then degrades to a ratio of 1:10 after column chromatography.

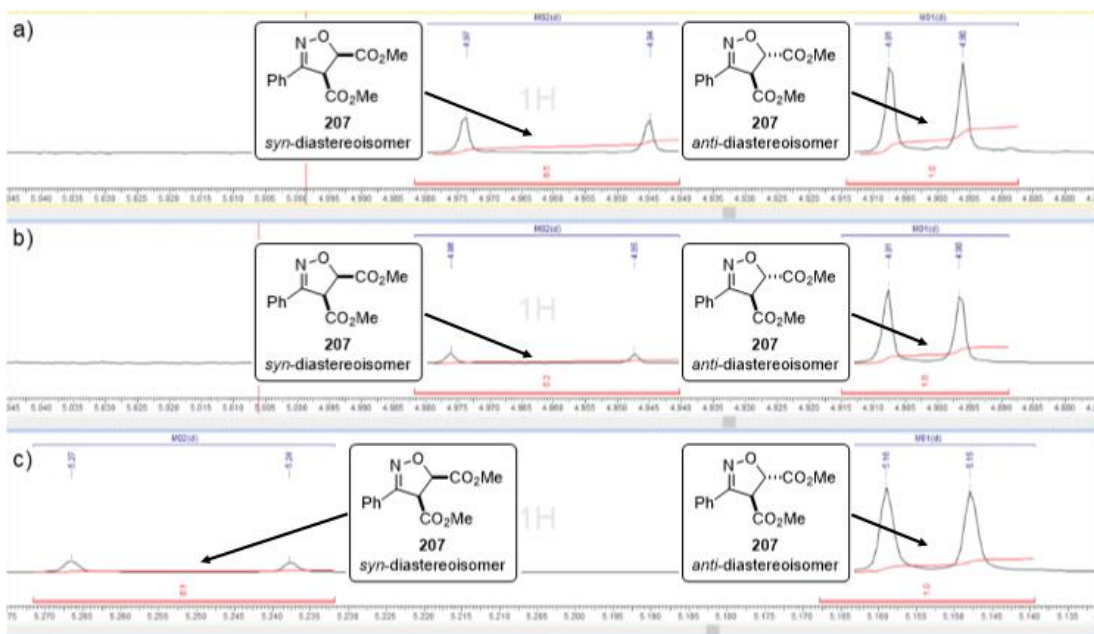


Figure 20: ^1H NMR extracts of the non-electrochemical reaction demonstrating instability of the *syn*-diastereoisomer. a) ^1H NMR extract of crude reaction mixture in $\text{MeCN-}d_3$; b) ^1H NMR extract of reaction mixture after work up in $\text{MeCN-}d_3$; c) ^1H NMR extract of chromatographed reaction mixture in $\text{DMSO-}d_6$.

^1H NMR analysis of the time-course of the electrochemical reaction shows that the *anti*-diastereoisomer is formed from the start of the reaction, with less than 10% *syn*-diastereoisomer formed throughout the reaction (**Figure 21**). Analysis of the electrochemical reaction between benzaldehyde oxime and dimethyl fumarate is shown in **Figure 22**, and shows a similar profile to the reaction with dimethyl maleate. These results support the hypothesis of an alternative mechanism when employing dimethyl fumarate or dimethyl maleate. Both these profiles are indicative of a radical mechanism as the *anti*-diastereoisomer is formed from the start of the reaction; conversion from *syn* to *anti* would be observed if the electrochemical reaction was a true pericyclic reaction (in the case of employing **203** as dipolarophile).

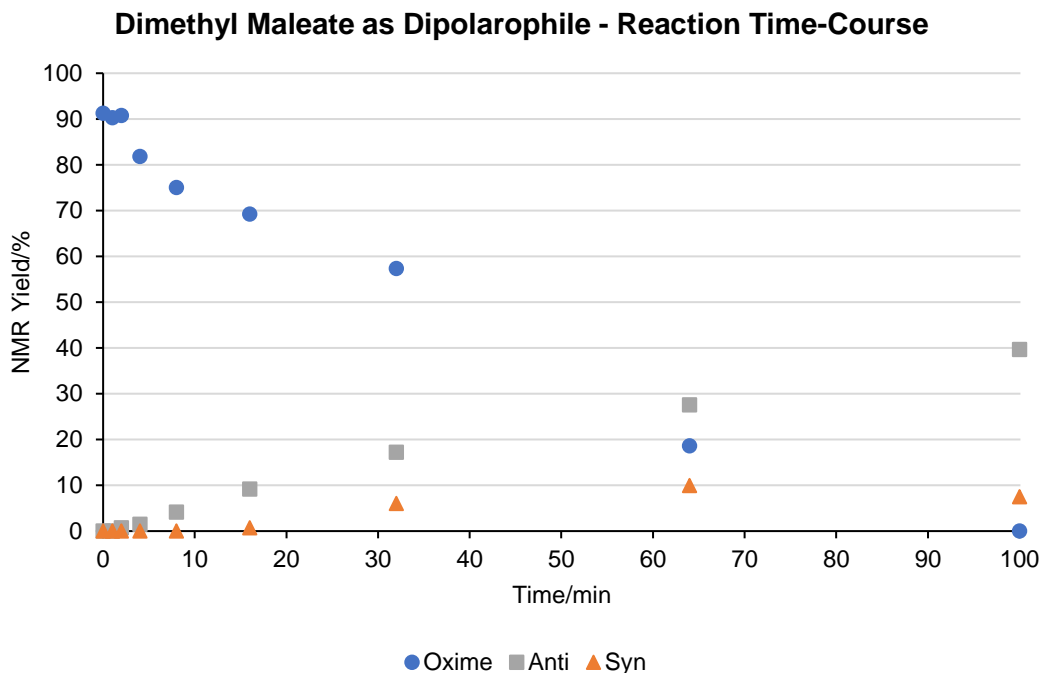


Figure 21: ^1H NMR analysis of the reaction time-course for the electrochemical reaction between benzaldehyde oxime and dimethyl maleate.

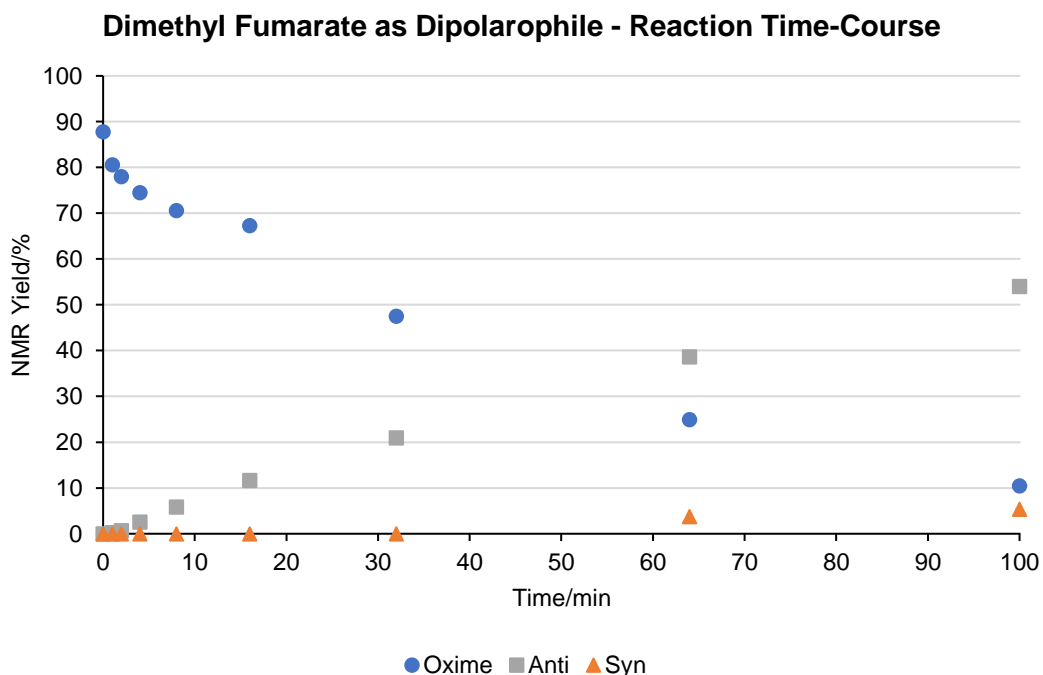


Figure 22: ^1H NMR analysis of the reaction time-course for the electrochemical reaction between benzaldehyde oxime and dimethyl fumarate.

By plotting the ^1H NMR yields of the *anti*- and *syn*-diastereoisomers from the electrochemical reaction between **199a** and **203/208** (Figure 23), it has been shown

that the rate of reaction with the *trans*-dipolarophile (**208**) is faster than the rate when employing the *cis*-dipolarophile (**203**); this finding is consistent with the literature.

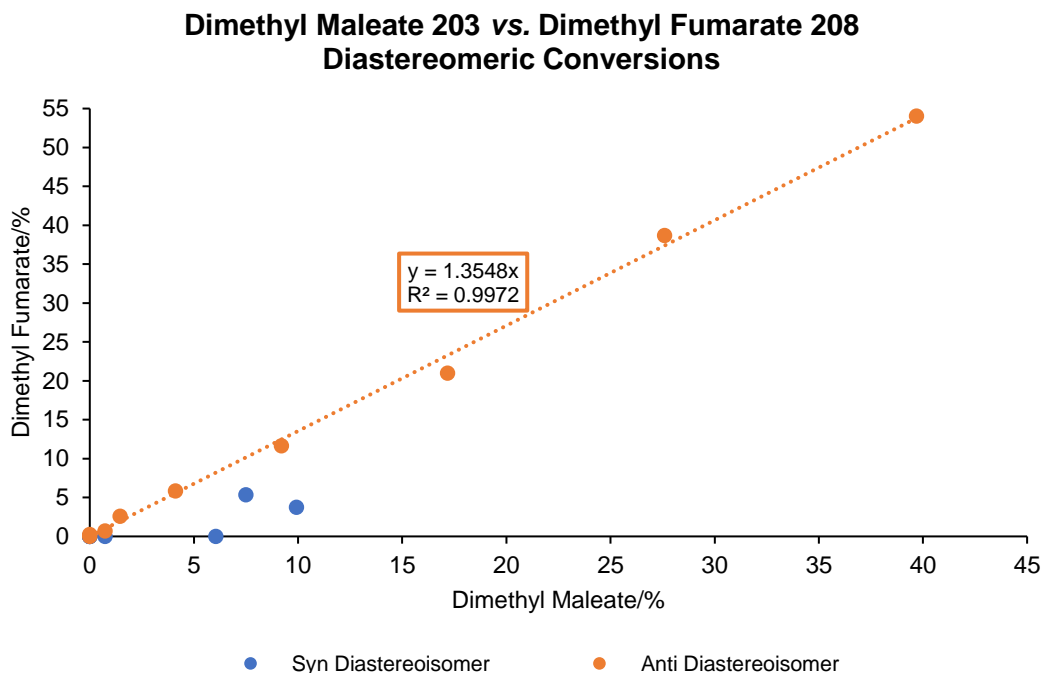


Figure 23: A plot of the NMR yields of each of the diastereoisomers for both dimethyl fumarate and dimethyl maleate. i.e. *anti* % vs. *anti* % for both dipolarophiles and *syn* % vs. *syn* % for both dipolarophiles.

An alternative analysis in which the *syn* vs. *anti* ^1H NMR yields for each of the reactions employing **203** and **208** as dipolarophiles was plotted and gave **Figure 24**. This graph shows that each diastereoisomer (for both dipolarophiles) is formed at different times during the reaction, which is indicative of a mechanism that facilitates the preferential formation of the *anti*-diastereoisomer, where the *syn*-diastereoisomer only emerges later, i.e. not from $t = 0$.

Syn vs. Anti - Both Dimethyl Maleate 203 and Dimethyl Fumarate 208

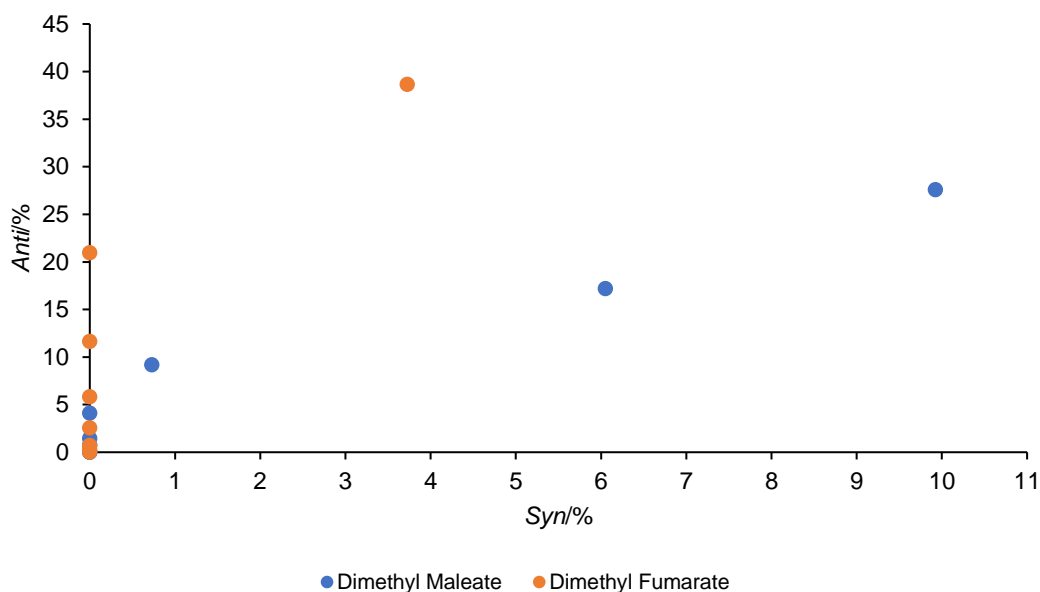
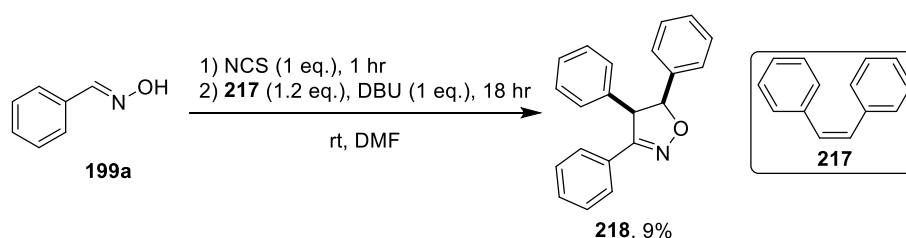


Figure 24: A plot of the NMR yields of *syn* vs. *anti* diastereoisomers for each of dimethyl maleate and dimethyl fumarate.

Interestingly, when *cis*-stilbene **217** was employed as dipolarophile, under non-electrochemical conditions, only the expected *syn*-substituted isoxazoline **218** was observed (**Scheme 65**, also Entry 3, **Table 3**). However, *cis*-stilbene did not demonstrate reactivity under electrochemical conditions. Still, this result suggests that dimethyl maleate and dimethyl fumarate may be reacting *via* a different mechanism. This may be a step-wise mechanism, as detailed above. Alternatively, due to the likely higher pK_a of the α -carboxyl protons of **205**, epimerisation by base is more facile when compared with the pK_a of the α -phenyl protons of **218**.



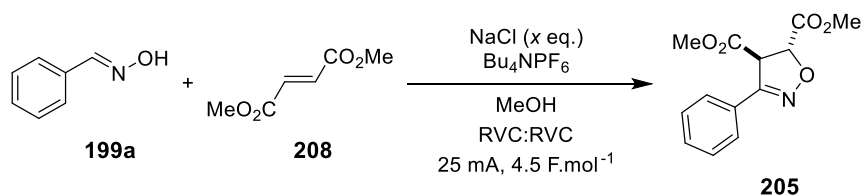
Scheme 65: Employing *cis*-stilbene as dipolarophile gives only the *syn*-configured isoxazoline, under chemical conditions.

Due to the observed epimerisation of *syn*-isoxazolines under a range of conditions, during the reaction, work-up and purification, it is challenging to deconvolute the true

source of *anti*-isoxazoline product. This is possibly due to a combination of the above described mechanisms, with a radical pathway the most likely cause.

3.1.2. External Electrolyte Screen

Attention was turned to explore whether a supporting electrolyte, as well as the mediator, could be of benefit to the reaction. The electrolyte Bu_4NPF_6 was chosen for this reaction, due to it being a common electrolyte employed in electrochemical syntheses; the external electrolyte was used at a concentration of 0.1 M, in line with the electrochemical literature.^{10d} With no NaCl mediator in solution, the isoxazoline was obtained in 8% yield (Entry 2, **Table 2**). This result may suggest an alternative mechanism to the current hypothesis; the plausible mechanisms are discussed further later (Section 3.2.9). Use of 0.5 equivalents of mediator also gave only 8% yield (Entry 3). This represented a marked decrease in efficiency of reaction (Entry 1 vs. Entry 3). Increasing the mediator loading to 100 mol% (Entry 4) improved reaction progression but increasing further was detrimental (Entry 5). Employing an alternative quaternary ammonium salt electrolyte, Et_4NBF_4 (Entry 6), showed an increased yield, although lower than when excluding a supporting electrolyte (Entry 1 vs. Entry 6). This screen demonstrated that these supporting electrolytes were detrimental to reaction progression, therefore no supporting electrolytes were employed in subsequent experiments.

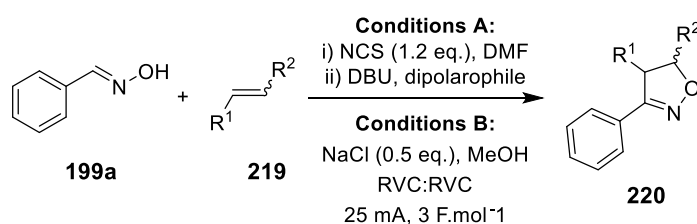


Entry	External Electrolyte	NaCl (x)/eq.	dr ^a (<i>anti:syn</i>)	205/%
1	-	0.5	9:1	76
2	Bu_4NPF_6	0	33:1	8
3	Bu_4NPF_6	0.5	33:1	8
4	Bu_4NPF_6	1	14:1	33
5	Bu_4NPF_6	2	50:1	14
6	Et_4NBF_4	0.5	25:1	39

Table 2: Conditions: Oxime (0.5 mmol), dimethyl fumarate (5 eq.), NaCl (x eq.), Bu_4NPF_6 (1.4 eq.), MeOH (0.07 M), RVC anode, RVC cathode, 25 mA, 4.5 F.mol⁻¹. ^aDiastereomeric ratio determined by ¹H NMR. RVC = reticulated vitreous carbon.

Further scoping was initiated; a comparison of the non-electrochemical and electrochemical conditions was performed, and the results are illustrated in **Table 3**. Under chemical conditions, dimethyl fumarate and dimethyl maleate furnished

isoxazoline **205** in 49% (Entry 1) and 33% (Entry 2), respectively. However, under electrochemical conditions, dimethyl fumarate gave **205** in 76% and dimethyl maleate gave **205** in 36%. While there is negligible difference between the conditions used for the *cis*-alkene, the electrochemical conditions were superior with dimethyl fumarate. Interestingly, when comparing the diastereomeric ratios, the *anti*-configured isoxazoline was favoured in all cases, but dimethyl maleate under electrochemical conditions gave almost exclusively the *anti*-product, with a ratio of 33:1 *anti:syn*. Both *cis*-stilbene and styrene demonstrated no reactivity under the electrochemical conditions (Entries 3 and 4). On the other hand, *tert*-butyl acrylate under both conditions gave similar yields of **221a**, with the same observed regioisomeric ratio.



Entry	Dipolarophile	Product	Conditions A: 220 (dr)^a/%	Conditions B: 220 (dr)^a/%
1			205 , 49 (20:1)	205 , 76 (9:1)
2			205 , 33 (9:1)	205 , 36 (33:1)
3			218 , 9 ^b	218 , NR
4			201 , 58	201 , NR
5			221a , 55 (20:1) ^c	221a , 41 (20:1) ^c

Table 3: Conditions A: Oxime (1 eq.), NCS (1.2 eq.), DMF, rt, 1 hr then, DBU (1 eq.), dipolarophile (1.2 eq.), rt, 18 hr. **Conditions B:** Oxime (0.5 mmol), dipolarophile (5 eq.), NaCl (0.5 eq.), MeOH (0.07 M), RVC:RVC, 25 mA, 4.5 F.mol⁻¹. ^aDiastereomeric ratio determined by ¹H NMR of chromatographed products; ^bNo *anti*-diastereoisomer observed; ^cRegioisomeric ratio, determined by ¹H NMR of chromatographed products. NCS = *N*-chlorosuccinimide, DMF = *N,N*-dimethylformamide, DBU = 1,8-diazabicyclo[5.4.0]undec-7-ene, rt = room temperature, RVC = reticulated vitreous carbon, NR = no reaction.

3.2. Optimisation of Electrochemical Reaction

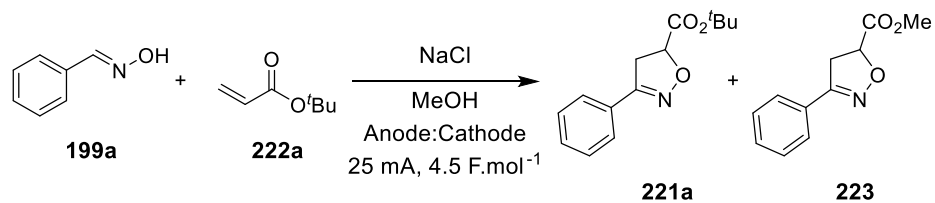
The initial scoping reactions provided a solid foundation to allow the progression of the work to a formal optimisation process. Optimising for the reaction between the electron-neutral (*E*)-benzaldehyde oxime and *tert*-butyl acrylate was carried out by devising thorough screens that explored electrode material, mediator, solvent and charge transferred. All yields quoted are with respect to starting aldoxime.

3.2.1. Electrode Material Screen

It was deemed necessary to optimise for a different dipolarophile. This decision was made since the reaction with dimethyl fumarate gave full consumption of aldoxime and a good isolated yield (76% Entry 1, **Table 3**). With a starting position that is half-way to the ideal outcome of quantitative conversion and high (>85%) isolated yield, the increase or decrease in yield and conversion will be more pronounced and allow more informed decisions on the conditions and variables.

So far, an electrode pairing of RVC anode and RVC cathode had been used in all electrolysis reactions and gave an isolated yield of 27% (Entry 1, **Table 4**). Upon substituting with graphite electrodes, a decreased yield of desired product was obtained (11%, Entry 2, **Table 4**), however the methyl ester substituted isoxazoline **223** was also observed in a ratio of 1:2.8 (**221a:223**). As detailed in the synthesis of isoxazolines *via* a non-electrochemical route (Section 1.3), a base is usually present to facilitate the elimination of HCl from the hydroxyimoyl chloride starting material to give the nitrile oxide. It was postulated that the methanol conjugate base (methoxide), formed from the reduction of methanol at the counter electrode, could be responsible in facilitating the elimination. From this hypothesis, stainless-steel (SS) and platinum were investigated as cathodes since these materials have a higher propensity for hydrogen evolution. Combinations of electrodes that used a SS or Pt cathode all gave similar isolated yields of desired products (Entries 3 - 8), although also in all the cases with these combinations, the major isolated product was **223** (with the exception of those combinations using RVC as the anodic material). Nonetheless, it was decided that the best combination of electrodes was graphite for the anode and stainless-steel for the cathode. This decision was made for three reasons: 1) it gave the highest total conversion to products (58%), 2) the reaction profile was cleanest (by LCMS analysis) and 3) they are the cheapest combination of electrodes. It was envisioned that the

formation of **223** could be avoided by a simple solvent switch and so the undesirable ratio of products was not a concern at this point.

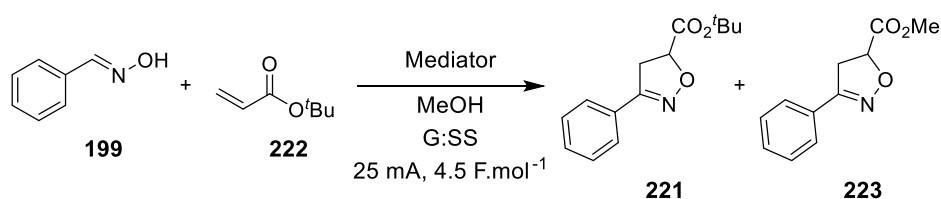


Entry	Anode	Cathode	Ratio 221a:223	Isolated Yield 221a (223)/%
1	RVC	RVC	6.8:1	27 (4)
2	G	G	1:2.8	11 (31)
3	RVC	SS	2.6:1	31 (12)
4	RVC	Pt	4.1:1	37 (9)
5	G	SS	1:3.1	14 (44)
6	G	Pt	1:3	13 (39)
7	GC	Pt	1:3	12 (36)
8	GC	SS	1:1.8	17 (30)

Table 4: Conditions: Oxime (0.5 mmol), *tert*-butyl acrylate (5 eq.), NaCl (0.5 eq.), MeOH (0.07 M), 25 mA, 4.5 F.mol⁻¹; RVC = reticulated vitreous carbon; G = graphite; SS = stainless steel; GC = glassy carbon.

3.2.2. Mediator/Electrolyte Screen

It was found that the mediator for the reaction allowed sufficient conductivity of the reaction solution such that an additional electrolyte was not needed. Therefore, for much of the investigation, the mediator is both mediator of the reaction and supporting electrolyte; any discussion of additional electrolytes will be more specific. It is integral that there is enough salt in solution so that the conductivity of the solution is not impaired and that the halide anion, which is assumed to be the mediator, is available to be oxidised. Other research groups in this area have used halides other than chloride as mediators (Section 1.1.6) and thus, these have been included in the mediator screen. Upon switching the halide to bromide (Entry 2, **Table 5**) a poor conversion of 20% was achieved, but with iodide (Entry 3) a comparable total conversion (60%) and moderate isolated yield (35%) of **221a** was attained. As with the previous screen, both the desired *tert*-butyl ester **221a** and methyl ester products **223** were observed in the ¹H NMR spectra, with isolated yields of the methyl ester by-product in parentheses. The sodium halide salts are sparingly soluble in organic solvents such as acetonitrile (MeCN) or dimethyl sulfoxide (DMSO), and therefore use of tetraalkylammonium halides as mediators may allow alternative solvents to be explored. Exploration of these tetraalkylammonium salts as mediators was carried out on the assumption that this is no ion pairing effect and that the cation is simply a spectator and aids solubility. Tetraethylammonium halide salts were employed as the tetraethylammonium (Et₄N⁺) counterion is one of the more commonly used cations in the electrochemical literature. A good total conversion of 74% was achieved when using Et₄NCl, however only a poor isolated yield of both reaction products was observed (21% for **221a** and 27% for **223**). Et₄NI (Entry 6) gave comparable conversions and isolated yields to both NaCl and Et₄NCl. Et₄NBr as mediator was omitted from the screen as NaBr showed little promise as a potential halide source. Additionally, due to very high potentials observed (>10 V), NHPI (**224**), TEMPO (**225**) and ABNO (**226**) displayed no reactivity (Entries 7 - 9). It would be interesting to test these mediators in combination with an electrolyte. Solvent switch from MeOH to MeCN gave a poor NMR conversion of 14% (Entry 5). However, this is an interesting result as some conversion was observed in the absence of MeOH and therefore conjugate methoxide base. Although the use of Et₄NCl gave a ratio of 1:1 of **221a**:**223**, it also gave the highest conversion (74%, Entry 4) and so it was decided to employ Et₄NCl as the mediator in subsequent experiments.



Entry	Mediator	NMR Conversion (221a + 223) ^a /%	Ratio ^b 221a:223	Isolated Yield 221a (223)/%
1	NaCl	63	2:1	22 (27)
2	NaBr	20	3:1	- (-)
3	NaI	60	1.5:1	35 (22)
4	Et₄NCl	74	1:1	21 (27)
5 ^c	Et ₄ NCl	14	∞ ^d	- (-)
6	Et ₄ NI	62	2:1	32 (21)
7	224	Abandoned ^e	-	-
8	225	Abandoned ^e	-	-
9	226	Abandoned ^e	-	-

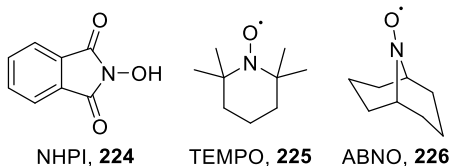


Table 5: Conditions: Oxime (0.5 mmol), *tert*-butyl acrylate (5 eq.), mediator (0.5 eq.), MeOH (0.07 M), G anode, SS cathode, 25 mA, 4.5 F.mol⁻¹. ^a¹H NMR yield using benzyl benzoate as internal standard; ^bDetermined by ¹H NMR of the chromatographed products; ^cMeCN used instead of MeOH; ^dNo methyl ester by-product observed; ^eReaction did not reach completion due to insufficient conductivity. G = graphite; SS = stainless steel; NHPI = *N*-hydroxyphthalimide; TEMPO = 2,2,6,6-tetramethylpiperidine *N*-oxyl; ABNO = 9-azabicyclo[3.3.1]nonane *N*-oxyl.

3.2.3. Reproducibility of Carousel

It was at this point in the investigation that it was decided that the reproducibility of the IKA ElectraSyn carousel should be tested. Up until then, the protocol had been thus: the reaction was performed in positions 1 - 5 of the carousel for the required length of time (or charge transferred) and, once reaction was complete, a sample was taken of the crude reaction mixture. The sample was blown down to dryness under a stream of nitrogen (at 40 °C). Once dry, the sample was weighed and submitted to ^1H NMR analysis using benzyl benzoate as internal standard in $\text{DMSO-}d_6$ to determine conversion. To test the reproducibility of the carousel, five identical reactions (shown in **Table 6**) were placed in positions 1 - 5 in the carousel, and the electrochemical reaction was carried out. By taking three samples from each reaction post-electrolysis, the reproducibility of sampling could also be tested. The results are detailed in **Table 6**. It shows that all results, across the five positions, had an error of 13%, within a confidence level of 95%. Upon inspection of the error bars in **Figure 25**, it was demonstrated that there is no significant difference between the positions on the carousel. However, looking at the results in more detail (**Table 6a**), there is a broad range in the NMR conversions that were observed, and this is represented by the large standard deviations. This notable variation may be attributed to the technique which was used to add the NMR standard to the blown down crude reaction samples: the NMR standard was added from a pre-prepared stock solution in $\text{DMSO-}d_6$ *via* a syringe. With only 50 μL of standard added from a 1 mL syringe, it is likely there was a large variability in the actual amount of standard present in the ^1H NMR. This was problematic as all NMR conversion calculations were based on an assumed concentration of standard in reaction samples.

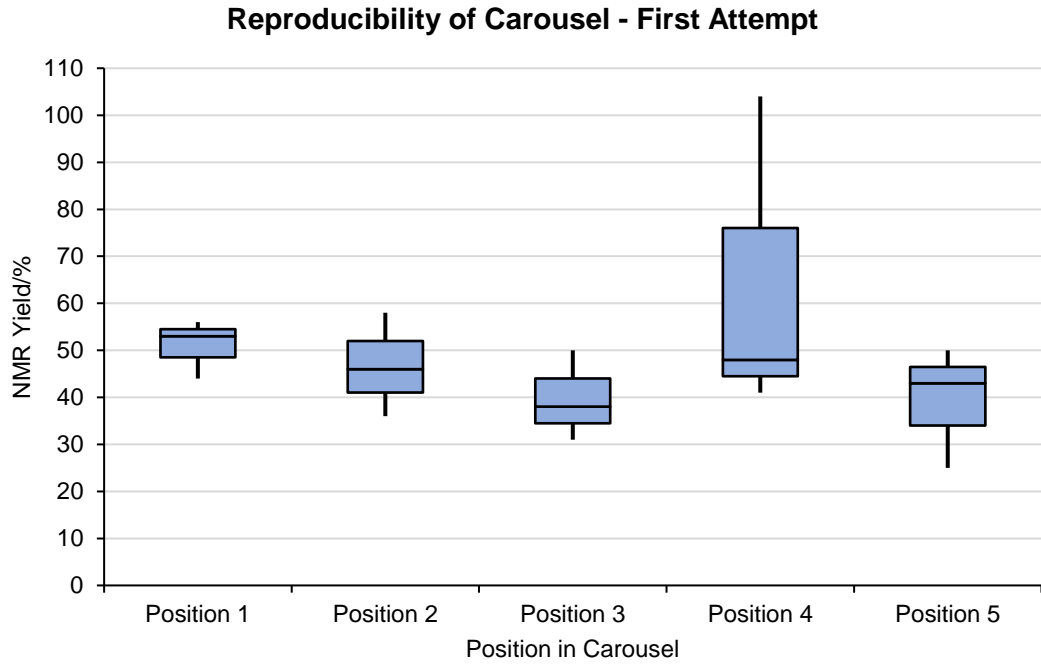
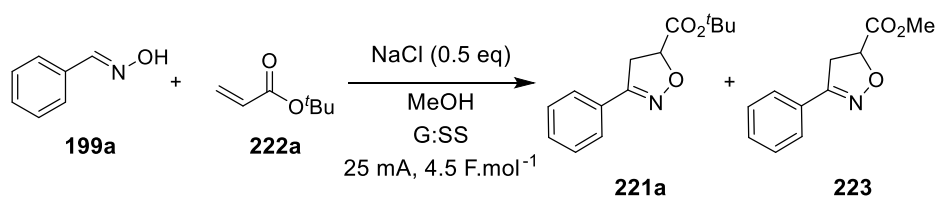


Figure 25: A pictorial representation of the data shown in **Table 6**.



Entry	Position	221a NMR Yield ^a /%	223 NMR Yield ^a /%	Total NMR Conversion ^{a,b} /%
1	1	32 / 34 / 28 (31)	21 / 22 / 16 (20)	53 / 56 / 44 (51±6)
2	2	19 / 31 / 25 (25)	17 / 27 / 21 (22)	36 / 58 / 46 (47±11)
3	3	30 / 18 / 26 (25)	20 / 13 / 12 (15)	50 / 31 / 38 (40±10)
4	4	66 / 31 / 26 (41)	38 / 17 / 15 (23)	104 / 48 / 41 (64±35)
5	5	24 / 14 / 28 (22)	19 / 11 / 22 (17)	43 / 25 / 50 (39±13)

Table 6a: Conditions: Oxime (0.5 mmol), tert-butyl acrylate (5 eq.), NaCl (0.5 eq.), MeOH (0.07 M), 25 mA, 4.5 F.mol⁻¹; ^a¹H NMR yield using benzyl benzoate as internal standard; ^bNumber in parentheses is mean average ± one standard deviation; G = graphite; SS = stainless steel.

Position Statistical Analysis

	221a NMR Data	223 NMR Data	Total NMR Conversion Data
Mean	29	19	48
Standard Error	3	1	5
Standard Deviation	8	3	10
Confidence Level (95%)	9	4	13
Range	19	5	25

Table 6b: Statistical analysis was performed on each of the yield/conversion data across the position in the IKA Carousel.

To combat the significant variability in the calculated NMR conversions, a new sampling technique was devised: the original protocol was used, except that instead of using a standard solution, the benzyl benzoate was weighed directly into the sample and the solution made from the mixture of sample and standard. The results from the reproducibility screen using this alternative sampling method are shown in **Table 7**. First of all, it was determined that the error between the positions was the same as with the previous sampling technique, with the conversions differing by 13%, within a 95% confidence level (**Table 7b**). Furthermore, it was also observed that the new sampling technique had made no difference to the range of conversions calculated for the total NMR conversion, but many of the standard deviations had decreased slightly in magnitude. Moreover, it can be clearly seen that there is no significant difference between the positions of the carousel as the error bars in **Figure 26** overlap with each other.

These reproducibility screens have given an error for the carousel that is compounded by the error in the sampling method. To this end, as a result of this screen, the decision was made to use NMR conversions only as a semi-quantitative measure and instead collect isolated yields for all future experiments and quantitative comparisons.

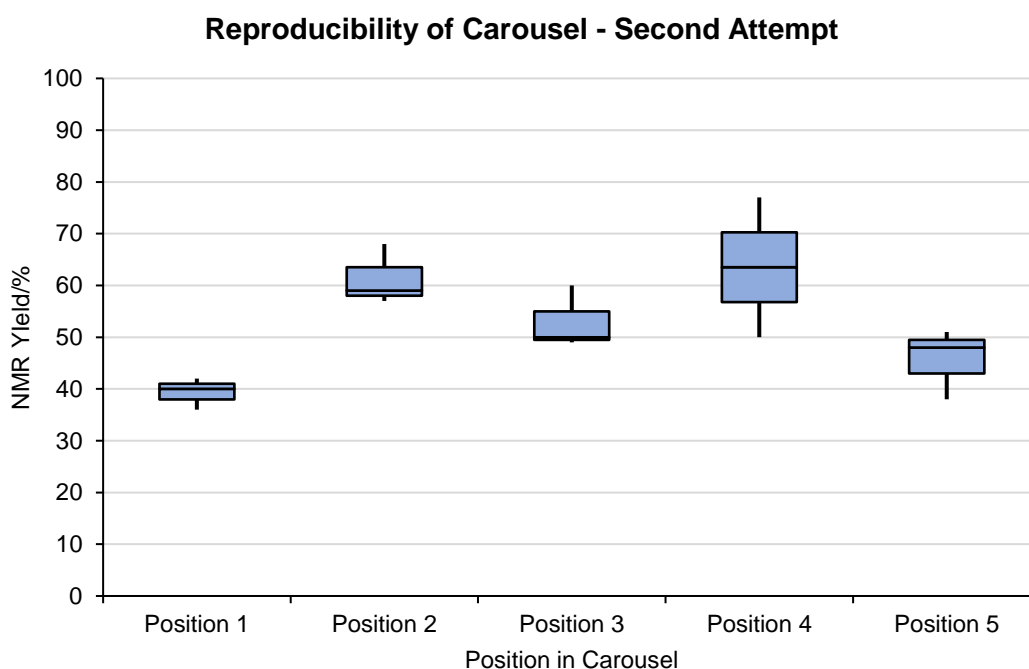
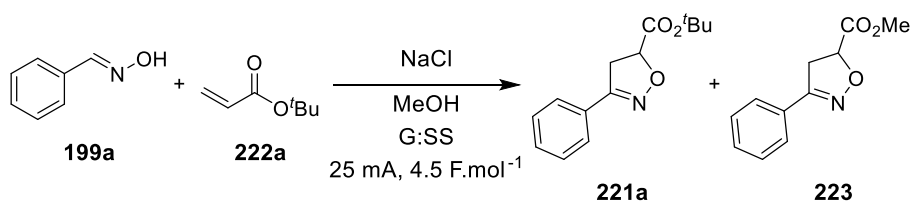


Figure 26: A pictorial representation of the data shown in **Table 7**.



Entry	Position	221a NMR Yield ^a /%	223 NMR Yield ^a /%	Total NMR Conversion ^{a,b} /%
1	1	27 / 23 / 26 (25)	15 / 13 / 14 (14)	42/ 36/ 40 (39±3)
2	2	35 / 40 / 34 (36)	24 / 28 / 23 (25)	59 / 68 / 57 (61±6)
3	3	32 / 38 / 31 (34)	18 / 22 / 18 (19)	50 / 60 / 49 (53±6)
4	4	28 / 44 (36)	22 / 33 (28)	50 / 77 (64±19)
5	5	28 / 21 / 28 (26)	20 / 17 / 23 (20)	48 / 38 / 51 (46±7)

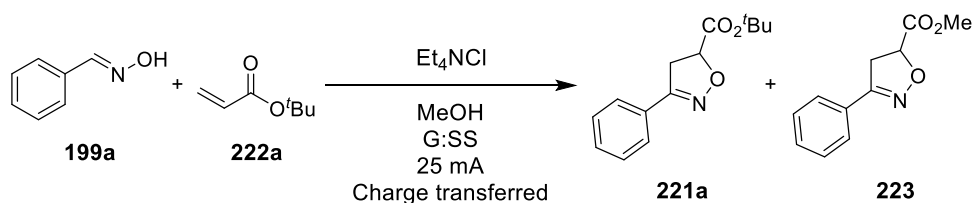
Table 7a: Conditions: Oxime (0.5 mmol), tert-butyl acrylate (5 eq.), NaCl (0.5 eq.), MeOH (0.07 M), 25 mA, 4.5 F.mol⁻¹; ^aH NMR yield using benzyl benzoate as internal standard; ^bNumber in parentheses is mean average ± one standard deviation; G = graphite; SS = stainless steel.

Position Statistical Analysis			
	221a NMR Data	223 NMR Data	Total NMR Conversion Data
Mean	31	21	53
Standard Error	2	2	5
Standard Deviation	5	2	10
Confidence Level (95%)	7	7	13
Range	11	14	24

Table 7b: Statistical analysis was performed on each of the yield/conversion data across the position in the IKA Carousel.

3.2.4. Charge Transferred Screen

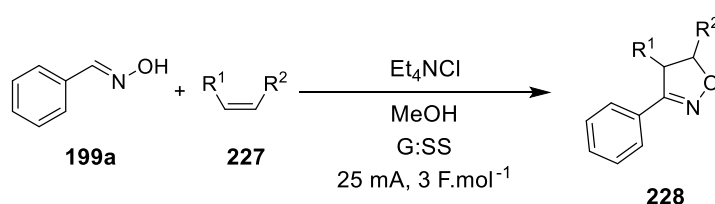
During previous screens and initial scoping reactions, over-oxidised products (to isoxazoles when using dimethyl maleate or dimethyl fumarate as dipolarophiles) or transesterification products (to the methyl ester when using *tert*-butyl acrylate as dipolarophile) were observed. Either side product could be due to extended reaction. Lowering the charge transferred ($F.mol^{-1}$) could have a two-fold effect: i) it would reduce the reaction time and ii) less charge would be transferred and so over-oxidation is less likely to occur. Charge transferred, or $F.mol^{-1}$, can be thought of as “equivalents of electrons” being introduced to the reaction system, so lowering the charge transferred is likely to have a similar effect to lowering reagent or catalyst loadings in traditional chemical reactions. It is noted that it is anticipated that a charge of $2 F.mol^{-1}$ is expected to be required for full consumption of starting material; the overall process, assuming a mechanism similar to the Shono work, is expected to require two molar equivalents of electrons. A quantity of charge transfer screen was designed to explore this factor as well as to understand the point at which significant over-oxidation or transesterification occurs. The results from the charge transferred screen are shown in **Table 8**. It was observed that the yield of desired product increased until a maximum was reached at $3 F.mol^{-1}$ (63%, Entry 3), after which transferring more charge was detrimental. Furthermore, transferring just $3 F.mol^{-1}$ gave a favourable distribution of products with a ratio of 7:1 in favour of **221a**.



Entry	Charge Transferred/ $F.mol^{-1}$	Ratio 221a:223	(221a + 223)/%
1 ^{a,b}	1	-	19
2 ^{a,b}	2	-	43
	3	7:1	63
4	4	2:1	52
5	5	6:1	39

Table 8: Conditions: Oxime (0.5 mmol), *tert*-butyl acrylate (5 eq.) Et_4NCl (0.5 eq.), MeOH (0.07 M), G anode, SS cathode, 25 mA, [charge transferred]. ^aIsolated with unreacted oxime starting material; ^bStrength 1H NMR, using benzyl benzoate as internal standard, used to determine yield. G = graphite; SS = stainless steel.

Following this screen, a small substrate scope was initiated to test the conditions attained so far and the results are illustrated in **Table 9**. Styrene as dipolarophile gave low conversion with only 3% desired product observed in the ^1H NMR of the crude reaction mixture (Entry 2). Encouragingly, switching the mediator to Et_4NI furnished the desired isoxazoline **201** in 18% yield (Entry 3). This represented the first time that styrene derived products had been isolated. Dimethyl maleate, which had previously given **205** in 36% yield (albeit with RVC electrodes, Entry 6, **Table 1**), demonstrated improved reactivity under these reaction conditions, furnishing isoxazoline **205** in 46%, along with 53% of the corresponding isoxazole (Entry 4). For the most part, the charge transferred screen was a success and reduced the formation of **223**, when



Entry	Dipolarophile	228 /%
1		221a (223) , 55 (8)
2		201 , 3 ^a
3 ^b		201 , 18
4		205 (206) , 46 (53 ^c); dr (205) = 9:1

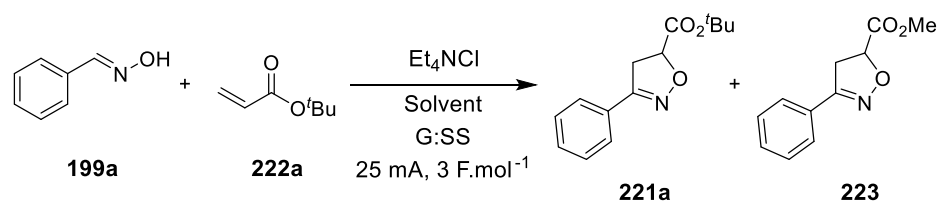
Table 9: Conditions: Oxime (0.5 mmol), dipolarophile (5 eq.), Et_4NCl (0.5 eq.), MeOH (0.07 M), G anode, SS cathode, 25 mA, 3 F.mol⁻¹. ^a ^1H NMR yield using benzyl benzoate as internal standard; ^b Et_4NI as mediator; ^cCo-eluted with dipolarophile, strength ^1H NMR using benzyl benzoate as standard to give yield. G = graphite; SS = stainless steel.

using *tert*-butyl acrylate as dipolarophile. However, it did fail to reduce the formation of the over-oxidised isoxazole product **206**, when employing dimethyl maleate as dipolarophile. Further screening was necessary to avoid over-oxidation.

3.2.5. Solvent Screen

It was found that when using methanol as solvent, dimethyl fumarate did not fully dissolve. If other dipolarophiles demonstrated poor solubility in methanol, the conductivity of the solution could be impacted, as the dipolarophile may not possess sufficient conductivity properties to allow charge to pass through solution. If an excess of dipolarophile is required, the dipolarophile could impact stirring, which would also impact mass transport of reactants to the electrode, affecting the efficiency of the reaction. It has been previously demonstrated that some solvents show enhanced properties within reactions that produce radical species; these include 1,1,1,3,3,3-hexafluoroisopropanol (HFIP), 1,1,1-trifluoroethanol (TFE) and other fluorinated alcoholic solvents. Additionally, it has been reported that these fluorinated alcohols can stabilise reactive intermediates, such as radicals or charged species, through solvation, and in some cases facilitate electron transfer.⁹⁴ Additionally, as previously mentioned (Section 3.2.1), the solvent could be performing a dual role: it is the solvent for the reaction and its conjugate base may facilitate the elimination of HCl to form the nitrile oxide, in so much as balancing the pH of the reaction mixture. As a result, MeOH and HFIP were investigated in a thorough screening process, with MeCN used as a co-solvent, to explore the effect of decreasing concentrations of alcoholic solvent on the reaction.

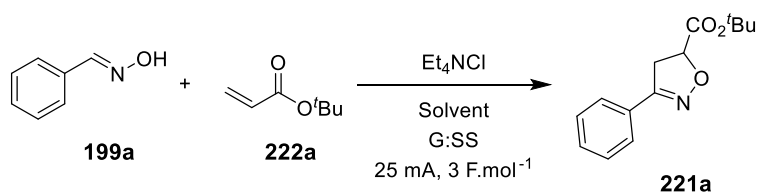
Firstly, a screen involving a MeOH:MeCN solvent system was devised and carried out and the results are shown in **Table 10**. Previously, MeOH as the solvent gave conversion to desired products, with the methyl ester by-product the major product (Entry 1). However, lowering the charge transferred increased both conversion and ratio of products (63%, 7:1, Entry 2). Reducing the MeOH content (and replacing with MeCN to maintain the same reaction volume) had a detrimental effect on the conversion (Entries 3 - 6), although a concurrent decrease in the conversion to **223** was also observed. Furthermore, it was demonstrated that 1 equivalent of MeOH was sufficient to give conversion to desired product with no methyl ester by-product observed (Entry 5). Intriguingly, an isolated yield of 36% of **221a** was obtained in the absence of MeOH; this result demonstrated that a conjugate base may not be needed for the progression of the reaction and supports the hypothesis of a radical reaction pathway.



Entry	Solvent	Solvents Ratio	% Alcohol (eq.)	Ratio 221a:223	221a + 223/%
1 ^a	MeOH	-	100 (340)	1:2	48
2	MeOH	-	100 (340)	7:1	63
3	MeOH:MeCN	1:1	50 (170)	5:1	47
4	MeOH:MeCN	1:9	10 (34)	22:1	45
5	MeOH:MeCN	-	0.3 (1)	-	50
6	MeCN	-	0 (0)	-	36

Table 10: Conditions: Oxime (0.5 mmol), *tert*-butyl acrylate (5 eq.), Et₄NCl (0.5 eq.), solvent (0.07 M), G anode, SS cathode, 25 mA, 3 F.mol⁻¹. ^a4.5 F.mol⁻¹ charge transferred. G = graphite; SS = stainless steel.

A second solvent screen was performed using a HFIP:MeCN solvent system. The results of this screen are shown in **Table 11**. It is noteworthy that no transesterification by-product, or any other identifiable by-products, were observed in either LCMS or ¹H NMR analyses of the crude mixtures. Lowering the HFIP content (Entries 2 - 6) provided an increase in conversion with a 1% HFIP in MeCN mixture, affording **221a** in 73% isolated yield (Entry 6). Further decrease in HFIP equivalents had a marginal effect on the conversion (Entries 7 - 9). Interestingly a sub-stoichiometric amount of HFIP was sufficient to allow reaction progression (Entries 8 and 9), with 10 mol% HFIP furnishing **221a** in 61% (Entry 9). This result highlights that additive levels of HFIP are enough for reaction to be observed and that HFIP is superior and was providing a greater beneficial effect on the reaction over MeOH. DCM, DMSO and water with 1.3 equivalents of HFIP all gave no reaction as the potentials observed were greater than 10 V, presumably due to the poor conductivity of the reaction solutions (Entries 10 - 12). However, a combination of HFIP and DMF in a 1:99 ratio provided the desired isoxazoline in 52% isolated yield (Entry 13), which is a marked decrease from a HFIP:MeCN combination (52% vs. 73%).



Entry	Solvent(s)	Solvents Ratio	% Alcohol (eq.)	221a/%
1	HFIP	N/A	100 (129)	34 [n=2]
2	HFIP:MeCN	1:1	50 (65)	57
3	HFIP:MeCN	1:3	25 (32)	55
4	HFIP:MeCN	1:9	10 (7)	59
5	HFIP:MeCN	1:19	5 (3.3)	68
6	HFIP:MeCN	1:99	1 (1.3)	73 [n=2]
7	HFIP:MeCN	N/A	0.8 (1)	71
8	HFIP:MeCN	N/A	0.4 (0.5)	67
9	HFIP:MeCN	N/A	0.08 (0.1)	61
10	HFIP:CH ₂ Cl ₂	1:99	1 (1.3)	- ^a
11	HFIP:DMSO	1:99	1 (1.3)	- ^a
12	HFIP:H ₂ O	1:99	1 (1.3)	- ^a
13	HFIP:DMF	1:99	1 (1.3)	52

Table 11: Conditions: Oxime (0.5 mmol), *tert*-butyl acrylate (5 eq.), Et₄NCl (0.5 eq.), solvent (0.07 M), G anode, SS cathode, 25 mA, 3 F.mol⁻¹. ^aNo reaction observed due to high potentials (>10 V). G = graphite, SS = stainless steel; HFIP = 1,1,1,3,3,3-hexafluoroisopropanol; DMSO = dimethyl sulfoxide; DMF = *N,N*-dimethylformamide

3.2.6. Additive Screen

With HFIP at additive levels giving the best yield, attention was turned to other additives. The choice of additive was based upon the pK_a value for a given additive. This was to test the hypothesis of whether the conjugate base of the additive was responsible for promoting the reaction. The results of the additive screen are shown in **Table 12**. All additives, with exception of t BuOH, had a positive impact on the progression of the reaction (with respect to MeCN alone). Interestingly, there seems to be little correlation between the pK_a values (either in DMSO or water) and isolated yields: both more acidic (Entry 4 and 5) and more basic (Entries 2, 3, 6 and 7) additives displayed decreased isolated yields (vs. HFIP, **Figure 27**). Addition of a base was detrimental to the reaction progression, with DIPEA and Et_3N both giving no reaction (Entries 12 and 13), and pyridine giving a decreased yield of 58% (Entry 14). It is noteworthy that in all cases little, or no, remaining oxime was observed in either LCMS or 1H NMR analysis of the crude mixtures; no identifiable by-products could be determined either.

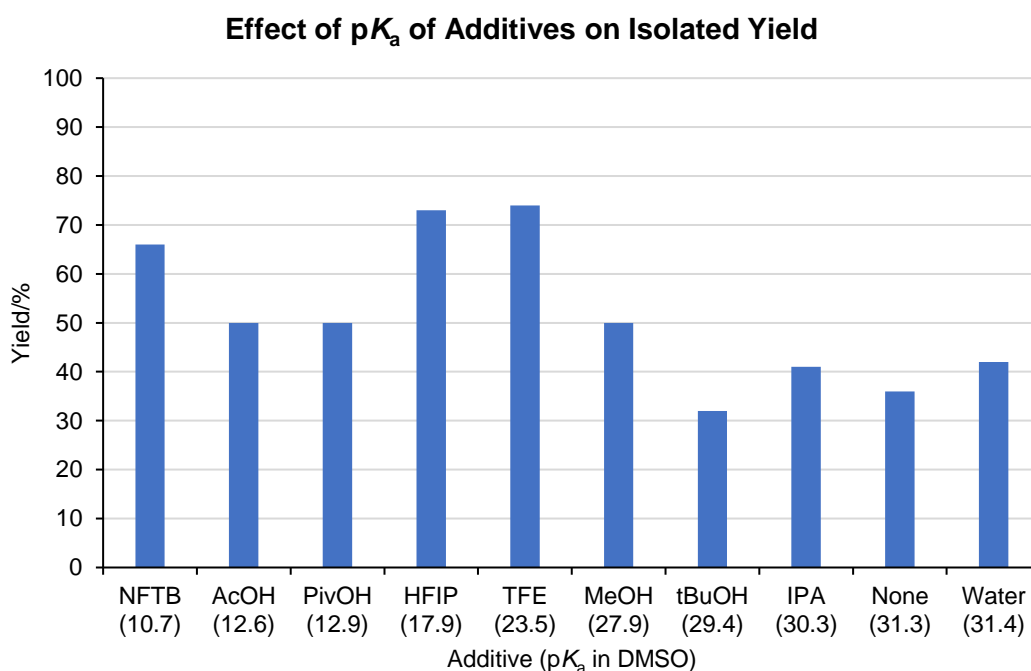
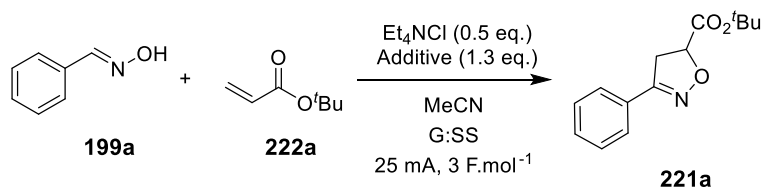


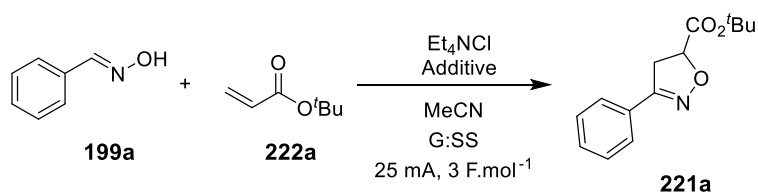
Figure 27: Pictorial representation of the data shown **Table 12**; no other additives have a more significant effect on the yield than HFIP, which gives the highest isolated yield.



Entry	Additive	p <i>K</i> _a in DMSO ⁹⁵ (H ₂ O ⁹⁶)	221a/%
1	HFIP	17.9 (9.3)	73 [n=3]
2	IPA	30.3 (16.5)	41
3	H ₂ O	31.4 (15.7)	42
4	AcOH	12.6 (4.8)	50
5	PivOH	12.9 (5.0)	46
6	^t BuOH	29.4 (17.0)	32
7	MeOH	27.9 (15.5)	50
8	-	31.3 (-)	36
9	TFE	23.5 (-)	74
10	FCH ₂ CH ₂ OH	- (-)	35
11	(CF ₃) ₃ COH	10.7 (-)	66
12 ^a	HFIP	17.9 (9.3)	-
13 ^b	HFIP	17.9 (9.3)	-
14 ^c	HFIP	17.9 (9.3)	58

Table 12: Conditions: Oxime (0.5 mmol), *tert*-butyl acrylate (5 eq.), Et₄NCl (0.5 eq.), Additive (1.3 eq.), MeCN (0.07 M), G anode, SS cathode, 25 mA, 3 F.mol⁻¹. ^a1.5 eq. DIPEA added; ^b1.5 eq. Et₃N added; ^c1.5 eq. pyridine added. G = graphite; SS = stainless steel; HFIP = 1,1,1,3,3,3-hexafluoroisopropanol; IPA = isopropanol; TFE = 1,1,1-trifluoroethanol; DIPEA = diisopropylethylamine.

Further alcoholic additives were also screened, namely substituted phenols. Phenol has a very similar p*K*_a as HFIP (18.0 vs. 17.9 in DMSO) and so would allow the exploration of the hypothesis that p*K*_a is the parameter that is responsible for HFIP's superior behaviour in the reaction. However, the results in **Table 13** show that this is not the case as phenol gave no reaction (presumably due to poor conductivity of solution, Entry 2), while 4-nitrophenol and 4-methoxyphenol gave drastically poorer yields of desired isoxazoline (Entries 3 and 4).



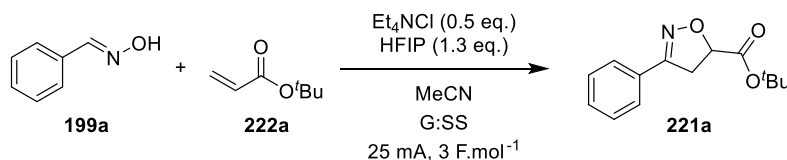
Entry	Additive	p <i>K</i> _a in DMSO ^{95a, 97} (H ₂ O ⁹⁶)	221a/%
1	HFIP	17.9 (9.3)	73
2	phenol	18.0 (-)	- ^a
3	4-nitrophenol	10.8 (-)	32
4	4-methoxyphenol	19.1 (-)	0

Table 13: Conditions: Oxime (0.5 mmol), *tert*-butyl acrylate (5 eq.), additive (1.3 eq.), Et₄NCl (0.5 eq.), MeCN (0.07 M), G anode, SS cathode, 25 mA, 3 F.mol⁻¹. ^aNo reaction observed due to high potential (>10 V). G = graphite; SS = stainless-steel; HFIP = 1,1,1,3,3,3-hexafluoroisopropanol.

Although only p*K*_a was explored, other properties such as nucleophilicity of conjugate base, H-bond donating ability and oxidation potential (all of which were not explored), could be responsible for the observed reactivity and could dominate any effects of p*K*_a on the efficiency of the reaction.

3.2.7. Reproducibility of Electrodes

The durability and reproducibility of the electrodes used for the reactions was tested. Experiments using the same set of graphite (G) and stainless-steel (SS) electrodes were designed. The ^1H NMR yield of nine consecutive uses of the same pair of electrodes, as well as isolated yields for selected experiments were obtained. The durability reactions were all performed in the same cell in the same position every time to eliminate variability between experiments. Only washing the electrodes with MeCN and water was conducted between each use; no polishing of electrodes was carried out. All results are shown in **Figure 28**. It is clear to see that the electrodes show no passivation as there were very minor differences between the NMR yields obtained. All the differences are within error of the sampling procedure. There was slightly more variability in the isolated yields, but they are all in good agreement with the NMR yields.



Electrode Control Experiments

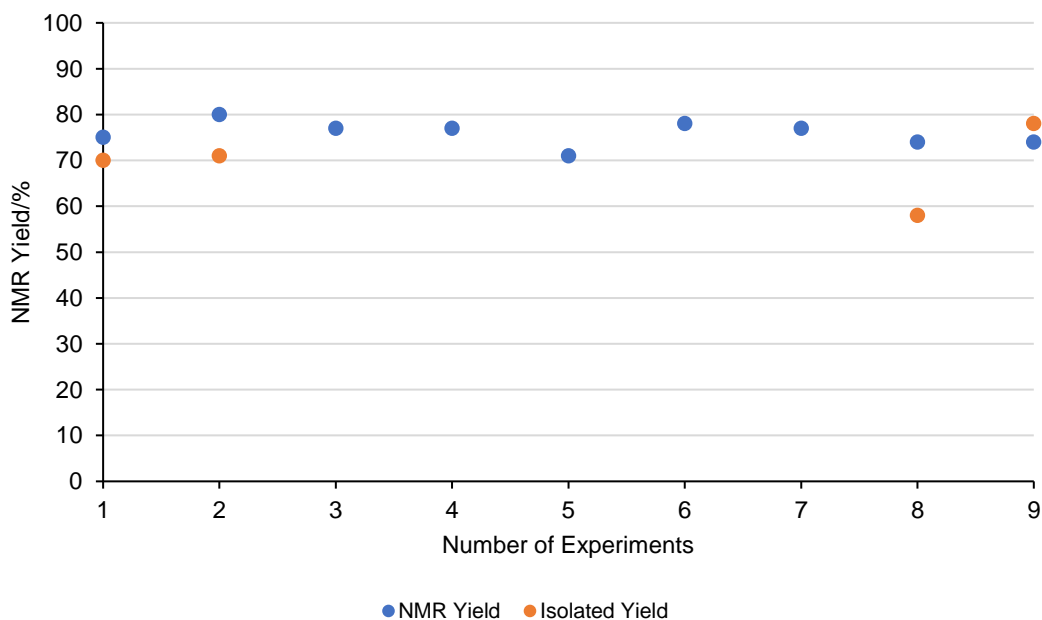
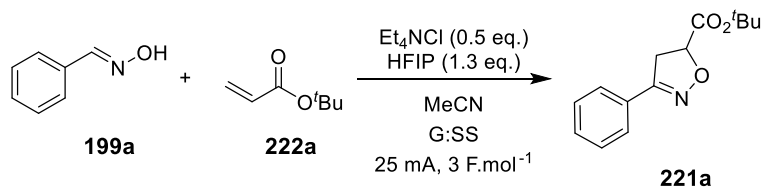


Figure 28: Durability experiments show that at least nine experiments can be conducted on a single set of electrodes, with no passivation or decrease in reactivity.

3.2.8. Further Screening of Conditions

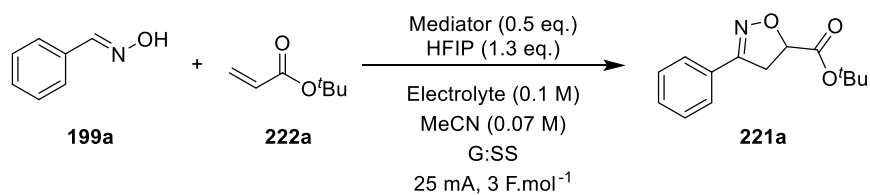
An additional charge transferred screen was performed on the HFIP:MeCN conditions to determine whether 3 F.mol⁻¹ was the optimal amount of charge to transfer. The charge transferred was varied from 1 - 5 F.mol⁻¹ in equal increments of 1 F.mol⁻¹. It was observed that the yield of desired product increased with transferred charge up until 3 F.mol⁻¹, at which point no further conversion was seen (**Table 14**). Pleasingly, no deleterious reaction was observed either.



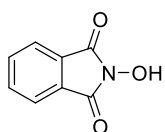
Entry	Charge Transferred/F.mol ⁻¹	221a/%
1 ^{a,b}	1	13
2 ^{a,b}	2	33
3	3	73
4	4	75
5	5	73

Table 14: Conditions: Oxime (0.5 mmol), *tert*-butyl acrylate (5 eq.), Et₄NCl (0.5 eq.), HFIP (1.3 eq.), MeCN (0.07 M), G anode, SS cathode, 25 mA, [charge transferred]. ^aIsolated with unreacted oxime starting material; ^b¹H NMR yield, using benzyl benzoate as internal standard, used to determine yield. HFIP = 1,1,1,3,3,3-hexafluoroisopropanol; G = graphite; SS = stainless steel.

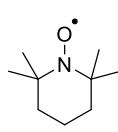
While the optimum conditions were in hand, further investigation into alternative mediators was carried out to explore the effect these alternative mediators have on the reaction outcome; electrolytes were also investigated. All other mediators gave only poor yields of desired isoxazoline (Entries 2 - 6, **Table 15**). Furthermore, no mediator and addition of an electrolyte also resulted in poor yields (Entries 7 - 9). However, these results demonstrate that direct oxidation of the **199a** can occur, allowing the reaction to proceed, albeit at a lower efficiency. An alternative positive counter ion for the mediator, ⁿBu₄N⁺, gave only a slight decrease in isolated yield of 74% (Entry 10, vs. 78%). Using an electrolyte in addition to a mediator results in a decrease in efficiency of reaction, with isolated yields of 63% and 61% (Entries 11 and 12, respectively). This additional screen demonstrates that Et₄NCl is the more superior mediator for this reaction among the mediators and electrolytes tested.



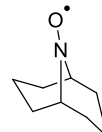
Entry	Mediator	Electrolyte	221a/%
1	Et ₄ NCl	-	78
2	224	Et ₄ NBF ₄	17
3	224	ⁿ Bu ₄ NPF ₆	14
4	224	Et ₄ NOTs	19
5	225	Et ₄ NBF ₄	6
6	226	Et ₄ NOTs	5
7	-	Et ₄ NBF ₄	16
8	-	ⁿ Bu ₄ NPF ₆	13
9	-	Et ₄ NOTs	24
10	ⁿ Bu ₄ NCl	-	74
11	Et ₄ NCl	Et ₄ NBF ₄	63
12	Et ₄ NCl	Et ₄ NOTs	61



NHPI, **224**



TEMPO, **225**

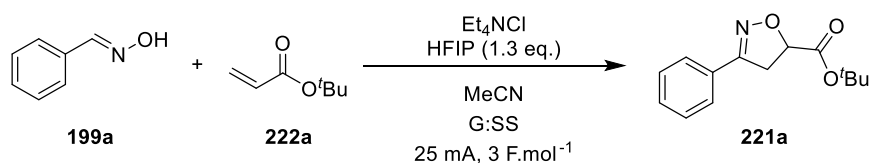


ABNO, **226**

Table 15: Conditions: Oxime (0.5 mmol), *tert*-butyl acrylate (5 eq.), HFIP (1.3 eq.), mediator (0.5 eq.), electrolyte (0.1 M), MeCN (0.07 M), G anode, SS cathode, 25 mA, 3 F.mol⁻¹. HFIP = 1,1,1,3,3,3-hexafluoroisopropanol; G = graphite, SS = stainless-steel; NHPI = *N*-hydroxyphthalimide; TEMPO = 2,2,6,6-tetramethylpiperidine *N*-oxyl; ABNO = 9-azabicyclo[3.3.1]nonane *N*-oxyl.

Attention was turned to attempting to scale up the electrochemical reaction in the same reaction vessel. To achieve this, a concentration screen was devised, exploring the effect of concentration on the reaction. A higher concentration would allow higher productivities, leading to larger scale reactions. The same volume of reaction mixture (7 mL) was used for all experiments in this screen. Unfortunately, increasing concentration only served to give a decreased yield of desired isoxazoline (**Table 16**). However, these reactions were performed under the same galvanostatic conditions as the optimised conditions, with an applied current of 25 mA transferring a charge of 3 F.mol⁻¹. As there was a higher concentration of starting materials, a larger current, and therefore longer electrolysis time, would be required to fully consume all reactants. The need for a higher charge for a more concentrated reaction is

demonstrated by the scaled-up reaction shown later (**Scheme 70**), in which a current of 72.5 mA for 5 mmol of starting oxime was required for the full consumption of starting materials and an isolated yield of 59%.

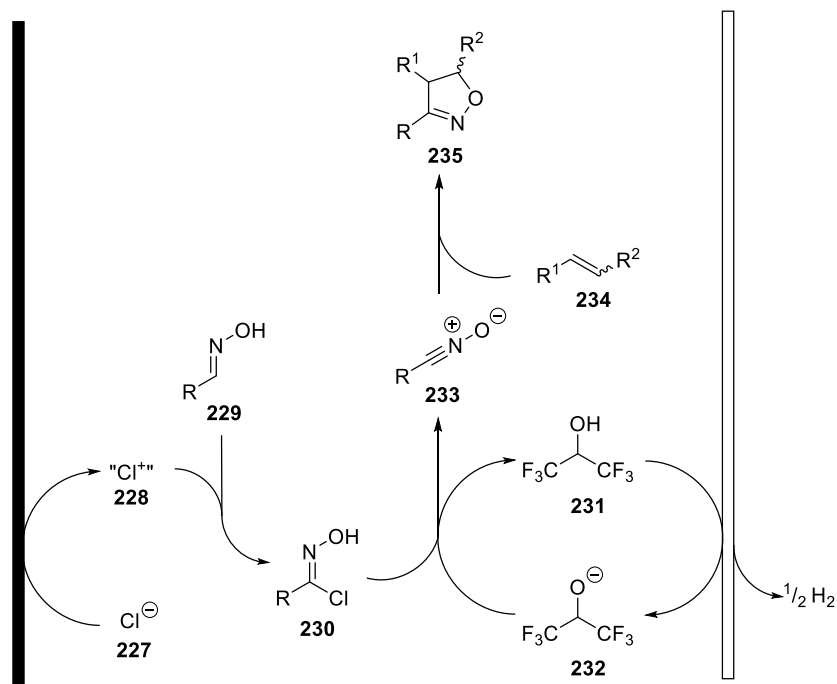


Entry	[199a]/M	[Et ₄ NCl]/M (eq.)	221a/%
1	0.07	0.035 (0.5)	78
2	0.5	0.035 (0.07)	- ^a
3	0.5	0.25 (0.5)	31
4	0.25	0.035 (0.07)	21
5	0.25	0.125 (0.5)	40

Table 16: Conditions: Oxime, *tert*-butyl acrylate (5 eq.), HFIP (1.3 eq.), Et₄NCl, MeCN, G anode, SS cathode, 25 mA, 3 F.mol⁻¹. ^aNo reaction observed to high potential (>10 V). HFIP = 1,1,1,3,3,3-hexafluoroisopropanol; G = graphite; SS = stainless-steel.

3.2.9. Initial Proposed Reaction Pathway

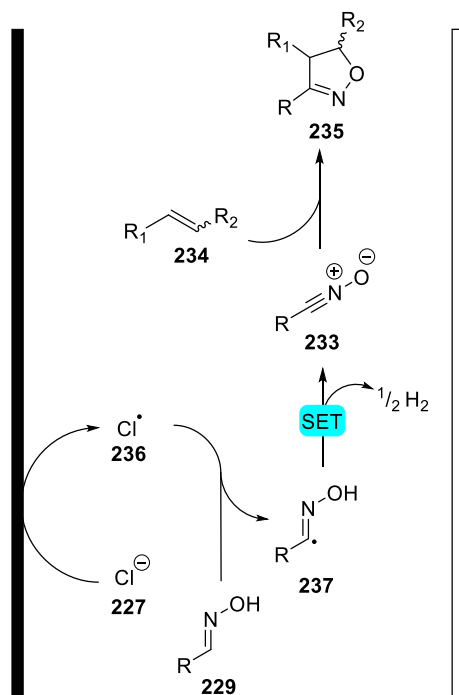
From the results gathered so far, two plausible reaction pathways were envisioned: the “classical” electrophilic chlorine pathway (**Scheme 66**) and a radical pathway (**Scheme 67**). The first possibility involves the oxidation of the chloride anion **227** to an electrophilic species **228** (**Scheme 66**). This electrophilic species is unlikely to be a free cationic chlorine species, it would either combine with chloride to form chlorine, or adventitious water would allow the formation of hypochlorous acid. Regardless, chlorination of oxime **229** would give **230**. HFIP conjugate base **232** (formed from the reduction of HFIP at the cathode, liberating hydrogen) could then facilitate the elimination of HCl, returning HFIP and fashioning nitrile oxide **233**. 1,3-Dipolar cycloaddition with **234** would give desired isoxazoline **235**. This pathway accounts for the observed “catalytic” nature of HFIP. However, it does not account for the fact that, in the absence of both chloride mediator and HFIP, conversion to product is observed.



Scheme 66: The proposed reaction pathway invoking the oxidation of the chloride mediator to an electrophilic species that can result in the formation of an hydroxyimoyl chloride, a well-known pre-cursor to nitrile oxides.

On the other hand, invoking a radical mechanism may account for the inherent reactivity observed in the absence of some reaction components (**Scheme 67**). In this proposed reaction pathway, a single electron oxidation of chloride **227** to the radical **236** could take place at the anode. Oxidation of the nitrogen centre of oxime **229** by

chloride radical **236** (and subsequent tautomerisation) would give hydroxyiminyl radical **237** and upon further oxidation, would fashion nitrile oxide **233**. Subsequent dipolar cycloaddition with dipolarophile **234** would furnish desired isoxazoline **235**. A radical reaction pathway may account for the reactivity in the absence of mediator as direct oxidation of oxime **229** to the hydroxyiminyl radical could take place at the anode. The lower reactivity in absence of a halide suggests that this oxidation event is much more difficult than oxidation by a halide radical. Furthermore, the reactivity observed in the absence of conjugate base (from the HFIP solvent) could be explained by proposing that the hydroxyl proton of oxime **237** could be eliminated by reduction at the cathode, with concurrent evolution of hydrogen. However, it is unlikely that the reactive species formed at the anode diffuses to the cathode to allow this to occur. An alternative explanation, could be the balancing on the reaction mixture pH by reduction of adventitious water as no effort was made to exclude moisture or air.



Scheme 67: A radical pathway can be used to account for the interesting results obtained when performing the electrolysis in the absence of mediator or HFIP additive.

3.3. Design of Experiments

Statistical Design of Experiments (DoE) is a powerful tool for both the medicinal and process chemist. It is often used to assist in the optimisation of processes. DoE is not only valuable in providing a streamlined and facile method for optimising reactions but is also extremely useful for determining the interaction between each reaction parameter. As described thus far, the chemist would approach an optimisation by varying one variable at a time (OVAT), i.e. changing one variable while keeping all others constant and after finding the best outcome, that variable is then kept constant and a different variable is explored. Although this is a “tried and tested” method, oftentimes only a local maximum of yield is achieved. This is because no information can be gleaned about the interactions between the variables. On the other hand, DoE can provide a more robust approach to optimisation that will allow the chemist to achieve a global maximum of yield (or other response). However, by employing DoE, a larger number of experiments are likely to be needed to achieve the desired outcome. This is due to the requirement for enough data to allow a statistical analysis to be performed; OVAT approaches rarely provide sufficient data for this analysis. Recent reviews^{92a, 92b} and reports from a process group at GSK^{92c, 92d} have shown that DoE can be employed as a tool to allow a rapid optimisation process.

There are several varieties of statistical DoE designs and the choice of which one to use is usually decided by a compromise between the number of experiments to be conducted and the level of information that is required. For example, if one wishes to simply screen a reaction, a low-resolution factorial design will suffice. Resolution is the measure of the amount of confounding, i.e. lower resolution designs have higher confounding in which interactions between variables are likely to be difficult to deconvolute. Factorial designs can be employed in a full or fractional manner, and these can be envisioned as cubes which represent the experimental region being explored (**Figure 29**). For example, when employing a three-factor full-factorial design, in which low and high values of the variables are used as the limits of the experimental parameters, experiments represented by all vertices and the centre point of the cube are conducted (**Figure 29a**). Oftentimes, the centre point experiment is repeated three times to gain information on the reproducibility and determine the background noise of the reaction. Thus, when screening three factors, 11 experiments would be required to provide enough information for a rigorous statistical analysis to

be performed. Alternatively, a half factorial design (**Figure 29b**) can be utilised and this would reduce the number of experiments to seven but, as mentioned before, this will introduce high confounding of the factors. Furthermore, if a response curve is required, or if a non-linear response is observed when attempting a factorial design, a more appropriate design in which a larger number of experiments are conducted is necessary. These designs can be represented as hyper-cubes. The Box-Benkhen (**Figure 29c**) and the Central Composite Face (CCF, **Figure 29d**) are designs that will support such non-linear responses. Essentially, a Box-Benkhen design is a full factorial design but additional experiments that are represented by the points at the centre of the cube edges are conducted, and these additional experiments will allow a surface in the approximation of a sphere to be modelled (**Figure 29c**). Moreover, a CCF design is also derived from a full factorial design but the additional experiments to be conducted are at the centre of the faces of the hyper-cube (**Figure 29d**). These experiments will approximate the response sphere more accurately than the Box-Benkhen design. Both of these designs, in which a response-surface model is required, are most useful when optimising a reaction and greater understanding of the interactions between factors is required. Often, these designs will be used in a process setting to both optimise the reaction and determine the robustness of a given process.

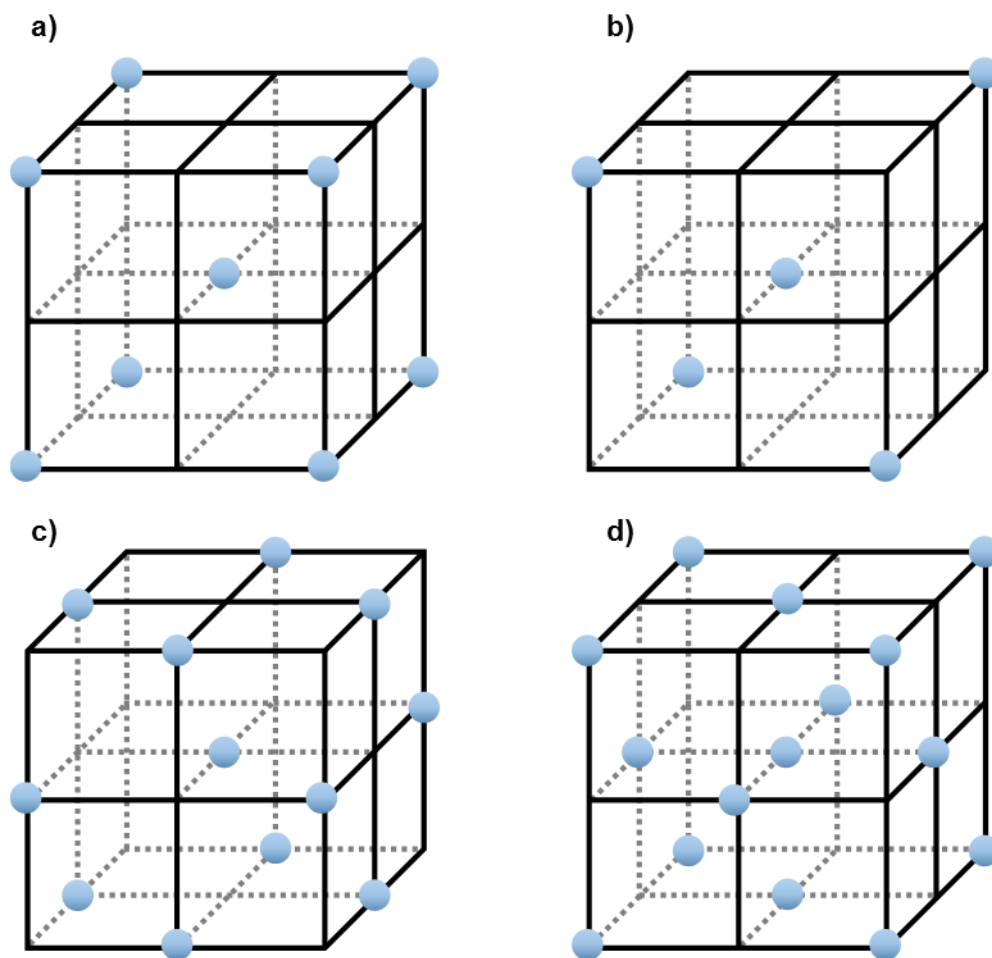


Figure 29: a) Full factorial design is useful for screening factors in a rationally designed way and can allow some deconvolution of interactions between factors; b) Half-factorial designs require fewer experiments than full factorial designs but are low resolution and high confounding of factors is observed; c) Box-Benken design is used when a non-linear response is observed and a response-surface model is desired; d) Central Composite Face (CCF) designs allow a more accurate response-surface to be modelled and is useful for optimisation of reactions or determining robustness of processes.

During this investigation, a three-factor full factorial design was employed. The factors that were explored were stir speed, mediator equivalents and dipolarophile equivalents. The limits of these factors were chosen to be symmetrical around the optimal conditions that were in hand at the time: for stir speed, limits of 200 - 600 rpm were chosen, while the limits for mediator and dipolarophile equivalents were 0.1 - 2.5 and 1 - 9 equivalents, respectively. However, when attempting the first DoE experiments with 0.1 eq. of Et_4NCl , it was found that the reaction did not possess the required conductivity to allow the electrochemical cell to reach the desired current. A large potential was observed and due to the safety limits of the IKA ElectraSyn, the current was decreased to ensure that that the potential did not rise above 30 V (across

the four reactions on the carousel). To remedy this, it was decided that the lower limit for the mediator equivalents was to be 0.5 equivalents, with the upper limit remaining at 2.5 equivalents. The factors that were kept constant in this DoE were HFIP equivalents (at 1.3 eq.), MeCN solvent (at 0.07 M), current (at 25 mA), charge transferred (at 3 F.mol⁻¹) and electrode materials (with graphite anode and stainless-steel cathode). All reactions were conducted on a 0.5 mmol scale and isolated yields were obtained after column chromatography.

The results of this DoE optimisation are illustrated in the following figures and demonstrate the effect of each factor on the outcome of the reaction. The mid-point experiments gave similar yields, which meant that the reaction was reproducible and that the results from the DoE were statistically relevant.

Firstly, stir speed had negligible effect on the outcome of the reaction. It can be seen in **Figure 30** that there is a small parabolic trend in which 400 rpm is the optimum stir speed. These results indicate that stir speed does not strongly influence the reaction and can be discounted from further optimisations. Alternatively, it could be that the reactor design does not allow sufficient mass transfer, or the electron transfer is the rate-determining step.

Isolated Yield vs. Stir Speed

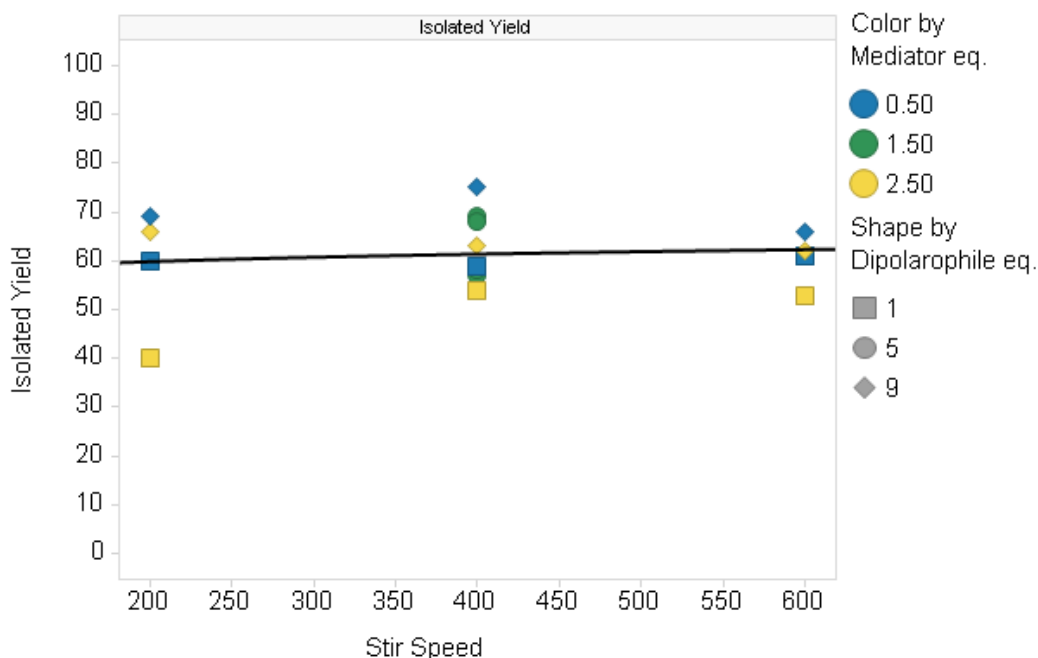


Figure 30: The results from the DoE show the effect of stir speed on isolated yield; stir speed has a negligible effect on the outcome of the reaction.

Secondly, the equivalents of mediator showed a more responsive trend: increasing the loading of mediator, decreased the conversion (**Figure 31**). Concurrently, during the reactions it was observed that the cells in which the higher loadings of mediator were present displayed lower potentials. This could be a factor that can explain why the yields dropped off with higher mediator equivalents. The overall trend is still apparent and a conclusion that increasing mediator is detrimental to the reaction progression could be drawn. Therefore, the mediator loading for the protocol remained at 0.5 equivalents.

Isolated Yield vs. Mediator eq.

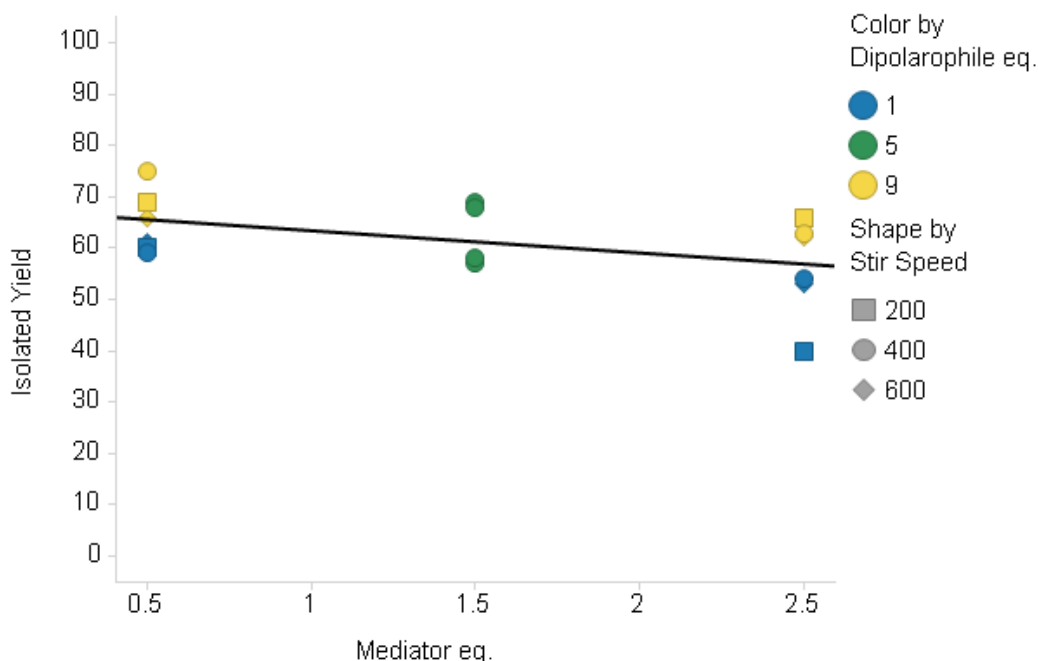


Figure 31: Employing more mediator has a detrimental effect on the reaction outcome, as shown by the trend that can be elucidated from the results from DoE.

Finally, the effect of dipolarophile equivalents was analysed. In this case, a correlation suggesting that increasing dipolarophile equivalents had a positive effect on conversion is apparent (**Figure 32**). This result would be expected as 1,3-dipolar cycloaddition is competing with the reduction of the nitrile oxide intermediate at the cathode and so higher concentrations of dipolarophile will favour the cycloaddition pathway.

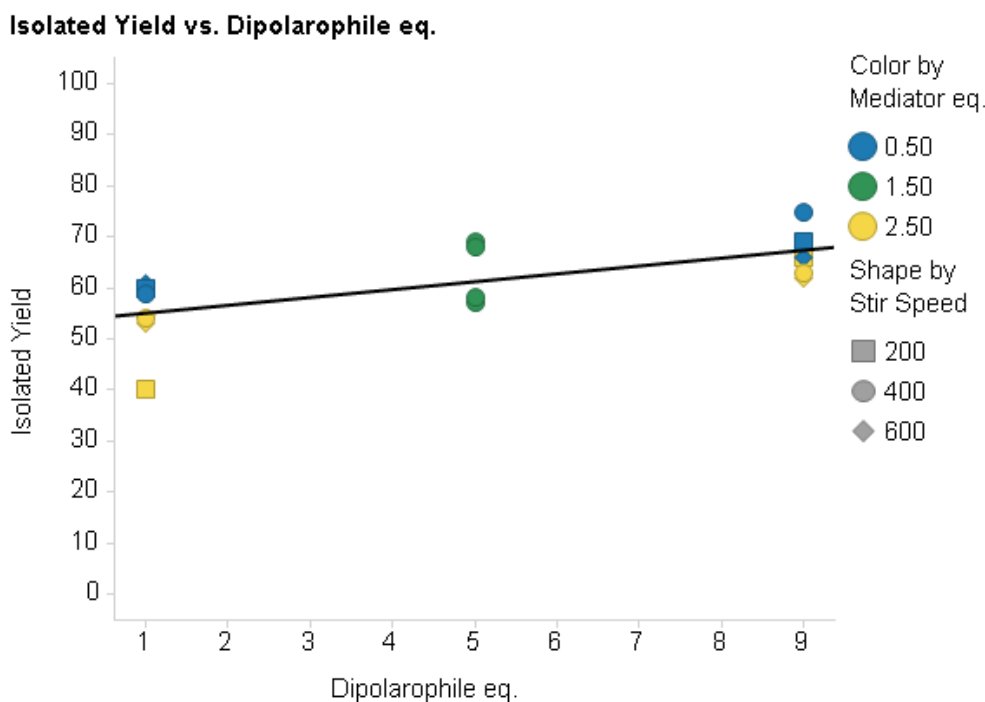
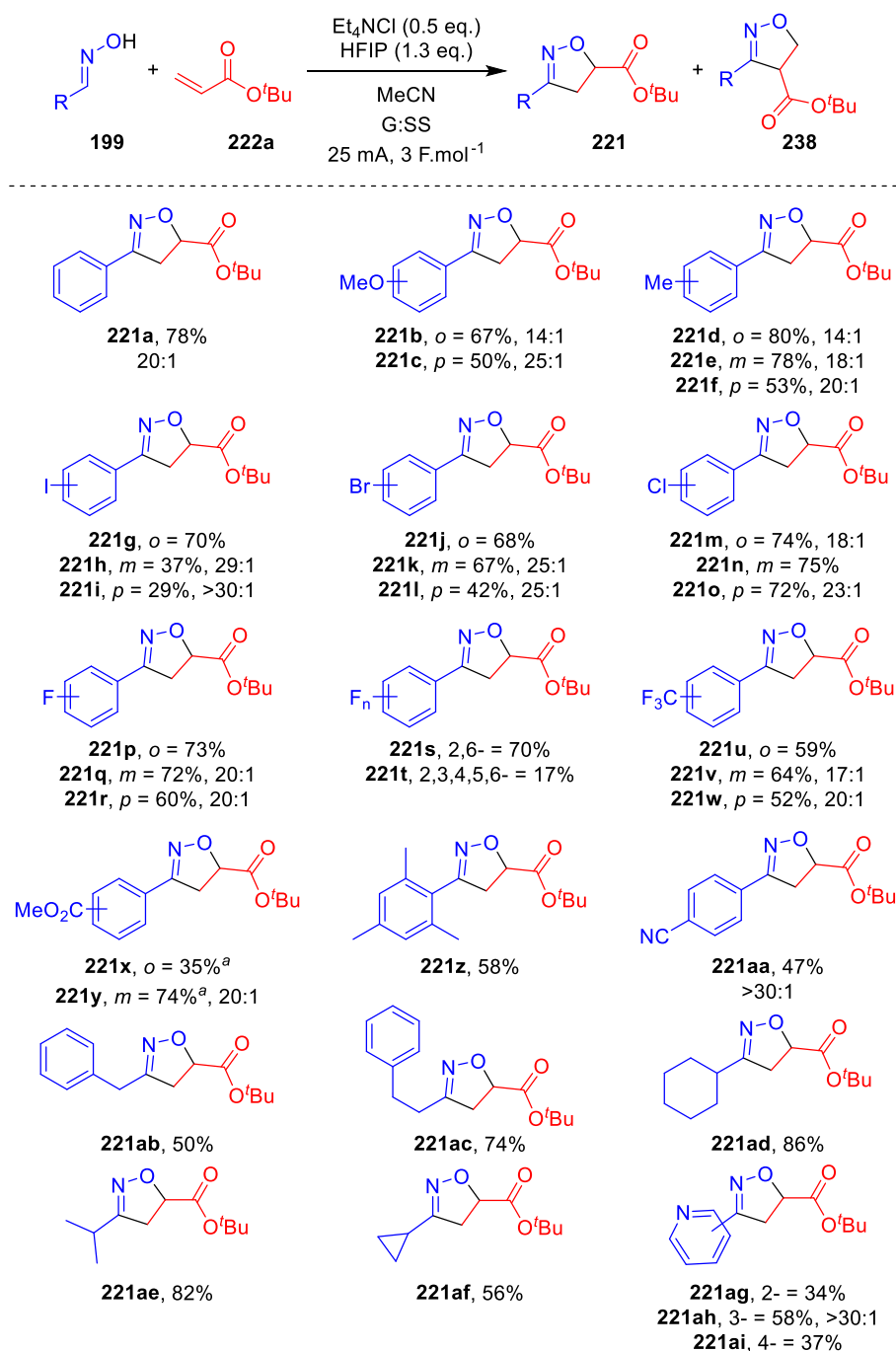


Figure 32: Analysis of the effect of the dipolarophile equivalents on the isolated yield of the electrochemically enabled 1,3-dipolar cycloaddition reaction showed that increasing the equivalents of dipolarophile gave an increased isolated yield.

Overall, instead of the DoE providing an optimisation of the reaction conditions, it became a tool for determining the robustness of the reaction to minor changes in the factors that were explored. Going beyond the limits that were imposed on this design is likely to have a larger impact on the result of the reaction. On the other hand, going beyond the limits set is unlikely to yield a useful protocol. The aim of this investigation was to develop a procedure that is less impactful to the environment, employ smaller amounts of toxic chemicals, and provide an overall greener approach to the synthesis of substituted isoxazolines. Thus, the conditions that were employed prior to the DoE seem to provide a local maximum of yield, and can also tolerate minor differences in stir speed, mediator equivalents and dipolarophile equivalents.

3.4. Substrate Scope

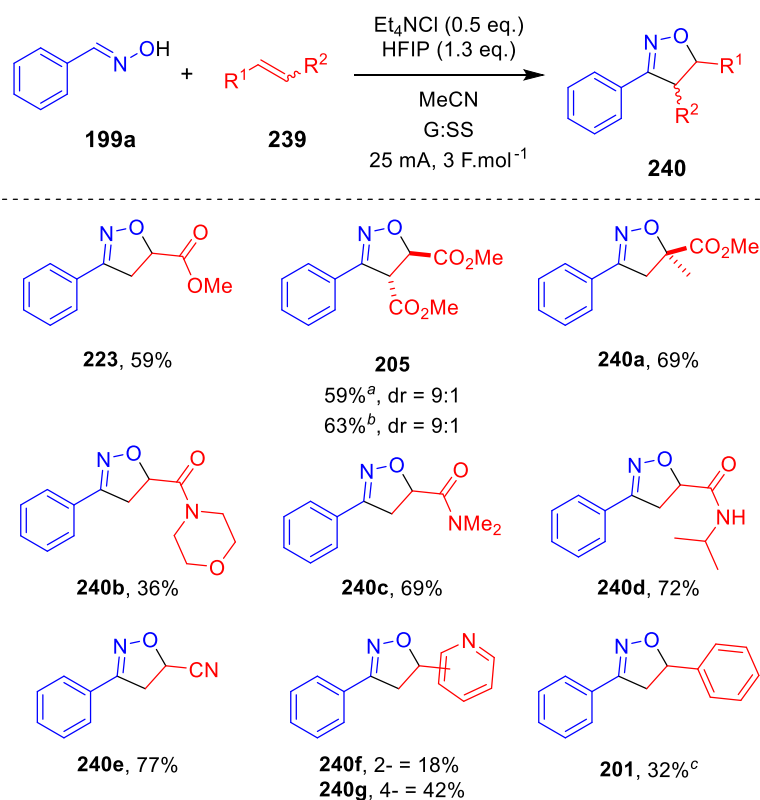
With optimised conditions in hand, attention was turned to a substrate scope in the oxime partner. Both electron-rich (**199b** - **199f** and **199z**; **Scheme 68**) and electron-poor (**199g** - **199y** and **199aa**) benzaldehyde oximes were well tolerated, with moderate to good yields achieved. Interestingly, the substitution on the phenyl ring had a marked effect on the yield of the reaction; in general, meta-substitution gave the highest yield but with poorer observed regioselectivity. Of note, methyl ester-substituted benzaldehyde oximes (**199x** and **199y**) required more charge transferred, when compared to other oximes. Furthermore, it is demonstrated that potentially electroactive groups such as I and Br were tolerated to a useful extent, with these moieties providing a chemical handle for further downstream chemistry (**199g** - **199i** and **199j** - **199l**, respectively). Mesityl oxime was smoothly converted to the corresponding isoxazoline **221z** in 58% yield. Perhaps most significantly, alkyl oximes are well tolerated with **221ab** - **221af** isolated in good yields. Curiously, the number of methylene units between the oxime functionality and the phenyl group had a large influence on the outcome of the reaction, with **221ac** isolated in 74% and **221ab** in 50% yield. Of note, cyclopropyl-substituted isoxazoline **221af** was isolated in serviceable 56% yield, suggesting that any radical intermediates generated under the reaction conditions could participate in a reaction without unproductive intrusion of competing side reactions; ring opening of the strained functionality is one such unproductive side reaction. This result is also highly indicative of a mechanism that does not involve radical C–H abstraction to form a hydroxyiminyl radical intermediate. Pyridyl aldoximes (**199ag** - **199ai**) were tolerated under the electrochemical reaction conditions, with no observed N-oxide or Minisci-type side products observed in the crude reaction mixture (by LCMS or ¹H NMR).



Scheme 68: Substrate scope in aldoxime. Conditions: Oxime (0.5 mmol), dipolarophile (5 eq.), Et₄NCl (0.5 eq.), HFIP (1.3 eq.), MeCN (7 mL), G anode, SS cathode, 25 mA, 3 F.mol⁻¹. ^a5 F.mol⁻¹ charge transferred. HFIP = 1,1,1,3,3,3-hexafluoroisopropanol; G = graphite; SS = stainless steel.

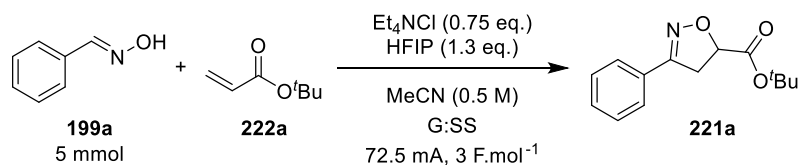
Attention was then turned to scope in dipolarophile reaction partner (**Scheme 69**). Methyl acrylate and amides are tolerated, with the corresponding isoxazolines **223** and **240b** - **240d** isolated in good yields. Pleasingly, medicinally relevant amide substituted isoxazoline **240d** was obtained in 36% isolated yield. Acrylonitrile

participated in the electrochemical reaction without incident, providing **240e** in a good 77% isolated yield. 1,3-Dipolar cycloaddition with disubstituted alkene dimethyl fumarate gave **205** in 59% with a diastereomeric of 9:1 in favour of the expected *anti*-diastereoisomer. As expected from earlier studies (Section 3.1.1), when employing dimethyl maleate as the dipolarophile, the same diastereomeric ratio of 9:1 in favour of the *anti*-diastereoisomer was observed, which is in contrast with the literature.⁷¹ Takeda and co-workers showed that when employing dimethyl maleate as a dipolarophile in their *t*-BuOI-mediated synthesis of isoxazolines, a diastereomeric ratio of 89:11 in favour of the *syn*-diastereoisomer was observed. Under the optimised conditions, styrene was not tolerated. However, upon switching the mediator to Et₄NI, solvent to MeOH and transferring a charge of 5 F.mol⁻¹, the phenyl-substituted isoxazoline **201** was isolated in 32% yield. It is suspected that styryl derived dipolarophiles are not well tolerated in this reaction due to the propensity for these species to polymerise under electrochemical conditions. Gratifyingly, the broadness of the methodology is exemplified by isolation of **240f** and **240g** in poor to moderate yields having employed vinyl pyridines as dipolarophiles.



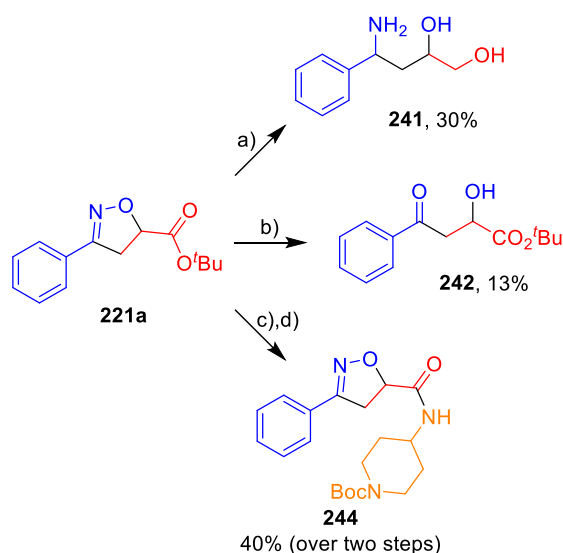
Scheme 69: Substrate scope in dipolarophile partner. Conditions: **199a** (0.5 mmol), dipolarophile (5 eq.), Et_4NCl (0.5 eq.), HFIP (1.3 eq.), MeCN (7 mL), G anode, SS cathode, 25 mA, 3 F.mol⁻¹. ^aDimethyl fumarate employed as dipolarophile; ^bDimethyl maleate employed as dipolarophile; ^cTEAI as mediator, no HFIP, MeOH as solvent, 5 F.mol⁻¹ charge transferred. HFIP = 1,1,1,3,3,3-hexafluoroisopropanol; G = graphite; SS = stainless steel.

To demonstrate the versatility of the electrochemical procedure, a scale-up reaction was performed. (*E*)-Benzaldehyde oxime **199a** subjected to the electrochemical conditions on a 5 mmol scale, coupling with *tert*-butyl acrylate **222a** to give isoxazoline **221a** in 58% isolated yield (**Scheme 70**). A higher current (72.5 mA vs. 25 mA) and higher concentration (0.5 M vs. 0.07 M), whilst transferring a total charge of 3 F.mol⁻¹, was required for the reaction to proceed; this translated to an increase reaction time of 5.5 hours (vs. 100 min). Although a lower yield was obtained (59%, vs. 78%), this experiment demonstrates the capability for this reaction to be scaled-up with only a moderate loss in efficiency. The ratios with which the current and concentration were scaled were influenced by the scale-up procedure from Wang and co-workers.⁹⁸



Scheme 70: The electrochemical synthesis of isoxazoline **221a** was scaled-up to a 5 mmol scale, demonstrating the versatility of this procedure.

The utility of the electrosynthesised isoxazoline products is shown in **Scheme 71**. Firstly, reduction by lithium aluminium hydride gave access to amino diol **241** in a modest isolated yield of 30%. Secondly, milder reduction conditions of iron powder and ammonium chloride provided **242** in 13%, with the *tert*-butyl ester group remaining intact. Hydrolysis with aqueous LiOH, followed by amide coupling with an amine, yielded isoxazoline **244** bearing functionality that is desirable for a fragment in a medicinal chemistry setting. It is noteworthy that these results are unoptimised and are simply examples of chemistry that can be used to reveal masked motifs and further functionalise the isoxazolines.



Scheme 71: Conditions a): LiAlH₄ (1.2 eq.), THF, 0 – rt; **Conditions b):** Fe powder (10 eq.), H₄NCl (10 eq.), EtOH:H₂O (1:1), 90 °C; **Conditions c):** LiOH_{aq} (3 eq.) EtOH, rt; **Conditions d):** amine (1.2 eq.), NMI (2.2 eq.), TCFH (1.2 eq.), DMF, rt. NMI = *N*-methylimidazole; TCFH = *N*-(chloro(dimethylamino)methylene)-*N*-methylmethanaminium hexafluorophosphate (V).

3.5. Reaction Kinetic Analysis

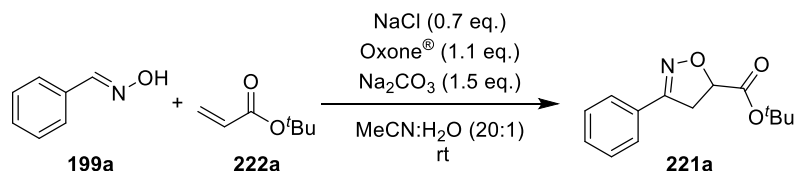
Reaction kinetic analysis and profiling is a powerful tool for probing reaction pathways. It was the intention to use *in-situ* IR monitoring of a non-electrochemical reaction and compare this reaction profile to the analogous electrochemical reaction, in an attempt to find commonalities between the two. Profiling in real time using ReactIR may allow the observation of any intermediates.

Hammett analysis of the electrochemical reaction between substituted aldoximes and *tert*-butyl acrylate was conducted to gain information on the kinetics of the reaction. This information could lead to understanding the nature of the transition state, through understanding how the electronics of the substrates affects the rate of reaction.

3.5.1. *In-situ* IR Monitoring

The mechanism was probed with *in-situ* IR monitoring. Reference spectra, taken with the commercially available ReactIR experimental set up, were used to determine which peaks corresponded to product or starting material. Difference spectra from these reference spectra were utilised to distinguish between peaks. All IR peak wave numbers shown on the following graphs are likely to be single bond vibrations.

Firstly, the non-electrochemical method described by Zhao and co-workers⁹⁹ (**Figure 33**) was monitored and provided a reference reaction profile to compare with the electrochemical method described herein. The non-electrochemical profile shows an initial rate that is commensurate with the consumption of aldoxime **199a**; the authors propose that the Oxone[®] and aldoxime initially form hydroxyimoyl chloride. Once the oxime is consumed, a faster rate of reaction is observed as the intermediate is converted to nitrile oxide; the subsequent 1,3-dipolar cycloaddition of the dipole is assumed to be fast.



Normalised IR Absorbance vs. Time

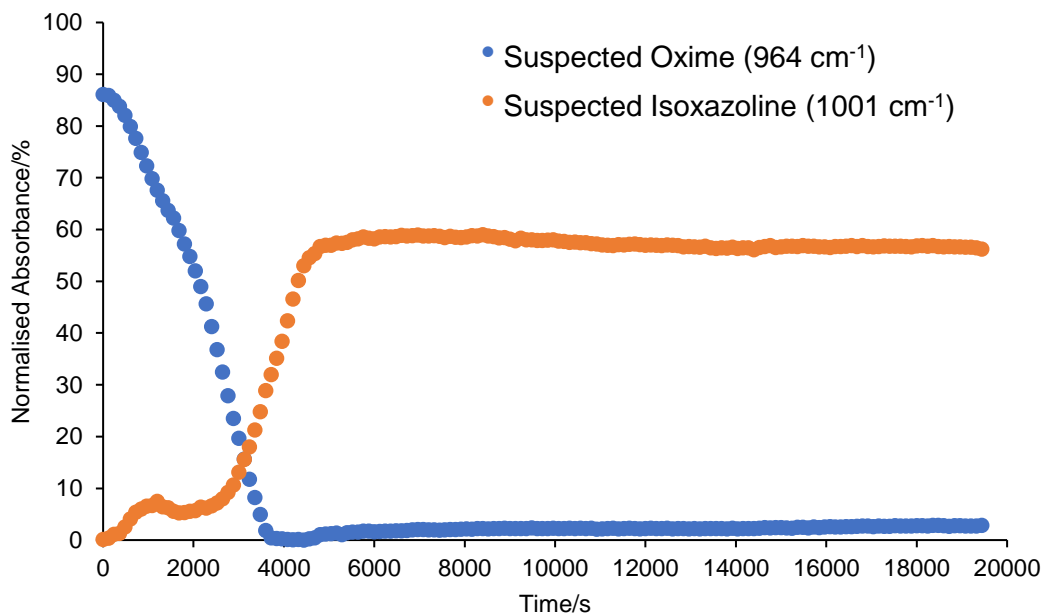


Figure 33: *In-situ* IR reaction profile of the non-electrochemical reaction described by Zhao and co-workers; t = 0 refers to the time Oxone[®] was added.

Comparing this to the electrochemical reaction profile (**Figure 34**), a different reaction profile is observed suggesting an alternative mechanism. The IR probe is only able to monitor the bulk solution and, as electrochemistry is a surface-mediated method with reactive intermediates reacting within the diffusion layer, it is unlikely that highly reactive species will be observed in the bulk solution. However, it can be seen that there is a fast initial rate, which slows to a linear rate of product formation over the time-course of the reaction. The faster initial rate could be explained by the fact that there is a high local concentration of reactants at the electrode surface prior to the application of electricity. This high local concentration is consumed quickly, as the electron transfer is assumed to be very fast, after which the reaction is now under mass transport control to and from the electrode. More clearly, the reaction (as monitored in the bulk) appears to be pseudo-zero order in oxime, which decays linearly for the majority of the reaction. This explanation is likely to be an incomplete picture of what is being monitored as the surface electrochemistry and mass transfer

of reagents could have higher impact on the observations. Although this does not give definitive information on the exact reaction mechanism, it does serve to demonstrate the ability for monitoring electrochemical reactions in the Electra-Syn 2.0.

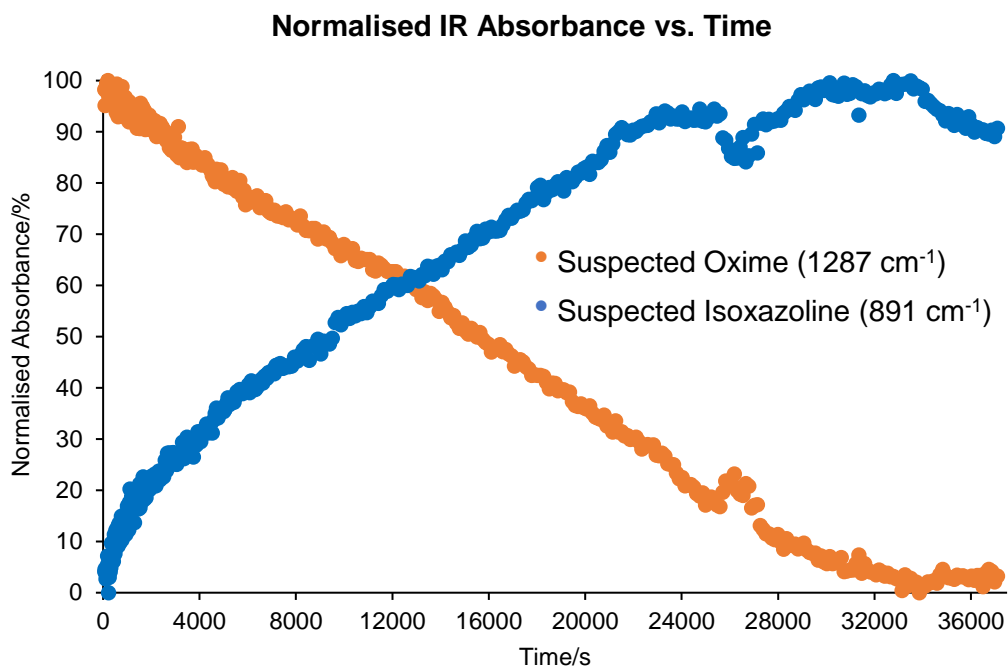
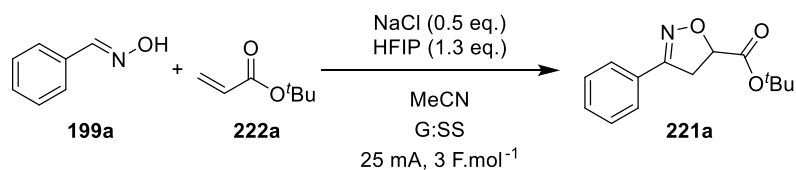


Figure 34: *In-situ* IR reaction profile of the electrochemical reaction developed in this investigation.

3.5.2. ¹H NMR Monitoring

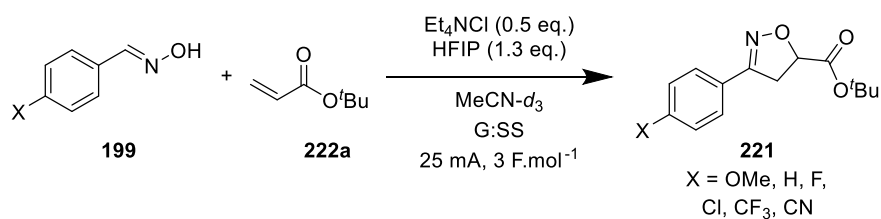
3.5.2.1. Hammett Analysis – σ_p

¹H NMR kinetic analysis of the electrochemical reaction was carried out with the intention of determining information about the rate-limiting step of the overall electrochemical process. Hammett analysis of the maximum rates and rate of reaction after the initial phase was performed, using the *para*-substituted benzaldehyde oximes shown in **Scheme 72**. In these Hammett analyses, the observed rate (k_{obs}) was used; strictly speaking, the analysis should be conducted using the rate constant for the reaction, which is determined by carrying out the reaction at different concentrations and measuring the rate. However, as all the reactions monitored were conducted at the same concentration, the rate is directly proportional to the rate constant and therefore, in this instance, the rate can be used as a proxy for the rate constant. As the reaction is a surface-mediated reaction, changing the concentration of the reaction can change the way the reactants interact with the surface of the electrode; there would be a smaller effective surface area of electrode if there is a high concentration. This change in interaction could lead to rate analyses that are complicated with surface effects and therefore it would be difficult to deconvolute these surface effects from electronic effects of the reactants. The Hammett equation is defined as follows:¹⁰⁰

$$\log\left(\frac{k_x}{k_H}\right) = \rho\sigma$$

Equation 2: Hammett equation, where k_x = observed rate constant of substituted aldoxime reaction, k_H = observed rate constant of unsubstituted aldoxime reaction, ρ = reaction constant and σ = substituent constant.

The values for σ_p were acquired from the Chemical Review by Hansch, Leo and Taft, which provides an exhaustive list of many different parameters.¹⁰¹ Plotting the left-hand side of **Equation 2** vs. σ should, for a reaction obeying a single mechanistic regime, give a line of gradient ρ , which will provide information on the effect of the electronics of the phenyl ring on the reaction. All analyses to follow assume that the electron transfer is fast, with subsequent slower chemical steps. A further assumption is that these analyses will also provide information on the rate-determining chemical step.



Scheme 72: The electrochemical reaction performed for the Hammett analysis; the reaction was followed by ^1H NMR, using benzyl benzoate as external standard.

The Hammett analysis of the maximum rates is shown in **Figure 35** with the values of the data points detailed in **Table 17**. The maximum rates were determined by performing the electrochemical reaction detailed in **Scheme 72**, following reaction progression by ^1H NMR, using benzyl benzoate as an external standard. Plotting the concentration (M) vs. time (s) gives a rate profile of each reaction (see Experimental Section 6.11. for all rate plots). A straight-line trend was fitted to the first zero value point that had two subsequent non-zero values; the gradient (M.s^{-1}) of this line is the maximum rate of reaction up to 300 s.

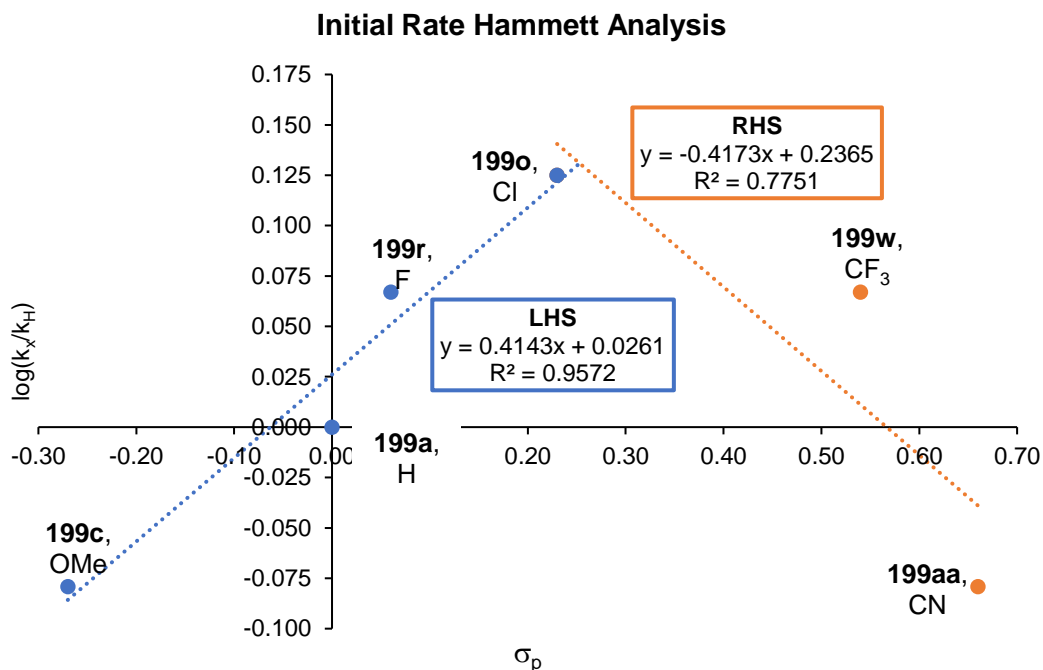


Figure 35: The Hammett plot of the initial rate of reaction for each substituted benzaldehyde oxime reaction; an inverse V-shaped plot suggests a change in rate-limiting step which is consistent with a 1,3-dipolar cycloaddition reaction.

An example of this analysis is shown in **Figure 36**. By plotting the values shown in **Table 17**, an inverted V-shaped plot was observed suggesting that there is a change

in rate-limiting step (or electronic contributions) upon going from electron-rich to electron-poor benzaldehyde oximes (**Figure 35**). This is consistent with 1,3-dipolar cycloaddition of nitrile oxides with dipolarophiles.⁷⁹ As nitrile oxides are ambiphilic dipoles, which means they react through either HOMO_{dipole}-LUMO_{dipolarophile} or LUMO_{dipole}-HOMO_{dipolarophile} frontier molecular orbital interactions (see Section 1.2.2.), this change in electronic contributions is consistent with the change in the interacting frontier molecular orbitals of the reactants. It is most likely that this Hammett plot derived from maximum rates describes the dipolar cycloaddition step and not the formation of the dipole itself (which is assumed to be fast due to highly reactive intermediate formed from the chlorination event). Having said this, steps prior to the cycloaddition could indeed contribute to the overall observed magnitude of the scale observed in constructions of the Hammett and related analyses. Similar to what is observed by ReactIR monitoring, there was a presumed high local concentration of reactants at the electrode surface at the start of the reaction. This local concentration is then depleted quickly as electron transfer will be fast and will likely provide information on the nature of the rate-limiting step. This is again assuming all other factors, such as electron transfer, are fast and do not contribute to this initial rate. Once depletion of the local concentration is achieved, the reaction is then under mass transport control. A similar Hammett plot is observed when using the well mixed-regime (after 300 s) observed rates (**Figure 37**). Again, this Hammett profile tentatively supports a 1,3-dipolar cycloaddition reaction of a nitrile oxide.

Substrate	σ_p	Initial k_{obs}	$\log(k_x/k_H)$
199c , OMe	-0.27	5×10^{-10}	-0.0792
199a , H	0	6×10^{-10}	0.0000
199r , F	0.06	7×10^{-10}	0.0669
199o , Cl	0.23	8×10^{-10}	0.1249
199w , CF ₃	0.54	7×10^{-10}	0.0669
199aa , CN	0.66	5×10^{-10}	-0.0792

Table 17: Values for σ_p taken from review by Hansch, Leo and Taft¹⁰¹ and values for k_{obs} acquired from straight-line analysis of the initial (first 300 s) rate from the rate profiles of each reaction.

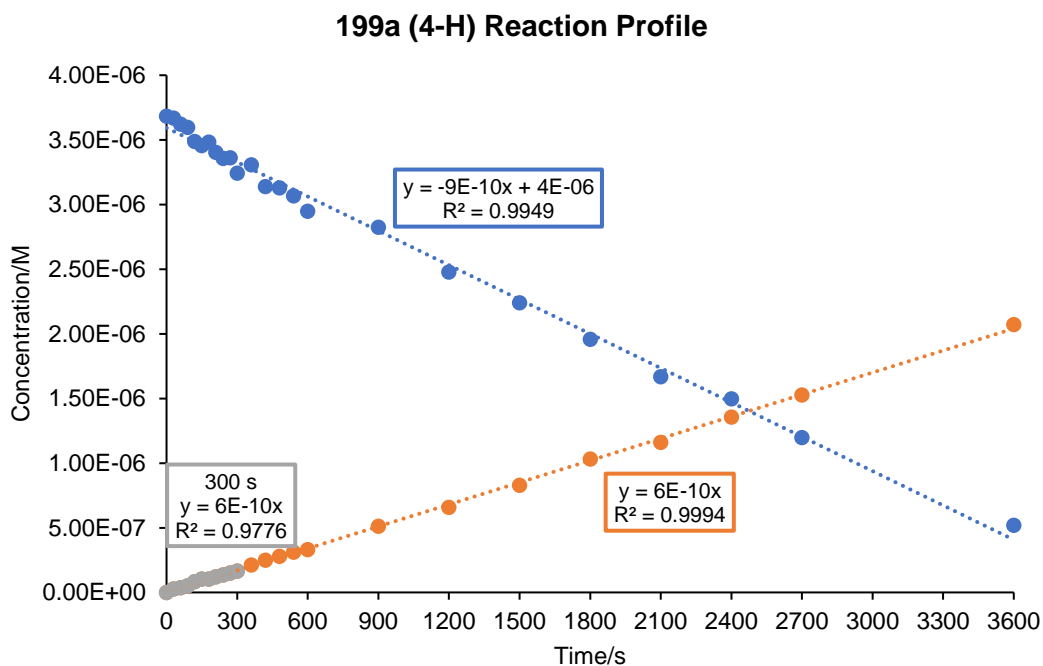


Figure 36: The rate profile of the electrochemical reaction between benzaldehyde oxime **199a** and *tert*-butyl acrylate **222a**, following reaction by ¹H NMR using benzyl benzoate as external standard. Blue = benzaldehyde oxime; orange = desired product, grey = initial rate of desired product.

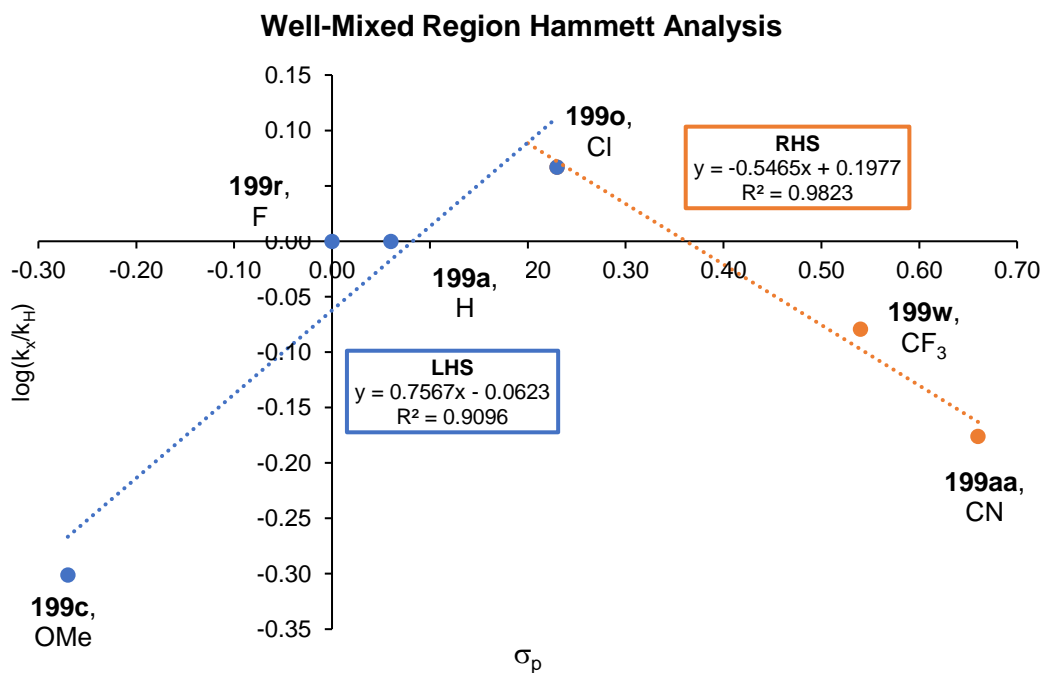


Figure 37: The Hammett plot for the well-mixed region of the rate profiles; it is likely the rates observed are pseudo-first order due to the well-mixed nature of this region of the rate profile.

While probing the electrochemical reaction with ^1H NMR to acquire data for Hammett and Swain-Lupton analyses (*vide infra*), it was found that the data for the reaction of 4-iodobenzaldehyde oxime appeared to be anomalous. The data for this reaction gave significantly lower concentrations of desired product than for the other halides profiled (F and Cl) and did not fit into the expected plot. It is possible that the iodo group may be participating in side-reactions, such as oxidation to hypervalent iodine species; this could then alter the observed kinetics and would render the data anomalous (when analysing all reactions together). Alternatively, it is also possible that the data collected on the 4-iodobenzaldehyde oxime electrochemical reaction were simply outliers. Future work in this area could be in the form of repeating the electrochemical reaction between 4-iodobenzaldehyde oxime and *tert*-butyl acrylate to determine which explanation is most applicable to the current data.

3.5.2.2. Hammett Analysis – σ_p^+

Alternative Hammett constants can be used to determine whether a charged species is formed during the transition state of a given reaction. In the case of a build-up of positive charge, Hammett-Brown σ_p^+ constants can be used.¹⁰¹ These Hammett-Brown constants take into consideration the increased effect of resonance on substituents that are electron-donating through resonance, such as alkoxy and halide group. If a given reaction, in particular the S_N1 reaction, is believed to develop a positive charge in the transition state, resonance electron-donating groups can stabilise this charge through quinoidal resonance forms. This would mean that electron-donating groups will exhibit rates much faster than would be expected when employing the original Hammett σ_p values. Conversely, electron-withdrawing groups cannot provide the same stabilisation of positive charge, and therefore σ_p values are still valid.

In the case of the electrochemical reaction described within this thesis, it is not expected that the reaction develops any particular charge. This is because, although nitrile oxide dipoles are charged species, they have small dipole moments (see Section 1.2.) and so using σ_p^+ Hammett-Brown constants are unlikely to change the outcome of the Hammett analysis. Furthermore, as it is assumed that the reaction process through a 1,3-dipolar cycloaddition pathway, no discrete intermediates are expected, charged or otherwise. Indeed, Hammett analysis of the maximum rate of reaction and σ_p^+ values, shown in **Figure 38**, demonstrates that there is a two-fold decrease in the proportionality constant, ρ , for both electron-donating groups (0.1877 vs. 0.4143) and electron-withdrawing substituents (-0.2677 vs. -0.4173). The overall shape of the Hammett plot is still consistent with a change in electronic demand in the rate-limiting step, and therefore indicative of a 1,3-dipolar cycloaddition reaction (which is therefore believed to be the rate-determining step). This alternative analysis demonstrates that it is unlikely that there is a build-up of positive charge in the transition state as electron-donating substituents retard the rate of reaction, rather than accelerating the rate of reaction. Furthermore, the correlation coefficient, R^2 , for the σ_p^+ Hammett analysis for the electron-donating groups is poorer than the correlation coefficient for the σ_p Hammett analysis (0.7419 vs. 0.9572). For electron-withdrawing groups, the σ_p^+ analysis has a similar disparity between the correlation coefficients (0.5991 vs. 0.7751). This would suggest that the traditional Hammett

analysis, employing standard σ_p Hammett constants, is a much better model for analysis the reaction mechanism than using σ_p^+ Hammett-Brown constants.

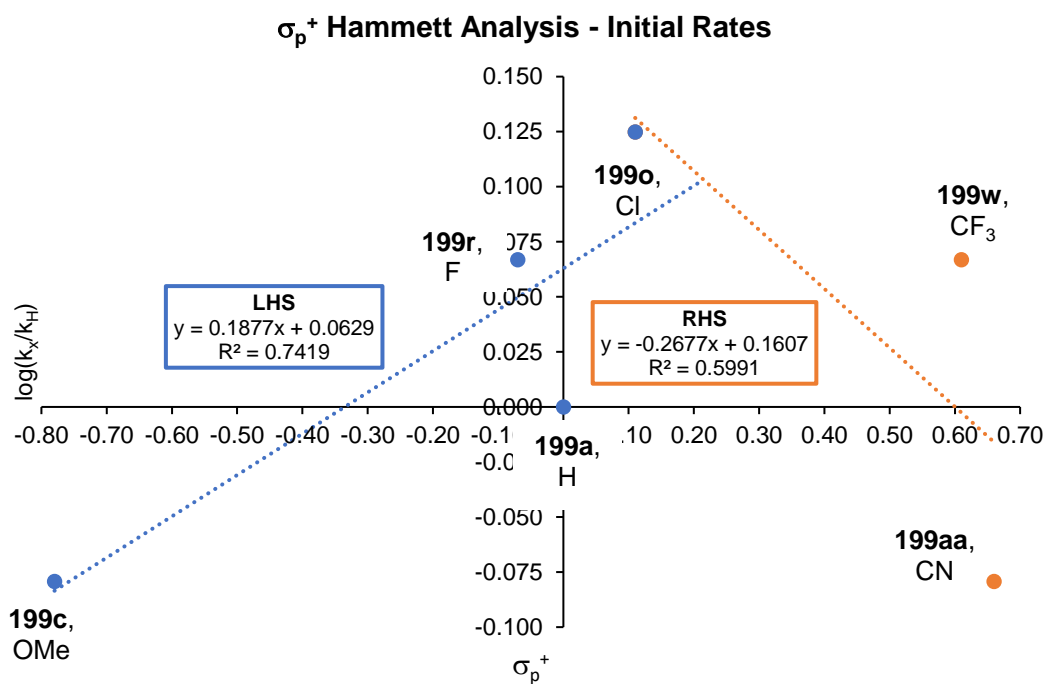


Figure 38: Alternative Hammett analysis using σ_p^+ Hammett-Brown constants instead of traditional σ_p constants.

3.5.2.3. Hammett Analysis – σ_p^-

Just as the Hammett analysis using σ_p^+ incorporates the effects of resonance from electron-donating groups, σ_p^- Hammett values take into consideration the enhanced resonance effects of electron-withdrawing substituents on a reaction that involves the development of a negative charge in the transition state. As shown in **Figure 39**, an inverse V-shaped plot is observed when using σ_p^- values with the maximum observed rates of reaction, consistent with 1,3-dipolar cycloaddition reactions of nitrile oxides. This is also consistent with the alternative Hammett analyses shown above. The proportionality coefficient for the resonance electron-donating substituents (left-hand side, **Figure 39**) is 0.4421, which is similar to the ρ value for the traditional Hammett analysis (0.4143, **Figure 35**). This is as expected as σ_p values for resonance electron-donating substituents are similar to σ_p^- values as electron-donating substituents cannot stabilise negative charge build up. Conversely, the ρ value for the electron-withdrawing substituents shows a two-fold decrease in value over the normal Hammett analysis (-0.2456 vs. -0.4173). This result would suggest that it is unlikely there is a build-up of negative charge in the transition state as electron-withdrawing substituents retard the rate of reaction, rather than accelerate the rate of reaction. Additionally, both correlation coefficients of the σ_p^- Hammett analysis are smaller in magnitude than for the normal Hammett analysis (0.8605 vs. 0.9572, left-hand side; 0.8995 vs. 0.7751, right-hand side), suggesting that the normal Hammett analysis is a much more reliable model than the σ_p^- Hammett analysis.

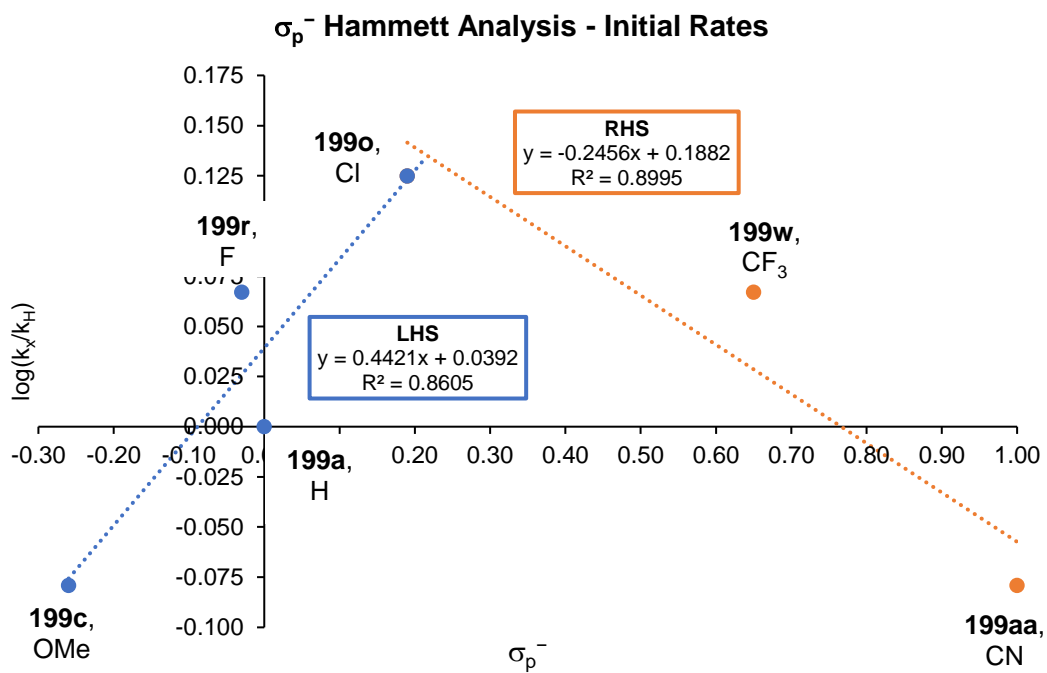


Figure 39: Alternative Hammett analysis using σ_p^- Hammett constants instead of traditional σ_p constants.

3.5.2.4. Swain-Lupton Analysis

Although Hammett analysis of reaction rates and equilibria is a powerful tool, this analysis fails to delineate more specific electronic contributions through resonance effects and field effects. Swain and Lupton made an assumption to redefine the Hammett parameters to separate out the field and resonance effects of substituents; this assumption also stipulates that the field and resonance effects are independent of each other, as in **Equation 3**:¹⁰²

$$\sigma = fF + rR$$

Equation 3: Swain-Lupton equation, separating out the field and resonance effects of substituents. f = weighted constant for field effects; F = field effects (both pure and inductive); r = weighted constant for resonance effects; R = resonance effects (average of electron donating and electron-accepting ability).

In the case of this investigation, f and r were calculated by employing the Solver function in Microsoft Excel, with the stipulation that $f + r = 1$ while maximising the correlation coefficient, R^2 . With these stipulations in place, it was found that for the electron-donating substituents (left-hand side, **Figure 40**), $f = 0.57$ and $r = 0.43$. For electron-withdrawing substituents (right-hand side, **Figure 40**), it was found that $f = 1$ and $r = 0$ (**Table 18**). It can be tentatively suggested that field effects dominate the rate of reaction for electron-withdrawing substituted benzaldehyde oximes, while for electron-donating substituted benzaldehyde oximes, field effects and resonance effects have similar influences over the rate of reaction.

Compound	Substituent	k_{obs}	$\log\left(\frac{k_x}{k_H}\right)$	f	r	F	R
199c	OMe	5×10^{-10}	-0.0792	0.5742	0.4258	0.29	-0.56
199a	H	6×10^{-10}	0.0000	0.5742	0.4258	0.03	0.00
199r	F	7×10^{-10}	0.0669	0.5742	0.4258	0.45	-0.39
199o	Cl	8×10^{-10}	0.0125	0.5742	0.4258	0.42	-0.19
199w	CF ₃	7×10^{-10}	0.0669	1.0000	0.0000	0.38	0.16
199aa	CN	5×10^{-10}	-0.0792	1.0000	0.0000	0.51	0.15

Table 18: Data used for Swain-Lupton analysis.

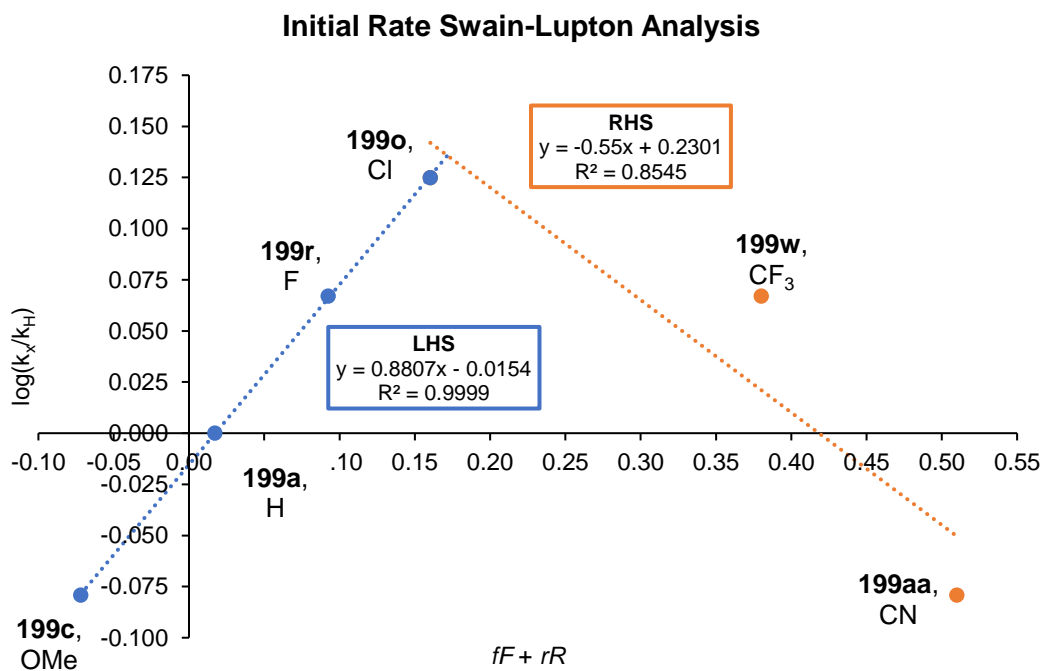


Figure 40: Swain-Lupton analysis of the initial rate of the electrochemical reaction between *para*-substituted benzaldehyde oximes and *tert*-butyl acrylate.

Furthermore, the Swain-Lupton analysis strengthens the hypothesis of 1,3-dipolar cycloaddition reaction of a nitrile oxide, with an inverse V-shaped plot observed (**Figure 40**). The ρ value for the electron-donating substituents of the Swain-Lupton analysis (**Figure 40**) is twice that of the ρ value for the same substituents in the traditional Hammett plot (0.8807 vs. 0.4143), with comparable correlation coefficients (0.9999 vs. 0.9572) suggesting that both plots are good models of the hypothesised reaction mechanism. For the electron-withdrawing substituents, both the ρ values (-0.5500 vs. -0.4173) and correlation coefficients (0.8545 vs. 0.7751) of the Swain-Lupton and Hammett analyses are similar, also supporting the proposed reaction mechanism of 1,3-dipolar cycloaddition.

3.5.2.5. Stir Speed Analysis

Although the stir speed of the electrochemical reaction was explored using DoE (see Section 3.3.), it was further probed using ^1H NMR and the model electrochemical reaction between (*E*)-benzaldehyde oxime and *tert*-butyl acrylate. More detailed information on the effect of stir speed was proposed to offer insight into the effects of mixing on the rate of reaction. As illustrated in **Figure 41**, the stir speed (200 - 600 rpm) has minimal effect on the rate of reaction – only in the absence of stirring is an effect observed. When the reaction is not stirred, the rate of reaction must be determined by the mass transport of material to and from the electrode surface. The mass transport is shown to be insufficient for the progress of the reaction as it does not go to completion, but levels out at approximately 50% NMR yield (**Figure 41**, red line). While there is only a slight difference in the rate of reaction between the different stir speeds analysed, the difference is within the error of the equipment (as determined above in Section 3.2.3). However, the small differences show that there could be a trend that shows that the slower the stir speed (between 0 and 200 rpm) the faster the rate of reaction. This could form part of further study into this electrochemical reaction from an engineering perspective. There is a high confidence that these results are real as the correlation coefficients of the three stir speeds with straight-line fits are excellent ($R^2 = 0.9923$, grey line; $R^2 = 0.9916$, blue line; $R^2 = 0.9877$, green line; **Figure 41**).

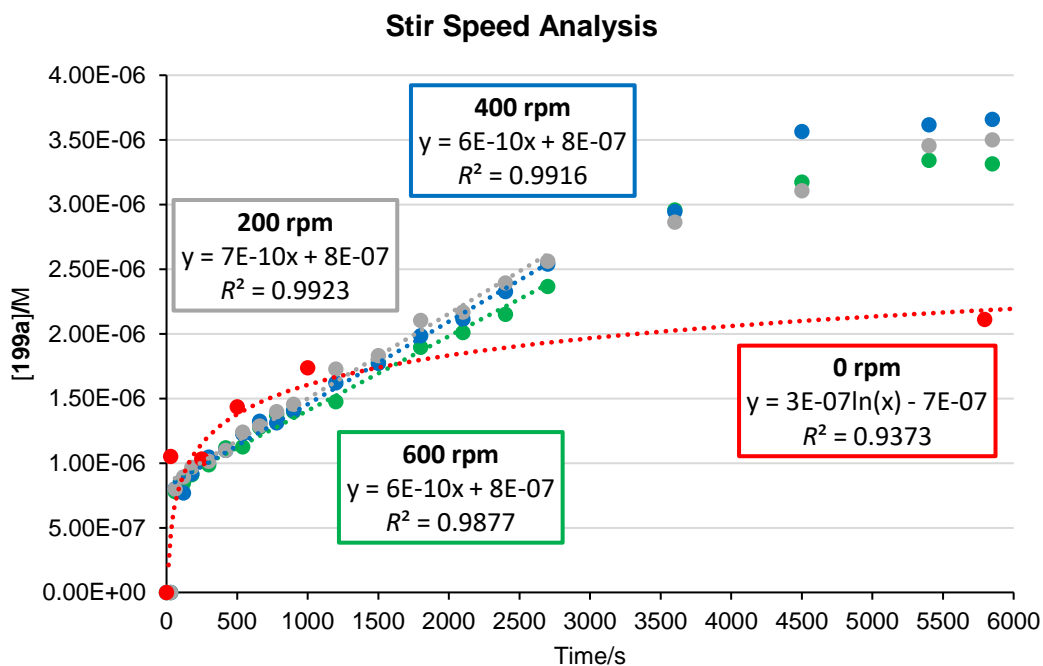


Figure 41: The effect of stir speed was further analysed by ^1H NMR, plotting the time-course of the reaction at each stir speed, using benzyl benzoate as an external standard. The y-axis plots concentration of isoxazoline product formed.

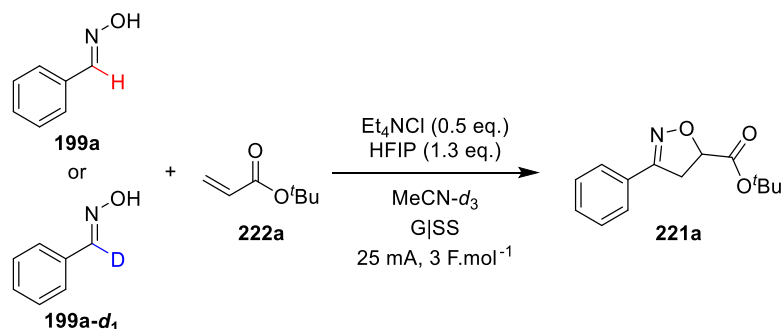
Expanding the scope of the stir speed analysis could give more detailed information on the effect of stir speed on the electrochemically enabled synthesis of isoxazolines. Including stir speeds of 100, 800 and 1000 rpm would be enough to sample the entire range of stir speeds that the ElectraSyn can achieve.

The acquired stir speed data suggested that all reactions in this study were above the threshold for being well-mixed, evidencing the mass-transport-limited pseudo-zero order profiles seen through complementary analyses (**Figure 35** and **Figure 37**).

3.5.2.6. Kinetic Isotope Effect

Having explored the effect of electronics on the rate of reaction, utilising the reaction between substituted benzaldehyde oximes and *tert*-butyl acrylate, attention was turned to explore whether there was a kinetic isotope effect. If a kinetic isotope effect (KIE) was to be observed, it would imply that there is a C–H bond broken (or formed) in the rate-limiting step (or product-determining step).

For the KIE experiments, it was decided that parallel experiments with a deuterated and non-deuterated benzaldehyde oxime employed.¹⁰³ As the non-deuterated benzaldehyde oxime had already been profiled, it only remained for the deuterated benzaldehyde oxime **199a-d₁** to be profiled (**Scheme 73**). The same conditions as was used in the Hammett and Swain-Lupton analyses were employed for the reaction profiling of **199a**, namely the reaction was followed by ¹H NMR, using benzyl benzoate as an external standard.



Scheme 73: The parallel reactions conducted for the determination of a possible kinetic isotope effect for the electrochemical reaction.

Figure 42 shows the profile of both **199a-d₁** (orange) and **199a** (blue). Comparison of the maximum rates shows that the reaction with **199a** has an initial rate of 6×10^{-10} M.s⁻¹, while the initial rate of **199a-d₁** is 4×10^{-10} M.s⁻¹. These rate values then give a secondary KIE of 1.5. This secondary KIE implied that there is C–H bond breaking (and/or bond forming) involved in the rate-limiting step, albeit the observed KIE is small. Our mechanistic hypothesis is supported by this KIE evidence as we propose that the rate-limiting step is most likely to be the formation of the nitrile oxide; the subsequent 1,3-dipolar cycloaddition is assumed to be fast.

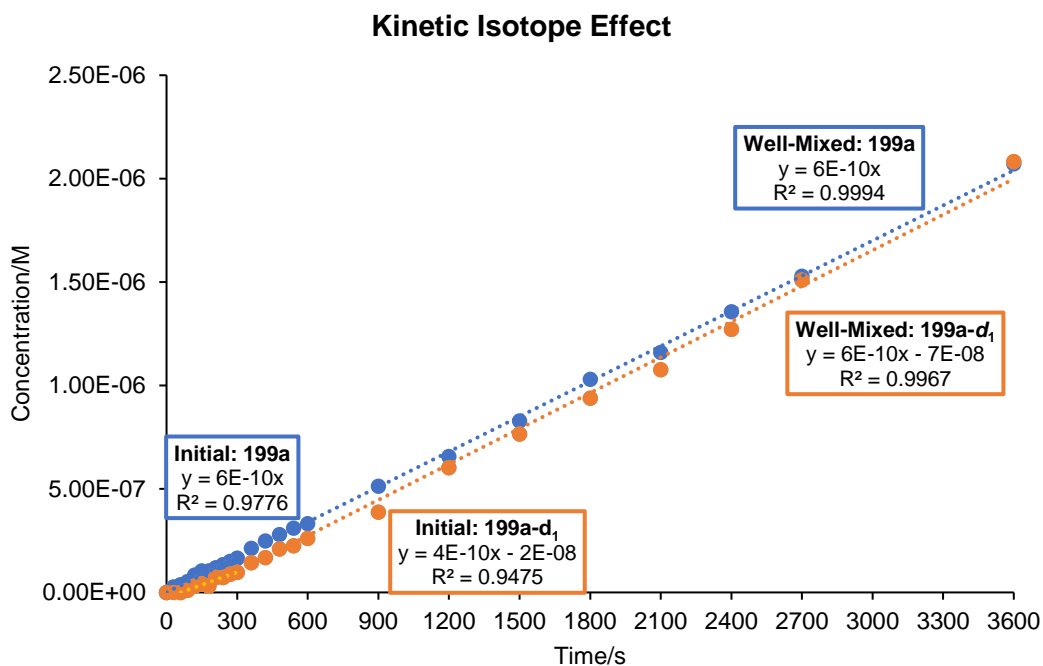


Figure 42: The ^1H NMR profiles of **199a** (blue) and **199a- d_1** (orange); analysis of the profiles for maximum rates and the rate of reaction of the well-mixed region supports the hypothesis of the formation of an intermediate nitrile oxide.

Interestingly, comparing the rates of the well-mixed region (after the initial phase of maximum rate), it can be seen that they are identical. This is not wholly unexpected as we propose that the rate of reaction in this region is dictated by mass transport (i.e. stirring of the reaction).

Overall, the secondary (perhaps negligible) KIE observed supports a mechanism in which C–H bond making/breaking does not feature. Furthermore it is more likely that the electrochemical reaction is under mass transport control, and therefore the rate is determined by current.

3.6. Cyclic Voltammetry Experiments

Cyclic voltammetry (CV) is an incredibly powerful tool for analysing electrochemical reactions. It can also be used as a supplementary tool for the study of the reaction pathway of an electrochemical reaction. For example, CV can determine which components of the reaction are likely to be oxidised first and therefore give an indication on the likely reaction pathway.

Throughout the CV experiments detailed below, the ferrocene redox couple was used as a reference. Most cyclic voltammograms are referenced to a standard hydrogen electrode (SHE) or saturated calomel electrode (SCE), however these are expensive and, in the case of SCE, can be toxic (SCE uses mercury). Instead, the standard of practice is to use ferrocene as the reference; ferrocene redox couples have been well-studied, and the electrode half-peak potential ($E_{\frac{p}{2}}$) can be used to reference to SCE or SHE. To calculate (and reference) to SCE or SHE, a ferrocene couple is obtained and the difference in $E_{\frac{p}{2}}$ is obtained. This calculated value can then be added to the $E_{\frac{p}{2}}$ value obtained from the desired analyte solution to give the reference half-peak potentials. Using half-peak potentials referenced to SCE or SHE allows more reliable comparisons between cyclic voltammograms as the $E_{\frac{p}{2}}$ are irrespective of the reversibility of the cyclic voltammogram; $E_{\frac{1}{2}}$ can only be used in the case of a reversible CV where the peak separation is ~ 60 mV.¹⁰⁴

Firstly, a figure containing all the ferrocene redox couples used as references is shown in **Figure 43**. It can be seen that there is very little difference between the CVs, demonstrating that there is no passivation of the platinum chip electrode throughout the cyclic voltammetry experiments. There was a concern that the chloride mediator may react irreversibly with the platinum chip to form chloroplatinate species and hence passivate the surface of the electrode chip. However, as the ferrocene redox couples do not change over the course of the experiments, this is unlikely to have happened. This also gives confidence in all the CVs obtained for the reaction components and combinations of components.

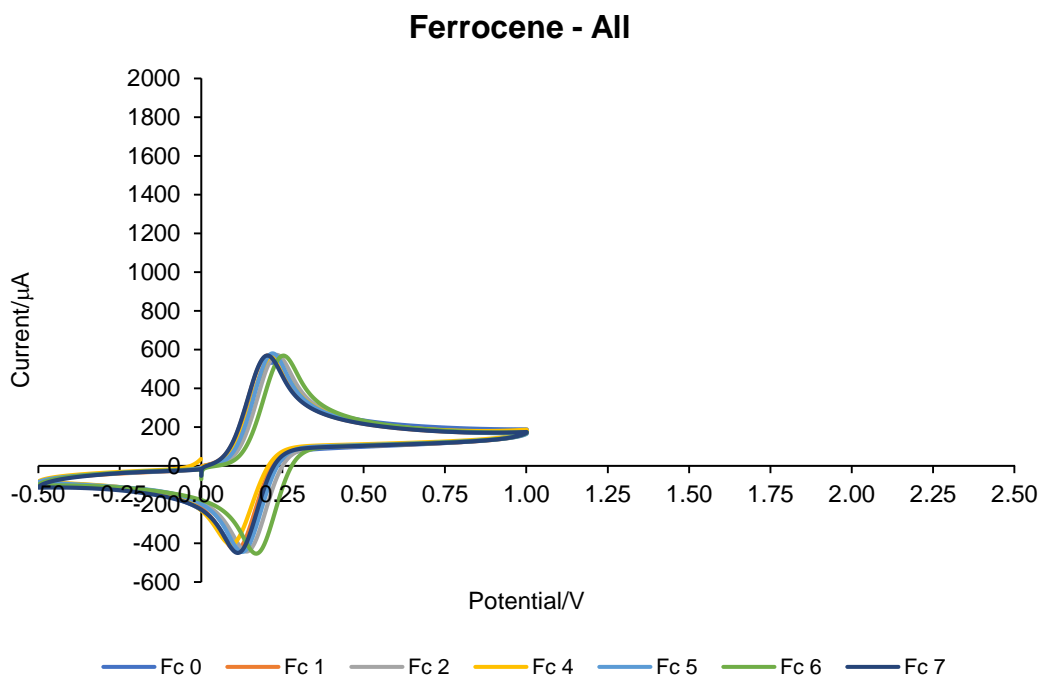


Figure 43: Cyclic voltammograms of the ferrocene redox couple, used as a reference for all CVs for the reaction components. Conditions: 10 mM ferrocene, 0.1 M $\text{Et}_4\text{NBF}_4\text{-MeCN}$, Pt chip electrode, 100 $\text{mV}\cdot\text{s}^{-1}$.

The CV of benzaldehyde oxime **199a** is shown in **Figure 44**. It is clear to see that there is an oxidation event at $E_{\frac{p}{2}} = 1.06 \text{ V}$ (vs. SCE), and a possible second oxidation event at $E_{\frac{p}{2}} = 1.26 \text{ V}$ (vs. SCE). As the height of the oxidative wave of the ferrocene couple is the same height as the oxidative waves of **199a**, it can be implied that both oxidative events for the analyte are one-electron processes.

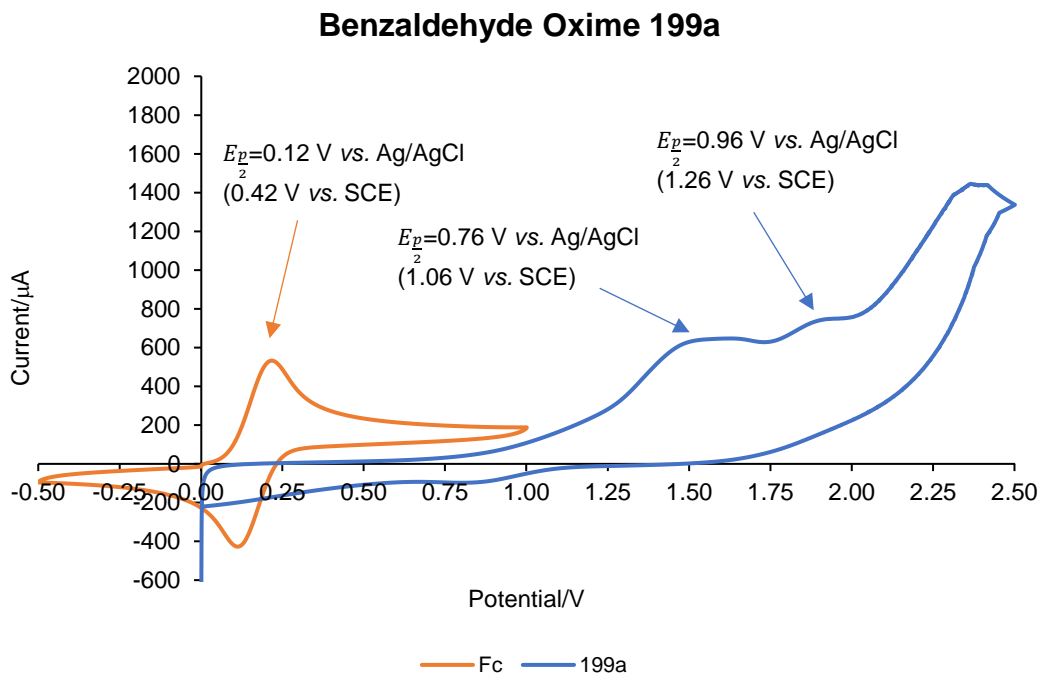


Figure 44: Cyclic voltammogram of a solution of benzaldehyde oxime **199a**. Conditions: 10 mM ferrocene, 0.1 M Et₄NBF₄-MeCN, Pt chip electrode, 100 mV.s⁻¹; 10 mM **199a**, 0.1 M Et₄NBF₄-MeCN, Pt chip electrode, 100 mV.s⁻¹. The potential scale is referenced to the Ag/AgCl of the Pt chip.

It was suspected that the peak at $E_p = 1.06$ V (vs. SCE) was formed from two peaks that are close together as the peak is quite broad. This was confirmed by repeating the cyclic voltammetry experiment (**Figure 45**, blue line). It is clear to see that there are three oxidative events. As all three oxidations occur at a similar peak current as the co-plotted ferrocene redox couple, it can be implied that these are oxidations of three separate species or functionalities. These functionalities can be on the same molecule as the different oxidation potentials mean that the electrons removed are from orbitals of different energies. A possible explanation for two of the oxidations could be that one peak is associated with the oxidation of the *N*-atom of the benzaldehyde oxime, while another peak is associated with the *O*-atom of the benzaldehyde oxime.

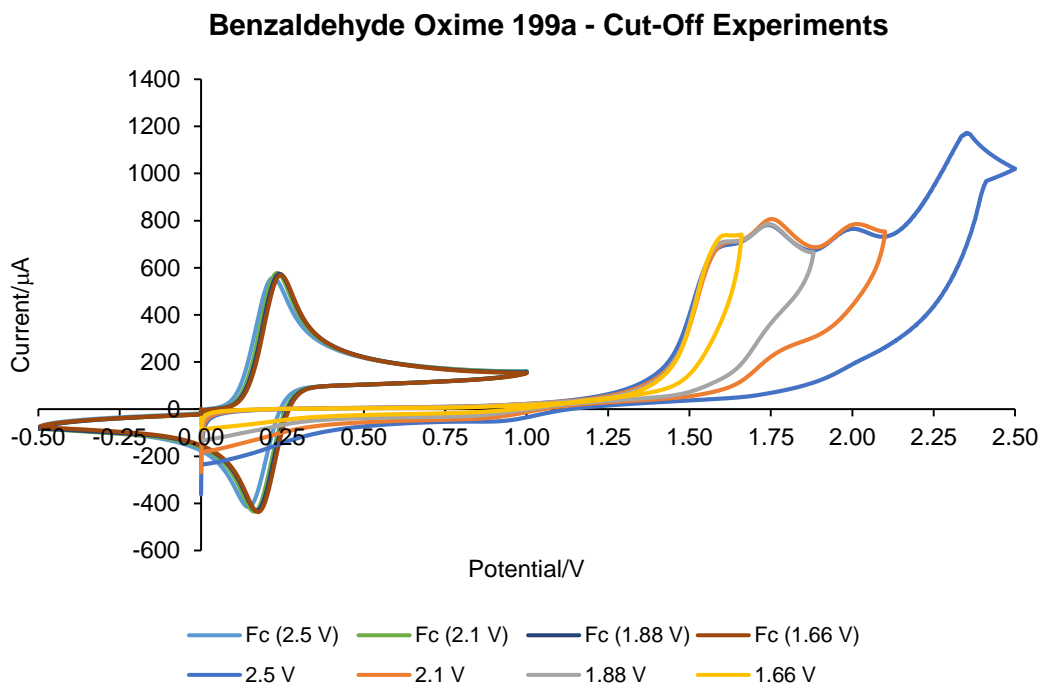


Figure 45: Repeated cyclic voltammogram of a solution of benzaldehyde oxime **199a**. Conditions: 10 mM ferrocene, 0.1 M $\text{Et}_4\text{NBF}_4\text{-MeCN}$, Pt chip electrode, $100 \text{ mV}\cdot\text{s}^{-1}$; 10 mM **199a**, 0.1 M $\text{Et}_4\text{NBF}_4\text{-MeCN}$, Pt chip electrode, $100 \text{ mV}\cdot\text{s}^{-1}$. The potential scale is referenced to the Ag/AgCl of the Pt chip.

Another intriguing feature of the CV of **199a** is the apparent small reductive current response at approximately 0.91 V (vs. Ag/AgCl). On the full CV, it is not possible to determine which oxidative event is responsible for the apparent reductive response. However, by performing the cyclic voltammetry experiment and reversing the potential just after each oxidation, it may be possible to determine which peak is responsible. Firstly, reversing the potential at 2.10 V (**Figure 45**, orange line) was performed and it was observed that there was no reductive response on the reverse way. This would suggest that the oxidation at 2.25 V (vs. Ag/AgCl) is responsible for the response on the reductive wave. To further confirm this, the potential was also reversed at 1.88 V (**Figure 45**, grey line) and 1.66 V (**Figure 45**, yellow line) and the CV shows no reductive response on the reverse wave, further implicating the peak at 2.25 V (vs. Ag/AgCl) as the culprit for the reduction.

Recording CVs at different scan rates (v) can provide information on the type of electron transfer (reversible or irreversible), as well as give a clue as to where the irreversible chemical steps occur. For a solution of **199a**, CVs were recorded at scan rates of 50, 100, 250 and $500 \text{ mV}\cdot\text{s}^{-1}$ (**Figure 46**). It can be seen that the peak potentials of the three oxidations remain very similar, with a very small shift to a more

positive potential. This is indicative of a reversible electron transfer, with the shape of the curves indicative of an irreversible chemical step after oxidation, i.e. EC mechanism.

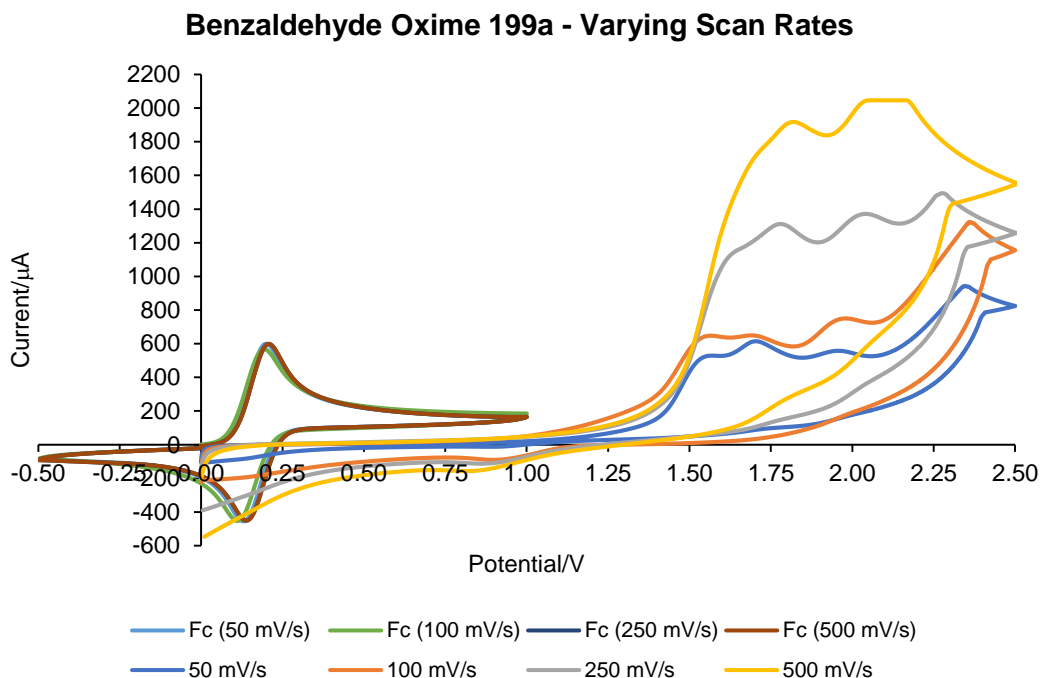


Figure 46: The cyclic voltammograms of a solution of benzaldehyde oxime **199a** at different scan rates. Conditions: 10 mM ferrocene, 0.1 M $\text{Et}_4\text{NBF}_4\text{-MeCN}$, Pt chip electrode, $100 \text{ mV}\cdot\text{s}^{-1}$; 10 mM **199a**, 0.1 M $\text{Et}_4\text{NBF}_4\text{-MeCN}$, Pt chip electrode, $[\nu] \text{ mV}\cdot\text{s}^{-1}$. The potential scale is referenced to the Ag/AgCl of the Pt

By plotting the peak potentials vs $\log(\nu)$, one can determine whether the electron transfer is reversible or irreversible; a plot of this kind for the solution of **199a** is shown in **Figure 47**. If the slope of the straight-line is $(+/-) 60 \text{ mV}\cdot\text{decade}^{-1}$, then the electron transfer is irreversible. As shown in **Figure 47**, all straight-lines associated with the three oxidations have slopes greater than $60 \text{ mV}\cdot\text{decade}^{-1}$, which is indicative of a reversible electron transfer (Peak 1 = $165.6 \text{ mV}\cdot\text{decade}^{-1}$; Peak 2 = $119.0 \text{ mV}\cdot\text{decade}^{-1}$; Peak 3 = $144.9 \text{ mV}\cdot\text{decade}^{-1}$).

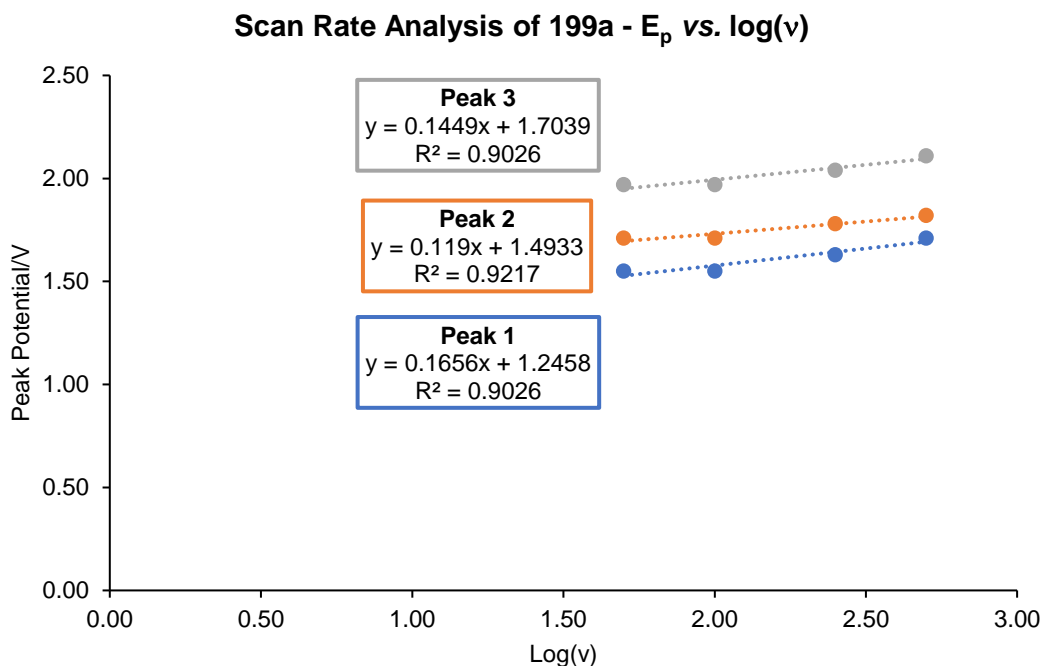


Figure 47: Analysis of the scan rates and plotting E_p vs. $\log(v)$ suggests that the electron transfers during the oxidations observed in the CV of a solution **199a** are reversible. Peak 1 = blue; Peak 2 = orange; Peak 3 = grey.

Furthermore, plotting the peak current (i_p) vs. square root of scan rate (\sqrt{v}) can provide information on whether the adsorption of the material onto the surface of the electrode occurs. A straight-line plot would allow the safe assumption that there is no adsorption to the surface of the electrode. **Figure 48** shows the peak current vs. square root of scan rate plot for a solution of **199a**. It can be seen that for all three oxidative peaks it can be assumed that there are no adverse adsorption effects. This would suggest that either the adsorption and desorption at the electrode is facile (i.e. facile inner-sphere electron transfer) or that the electron transfer is not *via* an adsorption event, but rather through solvent (i.e. tunnelling through an outer-sphere electron transfer). Alternatively, a reversible adsorption event could be occurring which does not lead to passivation of the electrode.

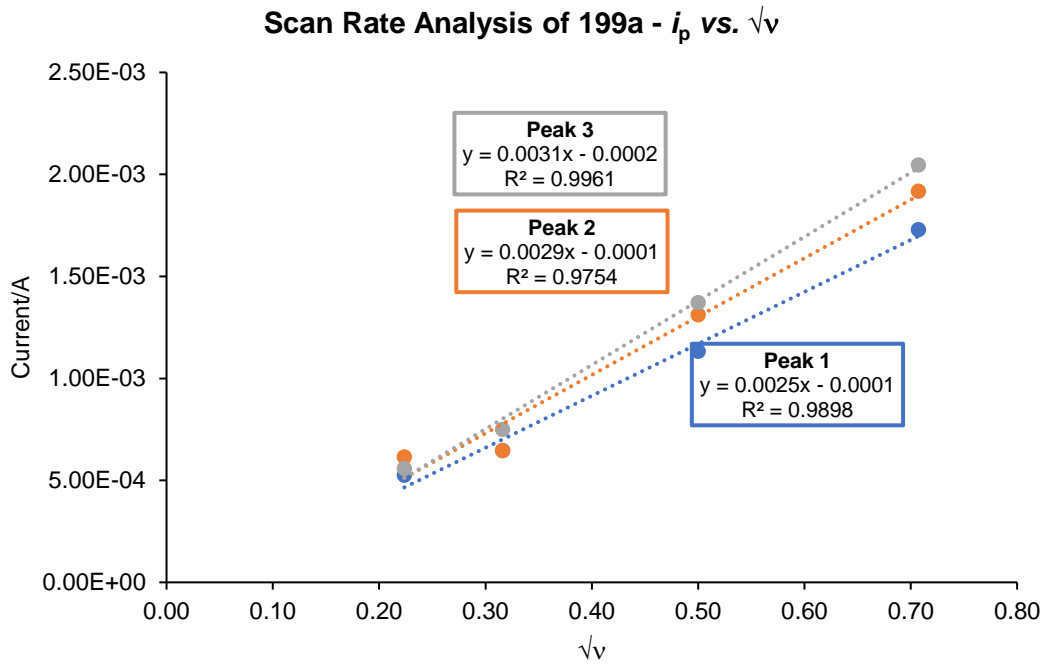


Figure 48: Analysis of the scan rates and plotting i_p vs. \sqrt{v} suggests that adsorption to the surface of the electrode is either non-existent or extremely facile. Peak 1 = blue; Peak 2 = orange; Peak 3 = grey.

Cyclic voltammetry of *tert*-butyl acrylate **222a** revealed that there is no oxidation of the dipolarophile in the range of potentials screened (**Figure 49**). This result suggests that a radical mechanism involving the oxidation and radical addition of the dipolarophile is an unlikely pathway.

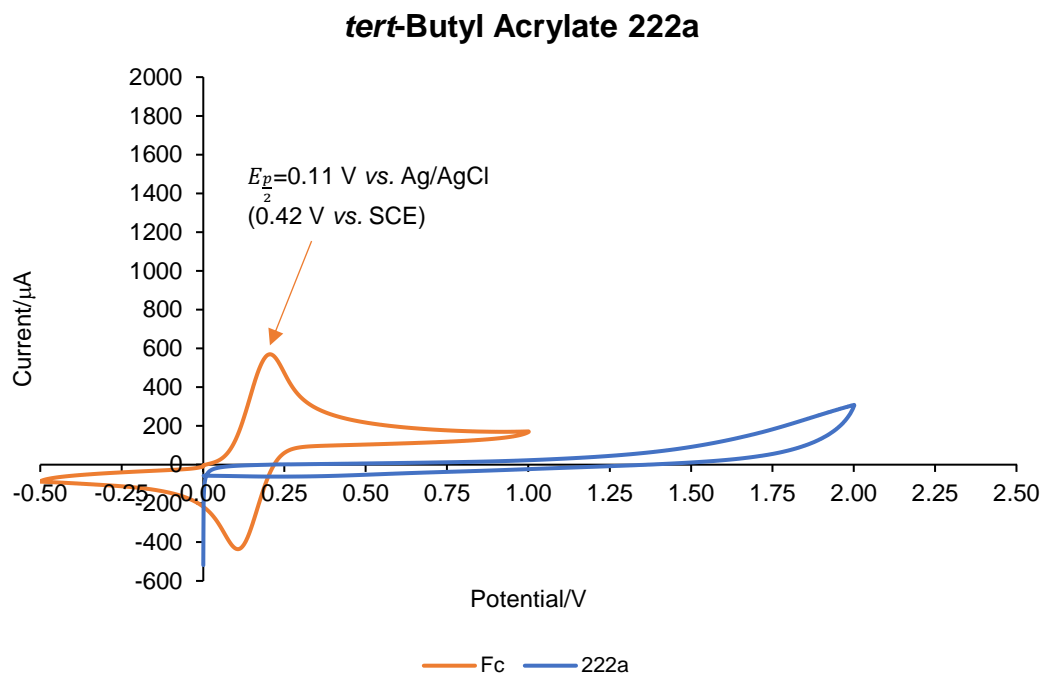


Figure 49: Cyclic voltammogram of a solution of *tert*-butyl acrylate **222a**. Conditions: 10 mM ferrocene, 0.1 M Et₄NBF₄-MeCN, Pt chip electrode, 100 mV.s⁻¹; 10 mM **222a**, 0.1 M Et₄NBF₄-MeCN, Pt chip electrode, 100 mV.s⁻¹. The potential scale is referenced to the Ag/AgCl of the Pt chip.

The profile of a solution of Et₄NCl shows a semi-reversible cyclic voltammogram (**Figure 50**). Oxidation of the chloride anions occurs at $E_{p/2} = 0.78$ V (vs. SCE). The couple is semi-reversible as the reductive peak height is smaller than the oxidative peak height. This could be explained by the fact that chloroplatinate species could be formed from the highly reactive oxidised chlorine species. Small amounts of platinum from the electrode used for the experiments could be in solution and are then able to react with the chloro species formed during the oxidative wave of the CV experiment. This semi-reversible redox couple of the mediator supports a mechanistic pathway in which chloride anions are acting as a mediator for the reaction. Furthermore, this CV of Et₄NCl also supports the proposed catalytic nature of the mediator, in so far as the CV displays a reversible oxidative event.

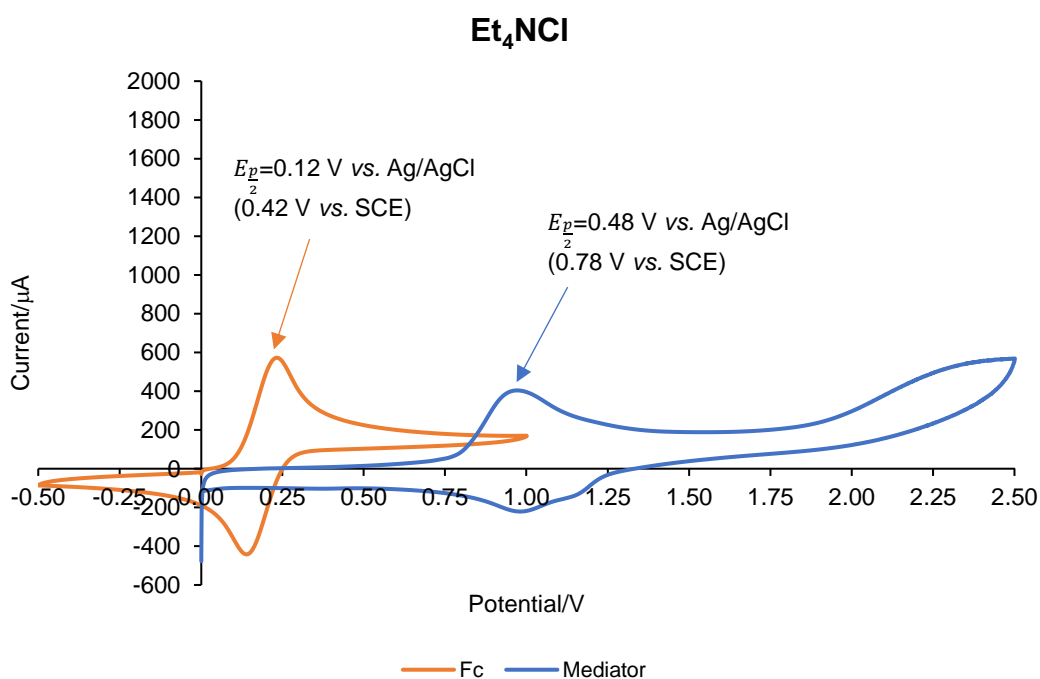


Figure 50: Cyclic voltammogram of a solution of Et₄NCl mediator. Conditions: 10 mM ferrocene, 0.1 M Et₄NBF₄-MeCN, Pt chip electrode, 100 mV.s⁻¹; 10 mM Et₄NCl, 0.1 M Et₄NBF₄-MeCN, Pt chip electrode, 100 mV.s⁻¹. The potential scale is referenced to the Ag/AgCl of the Pt chip.

It was observed that there were two reductive peaks in the CV of Et₄NCl. Similar to the CV experiments for **199a**, cut-off CV experiments were performed, reversing the potential at 1.25 V. This would give insight into which reductive peak belongs to the chloride redox couple. **Figure 51** shows this cut-off experiments and it can be seen that the first reductive peak at 1.12 V is not part of the chloride redox couple. This reductive peak may be associated with a chloroplatinate species that could form

during the CV of the mediator. It is also observed that in the CV of Et₄NCl, the ferrocene standard shifts between experiments; this would suggest that there may be passivation of the electrode surface. It is likely that this passivation is due to platinum having an affinity for forming chloroplatinate species under oxidative conditions. However, this is unavoidable in the case of this investigation as the chloride is of interest as it is the mediator/electrolyte for the electrochemical procedure developed herein.

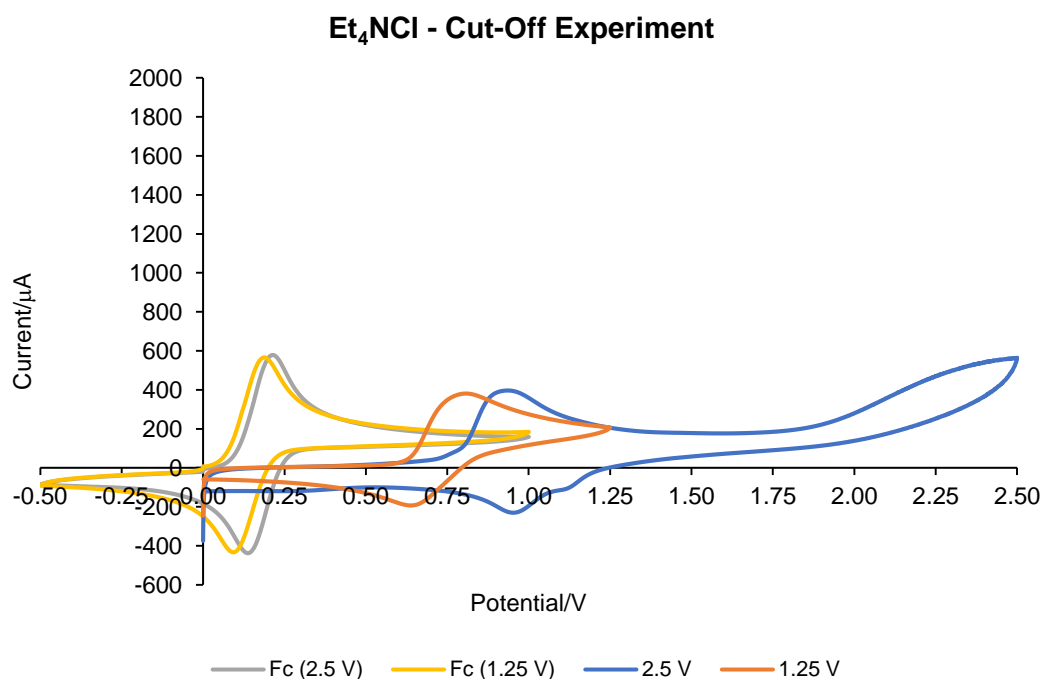


Figure 51: Cut-off CV experiments performed on a solution of Et₄NCl to determine which reductive peak is associated with the chloride redox couple. Conditions: 10 mM ferrocene, 0.1 M Et₄NBF₄-MeCN, Pt chip electrode, 100 mV.s⁻¹; 10 mM Et₄NCl, 0.1 M Et₄NBF₄-MeCN, Pt chip electrode, 100 mV.s⁻¹. The potential scale is referenced to the Ag/AgCl of the Pt chip.

The scan rate CV experiments that were performed for the solution of **199a** were also performed for a solution of Et₄NCl, with the CVs shown in **Figure 52**. As it is expected that the chloride redox couple is a reversible transformation, the peak potentials should not change when varying the scan rate. For the most part, this is what is observed. However, the 50 mV.s⁻¹ CV seems to be shifted to more positive potentials. As mentioned above, chloride may have adverse effects on the platinum surface of the electrode, and this may be causing the shift in observed peak potentials.

By plotting the peak current (i_p) vs. square root of scan rate (\sqrt{v}), a straight-line is obtained for both the oxidative (**Figure 53**) and reductive (**Figure 54**) wave. These

results are a strong indication that there is no adsorption (or facile adsorption/desorption) at the electrode surface.

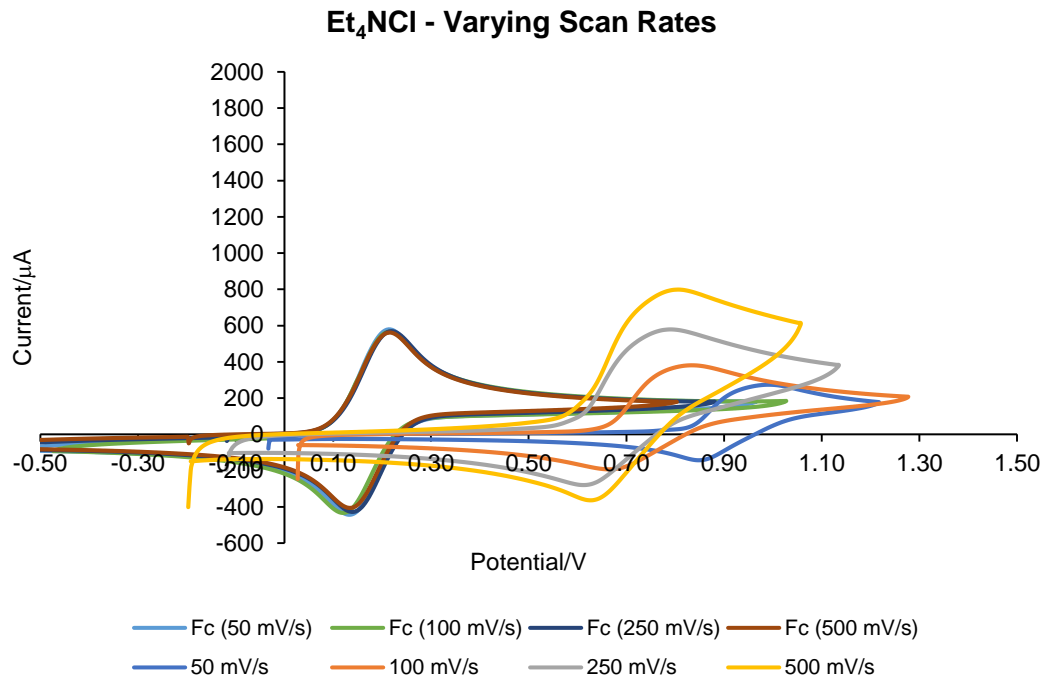


Figure 52: The cyclic voltammograms of a solution of Et₄NCl at different scan rates. Conditions: 10 mM ferrocene, 0.1 M Et₄NBF₄-MeCN, Pt chip electrode, 100 mV.s⁻¹; 10 mM Et₄NCl, 0.1 M Et₄NBF₄-MeCN, Pt chip electrode, [v] mV.s⁻¹. The potential scale is referenced to the Ag/AgCl of the Pt chip.

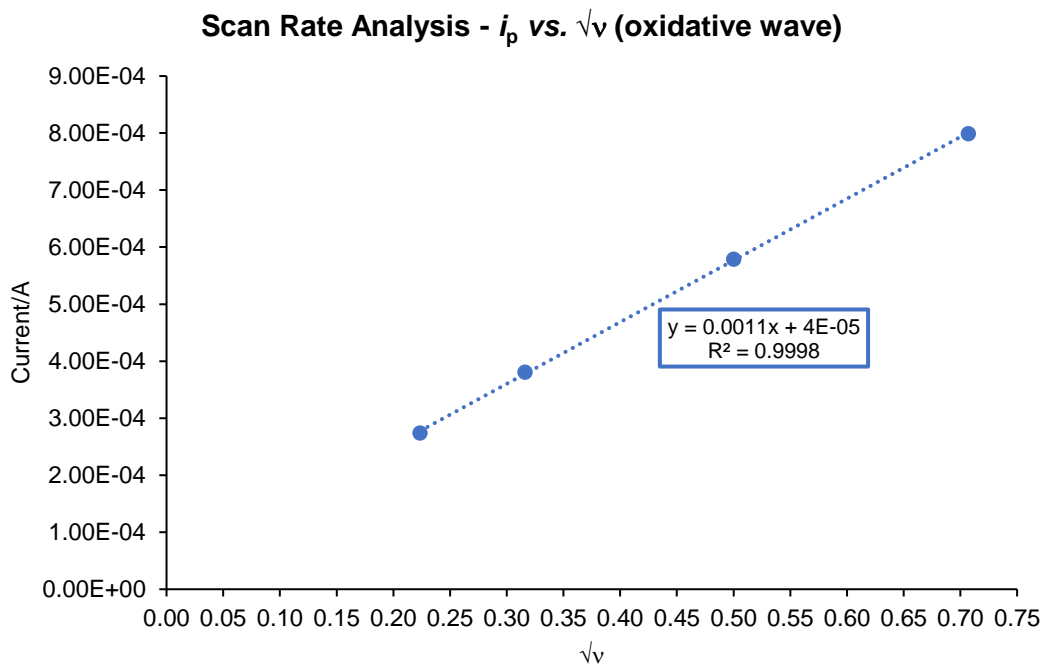


Figure 53: Analysis of the scan rates and plotting i_p vs. \sqrt{v} suggests that adsorption to the surface of the electrode is either non-existent or extremely facile for the oxidative wave of the Et₄NCl redox couple.

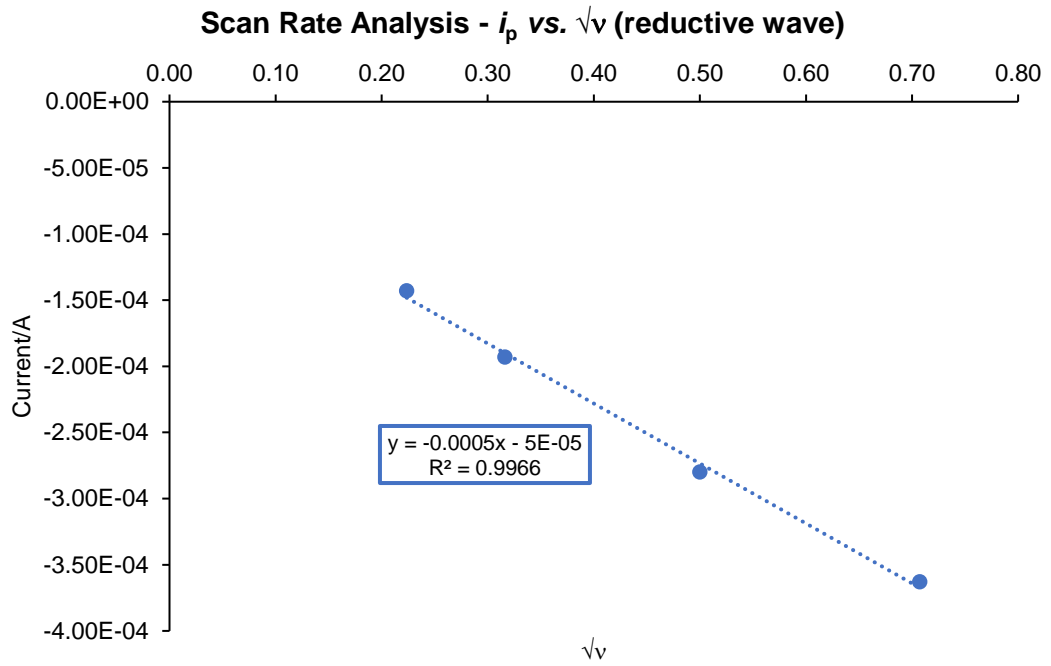


Figure 54: Analysis of the scan rates and plotting i_p vs. \sqrt{v} suggests that adsorption to the surface of the electrode is either non-existent or extremely facile for the reductive wave of the Et_4NCl redox couple.

A mixture of **199a** and HFIP was subjected to cyclic voltammetry. The CV displays a similar profile to that of **199a** by itself, but there appears to be a third oxidation event (**Figure 55**). All three oxidations occur at similar peak currents, suggesting that there is a minimum of three distinct species being oxidised in solution.

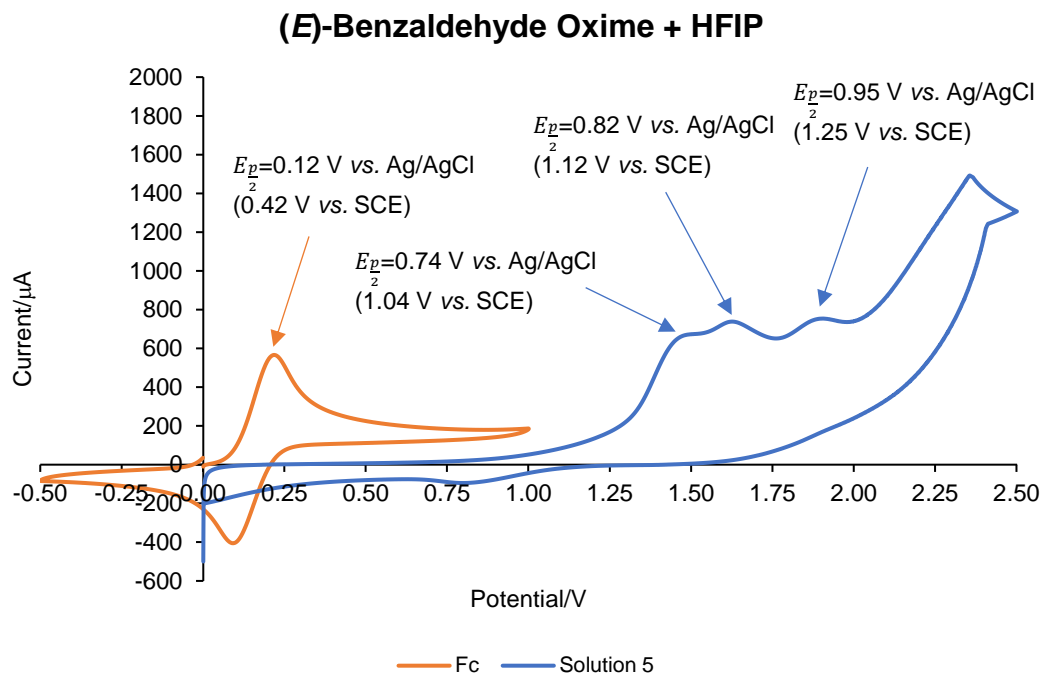


Figure 55: Cyclic voltammogram of a solution of (*E*)-benzaldehyde oxime and HFIP. Conditions: 10 mM ferrocene, 0.1 M Et₄NBF₄-MeCN, Pt chip electrode, 100 mV.s⁻¹; 10 mM **199a**, 13 mM HFIP, 0.1 M Et₄NBF₄-MeCN, Pt chip electrode, 100 mV.s⁻¹. HFIP = 1,1,1,3,3,3-hexafluoroisopropanol.

To determine the effect of the mediator on aldoxime **199a**, a cyclic voltammogram of a solution of **199a** and Et₄NCl (in the same stoichiometry as the reaction conditions, 0.5 eq.) was obtained (**Figure 56**). It shows a similar profile to both **Figure 44** and **Figure 55** in that three oxidation events are observed. One event (occurring at $E_{\frac{p}{2}} = 0.70$ V vs. SCE) is most likely to be the oxidation of the mediator as it occurs at a similar potential as Et₄NCl in **Figure 50** ($E_{\frac{p}{2}} = 0.70$ V vs. $E_{\frac{p}{2}} = 0.78$ V [vs. SCE]). The other two events correspond to oxidation of the aldoxime **199a**: an oxidation at $E_{\frac{p}{2}} = 1.14$ V (vs. SCE) and at $E_{\frac{p}{2}} = 1.34$ V (vs. SCE) are observed, both in line with the CV displayed in **Figure 44**. The CV in **Figure 56** is in line with the hypothesis that oxidation of the mediator occurs first. However, the CV suggests that the regeneration of chloride is slow and that it may not be catalytic in nature as there is no increased peak area when combining aldoxime and chloride. On the other hand, it does go some way to explain why, in the absence of mediator, the desired reaction still takes place. The CV clearly demonstrate that the aldoxime **199a** is electroactive and can be oxidised directly at the electrode.

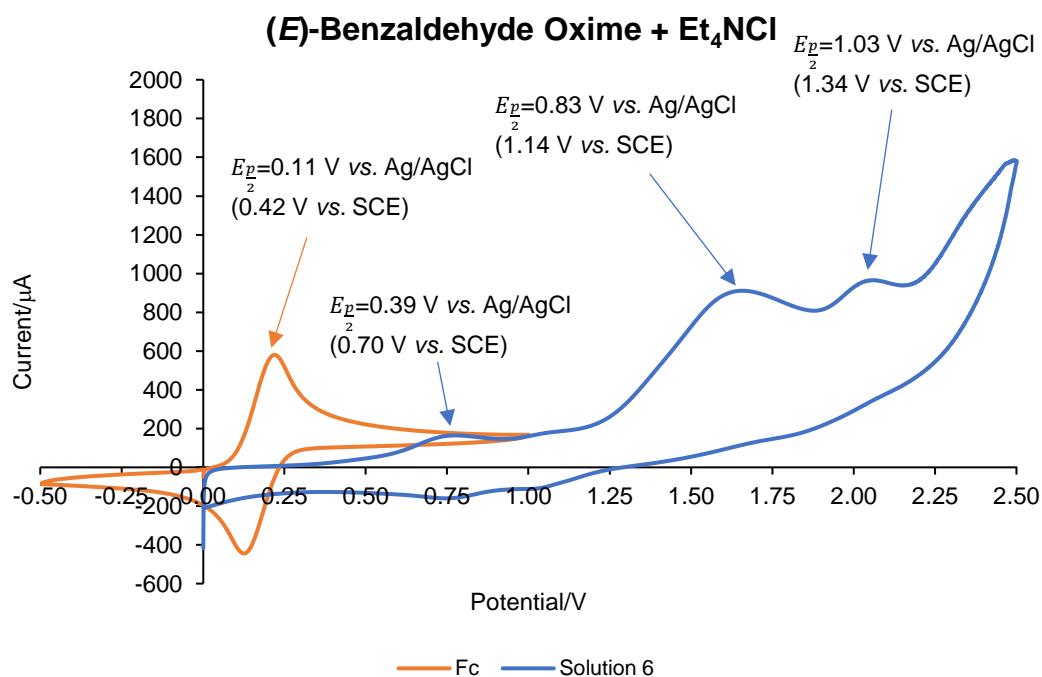


Figure 56: Cyclic voltammogram of a solution of (*E*)-benzaldehyde oxime and Et₄NCl. Conditions: 10 mM ferrocene, 0.1 M Et₄NBF₄-MeCN, Pt chip electrode, 100 mV.s⁻¹; 10 mM **199a**, 5 mM Et₄NCl, 0.1 M Et₄NBF₄-MeCN, Pt chip electrode, 100 mV.s⁻¹. The potential scale is referenced to the Ag/AgCl of the Pt chip.

Further cut-off experiments were performed on the solution of **199a** and Et₄NCl. Of interest was determining which oxidative peak the reductive peak at 1.10 V is associated with. **Figure 57** has the CVs of the cut-off experiments: the potential was reversed at 2.27 V, 2.00 V and 1.17 V. Similar to the CV of Et₄NCl, the reductive peak at 1.10 V can be associated with a species that is derived from subjecting the chloride mediator to highly oxidative conditions. Only when reversing the potential just after the chloride oxidation (at 1.17 V) does the reductive peak disappear.

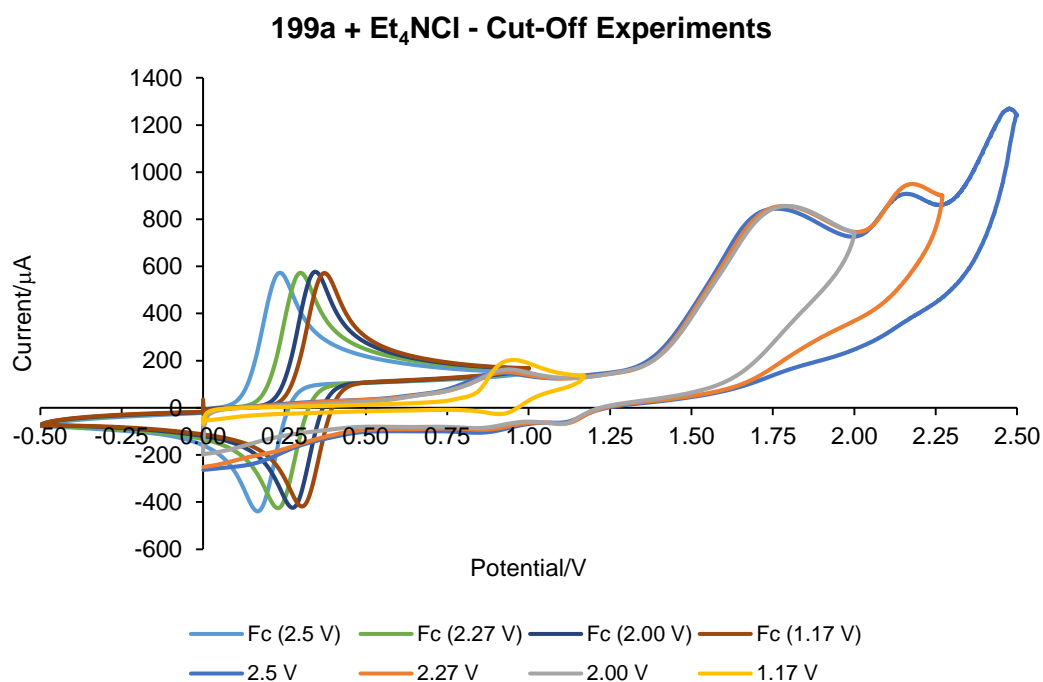


Figure 57: Cut-off CV experiments performed on a solution of **199a** and Et₄NCl to determine which oxidation the reductive peak at 1.10 V is associated with. Conditions: 10 mM ferrocene, 0.1 M Et₄NBF₄-MeCN, Pt chip electrode, 100 mV.s⁻¹; 10 mM **199a**, 5 mM Et₄NCl, 0.1 M Et₄NBF₄-MeCN, Pt chip electrode, 100 mV.s⁻¹. The potential scale is referenced to the Ag/AgCl of the Pt chip.

Varying the scan rate of the CV experiments was also conducted in order gain insight into the electrochemical behaviour of the mixture of **199a** and Et₄NCl; cyclic voltammetry was performed at 50, 100, 250, and 500 mV.s⁻¹. It is observed that the all oxidative events are likely to be electrochemically reversible as the peak potentials shift only very slightly (**Figure 58**).

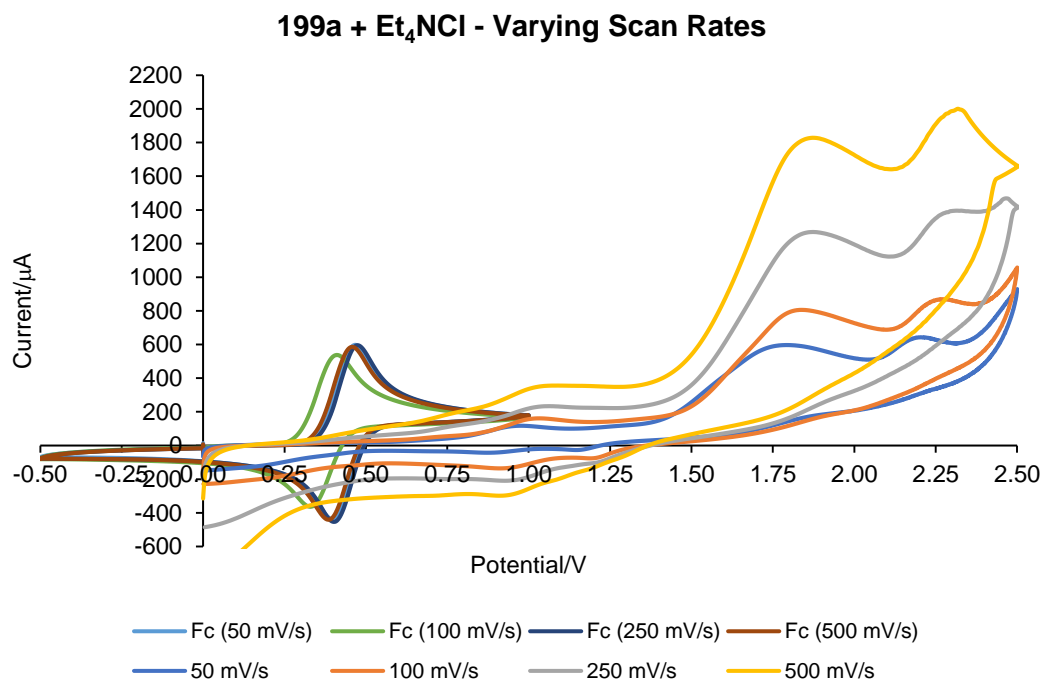


Figure 58: The cyclic voltammograms of a solution of **199a** and Et₄NCl at different scan rates. Conditions: 10 mM ferrocene, 0.1 M Et₄NBF₄-MeCN, Pt chip electrode, 100 mV.s⁻¹; 10 mM **199a**, 5 mM Et₄NCl, 0.1 M Et₄NBF₄-MeCN, Pt chip electrode, [v] mV.s⁻¹. The potential scale is referenced to the Ag/AgCl of the Pt chip.

A plot of the peak current (i_p) vs. square root of scan rate (\sqrt{v}) for each of the peaks observed all gave straight-lines which allows the assumption that the oxidations are all electrochemically reversible (**Figure 59**). The shape of the CVs can therefore be attributed to an irreversible chemical step that occurs after electron transfer.

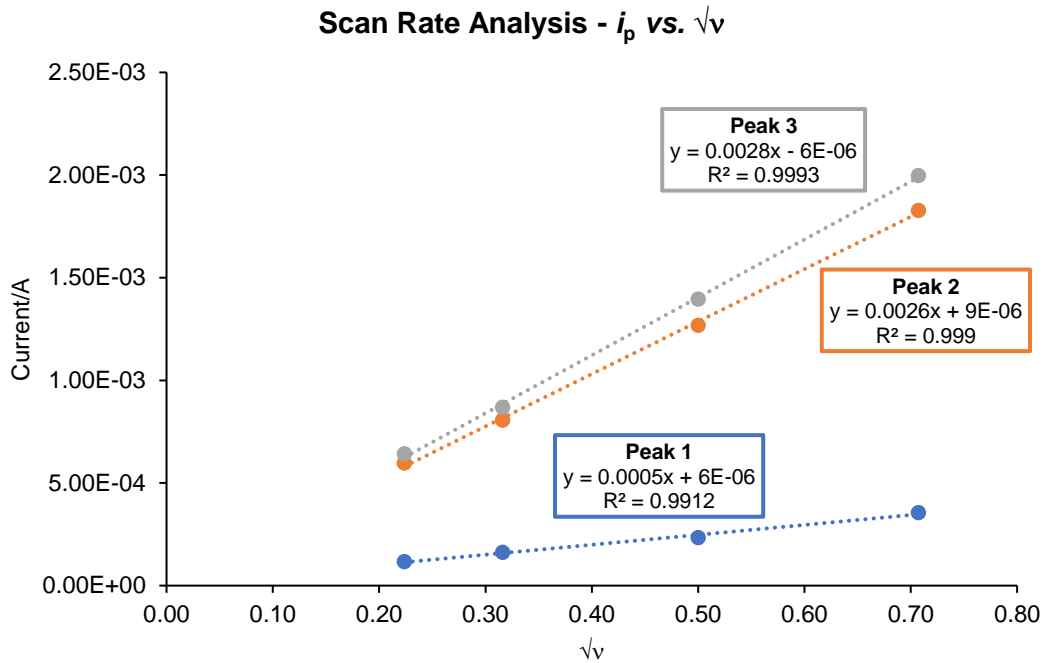


Figure 59: Analysis of the scan rates and plotting i_p vs. \sqrt{v} suggests that there is little adsorption or that adsorption is extremely facile. Peak 1 = blue; Peak 2 = orange; Peak 3 = grey.

Similarly, plotting peak potential (E_p) vs. log of the scan rate ($\log(v)$) also give straight-lines for all oxidative events (**Figure 60**). This suggests that adsorption/desorption at the electrode surface doesn't occur (i.e. electron transfer through solvent) or that it is extremely facile and has no detrimental effect on the electron transfer.

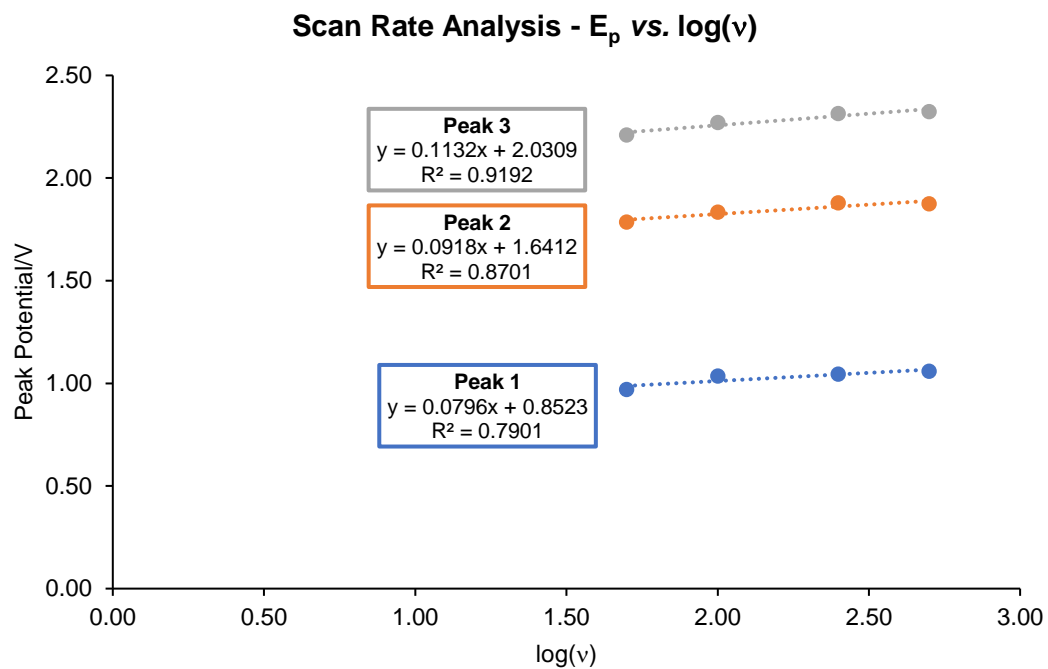


Figure 60: Analysis of the scan rates and plotting E_p vs. $\log(v)$ suggests that the electron transfers during the oxidations observed in the CV of a solution **199a** and Et_4NCl are reversible. Peak 1 = blue; Peak 2 = orange; Peak 3 = grey.

Analysis of the reaction mixture, using the same stoichiometry as for the optimised conditions, was conducted and the CV is shown in **Figure 61**. The profile has the same shape as in the previous cyclic voltammograms that have **199a** in the analyte mixture; three oxidation events are observed, one corresponding to the oxidation of mediator ($E_{p/2} = 0.62$ V vs. SCE) and two corresponding to the oxidation of **199a** ($E_{p/2} = 1.04$ V vs. SCE and $E_{p/2} = 1.24$ V vs. SCE).

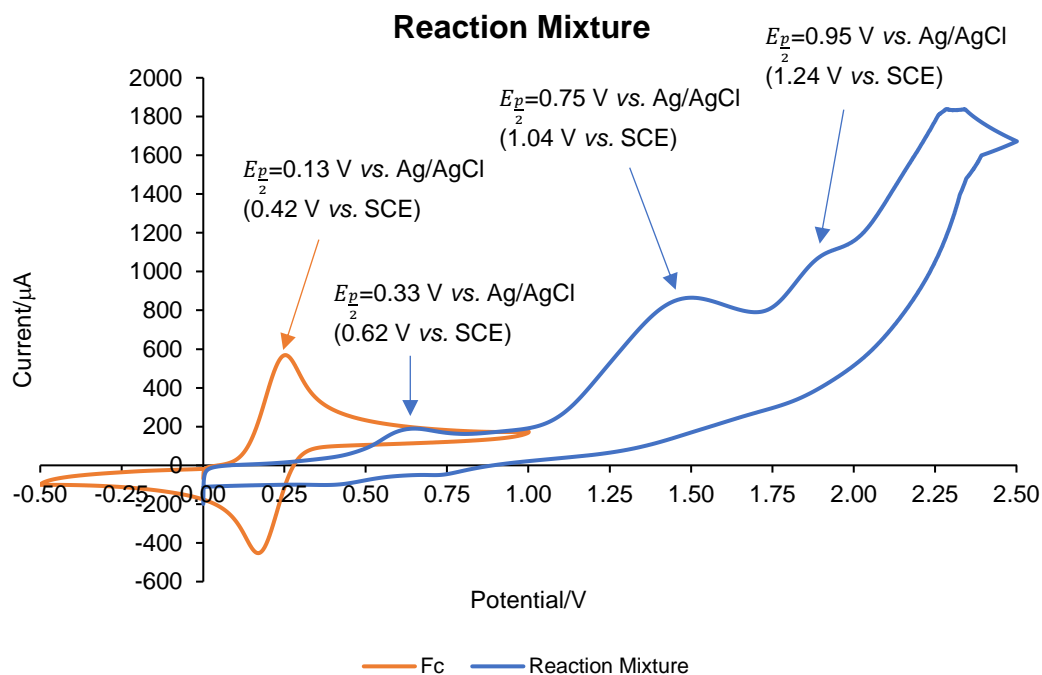


Figure 61: Cyclic voltammogram of a solution of reaction mixture. Conditions: 10 mM ferrocene, 0.1 M Et₄NBF₄-MeCN, Pt chip electrode, 100 mV.s⁻¹; 10 mM **199a**, 50 mM **222a**, 13 mM HFIP, 5 mM Et₄NCl, 0.1 M Et₄NBF₄-MeCN, Pt chip electrode, 100 mV.s⁻¹. HFIP = 1,1,1,3,3,3-hexafluoroisopropanol. The potential scale is referenced to the Ag/AgCl of the Pt chip.

All cyclic voltammograms of solutions that contain (*E*)-benzaldehyde oxime **199a** are examples of irreversible processes. Only those that contain Et₄NCl display some reversibility. The electrochemical behaviour of the reaction components supports a mechanism involving the oxidation of chloride, followed by a chlorination event.

Interestingly, a radical pathway cannot be fully discounted as the observed potentials during the electrochemical reaction between **199a** and **222a** are above the oxidation potentials of all components (as determined by CV experiments). This is shown in **Figure 62**: the potential displayed by the ElectraSyn was recorded alongside the potential displayed by a voltmeter that was attached directly to the electrodes. The

use of an external voltmeter would allow the comparison of observed potential difference (displayed by ElectroSyn) and actual potential difference (displayed by the voltmeter) between the working and counter electrodes. As can be seen in **Figure 62**, the potential at the anode (calculated by assuming half the potential difference is the potential at the anode) is above all components of the reaction. This suggests that not only is the reaction likely to be mediated by chloride oxidation, but direct oxidation of the aldoxime is highly probably, meaning that a radical pathway cannot not be fully ruled out.

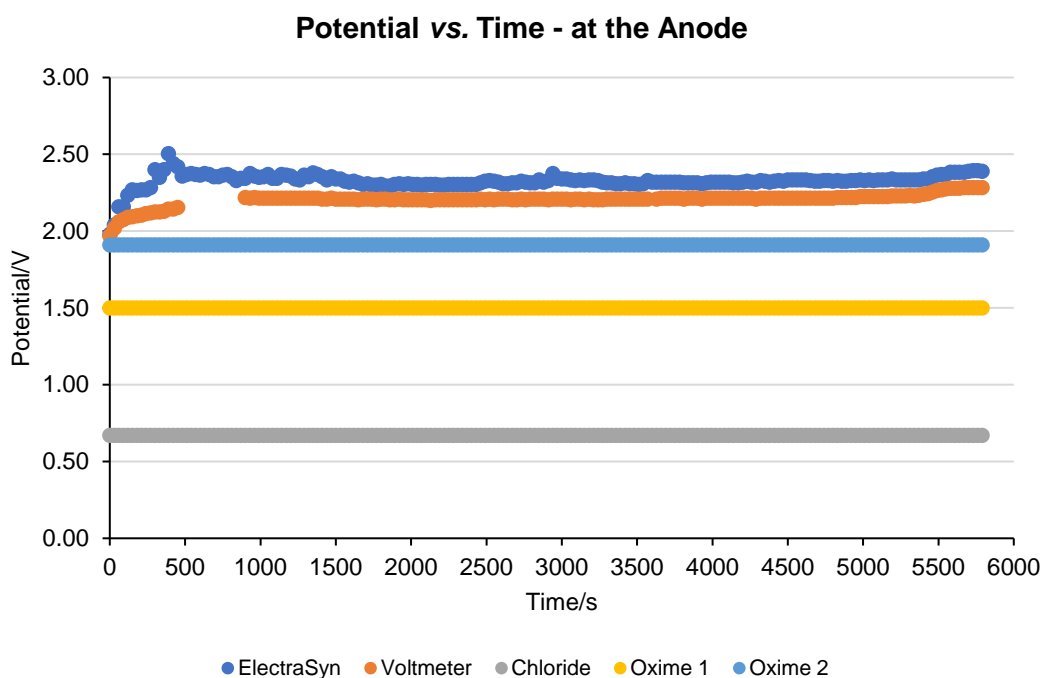
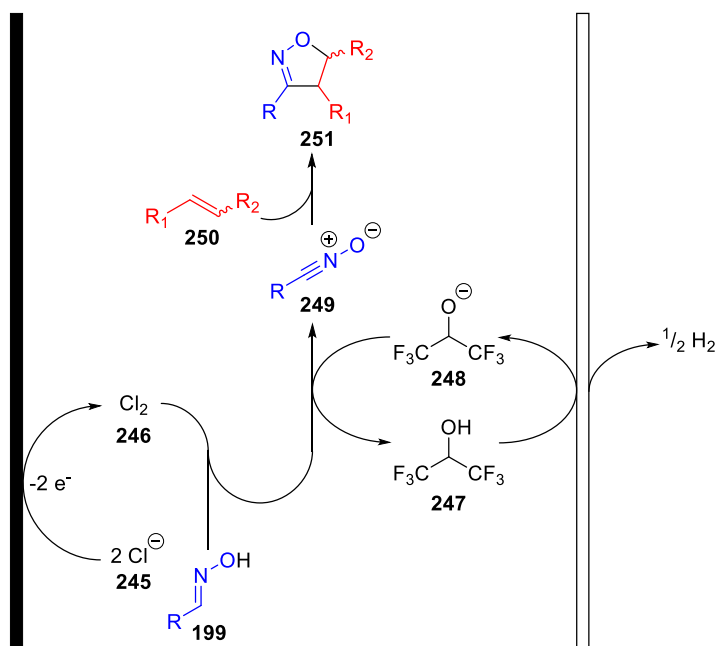


Figure 62: The observed (on the ElectroSyn) and actual (on the voltmeter) potential *versus* time shows that the potential at the anode is always above the potential of all reaction components, which means that a radical pathway cannot be discounted.

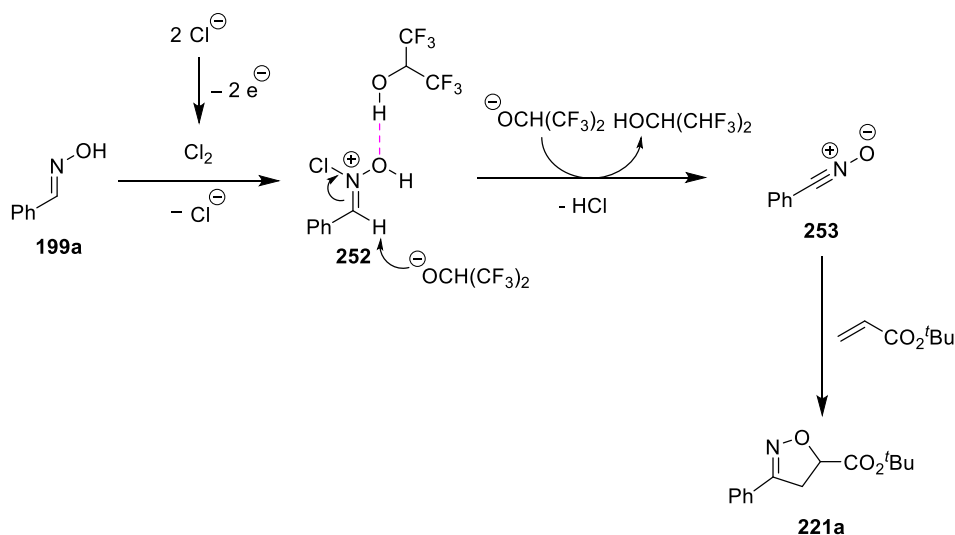
3.7. Revised Proposed Reaction Pathway

Following reaction profiling by ReactIR, ^1H NMR and cyclic voltammetry, the final proposed reaction pathway is shown in **Scheme 74**. This proposal is a combination of the reaction pathways alluded to above (Section 3.2.9). Two chloride anions **245** could undergo an oxidation event to generate chlorine **246** *in-situ*, which in combination with aldoxime **199** and subsequent oxidation events, furnish nitrile oxide **249**. The conjugate base could be formed from the reduction of HFIP at the cathode, producing hydrogen as a by-product. The nitrile oxide could then participate in 1,3-dipolar cycloaddition to give the desired substituted isoxazoline **251**.



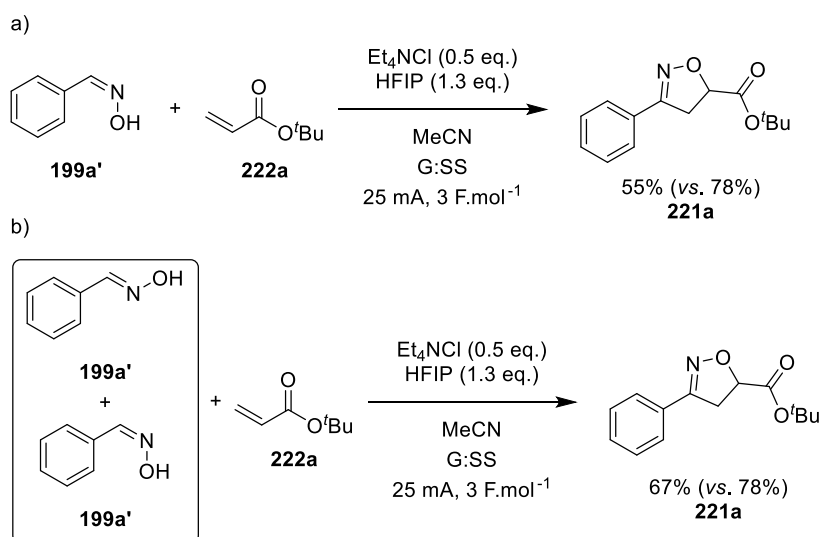
Scheme 74: Revised proposed reaction pathway, supported by control experiments, ReactIR profiling and ^1H NMR profiling.

A plausible reaction pathway leading to the formation of the nitrile oxide is shown in **Scheme 75**. As mentioned previously, oxidation of chloride ions could generate chlorine. Chlorination of the nitrogen, the most nucleophilic site on aldoxime **199a**, could give cationic species **252**. From species **252**, elimination of HCl and a proton (facilitated by the conjugate base of HFIP or direct reduction at the cathode) would give rise to the desired nitrile oxide that could participate in 1,3-dipolar cycloaddition with a dipolarophile. However, it is also true that an E1 elimination of chloride could also occur that could lead to the formation of a nitrile oxide; this would be independent of oxime stereochemistry.



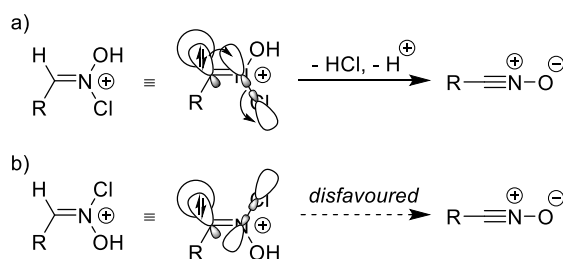
Scheme 75: The proposed pathway for the formation of the desired nitrile oxide intermediate for the electrochemically enabled 1,3-dipolar cycloaddition reaction.

The elimination pathway is supported by the control experiments shown in **Scheme 76**. Throughout the substrate scope detailed above, only the *E*-isomer of the aldoximes were subjected to the electrochemical conditions, with the geometric isomers having been separated by column chromatography. However, when employing (*Z*)-benzaldehyde oxime **199a'** as the nitrile oxide precursor, a diminished isolated yield of 55% of the desired isoxazoline was obtained (vs. 78%, **Scheme 76a**). Furthermore, electrolysing an equimolar amount of both geometric isomers of the aldoxime gave a moderately decreased isolated yield of 64% (vs. 78%, **Scheme 76b**).

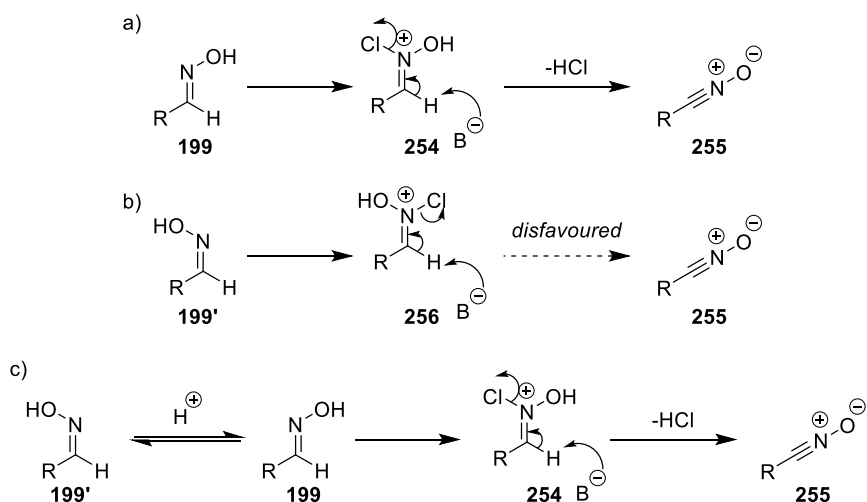


Scheme 76: Control experiments demonstrating the difference in reactivity between the geometric isomers of the aldoxime reaction partner.

Scheme 77 depicts an explanation for the difference in reactivity of the geometric isomers using molecular orbital theory. Bimolecular elimination (E2) reactions require an anti-periplanar arrangement of the groups that are being eliminated, i.e. there is a requirement for the correct orbital arrangement for elimination to take place. In the case of this reaction, the required arrangement to allow for the elimination of HCl means that the electrons from the C–H bond entering the N–Cl anti-bonding orbital. This would lead to weakening of the N–Cl bond during the elimination transition state and subsequent elimination can occur. When employing (*E*)-aldoximes (**199**, **Scheme 78a**), the anti-periplanar configuration required for elimination is satisfied upon chlorination of the nitrogen (**253**). However, the required configuration is not achieved when (*Z*)-aldoximes (**255**, **Scheme 78b**) are used. This necessitates the need for isomerisation from the *Z*-isomer to the *E*-isomer to occur in order for elimination to become favourable (**Scheme 78c**). It is known that, under acidic conditions, aldoximes can interconvert between geometric isomers.¹⁰⁵ It is therefore suggested that HFIP is acidic enough (pK_a 9.8 in DMSO) to facilitate the isomerisation event in order for elimination to occur. This isomerisation event is presumed to be slow and therefore a reaction in which a decrease in desired isoxazoline formation is observed. Although this isomerisation has not been observed, it is not unlikely that the isomerisation between geometric isomers is an equilibrium, such that only a very small proportion of *Z*-aldoxime is converted to the *E*-isomer; le Chatelier's principle dictates that as the *E*-isomer is consumed, more is formed from the isomerisation event, and so it is unlikely that any significant quantities of the *E*-isomer is observed in the reaction when employing *Z*-aldoxime. Alternatively, it is possible that, under a radical reaction pathway, the *Z*-aldoxime simply creates a higher barrier to nucleophilic radical attack.

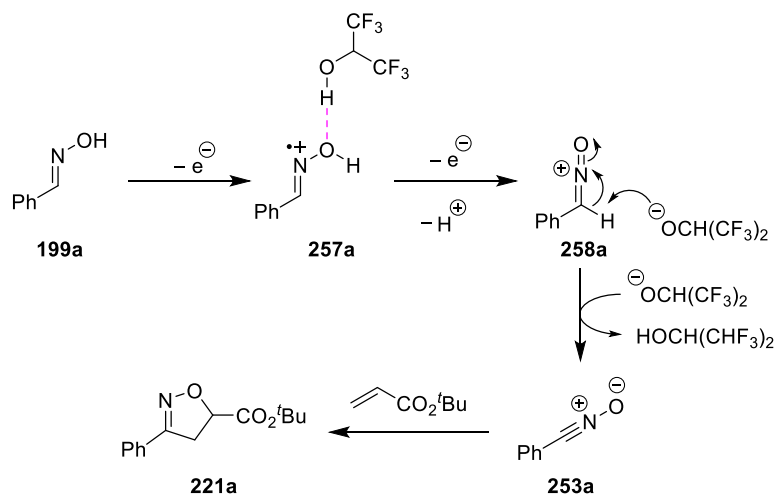


Scheme 77: For E2 elimination to occur, an anti-periplanar arrangement of leaving groups is required; this is satisfied by the (*E*)-aldoximes in the first instance.

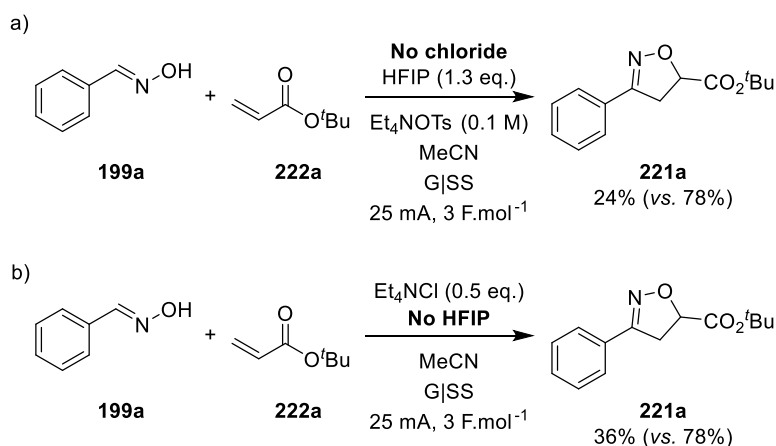


Scheme 78: In order for elimination to occur from (*Z*)-aldoximes, isomerisation to the (*E*)-isomer is required and hence the decrease in reactivity observed.

An alternative reaction mechanism involving a radical formation of the nitrile oxide (**Scheme 79**) is consistent with the control experiment in which, in the absence of chloride, the desired isoxazoline is obtained in 24% yield (**Scheme 80a**). This would suggest that direct oxidation of aldoxime could occur to give the hydroxyimoyl radical directly. It is possible that H-bonding with HFIP facilitates this direct oxidation mechanism as the oxidation potential of aldoxime **199a** was slightly lower in the presence of HFIP (*vide supra*). Furthermore, although HFIP is shown in the reaction pathway, it is not necessarily an integral part of the reaction but does increase the reaction efficiency. This is demonstrated by the control experiment which shows that, in the absence of HFIP, isoxazoline **221a** was isolated in 36% yield (**Scheme 80b**).



Scheme 79: An alternative radical pathway to the formation of the proposed nitrile oxide intermediate.



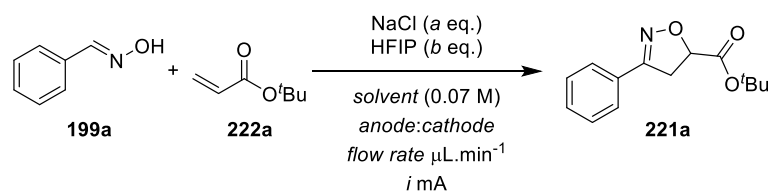
Scheme 80: Control experiments supporting the final proposed reaction pathway.

Both ReactIR and ¹H NMR profiling support the reaction pathway illustrated in **Scheme 74**. ReactIR shows pseudo-zero order reaction kinetics which is consistent with a surface-mediated reaction, as is expected of an electrochemical reaction due to the fast electron transfer as compared to the subsequent chemical steps. Moreover, both Hammett analysis and Swain-Lupton analysis of the electrochemical reaction suggests a 1,3-dipolar cycloaddition of a nitrile oxide, which is consistent with the proposed reaction pathway.

3.8. Flow Electrochemistry

Electrochemistry is inherently a green technology, possessing attributes such as lower energy costs and avoidance of toxic or expensive oxidants or reductants. However, one shortfall is the engineering requirements for scaling up electrochemistry. As it is a surface-mediated process, scaling up would require large reaction vessels with electrodes that have large surface areas. These parameters mean that scaling up an electrochemical procedure could prove to be expensive. It is possible to scale-out electrochemistry, with procedures making use of the carousel capabilities of the IKA ElectraSyn 2.0. However, an alternative to scaling-out in batch is scaling up in flow. Flow chemistry has many benefits including superior control over reactive intermediates. It would also provide a means to increase productivity of the electrochemical reaction.

The flow electrochemistry that will be described in this thesis was carried out in the Syrris FLUX electrochemical apparatus, with Syrris Asia pumps (see Experimental for further details). Optimisation of the flow electrochemical procedure was carried out using matrices of flow rates and currents (**Figure 63** - **Figure 67**), using the model substrates previously employed for the optimisation of the batch process (**Scheme 81**). Using matrices like those shown in **Figure 63** could allow a more expedient route to an optimised flow electrochemical reaction. The model substrates benzaldehyde oxime and *tert*-butyl acrylate were employed for the optimisation and monitored by LCMS and ¹H NMR with benzyl benzoate as external standard.



Scheme 81: The same model substrates used for the optimisation of the batch electrochemical process will be employed for the optimisation of flow procedure.

Optimisation was initiated by using the batch electrochemical conditions. The currents (*i*) and flow rates (FR) were chosen in order to limit the calculated charge transferred to $3 \text{ F}\cdot\text{mol}^{-1}$ across the diagonal (**Figure 63a**). This also means that the charge transferred increases towards the top right of the image and decreases towards the bottom left of the image. Starting with the diagonal, the batch solution was flowed through the electrochemical cell at the specified current and flow rate, with the ¹H

NMR yields shown in **Figure 63b** and mass balance (starting material + product ¹ **Figure 63c**. The NMR yields are of a 30 μL sample of the steady state flow stream, with benzyl benzoate added as an external standard; green represents the maximum NMR yield obtained (43%; FR = 118 $\mu\text{L}\cdot\text{min}^{-1}$, i = 30 mA, Q = 2.26 $\text{F}\cdot\text{mol}^{-1}$), while red represents the lowest NMR yield obtained (0%; FR = 74 $\mu\text{L}\cdot\text{min}^{-1}$, i = 50 mA, Q = 6.00 $\text{F}\cdot\text{mol}^{-1}$). First-pass full consumption of was not achieved under these conditions, with the best result providing a 2:1 ratio in favour of product and 27% NMR yield of starting material remaining (FR = 118 $\mu\text{L}\cdot\text{min}^{-1}$, i = 30 mA, Q = 2.26 $\text{F}\cdot\text{mol}^{-1}$; **Figure 63**).

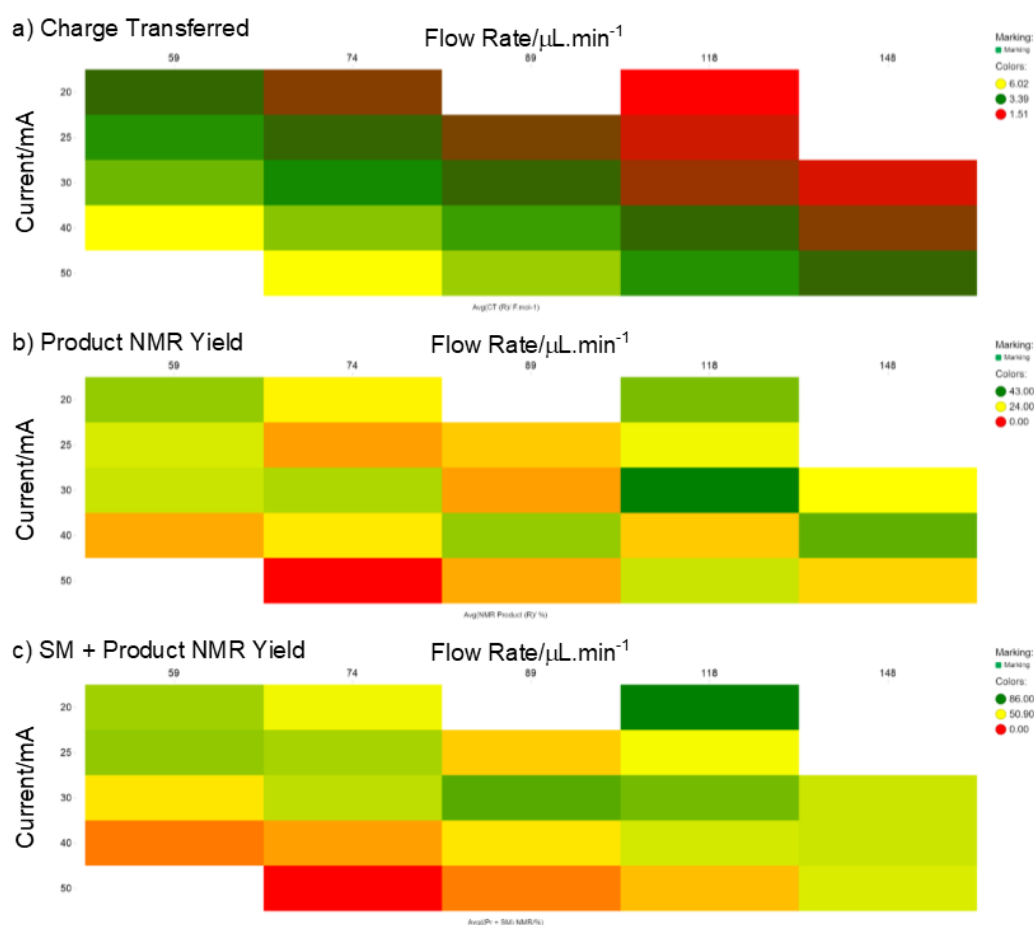


Figure 63: The initial results of the optimisation of the flow electrochemical procedure, using the batch conditions as a start point. Conditions: benzaldehyde oxime (1 eq.), *tert*-butyl acrylate (5 eq.), HFIP (1.3 eq.), Et_4NCl (0.5 eq.), MeCN (0.07 M), PVDF graphite anode, SS cathode, [flow rate], [current].

Moving on from the batch solution, it was decided that doubling the equivalents of mediator (from 0.5 eq. to 1 eq.) may provide a first-pass consumption of all starting material. As only around 50% yield was achieved, it could be that, under the flow conditions, the chloride mediator is no longer catalytic, and the flow reaction may

require a stoichiometric amount of mediator. To this end, an analogous solution, with 1 eq. mediator, was flowed through the electrochemical cell under the same conditions (**Figure 64**). Under these conditions, a 52% NMR yield (FR = 59 $\mu\text{L}\cdot\text{min}^{-1}$, $i = 20 \text{ mA}$, $Q = 3.01 \text{ F}\cdot\text{mol}^{-1}$, **Figure 64b**) of desired product was obtained, but only 12% starting material was observed, which is a two-fold improvement in consumption of starting material from the previous screen. Overall, this screen (with 1 eq. of mediator, **Figure 64**) provided better results, with the heat-map showing more green and yellow colours than in the heat-map from the standard batch conditions (**Figure 63**). However, a first-pass full consumption starting material was still not achieved.

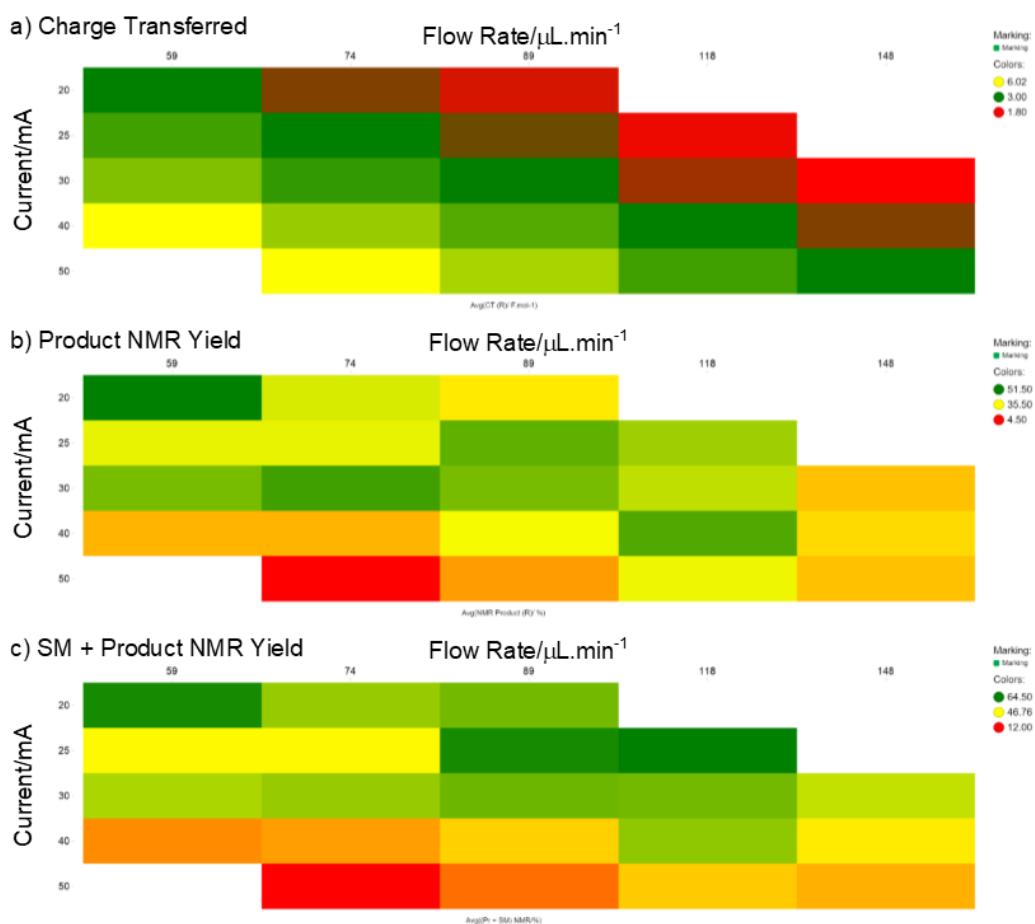


Figure 64: Exploration of higher loadings of mediator as part of the optimisation of the flow electrochemical procedure: Conditions: benzaldehyde oxime (1 eq.), *tert*-butyl acrylate (5 eq.), HFIP (1.3 eq.), Et₄NCl (1 eq.), MeCN (0.07 M), PVDF graphite anode, SS cathode, [flow rate], [current].

In an attempt to achieve full consumption on the first pass through the electrochemical cell, another solution with 1.4 equivalents (or 0.1 M) of mediator was flowed through the electrochemical cell. Alternative currents and flow rates were also investigated

with this solution and the results are presented in **Figure 65**. From previous results, it seemed likely that a slower flow rate may increase the efficiency of the reaction, and so exploration of flow rates below $59 \mu\text{L}\cdot\text{min}^{-1}$, as well as slightly above, was conducted. Again, flow rates were determined by the desired currents and calculated charge transferred, such that the diagonal of the matrices is $3.00 \text{ F}\cdot\text{mol}^{-1}$. It is clear to see that flow rates and currents that transfer a charge of greater than $7 \text{ F}\cdot\text{mol}^{-1}$ had a large detrimental effect on the outcome of the reaction (bottom left corner, **Figure 65b**). However, the best result was achieved with a flow rate of $44 \mu\text{L}\cdot\text{min}^{-1}$, current of 30 mA and $Q = 6.06 \text{ F}\cdot\text{mol}^{-1}$, giving an NMR yield of desired isoxazoline of 52% and no starting material was observed. Although, first-pass consumption of starting material was achieved, only a moderate yield of desired product was obtained, as well as a moderate mass balance (57%). This suggests that there are likely other processes occurring, impacting the formation of the product. This result was achieved with transferring a charge of $6.06 \text{ F}\cdot\text{mol}^{-1}$, over twice that which is transferred in the batch reaction and three times more than the theoretical amount of charge needed. It is possible this extra amount of charge could lead to polymerisation of starting materials which would severely impact the formation of desired product. For this reason, it was decided that 1 eq. of mediator was sufficient for the reaction and was used for further exploration of flow electrochemical conditions.

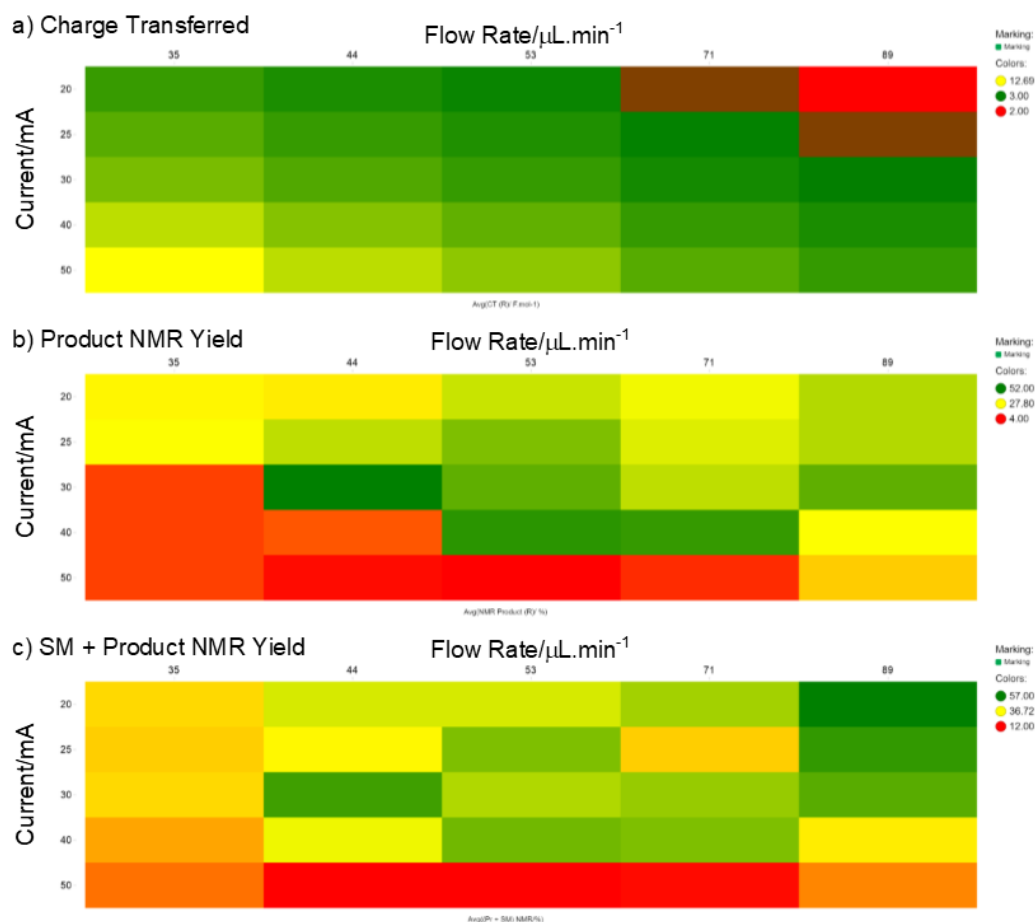


Figure 65: Exploration of slower flow rates and higher loadings of mediator as part of the optimisation of the flow electrochemical procedure: Conditions: benzaldehyde oxime (1 eq.), *tert*-butyl acrylate (5 eq.), HFIP (1.3 eq.), Et₄NCl (1.4 eq.), MeCN (0.07 M), PVDF graphite anode, SS cathode, [flow rate], [current].

An electrode combination of graphite anode and stainless-steel cathode had been used up to this point, similar to the batch electrochemical conditions in the IKA ElectraSyn 2.0. However, the graphite anode for the electrochemical flow cell is made from a polymeric material with graphite embedded in the polymer; there are two commercially available polymeric materials, PVDF (poly(vinylidene fluoride)) and PPS (polyphenylene sulfide). The PVDF graphite anode had been employed thus far. Further optimisation of the reaction required an exploration of the most suitable electrode combination, with both PVDF and PPS graphite anodes investigated in combination with either stainless-steel (SS) or platinum (Pt) cathodes. Specific flow rates and currents were chosen for the exploration of electrode materials, with results of the G (PPS):SS screen shown in **Figure 66**. Flow rates and currents were chosen as a mixture of the best results so far and repeats to give a diverse conditions space to investigate. It was found that the highest NMR yield obtained was 44% (FR = 74

$\mu\text{L}\cdot\text{min}^{-1}$, $i = 25 \text{ mA}$, $Q = 3.00 \text{ F}\cdot\text{mol}^{-1}$, **Figure 66b**), with 18% starting material remaining. Comparing this result to the analogous result from the previous screen with a PVDF graphite electrode (37%, **Figure 64b**), a 7% improvement in NMR yield is observed, as well as a marked improvement in mass balance (67% vs. 47%). However, when employing an electrode combination of PPS graphite anode and Pt cathode, the highest NMR yield and mass balance was achieved: 66% and 84%, respectively (FR = $95 \mu\text{L}\cdot\text{min}^{-1}$, $i = 30 \text{ mA}$, $Q = 2.80 \text{ F}\cdot\text{mol}^{-1}$, **Figure 67b**). This result did not give full consumption of starting material on first-time pass as 19% remaining benzaldehyde oxime was observed in the NMR sample. A direct comparison of the results at a flow rate of $74 \mu\text{L}\cdot\text{min}^{-1}$, applying a current of 25 mA and transferring a charge of $3.60 \text{ F}\cdot\text{mol}^{-1}$, shows that there is significant difference in NMR yield obtained (29%, SS vs. 55%, Pt).

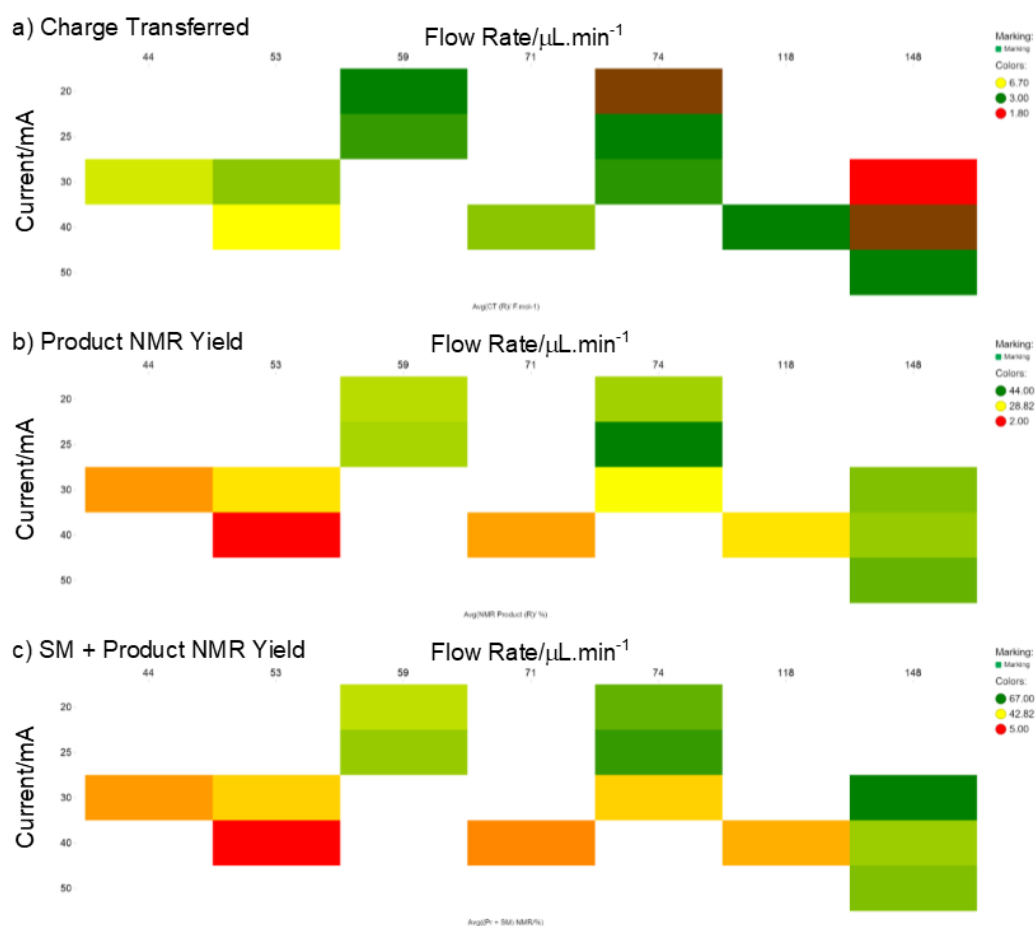


Figure 66: Exploration of PPS graphite anode and stainless-steel cathode electrode combination as part of the optimisation of the flow electrochemical procedure: Conditions: benzaldehyde oxime (1 eq.), *tert*-butyl acrylate (5 eq.), HFIP (1.3 eq.), Et₄NCl (1 eq.), MeCN (0.07 M), PPS graphite anode, SS cathode, [flow rate], [current].

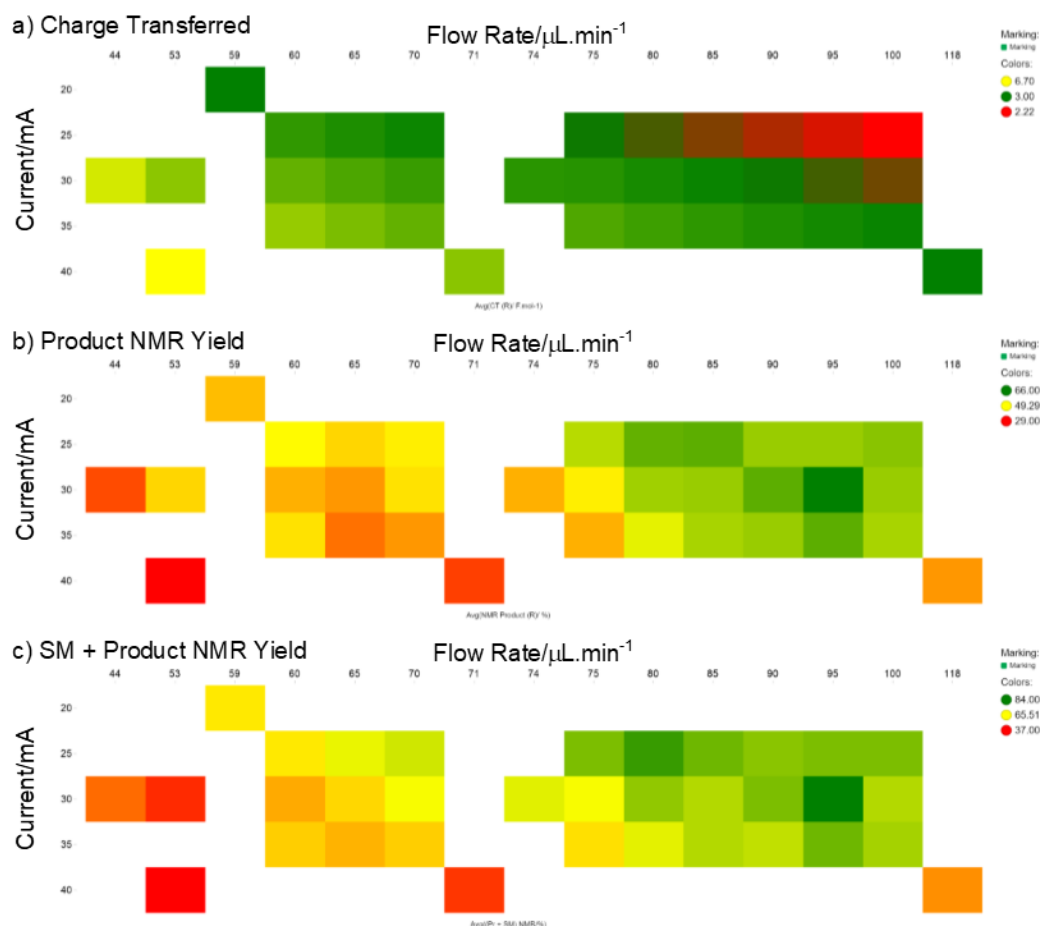
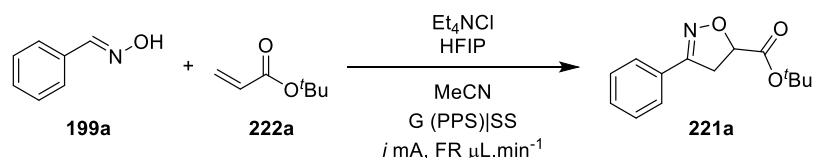


Figure 67: Exploration of PPS graphite anode and platinum cathode electrode combination as part of the optimisation of the flow electrochemical procedure: Conditions: benzaldehyde oxime (1 eq.), *tert*-butyl acrylate (5 eq.), HFIP (1.3 eq.), Et_4NCl (1 eq.), MeCN (0.07 M), PPS graphite anode, Pt cathode, [flow rate], [current].

Having still not achieved full consumption of starting aldoxime after the first pass through the electrochemical cell, attention was turned to exploring changes to the reaction conditions (dipolarophile equivalents, mediator equivalents and solvents). The results of this screen are shown in **Table 19**, where each solution was flowed at $53 \mu\text{L}\cdot\text{min}^{-1}$ at 30 mA. It was found that the dipolarophile equivalents could be decreased to 2.5 equivalents (39%, Entry 4 vs. 31%, Entry 2) with a marginal increase in NMR yield, but further decrease to 1.25 equivalents proved to be detrimental (24%, Entry 5 vs. 31%, Entry 2). Furthermore, removing HFIP from the reaction mixture almost completely shuts down the reaction with less than 10% NMR yield of desired observed (8%, Entry 6 and 5%, Entry 7 vs. 31%, Entry 2). Switching solvents to MeOH, and in the absence of HFIP, the reaction proceeds in a similar manner to the original solution (37%, Entry 8 vs. 31%, Entry 2), but decreasing the equivalents of

dipolarophile still proved to be detrimental (26%, Entry 9 vs. 31%, Entry 2). Using 1.2 equivalents of mediator, but otherwise identical conditions to Entry 2, a modest increase in NMR yield is observed (44%, Entry 10 vs. 31%, Entry 2).



Entry	222a eq.	Et ₄ NCl eq.	HFIP eq.	<i>i</i> / mA	FR/ μL.min ⁻¹	Q/ F.mol ⁻¹	221a/ % ^a	(199a+ 221a)/ % ^a
1 ^b	5	0.5	1.3	30	59	4.52	28	46
2 ^c	5	1	1.3	30	53	5.03	31	39
3 ^d	5	1.4	1.3	30	53	5.03	43	43
4	2.5	1	1.3	30	53	5.03	39	54
5	1.25	1	1.3	30	53	5.03	24	40
6	2.5	1	0	30	5.03	8	22	
7	1.25	1	0	30	53	5.03	5	17
8 ^e	2.5	1	0	30	53	5.03	37	41
9 ^e	1.25	1	0	30	53	5.03	26	30
10 ^f	5	1.2	1.3	30	80	3.33	44	61

Table 19: Exploration of dipolarophile equivalents, mediator equivalents and solvent. ^a1H NMR yield using benzyl benzoate as external standard; ^bG (PVDF):SS electrode combination used; ^cG (PPS):Pt electrode combination used; ^dG (PVDF):SS electrode combination used; ^eMeOH used as solvent; ^fG (PPS):Pt electrode combination used. G = graphite; PPS = polyphenylene sulfide; PVDF = poly(vinylidene fluoride); SS = stainless-steel; HFIP = 1,1,1,3,3,3-hexafluoroisopropanol; *i* = current; FR = flow rate; Q = charge transferred.

To test the apparent superiority of platinum as the cathodic material, two isolation experiments were conducted, with the progress of the reaction followed by ¹H NMR (using benzyl benzoate as external standard). The experiments were conducted at 53 μL.min⁻¹ at 30 mA, transferring a charge of 5.02 F.mol⁻¹, (Experiment 1, **Figure 68**) and 74 μL.min⁻¹ at 30 mA, transferring a charge of 3.60 F.mol⁻¹, (Experiment 2, **Figure 68**), taking in-stream samples every 20 minutes to assess the progress of the reaction. The experiments were conducted from the same batch of pre-prepared reaction solution and flowed the length of time required for 7 mL of electrolysed solution to be collected (or 0.5 mmol had been electrolysed, matching the isolated batch experiments). The results are shown in **Figure 68**, and it is shown that the faster flow rate provides a reaction that is more consistent between sampling. The slower flow

rate shows a decrease in efficiency the longer the reaction is allowed to continue. From these experiments, an isolated yield of 25% was achieved from Experiment 1 and 49% from Experiment 2, reflecting the NMR data that was collected during the reaction.

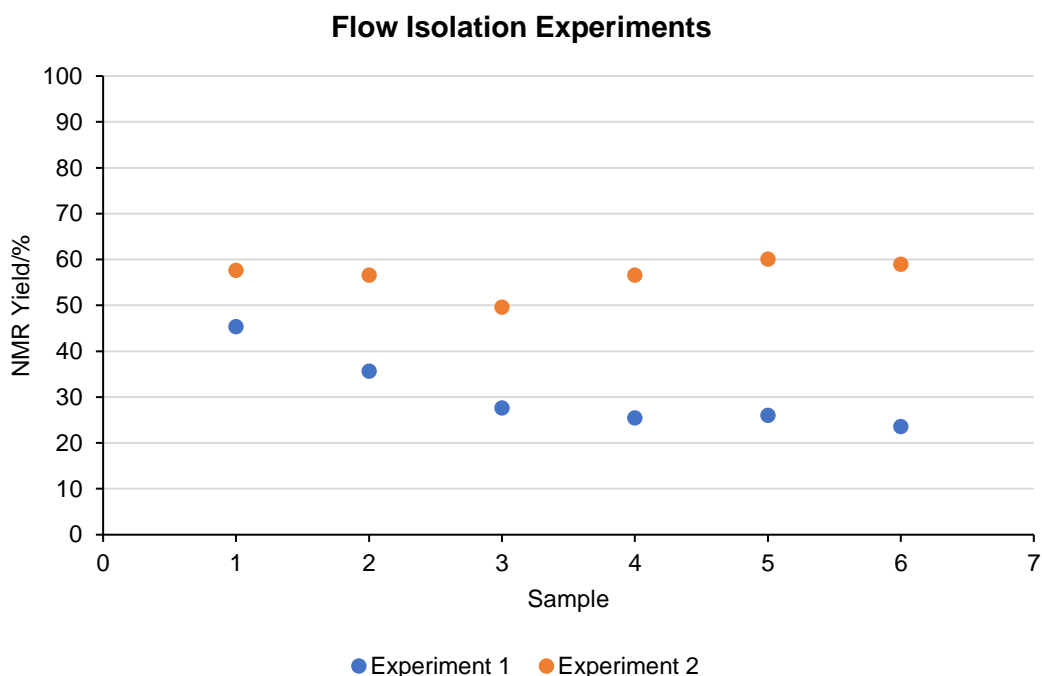


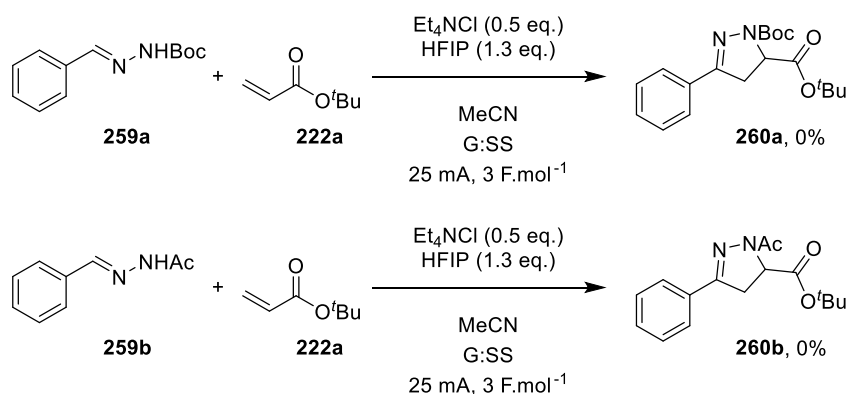
Figure 68: Flow isolation experiments to explore the superiority of platinum as the cathodic material. **Experiment 1 Conditions:** **199a** (1 eq.), **222a** (5 eq.), HFIP (1.3 eq.), Et₄NCl (1 eq.), G PPS anode, Pt cathode, 53 $\mu\text{L}\cdot\text{min}^{-1}$, 30 mA, 132 minutes flow time (7 mL final volume); **Experiment 2 Conditions:** **199a** (1 eq.), **222a** (5 eq.), HFIP (1.3 eq.), Et₄NCl (1 eq.), G PPS anode, Pt cathode, 74 $\mu\text{L}\cdot\text{min}^{-1}$, 30 mA, 95 minutes flow time (7 mL final volume).

To summarise, the adaption of the batch electrochemical reaction into a flow electrochemical setting has been carried out. Following partial optimisation of stoichiometry of reactants, flow rate and current, an isolated yield of 49% was achieved. However, this is not a fully optimised reaction as full consumption of starting material has not been successfully achieved. Further optimisation is required to achieve first-pass consumption of starting material and improve the isolated yield to at least the same as the batch process. Despite this, the work carried out so far has served to demonstrate that it is possible to adapt the batch reaction to a flow process.

3.9. Pyrazoline Synthesis and One-Pot Chemistry

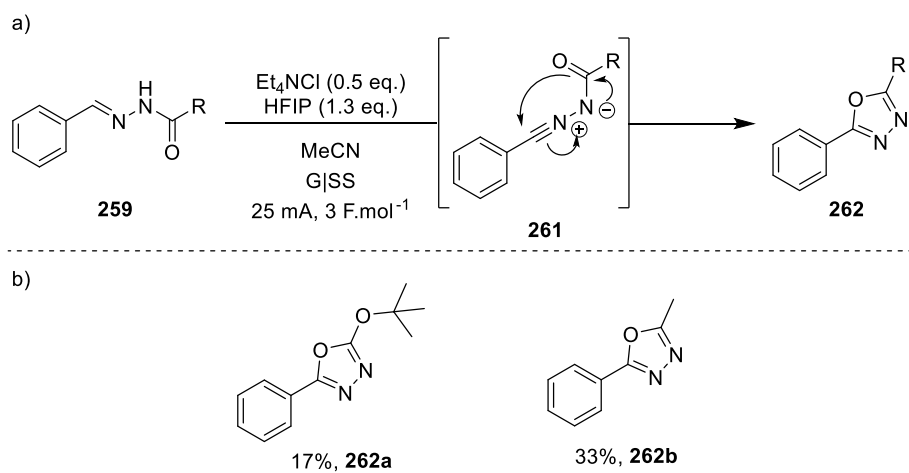
3.10.1. Attempted Pyrazoline Synthesis

Attempts were made to synthesise pyrazolines **260** from protected hydrazones **259**. (**Scheme 82**). Under the same electrochemical conditions used for the isoxazoline synthesis, the desired pyrazoline was not observed. However, it was found that hydrazones protected with carbonyl-containing protecting groups, for example Boc or acetyl, gave oxadiazoles (**Scheme 83**). This is likely to occur through an electrochemically generated nitrile imine (**259**, **Scheme 83a**), which could undergo an intramolecular rearrangement to give the oxadiazole (**Scheme 83a**).



Scheme 82: Attempted pyrazoline synthesis from protected hydrazones under identical electrochemical conditions for isoxazoline synthesis.

Subjecting hydrazones **259a** and **259b** to the electrochemical procedure, in the absence of dipolarophile, oxadiazoles **262a** and **262b** were isolated in 17% and 33%, respectively (**Scheme 83b**). Although these are low yields, they are also unoptimised and are promising results demonstrating that with further optimisation, a viable alternative to oxadiazole synthesis could be realised.



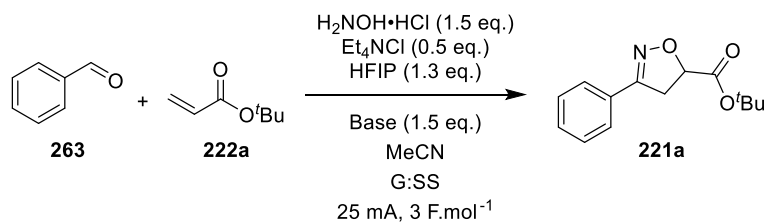
Scheme 83: Oxadiazole synthesis under electrochemical conditions developed for isoxazoline synthesis, in the absence of dipolarophile.

3.10.2. One-Pot Synthesis from Aldehydes

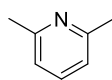
It can be envisioned that the electrochemical synthesis of isoxazolines could be more expedient if a one-pot procedure could be developed. Eliminating the initial need for a condensation reaction for the formation of the oximes would mean that the reaction time from aldehyde to isoxazoline would only be as long as the electrochemical reaction itself.

At first identical conditions as the optimised electrochemical procedure were tested, with the aldehyde and hydroxylamine added in place of aldoxime. This gave an isolated yield of 23% of desired isoxazoline (Entry 1, **Table 20**). A solvent switch to MeOH gave no reaction (Entry 2). Additional base was hypothesised to be beneficial for the formation of the aldoxime. Both 2,6-lutidine and DBU bases were explored, in combination with both MeCN and MeOH solvents; only a combination of 2,6-lutidine and MeCN gave a reasonable isolated yield of 25% (Entry 3), with the other combinations giving markedly lower yields or no reaction.

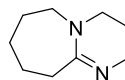
These results serve as a proof of concept for the one-pot procedure, with optimisation still required to give an isolated yield in the same region as the optimised electrochemical procedure. Other bases could be explored such as an inorganic base or alternative organic bases.



Entry	Base	Solvent	221a/%
1	-	MeCN	23
2	-	MeOH	-
3	264	MeCN	25
4	264	MeOH	12
5	265	MeCN	3
6	265	MeOH	-



264



265

Table 20: Conditions: **263** (0.5 mmol), **222a** (5 eq.), $\text{H}_2\text{NOH}\cdot\text{HCl}$ (1.5 eq.), Et_4NCl (1.3 eq.), HFIP (1.3 eq.), base (1.5 eq.), solvent (0.07 M), G anode, SS cathode, 25 mA, 3 $\text{F}\cdot\text{mol}^{-1}$. HFIP = 1,1,1,3,3,3-hexafluoroisopropanol; G = graphite; SS = stainless-steel.

4. Conclusion

In conclusion, the optimisation of the electrochemically enabled 1,3-dipolar cycloaddition between an aldoxime and an alkenyl dipolarophile was successfully carried out. Having started with an isolated yield of 41% for the synthesis of *tert*-butyl 3-phenyl-4,5-dihydroisoxazole-5-carboxylate **221a**, an improved reaction profile and yield were achieved with **221a** isolated in a good 78% yield. Optimisation of the reaction involved thorough screening of electrode material, mediator, solvent and charge transferred (i.e. electrolysis time). Furthermore, the electrochemical procedure was found to accommodate a range of functional groups, including halides and ester groups, providing 45 examples of substituted isoxazolines in up to 86% isolated yield. Of particular note, cyclohexyl, isopropyl and cyclopropyl aldoximes were successfully converted to the corresponding isoxazolines in moderate to good yields. These results demonstrate the capability of this methodology to compliment those methods already published, allowing the synthesis and utility of alkyl derived aldoximes which had previously proven to be elusive.

The electrochemical cycloaddition reaction was found to be robust and can withstand minor changes in stir speed, mediator equivalents and dipolarophile equivalents. This was explored using a statistical Design of Experiments (DoE) in which a three-factor full-factorial design was employed. A full factorial design allowed for the deconvolution of the interactions between the factors and the effects of the factors on the outcome of the reaction. It was found that stir speed had negligible effect on the reaction outcome, while increasing the loading of mediator was detrimental to the conversion to the desired isoxazoline. Conversely, increasing the equivalents of dipolarophile had a positive effect on the reaction progression. Although not explored by DoE, it was found that the optimised conditions can also withstand minor changes in charge transferred (electrolysis time) to some extent.

Furthermore, unexpected diastereoselectivity was observed when employing either dimethyl maleate **203** or dimethyl fumarate **208** as dipolarophiles: a diastereomeric ratio of 9:1 in favour of the *anti*-configured substituted isoxazoline was achieved. This contrasts with the theory that was discussed in Section 1.2.5. in which it was predicted that *cis*-alkenes should give the *syn*-configured isoxazolines, while *trans*-alkenes should give almost exclusively the *anti*-configured product. The major diastereoisomer was shown to be the *anti*-configuration and evidence for this was

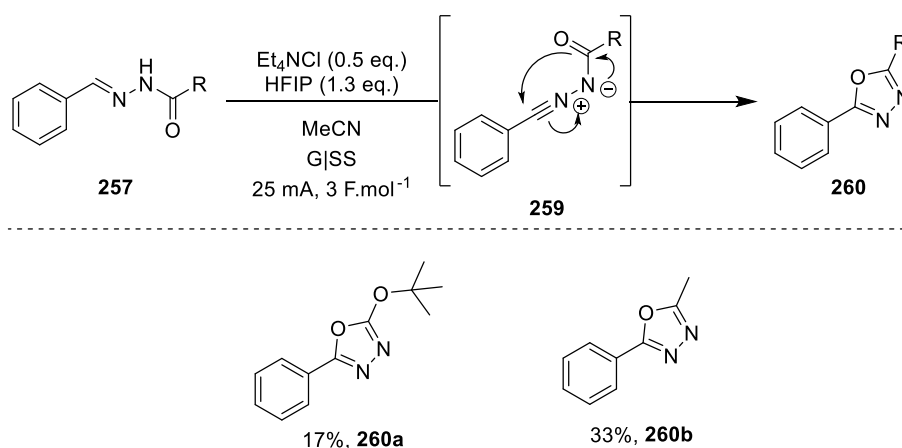
supplied by the J -couplings observed in the ^1H NMR spectra. Further exploration of this observed diastereoselectivity, with ^1H NMR reaction profiling and synthesis of products *via* non-electrochemical means, has led to the hypothesis that 1,2-disubstituted acrylates react *via* an alternative mechanism. However, all the experiments conducted under a range of conditions have still made it challenging to fully deconvolute the true source of the unexpected diastereoselectivity.

ReactIR proved to be a powerful tool for probing the electrochemical reaction between benzaldehyde oxime and *tert*-butyl acrylate. Comparison between the IR profile of a non-electrochemical 1,3-dipolar cycloaddition reaction and the electrochemical 1,3-dipolar cycloaddition reaction developed herein, allowed the observation that the electrochemical reaction proceeds under pseudo-first order reaction kinetics, such that the assumption that the electron transfer is not rate-limiting can be made. This result is consistent with a surface-mediated reaction, as would be expected of an electrochemical reaction. Furthermore, this reaction profiling by ReactIR has demonstrated the ability to probe an electrochemical reaction *in-situ*, without any complications.

Additional reaction profiling was conducted using ^1H NMR. Maximum rate analysis of the reaction between *para*-substituted benzaldehyde oximes and *tert*-butyl acrylate was carried out, providing sufficient data to conduct both Hammett and Swain-Lupton analyses. Both analyses gave an inverse V-shaped plot, which is indicative of a 1,3-dipolar cycloaddition of nitrile oxides. A change in rate-limiting step (or electronic contributions) is consistent with a change in interacting frontier molecular orbitals; nitrile oxides are ambiphilic dipoles and can interact through a $\text{HOMO}_{\text{dipole}}-\text{LUMO}_{\text{dipolarophile}}$ or $\text{LUMO}_{\text{dipole}}-\text{HOMO}_{\text{dipolarophile}}$ interaction, depending on the relative energies of the specific reaction. The change in the electronic contributions is therefore suggestive of the switch in interacting frontier molecular orbitals. The Hammett and Swain-Lupton analysis, in combination with control experiments, point to a reaction pathway involving a chlorination event, followed by elimination of HCl to give a nitrile oxide; subsequent 1,3-dipolar cycloaddition with a dipolarophile is then thought to occur.

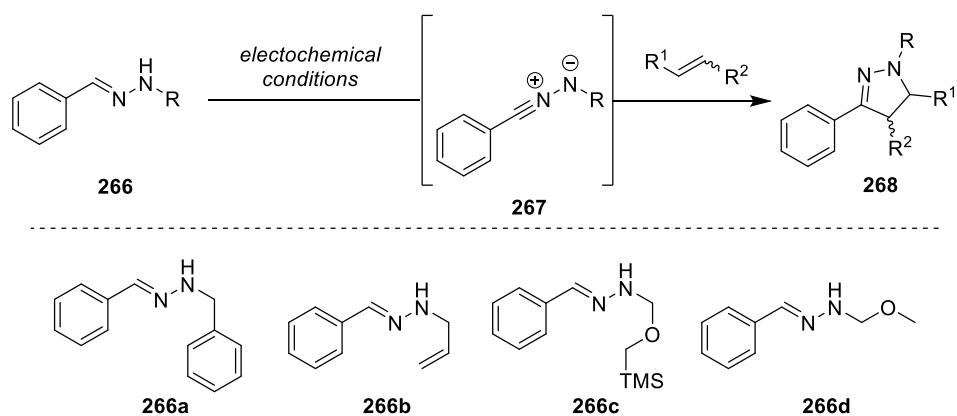
5. Future Work

In the future, development of an electrochemical methodology for the synthesis of oxadiazoles would be of benefit to the chemical community. During this investigation, it was found that hydrazones protected with protecting groups containing carbonyl functionalities exclusively gave oxadiazoles when subjected to the electrochemical conditions. Boc-protected hydrazone **259a** gave oxadiazole **262a** in 17% isolated yield, while oxadiazole **262b** was furnished from acetyl-protected hydrazone **259b** in 33% yield (**Scheme 84**). These are unoptimised results and with careful consideration of reaction conditions and substrates, it is possible this could provide a greener and inexpensive entry into oxadiazoles.



Scheme 84: Oxadiazole synthesis under identical electrochemical conditions to isoxazoline synthesis, in the absence of dipolarophile.

Alternatively, it could be envisioned that a hydrazone protected with a group containing no carbonyl functionality may provide the corresponding pyrazoline, under similar electrochemical conditions to the isoxazoline synthesis. This would presumably proceed through a nitrile imine intermediate, that could be generated electrochemically, analogous the electrochemical generation of a nitrile oxide from aldoximes. Protecting groups for this chemistry could include benzyl **266a**, allyl **266b**, SEM **266c** and MOM **266d** (**Scheme 85**).



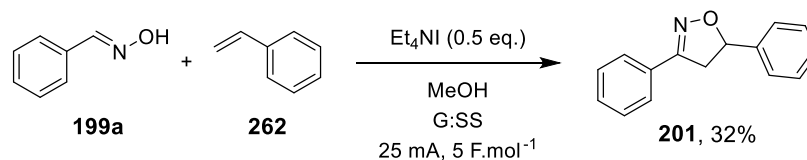
Scheme 85: Electrochemically enabled pyrazoline synthesis from hydrazones protected with groups that contain no carbonyl functionality.

To compliment the mechanistic work already carried out herein, computational chemistry could prove to be a powerful tool for modelling and predicting the mechanistic hypotheses. These models and predictions could prove to be vital for pinning down a real reaction pathway. To this end, work is currently being carried out to provide this further detailed information.

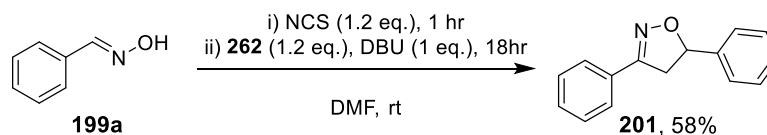
Further future work could be to fully optimise the electrochemical isoxazoline synthesis in flow. The current results have proven to be very promising, with the desired isoxazoline isolated in 49% from the reaction between benzaldehyde oxime and *tert*-butyl acrylate. However, full consumption of starting material in the first pass through the electrochemical cell has not been achieved to date and so there is scope to improve. Should this adaption into flow prove fruitful, it would greatly increase the productivity and impact that this electrochemical reaction could have on the chemical community, and indeed in an industrial setting. Optimisation of the flow process may require an alternative electrochemical flow cell, such as the Ammonite^{®106} or Vapourtec's flow electrochemical cell.¹⁰⁷ Alternatively, a bespoke flow electrochemical cell for the IKA ElectraSyn 2.0 could be employed: Kevin Lam of University of Greenwich developed a 3D printed flow cell that can fit on top of the ElectraSyn and provide flow capability.¹⁰⁸ This bespoke flow cell would allow use of electrodes and cell that were used for the original optimisation, eliminating much of the variability when switching equipment.

Other future work will involve improving the reaction scope by adapting the conditions to include alternate dipolarophiles, other than those with electron-withdrawing substituents. So far only a poor 32% isolated yield of **201** (**Scheme 86**) has been

achieved; to increase the impact this protocol can have to the chemical community, this type of reactivity is essential. As **201** can be isolated in 58% yield from a non-electrochemical method (**Scheme 87**), it is likely that the reduced yield under electrochemical conditions is caused by styrene reacting at an electrode. Bespoke optimisation of styrenyl dipolarophiles is most likely required, with re-optimisation of electrode materials, solvent and mediator.



Scheme 86: The current best result for the electrochemical 1,3-dipolar cycloaddition between benzaldehyde oxime and styrene, mediated by an iodide salt.



Scheme 87: Synthesis of **201** by a non-electrochemical method, demonstrating that the styrene dipolarophile may be reacting at an electrode under electrochemical conditions.

6. Experimental

6.1. General Experimental Data Methods

All chemicals were purchased from Sigma Aldrich or Alfa Aesar and used as received, with no purification. All electrolytes were purchased at electrochemical analysis purity grade and used as received, with no purification. All solvents were used, without purification, from SureSeal Sigma Aldrich solvent bottles. Solvents used for column chromatography were of HPLC grade.

Nuclear Magnetic Resonance Spectroscopy (NMR)

NMR spectra were recorded using a Bruker AV-400 (^1H = 400 MHz, ^{13}C = 101 MHz, ^{19}F = 376 MHz), AV-500 (^1H = 500 MHz, ^{13}C = 126 MHz) or AV-600 (^1H = 600 MHz, ^{13}C = 151 MHz). Chemical shifts (δ) are reported in parts per million (ppm) relative to tetramethylsilane and DMSO and coupling constants (J) in Hz. The following abbreviations are used for multiplicities: s = singlet; br. s = broad singlet; d = doublet; t = triplet; q = quartet; app. q = apparent quartet; m = multiplet; quin. = quintet; dd = doublet of doublets; dt = doublet of triplets; td = triplet of doublets; qd = quartet of doublets; ddd = doublet of doublet of doublets; ddt = doublet of doublet of triplets; dtd = doublet of triplet of doublets; dtt = doublet of triplet of triplets. If not specifically stated, the NMR experiments were run at 30 °C and ^{19}F and ^{13}C were run in ^1H -decoupled mode.

Liquid Chromatography Mass Spectrometry (LCMS)

Reaction progress and final LCMS analyses were conducted using the method below.

LCMS Method

The liquid chromatography (LC) analysis was conducted on an Acquity UPLC CSH C_{18} column (50 mm x 2.1 mm internal diameter, 1.7 μm packing diameter) at 40 °C using a 0.3 μL injection volume.

The solvents employed were:

A = 10 mM ammonium bicarbonate in water adjusted to pH 10 with ammonia solution.

B = Acetonitrile.

The gradient employed was:

Time/min	Flow Rate/mL.min ⁻¹	%A	%B
0.00	1	97	3
0.05	1	97	3
1.50	1	5	95
1.90	1	5	95
2.00	1	97	3

The UV detection was a summed signal from a wavelength of 210 nm to 350 nm. Mass spectra were recorded on a Waters ZQ mass spectrometer using alternate-scan positive and negative electrospray ionisation (ES⁺ and ES⁻) with a scan range of 100 to 1000 amu, scan time of 0.27 s and an inter-scan delay of 0.10 s.

High Resolution Mass Spectrometry (HRMS)

High-resolution mass spectra were recorded on a Micromass Q-ToF Ultima hybrid quadrupole time-of-flight mass spectrometer, with analytes separated on by Agilent 1100 Liquid Chromatography equipped with a Phenomenex Luna C₁₈ (2) reversed phase column (100 mm x 2.1 mm, 3 µm packing diameter). LC conditions were 0.5 mL.min⁻¹ flow rate, 35 °C, injection volume 2 - 5 µL. Gradient elution with (A) water containing 0.1% (v/v) formic acid and (B) acetonitrile containing 0.1% (v/v) formic acid. Gradient conditions were initially 5% B, increasing linearly to 100% B over 6 min, remaining at 100% B for 2.5 min then decreasing linearly to 5% B over 1 min followed by an equilibration period of 2.5 min prior to the next injection. Mass to charge ratios (*m/z*) are reported in Daltons.

Column Chromatography

Automated column chromatography was conducted on a Teledyne Isco Combiflash Rf system using RediSep Rf Silica cartridges (for normal phase), or Biotage KP-C₁₈-HS cartridges (for reverse phase) of appropriate size. Elution utilised standard HPLC grade solvents provided by Sigma Aldrich, with the desired modifier (for reverse phase) added in-house, unless otherwise stated.

Infrared Spectroscopy (IR)

IR spectra were recorded using a Perkin Elmer Spectrum One spectrometer. Absorption frequencies (*v*_{max}) are reported in wavenumbers (cm⁻¹).

Melting Point

Melting points were measured on a BÜCHI Melting Point M-560 melting point apparatus.

Electrochemical Apparatus

All electrochemical reactions were performed on an IKA ElectraSyn 2.0. All electrodes and electrode materials were purchased directly from IKA and used as received. Where appropriate, the IKA Carousel was used.

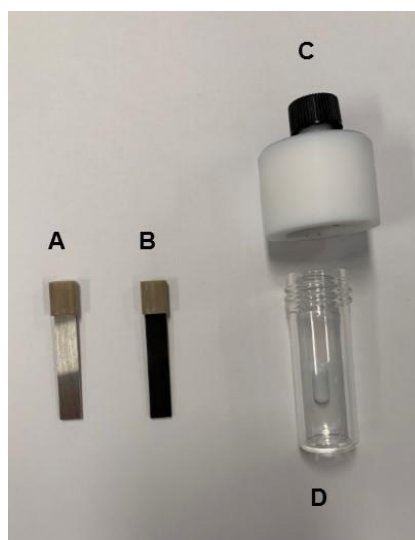


Figure S1: Components of the IKA ElectraSyn 2.0 electrochemical cell: A) stainless steel electrode; B) graphite electrode; C) lid of the electrochemical cell; D) 10 mL vial with stirrer bar.



Figure S2: Complete electrochemical cell, ready to be subjected to electrolysis on ElectraSyn 2.0.

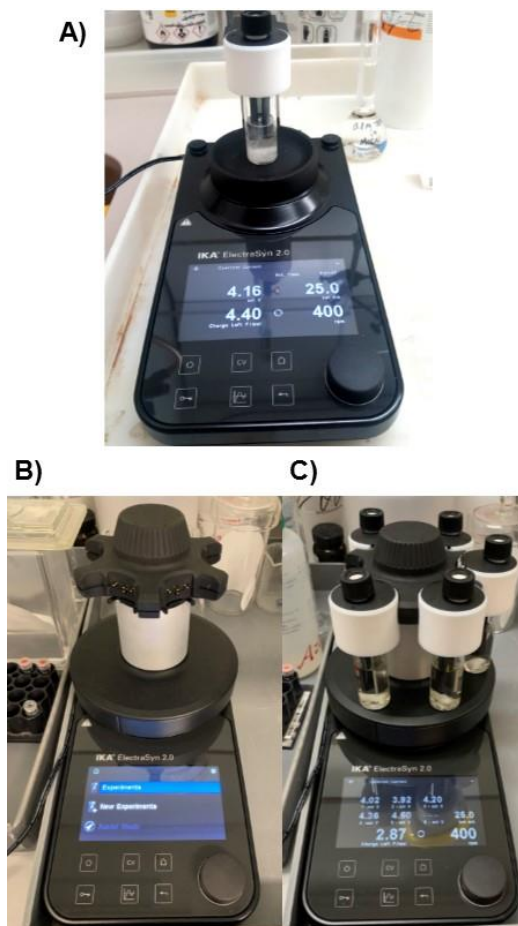


Figure S3: A) ElectraSyn 2.0 configured for single cell set up; B) ElectraSyn 2.0 configured for carousel reactions; C) ElectraSyn 2.0 and carousel used to allow multiple reactions to be electrolysed as the same time.

ReactIR Apparatus

In-situ IR experiments were conducted using the Mettler Toledo ReactIR 15 apparatus with 6.35 mm (1.5 m fibre) probe attached; probe used had diamond window and made of Alloy 22 (https://www.mt.com/gb/en/home/products/L1_AutochemProducts/ReactIR/ReactIR-15.html; Date access: 18/11/2019). All data was processed and analysed using iC IR 7.0 Mettler Toledo software provided with equipment, then exported to Microsoft Excel to produce the graphs shown in publication.

Flow Electrochemical Apparatus

The flow apparatus is the Asia Flux Module commercialised by Syrris Ltd. A Syrris Asia Syringe pump was used, equipped with Asia Yellow Syringes (100 μ L/50 μ L). The Syrris FLUX microfluidic cell was supplied by Syrris Ltd. The anode was made of

either carbon filled polyvinylidene fluoride (PVDF) or carbon filled with polyphenylene sulfide (PPS), the cathode of stainless-steel or platinum coated stainless-steel, the spacer of perfluoroelastomer (FFKM, TRPlast 330B, 500 μm thickness and the gasket of polyether ether ketone (PEEK). The microfluidic cell parameters are: channel depth 250 μm , channel width 1.50 mm, channel length 600 mm, surface area of channel 900 mm^2 , the channel volume 225 μL . All modules were connected by PTFE tubing and end fittings. All electrodes, microfluidic cell components and fittings were purchased from Syrris Ltd and used as supplied.



Figure S4: Syrris Asia pump and Syrris FLUX electrochemical module used for the adaption of the batch electrochemical reaction into flow.

Cyclic Voltammetry Equipment

Cyclic Voltammetry experiments were conducted on the Ana Fleuve chip-based system by Zimmer and Peacock (<https://www.zimmerpeacocktech.com/products/ana-fleuve/>; Date accessed: 05/02/2020). The experiments were conducted in MeCN (Sigma Aldrich SureSeal) with 0.1 M Et_4NBF_4 as electrolyte. All solutions of analytes were made as 10 mM solutions. All analytes were referenced to Ferrocene (10 mM in 0.1 M $\text{Et}_4\text{NBF}_4/\text{MeCN}$). The electrode chip material was platinum (both anode and cathode), with a Ag/AgCl reference electrode (<https://www.zimmerpeacocktech.com/products/electrochemical-sensors/bare-platinum-chemically-resistant-sensors/>; Date accessed: 05/02/2020). The CVs were recorded using the software provided by Zimmer and Peacock

(<https://www.zimmerpeacocktech.com/knowledge-base/software/>; Date accessed: 05/02/2020), with the data exported to Microsoft Excel for further data manipulation and cyclic voltammogram generation.

Voltmeter Apparatus

Experiments involving the use of a voltmeter were conducted in a cell in which wires were wrapped around the anode and cathode as shown in **Figure S5**. The voltmeter was then attached using the crocodile clip attachments (**Figure S6**). All wiring was secured using electrical tape. Data was recorded using a webcam that took pictures every 30 seconds (**Figure S7** and **Figure S8**). The potentials were extracted from the pictures captured and then analysed using Microsoft Excel.



Figure S5: Wires for the voltmeter were wrapped around the anode and cathode and fed up through the lid of the ElectroSyn vial.



Figure S6: The complete vial used for experiments that involved the use of a voltmeter.

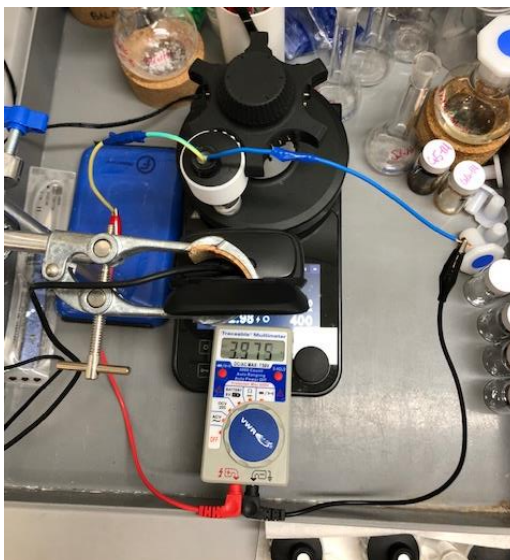


Figure S7: The experimental set-up for the recording of the observed potential difference, as displayed on the ElectraSyn, and actual potential difference, as displayed by the voltmeter.



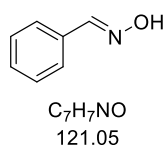
Figure S8: An alternative view of the experimental set up for recording the observed and actual potential difference of the electrochemical reaction.

6.2. General Experimental Procedures

6.2.1. General Procedure 1 for Oxime Synthesis (GP1)

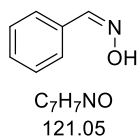
To a round-bottomed flask containing a stirrer bar, potassium carbonate (1.5 eq.) and hydroxylamine hydrochloride (1.5 eq.) were added, followed by Methanol (0.5 M) and aldehyde (1 eq.). The suspension was then allowed to stir at ambient temperature. The reaction was followed by TLC or LCMS, if appropriate. Once complete by TLC (or LCMS), the reaction mixture was concentrated *in vacuo*. The residue was taken up in water (30 mL) and EtOAc (25 mL). The phases were separated, and the aqueous layer was extracted with EtOAc (2 x 25 mL). The combined organics were washed with brine (30 mL), dried (hydrophobic frit) and concentrated *in vacuo* to give the crude mixture. The crude mixture was purified by column chromatography on silica gel, eluting with EtOAc/cyclohexane to afford the desired product.

(*E*)-Benzaldehyde oxime (**199a**) and (*Z*)-benzaldehyde oxime (**199a'**)



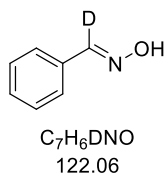
To a round-bottomed flask containing a stirrer bar, potassium carbonate (6880 mg, 49.80 mmol) and hydroxylamine hydrochloride (3488 mg, 50.20 mmol) were added, followed by MeOH (150 mL) and benzaldehyde (5 mL, 49.20 mmol). The suspension was then allowed to stir at ambient temperature. The reaction was followed by TLC (25% EtOAc in cyclohexane). After 4 hours, the reaction mixture was concentrated *in vacuo*. The residue was taken up in water (100 mL) and EtOAc (100 mL). The phases were separated, and the aqueous layer was extracted with EtOAc (2 x 50 mL). The combined organics were washed with brine (50 mL), dried (hydrophobic frit) and concentrated *in vacuo* to give the crude mixture. The crude mixture was submitted to column chromatography on silica gel (120 g, 0 - 25% EtOAc in cyclohexane over 25 CVs, affording (*E*)-benzaldehyde oxime **199a** (4893 mg, 40.40 mmol, 82%) as a colourless oil and (*Z*)-benzaldehyde oxime **199a'** (319 mg, 2.63 mmol, 5%) as a white solid (MP (CH₂Cl₂): 117.4 - 120.9 °C).

199a: ¹H NMR (400 MHz, DMSO-*d*₆) δ ppm 11.20 (1H, s), 8.13 (1H, s), 7.56 - 7.61 (2H, m), 7.34 - 7.43 (3H, m); ¹³C NMR (101 MHz, DMSO-*d*₆) δ ppm 148.0, 133.0, 129.2, 128.6, 126.3; LCMS: *t*_R = 0.74 min, area% = 97%, [M-H]⁻ 120 (100). Data consistent with literature synthesis.⁷⁶



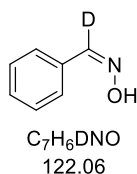
199a': 1H NMR (400 MHz, DMSO- d_6) δ ppm 11.58 (1H, s), 7.94 - 7.98 (2H, m), 7.37 - 7.46 (4H, m); ^{13}C NMR (101 MHz, DMSO- d_6) δ ppm 144.7, 131.0, 130.3, 129.4, 128.3; LCMS: t_R = 0.74 min, area% = 87%, $[M-H]^-$ 120 (100); IR ν_{max} (thin film): 3159, 3062, 3020, 2812, 1650, 1434, 690 cm^{-1} ; HRMS (ESI-QToF): calculated for $[M+H]^+$ 122.0528, found 122.0610.

(E)-Benzaldehyde- α - d_1 oxime (199a- d_1) and (Z)-benzaldehyde- α - d_1 oxime (199a- d_1')



To a round-bottomed flask containing a stirrer bar, hydroxylamine hydrochloride (925 mg, 13.31 mmol) and potassium carbonate (1837 mg, 13.29 mmol) were added followed by MeOH- d_4 (18 mL) and benzaldehyde- α - d_1 (900 μ L, 8.86 mmol). The resulting suspension was allowed to stir at ambient temperature. The reaction was followed by TLC (20% EtOAc/cyclohexane). After stirring for 4 hours, the reaction mixture was concentrated *in vacuo*. The residue was taken up in water (25 mL) and extracted with EtOAc (3 x 25 mL). The combined organic layers were washed with brine (25 mL), dried (hydrophobic frit) and concentrated *in vacuo* to give the crude mixture. The crude mixture was dissolved in DCM (2 mL) and submitted to column chromatography on silica gel (40 g, 0 - 20% EtOAc in cyclohexane over 20 CVs). Appropriate fractions were combined and concentrated *in vacuo* to afford (E)-benzaldehyde- α - d_1 oxime **199a- d_1** (522 mg, 4.27 mmol, 48%) as a colourless oil and (Z)-benzaldehyde- α - d_1 oxime **199a- d_1'** (69 mg, 0.56 mmol, 6%) as a white solid (MP (CH_2Cl_2): 128.7 - 130.1 $^{\circ}C$).

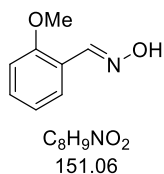
199a- d_1 : 1H NMR (400 MHz, DMSO- d_6) δ ppm 11.20 (1H, s), 7.57 - 7.62 (2H, m), 7.35 - 7.43 (3H, m); ^{13}C NMR (101 MHz, DMSO- d_6) δ ppm 147.8 (t, $^1J_{C-D}$ = 26 Hz), 133.0, 129.2, 128.6, 126.3; LCMS: t_R = 0.78 min, area% = 100%, $[M-H]^-$ 121 (100); IR ν_{max} (thin film): 3264, 3059, 3030, 2854, 1623, 1577, 1499, 1446, 1238, 1045, 946, 792, 738, 692, 637 cm^{-1} ; HRMS: calculated for $[M+H]^+$ 123.0684, found 123.0694.



199a- d_1' : 1H NMR (400 MHz, DMSO- d_6) δ ppm 11.57 (1H, s), 7.94 - 7.99 (2H, m), 7.39 - 7.47 (3H, m); ^{13}C NMR (101 MHz, DMSO- d_6) δ ppm 144.3 (t, $^1J_{C-D}$ = 26 Hz), 131.0, 130.3, 129.4, 128.3; LCMS: t_R = 0.78 min, area% = 100%, $[M-H]^-$ 121 (100); IR ν_{max} (thin film): 3158, 3021, 2812, 1640,

1490, 1434, 1202, 1059, 1026, 888, 821, 776, 730, 689 cm^{-1} ; HRMS: calculated for $[\text{M}+\text{H}]^+$ 123.0684, found 123.0696.

(E)-2-Methoxybenzaldehyde oxime (199b)



Prepared according to **GP1**, using 2-methoxybenzaldehyde (610 μL , 5.05 mmol), stirring overnight and after work up, affording (*E*)-3-methoxybenzaldehyde oxime **199b** (748 mg, 4.95 mmol, 98%) as a white solid (MP (CH_2Cl_2): 91.0 - 93.8 $^\circ\text{C}$).

199c: ^1H NMR (400 MHz, $\text{DMSO}-d_6$) δ ppm 11.17 (1H, s), 8.29 (1H, s), 7.65 (1H, dd, $J = 7.6, 1.7$ Hz), 7.37 (1H, ddd, $J = 8.4, 7.6, 1.7$ Hz), 7.06 (1H, dd, $J = 8.4, 0.9$ Hz), 6.96 (1H, tt, $J = 7.6, 0.9$ Hz), 3.82 (3H, s); ^{13}C NMR (101 MHz, $\text{DMSO}-d_6$) δ ppm 156.8, 143.4, 130.7, 125.4, 120.9, 120.5, 111.7, 55.6; LCMS: $t_R = 0.81$ min, area% = 100%, $[\text{M}+\text{H}]^+$ 152 (100). Data consistent with literature synthesis.¹⁰⁹

(E)-3-Methoxybenzaldehyde oxime (269) and (Z)-3-methoxybenzaldehyde oxime (269')



Prepared according to **GP1**, using 3-methoxybenzaldehyde (610 μL , 5.00 mmol), stirring overnight and eluting with 0 - 25% EtOAc in cyclohexane over 20 CVs, affording (*E*)-3-methoxybenzaldehyde oxime **269** (640 mg, 4.23 mmol, 85%) as a colourless oil and (*Z*)-3-methoxybenzaldehyde oxime **269'** (32 mg, 0.21 mmol, 4%) as a colourless oil.

269: ^1H NMR (400 MHz, $\text{DMSO}-d_6$) δ ppm 11.20 (1H, s), 8.10 (1H, s), 7.27 - 7.35 (1H, m), 7.13 - 7.19 (2H, m), 6.94 (1H, s), 3.77 (3H, s); ^{13}C NMR (101 MHz, $\text{DMSO}-d_6$) δ ppm 159.4, 147.9, 134.4, 129.7, 118.9, 115.1, 111.2, 55.0; LCMS: $t_R = 0.80$ min, area% = 100%, $[\text{M}-\text{H}]^-$ 150 (100). Data consistent with literature synthesis.¹⁰⁹



269': ^1H NMR (400 MHz, $\text{DMSO}-d_6$) δ ppm 11.60 (1H, s), 7.58 (1H, dd, $J = 2.6, 1.5$ Hz), 7.51 (1H, dt, $J = 8.3, 1.0$ Hz), 7.38 (1H, s), 7.35 (1H, t, $J = 8.3$ Hz), 6.99 (1H, ddd, $J = 8.3, 2.6, 1.0$ Hz), 3.77 (3H, s); ^{13}C NMR (101 MHz, $\text{DMSO}-d_6$) δ ppm 158.9, 144.5, 132.2, 129.3, 122.8, 115.6, 115.1, 55.1; LCMS: $t_R = 0.79$ min, area% = 100%, $[\text{M}-\text{H}]^-$ 150 (100). Data consistent with literature synthesis.¹¹⁰

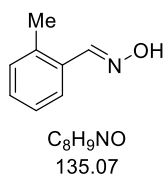
(E)-4-Methoxybenzaldehyde oxime (199c) and **(Z)-4-methoxybenzaldehyde oxime (199c')**

To a round-bottomed flask containing a stirrer bar, hydroxylamine hydrochloride (3141 mg, 45.20 mmol) and potassium carbonate (6247 mg, 45.20 mmol) were added, followed by MeOH (150 mL) and 4-methoxybenzaldehyde (5 mL, 41.10 mmol). The reaction mixture was stirred at ambient temperature. The reaction was followed by TLC (25% EtOAc in cyclohexane). After stirring overnight, the reaction mixture was concentrated *in vacuo*. The residue was partitioned between EtOAc (40 mL) and water (40 mL). The aqueous layer was extracted with EtOAc (2 x 25 mL). The combined organic layers were washed once with brine (25 mL), dried (hydrophobic frit) and concentrated *in vacuo* to give the crude mixture. The crude mixture was split into two batches. One batch was submitted to column chromatography on silica gel (120 g, 0 - 25% EtOAc in cyclohexane over 25 CVs), affording (E)-4-methoxybenzaldehyde oxime **199c** (2157 mg, 14.27 mmol, 80%) as a white solid (MP (CH₂Cl₂): 64.9 - 67.6 °C) and (Z)-4-methoxybenzaldehyde oxime **199c'** (99 mg, 0.66 mmol, 4%) as a white solid (MP (CH₂Cl₂): 132.2 - 134.1 °C).

199c: ¹H NMR (400 MHz, DMSO-*d*₆) δ ppm 10.92 (1H, s), 8.06 (1H, s), 7.50 - 7.54 (2H, m), 6.93 - 6.98 (2H, m), 3.77 (3H, s); ¹³C NMR (101 MHz, DMSO-*d*₆) δ ppm 160.0, 147.6, 127.8, 125.6, 114.1, 55.1; LCMS: t_R = 0.77 min, area% = 100%, [M-H]⁻ 150 (100). Data consistent with literature synthesis.⁷⁶

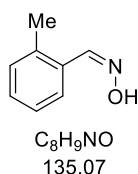


199c': ¹H NMR (400 MHz, DMSO-*d*₆) δ ppm 11.33 (1H, s), 7.92 - 7.96 (2H, m), 7.30 (1H, s), 6.95 - 7.00 (2H, m), 3.79 (3H, s); ¹³C NMR (101 MHz, DMSO-*d*₆) δ ppm 159.7, 144.2, 132.2, 124.1, 113.6, 55.1; LCMS: t_R = 0.77 min, area% = 100%, [M-H]⁻ 150 (100); IR ν_{max} (thin film): 3148, 3070, 3008, 2840, 2799, 1599, 1261, 829 cm⁻¹; HRMS (ESI-QToF): calculated for [M+H]⁺ 151.0633, found 152.0714.

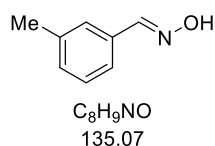
(E)-2-Methylbenzaldehyde oxime (199d) and **(Z)-2-methylbenzaldehyde oxime (199d')**

Prepared according to **GP1**, using 2-methylbenzaldehyde (600 μ L, 5.19 mmol), hydroxylamine hydrochloride (400 mg, 5.76 mmol, 1.1 eq.) and potassium carbonate (800 mg, 5.79 mmol, 1.1 eq.), stirring overnight and eluting with 0 - 20% EtOAc in cyclohexane over 25 CVs, affording (*E*)-2-methylbenzaldehyde oxime **199d** (612 mg, 4.53 mmol, 87%) as a pale-pink solid (MP (CH₂Cl₂): 49.2 - 50.8 °C) and (*Z*)-2-methylbenzaldehyde oxime **199d'** (23 mg, 0.17 mmol, 3%) as a colourless oil.

199d: ¹H NMR (400 MHz, DMSO-*d*₆) δ ppm 11.23 (1H, s), 8.32 (1H, s), 7.61 (1H, d, *J* = 7.8 Hz), 7.17 - 7.31 (3H, m), 2.38 (3H, s); ¹³C NMR (101 MHz, DMSO-*d*₆) δ ppm 147.0, 135.9, 131.1, 130.7, 128.9, 126.1, 125.9, 19.4; LCMS: *t*_R = 0.85 min, area% = 100%, [M-H]⁻ 134 (100). Data consistent with literature synthesis.¹¹⁰



199d': ¹H NMR (400 MHz, DMSO-*d*₆) δ ppm 11.23 (1H, s), 8.32 (1H, s), 7.61 (1H, d, *J* = 7.8 Hz), 7.17 - 7.30 (3H, m), 2.38 (3H, s); ¹³C NMR (101 MHz, DMSO-*d*₆) δ ppm 147.0, 135.9, 131.1, 130.7, 128.9, 126.1, 125.9, 19.4; LCMS: *t*_R = 0.85 min, area% = 97%, [M-H]⁻ 134 (100). Data consistent with literature synthesis.¹¹⁰

(E)-3-Methylbenzaldehyde oxime (199e)

Prepared according to **GP1**, using 3-methylbenzaldehyde (600 μ L, 5.10 mmol), hydroxylamine hydrochloride (395 mg, 5.68 mmol, 1.1 eq.) and potassium carbonate (775 mg, 5.61 mmol, 1.1 eq.), stirring overnight and eluting with 0 - 20% EtOAc in cyclohexane over 25 CVs, affording (*E*)-3-methylbenzaldehyde oxime **199e** (579 mg, 4.28 mmol, 84%) as a white solid (MP (CH₂Cl₂): 62.1 - 63.4 °C).

199e: ¹H NMR (400 MHz, DMSO-*d*₆) δ ppm 11.14 (1H, s), 8.08 (1H, s), 7.35 - 7.42 (2H, m), 7.28 (1H, t, *J* = 7.6 Hz), 7.18 (1H, d, *J* = 7.6 Hz), 2.31 (3H, s); ¹³C NMR (101 MHz, DMSO-*d*₆) δ ppm 148.1, 137.8, 133.0, 129.8, 128.5, 126.8, 123.5, 20.9; LCMS: *t*_R = 0.90 min, area% = 96%, [M-H]⁻ 134 (100). Data consistent with literature synthesis.¹¹⁰

(E)-4-Methylbenzaldehyde oxime (199f) and **(Z)-4-methylbenzaldehyde oxime (199f')**

Prepared according to **GP1**, using 4-methylbenzaldehyde (600 μ L, 5.09 mmol), hydroxylamine hydrochloride (360 mg, 5.18 mmol, 1.0 eq.) and potassium carbonate (713 mg, 5.16 mmol, 1.0 eq.), stirring overnight and eluting with 0 - 15% EtOAc in cyclohexane over 20 CVs, affording (*E*)-4-methylbenzaldehyde oxime **199f** (574 mg, 4.25 mmol, 83%) as a white solid (MP (CH_2Cl_2): 76.9 - 79.2 $^{\circ}C$) and (*Z*)-4-methylbenzaldehyde oxime **199f'** (32 mg, 0.24 mmol, 5%) as a white solid (MP (CH_2Cl_2): 114.5 - 118.1 $^{\circ}C$).

199f: 1H NMR (400 MHz, $DMSO-d_6$) δ ppm 11.06 (1H, s), 8.08 (1H, s), 7.47 (2H, d, $J = 8.2$ Hz), 7.20 (2H, d, $J = 8.2$ Hz), 2.31 (3H, s); ^{13}C NMR (101 MHz, $DMSO-d_6$) δ ppm 147.9, 138.8, 130.3, 129.2, 126.3, 20.9; LCMS: $t_R = 0.87$ min, area% = 96%, $[M-H]^-$ 134 (100); IR ν_{max} (thin film): 3114, 2986, 2916, 1608, 1513, 1435, 1286, 1180 cm^{-1} ; HRMS (ESI-QToF): calculated for $[M+H]^+$ 136.0762, found 136.0765. Data consistent with literature synthesis.¹¹⁰



199f': 1H NMR (400 MHz, $DMSO-d_6$) δ ppm 11.46 (1H, s), 7.86 (2H, d, $J = 7.5$ Hz), 7.35 (1H, s), 7.24 (2H, d, $J = 7.5$ Hz), 2.33 (3H, s); ^{13}C NMR (101 MHz, $DMSO-d_6$) δ ppm 144.6, 139.1, 130.3, 128.8, 128.5, 20.9; LCMS: $t_R = 0.87$ min, area% = 93%, $[M-H]^-$ 134 (100); IR ν_{max} (thin film): 3157, 3065, 3014, 2916, 2849, 2788, 1646, 1604, 1507, 1444, 1403, 1345, 1312, 1284 cm^{-1} ; HRMS (ESI-QToF): calculated for $[M+H]^+$ 136.0762, found 136.0764. Data consistent with literature synthesis.¹¹⁰

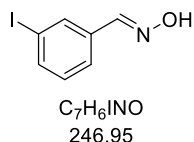
(E)-2-Iodobenzaldehyde oxime (199g)

Prepared according to **GP1**, using 2-iodobenzaldehyde (1161 mg, 5.00 mmol), stirring overnight and after work up, affording (*E*)-2-iodobenzaldehyde oxime **199g** (1193 mg, 4.83 mmol, 97%) as a white solid (MP (CH_2Cl_2): 103.6 - 110.3 $^{\circ}C$).

199g: 1H NMR (400 MHz, $DMSO-d_6$) δ ppm 11.60 (1H, s), 8.21 (1H, s), 7.91 (1H, dd, $J = 7.9, 1.1$ Hz), 7.72 (1H, dd, $J = 7.9, 1.7$ Hz), 7.42 (1H, tt, $J = 7.9, 1.1$ Hz), 7.15 (1H, td, $J = 7.9, 1.7$ Hz); ^{13}C NMR (101 MHz, $DMSO-d_6$) δ ppm 151.1, 139.4, 134.7, 131.1, 128.5, 126.7, 98.9; LCMS: $t_R = 1.02$, area% = 96%, $[M-H]^-$ 246 (100); IR ν_{max}

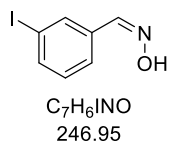
(thin film): 3165, 3053, 2994, 2859, 1583, 1557, 1472, 1430, 1315, 1279, 1209, 1011, 979, 868, 750, 702, 671, 629, 498 cm^{-1} ; HRMS (ESI-QToF): calculated for $[\text{M}+\text{H}]^+$ 247.9568, found 247.9570.

(E)-3-Iodobenzaldehyde oxime (199h) and **(Z)-3-iodobenzaldehyde oxime (199h')**



Prepared according to **GP1**, using 3-iodobenzaldehyde (1161 mg, 5.00 mmol), stirring overnight and eluting with 0 - 20% EtOAc in cyclohexane over 20 CVs, affording (*E*)-3-iodobenzaldehyde oxime **199h** (924 mg, 3.74 mmol, 75%) as a white solid (MP (CH_2Cl_2): 69.5 - 72.5 $^\circ\text{C}$). and a mixture of **199h** and (*Z*)-3-iodobenzaldehyde oxime **199h'** (4:1, 16 mg, 0.07 mmol, 1%) as a white solid.

199h: ^1H NMR (400 MHz, $\text{DMSO}-d_6$) δ ppm 11.38 (1H, s), 8.09 (1H, s), 7.94 (1H, t, $J = 1.8$ Hz), 7.73 (1H, ddd, $J = 7.8, 1.8, 1.1$ Hz), 7.61 (1H, dt, $J = 7.8, 1.1$ Hz), 7.20 (1H, t, $J = 7.8$ Hz); ^{13}C NMR (101 MHz, $\text{DMSO}-d_6$) δ ppm 146.7, 137.6, 135.3, 134.7, 130.8, 125.5, 95.0; LCMS: $t_R = 1.03$ min, area% = 100%, $[\text{M}-\text{H}]^-$ 246 (100); IR ν_{max} (thin film): 3295, 3076, 2967, 1557, 1475, 1417, 1310, 1263, 1201, 1064, 993, 928, 895, 875, 782, 671, 542, 460 cm^{-1} ; HRMS (ESI-QToF): calculated for $[\text{M}+\text{H}]^+$ 247.9572, found 247.9570.



199h': ^1H NMR (400 MHz, $\text{DMSO}-d_6$) δ ppm 11.81 (1H, s), 11.38 (s, *E*-isomer), 8.39 (1H, t, $J = 1.8$ Hz), 8.10 (s, *E*-isomer), 7.96 (1H, t, $J = 1.8$ Hz), 7.94 (t, $J = 1.8$ Hz, *E*-isomer), 7.77 (1H, ddd, $J = 7.9, 1.8, 1.1$ Hz), 7.73 (ddd, $J = 7.9, 1.8, 1.1$ Hz, *E*-isomer), 7.61 (dt, $J = 7.9, 1.1$ Hz, *E*-isomer), 7.40 (1H, s), 7.25 (1H, t, $J = 7.9$ Hz), 7.20 (t, $J = 7.9$ Hz, *E*-isomer); ^{13}C NMR (101 MHz, $\text{DMSO}-d_6$) δ ppm 146.7 (*E*-isomer), 143.2, 138.4, 137.9, 137.6 (*E*-isomer), 135.3 (*E*-isomer), 134.7 (*E*-isomer), 132.9, 130.8 (*E*-isomer), 130.5, 129.5, 125.5 (*E*-isomer), 95.0 (*E*-isomer), 94.6; LCMS: $t_R = 1.00$ min, area% = 78%, $[\text{M}-\text{H}]^-$ 246 (100); IR ν_{max} (thin film): 3182, 3054, 3020, 2914, 2849, 1556, 1456, 1414, 1350, 1294, 1267, 1189, 1064, 992, 943, 867, 778, 741, 680, 591 cm^{-1} . Spectra recorded on mixture.

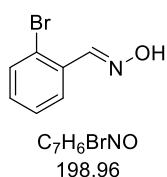
(E)-4-Iodobenzaldehyde oxime (199i) and **(Z)-4-iodobenzaldehyde oxime (199i')**

Prepared according to **GP1**, using 4-iodobenzaldehyde (1164 mg, 5.02 mmol), stirring overnight and eluting with 0 - 20% EtOAc in cyclohexane over 20 CVs, affording (*E*)-4-iodobenzaldehyde oxime **199i** (1089 mg, 4.41 mmol, 88%) as a white solid (MP (CH₂Cl₂): 119.0 - 122.0 °C) and (*Z*)-4-iodobenzaldehyde oxime **199i'** (84 mg, 0.34 mmol, 7%) as a white solid (MP (CH₂Cl₂): 156.0 - 161.1 °C).

199i: ¹H NMR (400 MHz, DMSO-*d*₆) δ ppm 11.32 (1H, s), 8.10 (1H, s), 7.76 (2H, dt, *J* = 8.3, 2.0 Hz), 7.38 (2H, dt, *J* = 8.3, 2.0 Hz); ¹³C NMR (101 MHz, DMSO-*d*₆) δ ppm 147.4, 137.5, 132.6, 128.2, 95.6; LCMS: *t*_R = 1.02 min, area% = 97%, [M-H]⁻ 246 (100); IR *v*_{max} (thin film): 3249, 1585, 1483, 1392, 1310, 1053, 1002, 949, 926, 864, 809, 666, 502, 458 cm⁻¹; HRMS (ESI-QToF): calculated for [M+H]⁺ 247.9572, found 247.9567.



199i': ¹H NMR (400 MHz, DMSO-*d*₆) δ ppm 11.75 (1H, s), 7.82 (2H, dt, *J* = 8.6, 2.2 Hz), 7.75 (2H, dt, *J* = 8.6, 2.2 Hz), 7.39 (1H, s); ¹³C NMR (101 MHz, DMSO-*d*₆) δ ppm 143.8, 137.2, 132.1, 130.3, 96.3; LCMS: *t*_R = 1.01 min, area% = 98%, [M-H]⁻ 246 (100); IR *v*_{max} (thin film): 3148, 3059, 3045, 2795, 1646, 1579, 1477, 1442, 1387, 1353, 1338, 1301, 1264, 1060, 1004, 948, 896, 855, 809, 740, 567 cm⁻¹; HRMS (ESI-QToF): calculated for [M+H]⁺ 247.9572, found 247.9570.

(E)-2-Bromobenzaldehyde oxime (199j)

Prepared according to **GP1**, using 2-bromobenzaldehyde (600 μL, 5.14 mmol), hydroxylamine hydrochloride (398 mg, 5.73 mmol, 1.1 eq.) and potassium carbonate (784 mg, 5.67 mmol, 1.1 eq.), stirring overnight and after work up, affording (*E*)-2-bromobenzaldehyde oxime **199j** (975 mg, 4.88 mmol, 95%) as a white solid (MP (CH₂Cl₂): 99.8 - 102.7 °C).

199j: ¹H NMR (400 MHz, DMSO-*d*₆) δ ppm 11.65 (1H, s), 8.32 (1H, s), 7.80 (1H, dd, *J* = 7.8, 1.7 Hz), 7.67 (1H, dd, *J* = 7.8, 1.2 Hz), 7.41 (1H, td, *J* = 7.8, 1.2 Hz), 7.33 (1H, td, *J* = 7.8, 1.7 Hz); ¹³C NMR (101 MHz, DMSO-*d*₆) δ ppm 146.7, 133.0, 131.8, 131.1, 128.0, 127.0, 122.4; LCMS: *t*_R = 0.98 min, area% = 94%, [M-H]⁻ 198 (100), 200 (100);

IR ν_{\max} (thin film): 3246, 1480, 1435, 1316, 1268, 1206, 1023, 970, 868, 746, 705, 680, 630, 489 cm^{-1} ; HRMS (ESI-QToF): calculated for $[\text{M}+\text{H}]^+$ 199.9711, found 199.9712.

(E)-3-Bromobenzaldehyde oxime (199k) and **(Z)-3-bromobenzaldehyde oxime (199k')**



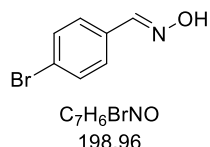
Prepared according to **GP1**, using 3-bromobenzaldehyde (600 μL , 5.15 mmol), stirring overnight and eluting with 0 - 25% TBME in cyclohexane over 20 CVs, affording (*E*)-3-bromobenzaldehyde oxime **199k** (846 mg, 4.23 mmol, 82%) as a white solid (MP (CH_2Cl_2): 75.0 - 77.2 $^\circ\text{C}$) and (*Z*)-4-bromobenzaldehyde oxime **199k'** (69 mg, 0.35 mmol, 7%) as a white solid (MP (CH_2Cl_2): 118.9 - 121.0 $^\circ\text{C}$).

199k: ^1H NMR (400 MHz, $\text{DMSO}-d_6$) δ ppm 11.42 (1H, s), 8.14 (1H, s), 7.77 (1H, t, $J = 1.7$ Hz), 7.61 (1H, dt, $J = 7.8, 1.1$ Hz), 7.57 (1H, ddd, $J = 8.0, 2.1, 1.1$ Hz), 7.36 (1H, t, $J = 7.8$ Hz); ^{13}C NMR (101 MHz, $\text{DMSO}-d_6$) δ ppm 146.8, 135.5, 131.8, 130.8, 128.8, 125.1, 121.9; LCMS: $t_R = 0.98$ min, area% = 98%, $[\text{M}-\text{H}]^-$ 198 (100), 200 (100); IR ν_{\max} (thin film): 3168, 3065, 2983, 2874, 2754, 1562, 1481, 1422, 1315, 1269, 1205, 1073, 976, 909, 779, 678 cm^{-1} ; HRMS (ESI-QToF): calculated for $[\text{M}+\text{H}]^+$ 199.9711, found 199.9713.



199k': ^1H NMR (400 MHz, $\text{DMSO}-d_6$) δ ppm 11.86 (1H, s), 8.23 (1H, t, $J = 1.7$ Hz), 7.92 (1H, dt, $J = 7.8, 1.2$ Hz), 7.61 (1H, ddd, $J = 8.1, 2.0, 1.0$ Hz), 7.45 (1H, s), 7.41 (1H, t, $J = 7.8$ Hz); ^{13}C NMR (101 MHz, $\text{DMSO}-d_6$) δ ppm 143.2, 132.9, 132.6, 132.1, 130.5, 129.2, 121.5; LCMS: $t_R = 0.96$ min, area% = 86%, $[\text{M}-\text{H}]^-$ 198 (100), 200 (100); IR ν_{\max} (thin film): 3146, 3065, 3013, 2804, 1644, 1558, 1460, 1415, 1330, 1270, 1191, 1074, 952, 897, 874, 749, 679, 459 cm^{-1} ; HRMS (ESI-QToF): calculated for $[\text{M}+\text{H}]^+$ 199.9711, found 199.9710.

(E)-4-Bromobenzaldehyde oxime (199l) and **(Z)-4-bromobenzaldehyde oxime (199l')**



Prepared according to **GP1**, using 4-bromobenzaldehyde (929 mg, 5.02 mmol), hydroxylamine hydrochloride (354 mg, 5.09 mmol, 1.0 eq.) and potassium carbonate (697 mg, 5.04 mmol, 1.0 eq.), stirring overnight and eluting with 0 - 15% EtOAc in cyclohexane over 20

CVs, affording (*E*)-4-bromobenzaldehyde oxime **199l** (859 mg, 4.29 mmol, 85%) as a white solid (MP (CH₂Cl₂): 118.4 - 119.7 °C) and (*Z*)-4-bromobenzaldehyde oxime **199l'** (60 mg, 0.30 mmol, 6%) as a white solid (MP (CH₂Cl₂): 152.2 - 156.2 °C).

199l: ¹H NMR (400 MHz, DMSO-*d*₆) δ ppm 11.34 (1H, s), 8.13 (1H, s), 7.57 - 7.62 (2H, m), 7.52 - 7.56 (2H, m); ¹³C NMR (101 MHz, DMSO-*d*₆) δ ppm 147.1, 132.3, 131.6, 128.2, 122.3; LCMS: t_R = 0.96 min, area% = 96%, [M-H]⁻ 198 (100), 200 (100); IR ν_{max} (thin film): 3256, 3050, 2996, 2911, 1588, 1489, 1397, 1397, 1316, 1299, 1282, 1210 cm⁻¹; HRMS (ESI-QToF): calculated for [M+H]⁺ 119.9711, found 199.9712. Data consistent with literature synthesis.¹¹¹



199l': ¹H NMR (400 MHz, DMSO-*d*₆) δ ppm 11.77 (1H, s), 7.89 - 7.94 (2H, m), 7.61 - 7.67 (2H, m), 7.43 (1H, s); ¹³C NMR (101 MHz, DMSO-*d*₆) δ ppm 143.6, 132.3, 131.3, 130.0, 122.7; LCMS: t_R = 0.96 min, area% = 92%, [M-H]⁻ 198 (100), 200 (90); IR ν_{max} (thin film): 3157, 3058, 3014, 2922, 2796, 1648, 1584, 1480, 1442, 1390, 1338 cm⁻¹; HRMS (ESI-QToF): calculated for [M+H]⁺ 199.9711, found 199.9713.

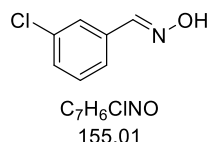
(*E*)-2-Chlorobenzaldehyde oxime (**199m**)



Prepared according to **GP1**, using 2-chlorobenzaldehyde (570 μL, 5.06 mmol), stirring overnight and after work up, affording (*E*)-2-chlorobenzaldehyde oxime **199m** (738 mg, 4.74 mmol, 94%) as a white solid (MP (CH₂Cl₂): 74.3 - 78.4 °C).

199m: ¹H NMR (400 MHz, DMSO-*d*₆) δ ppm 11.65 (1H, s), 8.36 (1H, s), 7.82 (1H, dd, *J* = 7.6, 2.0 Hz), 7.48 - 7.52 (1H, m), 7.34 - 7.44 (2H, m); ¹³C NMR (101 MHz, DMSO-*d*₆) δ ppm 144.5, 132.1, 130.8, 130.2, 129.8, 127.5, 126.7; LCMS: t_R = 0.94 min, area% = 100%, [M-H]⁻ 154 (100), 156 (25). Data consistent with literature synthesis.¹¹¹

(*E*)-3-Chlorobenzaldehyde oxime (**199n**)



Prepared according to **GP1**, using 3-chlorobenzaldehyde (570 μL, 5.03 mmol), stirring overnight and after work up, affording (*E*)-3-chlorobenzaldehyde oxime **199n** (735 mg, 4.73 mmol, 94%) as a white solid (MP (CH₂Cl₂): 71.2 - 72.3 °C)

199n: ^1H NMR (400 MHz, $\text{DMSO-}d_6$) δ ppm 11.43 (1H, s), 8.15 (1H, s), 7.61 - 7.64 (1H, m), 7.54 - 7.59 (1H, m), 7.41 - 7.45 (2H, m); ^{13}C NMR (101 MHz, $\text{DMSO-}d_6$) δ ppm 146.9, 135.2, 133.4, 130.5, 128.9, 125.9, 124.8; LCMS: t_R = 0.94 min, area% = 100%, $[\text{M-H}]^-$ 154 (100), 156 (25); IR ν_{max} (thin film): 3165, 3068, 2986, 2877, 2758, 1559, 1481, 1427, 1317, 1269, 1209, 1080, 975, 959, 945, 878, 780, 709, 678, 487 cm^{-1} ; HRMS (ESI-QToF): calculated for $[\text{M+H}]^+$ 156.0212, found 156.0215.

(E)-4-Chlorobenzaldehyde oxime (199o) and **(Z)-4-chlorobenzaldehyde oxime (199o')**



Prepared according to **GP1**, using 4-chlorobenzaldehyde (703 mg, 5.00 mmol), stirring overnight and eluting with 0 - 25% EtOAc in cyclohexane over 20 CVs, affording (*E*)-4-chlorobenzaldehyde oxime **199o** (612 mg, 3.94 mmol, 79%) as a white solid (MP (CH_2Cl_2): 111.5 - 113.6 $^\circ\text{C}$) and (*Z*)-4-chlorobenzaldehyde oxime **199o'** (45 mg, 0.29 mmol, 6%) as a white solid (MP (CH_2Cl_2): 143.6 - 146.8 $^\circ\text{C}$).

199: ^1H NMR (400 MHz, $\text{DMSO-}d_6$) δ ppm 11.33 (1H, s), 8.15 (1H, s), 7.61 (2H, dt, J = 8.6, 2.2 Hz), 7.46 (2H, dt, J = 8.6, 2.2 Hz); ^{13}C NMR (101 MHz, $\text{DMSO-}d_6$) δ ppm 147.0, 133.6, 132.0, 128.7, 128.0; LCMS: t_R = 0.94 min, area% = 100%, $[\text{M-H}]^-$ 154 (100), 156 (25). Data consistent with literature synthesis.¹¹¹



199o': ^1H NMR (400 MHz, $\text{DMSO-}d_6$) δ ppm 11.75 (1H, s), 7.99 (2H, dt, J = 8.8, 2.2 Hz), 7.50 (2H, dt, J = 8.8, 2.2 Hz), 7.44 (1H, s); ^{13}C NMR (101 MHz, $\text{DMSO-}d_6$) δ ppm 143.5, 133.8, 132.1, 129.7, 128.4; LCMS: t_R = 0.93 min, area% = 100%, $[\text{M-H}]^-$ 154 (100), 156 (25). Data consistent with literature synthesis.¹¹²

(E)-2-Fluorobenzaldehyde oxime (199p)



Prepared according to **GP1**, using 2-fluorobenzaldehyde (530 μL , 5.03 mmol), stirring overnight and eluting with 0 - 20% EtOAc in cyclohexane over 20 CVs, affording (*E*)-2-fluorobenzaldehyde oxime **199p** (654 mg, 4.70 mmol, 93%) as white solid (MP (CH_2Cl_2): 63.7 - 65.9 $^\circ\text{C}$).

199p: ^1H NMR (400 MHz, $\text{DMSO-}d_6$) δ ppm 11.56 (1H, s), 8.22 (1H, s), 7.74 (1H, td, J = 7.6, 1.9 Hz), 7.40 - 7.48 (1H, m), 7.20 - 7.29 (2H, m); ^{13}C NMR (101 MHz, DMSO-

d_6) δ ppm 159.7 (d, $^1J_{C-F} = 250$ Hz), 141.5 (d, $^3J_{C-F} = 3$ Hz), 131.1 (d, $^3J_{C-F} = 9$ Hz), 126.7 (d, $^3J_{C-F} = 3$ Hz), 124.7 (d, $^4J_{C-F} = 3$ Hz), 120.4 (d, $^2J_{C-F} = 11$ Hz), 115.9 (d, $^2J_{C-F} = 21$ Hz); ^{19}F NMR (376 MHz, DMSO- d_6) δ ppm -119.4 (1F, s); LCMS: $t_R = 0.82$ min, area% = 100%, $[M-H]^-$ 138 (100); IR ν_{max} (thin film): 3249, 3147, 3013, 2922, 1615, 1578, 1491, 1456, 1317, 1237, 1212, 1101, 980, 898, 808, 780, 748, 641 cm^{-1} ; HRMS (ESI-QToF): calculated for $[M+H]^+$ 140.0512, found 140.0510.

(E)-3-Fluorobenzaldehyde oxime (199q) and **(Z)-3-fluorobenzaldehyde oxime (199q')**



Prepared according to **GP1**, using 3-fluorobenzaldehyde (530 μ L, 5.00 mmol), stirring overnight and eluting with 0 - 20% EtOAc in cyclohexane over 20 CVs, affording (*E*)-3-fluorobenzaldehyde oxime **199q** (604 mg, 4.34 mmol, 87%) as white solid (MP (CH_2Cl_2): 68.2 - 69.8 $^{\circ}C$) and (*Z*)-3-fluorobenzaldehyde oxime **199q'** (37 mg, 0.26 mmol, 5%) as a white solid (MP (CH_2Cl_2): 92.1 - 94.7 $^{\circ}C$).

199q: 1H NMR (400 MHz, DMSO- d_6) δ ppm 11.41 (1H, s), 8.16 (1H, s), 7.36 - 7.48 (3H, m), 7.16 - 7.25 (1H, m); ^{13}C NMR (101 MHz, DMSO- d_6) δ ppm 162.2 (d, $^1J_{C-F} = 244$ Hz), 147.1 (d, $^3J_{C-F} = 3$ Hz), 135.5 (d, $^3J_{C-F} = 8$ Hz), 130.7 (d, $^3J_{C-F} = 8$ Hz), 122.6 (d, $^4J_{C-F} = 3$ Hz), 115.9 (d, $^2J_{C-F} = 22$ Hz), 112.5 (d, $^2J_{C-F} = 22$ Hz); ^{19}F NMR (376 MHz, DMSO- d_6) δ ppm -112.9 (1F, s); LCMS: $t_R = 0.82$ min, area% = 83%, $[M-H]^-$ 138 (100); IR ν_{max} (thin film): 3222, 3158, 3002, 2927, 2847, 1612, 1584, 1491, 1443, 1321, 1269, 1246, 1136, 953, 857, 775, 703, 677, 637 cm^{-1} ; HRMS (ESI-QToF): calculated for $[M+H]^+$ 140.0512, found 140.0511.



199q': 1H NMR (400 MHz, DMSO- d_6) δ ppm 11.84 (1H, s), 7.87 (1H, ddd, $J = 10.8, 2.7, 1.5$ Hz), 7.72 (1H, dt, $J = 7.8, 1.5$ Hz), 7.45 - 7.54 (2H, m), 7.23 - 7.30 (1H, m); ^{13}C NMR (101 MHz, DMSO- d_6) δ ppm 161.7 (d, $^1J_{C-F} = 243$ Hz), 143.5 (d, $^3J_{C-F} = 3$ Hz), 132.8 (d, $^3J_{C-F} = 8$ Hz), 130.3 (d, $^3J_{C-F} = 8$ Hz), 126.4 (d, $^4J_{C-F} = 3$ Hz), 116.6 (d, $^2J_{C-F} = 22$ Hz), 116.3 (d, $^2J_{C-F} = 22$ Hz); ^{19}F NMR (376 MHz, DMSO- d_6) δ ppm -112.9 (1F, s); LCMS: $t_R = 0.81$ min, area% = 97%, $[M-H]^-$ 138 (100); IR ν_{max} (thin film): 3179, 3019, 2837, 1648, 1582, 1479, 1430, 1356, 1276, 1235, 1140, 974, 914, 896, 873, 783, 679 cm^{-1} ; HRMS (ESI-QToF): calculated for $[M+H]^+$ 140.0512, found 140.0510.

(E)-4-Fluorobenzaldehyde oxime (199r) and **(Z)-4-fluorobenzaldehyde oxime (199r')**

Prepared according to **GP1**, using 4-fluorobenzaldehyde (1 mL, 9.32 mmol), hydroxylamine hydrochloride (648 mg, 9.32 mmol, 1.0 eq.), potassium carbonate (1288 mg, 9.32 mmol, 1.0 eq.) and MeOH (0.6 M), stirring for 3 hours and eluting with 0 - 20% EtOAc in cyclohexane over 25 CVs, affording (*E*)-4-fluorobenzaldehyde oxime **199r** (803 mg, 5.77 mmol, 62%) as white solid (MP (CH₂Cl₂): 88.4 - 89.7 °C) and (*Z*)-4-fluorobenzaldehyde oxime **199r'** (58 mg, 0.42 mmol, 4%) as a white solid.

199r: ¹H NMR (400 MHz, DMSO-*d*₆) δ ppm 11.20 (1H, s), 8.14 (1H, s), 7.61 - 7.67 (2H, m), 7.20 - 7.27 (2H, m); ¹³C NMR (101 MHz, DMSO-*d*₆) δ ppm 162.5 (d, ¹J_{C-F} = 246 Hz), 147.0, 129.6 (d, ⁴J_{C-F} = 4 Hz), 128.4 (d, ³J_{C-F} = 9 Hz), 115.6 (d, ²J_{C-F} = 22 Hz); ¹⁹F NMR (376 MHz, DMSO-*d*₆) δ ppm -111.9 (1F, s); LCMS: t_R = 0.78 min, area% = 94%, [M-H]⁻ 138 (100). Data consistent with literature synthesis.⁷⁶



199r': ¹H NMR (400 MHz, DMSO-*d*₆) δ ppm 11.62 (1H, s), 8.02 - 8.07 (2H, m), 7.42 (1H, s), 7.23 - 7.30 (2H, m); ¹³C NMR (101 MHz, DMSO-*d*₆) δ ppm 162.0 (d, ¹J_{C-F} = 248 Hz), 143.5, 132.8 (d, ³J_{C-F} = 9 Hz), 127.8 (d, ⁴J_{C-F} = 3 Hz), 115.2 (d, ²J_{C-F} = 21 Hz); ¹⁹F NMR (376 MHz, DMSO-*d*₆) δ ppm -110.4 (1F, s); LCMS: t_R = 0.78 min, area% = 84%, [M-H]⁻ 138 (100). Data consistent with literature synthesis.¹¹²

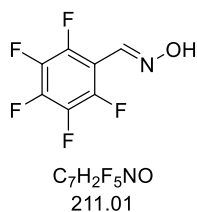
(E)-2,6-Difluorobenzaldehyde oxime (199s)

Prepared according to **GP1**, using 2,6-difluorobenzaldehyde (620 μL, 5.71 mmol), hydroxylamine hydrochloride (520 mg, 7.48 mmol, 1.3 eq.) and potassium carbonate (1042 mg, 7.54 mmol, 1.3 eq.) and stirring overnight, affording (*E*)-2,6-difluorobenzaldehyde oxime **199s** (811 mg, 5.16 mmol, 90%) as a white solid (MP (CH₂Cl₂): 116.1 - 118.5 °C).

199s: ¹H NMR (400 MHz, DMSO-*d*₆) δ ppm 11.80 (1H, s), 8.15 (1H, s), 7.47 (1H, tt, *J* = 8.4, 6.4 Hz), 7.13 - 7.23 (2H, m); ¹³C NMR (101 MHz, DMSO-*d*₆) δ ppm 159.9 (dd, ¹J_{C-F} = 253, ³J_{C-F} = 7 Hz), 138.5, 131.1 (t, ³J_{C-F} = 11 Hz), 112.1 (dd, ²J_{C-F} = 20, ⁴J_{C-F} = 7 Hz), 110.0 (t, ²J_{C-F} = 15 Hz); ¹⁹F NMR (376 MHz, DMSO-*d*₆) δ ppm -112.2 (2F, s); LCMS: t_R = 0.79 min, area% = 100%, [M-H]⁻ 156 (100); IR ν_{max} (thin film): 3271, 3010,

1621, 1564, 1471, 1270, 1231, 1208, 1026, 964, 951, 868, 785, 577, 552, 512 cm^{-1} ;
HRMS (ESI-QToF): calculated for $[\text{M}+\text{H}]^+$ 158.0413, found 158.0415.

(E)-2,3,4,5,6-Pentafluorobenzaldehyde oxime (199t)



Prepared according to **GP1**, using 2,3,4,5,6-pentafluorobenzaldehyde (620 μL , 5.02 mmol) and stirring overnight, affording (E)-2,3,4,5,6-difluorobenzaldehyde oxime **199t** (995 mg, 4.71 mmol, 94%) as an off-white solid (MP (CH_2Cl_2): 134.7 - 138.4 $^\circ\text{C}$).

199t: ^1H NMR (400 MHz, $\text{DMSO}-d_6$) δ ppm 12.21 (1H, s), 8.15 (1H, s); ^{13}C NMR (151 MHz, $\text{DMSO}-d_6$) δ ppm 144.2 (dddt, $^1J_{\text{C-F}} = 253$, $^2J_{\text{C-F}} = 12$, $^3J_{\text{C-F}} = 8$, $^4J_{\text{C-F}} = 4$, $^5J_{\text{C-F}} = 4$ Hz), 140.4 (dtt, $^1J_{\text{C-F}} = 253$, $^2J_{\text{C-F}} = 13$, $^2J_{\text{C-F}} = 13$, $^4J_{\text{C-F}} = 5$, $^4J_{\text{C-F}} = 5$ Hz), 137.1, 136.3 - 138.3 (m), 108.2 (td, $^2J_{\text{C-F}} = 14$, $^4J_{\text{C-F}} = 4$ Hz); ^{19}F NMR (376 MHz, $\text{DMSO}-d_6$) δ ppm 147.7 (1F, t, $^3J_{\text{F-F}} = 23$ Hz), -141.7 (4F, dd, $^3J_{\text{F-F}} = 23$, $^4J_{\text{F-F}} = 7$ Hz); LCMS: $t_{\text{R}} = 0.99$ min, area% = 89%, $[\text{M}-\text{H}]^-$ 210 (100); IR ν_{max} (thin film): 3299, 3008, 2237, 1649, 1519, 1494, 1422, 1381, 1319, 1159, 1134, 1024, 951, 785, 698, 645 cm^{-1} ; HRMS (ESI-QToF): calculated for $[\text{M}+\text{H}]^+$ 212.0131, found 212.0133.

(E)-2-(Trifluoromethyl)benzaldehyde oxime (199u)



Prepared according to **GP1**, using 2-(trifluoromethyl)benzaldehyde (660 μL , 5.00 mmol) and stirring overnight affording (E)-2-(trifluoromethyl)benzaldehyde oxime **199u** (817 mg, 4.32 mmol, 86%) as a white solid (MP (CH_2Cl_2): 80.7 - 86.7 $^\circ\text{C}$).

199u: ^1H NMR (400 MHz, $\text{DMSO}-d_6$) δ ppm 11.83 (1H, s), 8.30 (1H, q, $J = 2.4$ Hz), 8.00 (1H, d, $J = 7.8$ Hz), 7.79 (1H, d, $J = 7.8$ Hz), 7.71 (1H, t, $J = 7.8$ Hz), 7.61 (1H, t, $J = 7.8$ Hz); ^{13}C NMR (101 MHz, $\text{DMSO}-d_6$) δ ppm 144.0 (d, $^3J_{\text{C-F}} = 1$ Hz), 132.7, 130.6 (d, $^3J_{\text{C-F}} = 1$ Hz), 129.6, 126.9, 125.9 (q, $^2J_{\text{C-F}} = 6$ Hz), 125.8 (q, $^1J_{\text{C-F}} = 30$ Hz), 122.7; ^{19}F NMR (376 MHz, $\text{DMSO}-d_6$) δ ppm -57.3 (3F, s); LCMS: $t_{\text{R}} = 1.01$ min, area% = 98%, $[\text{M}-\text{H}]^-$ 188 (100); IR ν_{max} (thin film): 3258, 3029, 1580, 1494, 1448, 1313, 1278, 1171, 1117, 1035, 959, 935, 873, 761, 667, 637 cm^{-1} ; HRMS (ESI-QToF): calculated for $[\text{M}+\text{H}]^+$ 190.0479, found 190.0481.

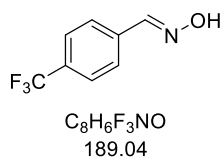
(E)-3-(Trifluoromethyl)benzaldehyde oxime (199v) and **(Z)-3-(trifluoromethyl)benzaldehyde oxime (199v')**

Prepared according to **GP1**, using 3-(trifluoromethyl)benzaldehyde (670 μ L, 5.01 mmol), stirring overnight and eluting with 0 - 20% EtOAc in cyclohexane over 20 CVs, affording (*E*)-3-(trifluoromethyl)benzaldehyde oxime **199v** (775 mg, 4.10 mmol, 82%) as a white solid (MP (CH_2Cl_2): 49.6 - 50.8 $^{\circ}C$) and a mixture of **199v** and (*Z*)-3-(trifluoromethyl)benzaldehyde oxime **199v'** (1:1.2, 69 mg, 0.36 mmol, 7%) as a white solid (MP (CH_2Cl_2): 48.4 - 49.3 $^{\circ}C$).

199v: 1H NMR (400 MHz, $DMSO-d_6$) δ ppm 11.50 (1H, s), 8.26 (1H, s), 7.88 - 7.94 (2H, m), 7.72 (1H, d, $J = 7.8$ Hz), 7.64 (1H, t, $J = 7.8$ Hz); ^{13}C NMR (151 MHz, $DMSO-d_6$) δ ppm 147.0, 134.2, 129.9 (d, $^4J_{C-F} = 1$ Hz), 129.8, 129.5 (q, $^2J_{C-F} = 32$ Hz), 125.5 (q, $^3J_{C-F} = 4$ Hz), 122.8 (q, $^3J_{C-F} = 4$ Hz), 124.0 (q, $^1J_{C-F} = 273$ Hz); ^{19}F NMR (376 MHz, $DMSO-d_6$) δ ppm -61.4 (3F, s); LCMS: $t_R = 1.01$ min, area% = 99%, $[M-H]^-$ 188 (100); IR ν_{max} (thin film): 3305, 1490, 1452, 1331, 1313, 1275, 1202, 1166, 1124, 1071, 949, 802, 696, 672 cm^{-1} ; HRMS (ESI-QToF): calculated for $[M+H]^+$ 190.01480, found 190.0477.

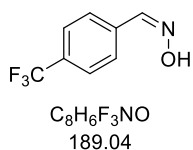


199v': 1H NMR (400 MHz, $DMSO-d_6$) δ ppm 11.96 (1H, s), 11.50 (s, *E-isomer*), 8.39 (1H, s), 8.27 (s, *E-isomer*), 8.22 (1H, d, $J = 8.1$ Hz), 7.88 - 7.93 (m, *E-isomer*), 7.61 - 7.80 (4H, m, *mixture of isomers*), 7.58 (1H, s); ^{13}C NMR (101 MHz, $DMSO-d_6$) δ ppm 146.9 (*E-isomer*), 143.3, 134.2 (*E-isomer*), 132.8 (q, $^1J_{C-F} = 244$ Hz), 129.9 (*E-isomer*), 129.8 (*E-isomer*), 129.6, 129.5 (q, $^2J_{C-F} = 32$ Hz, *E-isomer*), 129.1 (q, $^2J_{C-F} = 32$ Hz), 126.6 (q, $^3J_{C-F} = 4$ Hz), 125.8 (q, $^3J_{C-F} = 4$ Hz), 125.3 (q, $^3J_{C-F} = 4$ Hz), 122.8 (q, $^3J_{C-F} = 4$ Hz, *E-isomer*), 122.6 (q, $^3J_{C-F} = 4$ Hz); ^{19}F NMR (376 MHz, $DMSO-d_6$) δ ppm -61.3 (3F, s), -61.4 (s, *Z-isomer*); LCMS: $t_R = 0.99$ min, area% = 49%, $[M-H]^-$ 188 (100); IR ν_{max} (thin film): 3304, 2953, 2921, 2851, 1453, 1377, 1331, 1202, 1167, 1124, 1098, 1071, 949, 802, 695, 671 cm^{-1} ; HRMS (ESI-QToF): calculated for $[M+H]^+$ 190.01480, found 190.0477. Spectra recorded on mixture.

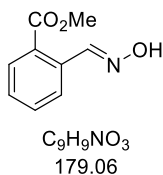
(E)-4-(Trifluoromethyl)benzaldehyde oxime (199w) and **(Z)-4-(trifluoromethyl)benzaldehyde oxime (199w')**

Prepared according to **GP1**, using 4-(trifluoromethyl)benzaldehyde (683 μ L, 5.00 mmol), hydroxylamine hydrochloride (349 mg, 5.02 mmol, 1.0 eq.) and potassium carbonate (697 mg, 5.04 mmol, 1.0 eq.), stirring overnight and eluting with 0 - 25% EtOAc in cyclohexane over 20 CVs, affording (*E*)-4-(trifluoromethyl)benzaldehyde oxime **199w** (723 mg, 3.82 mmol, 76%) as a white solid (MP (CH₂Cl₂): 101.9 - 104.1 °C) and (*Z*)-4-(trifluoromethyl)benzaldehyde oxime **199w'** (73 mg, 0.39 mmol, 8%) as a white solid (MP (CH₂Cl₂): 128.8 - 131.3 °C).

199w: ¹H NMR (400 MHz, DMSO-*d*₆) δ ppm 11.58 (1H, s), 8.25 (1H, s), 7.81 (2H, d, *J* = 8.3 Hz), 7.76 (2H, d, *J* = 8.3 Hz); ¹³C NMR (101 MHz, DMSO-*d*₆) δ ppm 147.1, 137.1, 129.1 (q, ²*J*_{C-F} = 32 Hz), 126.9, 125.6 (q, ³*J*_{C-F} = 4 Hz), 124.1 (q, ¹*J*_{C-F} = 272 Hz); ¹⁹F NMR (376 MHz, DMSO-*d*₆) δ ppm -61.3 (3F, s); LCMS: *t*_R = 1.02 min, area% = 100%, [M-H]⁻ 188 (100); IR ν_{max} (thin film): 3269, 1618, 1412, 1320, 1310, 970, 939, 872, 833 cm⁻¹; HRMS (ESI-QToF): calculated for [M+H]⁺ 190.0479, found 190.0484.



199w': ¹H NMR (400 MHz, DMSO-*d*₆) δ ppm 11.98 (1H, s), 8.16 (2H, d, *J* = 8.3 Hz), 7.81 (2H, d, *J* = 8.3 Hz), 7.57 (1H, s); ¹³C NMR (101 MHz, DMSO-*d*₆) δ ppm 143.5, 134.3, 130.8, 129.1 (q, ²*J*_{C-F} = 32 Hz), 125.2 (q, ³*J*_{C-F} = 3 Hz), 123.0 (q, ¹*J*_{C-F} = 84 Hz); ¹⁹F NMR (376 MHz, DMSO-*d*₆) δ ppm -61.3 (3F, s); LCMS: *t*_R = 1.00 min, area% = 95%, [M-H]⁻ 188 (100); IR ν_{max} (thin film): 3159, 3077, 3029, 2844, 1651, 1405, 1320, 1294 cm⁻¹; HRMS (ESI-QToF): calculated for [M+H]⁺ 190.0479, found 190.0482.

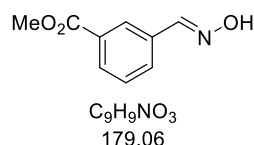
Methyl (E)-2-((hydroxyimino)methyl)benzoate (199x)

Prepared according to **GP1**, using methyl 2-formylbenzoate (823 mg, 5.01 mmol), stirring overnight and eluting with 0 - 20% EtOAc in cyclohexane over 20 CVs, affording methyl (*E*)-4-((hydroxyimino)methyl)benzoate **199x** (244 mg, 1.36 mmol, 27%) as a white solid (MP (CH₂Cl₂): 227.3 - 231.2 °C).

199x: ¹H NMR (400 MHz, DMSO-*d*₆) δ ppm 11.41 (1H, s), 8.65 (1H, s), 7.85 (2H, d, *J* = 8.1 Hz), 7.61 (1H, t, *J* = 7.6 Hz), 7.51 (1H, t, *J* = 7.6 Hz), 3.85 (3H, s); ¹³C NMR (101

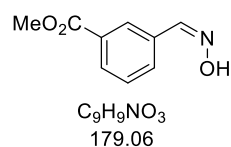
MHz, DMSO- d_6) δ ppm 166.7, 146.9, 133.0, 132.2, 130.0, 129.1, 128.8, 126.7, 52.3; LCMS: t_R = 0.80 min, area% = 96%, $[M-H]^-$ 178 (100); IR ν_{max} (thin film): 3186, 3012, 2956, 2869, 2228, 1710, 1573, 1489, 1433, 1294, 1256, 1205, 1134, 1080, 980, 871, 819, 756, 698, 637, 524 cm^{-1} ; HRMS (ESI-QToF): calculated for $[M+H]^+$ 180.0656, found 180.0664.

Methyl (*E*)-3-((hydroxyimino)methyl)benzoate (199y) and methyl (*Z*)-3-((hydroxyimino)methyl)benzoate (199y')



Prepared according to **GP1**, using methyl 3-formylbenzoate (823 mg, 5.01 mmol), stirring overnight and eluting with 0 – 20% EtOAc in cyclohexane over 20 CVs, affording methyl (*E*)-3-((hydroxyimino)methyl)benzoate **199y** (698 mg, 3.89 mmol, 78%) as a white solid (MP (CH_2Cl_2): 109.9 - 112.3 °C) and a mixture of **199y** and methyl (*Z*)-3-((hydroxyimino)methyl)benzoate **199y'** (2:1, 94 mg, 0.52 mmol, 10%) as a white solid.

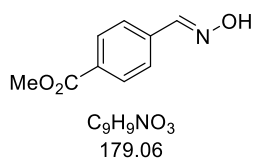
199y: 1H NMR (400 MHz, DMSO- d_6) δ ppm 11.39 (1H, s), 8.24 (1H, s), 8.18 (1H, t, J = 1.7 Hz), 7.95 (1H, dt, J = 7.7, 1.3 Hz), 7.86 (1H, dt, J = 7.7, 1.7 Hz), 7.56 (1H, t, J = 7.7 Hz), 3.87 (3H, s); ^{13}C NMR (101 MHz, DMSO- d_6) δ ppm 165.8, 147.3, 133.7, 130.7, 130.1, 129.6, 129.2, 126.9, 52.2; LCMS: t_R = 0.81 min, area% = 95%, $[M-H]^-$ 178 (100); IR ν_{max} (thin film): 3360, 2962, 1684, 1586, 1495, 1430, 1306, 1262, 1208, 1176, 1108, 960, 930, 819, 751, 684, 639, 535, 508 cm^{-1} ; HRMS (ESI-QToF): calculated for $[M+H]^+$ 180.0661, found 180.0662.



199y': 1H NMR (400 MHz, DMSO- d_6) δ ppm 11.82 (s, *Z-isomer*), 11.39 (1H, s), 8.63 (t, J = 1.7 Hz, *Z-isomer*), 8.24 (1H, s), 8.20 (t, J = 1.5 Hz, *Z-isomer*), 8.18 (1H, t, J = 1.7 Hz), 7.98 (dt, J = 7.9, 1.4 Hz, *Z-isomer*), 7.95 (1H, dt, J = 7.8, 1.5 Hz), 7.86 (1H, dt, J = 7.7, 1.5 Hz), 7.60 (t, J = 7.8 Hz, *Z-isomer*), 7.55 (s, *Z-isomer*), 7.56 (1H, t, J = 7.7 Hz), 3.87 - 3.88 (m, *both isomers*); ^{13}C NMR (101 MHz, DMSO- d_6) δ ppm 165.9, 165.8 (*E-isomer*), 147.3 (*E-isomer*), 143.8, 134.7, 133.7 (*E-isomer*), 130.9, 130.7 (*E-isomer*), 130.1 (*E-isomer*), 129.9, 129.7, 129.6 (*E-isomer*), 129.2 (*E-isomer*), 128.9, 126.9 (*E-isomer*), 52.2 (*both isomers*); LCMS: t_R = 0.80 min, area% = 33%, $[M-H]^-$ 178 (100) (*Z-isomer*); t_R = 0.81 min, area% = 67%, $[M-H]^-$ 178 (100) (*E-isomer*); IR ν_{max} (thin film): 3360, 2962, 1684, 1586, 1495, 1430, 1306, 1262, 1208, 1176, 1108, 960, 930, 819, 751, 684, 639, 535,

508 cm^{-1} ; HRMS (ESI-QToF): calculated for $[\text{M}+\text{H}]^+$ 180.0660, found 180.0663. Spectra recorded on mixture.

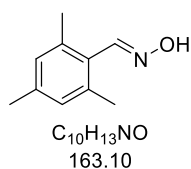
Methyl (*E*)-4-((hydroxyimino)methyl)benzoate (**270**)



Prepared according to **GP1**, using methyl 4-formylbenzoate (821 mg, 5.00 mmol), stirring overnight and eluting with 0 - 40% TBME in cyclohexane over 20 CVs, affording an inseparable mixture of methyl (*E*)-4-((hydroxyimino)methyl)benzoate **270** and methyl (*Z*)-4-((hydroxyimino)methyl)benzoate (13:1, 827 mg, 4.61 mmol, 92%) as a white solid (MP (CH_2Cl_2): 119.0 - 123.0 $^\circ\text{C}$).

270: ^1H NMR (400 MHz, $\text{DMSO}-d_6$) δ ppm 11.95 (s, *Z*-isomer), 11.56 (1H, s), 8.22 (1H, s), 8.09 (dt, $J = 8.6, 1.7$ Hz, *Z*-isomer), 8.01 (dt, $J = 8.6, 1.7$ Hz, *Z*-isomer), 7.97 (2H, dt, $J = 8.3, 1.7$ Hz), 7.73 (2H, dt, $J = 8.3, 1.7$ Hz), 7.54 (s, *Z*-isomer), 3.87 (s, *Z*-isomer), 3.86 (3H, s); ^{13}C NMR (101 MHz, $\text{DMSO}-d_6$) δ ppm 165.8, 147.4, 137.5, 129.8, 129.5, 126.5, 52.1; LCMS: $t_R = 0.82$ min, area% = 95%, $[\text{M}-\text{H}]^-$ 178 (100); IR ν_{max} (thin film): 3249, 3019, 1722, 1609, 1571, 1437, 1280, 1198, 1179, 1110, 1017, 949, 881, 849, 820, 763, 692, 503 cm^{-1} ; HRMS (ESI-QToF): calculated for $[\text{M}+\text{H}]^+$ 180.0661, found 180.0659. Spectra recorded on mixture.

(*E*)-2,4,6-Trimethylbenzaldehyde oxime (**199z**)



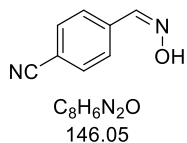
Prepared according to **GP1**, using 2,4,6-trimethylbenzaldehyde (750 μL , 5.09 mmol), hydroxylamine hydrochloride (357 mg, 5.14 mmol, 1.0 eq.) and potassium carbonate (707 mg, 5.12 mmol, 1.0 eq.), stirring overnight and after work up, affording (*E*)-2,4,6-trimethylbenzaldehyde oxime **199z** (719 mg, 4.40 mmol, 87%) as a white solid (MP (CH_2Cl_2): 115.5 - 120.0 $^\circ\text{C}$).

199z: ^1H NMR (400 MHz, $\text{DMSO}-d_6$) δ ppm 11.08 (1H, s), 8.30 (1H, s), 6.89 (2H, s), 2.30 (6H, s), 2.23 (3H, s); ^{13}C NMR (101 MHz, $\text{DMSO}-d_6$) δ ppm 147.4, 137.4, 136.5, 128.9, 127.2, 20.7, 20.6; LCMS: $t_R = 1.05$ min, area% = 100%, $[\text{M}-\text{H}]^-$ 162 (100); IR ν_{max} (thin film): 3245, 2965, 2916, 1609, 1487, 1443, 1375, 1298, 1197 cm^{-1} ; HRMS (ESI-QToF): calculated for $[\text{M}+\text{H}]^+$ 164.1075, found 164.1077.

(E)-4-((Hydroxyimino)methyl)benzonitrile (199aa) and **(Z)-4-((hydroxyimino)methyl)benzonitrile (199aa')**

Prepared according to **GP1**, using 4-formylbenzonitrile (658 mg, 5.00 mmol), hydroxylamine hydrochloride (350 mg, 5.04 mmol, 1.0 eq.) and potassium carbonate (704 mg, 5.09 mmol, 1.0 eq.), stirring overnight and eluting with 0 - 30% EtOAc in cyclohexane over 20 CVs, affording (*E*)-4-((hydroxyimino)methyl)benzonitrile **199aa** (567 mg, 3.88 mmol, 77%) as a white solid (MP (CH₂Cl₂): 178.7 - 180.4 °C) and (*Z*)-4-((hydroxyimino)methyl)benzonitrile **199aa'** (53 mg, 0.37 mmol, 7%) as a white solid (MP (CH₂Cl₂): 149.0 - 152.4 °C).

199aa: ¹H NMR (400 MHz, DMSO-*d*₆) δ ppm 11.70 (1H, s), 8.24 (1H, s), 7.84 - 7.87 (2H, m), 7.75 - 7.79 (2H, m); ¹³C NMR (101 MHz, DMSO-*d*₆) δ ppm 147.0, 137.6, 132.6, 127.0, 118.6, 111.3; LCMS: t_R = 0.72 min, area% = 100%, [M-H]⁺ 145 (100); IR ν_{max} (thin film): 3233, 3166, 3024, 2229, 1606, 1508, 1475, 1409, 1328, 1307, 1286, 1218 cm⁻¹; HRMS (ESI-QToF): calculated for [M+H]⁺ 147.0558, found [M+H]⁺ 147.0555.



199aa': ¹H NMR (400 MHz, DMSO-*d*₆) δ ppm 12.08 (1H, s), 8.11 - 8.14 (2H, m), 7.89 - 7.93 (2H, m), 7.57 (1H, s); ¹³C NMR (101 MHz, DMSO-*d*₆) δ ppm 143.4, 134.5, 132.3, 130.7, 118.5, 111.5; LCMS: t_R = 0.72 min, area% = 98%, [M-H]⁺ 145 (100); IR ν_{max} (thin film): 3144, 3067, 3010, 2842, 2225, 1463, 1403, 1288 cm⁻¹; HRMS (ESI-QToF): calculated for [M+H]⁺ 147.0558, found [M+H]⁺ 147.0560.

(E)-2-Phenylacetaldehyde oxime (199ab)

Prepared according to **GP1**, using 2-phenylacetaldehyde (590 μL, 5.04 mmol), hydroxylamine hydrochloride (362 mg, 5.21 mmol, 1.0 eq.) and potassium carbonate (705 mg, 5.10 mmol, 1.0 eq.), stirring overnight and after work up, affording (*E*)-2-phenylacetaldehyde oxime **199ab** (497 mg, 3.67 mmol, 73%) as a white solid (MP (CH₂Cl₂): 82.5 - 86.2 °C).

199ab: ¹H NMR (400 MHz, DMSO-*d*₆) δ ppm 11.00 (1H, s), 7.28 - 7.36 (2H, m), 7.17 - 7.27 (3H, m), 6.81 (1H, t, *J* = 5.4 Hz), 3.61 (2H, d, *J* = 5.4 Hz); ¹³C NMR (101 MHz, DMSO-*d*₆) δ ppm 148.3, 137.3, 128.6, 128.5, 126.2, 31.0; LCMS: t_R = 0.81 min, area%

= 90%, [M-H]⁻ 134 (100); IR ν_{\max} (thin film): 3182, 3086, 3028, 3859, 1661, 1598, 1496, 1453, 1436, 1420, 1326 cm⁻¹; HRMS (ESI-QToF): calculated for [M+H]⁺ 136.0763, found 136.0761.

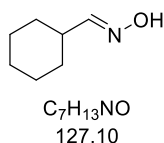
(E)-3-Phenylpropanal oxime (199ac)



Prepared according to **GP1**, using 3-phenylpropanal (660 μ L, 5.01 mmol), hydroxylamine hydrochloride (649 mg, 9.34 mmol, 1.9 eq.) and potassium carbonate (699 mg, 5.05 mmol, 1.0 eq.), stirring overnight and after work up, affording (*E*)-3-phenylpropanal oxime **199ac** (733 mg, 4.91 mmol, 98%) as a white solid (MP (CH₂Cl₂): 54.6 - 59.1 °C).

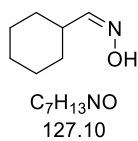
199ac: ¹H NMR (400 MHz, DMSO-*d*₆) δ ppm 10.78 (1H, s), 7.15 - 7.33 (5H, m), 6.66 (1H, t, *J* = 5.3 Hz), 2.74 (2H, t, *J* = 8.1 Hz), 2.52 - 2.57 (2H, m); ¹³C NMR (101 MHz, DMSO-*d*₆) δ ppm 149.5, 141.1, 128.3, 128.1, 125.9, 31.4, 26.1; LCMS: *t*_R = 0.88 min, area% = 90%, [M-H]⁻ 148 (100). Data consistent with literature synthesis.¹¹³

(E)-Cyclohexanecarbaldehyde oxime (199ad) and (Z)-cyclohexanecarbaldehyde oxime (199ad')



Prepared according to **GP1**, using cyclohexanecarbaldehyde (600 μ L, 4.95 mmol), hydroxylamine hydrochloride (352 mg, 5.07 mmol, 1.0 eq.) and potassium carbonate (688 mg, 4.98 mmol, 1.0 eq.), stirring overnight and eluting with 0 - 15% EtOAc in cyclohexane over 20 CVs, affording (*E*)-cyclohexanecarbaldehyde oxime **199ad** (357 mg, 2.81 mmol, 57%) as a colourless oil and (*Z*)-cyclohexanecarbaldehyde oxime **199ad'** (152 mg, 1.20 mmol, 24%) as a colourless oil.

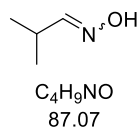
199ad: ¹H NMR (400 MHz, DMSO-*d*₆) δ ppm 10.32 (1H, s), 7.21 (1H, d, *J* = 5.6 Hz), 2.13 (1H, tdt, *J* = 10.8, 10.8, 5.8, 3.4, 3.4 Hz), 1.64 - 1.74 (4H, m), 1.09 - 1.33 (6H, m); ¹³C NMR (101 MHz, DMSO-*d*₆) δ ppm 153.3, 37.8, 30.0, 25.5, 25.0; LCMS: *t*_R = 0.87 min, area% = 80%, [M-H]⁻ 126 (100); IR ν_{\max} (thin film): 3211, 3091, 3023, 2924, 2852, 1663, 1449, 1328, 1264, 1229 cm⁻¹; HRMS (ESI-QToF): calculated for [M+H]⁺ 128.1075, found 128.1076.



199ad': ¹H NMR (400 MHz, DMSO-*d*₆) δ ppm 10.61 (1H, s), 6.45 (1H, d, *J* = 6.8 Hz), 2.81 (1H, tdt, *J* = 10.9, 10.9, 7.3, 3.5, 3.5 Hz), 1.56 - 1.70 (5H, m), 1.08 - 1.33 (5H, m); ¹³C NMR (101 MHz, DMSO-*d*₆) δ ppm 154.0,

33.1, 28.9, 25.5, 24.8; LCMS: $t_R = 0.90$ min, area% = 90%, $[M-H]^-$ 126 (100); IR ν_{max} (thin film): 3258, 3109, 2924, 2851, 1653, 1449, 1310, 1262 cm^{-1} ; HRMS (ESI-QToF): calculated for $[M+H]^+$ 128.1075, found 128.1074.

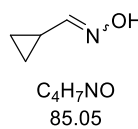
(Z)-Isobutyraldehyde oxime (199ae)



Prepared according to **GP1**, using isobutyraldehyde (2.3 mL, 25.20 mmol), stirring overnight and after work up, affording an inseparable mixture of (Z)-isobutyraldehyde oxime and (E)-isobutyraldehyde oxime **199ae** (2.3:1, 1321 mg, 15.16 mmol, 60%) as a colourless oil.

199ae: 1H NMR (400 MHz, DMSO- d_6) δ ppm 10.61 (s, *E-isomer*), 10.30 (1H, s), 7.24 (1H, d, $J = 5.6$ Hz), 6.45 (d, $J = 6.8$ Hz, *E-isomer*), 3.03 (dspt, $J = 7.1, 6.8, 6.8, 6.8, 6.8, 6.8$ Hz, *E-isomer*), 2.40 (1H, dsptd, $J = 7.0, 6.8, 1.2$ Hz), 1.01 (6H, d, $J = 6.8$ Hz), 0.96 (d, $J = 6.8$ Hz, *E-isomer*); ^{13}C NMR (101 MHz, DMSO- d_6) δ ppm 155.5 (*E-isomer*), 154.3, 28.7, 23.7 (*E-isomer*), 19.9, 19.4 (*E-isomer*); IR ν_{max} (thin film): 3257, 3100, 2966, 2873, 1652, 1466, 1385, 1313, 1280, 1103, 962, 941, 849, 696, 542, 463 cm^{-1} . Spectra recorded on mixture.

(Z)-Cyclobutanecarbaldehyde oxime (199af)



Prepared according to **GP1**, using cyclopropanecarbaldehyde (1 mL, 13.38 mmol), hydroxylamine hydrochloride (2.65 g, 38.10 mmol, 2.9 eq.) and potassium carbonate (5.30 g, 38.30 mmol, 2.9 eq.) and MeOH (0.13 M), stirring overnight and after work up, affording an inseparable mixture of (Z)-cyclopropanecarbaldehyde oxime and (E)-cyclopropanecarbaldehyde oxime **199af** (1.8:1, 923 mg, 10.85 mmol, 81%) as a white solid (MP (CH_2Cl_2): 91.4 - 95.8 $^{\circ}C$).

199af: 1H NMR (400 MHz, DMSO- d_6) δ ppm 10.50 (s, *E-isomer*), 10.20 (1H, s), 6.86 (1H, d, $J = 8.1$ Hz), 5.98 (d, $J = 8.8$ Hz, *E-isomer*), 2.11 (qt, $J = 8.4, 4.8$ Hz, *E-isomer*), 1.51 (1H, qt, $J = 8.2, 4.9$ Hz), 0.69 - 0.84 (4H, m, *mixture of geometric isomers*), 0.51 - 0.60 (4H, m, *mixture of geometric isomers*); ^{13}C NMR (101 MHz, DMSO- d_6) δ ppm 153.1 (*E-isomer*), 152.6, 10.7, 7.0 (*E-isomer*), 5.2 (*E-isomer*), 4.9; IR ν_{max} (thin film): 3172, 3089, 3016, 2872, 1661, 1459, 1433, 1330, 1297, 1193, 1102, 1061, 1031, 942, 871, 813, 697, 674 cm^{-1} . Spectra recorded on mixture.

(E)-Picolinaldehyde oxime (199ag)

Prepared according to **GP1**, using picolinaldehyde (480 μ L, 5.05 mmol), hydroxylamine hydrochloride (356 mg, 5.13 mmol, 1.0 eq.) and potassium carbonate (702 mg, 5.08 mmol, 1.0 eq.), stirring overnight and after work up, affording (*E*)-picolinaldehyde oxime **199ag** (544 mg, 4.45 mmol, 88%) as a white solid (MP (CH_2Cl_2): 113.0 - 115.0 $^\circ\text{C}$).

199ag: ^1H NMR (400 MHz, $\text{DMSO-}d_6$) δ ppm 11.63 (1H, s), 8.57 (1H, dt, $J = 4.8, 1.4$ Hz), 8.07 (1H, s), 7.82 (1H, td, $J = 7.7, 1.8$ Hz), 7.78 (1H, dt, $J = 7.7, 1.4$ Hz), 7.37 (1H, ddd, $J = 6.9, 4.8, 1.8$ Hz); ^{13}C NMR (101 MHz, $\text{DMSO-}d_6$) δ ppm 152.0, 149.3, 148.9, 136.7, 123.9, 119.7; LCMS: $t_R = 0.47$ min, area% = 99%, $[\text{M}+\text{H}]^+$ 123 (100). Data consistent with literature synthesis.¹¹⁴

(E)-Nicotinaldehyde oxime (199ah)

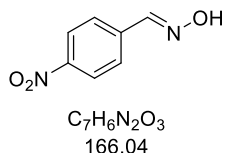
Prepared according to **GP1**, using nicotinaldehyde (470 μ L, 5.01 mmol), stirring overnight, and chromatographed on a 40 g silica column, eluting with 0 - 60% EtOAc in cyclohexane over 20 CVs affording an inseparable mixture of (*E*)-nicotinaldehyde oxime and (*Z*)-nicotinaldehyde oxime **199ah** (7:1, 506 mg, 4.14 mmol, 83%) as a white solid (MP (CH_2Cl_2): 146.8 - 149.4 $^\circ\text{C}$).

199ah: ^1H NMR (400 MHz, $\text{DMSO-}d_6$) δ ppm 11.91 (s, *Z*-isomer), 11.50 (1H, s), 9.05 (d, $J = 2.0$ Hz, *Z*-isomer), 8.75 (1H, d, $J = 1.9$ Hz), 8.56 (1H, dd, $J = 4.7, 1.7$ Hz), 8.40 (dt, $J = 7.9, 2.0$ Hz, *Z*-isomer), 8.20 (1H, s), 7.98 (1H, dt, $J = 7.7, 1.9$ Hz), 7.51 (s, *Z*-isomer), 7.47 (ddd, $J = 7.9, 4.9, 0.7$ Hz, *Z*-isomer), 7.42 (1H, ddd, $J = 7.7, 4.7, 0.6$ Hz); ^{13}C NMR (101 MHz, $\text{DMSO-}d_6$) δ ppm 150.8 (*Z*-isomer), 150.0, 149.8 (*Z*-isomer), 147.8, 145.7, 142.3 (*Z*-isomer), 137.2 (*Z*-isomer), 133.0, 128.9, 123.8, 123.5 (*Z*-isomer); LCMS: $t_R = 0.46$ min, area% = 94%, $[\text{M}+\text{H}]^+$ 123 (100); IR ν_{max} (thin film): 3164, 3055, 2946, 2847, 2697, 1637, 1582, 1518, 1411, 1311, 1257, 1124, 934, 881, 805, 703, 638, 514, 459 cm^{-1} ; HRMS (ESI-QToF): calculated for $[\text{M}+\text{H}]^+$ 123.0558, found 123.0558. Spectra recorded on mixture.

(E)-Isonicotinaldehyde oxime (199ai)

Prepared according to **GP1**, using isonicotinaldehyde (480 μ L, 5.10 mmol), stirring overnight, and chromatographed on a 40 g silica column, eluting with 0 - 60% EtOAc in cyclohexane over 20 CVs affording an inseparable mixture of (*E*)-isonicotinaldehyde oxime and (*Z*)-isonicotinaldehyde oxime **199ai** (14:1, 537 mg, 4.40 mmol, 86%) as a white solid (MP (CH_2Cl_2): 124.8 - 128.0 $^{\circ}C$).

199ai: 1H NMR (400 MHz, $DMSO-d_6$) δ ppm 12.15 (s, *Z*-isomer), 11.78 (1H, s), 8.67 (dd, $J = 4.4, 1.5$ Hz, *Z*-isomer), 8.59 (2H, dd, $J = 4.4, 1.7$ Hz), 8.17 (1H, s), 7.83 (dd, $J = 4.4, 1.5$ Hz, *Z*-isomer), 7.54 (2H, dd, $J = 4.4, 1.7$ Hz), 7.52 (s, *Z*-isomer); ^{13}C NMR (101 MHz, $DMSO-d_6$) δ ppm 150.2 (*Z*-isomer), 150.1, 146.6, 140.2, 123.8 (*Z*-isomer), 120.5; LCMS: $t_R = 0.45$ min, area% = 94%, $[M+H]^+$ 123 (100); IR ν_{max} (thin film): 3048, 2945, 2843, 2673, 2603, 1692, 1602, 1566, 1514, 1418, 1311, 1220, 987, 932, 883, 819, 736, 663, 646, 584, 535 cm^{-1} ; HRMS (ESI-QToF): calculated for $[M+H]^+$ 123.0558, found 123.0558. Spectra recorded on mixture.

(E)-4-Nitrobenzaldehyde oxime (199aj) and (Z)-4-nitrobenzaldehyde oxime (199aj')

Prepared according **GP1**, using 4-nitrobenzaldehyde (758 mg, 5.02 mmol), hydroxylamine hydrochloride (350 mg, 5.04 mmol) and potassium carbonate (694 mg, 5.02 mmol), stirring overnight and eluting with 0 - 25% EtOAc in cyclohexane over 20 CVs, affording (*E*)-4-nitrobenzaldehyde oxime **199aj** (676 mg, 4.07 mmol, 81%) as a white solid (MP (CH_2Cl_2): 132.2 - 134.2 $^{\circ}C$) and (*Z*)-4-nitrobenzaldehyde oxime **199aj'** (77 mg, 0.46 mmol, 9%) as a white solid (MP (CH_2Cl_2): 163.0 - 166.3 $^{\circ}C$).

199aj: 1H NMR (400 MHz, $DMSO-d_6$) δ ppm 11.82 (1H, s), 8.31 (1H, s), 8.23 - 8.28 (2H, m), 7.84 - 7.88 (2H, m); ^{13}C NMR (101 MHz, $DMSO-d_6$) δ ppm 147.5, 146.8, 139.4, 127.3, 123.9; LCMS: $t_R = 0.81$ min, area% = 100%, $[M-H]^-$ 165 (100). Data consistent with literature synthesis.⁷⁶



199aj': 1H NMR (400 MHz, $DMSO-d_6$) δ ppm 12.20 (1H, s), 8.27 - 8.32 (2H, m), 8.19 - 8.24 (2H, m), 7.65 (1H, s); ^{13}C NMR (101 MHz, $DMSO-d_6$) δ ppm 147.1, 143.0, 136.2, 131.3, 123.5; LCMS: $t_R = 0.81$

min, area% = 96%, [M-H]⁻ 165 (100); IR ν_{\max} (thin film): 3121, 3071, 3014, 2785, 1602, 1512, 1340, 838 cm⁻¹; HRMS (ESI-QToF): calculated for [M+H]⁺ 167.0457, found 167.0460.

(E)-N-(4-((hydroxyimino)methyl)phenyl)acetamide (271)



Prepared according to **GP1**, using *N*-(4-formylphenyl)acetamide (819 mg, 5.02 mmol), stirring overnight and after work up, affording (*E*)-*N*-(4-((hydroxyimino)methyl)phenyl)acetamide **271** (537 mg, 3.01 mmol, 60%) as a white solid (MP (CH₂Cl₂): 213.6

- 216.5 °C).

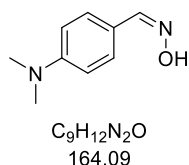
271: ¹H NMR (400 MHz, DMSO-*d*₆) δ ppm 11.01 (1H, s), 10.03 (1H, s), 8.05 (1H, s), 7.60 (2H, d, *J* = 8.8 Hz), 7.50 (2H, d, *J* = 8.8 Hz), 2.05 (3H, s); ¹³C NMR (101 MHz, DMSO-*d*₆) δ ppm 168.3, 147.6, 140.2, 127.6, 126.9, 118.8, 24.0; LCMS: *t*_R = 0.55 min, area% = 98%, [M-H]⁻ 177 (100); IR ν_{\max} (thin film): 3316, 3128, 3052, 2978, 2884, 2767, 1659, 1629, 1501, 1532, 1515, 1403, 1375, 1316, 1301, 1268, 1173, 938, 835, 667, 529, 460 cm⁻¹; HRMS (ESI-QToF): calculated for [M+H]⁺ 179.0821, found 179.0824.

(E)-4-(Dimethylamino)benzaldehyde oxime (272) and (Z)-4-(dimethylamino)benzaldehyde oxime (272')



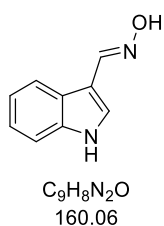
Prepared according to **GP1**, using 4-(dimethylamino)benzaldehyde (749 mg, 5.02 mmol), stirring overnight and eluting with 0 - 40% EtOAc in cyclohexane over 20 CVs (dry loaded from DCM:MeOH), affording (*E*)-4-(dimethylamino)benzaldehyde oxime **272** (470 mg, 2.86 mmol, 57%) as a white solid (MP (CH₂Cl₂): 149.7 - 152.4 °C) and (*Z*)-4-(dimethylamino)benzaldehyde oxime **272'** (109 mg, 0.66 mmol, 13%) as an off-white solid (MP (CH₂Cl₂): 135.3 - 138.1 °C).

272: ¹H NMR (400 MHz, DMSO-*d*₆) δ ppm 10.62 (1H, s), 7.96 (1H, s), 7.39 (2H, dt, *J* = 9.0, 2.2 Hz), 6.70 (2H, dt, *J* = 9.0, 2.2 Hz), 2.93 (6H, s); ¹³C NMR (101 MHz, DMSO-*d*₆) δ ppm 150.9, 148.0, 127.4, 120.5, 111.9, 39.8; LCMS: *t*_R = 0.85 min, area% = 100%, [M+H]⁺ 165 (100); IR ν_{\max} (thin film): 3203, 3134, 2910, 2801, 1601, 1557, 1524, 1444, 1359, 1301, 1224, 1185, 1168, 1125, 1065, 951, 867, 809, 727, 637, 570, 527, 493 cm⁻¹; HRMS (ESI-QToF): calculated for [M+H]⁺ 165.1028, found 165.1031. Data consistent with literature synthesis.¹¹¹



272': ¹H NMR (400 MHz, DMSO-*d*₆) δ ppm 11.00 (1H, s), 7.81 (2H, dt, *J* = 9.0, 2.2 Hz), 7.16 (1H, s), 6.70 (2H, dt, *J* = 9.0, 2.2 Hz), 2.95 (6H, s); ¹³C NMR (101 MHz, DMSO-*d*₆) δ ppm 150.5, 144.8, 131.9, 119.4, 111.1, 39.6; LCMS: *t*_R = 0.85 min, area% = 97%, [M+H]⁺ 165 (100); IR *v*_{max} (thin film): 3145, 2799, 1596, 1516, 1345, 1186, 1162, 1062, 904, 851, 811, 770, 658, 629 cm⁻¹; HRMS (ESI-QToF): calculated for [M+H]⁺ 165.1028, found 165.1029.

(*E*)-1*H*-Indole-3-carbaldehyde oxime (273) and (*Z*)-1*H*-indole-3-carbaldehyde oxime (273')

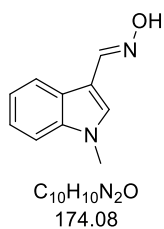


Prepared according to **GP1**, using 1*H*-indole-3-carbaldehyde (730 mg, 5.03 mmol), stirring overnight and eluting with 0 - 50% EtOAc in cyclohexane over 20 CVs (dry loaded from DCM:MeOH), affording (*E*)-1*H*-indole-3-carbaldehyde oxime **273** (319 mg, 1.99 mmol, 40%) as a white solid (MP (CH₂Cl₂): 185.5 - 192.7 °C) and (*Z*)-1*H*-indole-3-carbaldehyde oxime **273'** (68 mg, 0.42 mmol, 8%) as an off-white solid (MP (CH₂Cl₂): 120.8 - 124.2 °C).

273: ¹H NMR (400 MHz, DMSO-*d*₆) δ ppm 11.36 (1H, br s), 10.46 (1H, s), 8.26 (1H, s), 7.97 (1H, dt, *J* = 8.1, 1.0 Hz), 7.61 (1H, d, *J* = 1.2 Hz), 7.41 (1H, dt, *J* = 8.1, 1.0 Hz), 7.16 (1H, ddd, *J* = 8.1, 7.0, 1.2 Hz), 7.08 (1H, ddd, *J* = 8.1, 7.0, 1.2 Hz); ¹³C NMR (101 MHz, DMSO-*d*₆) δ ppm 144.5, 136.8, 128.3, 124.2, 122.2, 121.4, 119.9, 111.7, 109.5; LCMS: *t*_R = 0.70 min, area% = 100%, [M-H]⁻ 159 (100); IR *v*_{max} (thin film): 3398, 3279, 3119, 3055, 2845, 1634, 1542, 1456, 1415, 1334, 1308, 1248, 1103, 964, 910, 801, 746, 614, 525, 494 cm⁻¹; HRMS (ESI-QToF): calculated for [M+H]⁺ 161.0715, found 161.0716.

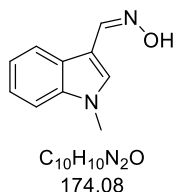


273': ¹H NMR (400 MHz, DMSO-*d*₆) δ ppm 11.54 (1H, br s), 11.14 (1H, s), 8.21 (1H, d, *J* = 2.4 Hz), 7.85 (1H, dt, *J* = 7.8, 1.0 Hz), 7.77 (1H, s), 7.44 (1H, dt, *J* = 7.9, 1.0 Hz), 7.16 (1H, ddd, *J* = 7.9, 6.9, 1.0 Hz), 7.10 (1H, ddd, *J* = 7.9, 6.9, 1.0 Hz); ¹³C NMR (101 MHz, DMSO-*d*₆) δ ppm 138.3, 134.9, 130.4, 126.1, 121.8, 119.8, 118.1, 111.7, 106.3; LCMS: *t*_R = 0.72 min, area% = 91%, [M-H]⁻ 159 (100); IR *v*_{max} (thin film): 3385, 3157, 3051, 3013, 2782, 1640, 1520, 1458, 1414, 1340, 1232, 1098, 929, 840, 745, 660, 588, 551, 461 cm⁻¹; HRMS (ESI-QToF): calculated for [M+H]⁺ 161.0715, found 161.0717.

(E)-1-Methyl-1H-indole-3-carbaldehyde oxime (274) and **(Z)-1-methyl-1H-indole-3-carbaldehyde oxime (274')**

Prepared according to **GP1**, using 1-methyl-1*H*-indole-3-carbaldehyde (798 mg, 5.01 mmol), stirring overnight and eluting with 0 - 50% EtOAc in cyclohexane over 20 CVs (dry loaded from DCM:MeOH), affording (*E*)-1-methyl-1*H*-indole-3-carbaldehyde oxime **274** (381 mg, 2.19 mmol, 44%) as a white solid (MP (CH₂Cl₂): 125.7 - 129.8 °C) and (*Z*)-1-methyl-1*H*-indole-3-carbaldehyde oxime **274'** (238 mg, 1.37 mmol, 27%) as an off-white solid (MP (CH₂Cl₂): 140.0 - 142.2 °C).

274: ¹H NMR (400 MHz, DMSO-*d*₆) δ ppm 10.49 (1H, s), 8.24 (1H, s), 7.98 (1H, dt, *J* = 7.8, 1.1 Hz), 7.59 (1H, s), 7.47 (1H, dt, *J* = 8.2, 1.1 Hz), 7.23 (1H, ddd, *J* = 8.2, 7.0, 1.1 Hz), 7.13 (1H, ddd, *J* = 7.8, 7.0, 1.1 Hz), 3.79 (3H, s); ¹³C NMR (101 MHz, DMSO-*d*₆) δ ppm 144.1, 137.3, 132.0, 124.6, 122.3, 121.5, 110.0, 106.6, 32.6; LCMS: *t*_R = 0.85 min, area% = 100%, [M-H]⁻ 173 (100); IR *v*_{max} (thin film): 3278, 3238, 3117, 2996, 2905, 1635, 1541, 1480, 1450, 1420, 1369, 1334, 1254, 1194, 1130, 1075, 809, 741, 614, 561 cm⁻¹; HRMS (ESI-QToF): calculated for [M+H]⁺ 175.0871, found 175.0874.

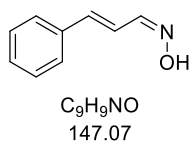


274': ¹H NMR (400 MHz, DMSO-*d*₆) δ ppm 11.19 (1H, s), 8.24 (1H, s), 7.87 (1H, dt, *J* = 7.9, 0.9 Hz), 7.77 (1H, s), 7.49 (1H, dt, *J* = 8.3, 0.9 Hz), 7.23 (1H, ddd, *J* = 8.3, 7.0, 0.9 Hz), 7.15 (1H, ddd, *J* = 7.9, 7.0, 0.9 Hz), 3.85 (3H, s); ¹³C NMR (101 MHz, DMSO-*d*₆) δ ppm 137.9, 135.4, 134.4, 126.6, 121.9, 120.0, 118.3, 110.0, 105.3, 32.7; LCMS: *t*_R = 0.85 min, area% = 100%, [M+H]⁺ 175 (100); IR *v*_{max} (thin film): 3146, 3045, 3007, 2861, 2788, 1631, 1519, 1475, 1458, 1332, 1240, 1202, 943, 872, 736, 527 cm⁻¹; HRMS (ESI-QToF): calculated for [M+H]⁺ 175.0871, found 175.0873.

(1E,2E)-Cinnamaldehyde oxime (275) and **(1Z,2E)-cinnamaldehyde oxime (275')**

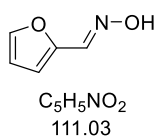
Prepared according to **GP1**, using cinnamaldehyde (630 μL, 5.01 mmol), stirring overnight and eluting with 0 - 25% EtOAc in cyclohexane over 20 CVs, affording (1*E*,2*E*)-cinnamaldehyde oxime **275** (449 mg, 3.05 mmol, 61%) as a white solid (MP (CH₂Cl₂): 71.6 - 74.5 °C) and (1*Z*,2*E*)-cinnamaldehyde oxime **275'** (243 mg, 1.65 mmol, 33%) as a white solid (MP (CH₂Cl₂): 131.8 - 135.1 °C).

275: ^1H NMR (400 MHz, $\text{DMSO-}d_6$) δ ppm 11.08 (1H, s), 7.88 - 7.93 (1H, m), 7.51 - 7.57 (2H, m), 7.34 - 7.39 (2H, m), 7.27 - 7.32 (1H, m), 6.89 - 6.92 (2H, m); ^{13}C NMR (101 MHz, $\text{DMSO-}d_6$) δ ppm 150.2, 136.5, 136.0, 128.7, 128.4, 126.7, 123.0; LCMS: t_R = 0.91 min, area% = 100%, $[\text{M-H}]^-$ 146 (100). Data consistent with literature synthesis.¹¹¹



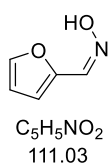
275': ^1H NMR (400 MHz, $\text{DMSO-}d_6$) δ ppm 11.21 (1H, s), 7.52 - 7.59 (2H, m), 7.28 - 7.42 (5H, m), 6.96 (1H, d, J = 15.4 Hz); ^{13}C NMR (101 MHz, $\text{DMSO-}d_6$) δ ppm 147.1, 137.8, 135.9, 128.9, 128.8, 127.1, 116.1; LCMS: t_R = 0.89 min, area% = 100%, $[\text{M-H}]^-$ 146 (100); IR ν_{max} (thin film): 3149, 3047, 3000, 2843, 1633, 1450, 1332, 1310, 1137, 978, 946, 920, 859, 750, 688, 546, 469 cm^{-1} ; HRMS (ESI-QToF): calculated for $[\text{M+H}]^+$ 148.0762, found 148.0763.

(E)-Furan-2-carbaldehyde oxime (276) and (Z)-furan-2-carbaldehyde oxime (276')



Prepared according to **GP1**, using furan-2-carbaldehyde (420 μL , 5.07 mmol), hydroxylamine hydrochloride (355 mg, 5.11 mmol, 1.0 eq.) and potassium carbonate (706 mg, 5.11 mmol, 1.0 eq.), stirring overnight and chromatographing on 80 g column, eluting with 0 - 20% TBME in cyclohexane over 20 CVs, affording (*E*)-furan-2-carbaldehyde oxime **276** (181 mg, 1.63 mmol, 32%) as a white solid (MP (CH_2Cl_2): 91.6 - 93.0 $^\circ\text{C}$) and (*Z*)-furan-2-carbaldehyde oxime **276'** (281 mg, 2.53 mmol, 50%) as a white solid (MP (CH_2Cl_2): 72.3 - 75.1 $^\circ\text{C}$).

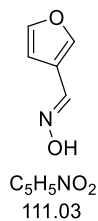
276: ^1H NMR (400 MHz, $\text{DMSO-}d_6$) δ ppm 11.76 (1H, s), 7.75 (1H, dd, J = 1.7, 0.7 Hz), 7.51 (1H, s), 7.19 (1H, d, J = 3.4 Hz), 6.63 (1H, ddt, J = 2.6, 1.7, 0.7, 0.7 Hz); ^{13}C NMR (101 MHz, $\text{DMSO-}d_6$) δ ppm 145.3, 143.3, 135.4, 116.3, 112.1; LCMS: t_R = 0.58 min, area% = 94%, $[\text{M-H}]^-$ 110 (100); IR ν_{max} (thin film): 3162, 3146, 3071, 3034, 3012, 2856, 2815, 2767, 1646, 1506, 1476, 1448, 1376, 1321, 1237 cm^{-1} ; HRMS (ESI-QToF): calculated for $[\text{M+H}]^+$ 112.0398, found 112.0398.



276': ^1H NMR (400 MHz, $\text{DMSO-}d_6$) δ ppm 11.21 (1H, s), 8.01 (1H, s), 7.72 - 7.74 (1H, m), 6.69 (1H, d, J = 3.4 Hz), 6.56 (1H, td, J = 2.4, 1.3 Hz); ^{13}C NMR (101 MHz, $\text{DMSO-}d_6$) δ ppm 147.8, 144.1, 138.8, 111.6, 111.5; LCMS: t_R = 0.58 min, area% = 94%, $[\text{M-H}]^-$ 110 (100); IR ν_{max} (thin film): 3218, 3132, 3050, 2981, 2911, 2848, 2783, 2708, 1566, 1502, 1439, 1418, 1387,

1288, 1270 cm^{-1} ; HRMS (ESI-QToF): calculated for $[\text{M}+\text{H}]^+$ 112.0398, found 112.0399. Data consistent with literature synthesis.¹¹⁵

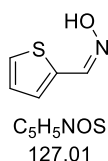
(*E*)-Furan-3-carbaldehyde oxime (277)



Prepared according to **GP1**, using furan-3-carbaldehyde (420 μL , 5.07 mmol), hydroxylamine hydrochloride (359 mg, 5.17 mmol, 1.0 eq.) and potassium carbonate (707 mg, 5.12 mmol, 1.0 eq.), stirring overnight and chromatographing on 80 g column, eluting with 0 - 20% TBME in cyclohexane over 20 CVs, affording (*E*)-furan-3-carbaldehyde oxime **277** (127 mg, 1.15 mmol, 23%) as a white solid (MP (CH_2Cl_2): 111.8 - 114.1 $^\circ\text{C}$).

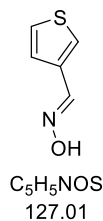
277: ^1H NMR (400 MHz, $\text{DMSO}-d_6$) δ ppm 11.53 (1H, s), 8.27 - 8.30 (1H, m), 7.70 (1H, t, $J = 1.7$ Hz), 7.36 (1H, s), 6.77 (1H, dd, $J = 2.0, 0.7$ Hz); ^{13}C NMR (151 MHz, $\text{DMSO}-d_6$) δ ppm 146.0, 142.9, 137.9, 116.6, 110.9 LCMS: $t_R = 0.55$ min, area% = 89%, $[\text{M}-\text{H}]^-$ 110 (100); IR ν_{max} (thin film): 3173, 3155, 3132, 3066, 3023, 2842, 2788, 1640, 1560, 1499, 1427, 1364, 1316, 1232 cm^{-1} ; HRMS (ESI-QToF): calculated for $[\text{M}+\text{H}]^+$ 112.0394, found 112.0395.

(*Z*)-Thiophene-2-carbaldehyde oxime (278)



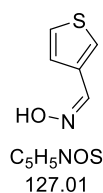
Prepared according to **GP1**, using thiophene-2-carbaldehyde (470 μL , 5.03 mmol), hydroxylamine hydrochloride (358 mg, 5.15 mmol, 1.0 eq.) and potassium carbonate (702 mg, 5.08 mmol, 1.0 eq.), stirring overnight and chromatographing on 80 g column, eluting with 0 - 20% TBME in cyclohexane over 20 CVs, affording (*Z*)-thiophene-2-carbaldehyde oxime **278** (521 mg, 4.09 mmol, 81%) as a white solid (MP (CH_2Cl_2): 140.3 - 142.3 $^\circ\text{C}$).

278: ^1H NMR (400 MHz, $\text{DMSO}-d_6$) δ ppm 11.81 (1H, s), 7.84 (1H, s), 7.73 (1H, dt, $J = 5.1, 1.2$ Hz), 7.47 (1H, dd, $J = 3.8, 1.2$ Hz), 7.13 (1H, dd, $J = 5.1, 3.8$ Hz); ^{13}C NMR (151 MHz, $\text{DMSO}-d_6$) δ ppm 139.7, 131.1, 131.0, 130.9, 126.1; LCMS: $t_R = 0.67$ min, area% = 92%, $[\text{M}-\text{H}]^-$ 126 (100); IR ν_{max} (thin film): 3012, 2856, 2756, 1630, 1433, 1416, 1347, 1306, 1232, 1213 cm^{-1} ; HRMS (ESI-QToF): calculated for $[\text{M}+\text{H}]^+$ 128.0170, found 128.0173.

(E)-Thiophene-3-carbaldehyde oxime (279) and **(Z)-thiophene-3-carbaldehyde oxime (279')**

Prepared according to **GP1**, using thiophene-3-carbaldehyde (450 μ L, 5.14 mmol), hydroxylamine hydrochloride (358 mg, 5.15 mmol, 1.0 eq.) and potassium carbonate (720 mg, 5.21 mmol, 1.0 eq.), stirring overnight and eluting with 0 - 20% EtOAc in cyclohexane over 20 CVs, affording a mixture of (*E*)-thiophene-3-carbaldehyde oxime and (*Z*)-thiophene-3-carbaldehyde oxime **279** (3:1, 355 mg, 2.79 mmol, 54%) as a white solid (MP (CH₂Cl₂): 126.6 - 129.5 °C) and (*Z*)-thiophene-3-carbaldehyde oxime **277'** (146 mg, 1.15 mmol, 22%) as a white solid (MP (CH₂Cl₂): 133.1 - 134.3 °C).

279: ¹H NMR (400 MHz, DMSO-*d*₆) δ ppm 11.49 (s, *Z*-isomer), 10.97 (1H, s), 8.22 (dd, *J* = 2.8, 1.3 Hz, *Z*-isomer), 8.15 (1H, s), 7.70 (1H, dd, *J* = 2.9, 1.3 Hz), 7.57 (1H, ddd, *J* = 5.1, 2.9, 0.6 Hz), 7.53 - 7.57 (m, *Z*-isomer), 7.49 (s, *Z*-isomer), 7.34 (1H, ddd, *J* = 5.1, 1.3, 0.6 Hz); ¹³C NMR (101 MHz, DMSO-*d*₆) δ ppm 143.7 (*Z*-isomer), 139.6 (*E*-isomer), 135.3 (*Z*-isomer), 132.1 (*E*-isomer), 130.2 (*E*-isomer), 129.3 (*E*-isomer), 127.3 (*Z*-isomer), 125.9 (*Z*-isomer), 125.6 (*E*-isomer), 124.4 (*Z*-isomer); LCMS: (*E* isomer) *t*_R = 0.65 min, area% = 59%, [M-H]⁻ 126 (100); (*Z* isomer) *t*_R = 0.67 min, area% = 34%. [M-H]⁻ 126 (100); IR ν_{max} (thin film): 3132, 3083, 3021, 2854, 2790, 1641, 1515, 1440, 1358, 1325, 1241, 1146, 977, 917, 841, 780, 695, 638 cm⁻¹; HRMS (ESI-QToF): calculated for [M+H]⁺ 128.0170, found 128.0170. Spectra recorded on mixture.



279': ¹H NMR (400 MHz, DMSO-*d*₆) δ ppm 11.49 (1H, s), 8.22 (1H, dd, *J* = 2.9, 1.2 Hz), 7.56 (1H, dd, *J* = 5.0, 2.9 Hz), 7.54 (1H, dd, *J* = 5.0, 1.2 Hz), 7.49 (1H, s); ¹³C NMR (101 MHz, DMSO-*d*₆) δ ppm 139.6, 132.1, 130.2, 129.3, 125.6; LCMS: *t*_R = 0.67 min, area% = 86%, [M-H]⁻ 126 (100); IR ν_{max} (thin film): 3132, 3069, 3021, 2860, 2785, 1461, 1515, 1440, 1358, 1324, 1241, 1146, 977, 917, 841, 780, 695, 638 cm⁻¹; HRMS (ESI-QToF): calculated for [M+H]⁺ 128.0170, found 128.0170.

***tert*-Butyl (*E*)-2-benzylidenehydrazine-1-carboxylate (259a)**

Prepared according to **GP1**, using benzaldehyde (510 μ L, 5.02 mmol), *tert*-butylhydrazinecarboxylate (672 mg, 5.09 mmol) and potassium carbonate (697 mg, 5.05 mmol, 1.0 eq.), stirring overnight, affording *tert*-butyl (*E*)-2-benzylidenehydrazine-1-

carboxylate **259a** (1065 mg, 4.83 mmol, 96%) as a white solid (MP (CH₂Cl₂): 190.8 - 192.2 °C).

259a: ¹H NMR (400 MHz, DMSO-*d*₆) δ ppm 10.86 (1H, br. s), 8.00 (1H, s), 7.57 - 7.62 (2H, m), 7.34 - 7.44 (3H, m), 1.47 (9H, s); ¹³C NMR (101 MHz, DMSO-*d*₆) δ ppm 152.9, 143.6, 135.1, 129.8, 129.2, 126.9, 79.9, 28.6; LCMS: t_R = 1.03 min, area% = 100%, [M-H]⁻ 219 (100); IR ν_{max} (thin film): 3248, 2982, 1689, 1525, 1487, 1447, 1369, 1247, 1150, 1055, 965, 859, 758, 692, 626 cm⁻¹. Data consistent with literature synthesis.¹¹³

(*E*)-*N*-Benzylideneacetohydrazide (**259b**)



Prepared according to **GP1**, using benzaldehyde (510 μL, 5.02 mmol), acetohydrazide (383 mg, 5.17 mmol) and potassium carbonate (708 mg, 5.12 mmol, 1.0 eq.), stirring overnight, affording (*E*)-*N*-benzylideneacetohydrazide **259b** (813 mg, 5.01 mmol, 100%)

as a white solid (MP (CH₂Cl₂): 138.6 - 140.3 °C).

259b: ¹H NMR (400 MHz, DMSO-*d*₆, mixture of rotamers) δ ppm 11.33 (s, *minor rotamer*), 11.21 (1H, s), 8.15 (s, *minor rotamer*), 7.98 (1H, s), 7.62 - 7.70 (2H, m), 7.36 - 7.48 (3H, m), 2.20 (3H, s), 1.95 (s, *minor rotamer*); ¹³C NMR (101 MHz, DMSO-*d*₆, mixture of rotamers) δ ppm 171.8, 165.5 (*minor rotamer*), 145.5 (*minor rotamer*), 142.4, 134.3 (*minor rotamer*), 134.2, 129.8 (*minor rotamer*), 129.5, 128.7, 128.7 (*minor rotamer*), 126.9 (*minor rotamer*), 126.6, 21.6 (*minor rotamer*), 20.2; LCMS: t_R = 0.71 min, area% = 100%, [M-H]⁻ 161 (100), [M+H]⁺ 163 (100); IR ν_{max} (thin film): 3081, 2975, 2870, 1671, 1393, 1341, 1137, 1020, 951, 900, 757, 689, 601, 513 cm⁻¹. Data consistent with literature synthesis.¹¹⁶

(*E*)-*N*-Benzylidene-4-methylbenzenesulfonohydrazide (**259c**)



Prepared according to **GP1**, using benzaldehyde (510 μL, 5.02 mmol), 4-methylbenzenesulfonohydrazide (958 mg, 5.14 mmol) and potassium carbonate (707 mg, 5.12 mmol, 1.0 eq.), stirring overnight, affording (*E*)-*N*-benzylidene-4-

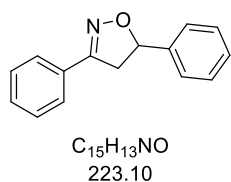
methylbenzenesulfonohydrazide **259c** (1138 mg, 4.15 mmol, 83%) as a white solid (MP (CH₂Cl₂): 119.4 - 123.8 °C).

259c: ¹H NMR (400 MHz, DMSO-*d*₆) δ ppm 11.40 (1H, s), 7.91 (1H, s), 7.74 - 7.78 (2H, m), 7.52 - 7.57 (2H, m), 7.36 - 7.43 (5H, m), 2.36 (3H, s); ¹³C NMR (101 MHz,

DMSO-*d*₆) δ ppm 146.9, 143.4, 136.1, 133.6, 130.0, 129.6, 128.7, 127.1, 126.7, 20.9;
LCMS: t_R = 0.81 min, area% = 95%, no appropriate mass ion; IR ν_{max} (thin film): 3225,
1596, 1495, 1437, 1364, 1311, 1226, 1161, 1093, 1043, 958, 815, 751, 664, 548 cm^{-1} ;
HRMS (ESI-QToF): calculated for [M+H]⁺ 275.0855, found 275.0849. Data
consistent with literature synthesis.¹¹⁷

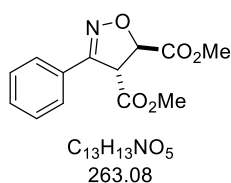
6.2.2. General Procedure 2 for Chemical Isoxazoline Synthesis (GP2)

To a microwave vial containing a stirrer bar, (*E*)-benzaldehyde oxime (1 eq.) was added followed by DMF (10 mL) and NCS (1.2 eq.). The resulting solution was stirred at ambient temperature for 1 hr. After 1 hr, dipolarophile (1.2 eq.) followed by DBU (1 eq.) were added, and the reaction mixture allowed to continue to stir at ambient temperature. After stirring overnight, the reaction mixture was diluted with water (40 mL) and extracted with EtOAc (3 x 20 mL). The combined organic layers were washed with aqueous 5% LiCl solution (5 x 10 mL), brine (20 mL) and dried (hydrophobic frit). The solvent was removed *in vacuo* to give the crude mixture. The crude mixture was submitted to column chromatography on silica gel, eluting with EtOAc/cyclohexane to afford the desired product.

3,5-Diphenyl-4,5-dihydroisoxazole (201)

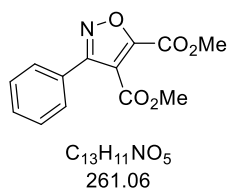
Prepared according to **GP2** using (*E*)-benzaldehyde oxime (5.01 mmol) and styrene as dipolarophile, eluting with 0 - 15% EtOAc in cyclohexane over 20 CVs, affording 3,5-diphenyl-4,5-dihydroisoxazole **201** (648 mg, 2.90 mmol, 58%) as a white solid (MP (CH₂Cl₂): 74.5 - 76.0 °C).

201: ¹H NMR (400 MHz, DMSO-*d*₆) δ ppm 7.69 - 7.75 (2H, m), 7.44 - 7.49 (3H, m), 7.31 - 7.42 (5H, m), 5.74 (1H, dd, *J* = 10.9, 8.6 Hz), 3.88 (1H, dd, *J* = 17.1, 10.9 Hz), 3.40 (1H, dd, *J* = 17.1, 8.6 Hz); ¹³C NMR (101 MHz, DMSO-*d*₆) δ ppm 156.4, 140.8, 130.1, 129.2, 128.7, 128.6, 128.0, 126.6, 126.1, 82.0, 42.1; LCMS: *t*_R = 1.18 min, area% = 100, [M+H]⁺ 224 (100); IR *v*_{max} (thin film): 3062, 3028, 2877, 1447, 1363, 893, 750, 686 cm⁻¹; HRMS (ESI-QToF): calculated for [M+H]⁺ 224.1075, found 224.1077.

Dimethyl (*anti*)-3-phenyl-4,5-dihydroisoxazole-4,5-dicarboxylate (205) from 208 (dimethyl fumarate)

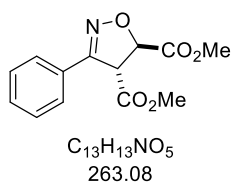
Prepared according to **GP2** using (*E*)-benzaldehyde oxime (4.99 mmol) and dimethyl fumarate as dipolarophile, eluting with 0 - 20% EtOAc in cyclohexane over 20 CVs, affording dimethyl (*anti*)-3-phenyl-4,5-dihydroisoxazole-4,5-dicarboxylate **205** (dr = 20:1, 647 mg, 2.46 mmol, 49%) as a colourless oil.

205: ^1H NMR (400 MHz, $\text{DMSO-}d_6$) δ ppm 7.69 - 7.74 (2H, m), 7.63 - 7.66 (m, *minor diastereoisomer*), 7.43 - 7.52 (3H, m), 5.59 (1H, d, $J = 4.4$ Hz), 5.25 (d, $J = 11.5$ Hz, *minor diastereoisomer*), 5.15 (1H, d, $J = 4.4$ Hz), 3.73 (3H, s), 3.71 (s, *minor diastereoisomer*), 3.66 (3H, s) 3.59 (s, *minor diastereoisomer*); ^{13}C NMR (101 MHz, $\text{DMSO-}d_6$) δ ppm 168.8, 168.4, 154.2, 130.6, 128.8, 127.4, 127.1, 81.3, 55.9, 53.0, 52.6. LCMS: $t_R = 0.95$ min, area% = 40%, $[\text{M}+\text{H}]^+$ 264 (50). Spectra recorded on mixture.



Dimethyl 3-phenylisoxazole-4,5-dicarboxylate **206** was also isolated (104 mg, 0.40 mmol, 8%) as a colourless oil. ^1H NMR (400 MHz, $\text{DMSO-}d_6$) δ ppm 7.63 - 7.68 (2H, m), 7.53 - 7.61 (3H, m), 3.96 (3H, s), 3.87 (3H, s); ^{13}C NMR (101 MHz, $\text{DMSO-}d_6$) δ ppm 161.1, 160.6, 159.1, 155.8, 131.0, 129.2, 127.7, 126.2, 115.2, 53.6, 53.3; LCMS: $t_R = 1.09$ min, area% = 96%, $[\text{M}+\text{H}]^+$ 262 (50); IR ν_{max} (thin film): 2955, 2913, 2889, 1736, 1609, 1580, 1462, 1439, 1402, 1320, 1306, 1283, 1219 cm^{-1} ; HRMS (ESI-QToF): calculated for $[\text{M}+\text{H}]^+$ 262.0715, found 262.0715. (N66689-100-2)

Dimethyl (*anti*)-3-phenyl-4,5-dihydroisoxazole-4,5-dicarboxylate (205) from 203 (dimethyl maleate)

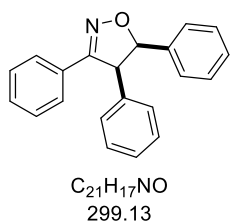


Prepared according to **GP2** using (*E*)-benzaldehyde oxime (5.13 mmol) and dimethyl maleate as dipolarophile, eluting with 0 - 25% EtOAc in cyclohexane over 20 CVs, affording dimethyl (*anti*)-3-phenyl-4,5-dihydroisoxazole-4,5-dicarboxylate **205** (dr = 8:1, 439 mg, 1.67 mmol, 33%) as a colourless oil.

205: ^1H NMR (400 MHz, $\text{DMSO-}d_6$) δ ppm 7.69 - 7.74 (2H, m), 7.63 - 7.67 (m, *minor diastereoisomer*), 7.43 - 7.52 (3H, m), 5.59 (1H, d, $J = 4.4$ Hz), 5.25 (d, $J = 11.5$ Hz, *minor diastereoisomer*), 5.15 (1H, d, $J = 4.4$ Hz), 3.73 (3H, s), 3.71 (s, *minor diastereoisomer*), 3.66 (3H, s), 3.59 (s, *minor diastereoisomer*); ^{13}C NMR (101 MHz, $\text{DMSO-}d_6$) δ ppm 168.8, 168.4, 154.2, 130.6, 128.8, 127.4, 127.1, 81.3, 55.9, 53.0, 52.6; LCMS: $t_R = 1.44$ min, area% = 100%, $[\text{M}+\text{H}]^+$ 300 (100); IR ν_{max} (thin film): 2956, 1739, 1436, 1232, 1012, 693 cm^{-1} ; HRMS (ESI-QToF): calculated for $[\text{M}+\text{H}]^+$ 264.0794, found 264.0870. Spectra recorded on mixture. Data consistent with **205** from dimethyl fumarate by **GP2**.

Dimethyl 3-phenylisoxazole-4,5-dicarboxylate **206** was also isolated as a mixture with remaining dimethyl maleate (269 mg, 60% purity, 20%).

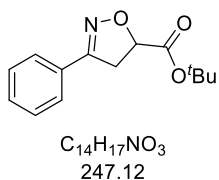
Syn-3,4,5-Triphenyl-4,5-dihydroisoxazole (218)



Prepared according **GP2** using (*E*)-benzaldehyde oxime (1.06 mmol), DMF (3 mL) and *cis*-stilbene as dipolarophile, stirring overnight. The crude mixture was submitted to column chromatography on silica gel eluting with 0 - 5% EtOAc cyclohexane over 20 CVs, affording *syn*-3,4,5-triphenyl-4,5-dihydroisoxazole **218** (29 mg, 0.10 mmol, 9%) as a white solid (MP (CH₂Cl₂): 164.4 - 166.7 °C).

218: ¹H NMR (400 MHz, DMSO-*d*₆) δ ppm 7.61 - 7.68 (2H, m), 7.34 - 7.41 (3H, m), 6.98 - 7.15 (8H, m), 6.89 - 6.95 (2H, m), 5.97 (1H, d, *J* = 9.5 Hz), 5.31 (1H, d, *J* = 9.5 Hz); ¹³C NMR (101 MHz, DMSO-*d*₆) δ ppm 135.2, 130.0, 128.8, 128.7, 128.1, 127.5, 127.2, 127.0, 126.6, 87.0, 56.9; LCMS: *t*_R = 1.44 min, area% = 100%, [M+H]⁺ 300 (100); IR *v*_{max} (thin film): 3066, 3028, 1496, 1446, 1365, 901, 691; HRMS (ESI-QToF): calculated for [M+H]⁺ 300.1310, found 300.1391.

tert-Butyl 3-phenyl-4,5-dihydroisoxazole-5-carboxylate (221a)



Prepared according to **GP2**, using (*E*)-benzaldehyde oxime (1.03 mmol), DMF (3 mL) and *tert*-butyl acrylate as dipolarophile, stirring for 1.5 hr. The crude mixture was submitted to column chromatography on silica gel eluting with 0 - 15% EtOAc in cyclohexane over 30 CVs, affording a mixture of *tert*-butyl 3-phenyl-4,5-dihydroisoxazole-5-carboxylate and *tert*-butyl 3-phenyl-4,5-dihydroisoxazole-4-carboxylate **221a** (20:1, 140 mg, 0.57 mmol, 55%) as a colourless oil.

221a: ¹H NMR (400 MHz, DMSO-*d*₆) δ ppm 7.67 - 7.72 (2H, m), 7.43 - 7.49 (3H, m), 5.12 (1H, dd, *J* = 11.7, 7.0 Hz), 4.76 (1H, dd, *J* = 11.3, 5.6 Hz, *minor regioisomer*), 4.65 (1H, dd, *J* = 9.0, 5.6 Hz, *minor regioisomer*), 4.54 (1H, dd, *J* = 11.3, 9.0 Hz, *minor regioisomer*), 3.74 (1H, dd, *J* = 17.4, 11.7 Hz), 3.54 (1H, dd, *J* = 17.2, 7.0 Hz), 1.45 (9H, s), 1.28 (9H, s, *minor regioisomer*); ¹³C NMR (101 MHz, DMSO-*d*₆) δ ppm 169.0, 156.0, 130.3, 128.8, 128.5, 126.7, 81.7, 78.1, 38.4, 27.5; LCMS: *t*_R = 1.13 min, area% = 100%, [M+H]⁺ 248 (100); IR *v*_{max} (thin film): 2977, 2925, 1732, 1355, 1154, 762 cm⁻¹

¹; HRMS (ESI-QToF): calculated for [M+H]⁺ 248.1287, found 248.1286. Spectra recorded on mixture

6.2.3. General Procedure 3 for Electrochemical Synthesis (GP3)

To a 10 mL ElectraSyn 2.0 reaction vessel containing a stirrer bar, oxime (0.5 mmol), dipolarophile (5 eq.) and Et₄NCl (0.5 eq.) were added followed by HFIP (1.3 eq.) and MeCN (0.07 M). The reaction mixture was electrolysed under a constant current of 25 mA with graphite (G) anode and stainless steel (SS) cathode and stirring at 400 rpm, until a current of 3 F.mol⁻¹ had been passed (100 min). The solution was analysed by LCMS (HpH). Following electrolysis, the reaction mixture was transferred to a round-bottomed flask, washing the electrodes with MeCN and acetone until washings ran clear, and concentrated *in vacuo* to give the crude mixture. The crude mixture was submitted to column chromatography on silica, eluting with EtOAc/cyclohexane to afford desired product.

***tert*-Butyl 3-phenyl-4,5-dihydroisoxazole-5-carboxylate (221a)**

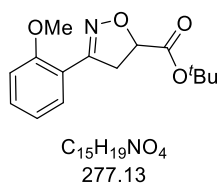
Prepared according to **GP3**, (*E*)-benzaldehyde oxime **199a**, using *tert*-butyl acrylate as dipolarophile, and eluting with 0 - 15% EtOAc in cyclohexane over 25 CVs, affording a mixture of *tert*-butyl 3-phenyl-4,5-dihydroisoxazole-5-carboxylate and *tert*-butyl 3-phenyl-4,5-dihydroisoxazole-4-carboxylate **221a** (20:1, 95 mg, 0.38 mmol, 76%) as a colourless oil.

221a: ¹H NMR (400 MHz, DMSO-*d*₆) δ ppm 7.66 - 7.73 (2H, m), 7.43 - 7.51 (3H, m), 5.12 (1H, dd, *J* = 11.7, 6.8 Hz), 4.76 (dd, *J* = 10.9, 5.6 Hz, *minor regioisomer*), 4.76 (dd, *J* = 8.6, 5.6 Hz, *minor regioisomer*), 4.54 (dd, *J* = 10.9, 8.6 Hz, *minor regioisomer*), 3.74 (1H, dd, *J* = 17.4, 11.7 Hz), 3.54 (1H, dd, *J* = 17.4, 6.8 Hz), 1.45 (9H, s), 1.28 (s, *minor regioisomer*); ¹³C NMR (101 MHz, DMSO-*d*₆) δ ppm 169.0, 156.0, 130.3, 128.8, 128.5, 126.7, 81.7, 78.1, 38.4, 27.5; LCMS: *t*_R = 1.16 min, area% = 100%, [M+H]⁺ 248 (100); IR *v*_{max} (thin film): 2978, 2926, 1732, 1498, 1448, 1393, 1368, 1354, 1302, 1250, 1226 cm⁻¹; HRMS (ESI-QToF): calculated for [M+H]⁺ 248.1287, found 248.1289. Spectra recorded on mixture. Data consistent with synthesis by **GP2**.

tert-Butyl 3-phenyl-4,5-dihydroisoxazole-5-carboxylate (221a)

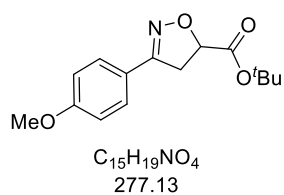
Prepared according to **GP3**, using (*E*)-benzaldehyde- α - d_1 oxime **199a-d₁**, *tert*-butyl acrylate as dipolarophile, and eluting with 0 - 15% EtOAc in cyclohexane over 25 CVs, affording a mixture of *tert*-butyl 3-phenyl-4,5-dihydroisoxazole-5-carboxylate and *tert*-butyl 3-phenyl-4,5-dihydroisoxazole-4-carboxylate **199a** (17:1, 88 mg, 0.36 mmol, 70%) as a colourless oil.

199a: 1H NMR (400 MHz, DMSO- d_6) δ ppm 7.66 - 7.73 (2H, m), 7.43 - 7.51 (3H, m), 5.12 (1H, dd, J = 11.6, 6.9 Hz), 4.76 (dd, J = 11.0, 5.9 Hz, *minor regioisomer*), 4.65 (dd, J = 8.9, 5.9 Hz, *minor regioisomer*), 4.54 (dd, J = 11.0, 8.9 Hz, *minor regioisomer*), 3.74 (1H, dd, J = 17.2, 11.6 Hz), 3.54 (1H, dd, J = 17.2, 6.9 Hz), 1.45 (9H, s), 1.28 (s, *minor regioisomer*); ^{13}C NMR (101 MHz, DMSO- d_6) δ ppm 169.0, 156.0, 130.3, 128.8, 128.5, 126.7, 81.7, 78.1, 38.4, 27.5; LCMS: t_R = 1.16 min, area% = 97%, $[M+H]^+$ 248 (60). Spectra recorded on mixture. Data consistent with synthesis by **GP2**.

tert-Butyl 3-(2-methoxyphenyl)-4,5-dihydroisoxazole-5-carboxylate (221b)

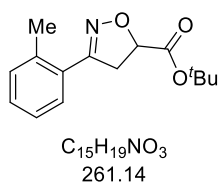
Prepared according to **GP3**, using (*E*)-2-methoxybenzaldehyde oxime **199b**, *tert*-butyl acrylate as dipolarophile, and eluting with 0 - 20% EtOAc in cyclohexane over 20 CVs, affording a mixture of *tert*-butyl 3-(2-methoxyphenyl)-4,5-dihydroisoxazole-5-carboxylate and *tert*-butyl 3-(2-methoxyphenyl)-4,5-dihydroisoxazole-4-carboxylate **221b** (15:1, 80 mg, 0.29 mmol, 57%) as a colourless oil.

221b: 1H NMR (400 MHz, DMSO- d_6) δ ppm 7.57 (1H, dd, J = 7.5, 1.8 Hz), 7.46 (1H, ddd, J = 8.5, 7.5, 1.8 Hz), 7.13 (1H, d, J = 8.5 Hz), 7.00 (1H, td, J = 7.5, 1.1 Hz), 5.06 (1H, dd, J = 11.6, 6.7 Hz), 4.72 (dd, J = 11.0, 7.8 Hz, *minor regioisomer*), 4.58 (dd, J = 11.0, 8.3 Hz, *minor regioisomer*), 4.49 (dd, J = 8.3, 7.8 Hz, *minor regioisomer*), 3.83 (3H, s), 3.71 (1H, dd, J = 17.7, 11.6 Hz), 3.52 (1H, dd, J = 17.7, 6.7 Hz), 1.44 (9H, s), 1.19 (s, *minor regioisomer*); ^{13}C NMR (101 MHz, DMSO- d_6) δ ppm 169.3, 157.3, 155.0, 131.7, 128.9, 120.6, 117.4, 112.2, 81.6, 77.9, 55.7, 40.9, 27.5; LCMS: t_R = 1.16 min, area% = 92%, $[M+H]^+$ 278 (100); IR ν_{max} (thin film): 2977, 2915, 2846, 1731, 1601, 1491, 1463, 1437, 1368, 1347, 1278, 1248, 1151, 1027, 891, 843, 757 cm^{-1} ; HRMS (ESI-QToF): calculated for $[M+H]^+$ 278.1392, found 278.1394. Spectra recorded on mixture.

***tert*-Butyl 3-(4-methoxyphenyl)-4,5-dihydroisoxazole-5-carboxylate (221c)**

Prepared according to **GP3**, using (*E*)-4-methoxybenzaldehyde oxime **199c**, *tert*-butyl acrylate as dipolarophile, and eluting with 0 - 15% EtOAc in cyclohexane over 25 CVs, affording a mixture of *tert*-butyl 3-(4-methoxyphenyl)-4,5-dihydroisoxazole-5-carboxylate and *tert*-butyl 3-(4-methoxyphenyl)-4,5-dihydroisoxazole-4-carboxylate **221c** (25:1, 69 mg, 0.25 mmol, 50%) as a colourless oil.

221c: ¹H NMR (400 MHz, DMSO-*d*₆) δ ppm 7.61 - 7.66 (2H, m), 6.99 - 7.03 (2H, m), 5.06 (1H, dd, *J* = 11.7, 6.8 Hz), 4.69 (dd, *J* = 10.8, 5.6 Hz, *minor regioisomer*), 4.61 (dd, *J* = 8.6, 5.6 Hz, *minor regioisomer*), 4.48 (dd, *J* = 10.8, 8.6 Hz, *minor regioisomer*), 3.80 (3H, s), 3.70 (1H, dd, *J* = 17.1, 11.7 Hz), 3.50 (1H, dd, *J* = 17.1, 6.8 Hz), 1.44 (9H, s), 1.30 (s, *minor regioisomer*); ¹³C NMR (101 MHz, DMSO-*d*₆) δ ppm 169.2, 160.8, 155.4, 128.4, 120.9, 114.2, 81.6, 77.9, 55.3, 38.6, 27.5; LCMS: *t*_R = 1.15 min, area% = 100%, [M+H]⁺ 278 (100); IR *v*_{max} (thin film): 2987, 2939, 2840, 1740, 1607, 1599, 1568, 1514, 1482, 1456, 1442, 1421, 1395, 1371, 1346, 1309, 1245, 1230 cm⁻¹; HRMS (ESI-QToF): calculated for [M+H]⁺-Bu 222.0767, found 222.0768. Spectra recorded on mixture.

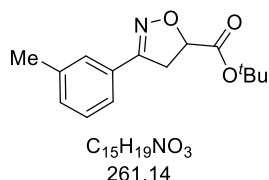
***tert*-Butyl 3-(2-methylphenyl)-4,5-dihydroisoxazole-5-carboxylate (221d)**

Prepared according to **GP3**, using (*E*)-2-methylbenzaldehyde oxime **199d**, *tert*-butyl acrylate as dipolarophile, and eluting with 0 - 25% EtOAc in cyclohexane over 25 CVs, affording a mixture of *tert*-butyl 3-(2-methylphenyl)-4,5-dihydroisoxazole-5-carboxylate and *tert*-butyl 3-(2-methylphenyl)-4,5-dihydroisoxazole-4-carboxylate **221d** (14:1, 106 mg, 0.41 mmol, 80%) as a colourless oil.

221d: ¹H NMR (400 MHz, DMSO-*d*₆) δ ppm 7.46 (1H, dd, *J* = 7.6, 1.2 Hz), 7.43 (dd, *J* = 7.6, 1.2 Hz, *minor regioisomer*), 7.26 - 7.39 (3H, m, *both regioisomers*), 5.06 (1H, dd, *J* = 11.5, 6.5 Hz), 4.80 (dd, *J* = 10.5, 8.1 Hz, *minor regioisomer*), 3.78 (1H, dd, *J* = 17.1, 11.5 Hz), 3.55 (1H, dd, *J* = 17.1, 6.5 Hz), 2.45 (3H, s), 2.39 (s, *minor regioisomer*), 1.45 (9H, s), 1.16 (s, *minor regioisomer*); ¹³C NMR (101 MHz, DMSO-*d*₆) δ ppm 169.1, 156.7, 136.9, 131.2, 129.5, 129.2, 127.7, 126.0, 81.7, 77.2, 40.9, 27.5, 22.1; LCMS: *t*_R = 1.25 min, area% = 100%, [M+H]⁺ 262 (100); IR *v*_{max} (thin film):

2978, 2929, 1731, 1456, 1368, 1374, 1226, 1152, 1000, 890, 842, 760, 719 cm^{-1} ; HRMS (ESI-QToF): calculated for $[\text{M}+\text{H}]^+$ 262.1439, found 262.1451. Spectra recorded on mixture.

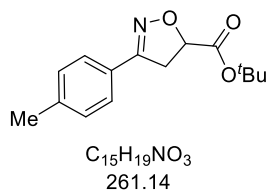
***tert*-Butyl 3-(3-methylphenyl)-4,5-dihydroisoxazole-5-carboxylate (221e)**



Prepared according to **GP3**, using (*E*)-3-methylbenzaldehyde oxime **199e**, *tert*-butyl acrylate as dipolarophile, and eluting with 0 - 25% EtOAc in cyclohexane over 25 CVs, affording a mixture of *tert*-butyl 3-(3-methylphenyl)-4,5-dihydroisoxazole-5-carboxylate and *tert*-butyl 3-(3-methylphenyl)-4,5-dihydroisoxazole-4-carboxylate **221e** (18:1, 103 mg, 0.39 mmol, 78%) as a colourless oil.

221e: ^1H NMR (400 MHz, $\text{DMSO-}d_6$) δ ppm 7.45 - 7.55 (2H, m), 7.26 - 7.39 (2H, m), 5.10 (1H, dd, $J = 11.7, 6.8$ Hz), 4.73 (dd, $J = 11.0, 5.9$ Hz, *minor regioisomer*), 4.63 (dd, $J = 8.5, 5.9$ Hz, *minor regioisomer*), 4.53 (dd, $J = 11.0, 8.5$ Hz, *minor regioisomer*), 3.72 (1H, dd, $J = 17.4, 11.7$ Hz), 3.52 (1H, dd, $J = 17.4, 6.8$ Hz), 2.35 (3H, s), 1.45 (9H, s), 1.29 (s, *minor regioisomer*); ^{13}C NMR (101 MHz, $\text{DMSO-}d_6$) δ ppm 169.1, 156.0, 138.1, 130.9, 128.7, 128.4, 127.2, 123.9, 81.7, 78.0, 38.5, 27.5, 20.8; LCMS: $t_R = 1.25$ min, area% = 100%, $[\text{M}+\text{H}]^+$ 262 (100); IR ν_{max} (thin film): 2979, 2933, 1731, 1456, 1368, 1225, 1151, 1001, 897, 819, 786, 693 cm^{-1} ; HRMS (ESI-QToF): calculated for $[\text{M}+\text{H}]^+$ 262.1439, found 262.1449. Spectra recorded on mixture.

***tert*-Butyl 3-(4-methylphenyl)-4,5-dihydroisoxazole-5-carboxylate (221f)**



Prepared according to **GP3**, using (*E*)-4-methylbenzaldehyde oxime **199f**, *tert*-butyl acrylate as dipolarophile, and eluting with 0 - 10% EtOAc in cyclohexane over 25 CVs, affording a mixture of *tert*-butyl 3-(4-methylphenyl)-4,5-dihydroisoxazole-5-carboxylate and *tert*-butyl 3-(4-methylphenyl)-4,5-dihydroisoxazole-4-carboxylate **221f** (20:1, 71 mg, 0.27 mmol, 53%) as a colourless oil.

221f: ^1H NMR (400 MHz, $\text{DMSO-}d_6$) δ ppm 7.56 - 7.60 (2H, m), 7.24 - 7.29 (2H, m), 5.09 (1H, dd, $J = 11.7, 6.8$ Hz), 4.71 (dd, $J = 11.2, 5.6$ Hz, *minor regioisomer*), 4.62 (dd, $J = 8.8, 5.6$ Hz, *minor regioisomer*), 4.51 (dd, $J = 11.2, 8.8$ Hz, *minor regioisomer*), 3.71 (1H, dd, $J = 17.4, 11.7$ Hz), 3.51 (1H, dd, $J = 17.4, 6.8$ Hz), 2.34 (3H, s), 1.44 (9H, s), 1.30 (s, *minor regioisomer*); ^{13}C NMR (101 MHz, $\text{DMSO-}d_6$) δ ppm 169.1, 155.8, 140.1, 129.3, 126.7, 125.7, 81.7, 78.0, 38.5, 27.5, 20.9; LCMS: $t_R = 1.22$ min,

area% = 99%, $[M+H]^+$ 262 (100); IR ν_{\max} (thin film): 2978, 2931, 1732, 1516, 1456, 1393, 1368, 1350, 1301, 1249, 1226, 1152 cm^{-1} ; HRMS (ESI-QToF): calculated for $[M+H]^+ \text{-}^t\text{Bu}$ 206.0812, found 206.0815. Spectra recorded on mixture.

***tert*-Butyl 3-(2-iodophenyl)-4,5-dihydroisoxazole-5-carboxylate (221g)**



Prepared according to **GP3**, using (*E*)-2-iodobenzaldehyde oxime **199g**, *tert*-butyl acrylate as dipolarophile, and eluting with 0 - 20% EtOAc in cyclohexane over 20 CVs, affording *tert*-butyl 3-(2-iodophenyl)-4,5-dihydroisoxazole-5-carboxylate **221g** (131 mg, 0.35 mmol, 70%) as a colourless oil.

221g: ^1H NMR (400 MHz, $\text{DMSO-}d_6$) δ ppm 7.99 (1H, dd, $J = 8.1, 1.7$ Hz), 7.50 (1H, td, $J = 7.6, 1.7$ Hz), 7.42 (1H, dd, $J = 7.6, 1.7$ Hz), 7.21 (1H, ddd, $J = 8.1, 7.6, 1.7$ Hz), 5.17 (1H, dd, $J = 11.7, 6.4$ Hz), 3.74 (1H, dd, $J = 17.3, 11.7$ Hz), 3.59 (1H, dd, $J = 17.3, 6.4$ Hz), 1.47 (9H, s); ^{13}C NMR (101 MHz, $\text{DMSO-}d_6$) δ ppm 168.8, 157.9, 140.0, 133.8, 131.3, 130.3, 128.4, 95.7, 81.8, 78.2, 41.2, 27.6; LCMS: $t_R = 1.26$ min, area% = 92%, $[M+H]^+$ 374 (60); IR ν_{\max} (thin film): 2978, 2932, 1729, 1583, 1470, 1432, 1368, 1338, 1225, 1147, 1066, 1009, 886, 840, 754 cm^{-1} ; HRMS (ESI-QToF): calculated for $[M+H]^+$ 374.0253, found 374.0252.

***tert*-Butyl 3-(3-iodophenyl)-4,5-dihydroisoxazole-5-carboxylate (221h)**

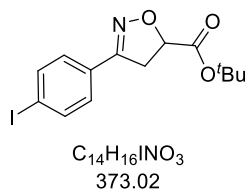


Prepared according to **GP3**, using (*E*)-3-iodobenzaldehyde oxime **199h**, *tert*-butyl acrylate as dipolarophile, and eluting with 0 - 20% EtOAc in cyclohexane over 20 CVs, affording a mixture of *tert*-butyl 3-(3-iodophenyl)-4,5-dihydroisoxazole-5-carboxylate and *tert*-butyl 3-(3-iodophenyl)-4,5-dihydroisoxazole-4-carboxylate **221h** (29:1, 69 mg, 0.19 mmol, 37%) as a white solid (MP (CH_2Cl_2): 74.0 - 80.7 $^\circ\text{C}$).

221h: ^1H NMR (400 MHz, $\text{DMSO-}d_6$) δ ppm 8.01 (1H, t, $J = 1.7$ Hz), 7.84 (1H, ddd, $J = 7.8, 1.7, 1.0$ Hz), 7.73 (1H, ddd, $J = 7.8, 1.7, 1.0$ Hz), 7.26 (1H, t, $J = 7.8$ Hz), 5.13 (1H, dd, $J = 11.9, 6.9$ Hz), 4.80 (dd, $J = 11.0, 5.9$ Hz, *minor regioisomer*), 4.68 (dd, $J = 8.7, 5.9$ Hz, *minor regioisomer*), 4.54 (dd, $J = 11.0, 8.7$ Hz, *minor regioisomer*), 3.73 (1H, dd, $J = 17.4, 11.9$ Hz), 3.55 (1H, dd, $J = 17.4, 6.9$ Hz), 1.45 (9H, s), 1.31 (s, *minor regioisomer*); ^{13}C NMR (101 MHz, $\text{DMSO-}d_6$) δ ppm 168.9, 155.0, 138.8, 134.9, 130.8, 130.6, 126.0, 95.1, 81.8, 78.4, 38.1, 27.5; LCMS: $t_R = 1.33$ min, area% = 93%, $[M+H]^+$ 374 (25); IR ν_{\max} (thin film): 2975, 2933, 1737, 1555, 1368, 1336, 1227, 1145, 1006,

971, 888, 867, 844, 786, 726, 686 cm^{-1} ; HRMS (ESI-QToF): calculated for $[\text{M}+\text{H}]^+$ 374.0253, found 374.0251. Spectra recorded on mixture.

***tert*-Butyl 3-(4-iodophenyl)-4,5-dihydroisoxazole-5-carboxylate (221i)**



Prepared according to **GP3**, using (*E*)-4-iodobenzaldehyde oxime **199i**, *tert*-butyl acrylate as dipolarophile, and eluting with 0 - 15% EtOAc in cyclohexane over 20 CVs, affording a mixture of *tert*-butyl 3-(4-iodophenyl)-4,5-dihydroisoxazole-5-carboxylate and *tert*-butyl 3-(4-iodophenyl)-4,5-dihydroisoxazole-4-carboxylate **221i** (32:1, 54 mg, 0.14 mmol, 29%) as a white solid (MP (CH_2Cl_2): 98.6 - 101.8 $^\circ\text{C}$).

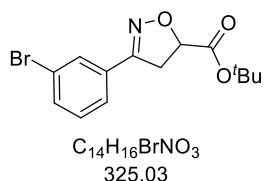
221i: ^1H NMR (400 MHz, $\text{DMSO}-d_6$) δ ppm 7.84 (2H, dt, $J = 8.6, 2.0$ Hz), 7.48 (2H, dt, $J = 8.6, 2.0$ Hz), 5.13 (1H, dd, $J = 11.9, 7.0$ Hz), 4.76 (1H, dd, $J = 11.0, 5.6$ Hz), 4.67 (dd, $J = 8.7, 5.6$ Hz, *minor regioisomer*), 4.53 (dd, $J = 11.0, 8.7$ Hz, *minor regioisomer*), 3.71 (1H, dd, $J = 17.4, 11.9$), 3.52 (1 H, dd, $J = 17.4, 6.9$ Hz), 1.44 (9H, s), 1.29 (s, *minor regioisomer*); ^{13}C NMR (101 MHz, $\text{DMSO}-d_6$) δ ppm 168.9, 155.6, 137.6, 128.6, 128.0, 97.2, 81.8, 78.4, 38.1, 27.5; LCMS: $t_R = 1.33$ min, area% = 97%, $[\text{M}+\text{H}]^+$ 374 (50); IR ν_{max} (thin film): 2978, 2930, 1737, 1587, 1481, 1347, 1225, 1149, 1006, 976, 901, 866, 821, 751, 536 cm^{-1} ; HRMS (ESI-QToF): calculated for $[\text{M}+\text{H}]^+$ 374.0249, found 374.0254. Spectra recorded on mixture.

***tert*-Butyl 3-(2-bromophenyl)-4,5-dihydroisoxazole-5-carboxylate (221j)**



Prepared according to **GP3**, using (*E*)-2-bromobenzaldehyde oxime **199j**, *tert*-butyl acrylate as dipolarophile, and eluting with 0 - 25% EtOAc in cyclohexane over 25 CVs, affording *tert*-butyl 3-(2-bromophenyl)-4,5-dihydroisoxazole-5-carboxylate **221j** (112 mg, 0.34 mmol, 68%) as a colourless oil.

221j: ^1H NMR (400 MHz, $\text{DMSO}-d_6$) δ ppm 7.75 (1H, dd, $J = 7.8, 1.2$ Hz), 7.46 - 7.56 (2H, m), 7.39 - 7.44 (1H, m), 5.17 (1H, dd, $J = 11.5, 6.4$ Hz), 3.77 (1H, dd, $J = 17.4, 11.5$ Hz), 3.61 (1H, dd, $J = 17.4, 6.4$), 1.46 (9H, s); ^{13}C NMR (101 MHz, $\text{DMSO}-d_6$) δ ppm 169.4, 156.9, 134.1, 132.1, 131.6, 130.4, 128.5, 121.5, 82.3, 78.8, 41.5, 28.1; LCMS: $t_R = 1.25$ min, area% = 93%, $[\text{M}+\text{H}]^+$ 326 (100), 328 (100); IR ν_{max} (thin film): 2978, 2933, 1730, 1589, 1474, 1429, 1368, 1342, 1225, 1150, 1001, 889, 841, 756 cm^{-1} ; HRMS (ESI-QToF): calculated for $[\text{M}+\text{H}]^+$ 326.0387, found 326.0396.

***tert*-Butyl 3-(3-bromophenyl)-4,5-dihydroisoxazole-5-carboxylate (221k)**

Prepared according to **GP3**, using (*E*)-3-bromobenzaldehyde oxime **199k**, *tert*-butyl acrylate as dipolarophile, and eluting with 0 - 20% EtOAc in cyclohexane over 20 CVs, affording a mixture of *tert*-butyl 3-(3-bromophenyl)-4,5-dihydroisoxazole-5-carboxylate and *tert*-butyl 3-(3-bromophenyl)-4,5-dihydroisoxazole-4-carboxylate **221k** (25:1, 110 mg, 0.34 mmol, 67%) as a colourless oil.

221k: ¹H NMR (400 MHz, DMSO-*d*₆) δ ppm 7.85 (1H, t, *J* = 1.9 Hz), 7.72 (1H, dt, *J* = 7.8, 1.3 Hz), 7.68 (1H, ddd, *J* = 7.8, 1.9, 1.3 Hz), 7.43 (1H, t, *J* = 7.8 Hz), 5.15 (1H, dd, *J* = 11.9, 7.0 Hz), 4.83 (dd, *J* = 10.9, 5.8 Hz, *minor regioisomer*), 4.70 (dd, *J* = 8.7, 5.8 Hz, *minor regioisomer*), 4.55 (dd, *J* = 10.9, 8.7 Hz, *minor regioisomer*), 3.74 (1H, dd, *J* = 17.4, 11.9 Hz), 3.57 (1H, dd, *J* = 17.4, 7.0 Hz), 1.45 (9H, s), 1.30 (s, *minor regioisomer*); ¹³C NMR (101 MHz, DMSO-*d*₆) δ ppm 168.8, 155.1, 133.0, 130.9, 130.8, 129.2, 125.7, 122.0, 81.8, 78.4, 38.1, 27.5; LCMS: *t*_R = 1.30 min, area% = 99%, [M+H]⁺ 326 (25), 328 (25); IR *v*_{max} (thin film): 2979, 2934, 1731, 1594, 1558, 1428, 1368, 1338, 1226, 1151, 1074, 996, 899, 841, 784, 683 cm⁻¹; HRMS (ESI-QToF): calculated for [M+H]⁺ 326.0387, found 326.0396. Spectra recorded on mixture.

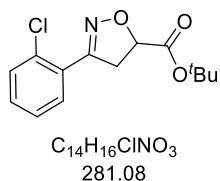
***tert*-Butyl 3-(4-bromophenyl)-4,5-dihydroisoxazole-5-carboxylate (221l)**

Prepared according to **GP3**, using (*E*)-4-bromobenzaldehyde oxime **199l**, *tert*-butyl acrylate as dipolarophile, and eluting with 0 - 15% EtOAc in cyclohexane over 25 CVs, affording a mixture of *tert*-butyl 3-(4-bromophenyl)-4,5-dihydroisoxazole-5-carboxylate and *tert*-butyl 3-(4-bromophenyl)-4,5-dihydroisoxazole-4-carboxylate **221l** (25:1, 69 mg, 0.21 mmol, 42%) as a white solid (MP (CH₂Cl₂): 72.8 - 75.0 °C).

221l: ¹H NMR (400 MHz, DMSO-*d*₆) δ ppm 7.62 - 7.69 (4H, m), 5.13 (1H, dd, *J* = 11.9, 6.8 Hz), 4.78 (dd, *J* = 11.0, 5.6 Hz, *minor regioisomer*), 4.68 (dd, *J* = 8.6, 5.6 Hz, *minor regioisomer*), 4.54 (dd, *J* = 11.0, 8.6 Hz, *minor regioisomer*), 3.73 (1H, dd, *J* = 17.4, 11.9 Hz), 3.54 (1H, dd, *J* = 17.4, 6.8 Hz), 1.44 (9H, s), 1.29 (s, *minor regioisomer*); ¹³C NMR (101 MHz, DMSO-*d*₆) δ ppm 168.9, 155.4, 131.8, 128.7, 127.7, 123.7, 81.8, 78.4, 38.2, 27.5; LCMS: *t*_R = 1.28 min, area% = 99%, [M+H]⁺ 326 (100), 328 (100); IR *v*_{max} (thin film): 2996, 2975, 2932, 1740, 1591, 1400, 1371, 1347, 1244, 1219, 1148

cm⁻¹; HRMS (ESI-QToF): calculated for [M+H]⁺-^tBu 269.9760, found 269.9759. Spectra recorded on mixture.

tert-Butyl 3-(2-chlorophenyl)-4,5-dihydroisoxazole-5-carboxylate (221m)



Prepared according to **GP3**, using (*E*)-2-chlorobenzaldehyde oxime **199m**, *tert*-butyl acrylate as dipolarophile, and eluting with 0 - 20% EtOAc in cyclohexane over 20 CVs, affording a mixture of *tert*-butyl 3-(2-chlorophenyl)-4,5-dihydroisoxazole-5-carboxylate and *tert*-butyl 3-(2-chlorophenyl)-4,5-dihydroisoxazole-4-carboxylate **221m** (18:1, 105 mg, 0.37 mmol, 74%) as a colourless oil.

221m: ¹H NMR (400 MHz, DMSO-*d*₆) δ ppm 7.72 (1H, t, *J* = 2.1 Hz), 7.68 (1H, dt, *J* = 7.7, 1.4 Hz), 7.55 (1H, ddd, *J* = 7.7, 2.1, 1.4 Hz), 7.49 (1H, t, *J* = 7.7 Hz), 5.15 (1H, dd, *J* = 11.7, 7.1 Hz), 4.83 (dd, *J* = 11.1, 5.8 Hz, *minor regioisomer*), 4.70 (dd, *J* = 8.8, 5.8 Hz, *minor regioisomer*), 4.55 (dd, *J* = 11.1, 8.8 Hz, *minor regioisomer*), 3.75 (1H, dd, *J* = 17.4, 11.7 Hz), 3.58 (1H, dd, *J* = 17.4, 7.1 Hz), 1.45 (9H, s), 1.29 (s, *minor regioisomer*); ¹³C NMR (101 MHz, DMSO-*d*₆) δ ppm 168.8, 155.2, 133.6, 130.7, 130.5, 130.1, 126.4, 125.3, 81.8, 78.4, 38.1, 27.5; LCMS: *t*_R = 1.28 min, area% = 99%, [M+H]⁺ 282 (20), 284 (5); IR *v*_{max} (thin film): 2979, 2930, 1733, 1597, 1562, 1430, 1368, 1339, 1226, 1154, 999, 903, 842, 788, 755, 685 cm⁻¹; HRMS (ESI-QToF): calculated for [M+H]⁺ 282.0893, found 282.0900. Spectra recorded on mixture.

tert-Butyl 3-(3-chlorophenyl)-4,5-dihydroisoxazole-5-carboxylate (221n)



Prepared according to **GP3**, using (*E*)-3-chlorobenzaldehyde oxime **199n**, *tert*-butyl acrylate as dipolarophile, and eluting with 0 - 20% EtOAc in cyclohexane over 20 CVs, affording *tert*-butyl 3-(3-chlorophenyl)-4,5-dihydroisoxazole-5-carboxylate **221n** (106 mg, 0.38 mmol, 75%) as a colourless oil.

221n: ¹H NMR (400 MHz, DMSO-*d*₆) δ ppm 7.56 - 7.63 (2H, m), 7.50 (1H, td, *J* = 7.7, 2.0 Hz), 7.44 (1H, td, *J* = 7.7, 1.5 Hz), 5.16 (1H, dd, *J* = 11.6, 6.5 Hz), 3.79 (1H, dd, *J* = 17.4, 11.6 Hz), 3.60 (1H, dd, *J* = 17.4, 6.5 Hz), 1.45 (9H, s); ¹³C NMR (101 MHz, DMSO-*d*₆) δ ppm 168.8, 155.3, 131.6, 131.5, 130.8, 130.5, 127.8, 127.5, 81.8, 78.3, 40.8, 27.5; LCMS: *t*_R = 1.23 min, area% = 100%, [M+H]⁺ 282 (100), 284 (25); IR *v*_{max} (thin film): 2979, 2930, 1733, 1591, 1476, 1434, 1368, 1345, 1300, 1236, 1153, 1038,

1002, 892, 842, 759 cm^{-1} ; HRMS (ESI-QToF): calculated for $[\text{M}+\text{H}]^+$ 282.0893, found 282.0900.

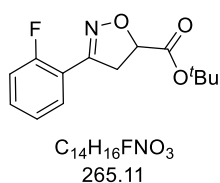
***tert*-Butyl 3-(4-chlorophenyl)-4,5-dihydroisoxazole-5-carboxylate (221o)**



Prepared according to **GP3**, using (*E*)-4-chlorobenzaldehyde oxime **199o**, *tert*-butyl acrylate as dipolarophile, and eluting with 0 - 20% EtOAc in cyclohexane over 20 CVs, affording a mixture of *tert*-butyl 3-(4-chlorophenyl)-4,5-dihydroisoxazole-5-carboxylate and *tert*-butyl 3-(4-chlorophenyl)-4,5-dihydroisoxazole-4-carboxylate **221o** (23:1, 102 mg, 0.36 mmol, 72%) as a white solid (MP (CH_2Cl_2): 69.5 - 70.7 $^\circ\text{C}$).

221o: ^1H NMR (400 MHz, $\text{DMSO}-d_6$) δ ppm 7.71 (2H, dt, $J = 8.6, 2.7$ Hz), 7.53 (2H, dt, $J = 8.6, 2.7$ Hz), 5.13 (1H, dd, $J = 11.9, 7.0$ Hz), 4.78 (dd, $J = 11.0, 5.6$ Hz, *minor regioisomer*), 4.68 (dd, $J = 8.6, 5.6$ Hz, *minor regioisomer*), 4.54 (dd, $J = 11.0, 8.6$ Hz, *minor regioisomer*), 3.73 (1H, dd, $J = 17.4, 11.9$ Hz), 3.54 (1H, dd, $J = 17.4, 7.0$ Hz), 1.44 (9H, s), 1.29 (s, *minor regioisomer*); ^{13}C NMR (101 MHz, $\text{DMSO}-d_6$) δ ppm 168.9, 155.3, 134.9, 128.9, 128.5, 127.4, 81.8, 78.4, 38.2, 27.5; LCMS: $t_R = 1.27$, area% = 100%, $[\text{M}+\text{H}]^+$ 282 (50), 284 (15); IR ν_{max} (thin film): 2975, 2934, 1724, 1602, 1495, 1349, 1298, 1259, 1149, 1089, 990, 894, 822, 782, 536 cm^{-1} ; HRMS (ESI-QToF): calculated for $[\text{M}+\text{H}]^+$ 282.0893, found 282.0899. Spectra recorded on mixture.

***tert*-Butyl 3-(2-fluorophenyl)-4,5-dihydroisoxazole-5-carboxylate (221p)**

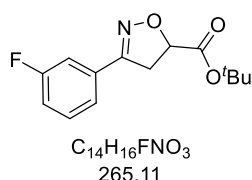


Prepared according to **GP3**, using (*E*)-2-fluorobenzaldehyde oxime **199p**, *tert*-butyl acrylate as dipolarophile and eluting with 0 - 20% EtOAc in cyclohexane over 20 CVs, affording a mixture of *tert*-butyl 3-(2-fluorophenyl)-4,5-dihydroisoxazole-5-carboxylate and *tert*-butyl 3-(2-fluorophenyl)-4,5-dihydroisoxazole-4-carboxylate **221p** (16:1, 97 mg, 0.37 mmol, 73%) as a colourless oil.

221p: ^1H NMR (400 MHz, $\text{DMSO}-d_6$) δ ppm 7.75 (1H, td, $J = 7.7, 1.7$ Hz), 7.49 - 7.58 (1H, m), 7.26 - 7.38 (2H, m), 5.12 (1H, dd, $J = 11.9, 6.8$ Hz), 4.71 - 4.78 (m, *minor regioisomer*), 4.55 - 4.67 (m, *minor regioisomer*), 3.77 (1H, ddd, $J = 17.4, 11.9, 1.7$ Hz), 3.55 (1H, ddd, $J = 17.4, 6.8, 1.7$ Hz), 1.45 (9H, s), 1.23 (s, *minor regioisomer*); ^{13}C NMR (101 MHz, $\text{DMSO}-d_6$) δ ppm 168.9, 159.6 (d, $^1J_{\text{C-F}} = 253$ Hz), 152.5 (d, $^3J_{\text{C-F}} = 4$ Hz), 132.3 (d, $^2J_{\text{C-F}} = 9$ Hz), 129.3 (d, $^3J_{\text{C-F}} = 3$ Hz), 124.8 (d, $^3J_{\text{C-F}} = 4$ Hz), 116.5 (d, $^2J_{\text{C-F}} = 22$ Hz), 116.4 (d, $^3J_{\text{C-F}} = 12$ Hz), 81.8, 78.0 (d, $^5J_{\text{C-F}} = 1$ Hz), 39.8 (d, $^4J_{\text{C-F}} =$

5 Hz), 27.5; ^{19}F NMR (376 MHz, $\text{DMSO-}d_6$) δ ppm -111.2 (1F, s), -112.0 (s, *minor regioisomer*); LCMS: t_R = 1.18 min, area% = 100%, $[\text{M}+\text{H}]^+$ 266 (100); IR ν_{max} (thin film): 2980, 2935, 1732, 1598, 1490, 1455, 1369, 1353, 1224, 1150, 1108, 1002, 901, 841, 815, 758, 651 cm^{-1} ; HRMS (ESI-QToF): calculated for $[\text{M}+\text{H}]^+$ 266.1188, found 266.1196. Spectra recorded on mixture.

***tert*-Butyl 3-(3-fluorophenyl)-4,5-dihydroisoxazole-5-carboxylate (221q)**



Prepared according to **GP3**, using (*E*)-3-fluorobenzaldehyde oxime **199q**, *tert*-butyl acrylate as dipolarophile and eluting with 0 - 15% EtOAc in cyclohexane over 20 CVs, affording a mixture of *tert*-butyl 3-(3-fluorophenyl)-4,5-dihydroisoxazole-5-carboxylate and *tert*-butyl 3-(3-fluorophenyl)-4,5-dihydroisoxazole-4-carboxylate **221q** (20:1, 96 mg, 0.36 mmol, 72%) as a colourless oil.

221q: ^1H NMR (400 MHz, $\text{DMSO-}d_6$) δ ppm 7.48 - 7.58 (3H, m), 7.28 - 7.38 (1H, m), 5.15 (1H, dd, J = 11.9, 7.0 Hz), 4.81 (dd, J = 11.0, 5.6 Hz, *minor regioisomer*), 4.70 (dd, J = 8.6, 5.6 Hz, *minor regioisomer*), 4.55 (dd, J = 11.0, 8.6 Hz, *minor regioisomer*), 3.74 (1H, dd, J = 17.4, 11.9 Hz), 3.56 (1H, dd, J = 17.4, 7.0 Hz), 1.45 (9H, s), 1.29 (s, *minor regioisomer*); ^{13}C NMR (101 MHz, $\text{DMSO-}d_6$) δ ppm 168.9, 162.1 (d, $^1J_{\text{C-F}}$ = 244 Hz), 155.4 (d, $^4J_{\text{C-F}}$ = 4 Hz), 130.9 (d, $^3J_{\text{C-F}}$ = 8 Hz), 130.7 (d, $^3J_{\text{C-F}}$ = 8 Hz), 122.9 (d, $^4J_{\text{C-F}}$ = 3 Hz), 117.1 (d, $^2J_{\text{C-F}}$ = 21 Hz), 113.5 (d, $^2J_{\text{C-F}}$ = 23 Hz), 81.8, 78.4, 38.2, 27.5; ^{19}F NMR (376 MHz, $\text{DMSO-}d_6$) δ ppm -112.3 (1F, s), -112.8 (s, *minor regioisomer*); LCMS: t_R = 1.19 min, area% = 100%, $[\text{M}+\text{H}]^+$ 266 (30); IR ν_{max} (thin film): 2980, 2938, 1732, 1613, 1576, 1494, 1451, 1368, 1342, 1226, 1189, 1150, 1002, 890, 829, 786, 684 cm^{-1} ; HRMS (ESI-QToF): calculated for $[\text{M}+\text{H}]^+$ 266.1188, found 266.1197. Spectra recorded on mixture.

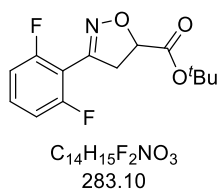
***tert*-Butyl 3-(4-fluorophenyl)-4,5-dihydroisoxazole-5-carboxylate (221r)**



Prepared according to **GP3**, using (*E*)-4-fluorobenzaldehyde oxime **199r**, *tert*-butyl acrylate as dipolarophile and eluting with 0 - 15% EtOAc in cyclohexane over 25 CVs, affording a mixture of *tert*-butyl 3-(4-fluorophenyl)-4,5-dihydroisoxazole-5-carboxylate and *tert*-butyl 3-(4-fluorophenyl)-4,5-dihydroisoxazole-4-carboxylate **221r** (20:1, 80 mg, 0.30 mmol, 60%) as a colourless oil.

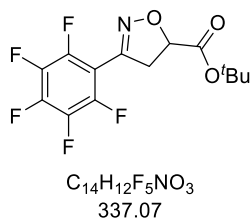
221r: ^1H NMR (400 MHz, $\text{DMSO-}d_6$) δ ppm 7.72 - 7.79 (2H, m), 7.27 - 7.34 (2H, m), 5.12 (1H, dd, $J = 11.7, 7.1$ Hz), 4.78 (dd, $J = 10.9, 5.5$ Hz, *minor regioisomer*), 4.67 (dd, $J = 8.6, 5.5$ Hz, *minor regioisomer*), 4.53 (dd, $J = 10.9, 8.6$ Hz, *minor regioisomer*), 3.73 (1H, dd, $J = 17.4, 11.7$ Hz), 3.55 (1H, dd, $J = 17.4, 7.1$ Hz), 1.44 (9H, s), 1.29 (s, *minor regioisomer*); ^{13}C NMR (101 MHz, $\text{DMSO-}d_6$) δ ppm 169.0, 163.1 (d, $^1J_{\text{C-F}} = 248$ Hz), 155.2, 129.1 (d, $^3J_{\text{C-F}} = 9$ Hz), 125.1 (d, $^4J_{\text{C-F}} = 3$ Hz), 115.9 (d, $^2J_{\text{C-F}} = 22$ Hz), 81.7, 78.2, 38.5, 27.5; ^{19}F NMR (376 Hz, $\text{DMSO-}d_6$) δ -110.1 (1F, s), -110.5 (s, *minor regioisomer*); LCMS: $t_{\text{R}} = 1.17$ min, area% = 100%, $[\text{M}+\text{H}]^+$ 266 (50); IR ν_{max} (thin film): 2980, 2933, 1732, 1603, 1514, 1479, 1458, 1436, 1411, 1394, 1369, 1349, 1300 cm^{-1} ; HRMS (ESI-QToF): calculated for $[\text{M}+\text{H}]^+ \text{-}^t\text{Bu}$ 210.0564, found 210.0569. Spectra recorded on mixture.

***tert*-Butyl 3-(2,6-difluorophenyl)-4,5-dihydroisoxazole-5-carboxylate (221s)**



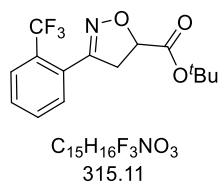
Prepared according to **GP3**, using (*E*)-2,6-difluorobenzaldehyde oxime **199s**, *tert*-butyl acrylate as dipolarophile, and eluting with 0 - 20% EtOAc in cyclohexane over 20 CVs, affording *tert*-butyl 3-(2,6-difluorophenyl)-4,5-dihydroisoxazole-5-carboxylate **221s** (101 mg, 0.36 mmol, 70%) as a white solid (MP (CH_2Cl_2): 91.6 - 94.2 $^\circ\text{C}$).

221s: ^1H NMR (400 MHz, $\text{DMSO-}d_6$) δ ppm 7.59 (1H, tt, $J = 8.6, 6.4$ Hz), 7.25 (2H, t, $J = 8.6$ Hz), 5.16 (1H, dd, $J = 11.7, 6.6$ Hz), 3.72 (1H, ddt, $J = 17.7, 11.7, 1.0, 1.0$ Hz), 3.51 (1H, ddt, $J = 17.7, 6.6, 1.0, 1.0$ Hz), 1.45 (9H, s); ^{13}C NMR (101 MHz, $\text{DMSO-}d_6$) δ ppm 168.7, 159.8 (dd, $^1J_{\text{C-F}} = 253, ^3J_{\text{C-F}} = 7$ Hz), 148.1 (t, $^3J_{\text{C-F}} = 3$ Hz), 132.5 (t, $^3J_{\text{C-F}} = 11$ Hz), 112.4 (dt, $^2J_{\text{C-F}} = 21, ^4J_{\text{C-F}} = 3$ Hz), 106.6 (t, $^3J_{\text{C-F}} = 17$ Hz), 81.9, 77.8, 40.8 (t, $^4J_{\text{C-F}} = 3$ Hz), 27.5; ^{19}F NMR (376 MHz, $\text{DMSO-}d_6$) δ ppm -109.1 (2F, s); LCMS: $t_{\text{R}} = 1.17$ min, area% = 100%, $[\text{M}+\text{H}]^+$ 284 (100); IR ν_{max} (thin film): 3006, 2988, 2935, 1728, 1627, 1462, 1310, 1234, 1153, 1029, 1000, 988, 880, 841, 790, 721 cm^{-1} ; HRMS (ESI-QToF): calculated for $[\text{M}+\text{H}]^+$ 284.1094, found 284.1102.

tert-Butyl 3-(2,3,4,5,6-pentafluorophenyl)-4,5-dihydroisoxazole-5-carboxylate (221t)

Prepared according to **GP3**, using (*E*)-2,3,4,5,6-pentafluorobenzaldehyde oxime **199t**, *tert*-butyl acrylate as dipolarophile, and eluting with 0 - 20% EtOAc in cyclohexane over 20 CVs, affording *tert*-butyl 3-(2,3,4,5,6-pentafluorophenyl)-4,5-dihydroisoxazole-5-carboxylate **221t** (29 mg, 0.09 mmol, 17%) as a colourless oil.

221t: ¹H NMR (400 MHz, DMSO-*d*₆) δ ppm 5.23 (1H, dd, *J* = 12.0, 6.6 Hz), 3.75 (1H, ddt, *J* = 17.6, 12.0, 1.2, 1.2 Hz), 3.53 (1H, ddt, *J* = 17.6, 6.6, 1.2, 1.2 Hz), 1.45 (9H, s); ¹³C NMR (176 MHz, DMSO-*d*₆) δ ppm 168.3, 147.4 (br d, ³*J*_{C-F} = 2 Hz), 144.4 (dddt, ¹*J*_{C-F} = 253, ²*J*_{C-F} = 12, ³*J*_{C-F} = 8, ³*J*_{C-F} = 4, ⁴*J*_{C-F} = 4 Hz), 141.2 (dtt, ¹*J*_{C-F} = 253, ²*J*_{C-F} = 15, ²*J*_{C-F} = 15 Hz, ³*J*_{C-F} = 5 Hz, ⁴*J*_{C-F} = 5 Hz), 136.3 - 138.6 (m), 104.9 (td, ²*J*_{C-F} = 15, ³*J*_{C-F} = 4 Hz), 82.6, 78.8, 40.1 (t, ⁴*J*_{C-F} = 5 Hz), 40.0, 27.5; ¹⁹F NMR (376 MHz, DMSO-*d*₆) δ ppm 149.9 (1F, tt, ³*J*_{F-F} = 23, ⁴*J*_{F-F} = 3 Hz), -137.7 (2F, t, ³*J*_{F-F} = 5 Hz), -137.8 (2F, t, ³*J*_{F-F} = 5 Hz); LCMS: *t*_R = 1.28 min, area% = 95%, no appropriate mass ion; IR *v*_{max} (thin film): 2982, 2930, 1738, 1657, 1576, 1525, 1489, 1370, 1346, 1230, 1155, 1073, 989, 922, 811, 794 cm⁻¹; HRMS (ESI-QToF): calculated for [M+H]⁺ 338.0811, found 338.0817.

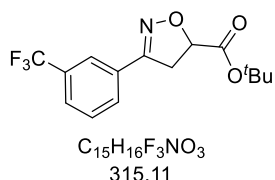
tert-Butyl 3-(2-(trifluoromethyl)phenyl)-4,5-dihydroisoxazole-5-carboxylate (221u)

Prepared according to **GP3**, using (*E*)-2-(trifluoromethyl)benzaldehyde oxime **199u**, *tert*-butyl acrylate as dipolarophile and eluting with 0 - 15% EtOAc in cyclohexane over 20 CVs, affording *tert*-butyl 3-(2-(trifluoromethyl)phenyl)-4,5-dihydroisoxazole-5-carboxylate **221u** (93 mg, 0.29 mmol, 59%) as a colourless oil.

221u: ¹H NMR (400 MHz, DMSO-*d*₆) δ ppm 7.87 (1H, dd, *J* = 7.6, 0.7 Hz), 7.79 (1H, td, *J* = 7.6, 0.7 Hz), 7.71 (1H, tt, *J* = 7.6, 0.7 Hz), 7.66 (1H, dt, *J* = 7.6, 0.7 Hz), 5.19 (1H, dd, *J* = 11.7, 5.9 Hz), 3.74 (1H, dd, *J* = 17.4, 11.7 Hz), 3.47 (1H, dd, *J* = 17.4, 5.9 Hz), 1.45 (9H, s); ¹³C NMR (101 MHz, DMSO-*d*₆) δ ppm 168.8, 155.0, 132.7, 130.7, 130.3, 127.5 (q, ³*J*_{C-F} = 1 Hz), 127.1 (q, ²*J*_{C-F} = 31 Hz), 126.7 (q, ³*J*_{C-F} = 5 Hz), 123.6 (q, ¹*J*_{C-F} = 274 Hz), 81.7, 78.2, 42.3 (app. d, ⁵*J*_{C-F} = 1 Hz), 27.5; ¹⁹F NMR (376 MHz,

DMSO- d_6) δ ppm -57.5 (3F, s); LCMS: t_R = 1.24 min, area% = 99%, $[M+H]^+$ 316 (20); IR ν_{max} (thin film): 2981, 2935, 1733, 1604, 1580, 1450, 1369, 1314, 1151, 1129, 1074, 1036, 1004, 891, 842, 770 cm^{-1} ; HRMS (ESI-QToF): calculated for $[M+H]^+ \cdot ^tBu$ 260.0534, found 260.0535.

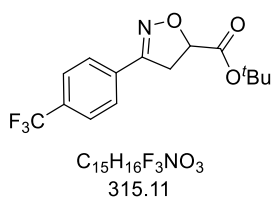
tert-Butyl 3-(3-(trifluoromethyl)phenyl)-4,5-dihydroisoxazole-5-carboxylate (221v)



Prepared according to **GP3**, using (*E*)-3-(trifluoromethyl)benzaldehyde oxime **199v**, *tert*-butyl acrylate as dipolarophile and eluting with 0 - 15% EtOAc in cyclohexane over 20 CVs, affording a mixture of *tert*-butyl 3-(3-(trifluoromethyl)phenyl)-4,5-dihydroisoxazole-5-carboxylate and *tert*-butyl 3-(3-(trifluoromethyl)phenyl)-4,5-dihydroisoxazole-4-carboxylate **221v** (17:1, 101 mg, 0.32 mmol, 64%) as a colourless oil.

221v: 1H NMR (400 MHz, DMSO- d_6) δ ppm 8.01 (1H, d, J = 7.8 Hz), 7.97 (1H, s), 7.85 (1H, dt, J = 7.8, 0.7 Hz), 7.72 (1H, tt, J = 7.8, 0.7 Hz), 5.18 (1H, dd, J = 11.9, 7.0 Hz), 4.93 (dd, J = 11.0, 5.6 Hz, *minor regioisomer*), 4.74 (dd, J = 8.7, 5.6 Hz, *minor regioisomer*), 4.57 (dd, J = 11.0, 8.7 Hz, *minor regioisomer*), 3.81 (1H, dd, J = 17.4, 11.9 Hz), 3.64 (1H, dd, J = 17.4, 7.0 Hz), 1.45 (9H, s), 1.26 (s, *minor regioisomer*); ^{13}C NMR (101 MHz, DMSO- d_6) δ ppm 168.8, 155.4, 130.1, 129.6 (q, $^3J_{C-F}$ = 32 Hz), 130.1 (q, $^2J_{C-F}$ = 106 Hz), 126.8 (q, $^4J_{C-F}$ = 4 Hz), 123.1 (q, $^4J_{C-F}$ = 4 Hz), 123.8 (br q, $^1J_{C-F}$ = 273 Hz), 81.8, 78.6, 38.1, 27.5; ^{19}F NMR (376 MHz, DMSO- d_6) δ ppm -61.3 (3F, s), -61.4 (s, *minor regioisomer*); LCMS: t_R = 1.29 min, area% = 99%, $[M+H]^+$ 316 (25); IR ν_{max} (thin film): 2982, 2940, 1733, 1458, 1434, 1370, 1310, 1153, 1124, 1072, 906, 803, 695 cm^{-1} ; HRMS (ESI-QToF): calculated for $[M+H]^+$ 316.1156, found 316.1165. Spectra recorded on mixture.

tert-Butyl 3-(4-(trifluoromethyl)phenyl)-4,5-dihydroisoxazole-5-carboxylate (221w)

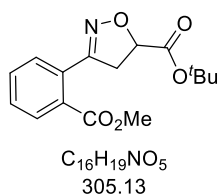


Prepared according to **GP3**, using (*E*)-4-(trifluoromethyl)benzaldehyde oxime **199w**, *tert*-butyl acrylate as dipolarophile and eluting with 0 - 20% EtOAc in cyclohexane over 25 CVs, affording a mixture of *tert*-butyl 3-(4-(trifluoromethyl)phenyl)-4,5-dihydroisoxazole-5-

carboxylate (83 mg, 0.26 mmol, 52%) and *tert*-butyl 3-(4-(trifluoromethyl)phenyl)-4,5-dihydroisoxazole-4-carboxylate **221w** as a white solid (MP (CH₂Cl₂): 88.3 - 90.3 °C).

221w: ¹H NMR (400 MHz, DMSO-*d*₆) δ ppm 7.89 - 7.94 (2H, m), 7.81 - 7.85 (2H, m), 5.19 (1H, dd, *J* = 11.7, 7.1 Hz), 4.87 (dd, *J* = 11.0, 5.6 Hz, *minor regioisomer*), 4.73 (dd, *J* = 8.7, 5.6 Hz, *minor regioisomer*), 4.59 (dd, *J* = 11.0, 8.7 Hz, *minor regioisomer*), 3.79 (1H, dd, *J* = 17.5, 11.7 Hz), 3.60 (1H, dd, *J* = 17.5, 7.1 Hz), 1.45 (9H, s), 1.28 (s, *minor regioisomer*); ¹³C NMR (101 MHz, DMSO-*d*₆) δ 168.8, 155.4, 132.4, 130.2 (q, ²*J*_{C-F} = 32 Hz), 127.5, 125.7 (q, ³*J*_{C-F} = 4 Hz), 81.9, 78.7, 38.0, 27.5 (CF₃ quaternary carbon not observed); ¹⁹F NMR (376 MHz, DMSO-*d*₆) δ -61.4 (3F, s), -61.3 (s, *minor regioisomer*); LCMS: *t*_R = 1.29 min, area% = 100%, [M+H]⁺ 316 (100); IR *v*_{max} (thin film): 2981, 2939, 1733, 1442, 1412, 1394, 1372, 1325, 1254, 1232 cm⁻¹; HRMS (ESI-QToF): calculated for [M+Na]⁺ 338.0980, found 338.0975. Spectra recorded on mixture.

***tert*-Butyl 3-(2-(methoxycarbonyl)phenyl)-4,5-dihydroisoxazole-5-carboxylate (221x)**



Prepared according to **GP3**, using methyl (*E*)-2-((hydroxyimino)methyl)benzoate **199x**, *tert*-butyl acrylate as dipolarophile, and eluting with 0 - 20% EtOAc in cyclohexane over 20 CVs, affording *tert*-butyl 3-(2-(methoxycarbonyl)phenyl)-4,5-dihydroisoxazole-5-carboxylate **221x** (54 mg, 0.18 mmol, 35%) as

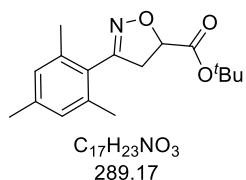
a colourless oil.

221x: ¹H NMR (400 MHz, DMSO-*d*₆) δ ppm 7.80 (1H, dd, *J* = 7.6, 1.5 Hz), 7.67 (1H, td, *J* = 7.6, 1.5 Hz), 7.60 (1H, td, *J* = 7.6, 1.5 Hz), 7.54 (1H, dd, *J* = 7.6, 1.5 Hz), 5.14 (1H, dd, *J* = 11.6, 6.5 Hz), 3.79 (3H, s), 3.67 (1H, dd, *J* = 17.2, 11.6 Hz), 3.47 (1H, dd, *J* = 17.2, 6.5 Hz), 1.47 (9H, s); ¹³C NMR (101 MHz, DMSO-*d*₆) δ ppm 168.9, 167.1, 156.6, 131.9, 130.5, 130.0, 129.5, 129.3, 128.6, 81.7, 78.1, 52.3, 41.0, 27.5; LCMS: *t*_R = 1.13 min, area% = 92%, [M+H]⁺ 306 (60); IR *v*_{max} (thin film): 2980, 1721, 1598, 1434, 1368, 1265, 1150, 1091, 1004, 842, 758, 705 cm⁻¹; HRMS (ESI-QToF): calculated [M+H]⁺-^tBu 250.0719, found 250.0717.

***tert*-Butyl 3-(3-(methoxycarbonyl)phenyl)-4,5-dihydroisoxazole-5-carboxylate (221y)**

Prepared according to **GP3**, using methyl (*E*)-3-((hydroxyimino)methyl)benzoate oxime **199y**, *tert*-butyl acrylate as dipolarophile, and eluting with 0 - 20% EtOAc in cyclohexane over 20 CVs, affording a mixture of *tert*-butyl 3-(3-(methoxycarbonyl)phenyl)-4,5-dihydroisoxazole-5-carboxylate and *tert*-butyl 3-(3-(methoxycarbonyl)phenyl)-4,5-dihydroisoxazole-4-carboxylate **221y** (20:1, 113 mg, 0.37 mmol, 74%) as a white solid (MP (CH₂Cl₂): 77.1 - 84.8 °C).

221y: ¹H NMR (400 MHz, DMSO-*d*₆) δ ppm 8.23 (1H, t, *J* = 1.5 Hz), 8.05 (1H, dt, *J* = 7.8, 1.5 Hz), 7.97 (1H, dt, *J* = 7.8, 1.5 Hz), 7.64 (1H, t, *J* = 7.8 Hz), 5.17 (1H, dd, *J* = 11.7, 6.8 Hz), 4.86 (dd, *J* = 11.0, 5.9 Hz, *minor regioisomer*), 4.71 (dd, *J* = 8.8, 5.9 Hz, *minor regioisomer*), 4.59 (dd, *J* = 11.0, 8.8 Hz, *minor regioisomer*), 3.89 (3H, s), 3.81 (1H, dd, *J* = 17.4, 11.7 Hz), 3.61 (1H, dd, *J* = 17.4, 6.8 Hz), 1.46 (9H, s), 1.41 (s, *minor regioisomer*); ¹³C NMR (101 MHz, DMSO-*d*₆) δ ppm 168.9, 165.6, 155.5, 131.3, 130.7, 130.2, 129.5, 129.1, 127.0, 81.8, 78.5, 52.3, 38.2, 27.5; LCMS: *t*_R = 1.17 min, area% = 99%, [M+H]⁺ 306 (50); IR *v*_{max} (thin film): 2975, 1720, 1436, 1347, 1255, 1223, 1148, 1004, 980, 897, 841, 823, 754, 732, 689 cm⁻¹; HRMS (ESI-QToF): calculated for [M+H]⁺ 306.1337, found 306.1339. Spectra recorded on mixture.

***tert*-Butyl 3-mesityl-4,5-dihydroisoxazole-5-carboxylate (221z)**

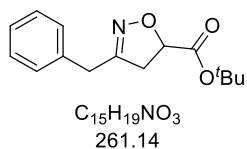
Prepared according to **GP3**, using (*E*)-2,4,6-trimethylbenzaldehyde oxime **199z**, *tert*-butyl acrylate as dipolarophile and eluting with 0 - 10% EtOAc in cyclohexane over 25 CVs, affording *tert*-butyl 3-mesityl-4,5-dihydroisoxazole-5-carboxylate **221z** (85 mg, 0.30 mmol, 58%) as a colourless oil.

199z: ¹H NMR (400 MHz, DMSO-*d*₆) δ ppm 6.92 (2H, s), 5.12 (1H, dd, *J* = 11.6, 5.1 Hz), 3.58 (1H, dd, *J* = 17.7, 11.6 Hz), 3.27 (1H, dd, *J* = 17.7, 5.1 Hz), 2.24 (3H, s), 2.14 (6H, s), 1.46 (9H, s); ¹³C NMR (101 MHz, DMSO-*d*₆) δ ppm 169.5, 156.5, 138.3, 136.1, 128.1, 125.3, 81.6, 77.3, 42.3, 27.5, 20.6, 19.0; LCMS: *t*_R = 1.32 min, area% = 95%, [M+H]⁺ 290 (100); IR *v*_{max} (thin film): 2978, 2927, 1732, 1611, 1456, 1393, 1368, 1327, 1297, 1225, 1155 cm⁻¹; HRMS (ESI-QToF): calculated for [M+H]⁺-^tBu 239.1125, found 239.1128.

***tert*-Butyl 3-(4-cyanophenyl)-4,5-dihydroisoxazole-5-carboxylate (221aa)**

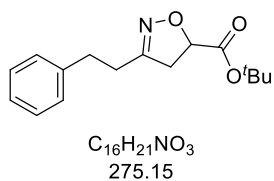
Prepared according to **GP3**, using (*E*)-4-((hydroxyimino)methyl)benzotrile **199aa**, *tert*-butyl acrylate as dipolarophile and eluting with 0 - 20% EtOAc in cyclohexane over 25 CVs, affording a mixture of *tert*-butyl 3-(4-cyanophenyl)-4,5-dihydroisoxazole-5-carboxylate and *tert*-butyl 3-(4-cyanophenyl)-4,5-dihydroisoxazole-4-carboxylate **221aa** (33:1, 65 mg, 0.24 mmol, 47%) as a white solid (MP (CH₂Cl₂): 92.6 - 95.0 °C).

221aa: ¹H NMR (400 MHz, DMSO-*d*₆) δ ppm 7.92 - 7.95 (2H, m), 7.86 - 7.89 (2H, m), 5.20 (1H, dd, *J* = 12.0, 7.1 Hz), 4.87 (dd, *J* = 11.0, 5.4 Hz, *minor regioisomer*), 4.75 (dd, *J* = 8.8, 5.6 Hz, *minor regioisomer*), 4.58 (dd, *J* = 11.0, 8.8 Hz, *minor regioisomer*), 3.77 (1H, dd, *J* = 17.6, 12.0 Hz), 3.59 (1H, dd, *J* = 17.6, 7.1 Hz), 1.45 (9H, s), 1.28 (s, *minor regioisomer*); ¹³C NMR (101 MHz, DMSO-*d*₆) δ ppm 168.7, 155.4, 132.7, 132.7, 127.5, 118.3, 112.5, 81.9, 78.8, 37.9, 27.5; LCMS: *t*_R = 1.12 min, area% = 100%, [M+H]⁺ 273 (10); IR *v*_{max} (thin film): 3090, 2983, 2935, 2227, 1736, 1601, 1460, 1431, 1405, 1393, 1368, 1351, 1247, 1223 cm⁻¹; HRMS (ESI-QToF): calculated for [M+Na]⁺ 295.1059, found 295.1059. Spectra recorded on mixture.

***tert*-Butyl 3-benzyl-4,5-dihydroisoxazole-5-carboxylate (221ab)**

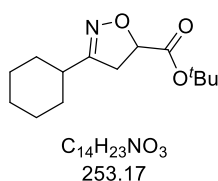
Prepared according to **GP3**, using (*E*)-2-phenylacetaldehyde oxime **199ab**, *tert*-butyl acrylate as dipolarophile and eluting with 0 - 20% EtOAc in cyclohexane over 25 CVs, affording *tert*-butyl 3-benzyl-4,5-dihydroisoxazole-5-carboxylate **221ab** (66 mg, 0.25 mmol, 50%) as a colourless oil.

221ab: ¹H NMR (400 MHz, DMSO-*d*₆) δ ppm 7.31 - 7.36 (2H, m), 7.21 - 7.29 (3H, m), 4.88 (1H, dd, *J* = 11.5, 6.1 Hz), 3.68 (2H, q, *J* = 15.6 Hz), 3.18 (1H, ddt, *J* = 17.4, 11.5, 0.9, 0.9 Hz), 2.93 (1H, ddt, *J* = 17.4, 6.1, 0.9, 0.9 Hz), 1.37 (9H, s); ¹³C NMR (101 MHz, DMSO-*d*₆) δ ppm 169.2, 157.2, 135.8, 128.7, 128.5, 126.8, 81.4, 77.2, 32.4, 27.4, ArCH₂ under DMSO-*d*₆ peak (confirmed by HSQC/HMBC); LCMS: *t*_R = 1.17 min, area% = 100%, [M+H]⁺ 262 (100); IR *v*_{max} (thin film): 2979, 2932, 1733, 1496, 1455, 1368, 1229, 1153, 1001, 842, 702 cm⁻¹; HRMS (ESI-QToF): calculated for [M+H]⁺ 262.1443, found 262.1441.

tert-Butyl 3-phenethyl-4,5-dihydroisoxazole-5-carboxylate (221ac)

Prepared according to **GP3**, using (*E*)-3-phenylpropanal oxime **199ac**, *tert*-butyl acrylate as dipolarophile and eluting with 0 - 20% EtOAc in cyclohexane over 25 CVs, affording *tert*-butyl 3-phenethyl-4,5-dihydroisoxazole-5-carboxylate **221ac** (103 mg, 0.38 mmol, 74%) as a colourless oil.

221ac: ¹H NMR (400 MHz, DMSO-*d*₆) δ ppm 7.17 - 7.31 (5H, m), 4.85 (1H, dd, *J* = 11.5, 6.8 Hz), 3.27 (1H, dd, *J* = 17.6, 11.5 Hz), 3.08 (1H, dd, *J* = 17.6, 6.8 Hz), 2.83 (2H, t, *J* = 7.3 Hz), 2.61 (2H, t, *J* = 7.3 Hz), 1.42 (9 H, s); ¹³C NMR (101 MHz, DMSO-*d*₆) δ ppm 169.3, 157.7, 140.6, 128.2, 128.2, 126.0, 81.4, 76.8, 40.6, 31.6, 28.2, 27.5; LCMS: *t*_R = 1.20 min, area% = 100%, [M+H]⁺ 276 (50); IR *v*_{max} (thin film): 2978, 2926, 2854, 1732, 1455, 1368, 1227, 1153, 1006, 871, 842, 751, 700 cm⁻¹; HRMS (ESI-QToF): calculated for [M+H]⁺ 276.1626, found 276.1637.

tert-Butyl 3-cyclohexyl-4,5-dihydroisoxazole-5-carboxylate (221ad)

Prepared according to **GP3**, using (*E*)-cyclohexanecarbaldehyde oxime **199ad**, *tert*-butyl acrylate as dipolarophile and eluting with 0 - 15% EtOAc in cyclohexane over 25 CVs, affording *tert*-butyl 3-cyclohexyl-4,5-dihydroisoxazole-5-carboxylate **221ad** (110 mg, 0.43 mmol, 86%) as a colourless oil.

221ad: ¹H NMR (400 MHz, DMSO-*d*₆) δ ppm 4.83 (1H, dd, *J* = 11.4, 6.4 Hz), 3.26 (1H, ddd, *J* = 17.3, 11.4, 0.7 Hz), 3.06 (1H, ddd, *J* = 17.3, 6.4, 0.7 Hz), 2.31 - 2.42 (1H, m), 1.74 - 1.84 (2H, m), 1.66 - 1.73 (2H, m), 1.56 - 1.65 (1H, m), 1.42 (9H, s), 1.15 - 1.34 (5H, m); ¹³C NMR (101 MHz, DMSO-*d*₆) δ ppm 169.3, 161.6, 81.3, 76.7, 36.0, 29.7, 27.5, 25.3, 25.0; LCMS: *t*_R = 1.24 min, area% = 92%, [M+H]⁺ 254 (100); IR *v*_{max} (thin film): 2978, 2929, 2854, 1732, 1449, 1368, 1225, 1151, 994, 872, 842, 806 cm⁻¹; HRMS (ESI-QToF): calculated for [M+H]⁺ 254.1751, found 254.1756.

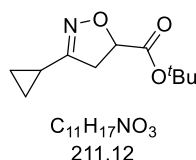
tert-Butyl 3-isopropyl-4,5-dihydroisoxazole-5-carboxylate (221ae)

Prepared according to **GP3**, using (*Z*)-isobutyraldehyde oxime **199ae**, *tert*-butyl acrylate as dipolarophile and eluting with 0 - 20% EtOAc in cyclohexane over 25 CVs, affording *tert*-butyl 3-isopropyl-

4,5-dihydroisoxazole-5-carboxylate **221ae** (87 mg, 0.41 mmol, 82%) as a colourless oil.

221ae: ^1H NMR (400 MHz, DMSO- d_6) δ ppm 4.85 (1H, dd, $J = 11.4, 6.5$ Hz), 3.27 (1H, ddd, $J = 17.4, 11.4, 0.7$ Hz), 3.07 (1H, ddd, $J = 17.4, 6.5, 0.7$ Hz), 2.66 (1H, spt, $J = 6.9$ Hz), 1.42 (9H, s), 1.09 (6H, d, $J = 6.9$ Hz); ^{13}C NMR (101 MHz, DMSO- d_6) δ ppm 169.3, 162.6, 81.3, 76.9, 38.7, 27.5, 26.9, 19.8, 19.7; LCMS: $t_{\text{R}} = 1.05$ min, area% = 98%, $[\text{M}+\text{H}]^+$ 214 (100); IR ν_{max} (thin film): 2971, 2933, 2876, 1732, 1459, 1368, 1291, 1226, 1152, 1088, 994, 875, 842 cm^{-1} ; HRMS (ESI-QToF): calculated for $[\text{M}+\text{H}]^+$ 214.1439, found 214.1442.

tert-Butyl 3-cyclopropyl-4,5-dihydroisoxazole-5-carboxylate (221af)



Prepared according to **GP3**, using (*Z*)-cyclopropanecarbaldehyde oxime **199af**, *tert*-butyl acrylate as dipolarophile and eluting with 0 - 20% EtOAc in cyclohexane over 25 CVs, affording *tert*-butyl 3-cyclopropyl-4,5-dihydroisoxazole-5-carboxylate **221af** (59 mg, 0.28 mmol, 56%) as a white solid (MP (CH_2Cl_2): 91.4 - 95.8 $^{\circ}\text{C}$).

221af: ^1H NMR (400 MHz, DMSO- d_6) δ ppm 4.83 (1H, dd, $J = 11.5, 6.6$ Hz), 3.12 (1H, dd, $J = 17.1, 11.5$ Hz), 2.88 (1H, dd, $J = 17.1, 6.6$ Hz), 1.78 (1H, tt, $J = 8.3, 5.0$ Hz), 1.42 (9H, s), 0.82 - 0.88 (2H, m), 0.71 - 0.76 (2H, m); ^{13}C NMR (101 MHz, DMSO- d_6) δ ppm 169.2, 160.2, 81.4, 76.8, 38.2, 27.5, 8.3, 5.6, 5.2 LCMS: $t_{\text{R}} = 0.97$ min, area% = 100%, $[\text{M}+\text{H}]^+$ 212 (100); IR ν_{max} (thin film): 2978, 2913, 2849, 1732, 1615, 1458, 1368, 1293, 1235, 1154, 1001, 915, 875, 843 cm^{-1} ; HRMS (ESI-QToF): calculated for $[\text{M}+\text{H}]^+$ 212.1283, found 212.1286.

tert-Butyl 3-(pyridin-2-yl)-4,5-dihydroisoxazole-5-carboxylate (221ag)



Prepared according to **GP3**, using (*E*)-picolinaldehyde oxime **199ag**, *tert*-butyl acrylate as dipolarophile and eluting with 0 - 25% EtOAc in cyclohexane over 25 CVs, affording *tert*-butyl 3-(pyridin-2-yl)-4,5-dihydroisoxazole-5-carboxylate **221ag** (42 mg, 0.17 mmol, 34%) as a colourless oil.

221ag: ^1H NMR (400 MHz, DMSO- d_6) δ ppm 8.65 (1H, dt, $J = 4.9, 1.5$ Hz), 7.86 - 7.95 (2H, m), 7.48 (1H, ddd, $J = 7.0, 4.9, 1.5$ Hz), 5.17 (1H, dd, $J = 11.7, 6.8$ Hz), 3.77 (1H, dd, $J = 17.9, 11.7$ Hz), 3.56 (1H, dd, $J = 17.9, 6.8$ Hz), 1.44 (9H, s); ^{13}C NMR (101

MHz, DMSO- d_6) δ ppm 168.9, 157.6, 149.5, 147.9, 137.0, 124.9, 121.4, 81.8, 78.6, 38.3, 27.5; LCMS: t_R = 1.00 min, area% = 96%, $[M+H]^+$ 249 (100); IR ν_{max} (thin film): 2979, 2935, 1732, 1584, 1473, 1441, 1367, 1224, 1151, 991, 898, 841, 781, 743 cm^{-1} ; HRMS (ESI-QToF): calculated for $[M+H]^+ - tBu$ 193.0613, found 193.0614.

***tert*-Butyl 3-(pyridin-3-yl)-4,5-dihydroisoxazole-5-carboxylate (221ah)**



Prepared according to **GP3**, using (*E*)-nicotinaldehyde oxime **199ah**, *tert*-butyl acrylate as dipolarophile and eluting with 0 - 60% EtOAc in cyclohexane over 20 CVs, affording a mixture of *tert*-butyl 3-(pyridin-3-yl)-4,5-dihydroisoxazole-4-carboxylate **221ah** (69:1, 72 mg, 0.29 mmol, 58%) as a pale-yellow solid (MP (CH₂Cl₂): 72.2 - 75.5 °C).

221ah: ¹H NMR (400 MHz, DMSO- d_6) δ ppm 8.87 (1H, dd, J = 2.2, 0.9 Hz), 8.66 (1H, dd, J = 4.8, 1.8 Hz), 8.09 (1H, dt, J = 8.0, 1.8 Hz), 7.50 (1H, ddd, J = 8.0, 4.8, 0.9 Hz), 5.17 (1H, dd, J = 11.9, 7.0 Hz), 4.90 (dd, J = 11.0, 5.6 Hz, *minor regioisomer*), 4.73 (dd, J = 8.6, 5.6 Hz, *minor regioisomer*), 4.55 (dd, J = 11.0, 8.6 Hz, *minor regioisomer*), 3.78 (1H, dd, J = 17.4, 11.9 Hz), 3.61 (1H, dd, J = 17.4, 7.0 Hz), 1.45 (9H, s), 1.27 (s, *minor regioisomer*); ¹³C NMR (101 MHz, DMSO- d_6) δ ppm 168.8, 154.3, 151.1, 147.6, 134.0, 124.6, 123.8, 81.8, 78.3, 38.0, 27.5; LCMS: t_R = 0.91 min, area% = 100%, $[M+H]^+$ 249 (100); IR ν_{max} (thin film): 2976, 2933, 1744, 1590, 1408, 1350, 1223, 1149, 1004, 904, 867, 812, 706 cm^{-1} ; HRMS (ESI-QToF): calculated for $[M+H]^+$ 249.1266, found 249.1277. Spectra recorded on mixture.

***tert*-Butyl 3-(pyridin-4-yl)-4,5-dihydroisoxazole-5-carboxylate (221ai)**



Prepared according to **GP3**, using (*E*)-isonicotinaldehyde oxime **199ai**, *tert*-butyl acrylate as dipolarophile and eluting with 0 - 60% EtOAc in cyclohexane over 20 CVs, affording *tert*-butyl 3-(pyridin-4-yl)-4,5-dihydroisoxazole-5-carboxylate **221ai** (46 mg, 0.19 mmol, 37%) as a colourless oil.

221ai: ¹H NMR (400 MHz, DMSO- d_6) δ ppm 8.68 (2H, dd, J = 4.4, 1.7 Hz), 7.64 (2H, dd, J = 4.4, 1.7 Hz), 5.21 (1H, dd, J = 12.0, 7.1 Hz), 3.76 (1H, dd, J = 17.5, 12.0 Hz), 3.57 (1H, dd, J = 17.5, 7.1 Hz), 1.45 (9H, s); ¹³C NMR (101 MHz, DMSO- d_6) δ ppm 168.6, 155.2, 150.3, 135.6, 120.8, 81.9, 78.8, 37.6, 27.5; LCMS: t_R = 0.92 min, area%

= 100%, $[M+H]^+$ 249 (100); IR ν_{\max} (thin film): 2980, 2935, 1732, 1598, 1409, 1367, 1358, 1226, 1001, 905, 820, 671, 557 cm^{-1} ; HRMS (ESI-QToF): calculated for $[M+H]^+$ 249.1266, found 249.1276.

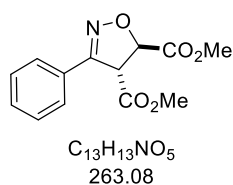
Methyl 3-phenyl-4,5-dihydroisoxazole-5-carboxylate (**223**)



Prepared according to **GP3**, using (*E*)-benzaldehyde oxime **199a**, methyl acrylate as dipolarophile, and eluting with 0 - 20% EtOAc in cyclohexane over 25 CVs, affording methyl 3-phenyl-4,5-dihydroisoxazole-5-carboxylate **223** (53 mg, 0.26 mmol, 59%) as a colourless oil.

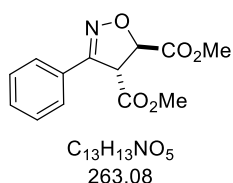
223: ^1H NMR (400 MHz, $\text{DMSO-}d_6$) δ ppm 7.67 - 7.72 (2H, m), 7.43 - 7.51 (3H, m), 5.29 (1H, dd, $J = 11.7, 6.6$ Hz), 3.78 (1H, dd, $J = 17.3, 11.7$ Hz), 3.72 (3H, s), 3.64 (1H, dd, $J = 17.3, 6.6$ Hz); ^{13}C NMR (101 MHz, $\text{DMSO-}d_6$) δ ppm 170.4, 156.2, 130.4, 128.8, 128.4, 126.8, 77.5, 52.3, 38.4; LCMS: $t_R = 0.89$ min, area% = 99%, $[M+H]^+$ 206 (100); IR ν_{\max} (thin film): 2954, 2923, 2851, 1741, 1498, 1447, 1438, 1355, 1284, 1215 cm^{-1} ; HRMS (ESI-QToF): calculated for $[M+H]^+$ 206.0818, found 206.0815.

Dimethyl (*anti*)-3-phenyl-4,5-dihydroisoxazole-4,5-dicarboxylate (**205**) from **208**



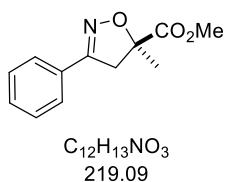
Prepared according to **GP3**, using (*E*)-benzaldehyde oxime **199a**, dimethyl fumarate as dipolarophile and eluting with 0 - 20% EtOAc in cyclohexane over 20 CVs, affording dimethyl (*anti*)-3-phenyl-4,5-dihydroisoxazole-4,5-dicarboxylate **205** (dr = 9:1, 78 mg, 0.30 mmol, 59%).

205: ^1H NMR (400 MHz, $\text{DMSO-}d_6$) δ ppm 7.69 - 7.76 (2H, m), 7.61 - 7.67 (m, *minor diastereoisomer*), 7.42 - 7.55 (3H, m), 5.61 (d, $J = 11.5$ Hz, *minor diastereoisomer*), 5.59 (1H, d, $J = 4.5$ Hz), 5.25 (d, $J = 11.5$ Hz, *minor diastereoisomer*), 5.16 (1H, d, $J = 4.5$ Hz), 3.73 (3H, s), 3.71 (s, *minor diastereoisomer*), 3.66 (3H, s), 3.59 (s, *minor diastereoisomer*); ^{13}C NMR (101 MHz, $\text{DMSO-}d_6$) δ ppm 168.8, 168.4, 154.2, 130.6, 129.0 (*minor diastereoisomer*), 128.8, 127.4, 127.1, 126.6 (*minor diastereoisomer*), 81.3, 55.9, 53.0, 52.6; LCMS: $t_R = 0.97$ min, area% = 83%, $[M+H]^+$ 264 (30). Spectra recorded on mixture. Data consistent with synthesis by **GP2**.

Dimethyl (*anti*)-3-phenyl-4,5-dihydroisoxazole-4,5-dicarboxylate (205) from **203**

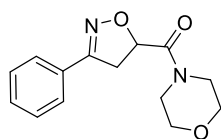
Prepared according to **GP3**, (*E*)-benzaldehyde oxime **199a**, using dimethyl maleate as dipolarophile and eluting with 0 - 25% EtOAc in cyclohexane over 25 CVs, affording dimethyl *anti*-3-phenyl-4,5-dihydroisoxazole-4,5-dicarboxylate **205** (dr = 9:1, 83 mg, 0.32 mmol, 63%).

205: ¹H NMR (400 MHz, DMSO-*d*₆) δ ppm 7.69 - 7.76 (2H, m), 7.61 - 7.67 (m, *minor diastereoisomer*), 7.42 - 7.55 (3H, m), 5.61 (d, *J* = 11.5 Hz, *minor diastereoisomer*), 5.59 (1H, d, *J* = 4.5 Hz), 5.25 (d, *J* = 11.5 Hz, *minor diastereoisomer*), 5.16 (1H, d, *J* = 4.5 Hz), 3.73 (3H, s), 3.71 (s, *minor diastereoisomer*), 3.66 (3H, s), 3.59 (s, *minor diastereoisomer*); ¹³C NMR (101 MHz, DMSO-*d*₆) δ ppm 168.8, 168.4, 154.2, 130.6, 129.0 (*minor diastereoisomer*), 128.8, 127.4, 127.1, 126.6 (*minor diastereoisomer*), 81.3, 55.9, 53.0, 52.6; LCMS: t_R = 0.97 min, area% = 83%, [M+H]⁺ 264 (30). Spectra recorded on mixture. Data consistent with synthesis by **GP2**.

Methyl 5-methyl-3-phenyl-4,5-dihydroisoxazole-5-carboxylate (240a)

Prepared according to **GP3**, using (*E*)-benzaldehyde oxime **199a**, methyl methacrylate as dipolarophile, and eluting with 0 - 20% EtOAc in cyclohexane over 25 CVs, affording methyl 5-methyl-3-phenyl-4,5-dihydroisoxazole-5-carboxylate **240a** (77 mg, 0.35 mmol, 69%) as a colourless oil.

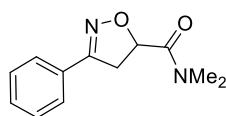
240a: ¹H NMR (400 MHz, DMSO-*d*₆) δ ppm 7.63 - 7.70 (2H, m), 7.43 - 7.50 (3H, m), 3.84 (1H, d, *J* = 17.6 Hz), 3.72 (3H, s), 3.45 (1H, d, *J* = 17.6 Hz), 1.60 (3H, s); ¹³C NMR (101 MHz, DMSO-*d*₆) δ ppm 171.8, 156.3, 130.3, 128.8, 128.6, 126.6, 85.6, 52.6, 44.2, 22.9; LCMS: t_R = 0.99 min, area% = 100%, [M+H]⁺ 220 (100); IR ν_{max} (thin film): 2997, 2955, 1746, 1595, 1568, 1498, 1435, 1361, 1281, 1197, 1095, 979, 908, 883, 760, 689 cm⁻¹; HRMS (ESI-QToF): calculated for [M+H]⁺ 220.0973, found 220.0976.

Morpholino(3-phenyl-4,5-dihydroisoxazol-5-yl)methanone (240b)

C₁₄H₁₆N₂O₃
260.12

Prepared according to **GP3**, using (*E*)-benzaldehyde oxime **199a**, 1-morpholinoprop-2-en-1-one as dipolarophile, and eluting with 0 - 20% EtOAc in cyclohexane over 20 CVs (product co-eluted with unreacted dipolarophile) and then submitted to a second column chromatography eluting with 0 - 100% EtOAc in cyclohexane over 20 CVs, affording morpholino(3-phenyl-4,5-dihydroisoxazol-5-yl)methanone **240b** (47 mg, 0.18 mmol, 36%) as a white solid (MP (CH₂Cl₂): 132.1 - 133.8 °C).

240b: ¹H NMR (400 MHz, DMSO-*d*₆) δ ppm 7.67 - 7.73 (2H, m), 7.44 - 7.51 (3H, m), 5.60 (1H, dd, *J* = 11.2, 7.1 Hz), 3.83 (1H, dd, *J* = 17.0, 7.1 Hz), 3.44 - 3.73 (9H, m); ¹³C NMR (101 MHz, DMSO-*d*₆) δ ppm 166.3, 156.7, 130.3, 128.8, 128.7, 126.7, 76.7, 66.1, 65.9, 45.7, 42.2, 36.7; LCMS: *t*_R = 0.80 min, area% = 100%, [M+H]⁺ 261 (100); IR *v*_{max} (thin film): 2969, 2858, 1657, 1444, 1360, 1275, 1236, 1113, 1066, 1029, 990, 888, 842, 767, 693 cm⁻¹; HRMS (ESI-QToF): calculated for [M+H]⁺ 261.1239, found 261.1251.

***N,N*-Dimethyl-3-phenyl-4,5-dihydroisoxazole-5-carboxamide (240c)**

C₁₂H₁₄N₂O₂
218.11

Prepared according to **GP3**, using (*E*)-benzaldehyde oxime **199a**, *N,N*-dimethylacrylamide as dipolarophile, and eluting with 0 - 50% EtOAc in cyclohexane over 25 CVs, affording *N,N*-dimethyl-3-phenyl-4,5-dihydroisoxazole-5-carboxamide **240c** (77 mg, 0.35 mmol, 69%) as a colourless oil.

240c: ¹H NMR (400 MHz, DMSO-*d*₆) δ ppm 7.67 - 7.73 (2H, m), 7.43 - 7.49 (3H, m), 5.58 (1H, dd, *J* = 11.2, 7.3 Hz), 3.80 (1H, dd, *J* = 16.9, 7.3 Hz), 3.54 (1H, dd, *J* = 16.9, 11.2 Hz), 3.12 (3H, s), 2.89 (3H, s); ¹³C NMR (101 MHz, DMSO-*d*₆) δ ppm 167.4, 156.6, 130.2, 128.8 (1 x 1C, 1 x 2C), 126.6, 77.0, 36.8, 36.6, 35.3; LCMS: *t*_R = 0.78 min, area% = 100%, [M+H]⁺ 219 (100); IR: *v*_{max} (thin film): 2933, 1647, 1497, 1446, 1401, 1357, 1260, 1148, 890, 761, 691, 541 cm⁻¹; HRMS (ESI-QToF): calculated for [M+H]⁺ 219.1133, found 219.1139.

***N*-Isopropyl-3-phenyl-4,5-dihydroisoxazole-5-carboxamide (240d)**

Prepared according to **GP3**, using (*E*)-benzaldehyde oxime **199a**, *N*-isopropylacrylamide as dipolarophile, and eluting with 0 - 20% EtOAc in cyclohexane over 25 CVs, affording *N*-isopropyl-3-phenyl-4,5-dihydroisoxazole-5-carboxamide **240d** (83 mg, 0.36 mmol, 72%) as a white solid (MP (CH₂Cl₂): 125.3 - 126.4 °C).

240d: ¹H NMR (400 MHz, DMSO-*d*₆) δ ppm 8.02 (1H, br d, *J* = 7.3 Hz), 7.66 - 7.73 (2H, m), 7.42 - 7.51 (3H, m), 5.02 (1H, dd, *J* = 11.5, 7.3 Hz), 3.89 (1H, dspt, *J* = 8.1, 6.6), 3.65 (1H, dd, *J* = 17.1, 11.5 Hz), 3.53 (1H, dd, *J* = 17.1, 7.3 Hz), 1.08 (6H, dd, *J* = 8.1, 6.6 Hz); ¹³C NMR (101 MHz, DMSO-*d*₆) δ ppm 168.2, 156.3, 130.2, 128.8, 128.7, 126.7, 79.1, 40.5, 38.3, 22.1, 22.0; LCMS: *t*_R = 0.91 min, area% = 100%, [M+H]⁺ 233 (100); IR *v*_{max} (thin film): 3366, 2968, 2918, 1649, 1521, 1447, 1335, 1153, 1015, 947, 860, 757, 688 cm⁻¹; HRMS (ESI-QToF): calculated for [M+H]⁺ 233.1286, found 233.1301.

3-Phenyl-4,5-dihydroisoxazole-5-carbonitrile (240e)

Prepared according to **GP3**, using (*E*)-benzaldehyde oxime **199a**, acrylonitrile as dipolarophile, and eluting with 0 - 20% EtOAc in cyclohexane over 20 CVs, affording 3-phenyl-4,5-dihydroisoxazole-5-carbonitrile **240e** (66 mg, 0.39 mmol, 77%) as a white solid (MP (CH₂Cl₂): 83.8 - 85.7 °C).

240e: ¹H NMR (400 MHz, DMSO-*d*₆) δ ppm 7.69 - 7.75 (2H, m), 7.46 - 7.55 (3H, m), 5.83 (1H, dd, *J* = 10.6, 5.8 Hz), 3.96 (1H, dd, *J* = 17.4, 5.8 Hz), 3.89 (1H, dd, *J* = 17.4, 10.6 Hz); ¹³C NMR (101 MHz, DMSO-*d*₆) δ ppm 157.4, 131.0, 128.9, 127.5, 127.1, 118.3, 66.9, 40.3; LCMS: *t*_R = 0.91 min, area% = 100%, [M+H]⁺ 173 (100); IR *v*_{max} (thin film): 1602, 1570, 1499, 1448, 1356, 1054, 940, 886, 768, 692 cm⁻¹; HRMS (ESI-QToF): calculated for [M+H]⁺ 173.0715, found 173.0715.

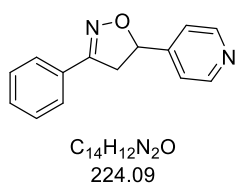
3-Phenyl-5-(pyridin-2-yl)-4,5-dihydroisoxazole (240f)

Prepared according to **GP3**, using (*E*)-benzaldehyde oxime **199a**, 2-vinylpyridine as dipolarophile, and eluting with 0 - 30% EtOAc in cyclohexane over 20 CVs, affording 3-phenyl-5-(pyridin-2-yl)-

4,5-dihydroisoxazole **240f** (20 mg, 0.09 mmol, 18%) as a pale-yellow oil.

240f: ^1H NMR (400 MHz, DMSO- d_6) δ ppm 8.58 (1H, ddd, $J = 4.9, 2.0, 1.1$ Hz), 7.84 (1H, td, $J = 7.7, 2.0$ Hz), 7.70 - 7.74 (2H, m), 7.52 (1H, dt, $J = 7.6, 1.1$ Hz), 7.44 - 7.48 (3H, m), 7.37 (1H, ddd, $J = 7.6, 4.9, 1.1$ Hz), 5.80 (1H, dd, $J = 11.1, 7.6$ Hz), 3.86 (1H, dd, $J = 17.2, 11.1$ Hz), 3.72 (1H, dd, $J = 17.2, 7.6$ Hz); ^{13}C NMR (101 MHz, DMSO- d_6) δ ppm 158.9, 156.4, 149.3, 137.1, 130.1, 129.1, 128.8, 126.7, 123.3, 121.3, 82.2, 40.1; LCMS: $t_{\text{R}} = 0.97$ min, area% = 100%, $[\text{M}+\text{H}]^+$ 225 (100); IR ν_{max} (thin film): 3059, 2930, 1590, 1436, 1356, 1149, 996, 896, 759, 692 cm^{-1} ; HRMS (ESI-QToF): calculated for $[\text{M}+\text{H}]^+$ 225.1028, found 225.1028.

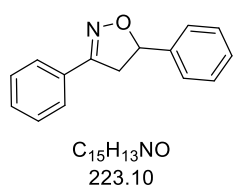
3-Phenyl-5-(pyridin-4-yl)-4,5-dihydroisoxazole (**240g**)



Prepared according to **GP3**, using (*E*)-benzaldehyde oxime **199a**, 4-vinylpyridine as dipolarophile, and eluting with 0 - 50% EtOAc in cyclohexane over 20 CVs, affording 3-phenyl-5-(pyridin-4-yl)-4,5-dihydroisoxazole **240g** (48 mg, 0.21 mmol, 42%) as a white solid (MP (CH_2Cl_2): 94.2 - 96.6 $^{\circ}\text{C}$).

240g: ^1H NMR (400 MHz, DMSO- d_6) δ ppm 8.59 (2H, dd, $J = 4.4, 1.7$ Hz), 7.69 - 7.73 (2H, m), 7.44 - 7.49 (3H, m), 7.40 (2H, dd, $J = 4.4, 1.7$ Hz), 5.80 (1H, dd, $J = 11.1, 7.6$ Hz), 3.95 (1H, dd, $J = 17.2, 11.1$ Hz), 3.43 (1H, dd, $J = 17.2, 7.6$ Hz); ^{13}C NMR (101 MHz, DMSO- d_6) δ ppm 156.4, 149.9, 149.7, 130.3, 128.8, 128.8, 126.7, 120.7, 80.2, 42.0; LCMS: $t_{\text{R}} = 0.91$ min, area% = 99%, $[\text{M}+\text{H}]^+$ 225 (100); IR ν_{max} (thin film): 2921, 1600, 1559, 1494, 1447, 1415, 1355, 1316, 1220, 1074, 974, 939, 857, 800, 752, 688, 539 cm^{-1} ; HRMS (ESI-QToF): calculated for $[\text{M}+\text{H}]^+$ 225.1024, found 225.1038.

3,5-Diphenyl-4,5-dihydroisoxazole (**201**)



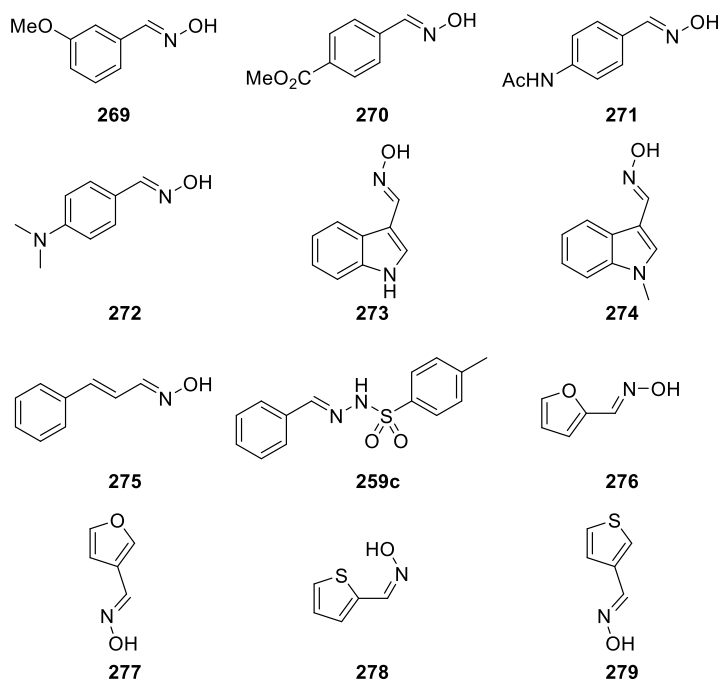
To a 10 mL ElectraSyn 2.0 reaction vessel containing a stirrer bar, (*E*)-benzaldehyde oxime **199a** (61 mg, 0.50 mmol), styrene (287 μL , 2.50 mmol) and Et_4NI (65 mg, 0.25 mmol) were added followed by MeOH (7 mL). The reaction mixture was electrolysed under a constant current of 25 mA with G anode and SS cathode and stirring at 400 rpm, until a current of 5 $\text{F}\cdot\text{mol}^{-1}$ had been passed. Following electrolysis, the reaction mixture was transferred to a round-bottomed flask, washing the electrodes with MeOH and acetone until washings ran clear, and concentrated *in vacuo* to give the crude mixture. The crude mixture was submitted to column chromatography on silica gel,

eluting with 0 - 15% EtOAc/cyclohexane over 20 CVs to afford 3,5-diphenyl-4,5-dihydroisoxazole **201** (36 mg, 0.16 mmol, 32%) as a white solid (MP (CH₂Cl₂): 72.5 - 73.6 °C).

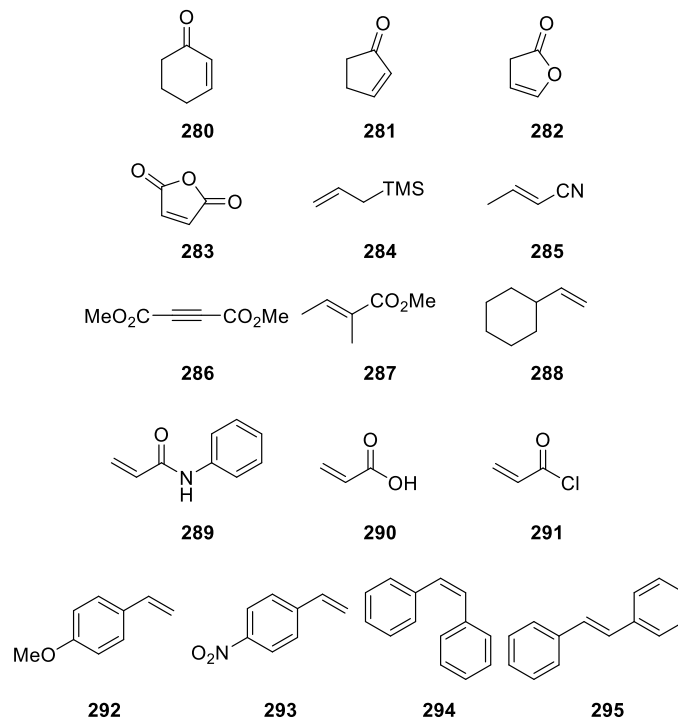
201: ¹H NMR (400 MHz, DMSO-*d*₆) δ ppm 7.69 - 7.75 (2H, m), 7.44 - 7.49 (3H, m), 7.31 - 7.43 (5H, m), 5.74 (1H, dd, *J* = 10.8, 8.6 Hz), 3.89 (1H, dd, *J* = 17.1, 10.8 Hz), 3.40 (1H, dd, *J* = 17.1, 8.6 Hz); ¹³C NMR (101 MHz, DMSO-*d*₆) δ ppm 156.4, 140.8, 130.1, 129.2, 128.8, 128.6, 128.0, 126.6, 126.1, 82.0, 42.1; LCMS: *t*_R = 1.20 min, area% = 100%, [M+H]⁺ 224 (100). Data consistent with synthesis by **GP2**.

6.2.4. Substrates Not Tolerated Under Electrochemical Conditions

The following aldoximes were not tolerated under the electrochemical conditions:



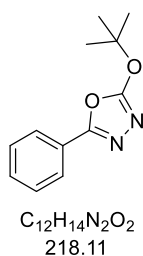
The following dipolarophiles were not tolerated under the electrochemical conditions:



6.2.5. Pyrazoline Synthesis Attempts

When attempting to employ the electrochemical methodology developed in the main publication to the synthesis of pyrazoles (*via* the corresponding hydrazones), it was observed that only rearrangement to the oxadiazole was achieved.

2-(*tert*-Butoxy)-5-phenyl-1,3,4-oxadiazole (**262a**)

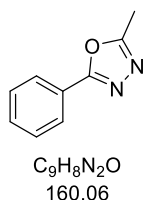


To a 10 mL ElectraSyn 2.0 reaction vessel containing a stirrer bar, *tert*-butyl (*E*)-2-benzylidenehydrazine-1-carboxylate **259a** (111 mg, 0.50 mmol), HFIP (70 μ L, 0.67 mmol, 1.3 eq.) and Et_4NCl (43 mg, 0.26 mmol, 0.5 eq.) were added followed by MeCN (7 mL). The reaction mixture was electrolysed under a constant current of 25 mA with G anode and SS cathode stirring at 400 rpm, until a current of 3 F.mol⁻¹ had been passed.

After electrolysis, the reaction mixture was transferred to a round-bottomed flask, washing the electrodes with MeCN until washings ran clear, and concentrated *in vacuo* to give the crude mixture. The crude mixture and submitted to column chromatography on silica gel (24 g, 0 - 20% EtOAc in cyclohexane over 25 CVs). Appropriate fractions were combined and concentrated *in vacuo* to afford 2-(*tert*-butoxy)-5-phenyl-1,3,4-oxadiazole **262a** (19 mg, 0.09 mmol, 17%) as a colourless oil.

262a: ¹H NMR (400 MHz, DMSO-*d*₆) δ ppm 7.85 - 7.91 (2H, m), 7.53 - 7.63 (3H, m), 1.61 (9H, s); ¹³C NMR (101 MHz, DMSO-*d*₆) δ ppm 154.4, 153.7, 131.4, 129.2, 125.2, 123.9, 28.8, 27.3; LCMS: t_R = 1.16 min, area% = 90%, [M+H]⁺ 219 (100); IR ν_{max} (thin film): 3213, 3148, 2980, 1766, 1735, 1615, 1497, 1450, 1353, 1251, 1153, 1065, 659, 931, 748, 686 cm⁻¹; HRMS (ESI-QToF): calculated for [2M+H]⁺ 437.2188, found 437.2190.

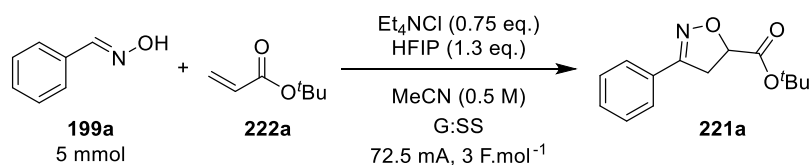
2-Methyl-5-phenyl-1,3,4-oxadiazole (**262b**)



To a 10 mL ElectraSyn 2.0 reaction vessel containing a stirrer bar, (*E*)-*N*-benzylideneacetohydrazide **259b** (82 mg, 0.50 mmol), HFIP (70 μ L, 0.67 mmol, 1.3 eq.) and Et_4NCl (45 mg, 0.27 mmol, 0.5 eq.) were added followed by MeCN (7 mL). The reaction mixture was electrolysed under a constant current of 25 mA with G anode and SS cathode stirring at 400 rpm, until a current of 3 F.mol⁻¹ had been passed. After electrolysis, the reaction mixture was transferred to a round-bottomed flask, washing the electrodes with MeCN

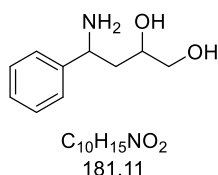
until washings ran clear, and concentrated *in vacuo* to give the crude mixture. The crude mixture and submitted to column chromatography on silica gel (24 g, 0 - 20% EtOAc in cyclohexane over 25 CVs). Appropriate fractions were combined and concentrated *in vacuo* to afford 2-methyl-5-phenyl-1,3,4-oxadiazole **262b** (27 mg, 0.165 mmol, 33%) as a colourless oil.

262b: ^1H NMR (400 MHz, DMSO- d_6) δ ppm 7.94 - 8.00 (2H, m), 7.56 - 7.65 (3H, m), 2.58 (3H, s); ^{13}C NMR (101 MHz, DMSO- d_6) δ ppm 163.9, 131.7, 129.3, 126.2, 123.5, 10.6; LCMS: t_{R} = 0.80 min, area% = 96%, $[\text{M}+\text{H}]^+$ 161 (100). Data consistent with literature synthesis.¹¹⁸

6.3. Electrochemical Synthesis of **221a** on 5 mmol Scale

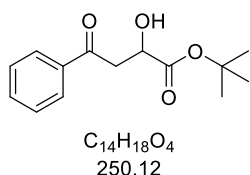
To a 20 mL ElectraSyn 2.0 reaction vessel containing a stirrer bar, (*E*)-benzaldehyde oxime **199a** (607 mg, 5.01 mmol), *tert*-butyl acrylate (1830 μL , 12.49 mmol), HFIP (700 μL , 6.65 mmol) and Et_4NCl (621 mg, 3.75 mmol) were added followed by MeCN (10 mL). The reaction mixture was electrolysed under a constant current of 72.5 mA with G anode and SS cathode stirring at 400 rpm, until a current of 3 F.mol⁻¹ had been passed (5.5 hours). Following electrolysis, the reaction mixture was transferred to a round-bottomed flask, washing with MeCN, and concentrated *in vacuo* to give the crude mixture. The crude mixture was submitted to column chromatography on silica gel (80 g, 0 - 15% EtOAc in cyclohexane over 15 CVs). Appropriate fractions were combined and concentrated *in vacuo* to afford a mixture of *tert*-butyl 3-phenyl-4,5-dihydroisxazole-5-carboxylate and *tert*-butyl 3-phenyl-4,5-dihydroisxazole-4-carboxylate **221a** as a pale-yellow oil (14:1, 713 mg, 2.88 mmol, 58%).

221a: ¹H NMR (400 MHz, DMSO-*d*₆) δ ppm 7.66 - 7.73 (2H, m), 7.42 - 7.51 (3H, m), 5.12 (1H, dd, J = 11.7, 7.0 Hz), 4.76 (dd, J = 11.0, 5.6 Hz, *minor regioisomer*), 4.65 (dd, J = 8.7, 5.6 Hz, *minor regioisomer*), 4.54 (dd, J = 11.0, 8.7 Hz, *minor regioisomer*), 3.74 (1H, dd, J = 17.2, 11.7 Hz), 3.54 (1H, dd, J = 17.2, 7.0 Hz), 1.45 (9H, s), 1.28 (s, *minor regioisomer*); ¹³C NMR (101 MHz, DMSO-*d*₆) δ ppm 169.0, 156.0, 130.3, 128.8, 128.5, 126.7, 81.7, 78.1, 38.4, 27.5; LCMS: t_{R} = 1.15 min, area% = 98%, [M+H]⁺ 248 (100). Spectra recorded on mixture. Data consistent with synthesis by **GP2**. (N74624-23)

6.4. Derivatisation of **221a****4-Amino-4-phenylbutane-1,2-diol (241)**

To a round-bottomed flask (containing a stirrer bar) that had been purged with cycles of vacuum and nitrogen (x 3), a solution of *tert*-butyl 3-phenyl-4,5-dihydroisoxazole-5-carboxylate **221a** (294 mg, 1.19 mmol) in THF (12 mL) was added. The solution was cooled to 0 °C in an ice bath. Once cool, lithium aluminium hydride (2 M in THF) (720 μ L, 1.44 mmol) was added slowly. The resulting yellow solution was stirred at 0 °C for 10 mins under N₂, before being allowed to warm to ambient temperature. After 1 hour at ambient temperature, the reaction mixture was diluted with Et₂O (15 mL) and cooled to 0 °C in an ice bath. Once cool, water (55 μ L) was added slowly, followed by aqueous 15% NaOH solution (55 μ L) and further water (165 μ L). The resulting suspension was allowed to warm to ambient temperature over 15 mins. After 15 mins, MgSO₄ (approx. 250 mg) was added and the suspension stirred for a further 15 mins at ambient temperature. After 15 mins, the suspension was filtered, washing with Et₂O (3 x 15 mL). The filtrate was concentrated *in vacuo* to afford the crude mixture. The crude mixture was submitted to column chromatography on silica gel (12 g, 0 - 50% EtOAc in cyclohexane over 15 CVs). Appropriate fractions were combined and concentrated to afford 4-amino-4-phenylbutane-1,2-diol **241** (65 mg, 0.36 mmol, 30%) as a white solid (MP (CH₂Cl₂): 80.4 - 82.3 °C).

241: ¹H NMR (400 MHz, DMSO-*d*₆) δ ppm 7.63 - 7.69 (2H, m), 7.42 - 7.48 (3H, m), 4.96 (1H, t, *J* = 5.7 Hz), 4.71 (1H, ddt, *J* = 10.9, 7.8, 4.8 Hz), 3.51 (2H, ddd, *J* = 5.7, 4.8, 2.1 Hz), 3.41 (1H, dd, *J* = 17.0, 10.9 Hz), 3.19 (1H, dd, *J* = 17.0, 7.8 Hz); ¹³C NMR (101 MHz, DMSO-*d*₆) δ ppm 156.2, 129.8, 129.6, 128.7, 126.4, 81.5, 62.3, 36.0; LCMS: *t*_R = 0.69 min, area% = 100%, [M-H]⁻ 180 (100); IR ν_{max} (thin film): 3377, 3053, 2920, 2849, 1596, 1497, 1446, 1357, 1251, 1102, 1039, 915, 891, 808, 753, 688, 618 cm⁻¹.

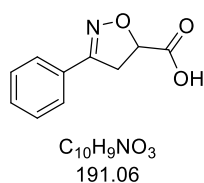
***tert*-Butyl 2-hydroxy-4-oxo-4-phenylbutanoate (242)**

To a round-bottomed flask containing a stirrer bar, ammonium chloride (537 mg, 10.04 mmol) was added followed by ethanol (16.9 mL) and water (20 mL). To the stirring solution, a solution of *tert*-butyl 3-phenyl-4,5-dihydroisoxazole-5-carboxylate **221a**

(247 mg, 1.00 mmol) in EtOH (3.1 mL) was added, followed by iron powder (557 mg, 9.97 mmol). The resulting colourless solution was heated to 80 °C with stirring. After reaching 80 °C, the solution turned orange. After stirring for 24 hrs, the reaction mixture had turned brown. The reaction temperature was increased to 90 °C and allowed to continue to stir. After stirring for further 72 hrs, the reaction was allowed to cool to ambient temperature. Once cooled, the reaction was diluted with EtOAc (50 mL) and filtered through a pad of Florisil under vacuum. The filtrate was washed with brine (75 mL), dried (hydrophobic frit) and concentrated *in vacuo* to give the crude mixture. After standing overnight at ambient temperature, the crude mixture was dissolved in DCM (1.5 mL) and submitted to column chromatography on silica gel (12 g, 0 - 20% EtOAc in cyclohexane over 20 CVs). Appropriate fractions were combined and concentrated *in vacuo* to afford *tert*-butyl 2-hydroxy-4-oxo-4-phenylbutanoate **242** (34 mg, 0.14 mmol, 13%) as a white solid (MP (CH₂Cl₂): 87.3 - 89.2 °C).

242: ¹H NMR (400 MHz, DMSO-*d*₆) δ ppm 7.92 - 7.99 (2H, m), 7.65 (1H, tt, *J* = 7.3, 1.2 Hz), 7.49 - 7.57 (2H, m), 5.45 (1H, d, *J* = 6.1 Hz), 4.41 (1H, q, *J* = 6.1 Hz), 3.30 (2H, d, *J* = 5.6 Hz), 1.39 (9H, s); ¹³C NMR (101 MHz, DMSO-*d*₆) δ ppm 197.3, 172.4, 136.6, 133.2, 128.7, 128.0, 80.3, 67.4, 42.6, 27.6; LCMS: *t*_R = 1.00 min, area% = 98%, [M+H]⁺ 251 (10); IR *v*_{max} (thin film): 3447, 3408, 2975, 2930, 1736, 1681, 1594, 1451, 1366, 1297, 1210, 1151, 1123, 1024, 847, 764, 692, 574 cm⁻¹; HRMS (ESI-QToF): calculated for [M+Na]⁺ 273.1103, found 273.1094.

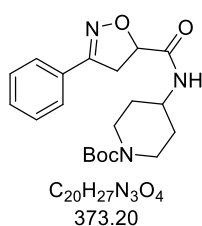
3-Phenyl-4,5-dihydroisoxazole-5-carboxylic acid (**290**)



To a round-bottomed flask containing a stirrer bar, *tert*-butyl 3-phenyl-4,5-dihydroisoxazole-5-carboxylate **221a** (479 mg, 1.94 mmol) was added, followed by EtOH (20 mL). To the resulting stirring solution, 0.5 M aqueous lithium hydroxide (12 mL, 6.00 mmol) was added. The reaction mixture was allowed to stir at ambient temperature. After stirring for 72 hours, the reaction mixture was quenched with aqueous 0.5 M aqueous HCl until a pH 4 was achieved. The resulting solution was extracted with EtOAc (3 x 30 mL). The combined organic layers were washed with brine (30 mL), dried (hydrophobic frit) and concentrated *in vacuo* to afford 3-phenyl-4,5-dihydroisoxazole-5-carboxylic acid **290** (211.4 mg, 1.12 mmol, 57%) as an orange solid (MP (CH₂Cl₂): 135.9 - 137.4 °C).

290: ^1H NMR (400 MHz, $\text{DMSO-}d_6$) δ ppm 7.67 - 7.72 (2H, m), 7.44 - 7.49 (3 H, m), 5.14 (1H, dd, $J = 11.7, 6.8$ Hz), 4.65 - 4.71 (m, *minor regioisomer*), 4.49 - 4.56 (m, *minor regioisomer*), 3.72 (1H, dd, $J = 17.2, 11.7$ Hz), 3.57 (1H, dd, $J = 17.2, 6.8$ Hz) [COOH interchangeable proton not observed]; ^{13}C NMR (101 MHz, $\text{DMSO-}d_6$) δ ppm 171.5, 156.0, 130.2, 128.8, 128.6, 126.7, 77.9, 38.4; LCMS: $t_R = 0.45$ min, area% = 91%, $[\text{M-H}]^-$ 190 (100); $t_R = 0.42$ min, area% = 9%, $[\text{M-H}]^-$ 190 (75) (*minor regioisomer*); IR ν_{max} (thin film): 3030, 1714, 1413, 1357, 1223, 977, 896, 753, 689, 617, 543 cm^{-1} . Data consistent with literature synthesis.¹¹⁹

tert-Butyl 4-(3-phenyl-4,5-dihydroisoxazole-5-carboxamido)piperidine-1-carboxylate (244)



To microwave vial containing a stirrer bar, 3-phenyl-4,5-dihydroisoxazole-5-carboxylic acid **290** (101 mg, 0.53 mmol) and *tert*-butyl 4-aminopiperidine-1-carboxylate (127 mg, 0.63 mmol) were added, followed by MeCN (2.5 mL) and 1-methyl-1*H*-imidazole (NMI, 88 μL , 1.11 mmol). While the resulting suspension was stirred, *N*-(chloro(dimethylamino)methylene)-*N*-methylmethanaminium hexafluorophosphate (V) (TCFH, 166 mg, 0.59 mmol) was added and the reaction mixture allowed to continue to stir at ambient temperature. After stirring for 4 hours, the reaction mixture was diluted with water (15 mL) and EtOAc (15 mL), and the phases separated. The aqueous layer was extracted with EtOAc (2 x 10 mL). The combined organic layers were washed with brine (15 mL), dried (hydrophobic frit) and concentrated *in vacuo* to give the crude mixture. After standing overnight at ambient temperature, the crude mixture was dissolved in DCM (2.5 mL) and submitted to column chromatography on silica gel (24 g, 0 - 50% EtOAc in cyclohexane over 15 CVs). Appropriate fractions were combined and concentrated *in vacuo* to afford *tert*-butyl 4-(3-phenyl-4,5-dihydroisoxazole-5-carboxamido)piperidine-1-carboxylate **244** (139 mg, 0.37 mmol 70%) as a white solid (MP (CH_2Cl_2): 137.2 - 139.8 $^\circ\text{C}$).

244: ^1H NMR (400 MHz, $\text{DMSO-}d_6$) δ ppm 8.17 (1H, d, $J = 8.1$ Hz), 7.66 - 7.73 (2H, m), 7.43 - 7.49 (3H, m), 5.05 (1H, dd, $J = 11.5, 7.3$ Hz), 3.87 (2H, br. d, $J = 9.8$ Hz), 3.78 (1H, ddt, $J = 15.0, 11.1, 4.1, 4.1$ Hz), 3.67 (1H, dd, $J = 17.2, 11.5$ Hz), 3.54 (1H, dd, $J = 17.2, 7.3$ Hz), 2.80 (1H, br s), 1.61 - 1.73 (2H, m), 1.29 - 1.44 (12H, m); ^{13}C NMR (101 MHz, $\text{DMSO-}d_6$) δ ppm 168.6, 156.3, 153.8, 130.3, 128.8, 128.6, 126.7, 79.0, 78.6, 46.0, 38.4, 31.0, 28.0; LCMS: $t_R = 1.09$ min, area% = 100%, $[\text{M+H}]^+$ 374

(25), 274 (100); IR ν_{max} (thin film): 3365, 2981, 2943, 2852, 1683, 1662, 1522, 1428, 1366, 1324, 1241, 1173, 1139, 954, 860, 767, 697 cm^{-1} ; HRMS (ESI-QToF): calculated for $[\text{M}+\text{H}]^+-\text{Boc}$ 274.1556, found 274.1557.

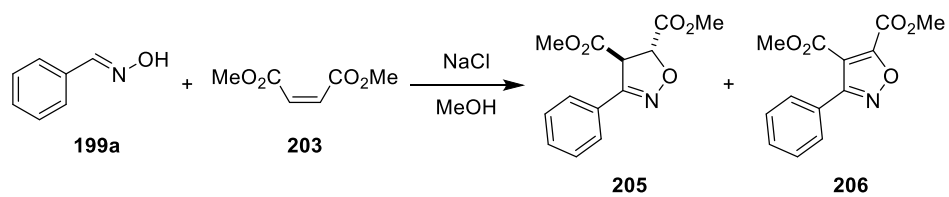
6.5. Initial Scoping

Initial scoping reactions were carried out using an IKA ElectraSyn 2.0.

6.5.1. Initial Scoping Reactions

To a 10 mL ElectraSyn 2.0 reaction vessel containing a stirrer bar, (*E*)-benzaldehyde oxime (0.5 mmol), dimethyl maleate (5 eq.) and sodium chloride (0.5 eq.) were added followed by methanol (0.07 M). The resulting suspension was stirred at ambient temperature for 5 mins to dissolve mediator. The reaction mixture was electrolysed under the desired constant current with a working electrode and counter electrode, until the desired current had been passed. The solution was analysed by LCMS. After electrolysis, the reaction mixture was transferred to a round-bottomed flask, washing the electrodes with MeOH until washings ran clear, and concentrated *in vacuo* to give the crude mixture. The residue was taken up in EtOAc (40 mL) and partitioned with water (50 mL), and the phases separated. The aqueous layer was extracted with EtOAc (2 x 25 mL). The combined organic layers were washed with brine (25 mL), dried (hydrophobic frit) and concentrated *in vacuo*. The crude mixture was submitted to column chromatography on silica gel, eluting with 0 - 30% EtOAc/cyclohexane over 25 CVs, to afford desired product.

Entry 1 (**Table 21**) was submitted to reverse phase column chromatography on X-Select C18 preparative column (30 x 100 mm, 15 - 85% MeCN in water with ammonium bicarbonate modifier over 30 mins). Appropriate fractions were combined and the MeCN removed *in vacuo*. The resulting aqueous layer was extracted with EtOAc (3 x 25 mL). The combined organic layers were washed with brine (25 mL), dried (hydrophobic frit) and concentrated *in vacuo* to afford dimethyl 3-phenylisoxazole-4,5-dicarboxylate **206** as a mixture with unreacted dimethyl maleate (35 mg, 0.13 mmol, 27%, 60% purity). Data consistent with the synthesis of **205** with dimethyl fumarate by **GP2**.

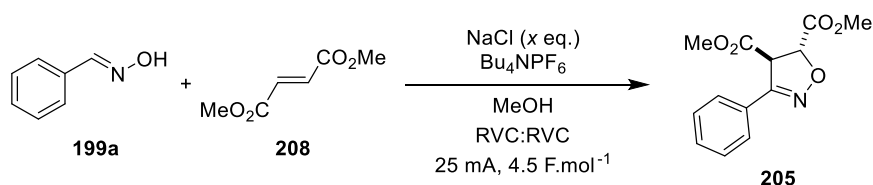


Entry	Anode	Cathode	Current/mA	Charge transferred/F.mol ⁻¹	Yield 205 (206)/%
1 ^a	G	G	25	5	0 (27)
2 ^a	RVC	RVC	16.8	2	14 (0)
3	RVC	RVC	11.4	2.6	28 (0)
4 ^{a,b}	RVC	RVC	25	3	15 (0)
5	RVC	RVC	25	4.5	27 (0)
6 ^c	RVC	RVC	25	4.5	36 (0)
7 ^d	RVC	RVC	25	4.5	76 (0)

Table 21: Conditions: Oxime (0.5 mmol), dimethyl maleate (5 eq.), NaCl (0.5 eq.), MeOH (0.07 M), [anode], [cathode], [current] mA, [charge transferred] F.mol⁻¹; ^aReaction conducted at 0.1 M concentration; ^b1 eq. NaCl used; ^cPolarity of the electrodes was switched every 15 mins; ^dDimethyl fumarate used instead of dimethyl maleate; G = graphite; RVC = reticulated vitreous carbon.

6.5.2. Additional Electrolyte Screen

To a 10 mL ElectraSyn 2.0 reaction vessel containing a stirrer bar, (*E*)-benzaldehyde oxime (0.5 mmol), dimethyl fumarate (5 eq.), Et₄NPF₆ (1.4 eq.) and sodium chloride (x eq.) were added followed by methanol (0.07 M). The resulting suspension was stirred at ambient temperature for 5 mins to dissolve mediator. The reaction mixture was electrolysed under a constant current of 25 mA with RVC anode and RVC cathode, until a current of 4.5 F.mol⁻¹ had been passed. The solution was analysed by LCMS. After electrolysis, the reaction mixture was transferred to a round-bottomed flask, washing the electrodes with MeOH until washings ran clear. The combined washings were concentrated *in vacuo* to give the crude mixture. The crude mixture was submitted to column chromatography on silica gel, dry loading from CH₂Cl₂ and eluting with 0 - 30% EtOAc/cyclohexane over 30 column volumes, to afford desired product.



Entry	NaCl (x)/eq.	205/%
1	0	8
2	0.5	8
3	1	33
4	2	14
5 ^a	0.5	39

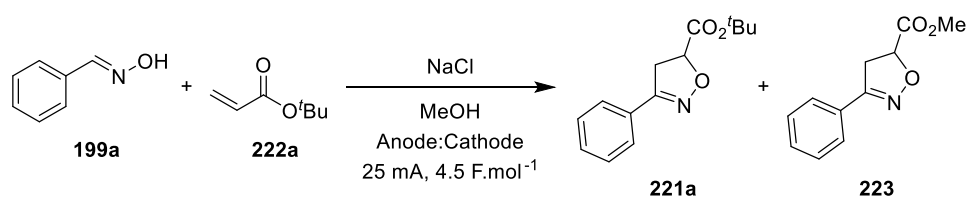
Table 22: Conditions: Oxime (0.5 mmol), dimethyl fumarate (5 eq.), NaCl (x eq.), Bu₄NPF₆ (1.4 eq.), MeOH (0.07 M), RVC anode, RVC cathode, 25 mA, 4.5 F.mol⁻¹; ^aEt₄NBF₄ used instead of Bu₄NPF₆; RVC = reticulated vitreous carbon.

6.6. Optimisation of Electrochemical Isoxazoline Procedure

The optimisation of the reaction was carried out using an IKA ElectraSyn 2.0 with IKA carousel.

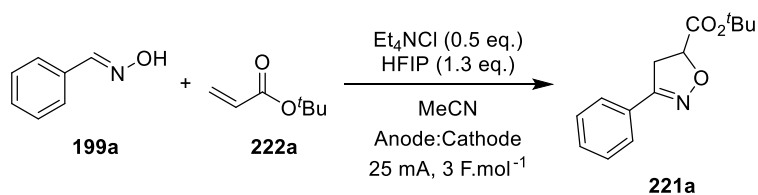
6.6.1. Electrode Material Screen

To a 10 mL ElectraSyn 2.0 reaction vessel containing a stirrer bar, (*E*)-benzaldehyde oxime (0.5 mmol), *tert*-butyl acrylate (5 eq.) and sodium chloride (0.5 eq.) were added followed by methanol (0.07 M). The resulting suspension was stirred at ambient temperature for 5 mins to dissolve mediator. The reaction mixture was electrolysed under a constant current of 25 mA with a working electrode and counter electrode, until a current of 4.5 F.mol⁻¹ had been passed. The solution was analysed by LCMS. After electrolysis, the reaction mixture was transferred to a round-bottomed flask, washing the electrodes with MeOH and acetone until washings ran clear, and concentrated *in vacuo* to give the crude mixture. The crude mixture was submitted to column chromatography on silica gel, eluting with 15% EtOAc in cyclohexane to give *tert*-butyl 3-phenyl-4,5-dihydroisoxazole-5-carboxylate **221a** and methyl 3-phenyl-4,5-dihydroisoxazole-5-carboxylate **223**. Data from all isolations was consistent with synthesis by **GP2** (and **GP3** for **223**).



Entry	Anode	Cathode	Isolated Yield 221a (223)/%
1	RVC	RVC	27 (4)
2	G	G	11 (31)
3	RVC	SS	31 (12)
4	RVC	Pt	37 (9)
5	G	SS	14 (44)
6	G	Pt	13 (39)
7	GC	Pt	12 (36)
98	GC	SS	17 (30)

Table 23: Conditions: Oxime (0.5 mmol), *tert*-butyl acrylate (5 eq.), NaCl (0.5 eq.), MeOH (0.07 M), anode, cathode, 25 mA, 4.5 F.mol⁻¹. RVC = reticulated vitreous carbon; G = graphite; SS = stainless steel; GC = glassy carbon.

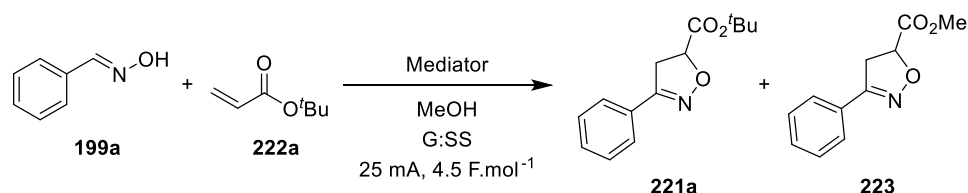


Entry	Anode	Cathode	Isolated Yield 221a/%
1	RVC	RVC	7
2	G	G	48
3	Pt	Pt	44
4	RVC	SS	30
5	RVC	Pt	23
6	G	SS	78
7	G	Pt	79
8	GC	SS	46

Table 24: Conditions: Oxime (0.5 mmol), *tert*-butyl acrylate (5 eq.), Et₄NCl (0.5 eq.), HFIP (1.3 eq.), MeCN (0.07 M), anode, cathode, 25 mA, 3 F.mol⁻¹. RVC = reticulated vitreous carbon; G = graphite; SS = stainless steel; GC = glassy carbon

6.6.2. Mediator Screen

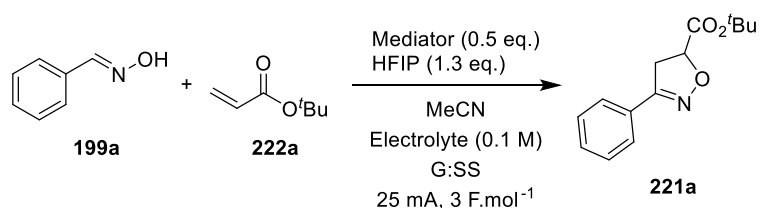
To a 10 mL ElectraSyn 2.0 reaction vessel containing a stirrer bar, (*E*)-benzaldehyde oxime (0.5 mmol), *tert*-butyl acrylate (5 eq.) and mediator (0.5 eq.) were added, followed by Methanol (0.07 M). Heterogenous mixtures were stirred at ambient temperature for 5 mins to dissolve mediator. The reaction mixture was electrolysed under a constant current of 25 mA with graphite anode and stainless-steel cathode, until a current of 4.5 F.mol⁻¹ had been passed. The solution was analysed by LCMS. After electrolysis, the reaction mixture was transferred to a round-bottomed flask, washing the electrodes with MeOH until washings ran clear, and concentrated *in vacuo* to give crude mixture. The crude mixture was analysed by ¹H NMR, using benzyl benzoate as internal standard. If isolated, the crude mixture was submitted to column chromatography on silica gel, eluting with 0 - 15% EtOAc/cyclohexane over 25 column volumes, to afford *tert*-butyl 3-phenyl-4,5-dihydroisoxazole-5-carboxylate **221a** and methyl 3-phenyl-4,5-dihydroisoxazole-5-carboxylate **223**.



Entry	Mediator	NMR Yield 221a (223) ^a /%	Isolated Yield 221a (223) ^b /%
1	NaCl	41 (22)	22 (27)
2	NaBr	15 (5)	- (-)
3	NaI	36 (24)	35 (22)
4	Et ₄ NCl	37 (37)	21 (27)
5 ^b	Et ₄ NCl	14 (0)	- (-)
6	Et ₄ NI	40 (22)	32 (21)
7	NHPI	- (-)	- (-)
8	TEMPO	- (-)	- (-)
9	ABNO	- (-)	- (-)

Table 25: Conditions: Oxime (0.5 mmol), *tert*-butyl acrylate (5 eq.), mediator (0.5 eq.), MeOH (0.07 M), G anode, SS cathode, 25 mA, 4.5 F.mol⁻¹; ^a¹H NMR yield using benzyl benzoate as internal standard; ^bMeCN used instead of MeOH; G = graphite; SS = stainless steel; NHPI = *N*-hydroxyphthalimide; TEMPO = 2,2,6,6-tetramethylpiperidine *N*-oxyl; ABNO = 9-azabicyclo[3.3.1]nonane *N*-oxyl.

Further screening of mediators was performed:



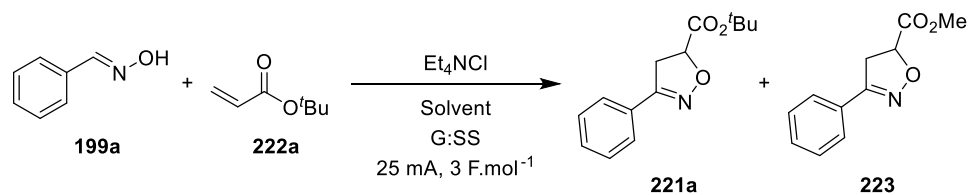
Entry	Mediator	Electrolyte (0.1 M)	Isolated Yield 221a /%
1	NHPI	Et ₄ NBF ₄	17
2	NHPI	ⁿ Bu ₄ NPF ₆	14
3	NHPI	Et ₄ NOTs	19
4	TEMPO	Et ₄ NBF ₄	6
5	ABNO	Et ₄ NOTs	5
6	-	Et ₄ NBF ₄	16
7	-	ⁿ Bu ₄ NPF ₆	13
8	-	Et ₄ NOTs	24
9	ⁿ Bu ₄ NCl	-	74
10	Et ₄ NCl	Et ₄ NBF ₄	63
11	Et ₄ NCl	Et ₄ NOTs	61

Table 26: Conditions: Oxime (0.5 mmol), *tert*-butyl acrylate (5 eq.), mediator (0.5 eq.), electrolyte 1.4 eq., 0.1 M, MeCN (0.07 M), G anode, SS cathode, 25 mA, 3 F.mol⁻¹. G = graphite; SS = stainless steel; NHPI = *N*-hydroxyphthalimide; TEMPO = 2,2,6,6-tetramethylpiperidine *N*-oxyl; ABNO = 9-azabicyclo[3.3.1]nonane *N*-oxyl.

6.6.3. Solvent Screen

To a 10 mL ElectraSyn 2.0 reaction vessel containing a stirrer bar, (*E*)-benzaldehyde oxime (0.5 mmol), *tert*-butyl acrylate (5 eq.) and Et₄NCl (0.5 eq.) were added followed by solvent mixture (0.07 M). The reaction mixture was electrolysed under a constant current of 25 mA with graphite anode and stainless-steel cathode, until a current of 3 F.mol⁻¹ had been passed. The solution was analysed by LCMS. After electrolysis, the reaction mixture was transferred to a round-bottomed flask, washing the electrodes with MeOH (or MeCN if HFIP is used) and acetone until washings ran clear, and concentrated *in vacuo* to give the crude mixture. The crude mixture was analysed by ¹H NMR, using benzyl benzoate as internal standard. If isolated, the crude product was submitted to column chromatography on silica gel, eluting with 0 - 15% EtOAc/cyclohexane over 25 column volumes, to afford *tert*-butyl 3-phenyl-4,5-dihydroisoxazole-5-carboxylate **221a** and methyl 3-phenyl-4,5-dihydroisoxazole-5-carboxylate **223**. Data is consistent with synthesis of **221a** by **GP2** and **223** from electrode material screen.

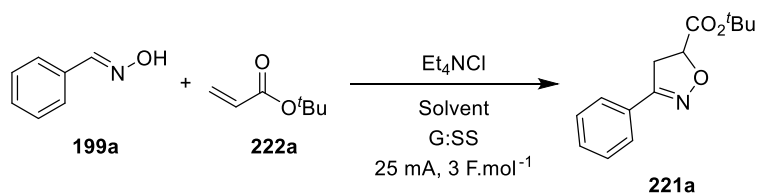
MeOH:MeCN Solvent Screening:



Entry	Solvent	Ratio	% Alcohol (eq.)	221a (223) ^a /%
1	MeOH	-	100 (340)	55 (8)
2	MeOH:MeCN	1:1	50 (170)	39 (8)
3	MeOH:MeCN	1:9	10 (34)	43 (2)
4	MeOH:MeCN	-	0.3 (1)	50 (0)
5	MeCN	-	0 (0)	36 (0)

Table 27: Conditions: Oxime (0.5 mmol), *tert*-butyl acrylate (5 eq.), Et₄NCl (0.5 eq.), solvent (0.07 M), G anode, SS cathode, 25 mA, 3 F.mol⁻¹; ^aYield in parentheses refers to the yield for the methyl ester by-product; G = graphite; SS = stainless steel.

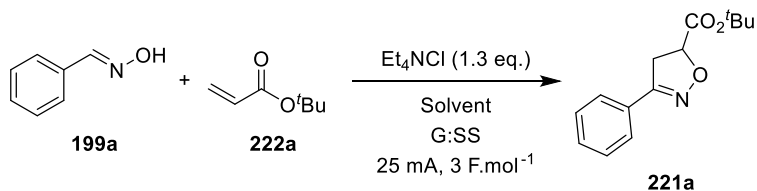
HFIP: MeCN Solvent Screening:



Entry	Solvent(s)	Ratio	% Alcohol (eq.)	221a/%
1	HFIP	-	100 (129)	32, 36
2	HFIP:MeCN	1:1	50 (65)	57
3	HFIP:MeCN	1:3	25 (32)	55
4	HFIP:MeCN	1:9	10 (7)	59
5	HFIP:MeCN	1:19	5 (3.3)	68
6	HFIP:MeCN	1:99	1 (1.3)	70, 76, 73
7	HFIP:MeCN	-	0.8 (1)	71
8	HFIP:MeCN	-	0.4 (0.5)	67
9	HFIP:MeCN	-	0.08 (0.1)	61

Table 28: Conditions: Oxime (0.5 mmol), *tert*-butyl acrylate (5 eq.), Et_4NCl (0.5 eq.), solvent (0.07 M), G anode, SS cathode, 25 mA, 3 F.mol^{-1} ; G = graphite, SS = stainless steel; HFIP = 1,1,1,3,3,3-hexafluoroisopropanol.

Further solvent screening:



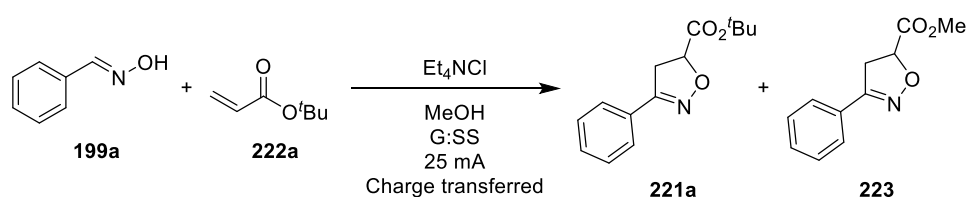
Entry	Solvent	Ratio	% Alcohol (eq.)	221a/%
1	HFIP:DCM	1:99	1 (1.3)	NR
2	HFIP:DMSO	1:99	1 (1.3)	NR
3	HFIP:H ₂ O	1:99	1 (1.3)	NR
4	HFIP:DMF	1:99	1 (1.3)	52
5	HFIP- <i>d</i> ₂ :MeCN- <i>d</i> ₃	1:99	1 (1.3)	75
6	HFIP:MeCN- <i>d</i> ₃	1:99	1 (1.3)	70

Table 29: Conditions: Oxime (0.5 mmol), *tert*-butyl acrylate (5 eq.), Et_4NCl (0.5 eq.), solvent (0.07 M), G anode, SS cathode, 25 mA, 3 F.mol^{-1} . G = graphite; SS = stainless steel; DCM = dichloromethane; DMSO = dimethyl sulfoxide; DMF = *N,N*-dimethylformamide.

6.6.4. Charge Transferred Screen

To a 10 mL ElectraSyn 2.0 reaction vessel containing a stirrer bar, (*E*)-benzaldehyde oxime (0.5 mmol), *tert*-butyl acrylate (5 eq.) and Et₄NCl (0.5 eq.) (and 1.3 eq. additive, if used) were added followed by solvent (0.07 M). The reaction mixture was electrolysed under a constant current of 25 mA with graphite anode and stainless-steel cathode, until the required charge had been transferred. The solution was analysed by LCMS. After electrolysis, the reaction mixture was transferred to a round-bottomed flask, washing the electrodes with MeOH and acetone until washings ran clear, and concentrated *in vacuo* to give the crude mixture. The crude product was submitted to column chromatography on silica gel, eluting with 0 - 15% EtOAc/cyclohexane over 25 column volumes, to afford *tert*-butyl 3-phenyl-4,5-dihydroisoxazole-5-carboxylate **221a** (and methyl 3-phenyl-4,5-dihydroisoxazole-5-carboxylate **223**, where appropriate). Data is consistent with synthesis of **221a** by **GP2** and **223** from the electrode material screen.

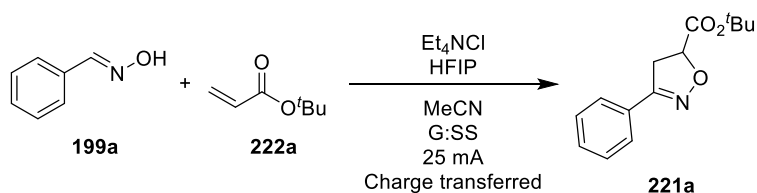
MeOH Screen:



Entry	Charge Transferred/F.mol ⁻¹	221a (223)/%
1 ^{a,b}	1	19 (0)
2 ^{a,b}	2	43 (0)
3	3	55 (8)
4	4	35 (17)
5	5	33 (6)

Table 30: Conditions: Oxime (0.5 mmol), *tert*-butyl acrylate (5 eq.) Et₄NCl (0.5 eq.), MeOH (0.07 M), G anode, SS cathode, 25 mA, [charge transferred]; ^aIsolated with unreacted oxime starting material; ^bStrength ¹H NMR used to determine yield, with benzyl benzoate as internal standard; G = graphite; SS = stainless steel.

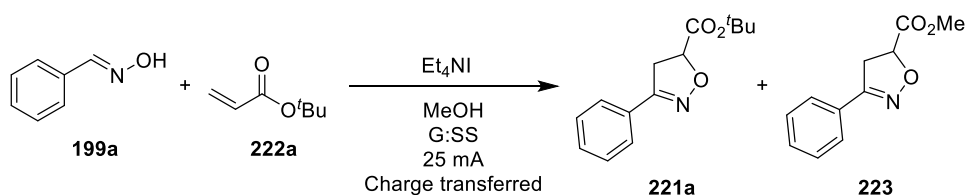
HFIP Screen:



Entry	Charge Transferred/F.mol ⁻¹	221a/%
1 ^{a,b}	1	13
2 ^{a,b}	2	33
3	3	73
4	4	75
5	5	73

Table 31: Conditions: Oxime (0.5 mmol), *tert*-butyl acrylate (5 eq.) Et_4NCl (0.5 eq.), MeOH (0.07 M), G anode, SS cathode, 25 mA, [charge transferred]; ^aIsolated with unreacted oxime starting material; ^bStrength ¹H NMR used to determine yield, with benzyl benzoate as internal standard; HFIP = 1,1,1,3,3,3-hexafluoroisopropanol; G = graphite; SS = stainless steel.

Charge transferred screen using Et_4NI as mediator:

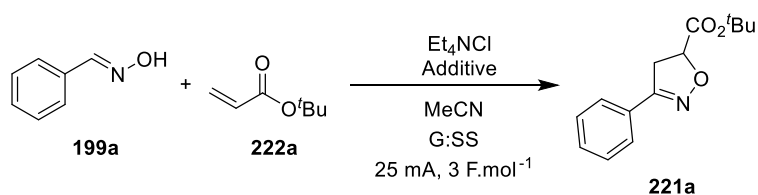


Entry	Charge Transferred/F.mol ⁻¹	221a (223)/%
1	1	33
2	2	41
3	3	39 (9)
4	4	50
5	5	38 (16)

Table 32: Conditions: Oxime (0.5 mmol), *tert*-butyl acrylate (5 eq.) Et_4NCl (0.5 eq.), MeOH (0.07 M), G anode, SS cathode, 25 mA, [charge transferred]; G = graphite; SS = stainless steel.

6.6.5. Additive Screen

To a 10 mL ElectraSyn 2.0 reaction vessel containing a stirrer bar, (*E*)-benzaldehyde oxime (0.5 mmol), *tert*-butyl acrylate (5 eq.), Et₄NCl (0.5 eq.) and additive (1.3 eq.) were added followed by MeCN (0.07 M). The reaction mixture was electrolysed under a constant current of 25 mA with graphite anode and stainless-steel cathode, until a current of 3 F.mol⁻¹ had been passed. The solution was analysed by LCMS. After electrolysis, the reaction mixture was transferred to a round-bottomed flask, washing the electrodes with MeCN and acetone until washings ran clear, and concentrated *in vacuo* to give the crude mixture. The crude product was submitted to column chromatography on silica gel, eluting with 0 - 15% EtOAc/cyclohexane over 25 Column volumes, to afford *tert*-butyl 3-phenyl-4,5-dihydroisoxazole-5-carboxylate **221a**. Data consistent with synthesis of **221a** by **GP2**.

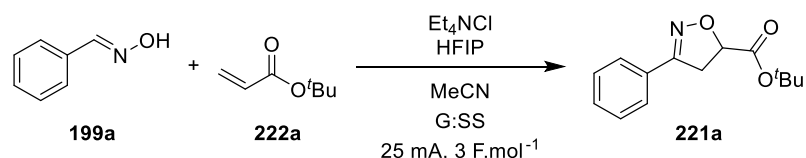


Entry	Base (1.5 eq.)	Additive	pK _a in DMSO (H ₂ O)	221a/%
1	-	HFIP	17.9 (9.3)	73 (n=3)
2	-	IPA	30.3 (16.5)	41
3	-	H ₂ O	31.4 (15.7)	42
4	-	AcOH	12.6 (4.8)	50
5	-	PivOH	12.9 (5.0)	46
6	-	^t BuOH	29.4 (17.0)	32
7	-	MeOH	27.9 (15.5)	50
8	-	-	31.3 (-)	36
9	-	TFE	23.5 (-)	74
10	-	FCH ₂ CH ₂ OH	- (-)	35
11	-	(CF ₃) ₃ COH	10.7 (-)	66
12	DIPEA	HFIP	17.9 (9.3)	-
13	Et ₃ N	HFIP	17.9 (9.3)	-
14	Py	HFIP	17.9 (9.3)	58

Table 33: Conditions: Oxime (0.5 mmol), *tert*-butyl acrylate (5 eq.), Et₄NCl (0.5 eq.), Additive (1.3 eq.), MeCN (0.07 M), G anode, SS cathode, 25 mA, 3 F.mol⁻¹; G = graphite; SS = stainless steel; HFIP = 1,1,1,3,3,3-hexafluoroisopropanol; IPA = isopropanol; TFE = trifluoroethanol; DIPEA = diisopropylethylamine; Py = pyridine.

6.6.6. Concentration Screen

To a 10 mL ElectraSyn 2.0 reaction vessel containing a stirrer bar, (*E*)-benzaldehyde oxime **199a**, tert-butyl acrylate **222a**, HFIP and Et₄NCl were added followed by MeCN (stoichiometry shown in **Table 34**). The reaction mixture was electrolysed under a constant current of 25 mA with G anode and SS cathode stirring at 400 rpm, until a current of 3 F.mol⁻¹ had been passed. The solution was analysed by LCMS (HPLC). After electrolysis, the reaction mixture was transferred to a round-bottomed flask, washing the electrodes with MeCN until washings ran clear, and concentrated *in vacuo* to give the crude mixture. The crude mixture was dissolved in DCM (2 mL) and submitted to column chromatography on silica gel (80 g, 0 - 15% EtOAc in cyclohexane over 20 CVs). Appropriate fractions were combined and concentrated *in vacuo* to afford the desired products. The data from all isolations was consistent with synthesis by **GP2**.



Entry	199a/mmol	222a/mmol	HFIP/mmol	Et ₄ NCl	Conc./M	Yield/%
1	3.76	18.75	4.99	0.26	0.5	-
2	3.76	18.75	4.99	1.88	0.5	31
3	1.87	9.37	2.50	0.25	0.25	21
4	1.88	9.37	2.50	0.94	0.25	40

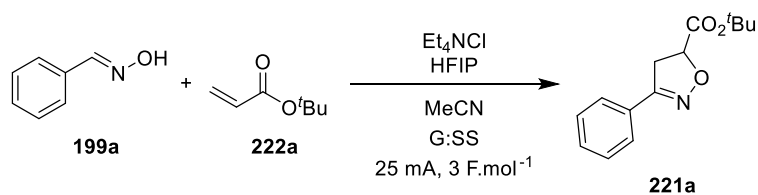
Table 34: Conditions: **199a**, **222a**, HFIP, Et₄NCl, MeCN, G anode, SS cathode, 25 mA, 3 F.mol⁻¹. HFIP = 1,1,1,3,3,3-hexafluoroisopropanol; G =graphite; SS = stainless-steel.

6.7. Design of Experiments

Design of experiments was carried out using the IKA ElectraSyn 2.0 with the IKA Carousel attached. The factorial Design of Experiments (DoE) was created using Design-Expert 10 software; stir speed was characterised as a categorical variable while mediator equivalents and dipolarophile equivalents were characterised as continuous variables. The range of stir speeds was 200 - 600 rpm. The range of mediator equivalents was 0.5 - 2.5 equivalents (with respect to oxime). The range of dipolarophile equivalents was 1 - 9 equivalents (with respect to oxime). The positions (1 - 5) were chosen at random using a random number generator. The following procedure was used for all experiments:

To a 10 mL ElectraSyn 2.0 reaction vessel containing a stirrer bar, (*E*)-benzaldehyde oxime (0.5 mmol), *tert*-butyl acrylate (*c* eq.), Et₄NCl (*b* eq.) and HFIP (1.3 eq.) were added followed by MeCN (0.07 M). The reaction mixture was electrolysed under a constant current of 25 mA with graphite anode and stainless-steel cathode at the desired stir speed (*a* rpm) in the desired position (*d*), until a current of 3 F.mol⁻¹ had been passed. The solution was analysed by LCMS. After electrolysis, the reaction mixture was transferred to a round-bottomed flask, washing the electrodes with MeCN and acetone until washings ran clear, and concentrated *in vacuo* to give the crude mixture. The crude product was submitted to column chromatography on silica gel, eluting with 0 - 15% EtOAc/cyclohexane over 25 column volumes, to afford *tert*-butyl 3-phenyl-4,5-dihydroisoxazole-5-carboxylate **221a**. Data is consistent with synthesis of **221a** by **GP2**.

DoE – Experiment Run List:

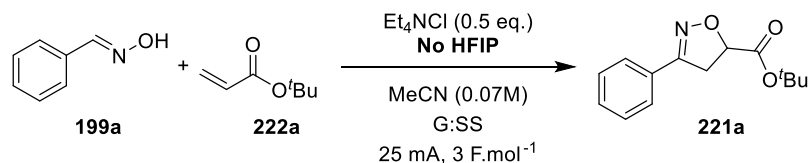


Entry	Run	Stir Speed (a)/rpm	Mediator (b)/eq.	Dipolarophile (c)/eq.	Position (d)	221a/%
1	1	200	0.5	1	2	60
2	1	200	0.5	9	5	69
3	1	200	2.5	1	1	40
4	1	200	2.5	9	3	66
5	2	400	0.5	1	2	59
6	2	400	0.5	9	5	75
7	2	400	1.5	5	2	69
8	2	400	1.5	5	3	57
9	3	400	1.5	5	1	58
10	3	400	1.5	5	5	68
11	3	400	2.5	1	1	54
12	3	400	2.5	9	3	63
13	4	600	0.5	1	4	61
14	4	600	0.5	9	1	66
15	4	600	2.5	9	5	62
16	4	600	2.5	1	3	53

Table 35: Conditions: Oxime (0.5 mmol), *tert*-butyl acrylate (*c* eq.), Et₄NCl (*b* eq.), HFIP (1.3 eq.), MeCN (0.07 M), G anode, SS cathode, position *d*, *a* rpm, 25 mA, 3 F.mol⁻¹; HFIP = 1,1,1,3,3,3-hexafluoroisopropanol; G = graphite; SS = stainless steel.

6.8. Control Experiments

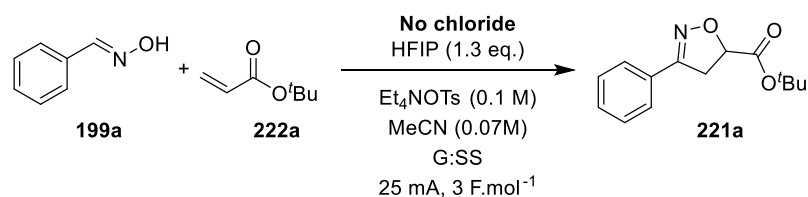
6.8.1. No HFIP Control



To a 10 mL ElectraSyn 2.0 reaction vessel containing a stirrer bar, (*E*)-benzaldehyde oxime **199a** (62 mg, 0.51 mmol), *tert*-butyl acrylate (366 μ L, 2.50 mmol) and Et₄NCl (42 mg, 0.26 mmol) were added followed by MeCN (7 mL). The reaction mixture was electrolysed under a constant current of 25 mA with G anode and SS cathode and stirring at 400 rpm, until a current of 3 F.mol⁻¹ had been passed. Following electrolysis, the reaction mixture was transferred to a round-bottomed flask, washing electrodes with MeCN and acetone until washings ran clear, and concentrated *in vacuo* to give the crude mixture. After standing overnight at ambient temperature, the crude mixture was submitted to column chromatography on silica gel (24 g, 0 - 15% EtOAc in cyclohexane over 25 CVs). Appropriate fractions were combined and concentrated *in vacuo* to afford *tert*-butyl 3-phenyl-4,5-dihydroisoxazole-5-carboxylate **221a** as a colourless oil (46 mg, 0.19 mmol, 36%).

221a: ¹H NMR (400 MHz, DMSO-*d*₆) δ ppm 7.65 - 7.74 (2H, m), 7.42 - 7.52 (3H, m), 5.12 (1H, dd, *J* = 11.7, 6.8 Hz), 3.74 (1H, dd, *J* = 17.4, 11.7 Hz), 3.54 (1H, dd, *J* = 17.4, 6.8 Hz), 1.45 (9H, s); ¹³C NMR (101 MHz, DMSO-*d*₆) δ ppm 169.0, 156.0, 130.3, 128.8, 128.5, 126.7, 81.7, 78.1, 38.4, 27.5; LCMS: *t*_R = 1.16 min, area% = 96%, [M+H]⁺ 248 (100). Data consistent with synthesis by **GP2**.

6.8.2. No Chloride Control

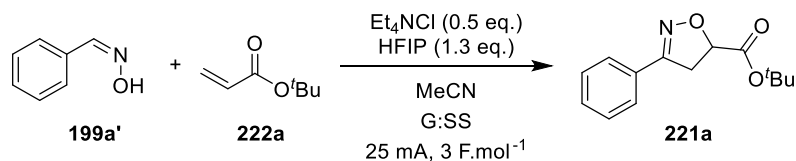


To a 10 mL ElectraSyn 2.0 reaction vessel containing a stirrer bar, (*E*)-benzaldehyde oxime **199a** (61 mg, 0.50 mmol), *tert*-butyl acrylate (366 μ L, 2.50 mmol), Et₄NOTs (213 mg, 0.71 mmol) and HFIP (70 μ L, 0.67 mmol) were added followed by MeCN (7 mL). The reaction mixture was electrolysed under a constant current of 25 mA with G anode and SS cathode stirring at 400 rpm, until a current of 3 F.mol⁻¹ had been passed. Following electrolysis, the reaction mixture was transferred to a round-bottomed flask, washing the electrodes with MeCN until washings ran clear, and concentrated *in vacuo* to give the crude mixture. After standing at ambient temperature overnight, the crude mixture was submitted to column chromatography on silica gel (24 g, 0 - 15% EtOAc in cyclohexane over 25 CVs). Appropriate fractions were combined and concentrated *in vacuo* to afford a mixture of *tert*-butyl 3-phenyl-4,5-dihydroisoxazole-5-carboxylate and *tert*-butyl 3-phenyl-4,5-dihydroisoxazole-4-carboxylate **221a** as a colourless oil (22:1, 30 mg, 0.12 mmol, 24%).

221a: ¹H NMR (400 MHz, DMSO-*d*₆) δ ppm 7.67 - 7.72 (2H, m), 7.43 - 7.50 (3H, m), 5.12 (1H, dd, *J* = 11.7, 6.9 Hz), 4.76 (dd, *J* = 11.0, 5.9 Hz, *minor regioisomer*), 4.65 (dd, *J* = 8.6, 5.9 Hz, *minor regioisomer*), 4.54 (dd, *J* = 11.0, 8.6 Hz, *minor regioisomer*), 3.74 (1H, dd, *J* = 17.4, 11.7 Hz), 3.54 (1H, dd, *J* = 17.4, 6.9 Hz), 1.45 (9H, s), 1.28 (s, *minor regioisomer*); LCMS: *t*_R = 1.15 min, area% = 89%, [M+H]⁺ 248 (100). Spectra recorded on mixture. Data consistent with synthesis by **GP2**.

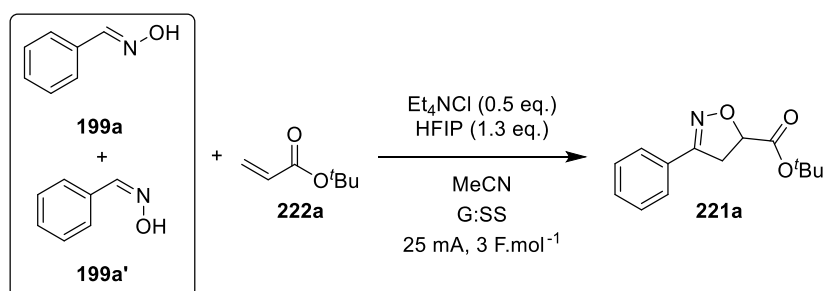
6.8.3. (Z)-Benzaldehyde oxime studies

6.8.3.1. 1 Equivalent (Z)-Benzaldehyde oxime



To a 10 mL ElectraSyn 2.0 reaction vessel containing a stirrer bar, (Z)-benzaldehyde oxime **199a'** (62 mg, 0.51 mmol), *tert*-butyl acrylate (366 μ L, 2.50 mmol), Et₄NCl (42 mg, 0.25 mmol) and HFIP (70 μ L, 0.67 mmol) were added followed by MeCN (7 mL). The reaction mixture was electrolysed under a constant current of 25 mA with G anode and SS cathode stirring at 400 rpm, until a current of 3 F.mol⁻¹ had been passed. After electrolysis, the reaction mixture was transferred to a round-bottomed flask, washing the electrodes with MeCN until washings ran clear, and concentrated *in vacuo* to give the crude mixture. The crude mixture submitted to column chromatography on silica gel (24 g, 0 - 15% EtOAc in cyclohexane over 25 CVs). Appropriate fractions were combined and concentrated *in vacuo* to afford a mixture of *tert*-butyl 3-phenyl-4,5-dihydroisoxazole-5-carboxylate and *tert*-butyl 3-phenyl-4,5-dihydroisoxazole-4-carboxylate **221a** as a colourless oil (19:1, 70 mg, 0.28 mmol, 55%).

221a: ¹H NMR (400 MHz, DMSO-*d*₆) δ ppm 7.67 - 7.72 (2H, m), 7.44 - 7.50 (3H, m), 5.12 (1H, dd, *J* = 11.7, 6.9 Hz), 4.76 (dd, *J* = 11.1, 5.9 Hz, *minor regioisomer*), 4.65 (dd, *J* = 8.6, 5.9 Hz, *minor regioisomer*), 4.54 (dd, *J* = 11.1, 8.6 Hz, *minor regioisomer*), 3.74 (1H, dd, *J* = 17.4, 11.7 Hz), 3.54 (1H, dd, *J* = 17.4, 6.9 Hz), 1.45 (9H, s), 1.28 (s, *minor regioisomer*); LCMS: *t*_R = 1.15 min, area% = 100%, [M+H]⁺ 248 (100). Spectra recorded on mixture. Data consistent with synthesis by **GP2**.

6.8.3.2. Equimolar (*E*)- and (*Z*)-benzaldehyde oxime

To a 10 mL ElectraSyn 2.0 reaction vessel containing a stirrer bar, (*E*)-benzaldehyde oxime (31 mg, 0.25 mmol), (*Z*)-benzaldehyde oxime (30 mg, 0.25 mmol), *tert*-butyl acrylate (366 μL , 2.50 mmol), HFIP (70 μL , 0.67 mmol) and Et_4NCl (42 mg, 0.25 mmol) were added followed by MeCN (7 mL). The reaction mixture was electrolysed under a constant current of 25 mA with G anode and SS cathode stirring at 400 rpm, until a current of 3 F.mol⁻¹ had been passed. After electrolysis, the reaction mixture was transferred to a round-bottomed flask, washing the electrodes with MeCN until washings ran clear, and concentrated *in vacuo* to give the crude mixture. The crude mixture and submitted to column chromatography on silica gel (24 g, 0 - 15% EtOAc in cyclohexane over 25 CVs). Appropriate fractions were combined and concentrated *in vacuo* to afford a mixture of *tert*-butyl 3-phenyl-4,5-dihydroisoxazole-5-carboxylate and *tert*-butyl 3-phenyl-4,5-dihydroisoxazole-4-carboxylate **221a** as a colourless oil (19:1, 83 mg, 0.34 mmol, 67%).

221a: ¹H NMR (400 MHz, DMSO-*d*₆) δ ppm 7.66 - 7.73 (2H, m), 7.43 - 7.50 (3H, m), 5.12 (1H, dd, $J = 11.7, 6.8$ Hz), 4.76 (dd, $J = 11.0, 5.9$ Hz, *minor regioisomer*), 4.65 (dd, $J = 8.6, 5.9$ Hz, *minor regioisomer*), 4.54 (dd, $J = 11.0, 8.6$ Hz, *minor regioisomer*), 3.74 (1H, dd, $J = 17.2, 11.7$ Hz), 3.54 (1H, dd, $J = 17.2, 6.8$ Hz), 1.45 (9H, s), 1.28 (s, *minor regioisomer*); LCMS: $t_{\text{R}} = 1.15$ min, area% = 99%, $[\text{M}+\text{H}]^+$ 248 (100). Spectra recorded on mixture. Data consistent with synthesis by **GP2**.

6.9. Flow Electrochemical Optimisation

6.9.1. General Procedure for Optimisation using Matrices

Flow optimisation was carried out in the Syrris FLUX electrochemical cell, using Syrris Asia syringe pumps with yellow syringes (100 μL /50 μL). Solutions for optimisation were prepared with (*E*)-benzaldehyde oxime, *tert*-butyl acrylate, HFIP (if applicable), Et_4NCl and MeCN (or MeOH, if applicable). The following solutions were prepared:

- R1 = (*E*)-benzaldehyde oxime (1 eq.), *tert*-butyl acrylate (5 eq.), HFIP (1.3 eq.), Et_4NCl (0.5 eq.), MeCN (0.07 M)
- S1 = (*E*)-benzaldehyde oxime (1 eq.), *tert*-butyl acrylate (5 eq.), HFIP (1.3 eq.), Et_4NCl (1 eq.), MeCN (0.07 M)
- S2 = (*E*)-benzaldehyde oxime (1 eq.), *tert*-butyl acrylate (5 eq.), HFIP (1.3 eq.), Et_4NCl (1.4 eq.), MeCN (0.07 M)
- S3 = (*E*)-benzaldehyde oxime (1 eq.), *tert*-butyl acrylate (2.5 eq.), HFIP (1.3 eq.), Et_4NCl (1 eq.), MeCN (0.07 M)
- S4 = (*E*)-benzaldehyde oxime (1 eq.), *tert*-butyl acrylate (1.25 eq.), HFIP (1.3 eq.), Et_4NCl (1 eq.), MeCN (0.07 M)
- S5 = (*E*)-benzaldehyde oxime (1 eq.), *tert*-butyl acrylate (2.5 eq.), Et_4NCl (1 eq.), MeCN (0.07 M)
- S6 = (*E*)-benzaldehyde oxime (1 eq.), *tert*-butyl acrylate (1.25 eq.), Et_4NCl (1 eq.), MeCN (0.07 M)
- S7 = (*E*)-benzaldehyde oxime (1 eq.), *tert*-butyl acrylate (2.5 eq.), Et_4NCl (1 eq.), MeOH (0.07 M)
- S8 = (*E*)-benzaldehyde oxime (1 eq.), *tert*-butyl acrylate (1.25 eq.), Et_4NCl (1 eq.), MeOH (0.07 M)
- S9 = (*E*)-benzaldehyde oxime (1 eq.), *tert*-butyl acrylate (5 eq.), Et_4NCl (1.2 eq.), MeCN (0.07 M)

A representative method is as follows and was used for all matrices shown below:

Solution R1 was flowed at $59 \mu\text{L}\cdot\text{min}^{-1}$ at 20 mA until steady state was reached, then 50 μL sample was collected. 30 μL was taken from the sample and 50 μL of standard solution (benzyl benzoate; 209.8 mg in 10 mL MeCN- d_3) was added and made up to 500 μL with further MeCN- d_3 ; this was submitted to ^1H NMR analysis. The remainder

of the 50 μL sample was diluted with 80 μL , and 100 μL was taken to be analysed by LCMS.

This procedure was repeated for the next flow rate and current until the desired conditions were completed.

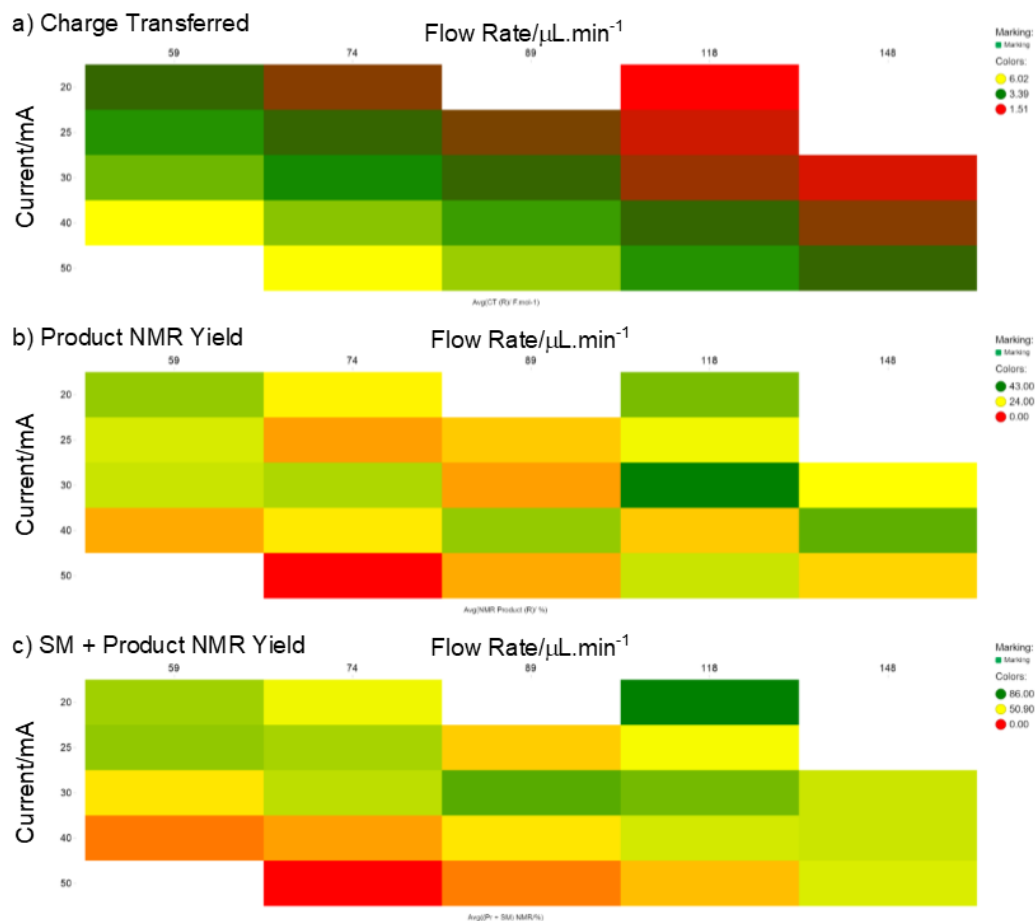


Figure S9: The initial results of the optimisation of the flow electrochemical procedure, using the batch conditions as a start point. Conditions: benzaldehyde oxime (1 eq.), *tert*-butyl acrylate (5 eq.), HFIP (1.3 eq.), Et_4NCl (0.5 eq.), MeCN (0.07 M), PVDF graphite anode, SS cathode, [flow rate], [current].

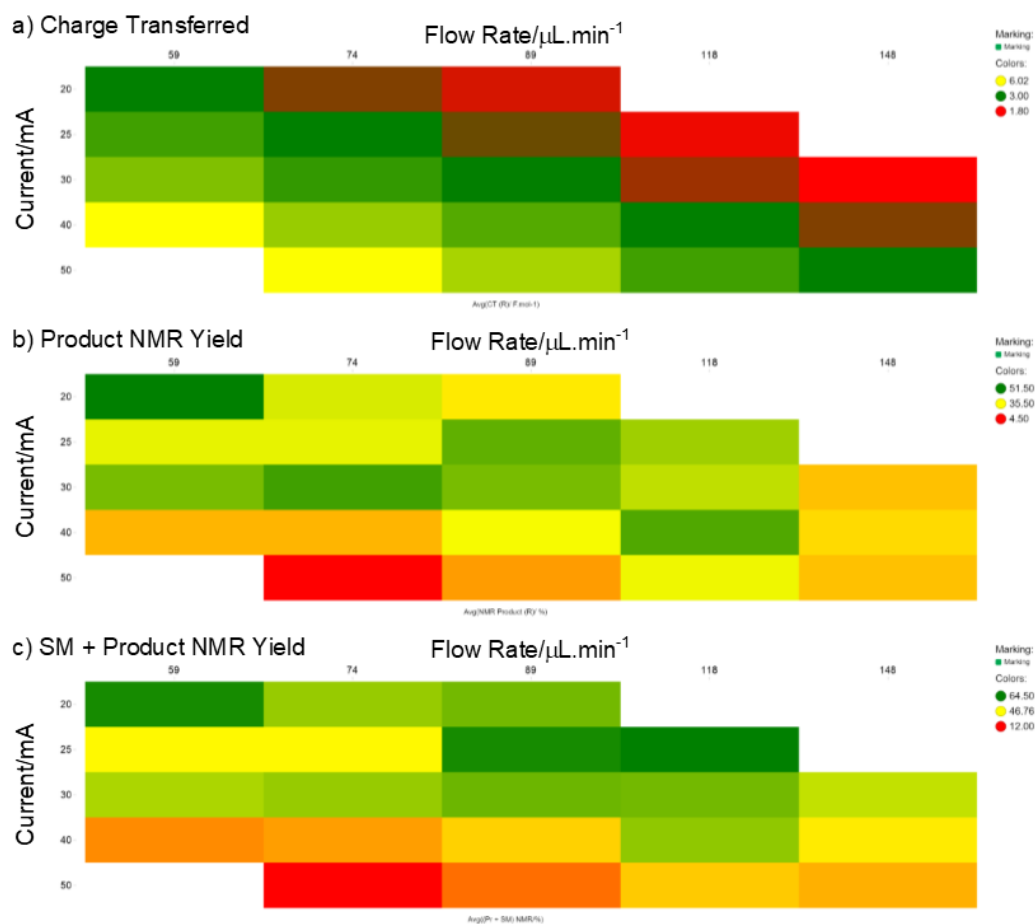


Figure S10: Exploration of higher loadings of mediator as part of the optimisation of the flow electrochemical procedure: Conditions: benzaldehyde oxime (1 eq.), *tert*-butyl acrylate (5 eq.), HFIP (1.3 eq.), Et₄NCl (1 eq.), MeCN (0.07 M), PVDF graphite anode, SS cathode, [flow rate], [current].

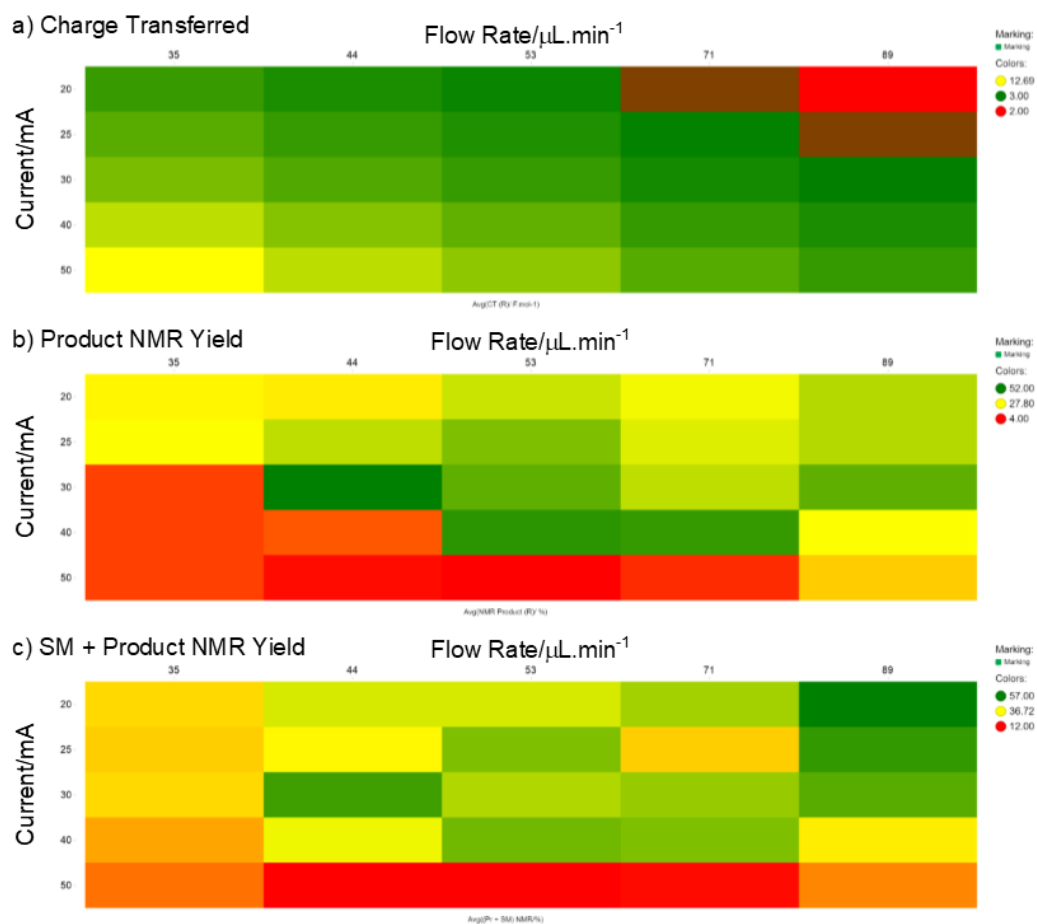


Figure S11: Exploration of slower flow rates and higher loadings of mediator as part of the optimisation of the flow electrochemical procedure: Conditions: benzaldehyde oxime (1 eq.), *tert*-butyl acrylate (5 eq.), HFIP (1.3 eq.), Et₄NCl (1.4 eq.), MeCN (0.07 M), PVDF graphite anode, SS cathode, [flow rate], [current].

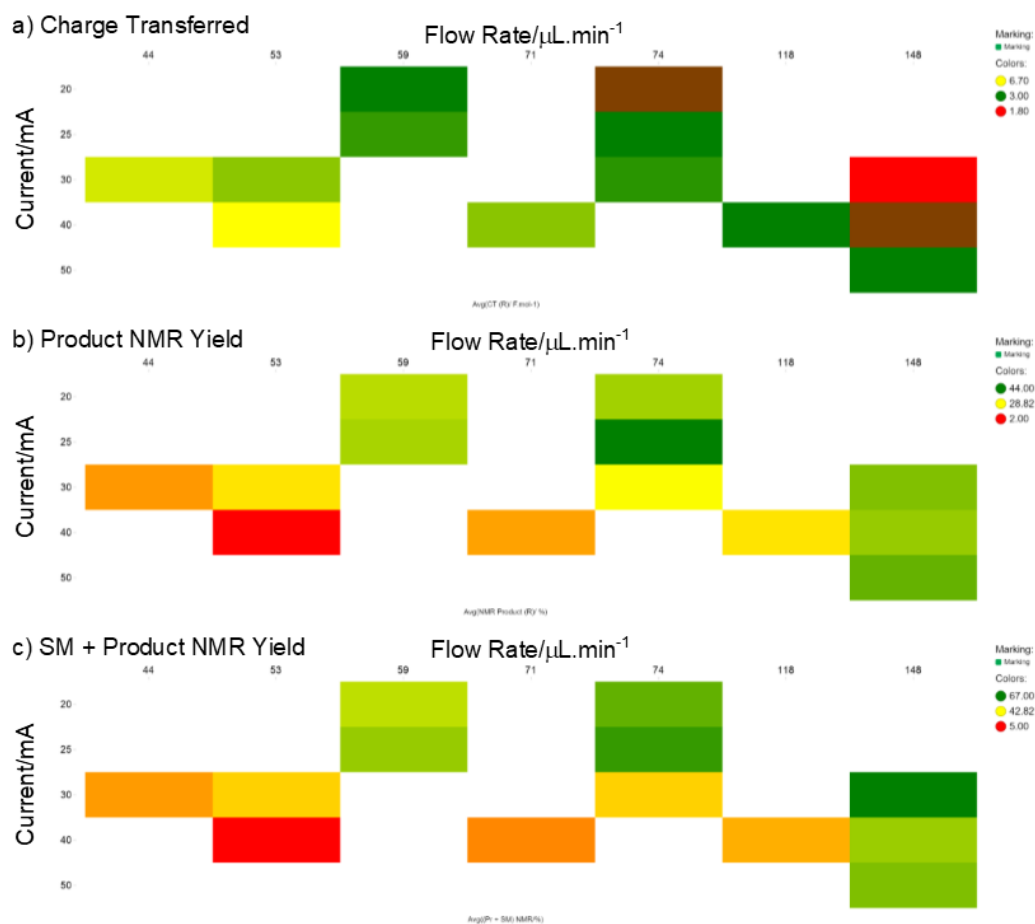


Figure S12: Exploration of PPS graphite anode and stainless-steel cathode electrode combination as part of the optimisation of the flow electrochemical procedure: Conditions: benzaldehyde oxime (1 eq.), *tert*-butyl acrylate (5 eq.), HFIP (1.3 eq.), Et₄NCl (1 eq.), MeCN (0.07 M), PPS graphite anode, SS cathode, [flow rate], [current].

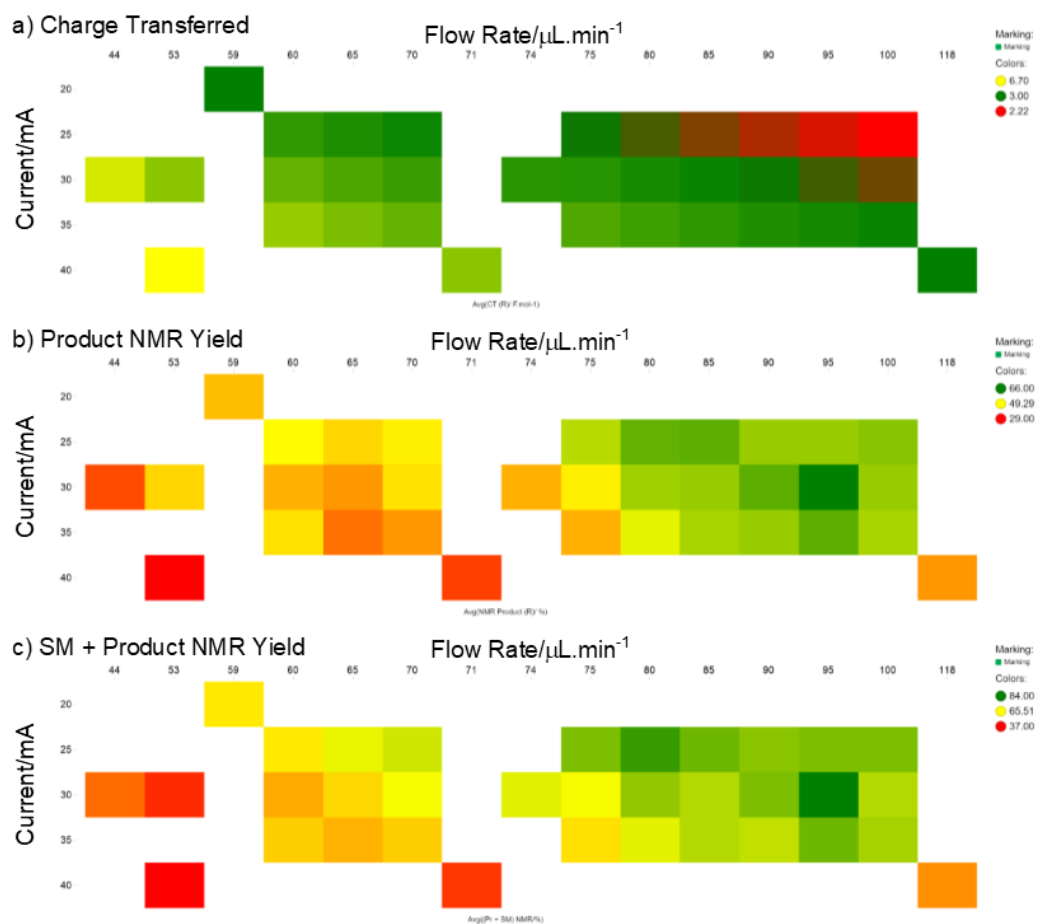
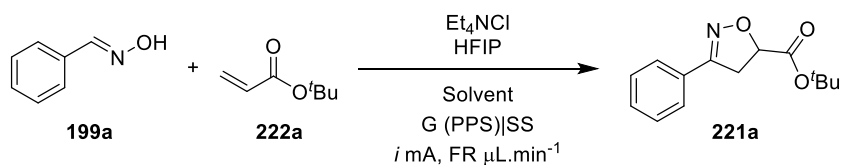


Figure S13: Exploration of PPS graphite anode and platinum cathode electrode combination as part of the optimisation of the flow electrochemical procedure: Conditions: benzaldehyde oxime (1 eq.), *tert*-butyl acrylate (5 eq.), HFIP (1.3 eq.), Et₄NCl (1 eq.), MeCN (0.07 M), PPS graphite anode, Pt cathode, [flow rate], [current].



Entry	222a eq.	Et ₄ NCl eq.	HFIP eq.	Solvent	<i>i</i> / mA	FR/ μL.min ⁻¹	221a/ % ^a	(199a+ 221a)/ % ^a
1 ^b	5	0.5	1.3	MeCN	30	59	28	46
2 ^c	5	1	1.3	MeCN	30	53	31	39
3 ^d	5	1.4	1.3	MeCN	30	53	43	43
4	2.5	1	1.3	MeCN	30	53	39	54
5	1.25	1	1.3	MeCN	30	53	24	40
6	2.5	1	0	MeCN	30	53	8	22
7	1.25	1	0	MeCN	30	53	5	17
8	2.5	1	0	MeOH	30	53	37	41
9	1.25	1	0	MeOH	30	53	26	30
10 ^e	5	1.2	1.3	MeCN	30	80	44	61

Table 36: Exploration of dipolarophile equivalents, mediator equivalents and solvent. ^a1H NMR yield using benzyl benzoate as external standard; ^bG (PVDF):SS electrode combination used; ^cG (PPS):Pt electrode combination used; ^dG (PVDF):SS electrode combination used; ^eG (PPS):Pt electrode combination used. G = graphite; PPS = polyphenylene sulfide; PVDF = poly(vinylidene fluoride); SS = stainless-steel; HFIP = 1,1,1,3,3,3-hexafluoroisopropanol; *i* = current; FR = flow rate.

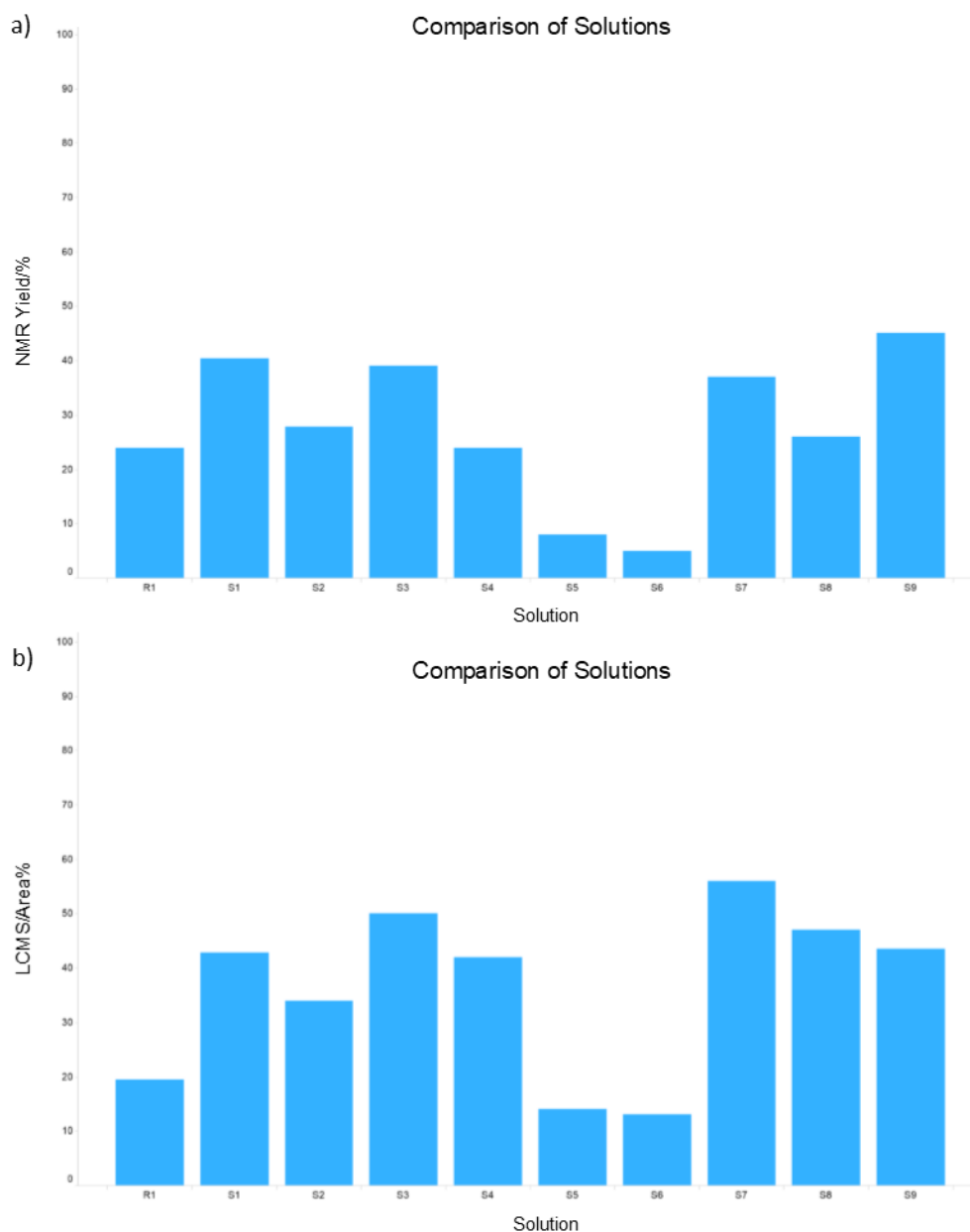


Figure S14: Exploration of dipolarophile equivalents, mediator equivalents and solvent. **Conditions:** All solutions were all flowed at $53 \text{ mL}\cdot\text{min}^{-1}$ at 30 mA, with 1 eq. benzaldehyde oxime. **R1** = *tert*-butyl acrylate (5 eq.), HFIP (1.3 eq.), Et_4NCl (0.5 eq.), MeCN (0.07 M); **S1** = *tert*-butyl acrylate (5 eq.), HFIP (1.3 eq.), Et_4NCl (1 eq.), MeCN (0.07 M); **S2** = *tert*-butyl acrylate (5 eq.), HFIP (1.3 eq.), Et_4NCl (1.4 eq.), MeCN (0.07 M); **S3** = *tert*-butyl acrylate (2.5 eq.), HFIP (1.3 eq.), Et_4NCl (1 eq.), MeCN (0.07 M); **S4** = *tert*-butyl acrylate (1.25 eq.), HFIP (1.3 eq.), Et_4NCl (1 eq.), MeCN (0.07 M); **S5** = *tert*-butyl acrylate (2.5 eq.), Et_4NCl (1 eq.), MeCN (0.07 M); **S6** = *tert*-butyl acrylate (1.25 eq.), Et_4NCl (1 eq.), MeCN (0.07 M); **S7** = *tert*-butyl acrylate (2.5 eq.), Et_4NCl (1 eq.), MeOH (0.07 M); **S8** = *tert*-butyl acrylate (1.25 eq.), Et_4NCl (1 eq.), MeOH (0.07 M); **S9** = *tert*-butyl acrylate (5 eq.), HFIP (1.3 eq.), Et_4NCl (1.2 eq.), MeCN (0.07 M).

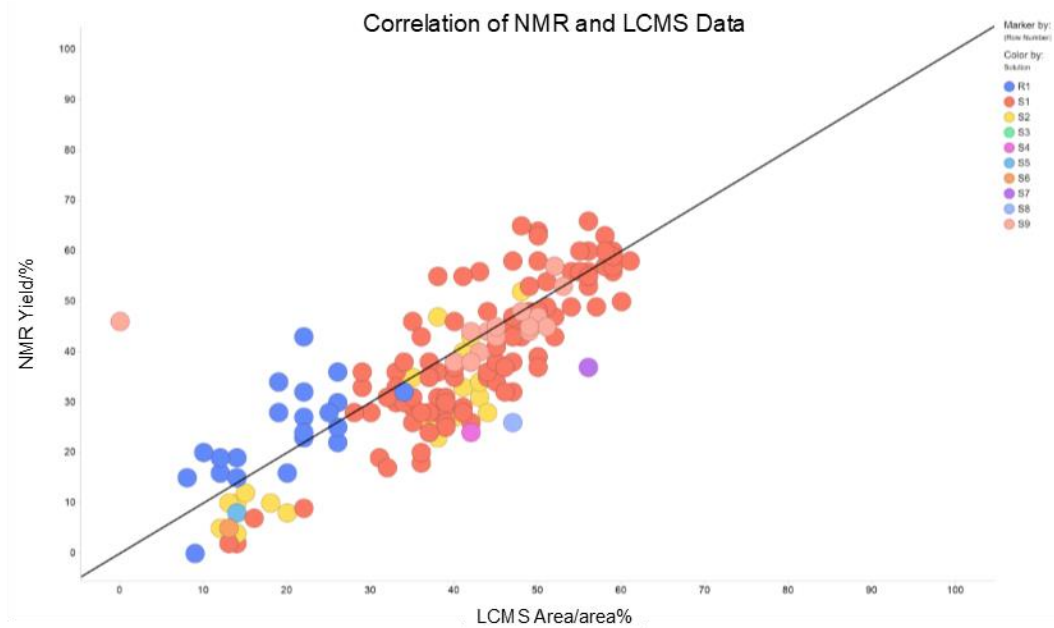
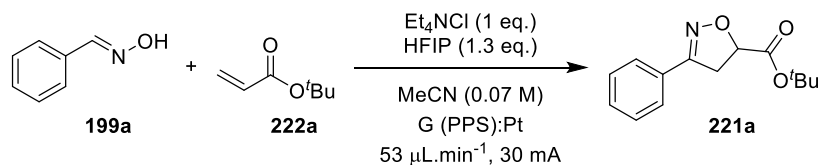


Figure S15: A graph illustrating the correlation between the LCMS and ¹

6.9.2. Isolation of Flow Experiments

Experiment 1:



A solution of (*E*)-benzaldehyde oxime **199a** (425 mg, 3.51 mmol), *tert*-butyl acrylate (2565 μL , 17.51 mmol), HFIP (490 μL , 4.65 mmol) and Et_4NCl (582 mg, 3.51 mmol) in MeCN (50 mL) was prepared. The solution was flowed at 53 $\mu\text{L}\cdot\text{min}^{-1}$ at a current of 30 mA until 7 mL (0.5 mmol, 132 minutes) was collected.

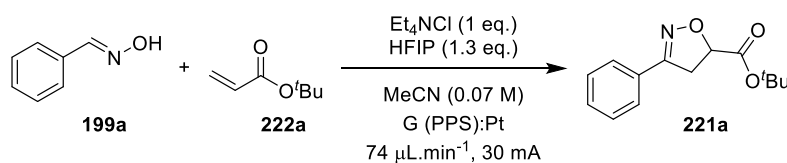
50 μL samples were collected every 20 mins. 30 μL was added to a 50 μL sample of standard solution (benzyl benzoate, 0.1 M MeCN- d_3) and made up to 500 μL with MeCN- d_3 and analysed by ^1H NMR. The remainder of the sample was diluted with 80 μL of MeCN and submitted to LCMS analysis.

Once 7 mL had been collected, the solution was blown down under N_2 at 40 $^\circ\text{C}$ to give the crude mixture.

After standing over the weekend at ambient temperature, the crude mixture was dissolved in DCM (2.5 mL) and submitted to column chromatography on silica gel (24 g, 0 - 15% EtOAc in cyclohexane over 20 CVs). Appropriate fractions were combined and concentrated *in vacuo* to afford *tert*-butyl 3-phenyl-4,5-dihydroisoxazole-5-carboxylate and *tert*-butyl 3-phenyl-4,5-dihydroisoxazole-4-carboxylate **221a** as a colourless oil (13:1, 36 mg, 25% - 85% purity).

221a: ^1H NMR (400 MHz, DMSO- d_6) δ ppm 7.66 - 7.73 (2H, m), 7.44 - 7.50 (3H, m), 5.12 (1H, dd, $J = 11.7, 6.8$ Hz), 4.76 (dd, $J = 11.1, 5.7$ Hz, *minor regioisomer*), 4.65 (dd, $J = 8.6, 5.8$ Hz, *minor regioisomer*), 4.54 (dd, $J = 11.1, 8.6$ Hz, *minor regioisomer*), 3.74 (1H, dd, $J = 17.4, 11.7$ Hz), 3.54 (1H, dd, $J = 17.4, 6.8$ Hz), 1.45 (9H, s), 1.28 (s, *minor regioisomer*); LCMS: $t_{\text{R}} = 1.16$ min, area% = 85%, $[\text{M}+\text{H}]^+$ 248 (100). Spectra recorded on mixture. Data consistent with synthesis by **GP2**.

Experiment 2:



A solution of (*E*)-benzaldehyde oxime **199a** (425 mg, 3.51 mmol), *tert*-butyl acrylate (2565 μL , 17.51 mmol), HFIP (490 μL , 4.65 mmol) and Et_4NCl (582 mg, 3.51 mmol) in MeCN (50 mL) was prepared. The solution was flowed at $74 \mu\text{L}\cdot\text{min}^{-1}$ at a current of 30 mA until 7 mL (0.5 mmol, 94 minutes) was collected.

50 μL samples were collected every 20 mins. 30 μL was added to a 50 μL sample of standard solution (benzyl benzoate, 0.1 M MeCN- d_3) and made up to 500 μL with MeCN- d_3 and analysed by ^1H NMR. The remainder of the sample was diluted with 80 μL of MeCN and submitted to LCMS analysis.

Once 7 mL had been collected, the solution was blown down under N_2 at 40°C to give the crude mixture.

After standing over the weekend at ambient temperature, the crude mixture was dissolved in DCM (2.5 mL) and submitted to column chromatography on silica gel (24 g, 0 - 15% EtOAc in cyclohexane over 20 CVs). Appropriate fractions were combined and concentrated *in vacuo* to afford *tert*-butyl 3-phenyl-4,5-dihydroisoxazole-5-carboxylate and *tert*-butyl 3-phenyl-4,5-dihydroisoxazole-4-carboxylate **221a** as a colourless oil (13:1, 72 mg, 49% - 85% purity).

221a: ^1H NMR (400 MHz, DMSO- d_6) δ ppm 7.67 - 7.73 (2H, m), 7.44 - 7.50 (3H, m), 5.12 (1H, dd, $J = 11.7, 7.0$ Hz), 4.76 (dd, $J = 11.0, 5.9$ Hz, *minor regioisomer*), 4.65 (dd, $J = 8.8, 5.9$ Hz, *minor regioisomer*), 4.54 (dd, $J = 11.0, 8.8$ Hz, *minor regioisomer*), 3.74 (1H, dd, $J = 17.4, 11.7$ Hz), 3.54 (1H, dd, $J = 17.4, 7.0$ Hz), 1.45 (9H, s), 1.28 (s, *minor regioisomer*); LCMS: $t_{\text{R}} = 1.16$ min, area% = 85%, $[\text{M}+\text{H}]^+ 248$ (100). Spectra recorded on mixture. Data consistent with synthesis by **GP2**.

The ^1H NMR data collected from the samples of both isolation flow experiments were plotted on a graph and showed that the faster flow rate ($74 \mu\text{L}\cdot\text{min}^{-1}$) provided a more consistent reaction profile (**Figure S16**).

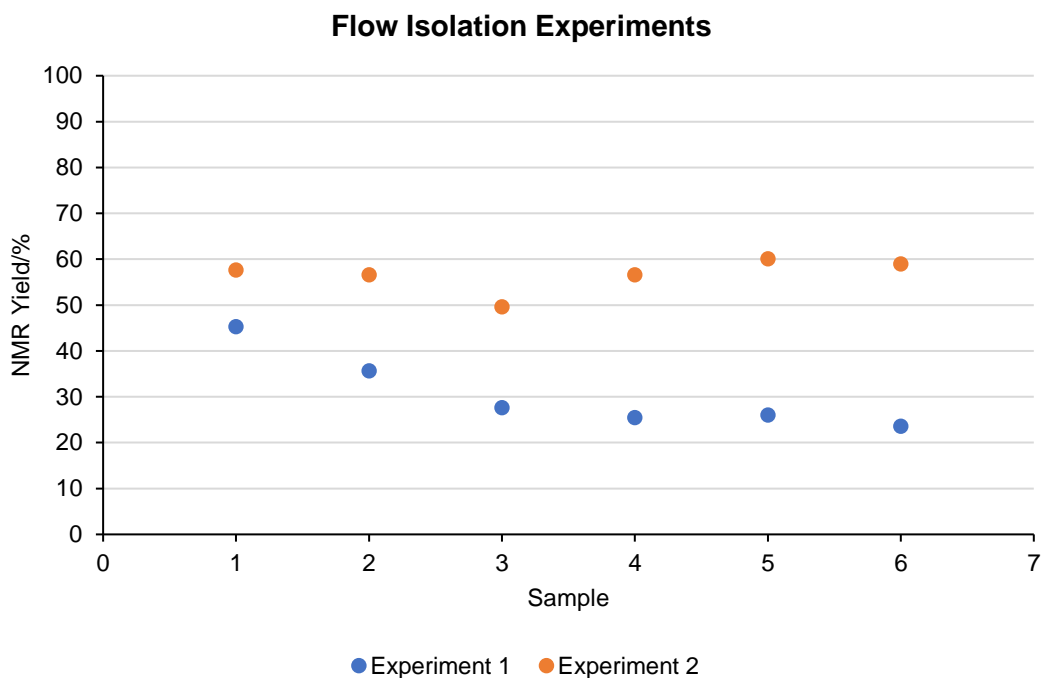
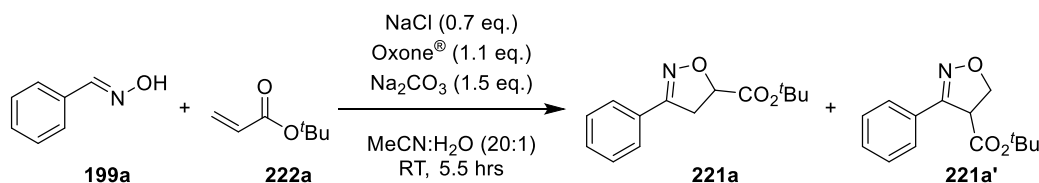


Figure S16: Flow isolation experiments to explore the superiority of platinum as the cathodic material. **Experiment 1 Conditions:** **199a** (1 eq.), **222a** (5 eq.), HFIP (1.3 eq.), Et_4NCl (1 eq.), G PPS anode, Pt cathode, $53 \text{ mL}\cdot\text{min}^{-1}$, 30 mA, 132 minutes flow time (7 mL final volume); **Experiment 2 Conditions:** **199a** (1 eq.), **222a** (5 eq.), HFIP (1.3 eq.), Et_4NCl (1 eq.), G PPS anode, Pt cathode, $74 \text{ mL}\cdot\text{min}^{-1}$, 30 mA, 95 minutes flow time (7 mL final volume).

6.10. ReactIR Experiments

6.10.1. Monitoring of Chemical Reaction



To a 25 mL multi-necked flask containing a stirrer bar, (*E*)-benzaldehyde oxime **199a** (341 mg, 2.81 mmol), *tert*-butyl acrylate (533 μ L, 3.64 mmol), NaCl (116 mg, 1.99 mmol) and Na₂CO₃ (445 mg, 4.20 mmol) were added, followed by water (550 μ L) and MeCN (11 mL). The ReactIR probe was placed into the reaction through the centre neck, ensuring the end of the probe was fully submerged and upright. IR spectra were recorded every 2 minutes from when the probe was in position.

The reaction mixture was allowed to stir for 5 mins and then Oxone[®] (1910 mg, 3.11 mmol) was added, after which IR spectra recording every 2 minutes was continued. The reaction mixture was allowed to continue to stir at ambient temperature.

After stirring for 5.5 hrs, the ReactIR probe was removed from the flask and the reaction mixture was quenched with aqueous 5% sodium metabisulfite (25 mL), diluted with water (20 mL) and extracted with EtOAc (3 x 25 mL). The combined organic layers were washed with brine (30 mL), dried (hydrophobic frit) and concentrated *in vacuo* to give the crude mixture. After standing for two days at ambient temperature, the crude mixture was submitted to column chromatography on silica gel (dry loaded from DCM, 40 g, 0 - 15% EtOAc in cyclohexane over 25 CVs). Appropriate fractions were combined and concentrated *in vacuo* to afford a mixture of *tert*-butyl 3-phenyl-4,5-dihydroisoxazole-5-carboxylate and *tert*-butyl 3-phenyl-4,5-dihydroisoxazole-4-carboxylate **221a** as a pale-yellow oil (430 mg, 1.74 mmol, 62%).

221a: ¹H NMR (400 MHz, DMSO-*d*₆) δ ppm 7.66 - 7.73 (2H, m), 7.43 - 7.51 (3H, m), 5.12 (1H, dd, *J* = 11.7, 6.8 Hz), 4.76 (dd, *J* = 11.0, 5.8 Hz, *minor regioisomer*), 4.65 (dd, *J* = 8.6, 5.8 Hz, *minor regioisomer*), 4.54 (dd, *J* = 11.0, 8.6 Hz, *minor regioisomer*), 3.74 (1H, dd, *J* = 17.4, 11.7 Hz), 3.54 (1H, dd, *J* = 17.4, 6.8 Hz), 1.45 (9H, s), 1.28 (s, *minor regioisomer*); LCMS: *t*_R = 1.16 min, area% = 100%, [M+H]⁺ 248 (100). Spectra recorded on mixture. Data consistent with synthesis by **GP2**.

All IR data was manipulated in the Mettler Toledo iC IR 7.0 software supplied with the ReactIR equipment before being exported to Microsoft Excel to create the desired graph, on which the LCMS sample data was co-plotted.

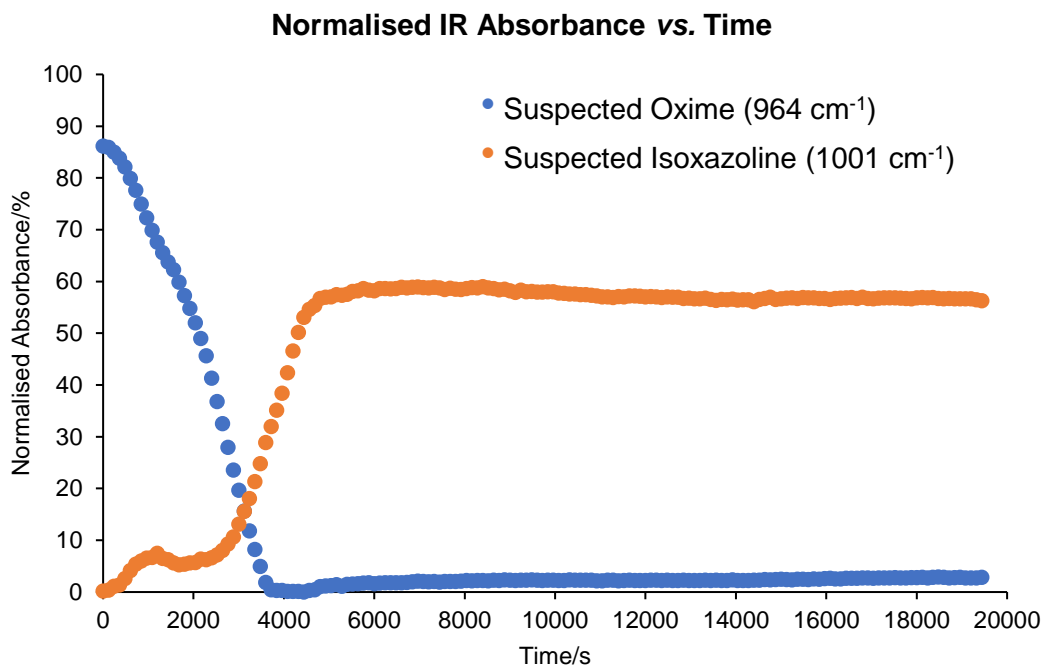
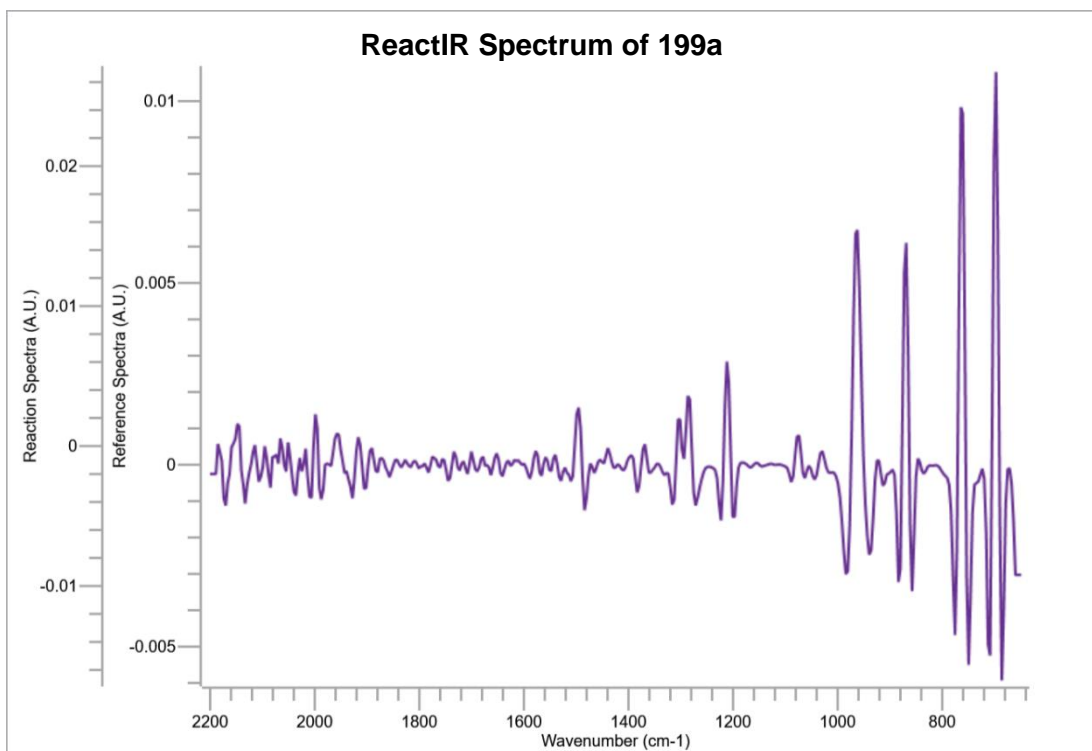
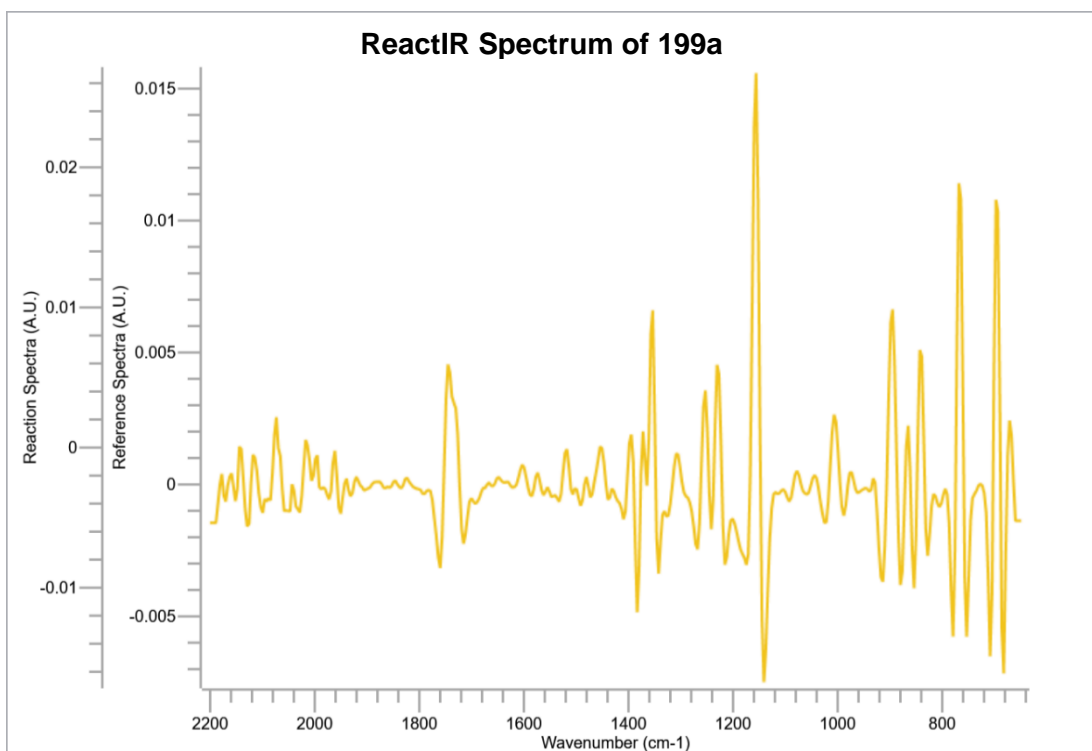


Figure S17: ReactIR spectrum of the non-electrochemical 1,3-dipolar cycloaddition reaction to form substituted isoxazoline **221a**.



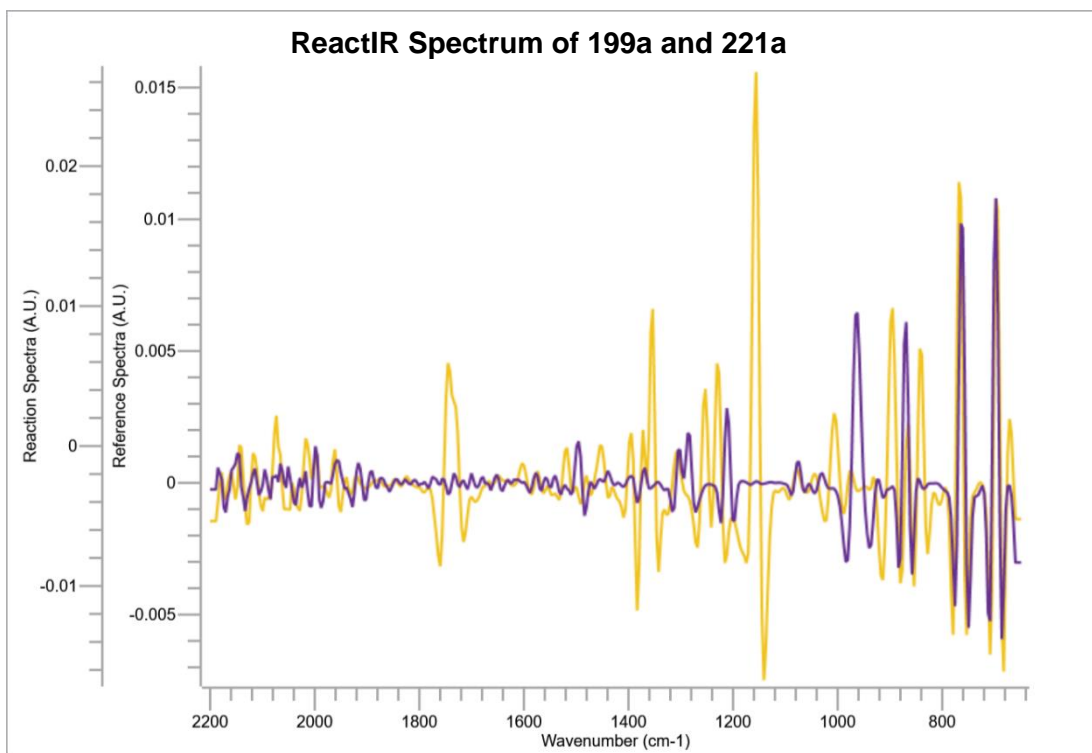
METTLER TOLEDO

Figure S18: The reference IR spectrum of the starting aldoxime **199a** used for the ReactIR experiments. Probing the non-electrochemical reaction.



METTLER TOLEDO

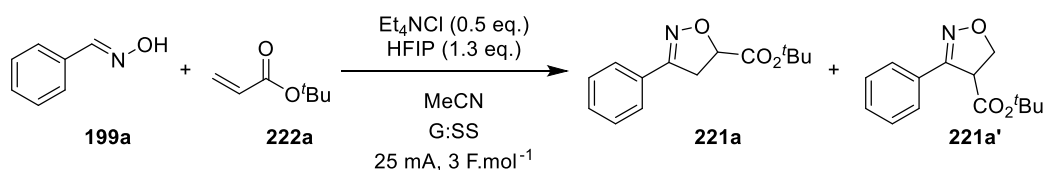
Figure S19: The reference IR spectrum of the desired product isoxazoline **221a** used for ReactIR experiments probing the electrochemical reaction.



METTLER TOLEDO

Figure S20: Reference IR spectra for **199a** and **221a** overlaid to determine distinct peaks to follow during ReactIR experiments probing the electrochemical reaction.

6.10.2. Monitoring of Electrochemical Reaction



To a 50 mL beaker, (*E*)-benzaldehyde oxime **199a** (341 mg, 2.81 mmol), *tert*-butyl acrylate (2051 μL , 14.00 mmol), HFIP (383 μL , 3.64 mmol) and Et_4NCl (234 mg, 1.41 mmol) were added, followed by MeCN (40 mL). The reaction mixture was electrolysed, open to air (with cotton wool to stop evaporation), under a constant current of 25 mA with G anode and SS cathode stirring at 600 rpm, until a current of 3 F.mol⁻¹ had been passed. IR spectra collection was initiated just prior to start of electrolysis to ensure that entire reaction was captured. IR spectra were collected every 15 secs for the first 30 mins, then every 30 secs for 30 mins, then every 60 secs for 1 hour, and every 2 mins for the remainder of the reaction.

Following electrolysis and standing overnight, the probe was removed, and the reaction mixture was transferred to a round-bottomed flask, washing the electrodes with MeCN until washings ran clear, and concentrated *in vacuo* to give the crude mixture. The crude mixture was submitted to column chromatography on silica gel (dry loaded from DCM, 40 g, 0 - 15% EtOAc in cyclohexane over 25 CVs). Appropriate fractions were combined and concentrated *in vacuo* to afford *tert*-butyl 3-phenyl-4,5-dihydroisoxazole-5-carboxylate and *tert*-butyl 3-phenyl-4,5-dihydroisoxazole-4-carboxylate **221a** as a colourless oil (390 mg, 1.58 mmol, 56%).

221a: ¹H NMR (400 MHz, DMSO-*d*₆) δ ppm 7.68 (2H, s), 7.42 - 7.51 (3H, m), 5.12 (1H, dd, $J = 11.9, 7.0$ Hz), 4.76 (dd, $J = 11.0, 5.7$ Hz, *minor regioisomer*), 4.65 (dd, $J = 8.6, 5.7$ Hz, *minor regioisomer*), 4.54 (dd, $J = 11.0, 8.6$ Hz, *minor regioisomer*), 3.74 (1H, dd, $J = 17.4, 11.9$ Hz), 3.54 (1H, dd, $J = 17.4, 7.0$ Hz), 1.45 (9H, s), 1.28 (s, *minor regioisomer*); LCMS: $t_{\text{R}} = 1.16$ min, area% = 99%, $[\text{M}+\text{H}]^+$ 248 (100). Spectra recorded on mixture. Data consistent with synthesis by **GP2**.

All IR data was manipulated in the Mettler Toledo iC IR 7.0 software supplied with the ReactIR equipment before being exported to Microsoft Excel to create the desired graph, on which the LCMS sample data was co-plotted.

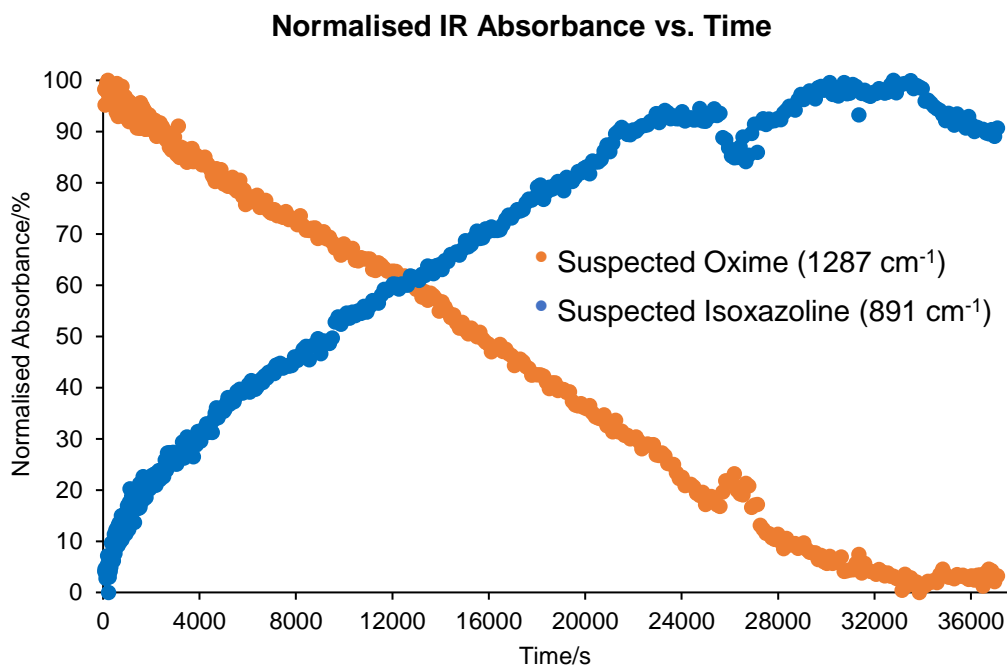
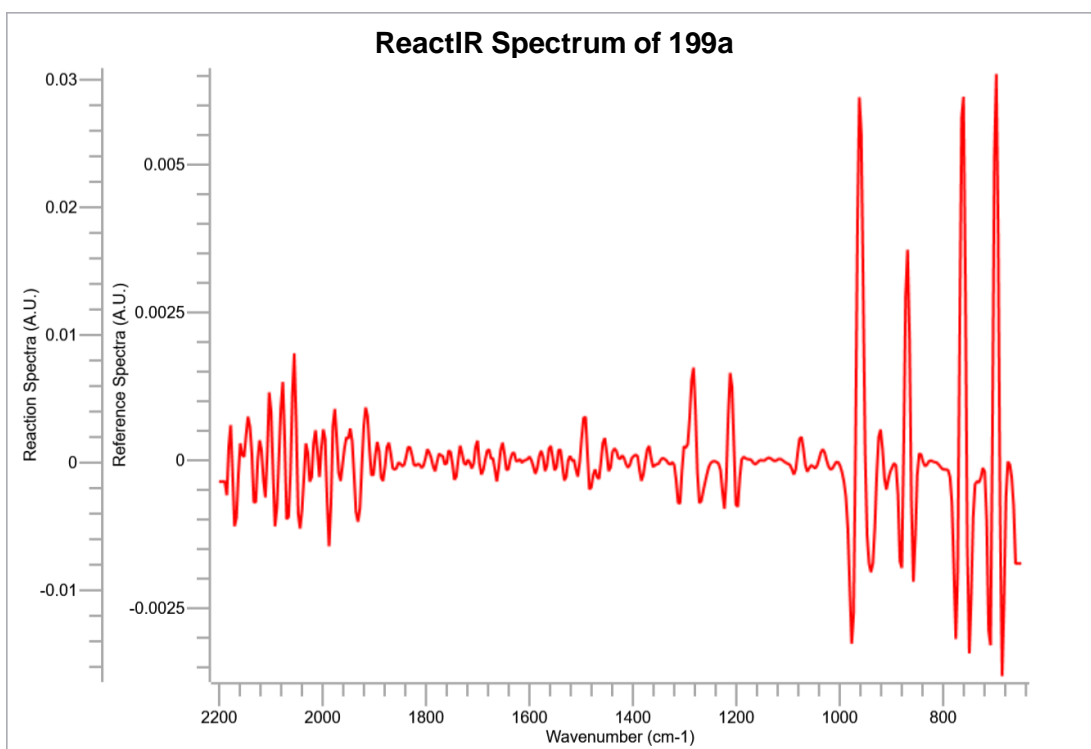
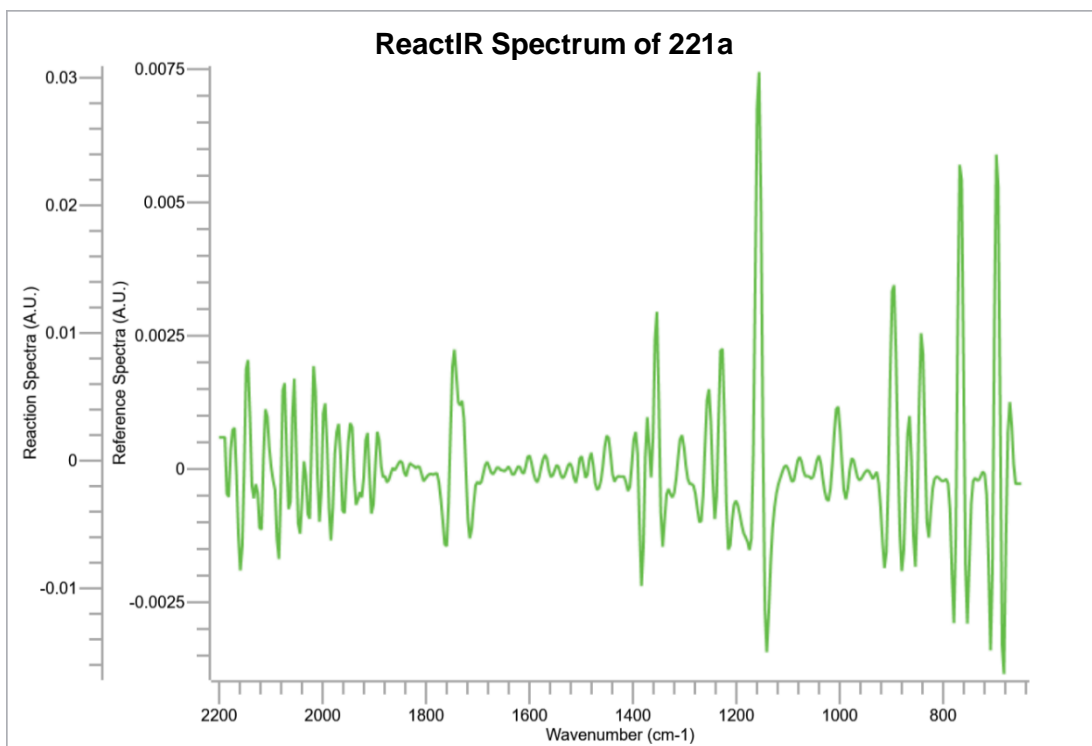


Figure S21: ReactIR spectrum of the electrochemically enabled 1,3-dipolar cycloaddition reaction to form substituted isoxazoline **221a**.



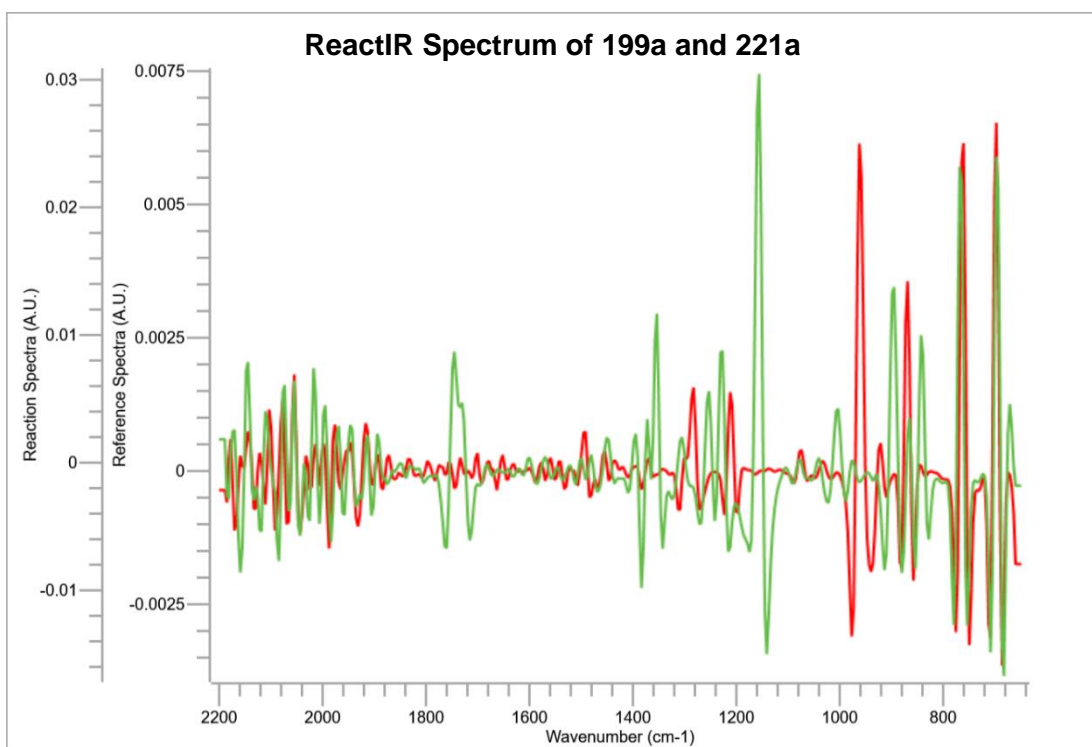
METTLER TOLEDO

Figure S22: The reference IR spectrum of the starting aldoxime **199a** used for the ReactIR experiments. Probing the electrochemical reaction.



METTLER TOLEDO

Figure S23: The reference IR spectrum of the desired product isoxazoline **221a** used for ReactIR experiments probing the electrochemical reaction.

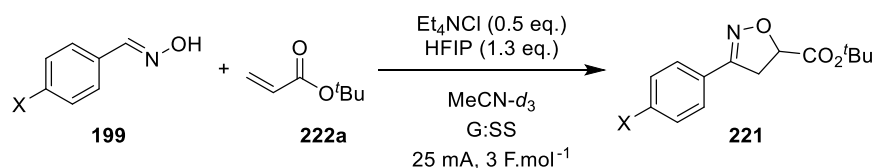


METTLER TOLEDO

Figure S24: Reference IR spectra for **199a** and **221a** overlaid to determine distinct peaks to follow during ReactIR experiments probing the electrochemical reaction.

6.11. Hammett Analysis

6.11.1. Maximum Rate Kinetic Analysis:



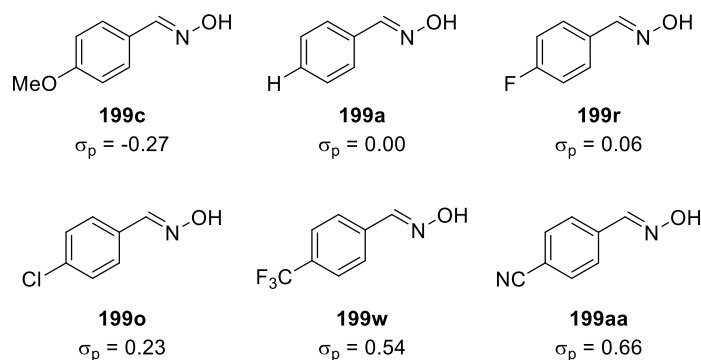
The maximum rate kinetic studies were performed following the reaction by ¹H NMR analysis using benzyl benzoate as external standard.

A general procedure for the NMR experiments is as follows:

To a 10 mL ElectraSyn 2.0 reaction vessel containing a stirrer bar, oxime (0.5 mmol), *tert*-butyl acrylate (5 eq.), HFIP (1.3 eq.) and Et_4NCl (0.5 eq.) were added followed by $\text{MeCN-}d_3$ (7 mL). The reaction mixture was electrolysed under a constant current of 25 mA with G anode and SS cathode stirring at 400 rpm, until a current of 3 F.mol⁻¹ had been passed.

The reaction was followed by ¹H NMR, taking samples at the following intervals: 0, 0.5, 1, 1.5, 2, 2.5, 3, 3.5, 4, 4.5, 5, 6, 7, 8, 9, 10, 15, 20, 25, 30, 35, 40, 45, 60 min. NMR samples were made from 30 μL of reaction mixture, 50 μL of NMR standard solution (benzyl benzoate, 0.1 M solution), and 420 μL of $\text{MeCN-}d_3$. NMR analysis was performed on a Bruker 700 MHz spectrometer with a $D1 = 2$ s. Every experiment was performed at least twice, and the graphs shown are an average of the two experiments. Initial rates were calculated by fitting a straight-line to the first 300 s (5 mins) of the reaction profile (or first zero value that had a subsequent non-zero value). Well-mixed rate refers to the rate of reaction for after 300 s (or 5 mins).

The following substrates were used for rate kinetic analysis:



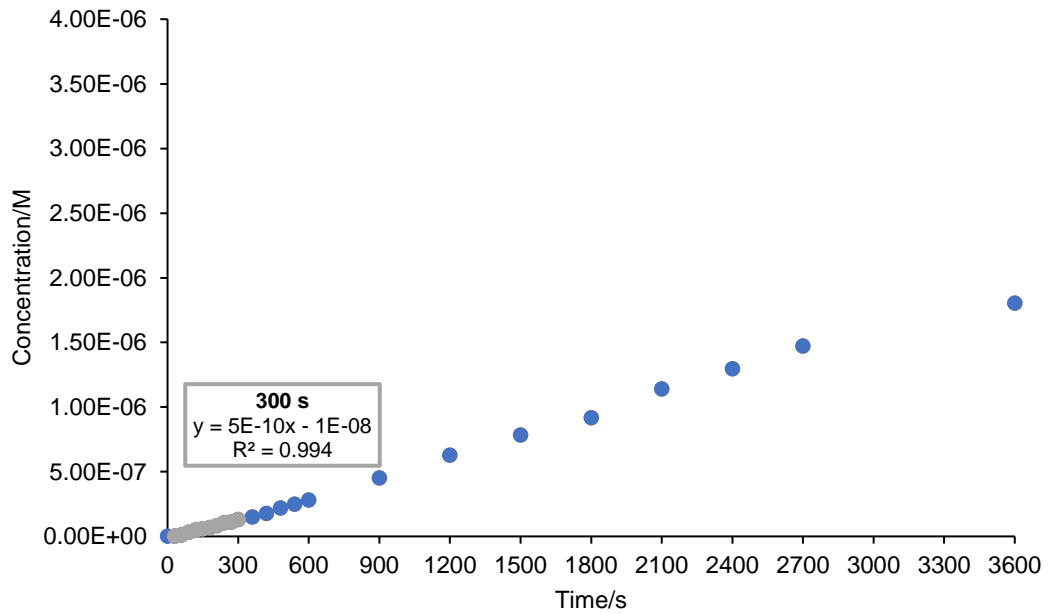
Points for analysis were chosen as the first zero value which had two subsequent non-zero points and then out to 300 s. The σ_p values were acquired from the review by Hansch and co-workers.¹⁰¹

The concentrations shown in each of the graphs is the concentration of material in the NMR sample and not the concentration of the reaction itself; no attempt has been made to scale the concentration in the NMR sample to the reaction concentration.

Mass and millimolar quantities of each substrate are shown in parentheses above each plot, with each experiment used in the average calculation separated by a semi-colon.

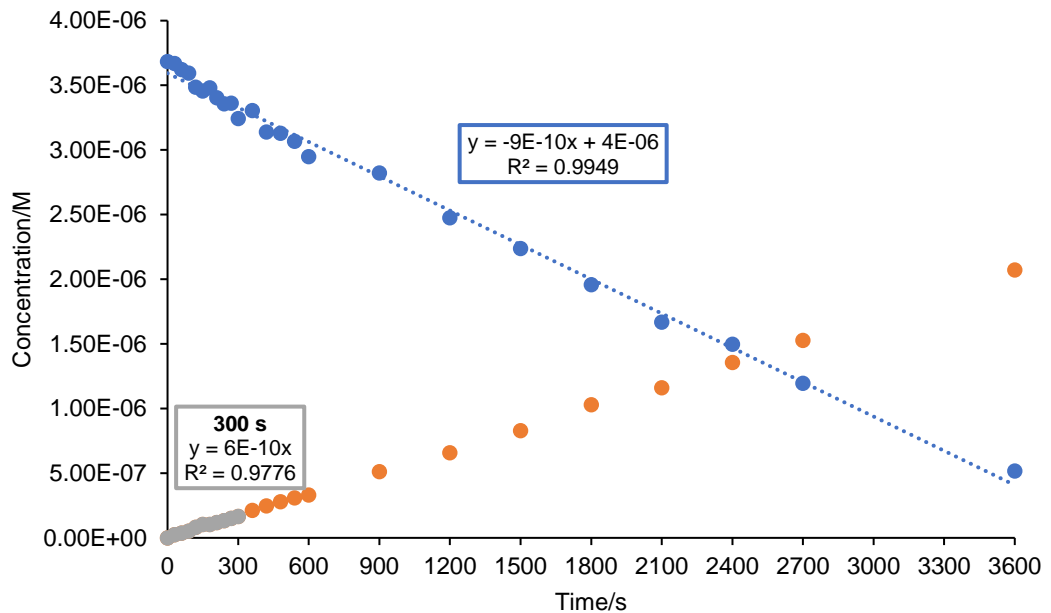
199c, X = OMe (76 mg/0.50 mmol; 77 mg/0.51 mmol) - $k_{obs} = 5 \times 10^{-10} \text{ M.s}^{-1}$

199c (X = OMe) - Concentration (Avg.)

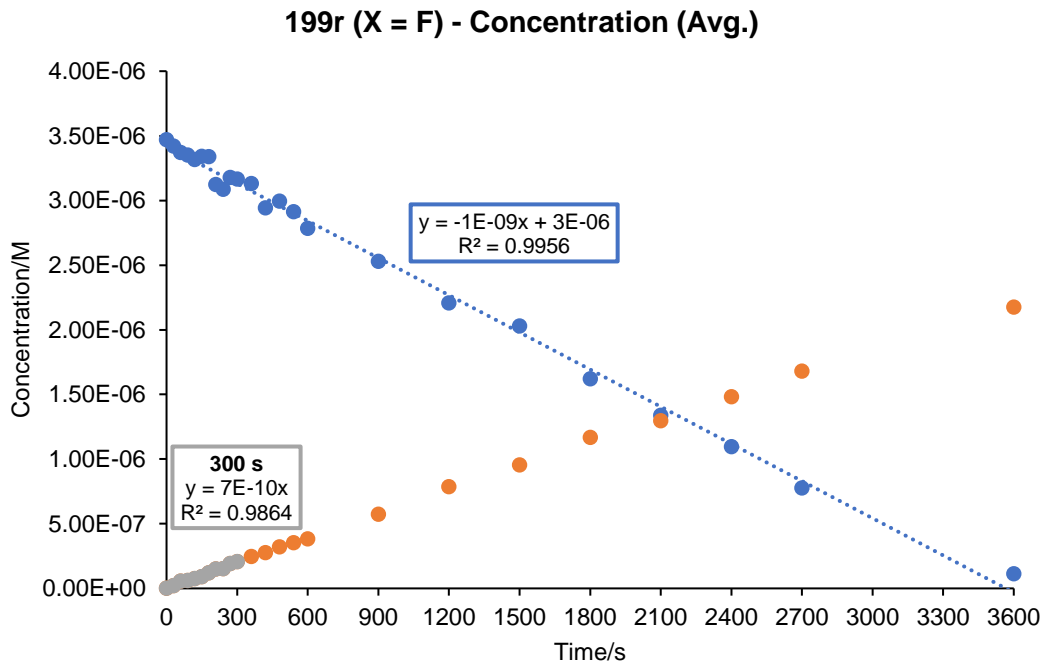


199a, X = H (61 mg/0.51 mmol; 61 mg/0.50 mmol) - $k_{obs} = 6 \times 10^{-10} \text{ M.s}^{-1}$

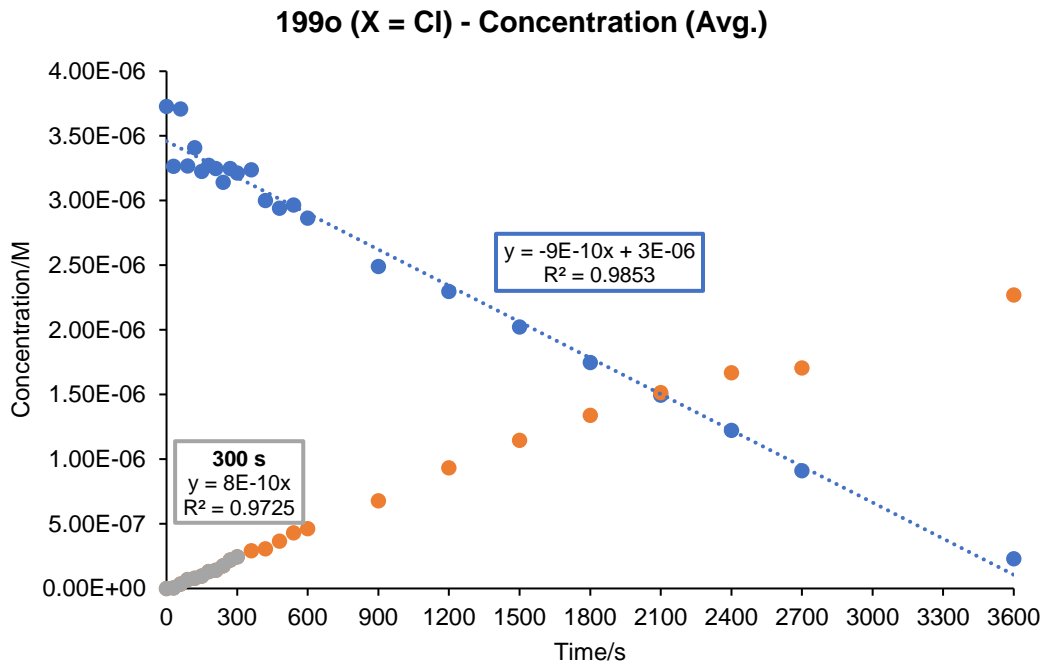
199a (X = H) - Concentration (Avg.)



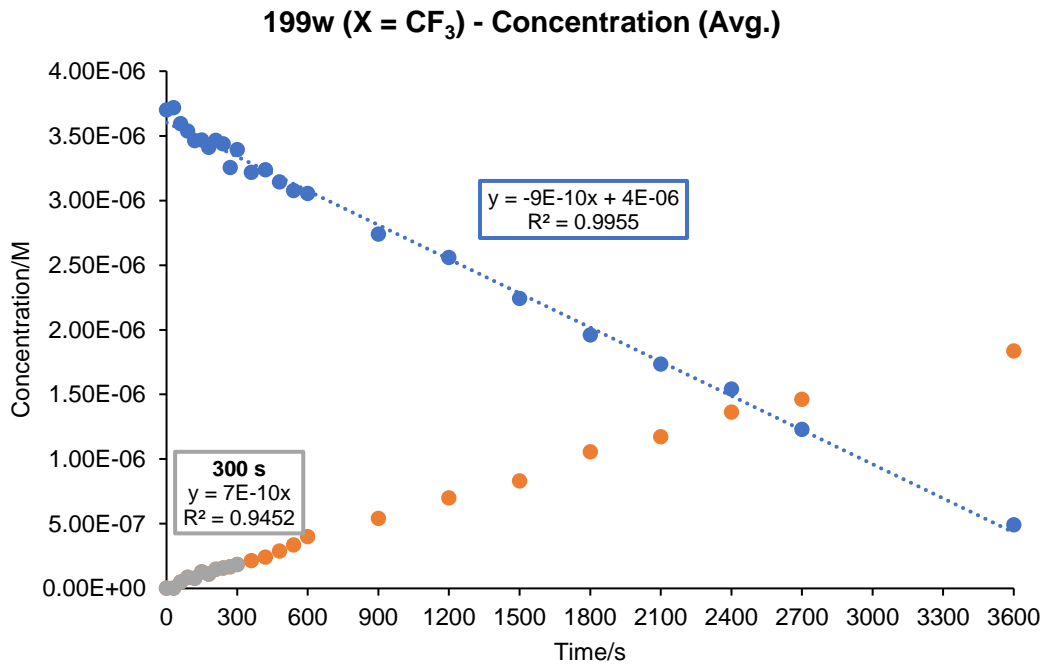
199r, X = F (70 mg/0.50 mmol; 70 mg/0.50 mmol - $k_{obs} = 7 \times 10^{-10} \text{ M.s}^{-1}$)



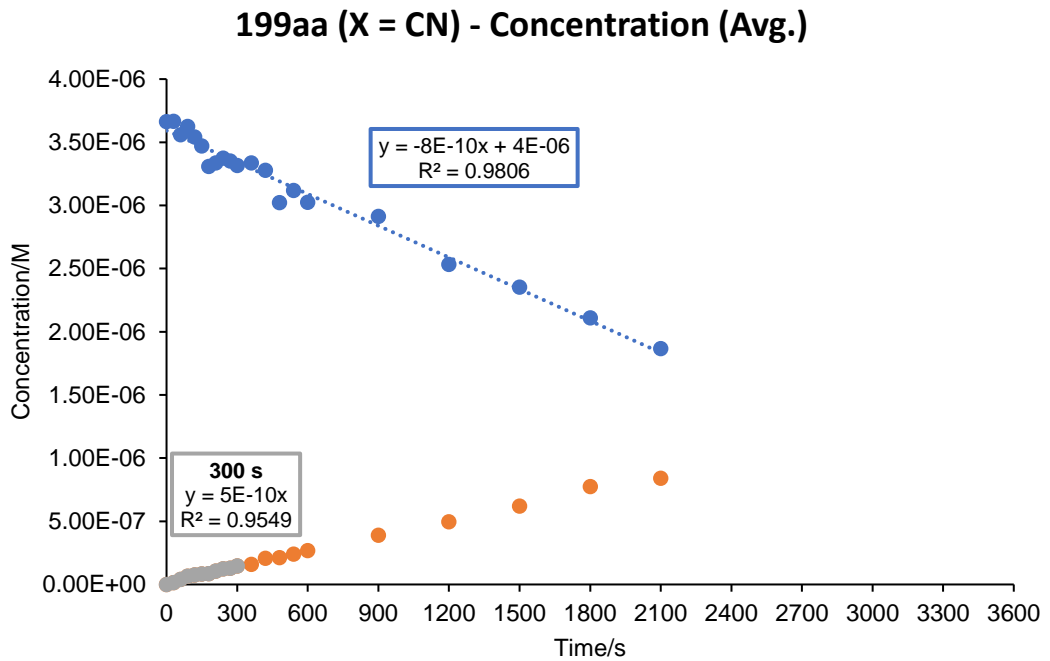
199o, X = Cl (79 mg/0.51 mmol; 78 mg/0.50 mmol; 79 mg/ 0.51 mmol) - $k_{obs} = 8 \times 10^{-10} \text{ M.s}^{-1}$



199w, X = CF₃ (95 mg/0.50 mmol; 95 mg/0.50 mmol) - k_{obs} = 7x10⁻¹⁰ M.s⁻¹



199aa, X = CN (74 mg/0.50 mmol; 74 mg/0.50 mmol; 73 mg/0.50 mmol) - k_{obs} = 5x10⁻¹⁰ M.s⁻¹



Compound	Substituent	σ_p	k_{obs}	$\log\left(\frac{k_x}{k_H}\right)$
199c	OMe	-0.27	5×10^{-10}	-0.0792
199a	H	0	6×10^{-10}	0.0000
199r	F	0.06	7×10^{-10}	0.0669
199o	Cl	0.23	8×10^{-10}	0.1249
199w	CF ₃	0.54	7×10^{-10}	0.0669
199aa	CN	0.66	5×10^{-10}	-0.0792

Table 37: Tabulated data used for the Initial rate Hammett Analysis in Figure S25.

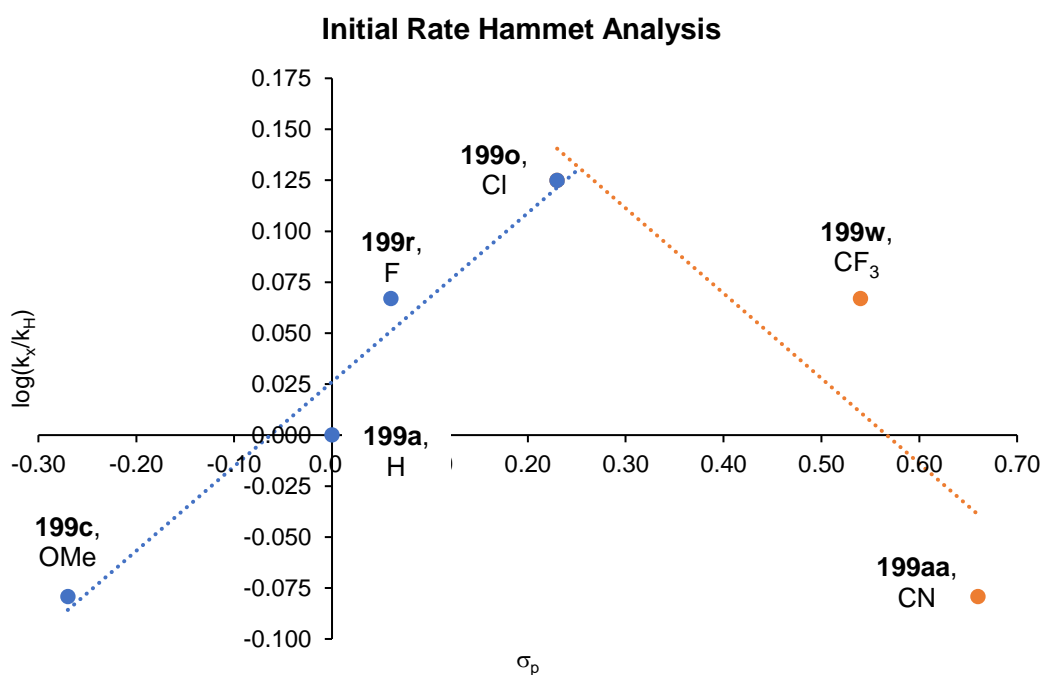


Figure S25: Hammett analysis of the maximum rates of reaction of the electrochemically enabled reaction of substituted benzaldehyde oximes, with the data consistent with a 1,3-dipolar cycloaddition reaction of a nitrile oxide.

6.11.2. Swain-Lupton Analysis

For Swain-Lupton analysis, the same ^1H NMR data and rates that were used for the Hammett analysis was employed.

To calculate f and r , the Excel Solver Function was used. The restrictions employed were maximising R^2 (correlation coefficient) while ensuring that r and f add up to 1. The data is shown in **Table 38**. The values for F and R were taken from the review by Hansch and co-workers.¹⁰¹

Compound	Substituent	k_{obs}	$\log\left(\frac{k_x}{k_H}\right)$	f	r	F	R
199c	OMe	5×10^{-10}	-0.1249	0.5742	0.4278	0.29	-0.56
199a	H	6×10^{-10}	0.0000	0.5742	0.4278	0.03	0.00
199r	F	7×10^{-10}	0.0512	0.5742	0.4278	0.45	-0.39
199o	Cl	8×10^{-10}	0.0969	0.5742	0.4278	0.42	-0.19
199w	CF_3	7×10^{-10}	0.0512	1.0000	0.0000	0.38	0.16
199aa	CN	5×10^{-10}	0.0000	1.0000	0.0000	0.51	0.15

Table 38: Data used for Swain-Lupton analysis shown in **Figure S26**.

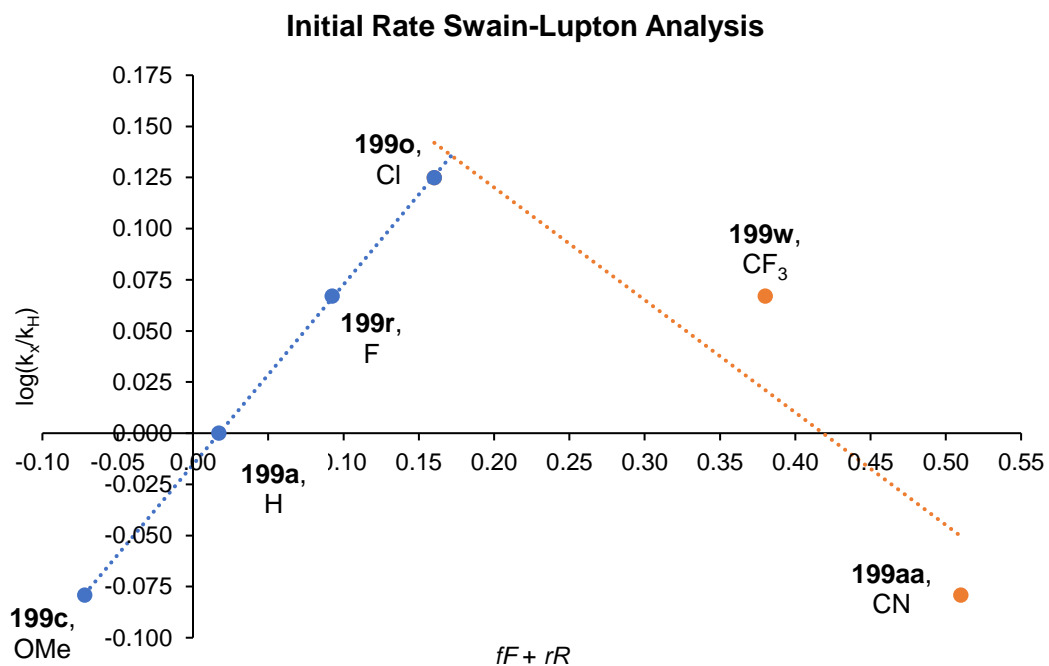


Figure S26: Swain-Lupton analysis of the maximum rates of reaction of the electrochemically enabled reaction of substituted benzaldehyde oximes, with the data consistent with a 1,3-dipolar cycloaddition reaction of a nitrile oxide.

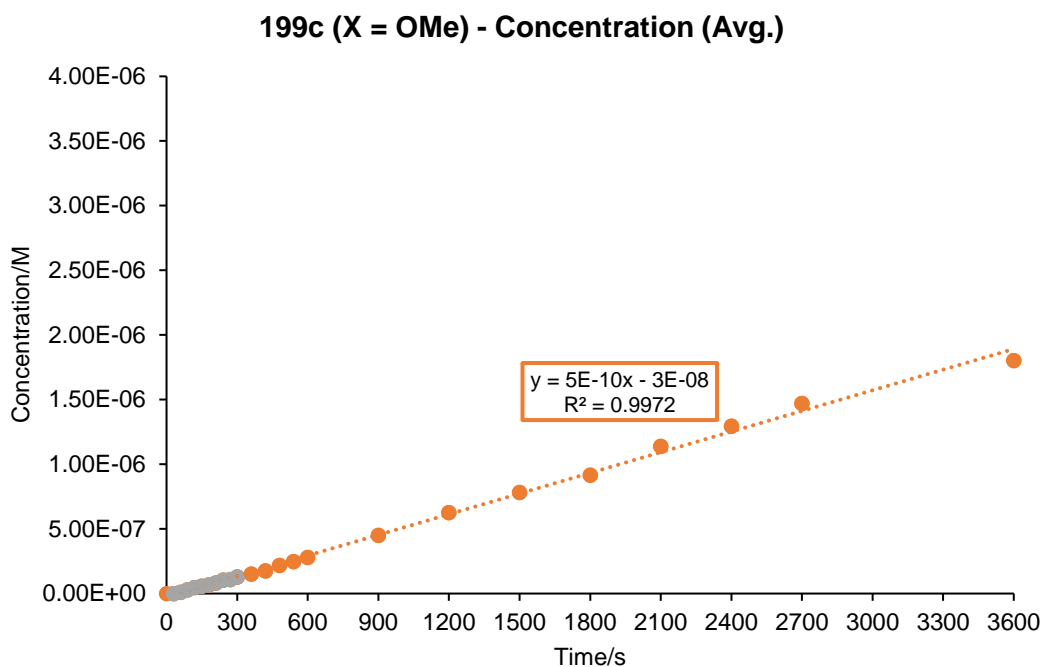
6.11.3. Well-Mixed Regime Kinetic Analysis

The ^1H NMR profiles for each of the reactions from the maximum rate kinetic study were re-analysed, with a trendline fitted to the well-mixed regime to give the k_{obs} for this regime.

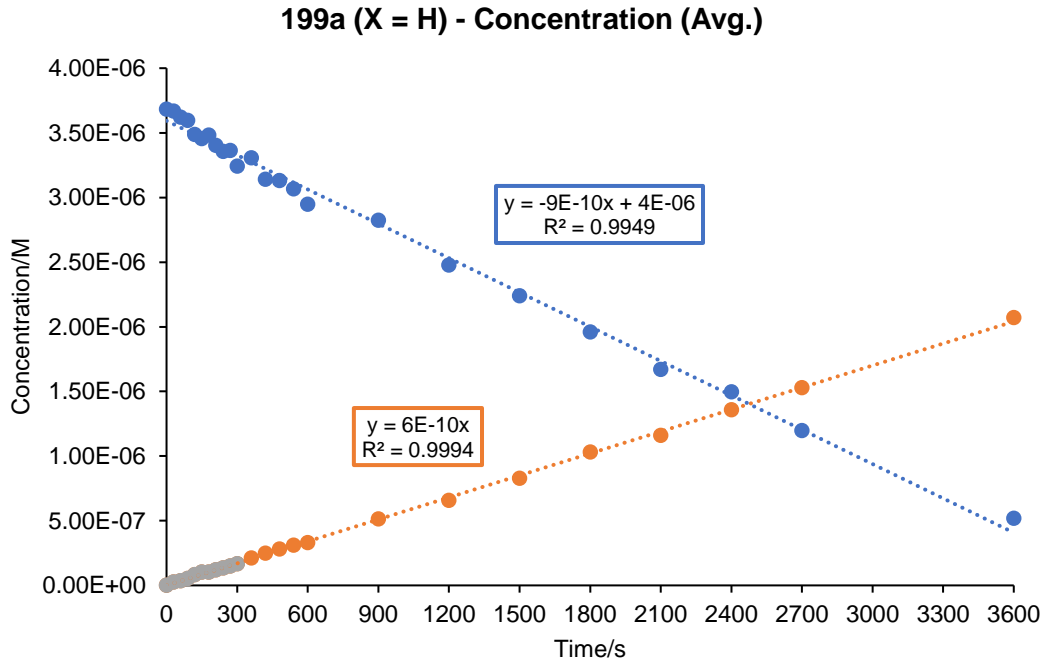
Points were chosen for straight-line fit by 300 seconds onwards.

Mass and millimolar quantities of each substrate are shown in parentheses above each plot, with each experiment used in the average calculation separated by a semi-colon.

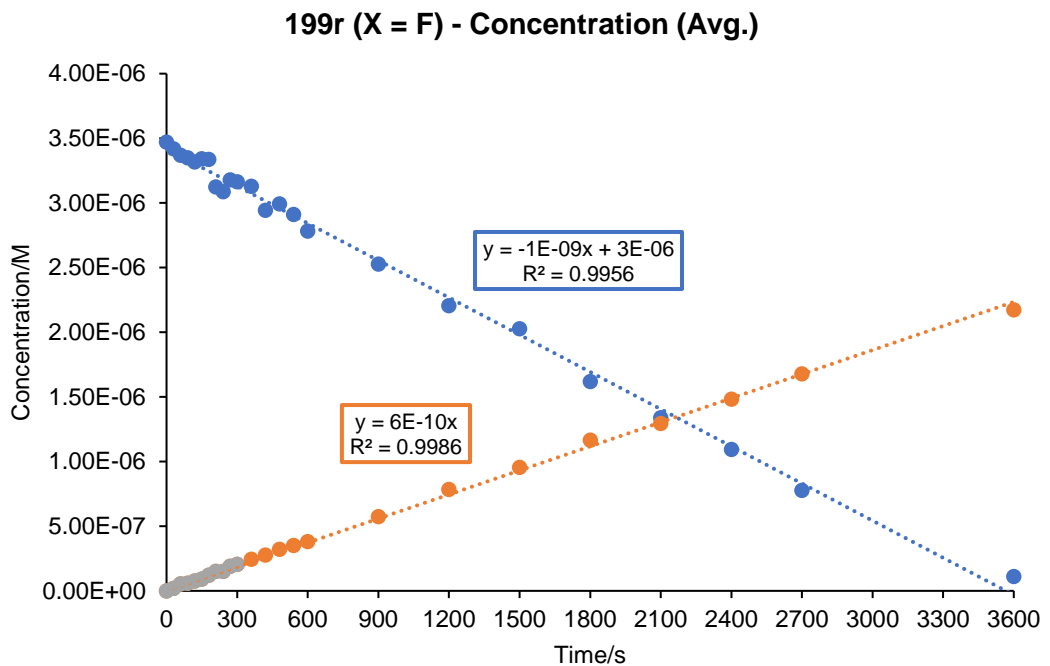
199c, X = OMe (76mg/0.50 mmol; 77 mg/0.51 mmol) - $k_{\text{obs}} = 5 \times 10^{-10} \text{ M.s}^{-1}$



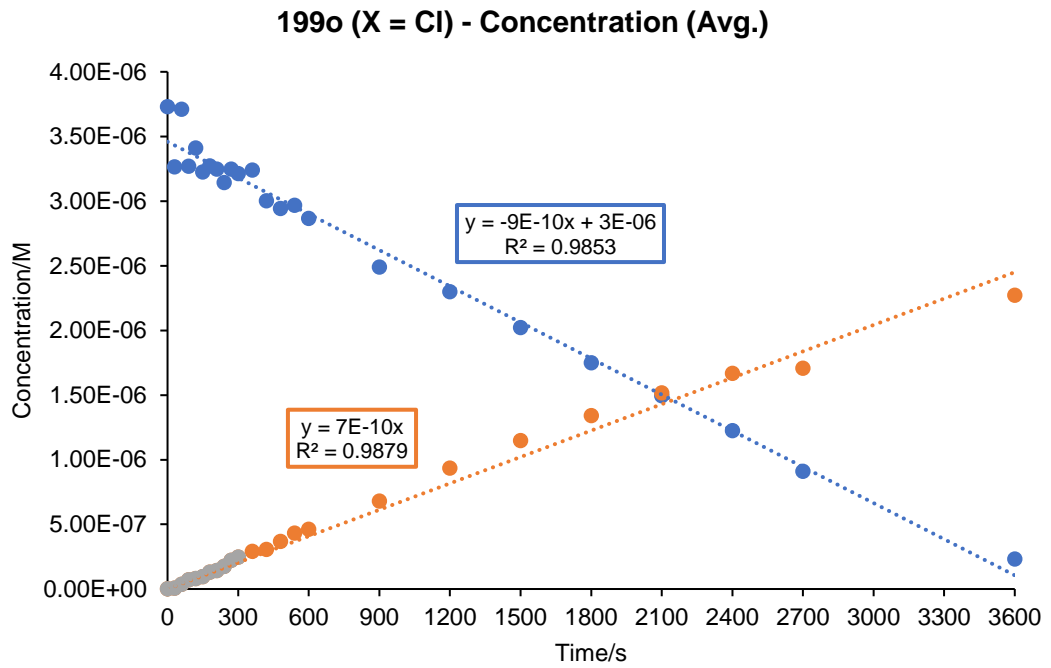
199a, X = H (61 mg/0.51 mmol; 61 mg/ 0.50 mmol) - $k_{obs} = 6 \times 10^{-10} \text{ M.s}^{-1}$



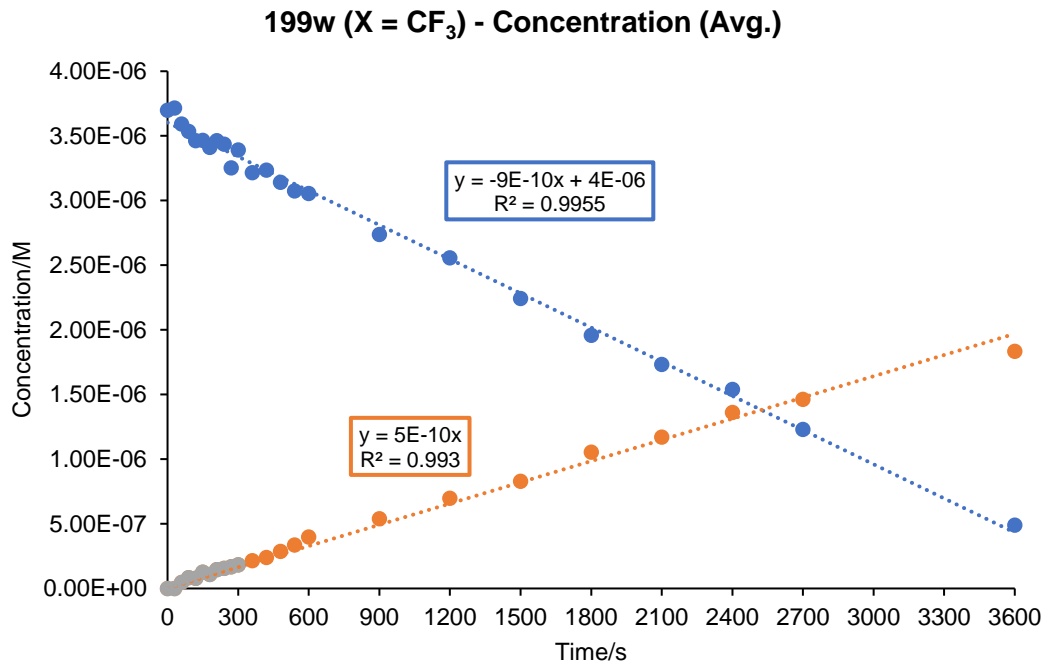
199r, X = F (70 mg/0.50 mmol; 70 mg/0.50 mmol) - $k_{obs} = 6 \times 10^{-10} \text{ M.s}^{-1}$



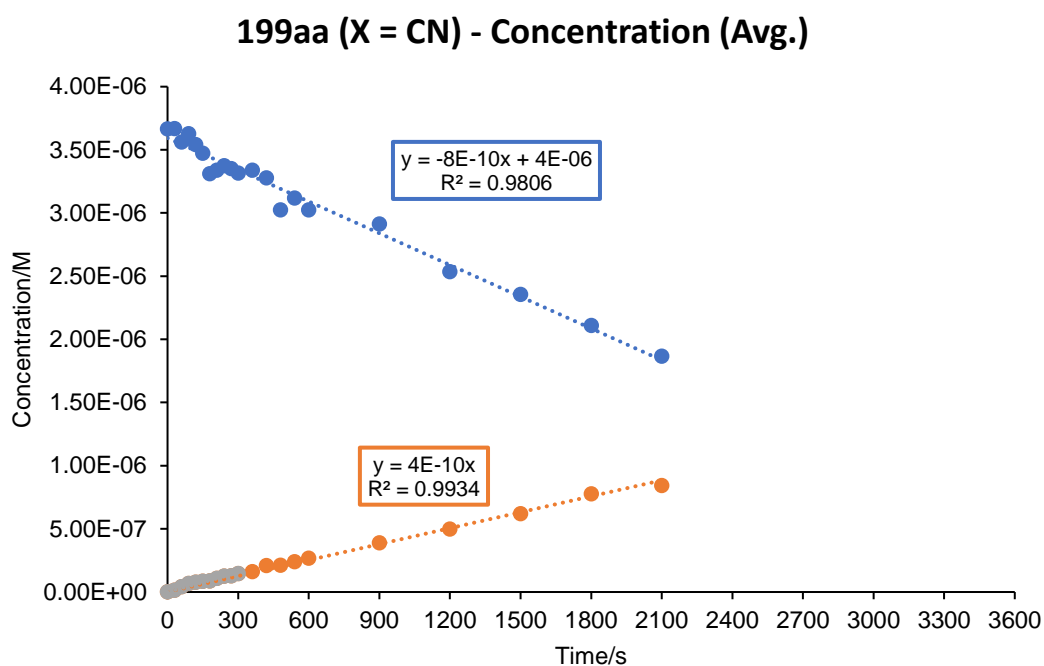
199o, X = Cl (79 mg/0.51 mmol; 78 mg/0.50 mmol; 79 mg/0.50 mmol) - $k_{obs} = 7 \times 10^{-10}$ M.s⁻¹



199w, X = CF₃ (95 mg/0.50 mmol; 95 mg/0.50 mmol) - $k_{obs} = 5 \times 10^{-10}$ M.s⁻¹



199aa, X = CN (74 mg/0.50 mmol; 74 mg/0.50 mmol; 73 mg/0.50 mmol) - $k_{\text{obs}} = 4 \times 10^{-10} \text{ M}\cdot\text{s}^{-1}$



Experiment employing **199aa** (X = CN) was removed from the ElectraSyn carousel after 2700 s due to high (>15 V) potentials observed.

Compound	Substituent	σ_p	k_{obs}	$\log\left(\frac{k_x}{k_H}\right)$
199c	OMe	-0.27	3×10^{-10}	-0.3010
199a	H	0	6×10^{-10}	0.0000
199r	F	0.06	6×10^{-10}	0.0000
199o	Cl	0.23	7×10^{-10}	0.0669
199w	CF ₃	0.54	5×10^{-10}	-0.0792
199aa	CN	0.66	4×10^{-10}	-0.1761

Table 39: Tabulated data used for the well-mixed regime Hammett Analysis shown in **Figure S27**.

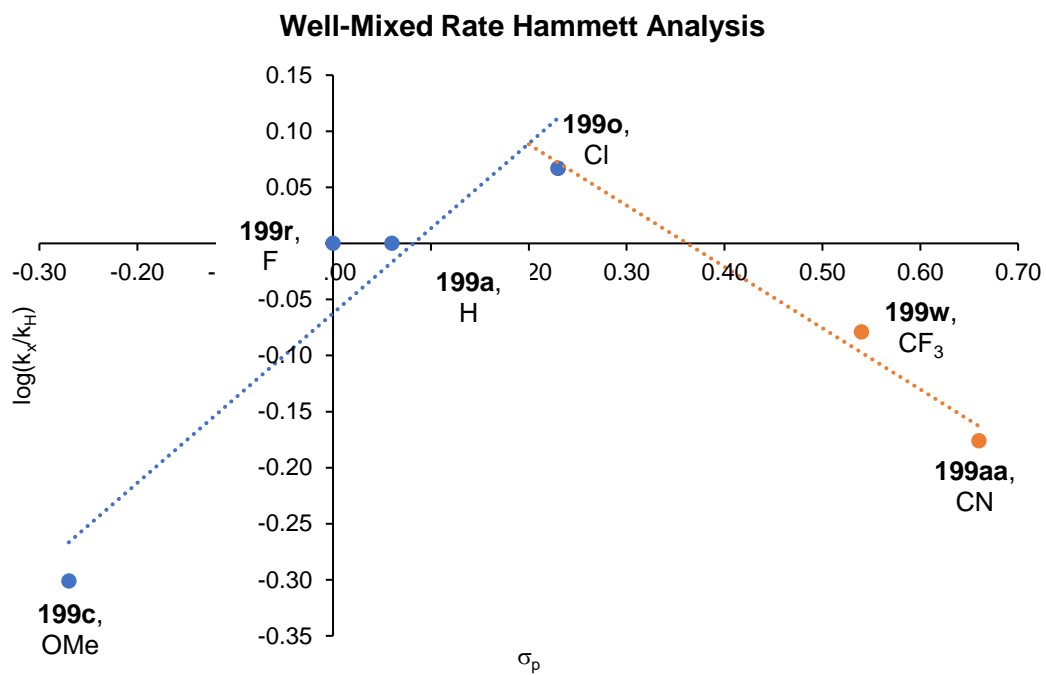
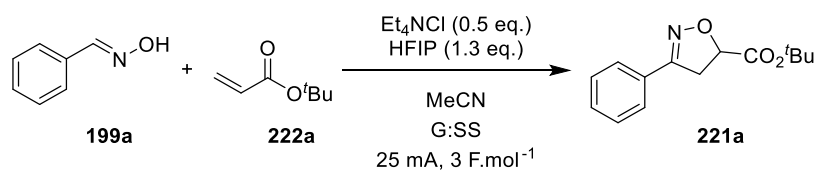


Figure S27: Hammett analysis of the well-mixed regime of the electrochemically enabled synthesis of isoxazolines from substituted benzaldehyde oximes.

6.11.4. Stir Speed Analysis



The effect of stir speed on the rate of reaction was analysed by ^1H NMR using the following procedure:

To a 10 mL ElectraSyn 2.0 reaction vessel containing a stirrer bar, (*E*)-benzaldehyde oxime **199a** (61 mg, 0.50 mmol), *tert*-butyl acrylate (366 μL , 2.50 mmol), HFIP (70 μL , 0.67 mmol) and Et_4NCl (42 mg, 0.25 mmol) were added followed by $\text{MeCN-}d_3$ (7 mL). The reaction mixture was electrolysed under a constant current of 25 mA with G anode and SS cathode stirring at the desired speed in position 1, until a current of 3 F.mol^{-1} had been passed. Stir speeds analysed were 200, 400 and 600 rpm.

The solution was followed by NMR (400 MHz spectrometer), taking samples at the following intervals: 0, 0.5, 2, 3, 5, 7, 9, 11, 13, 15, 20, 25, 30, 35, 40, 45, 60, 75, 90, 100 min.

For the reaction with no stirring, NMR samples were taken at 0, 0.5, 4.2, 8.3, 16.7, and 100 min.

NMR samples were made from 30 μL of reaction mixture, 50 μL of NMR standard solution (benzyl benzoate; 0.1 M solution), and 420 μL of $\text{MeCN-}d_3$.

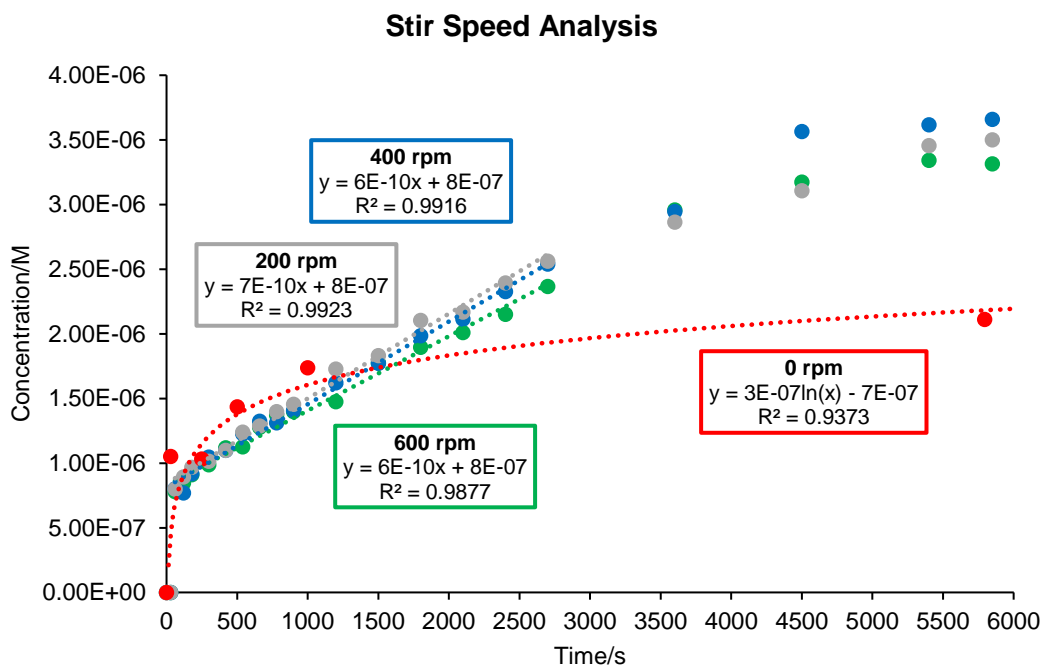
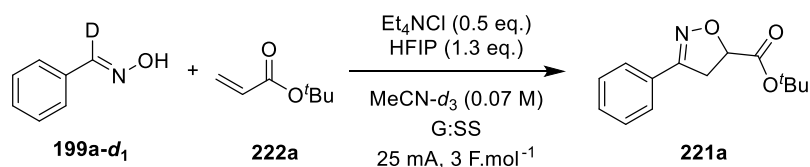


Figure S28: Analysis of the effect of stir speed on the electrochemically enabled synthesis of substituted isoxazolines from aldoximes.

6.11.5. Kinetic Isotope Effect Study



The kinetic isotope effect on the rate of reaction was analysed by ^1H NMR using the following procedure:

To a 10 mL ElectraSyn 2.0 reaction vessel containing a stirrer bar, (*E*)-benzaldehyde- α - d_1 oxime **199a-d₁** (62 mg, 0.51 mmol), *tert*-butyl acrylate (366 μL , 2.50 mmol), HFIP (70 μL , 0.67 mmol) and Et_4NCl (41 mg, 0.25 mmol) were added followed by MeCN-d_3 (7 mL). The reaction mixture was electrolysed under a constant current of 25 mA with G anode and SS cathode stirring at the desired speed in position 1, until a current of 3 F.mol^{-1} had been passed.

The reaction was followed by ^1H NMR, taking samples at the following intervals: 0, 0.5, 1, 1.5, 2, 2.5, 3, 3.5, 4, 4.5, 5, 6, 7, 8, 9, 10, 15, 20, 25, 30, 35, 40, 45, 60 min. NMR samples were made from 30 μL of reaction mixture, 50 μL of NMR standard solution (benzyl benzoate, 0.1 M solution), and 420 μL of MeCN-d_3 . NMR analysis was performed on a Bruker 700 MHz spectrometer with a $\text{D1} = 2 \text{ s}$. Every experiment was performed at least twice, and the graphs shown are an average of the two experiments. Initial rates were calculated by fitting a straight-line to the first 300 s (5 mins) of the reaction profile (or first zero value that had a subsequent non-zero value). Well-mixed rate refers to the rate of reaction for after 300 s (or 5 mins).

NMR samples were made from 30 μL of reaction mixture, 50 μL of NMR standard solution (benzyl benzoate; 0.1 M solution), and 420 μL of MeCN-d_3 .

The observed rates from the reaction with **199a** was compared with the observed rates from the reaction with **199a-d₁** to get a KIE value.

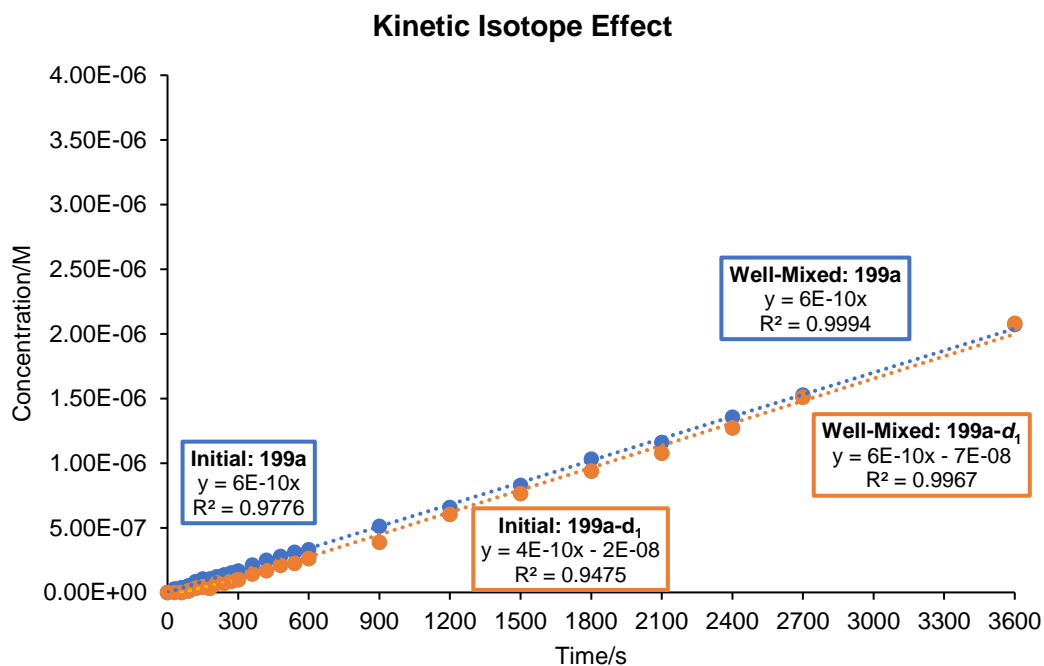


Figure S29: The ^1H NMR profiles of **199a** (blue) and **199a-d₁** (orange); analysis of the profiles for maximum rates and the rate of reaction of the well-mixed region supports the hypothesis of the formation of an intermediate nitrile oxide.

6.11.6. Alternative Hammett Analyses

Alternative methods for choosing points for straight-line fits were explored using the same data acquired during ^1H NMR analysis of *para*-substituted benzaldehyde oximes. All substituent parameters (σ_p , σ_p^- , σ_p^+) were acquired from the review by Hansch and co-workers.¹⁰¹

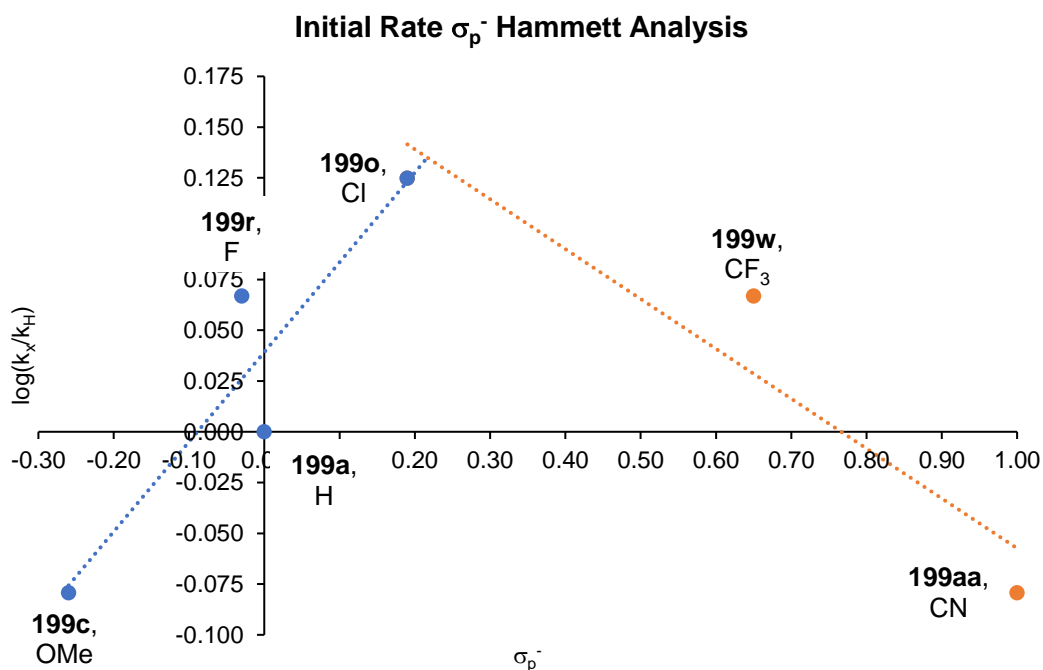


Figure S30: Maximum rate Hammett analysis using the σ_p^- substituent constant.

Maximum rate Hammett analysis using σ_p^- substituent constant is shown in **Figure S30**.

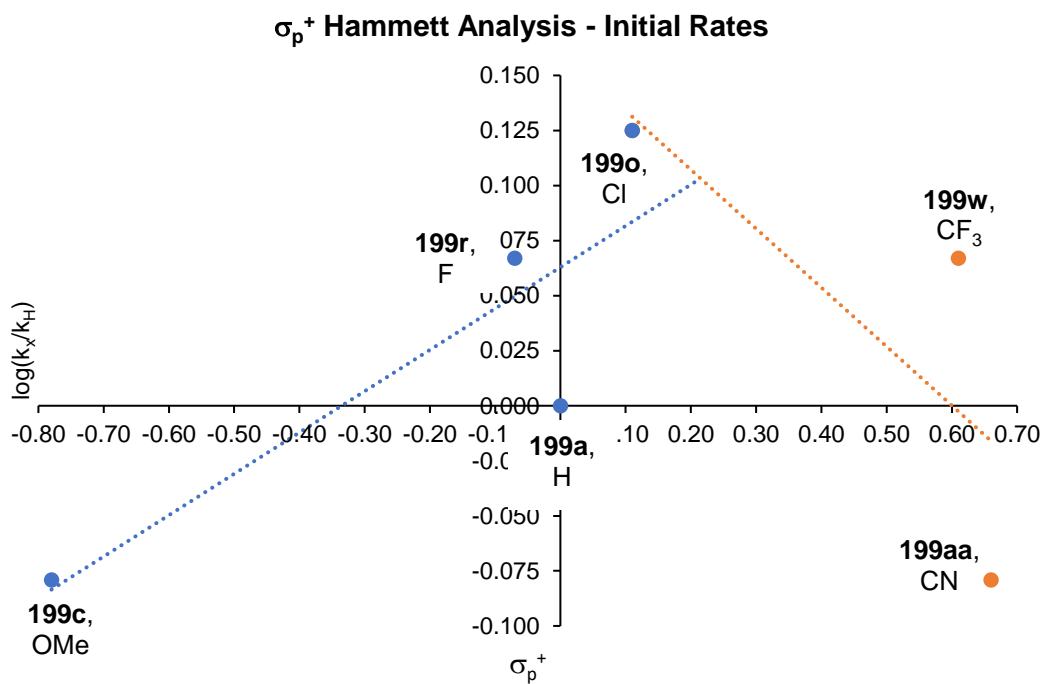


Figure S31: Maximum rate Hammett analysis using the σ_p^+ substituent constant.

Maximum rate Hammett analysis using σ_p^+ substituent constant is shown in **Figure S31**.

6.12. Cyclic Voltammetry

6.12.1. General Procedure for Cyclic Voltammetry

The general procedure for cyclic voltammetry experiments is as follows:

2 mL MeCN was flowed over the electrode (platinum electrode), followed by 1 mL of analyte solution. The CV was acquired using the following parameters: 3 segments, starting $V = 0$ V, mid- $V = 1.5$ V, finishing $V = 0$ V, scan rate = $100 \text{ mV}\cdot\text{s}^{-1}$, V step = 0.005 V. Once CV was obtained, the cell was flushed with 2 mL MeCN and the next solution was flowed onto the chip.

Between each different solution (Solutions 2 - 8), a CV of the ferrocene solution (Solution 1) was obtained for two reasons: 1) to check the state of the electrode (no fouling) and 2) to provide a reference for the preceding CVs of desired solutions.

Solutions were prepared with 10 mM analyte and 0.1 M electrolyte in MeCN. A CV was performed three times for each solution. The three CVs were averaged to give the cyclic voltammograms shown below.

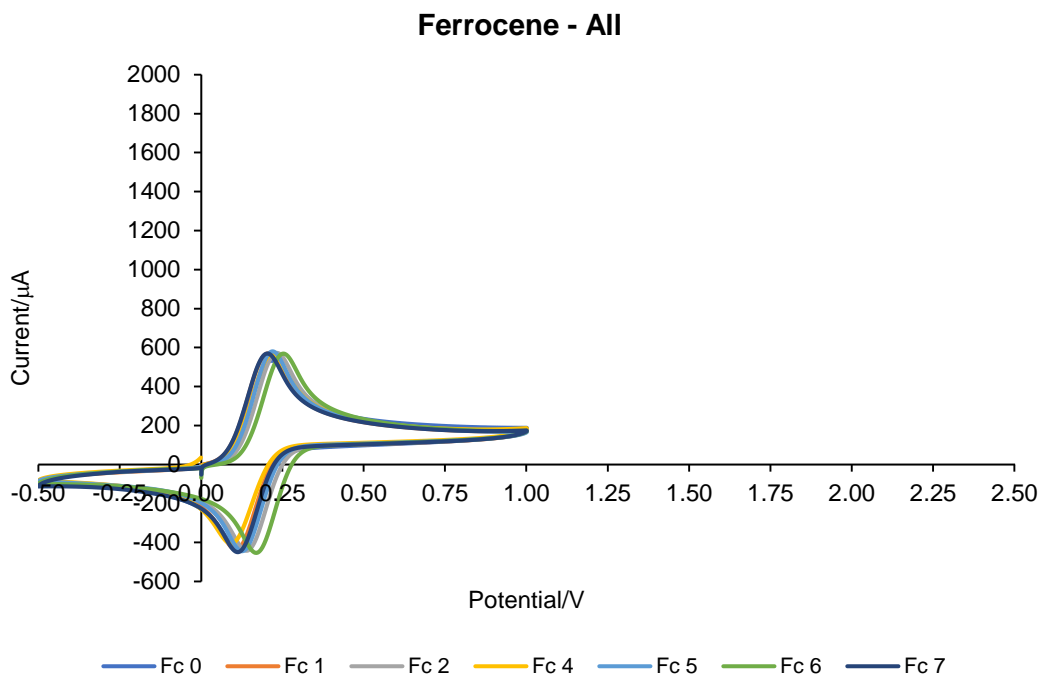
The following solutions were prepared:

- Solution 1 = Ferrocene (94 mg, 0.50 mmol) and Et_4NBF_4 (1085 mg, 5 mmol) in MeCN (50 mL)
- Solution 2 = (*E*)-benzaldehyde oxime (62 mg, 0.51 mmol) and Et_4NBF_4 (1086 mg, 5.00 mmol) in MeCN (50 mL)
- Solution 3 = *tert*-butyl acrylate (73 μL , 0.50 mmol) and Et_4NBF_4 (1085 mg, 5.00 mmol) in MeCN (50 mL)
- Solution 4 = Et_4NCl (86 mg, 0.52 mmol) and Et_4NBF_4 (1085 mg, 5.00 mmol) in MeCN (50 mL)
- Solution 5 = (*E*)-benzaldehyde oxime (31 mg, 0.26 mmol), HFIP (34 μL , 0.32 mmol) and Et_4NBF_4 (543 mg, 2.50 mmol) in MeCN (25 mL)
- Solution 6 = (*E*)-benzaldehyde oxime (32 mg, 0.26 mmol), Et_4NCl (22 mg, 0.13 mmol) and Et_4NBF_4 (543 mg, 2.50 mmol) in MeCN (25 mL)
- Solution 7 = (*E*)-benzaldehyde oxime (31.0 mg, 2.56 mmol), *tert*-butyl acrylate (183 μL , 1.25 mmol), HFIP (34 μL , 0.32 mmol), Et_4NCl (23 mg, 0.14 mmol) and Et_4NBF_4 (543 mg, 2.50 mmol) in MeCN (25 mL)

- Solution 8 = (*E*)-benzaldehyde oxime (31 mg, 0.25 mmol), HFIP (34 μ L, 0.32 mmol), Et₄NCl (22 mg, 0.13 mmol) and Et₄NBF₄ (543 mg, 2.50 mmol) in MeCN (25 mL)

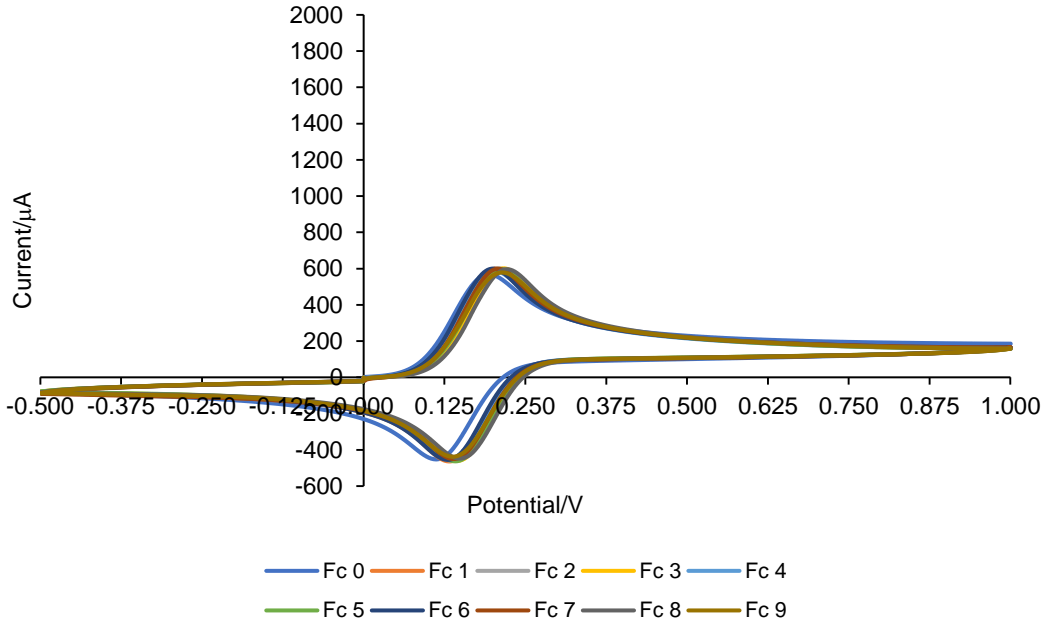
6.12.2. Cyclic Voltammograms

Ferrocene Solution (All cyclic voltammograms); 10 mM ferrocene, 0.1 M Et₄NBF₄-MeCN



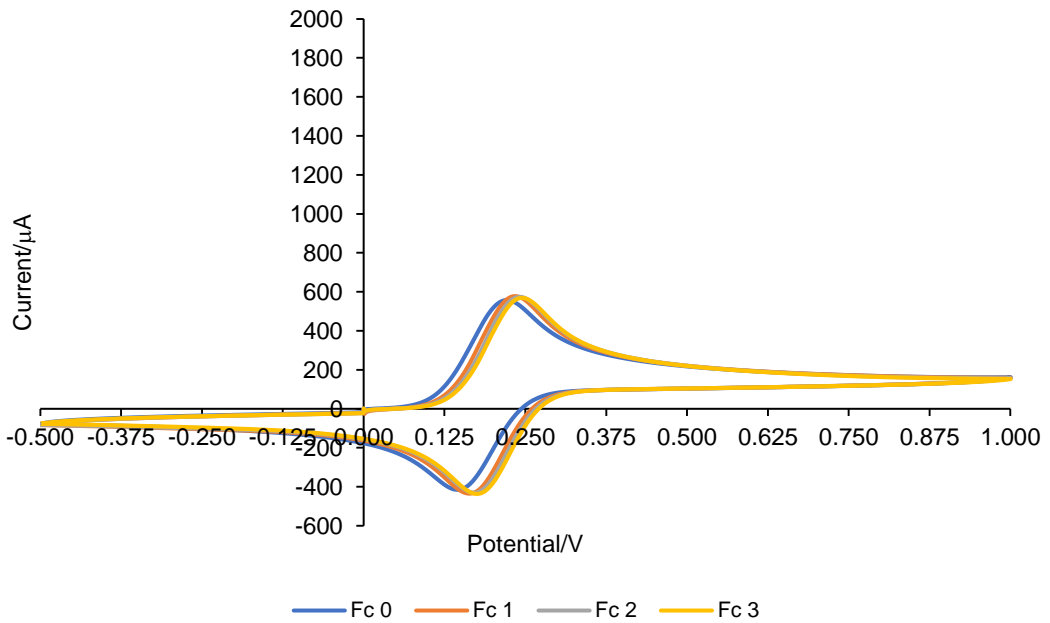
Ferrocene Solution – further Fc CVs associated with the scan rate experiments for Solution 2; 10 mM ferrocene, 0.1 M Et₄NBF₄-MeCN

Ferrocene - Solution 2 Scan Rate Analysis



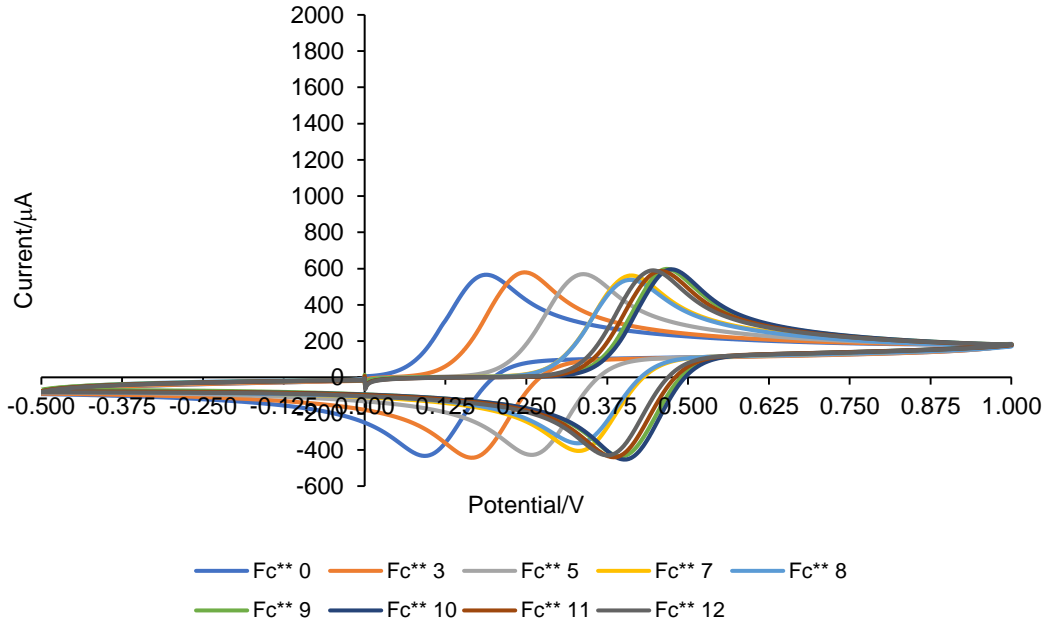
Ferrocene Solution – further Fc CVs associated with the cut-off experiments for solution 2; 10 mM ferrocene, 0.1 Et₄NBF₄-MeCN

Ferrocene - Solution 2 Cut-Off Experiments



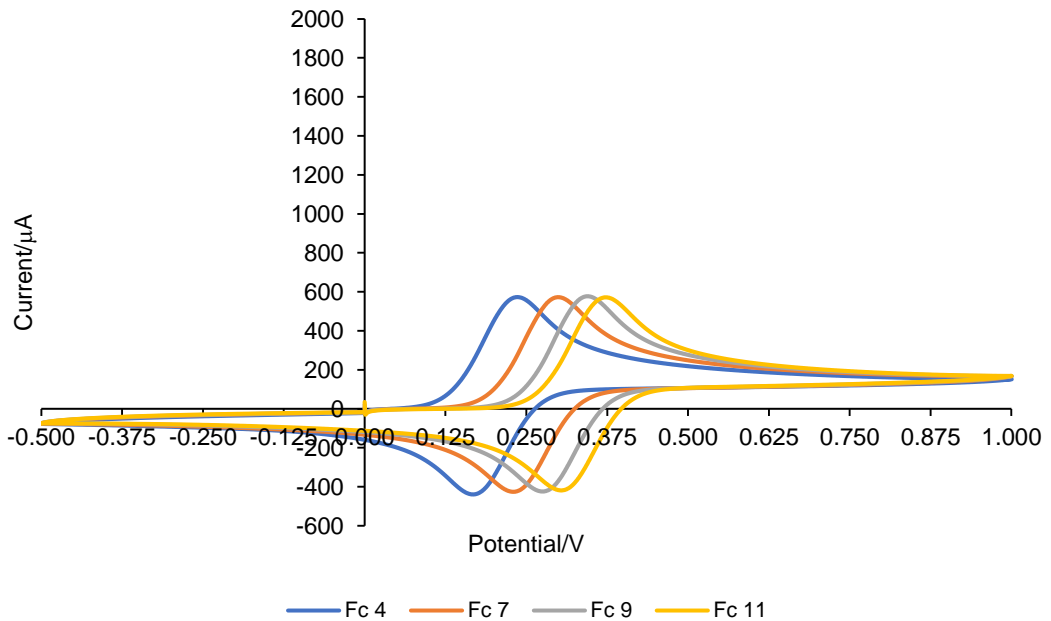
Ferrocene Solution – further Fc CVs associated with the scan rate and cut-off experiments for Solution 3; 10 mM ferrocene, 0.1 M Et₄NBF₄-MeCN

Ferrocene - Solution 3 Cut-Off and Scan Rate Experiments



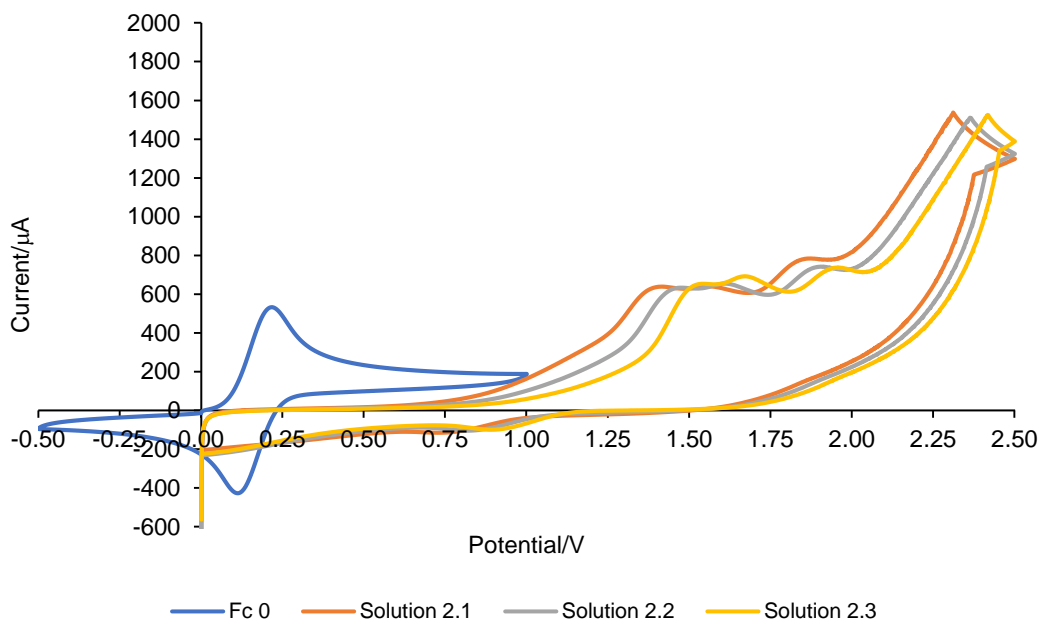
Ferrocene Solution – further Fc CVs associated with the cut-off experiments for Solution 4; 10 mM ferrocene, 0.1 M Et₄NBF₄-MeCN

Ferrocene - Solution 4 Cut-Off Experiments



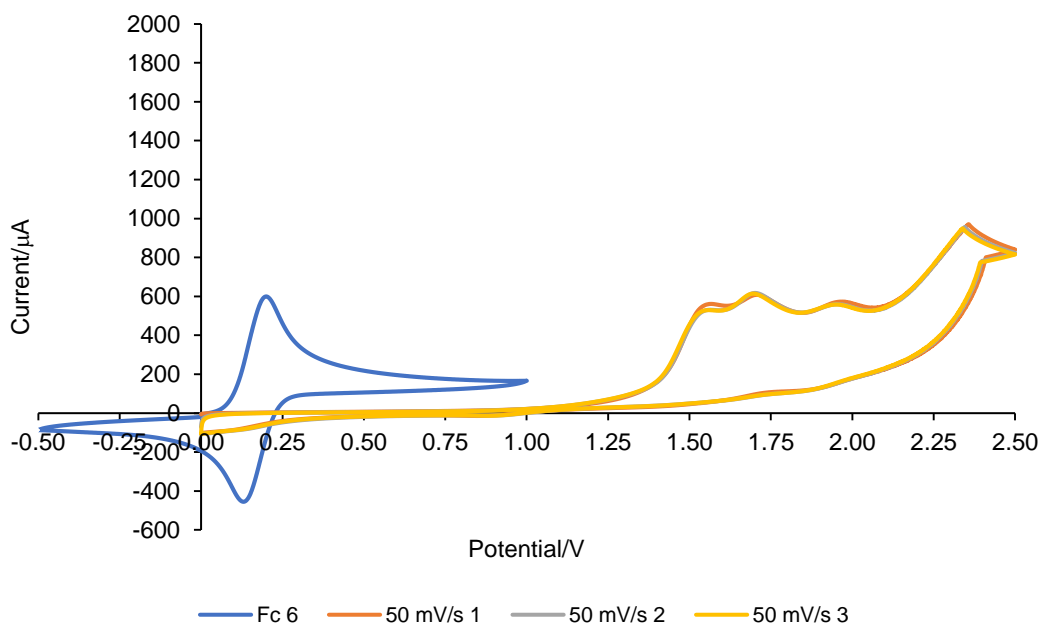
Solution 2 (including Ferrocene reference); 10 mM (*E*)-benzaldehyde oxime, 0.1 M Et₄BF₄-MeCN

Solution 2 CV

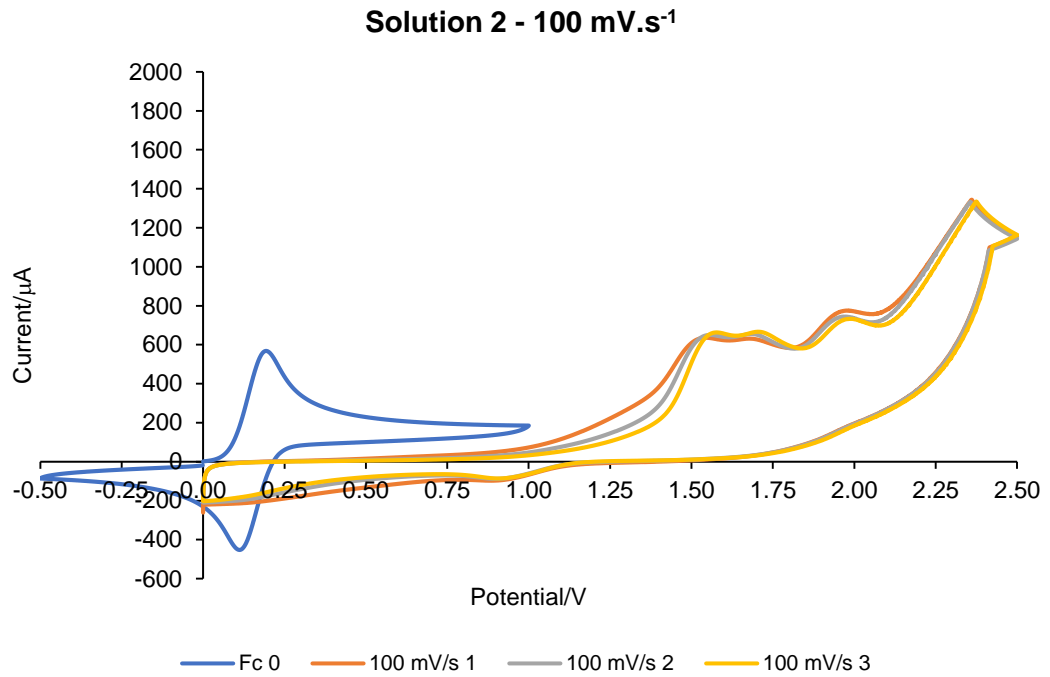


Solution 2 (including Ferrocene reference) – 50 mV.s⁻¹; 10 mM (*E*)-benzaldehyde oxime, 0.1 M ET₄NBF₄

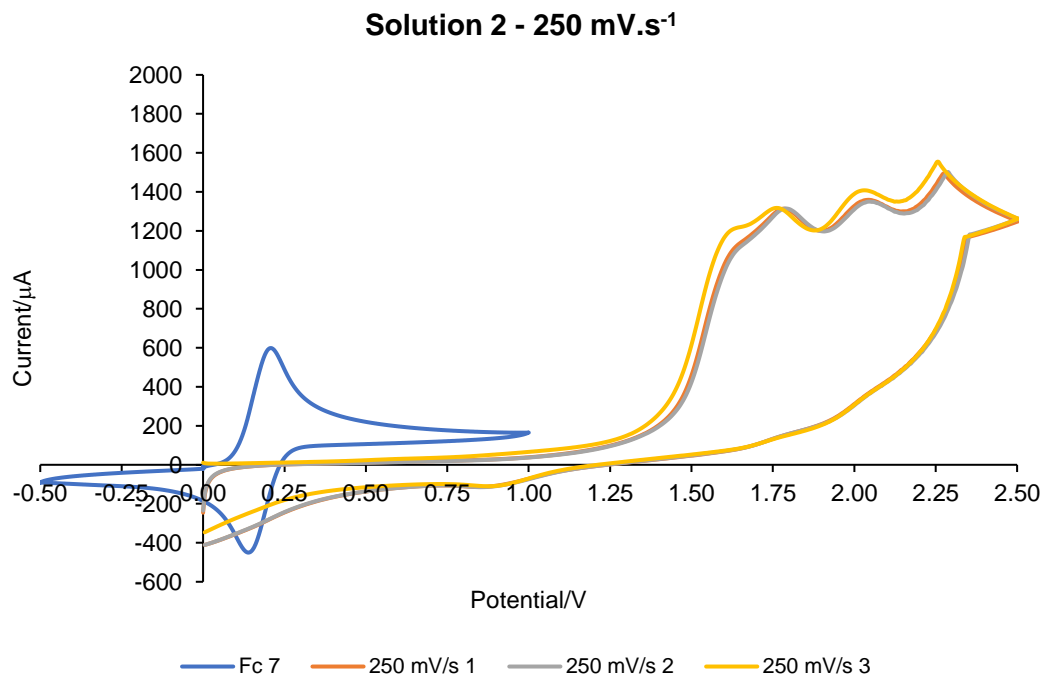
Solution 2 CV - 50 mV.s⁻¹



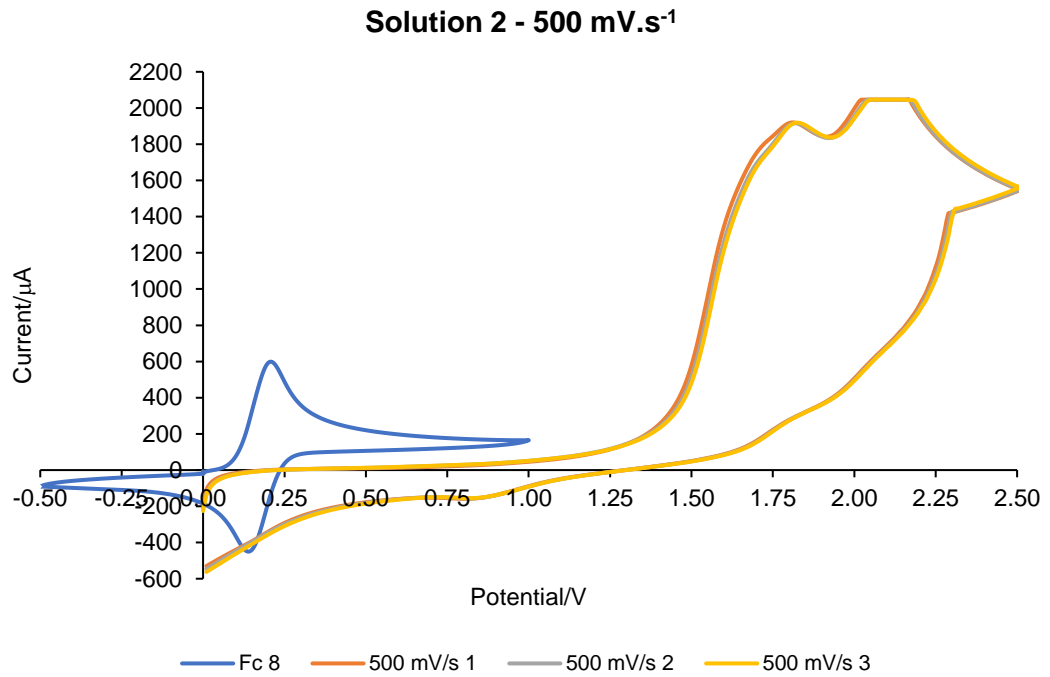
Solution 2 (including Ferrocene reference) – 100 mV.s⁻¹; 10 mM (*E*)-benzaldehyde oxime, 0.1 M Et₄NBF₄-MeCN



Solution 2 (including Ferrocene reference) – 250 mV.s⁻¹; 10 mM (*E*)-benzaldehyde oxime, 0.1 M Et₄NBF₄-MeCN



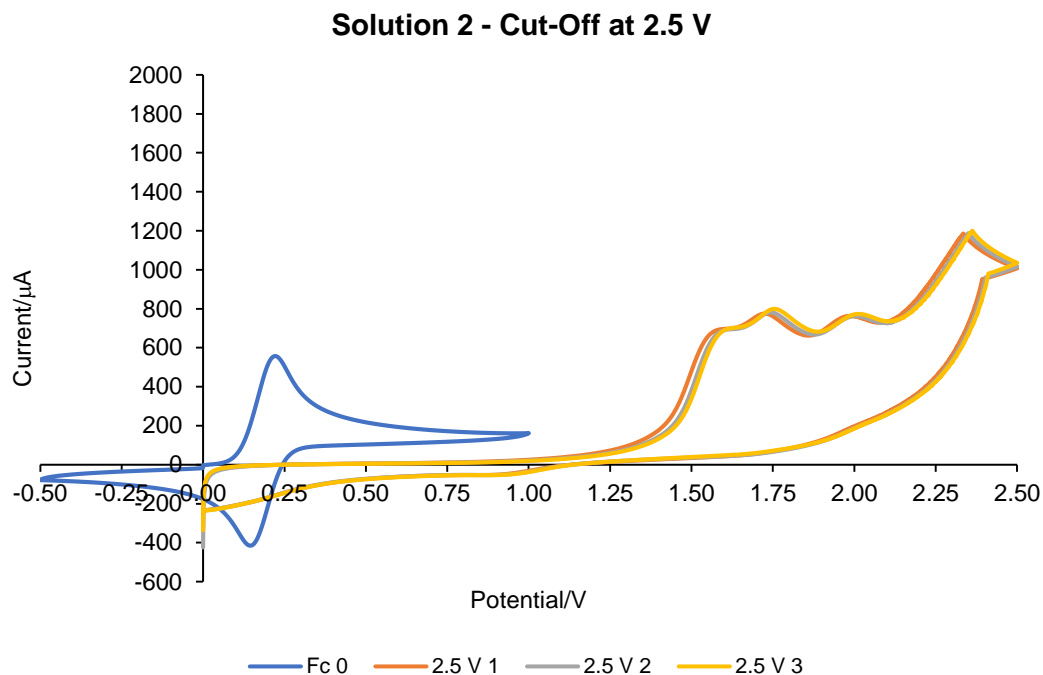
Solution 2 (including Ferrocene reference) – 500 mV.s⁻¹; 10 mM (E)-benzaldehyde oxime, 0.1 M Et₄NBF₄-MeCN



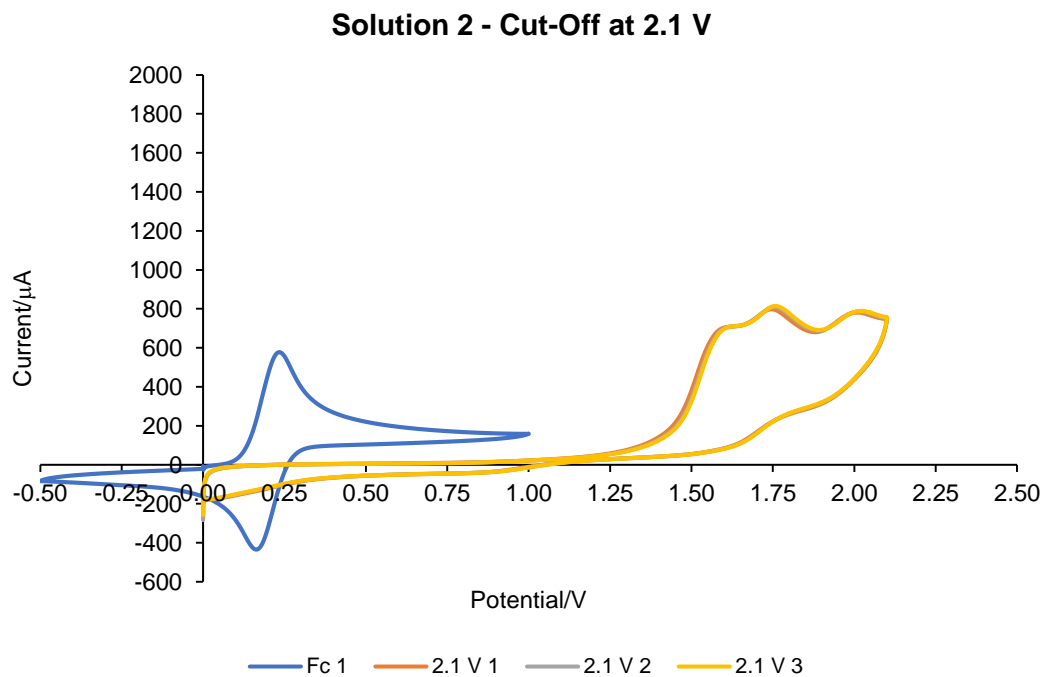
v/ mV.s ⁻¹	$\sqrt{v}/$ V ^{1/2} .s ^{-1/2}	Log(v)	E _p /V			i _p /x10 ⁻³ A		
			Peak 1	Peak 2	Peak 3	Peak 1	Peak 2	Peak 3
50	0.2236	1.6990	1.55	1.71	1.97	0.53	0.62	0.56
100	0.3162	2.0000	1.55	1.71	1.97	0.65	0.65	0.75
250	0.5000	2.3979	1.63	1.78	2.04	1.13	1.31	1.37
500	0.7071	2.6990	1.71	1.82	2.11	1.73	1.92	2.05

Table 40: Scan rate data used for the analysis of the cyclic voltammetry experiments for Solution 2.

Solution 2 (including Ferrocene reference) – cut-off at 2.5 V; 10 mV (*E*)-benzaldehyde oxime, 0.1 M Et₄NBF₄-MeCN

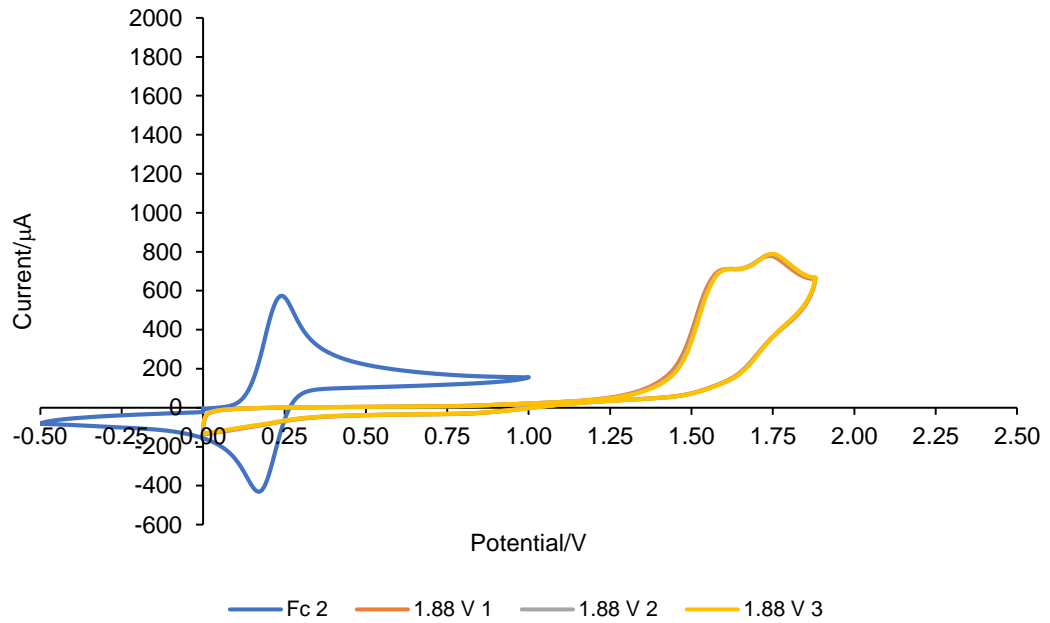


Solution 2 (including Ferrocene reference) – cut-off at 2.1 V; 10 mM (*E*)-benzaldehyde oxime, 0.1 M Et₄NBF₄-MeCN



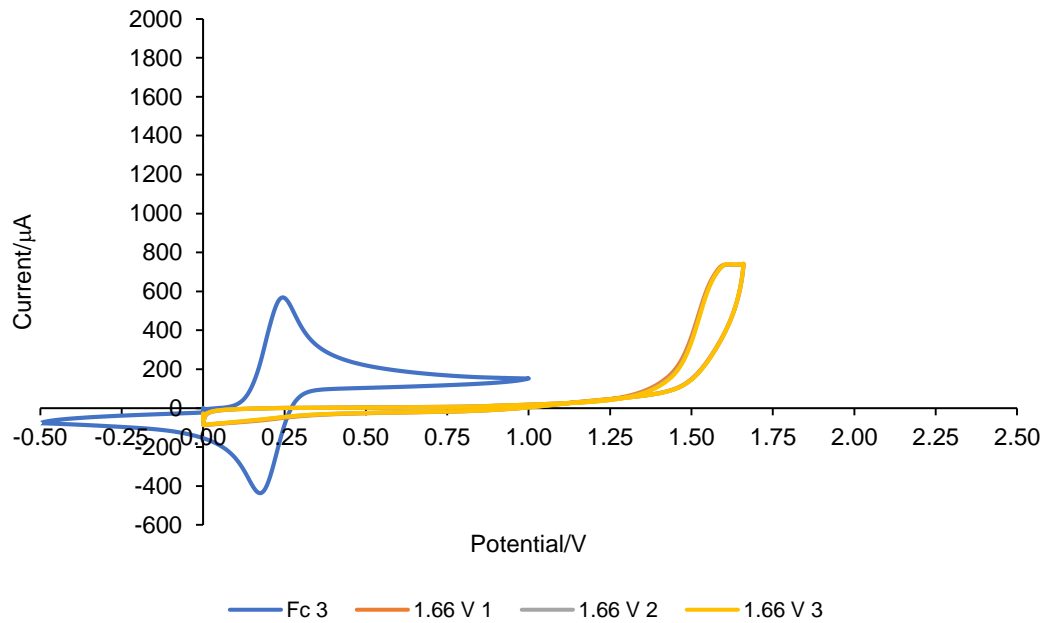
Solution 2 (including Ferrocene reference) – cut-off at 1.88 V; 10 mM (*E*)-benzaldehyde oxime, 0.1 M Et₄NBF₄-MeCN

Solution 2 - Cut-Off at 1.88 V

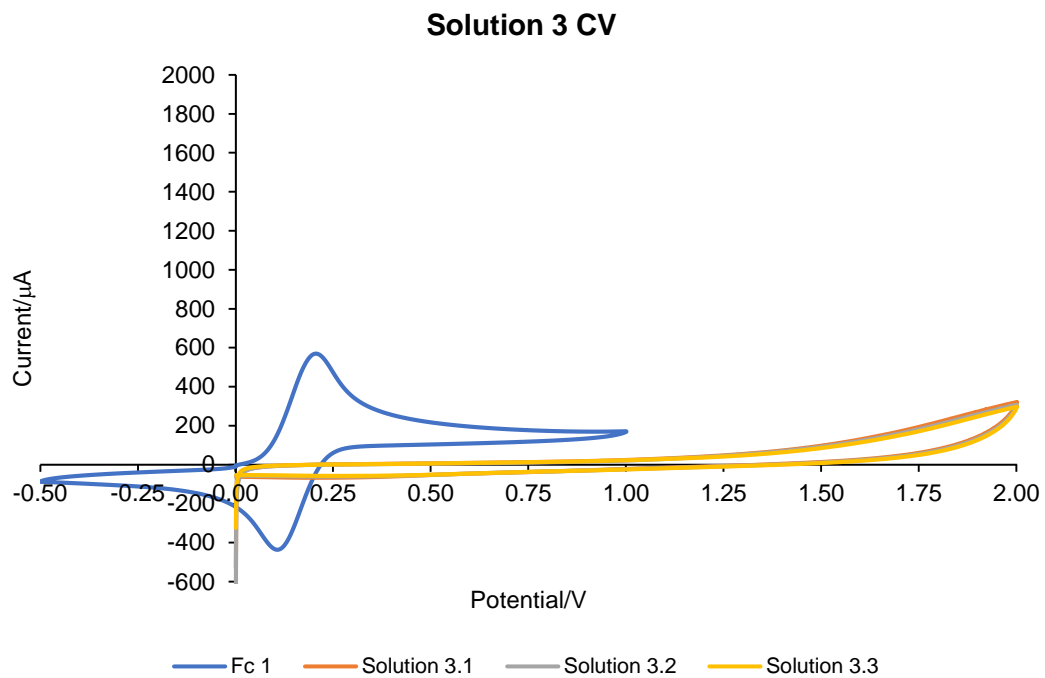


Solution 2 (including Ferrocene reference) – cut-off at 1.66 V; 10 mM (*E*)-benzaldehyde oxime, 0.1 M Et₄NBF₄-MeCN

Solution 2 - Cut-Off at 1.66 V

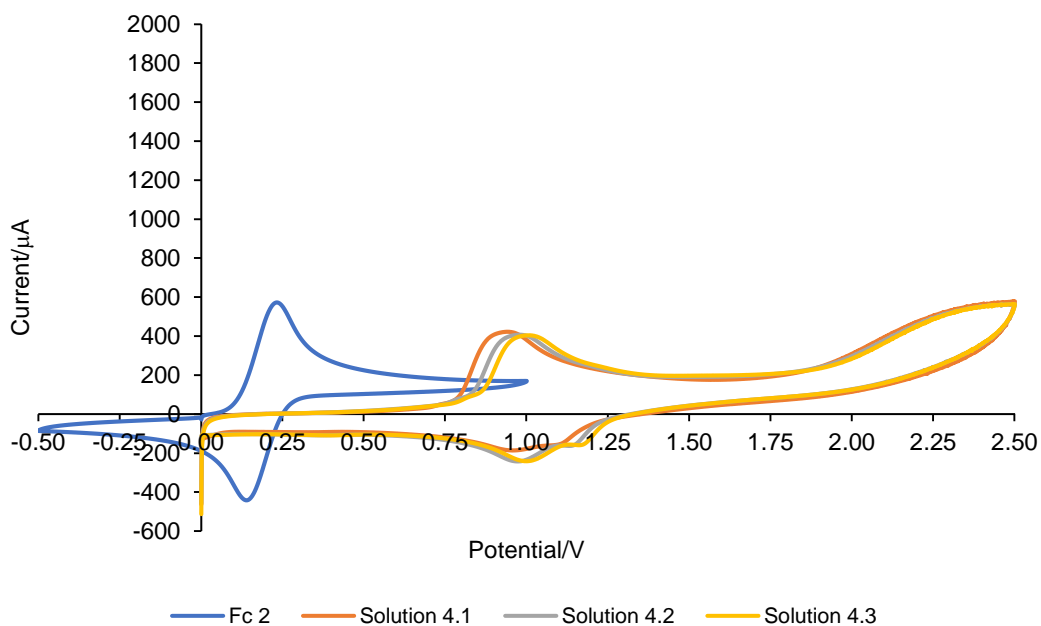


Solution 3 (including Ferrocene reference); 10 mM *tert*-butyl acrylate, 0.1 M Et₄BF₄-MeCN



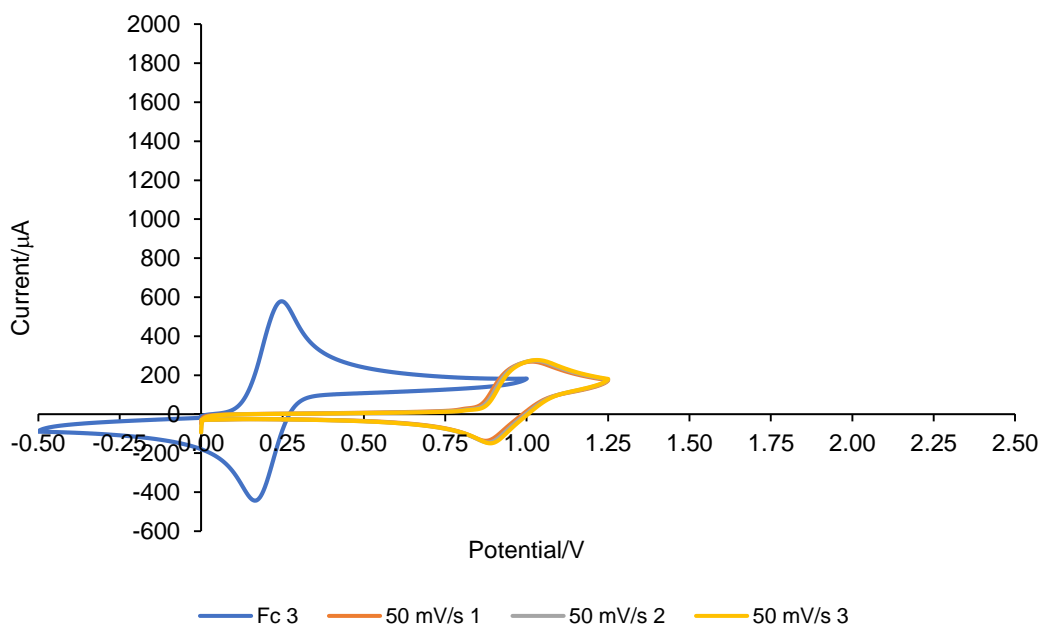
Solution 4 (including Ferrocene reference); 10 mM Et₄NCl, 0.1 M Et₄BF₄-MeCN

Solution 4 CV

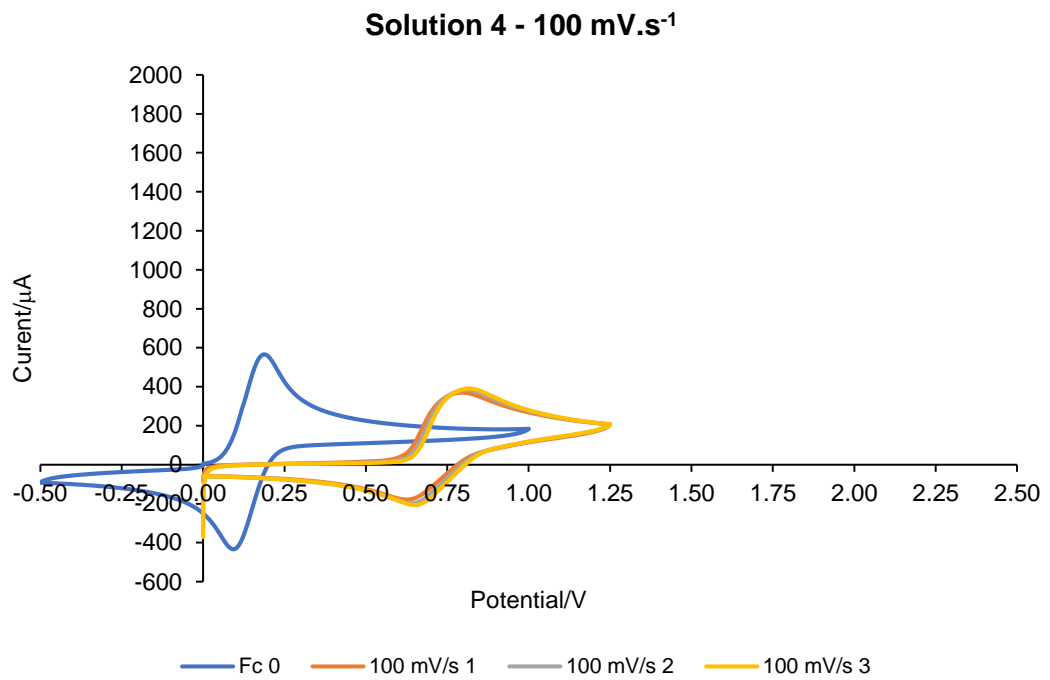


Solution 4 (including Ferrocene reference) – 50 mV.s⁻¹; 10 mM Et₄NCl, 0.1 M Et₄NBF₄-MeCN

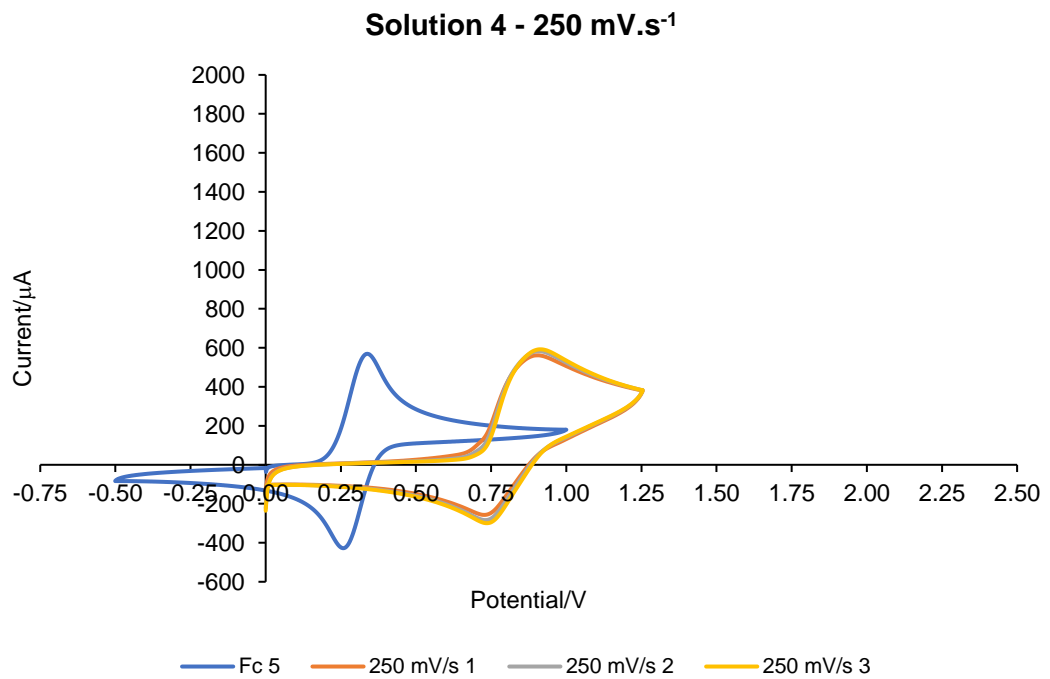
Solution 4 - 50 mV.s⁻¹



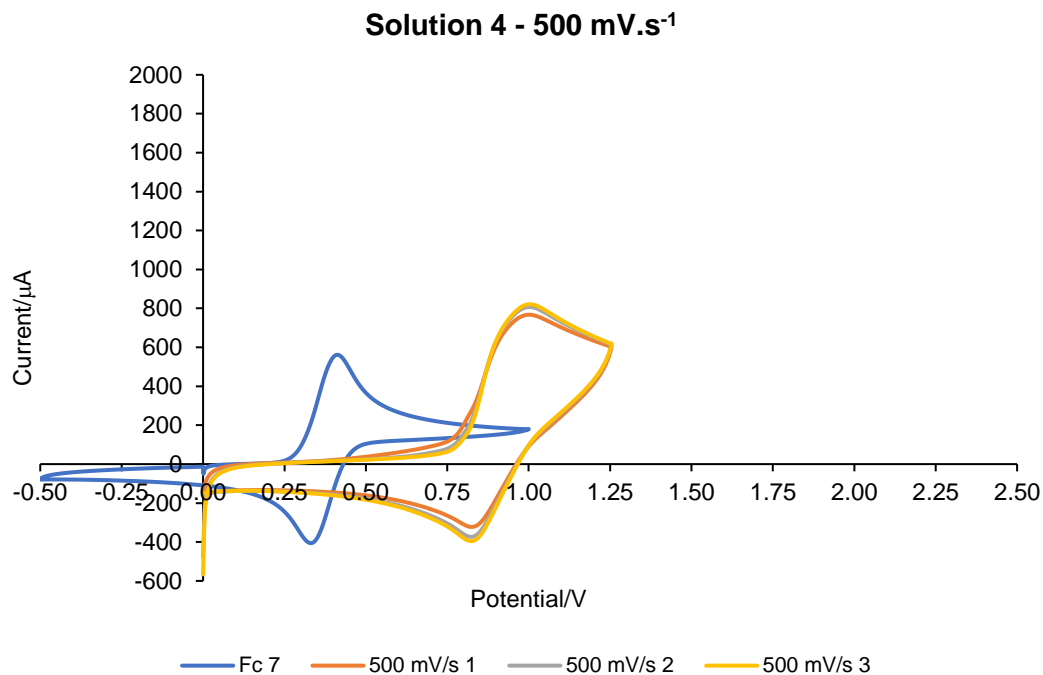
Solution 4 (including Ferrocene reference) – 100 mV.s⁻¹; 10 mM Et₄NCl, 0.1 M Et₄NBF₄-MeCN



Solution 4 (including Ferrocene reference) – 250 mV.s⁻¹; 10 mM Et₄NCl, 0.1 M Et₄NBF₄-MeCN



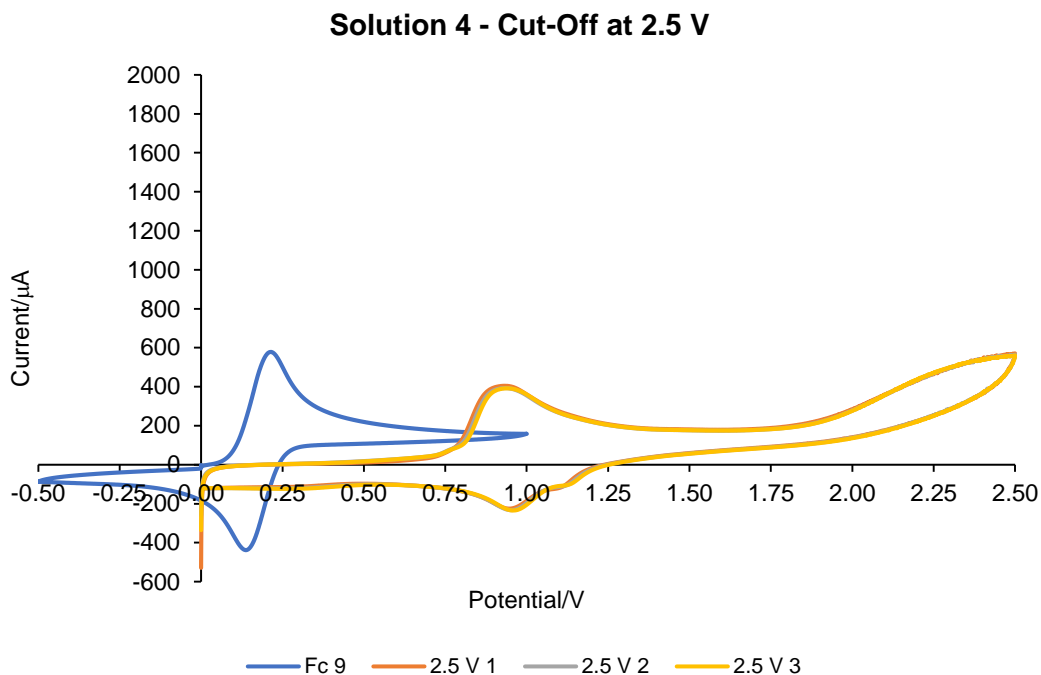
Solution 4 (including Ferrocene reference) – 500 mV.s⁻¹; 10 mM Et₄NCl, 0.1 M Et₄NBF₄-MeCN



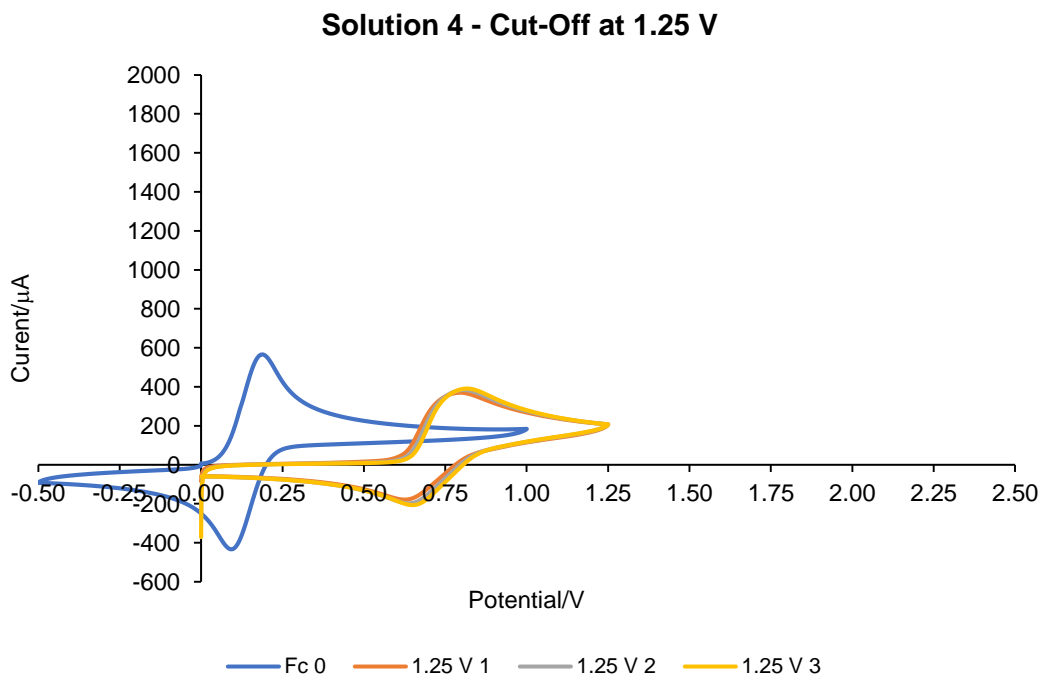
v/ mV.s ⁻¹	√v/ V ^{1/2} .s ^{-1/2}	Oxidative Wave		Reductive Wave		ΔE _p /mV
		E _p /V	i _p /x10 ⁻⁴ A	E _p /V	i _p /x10 ⁻⁴ A	
50	0.2236	1.023	2.74	0.885	-1.43	138
100	0.3162	0.803	3.81	0.639	-1.93	164
250	0.5000	0.909	5.79	0.730	-2.80	179
500	0.7071	1.004	7.99	0.829	-3.63	175

Table 41: Scan rate data used for the analysis of the cyclic voltammetry experiments for Solution 4.

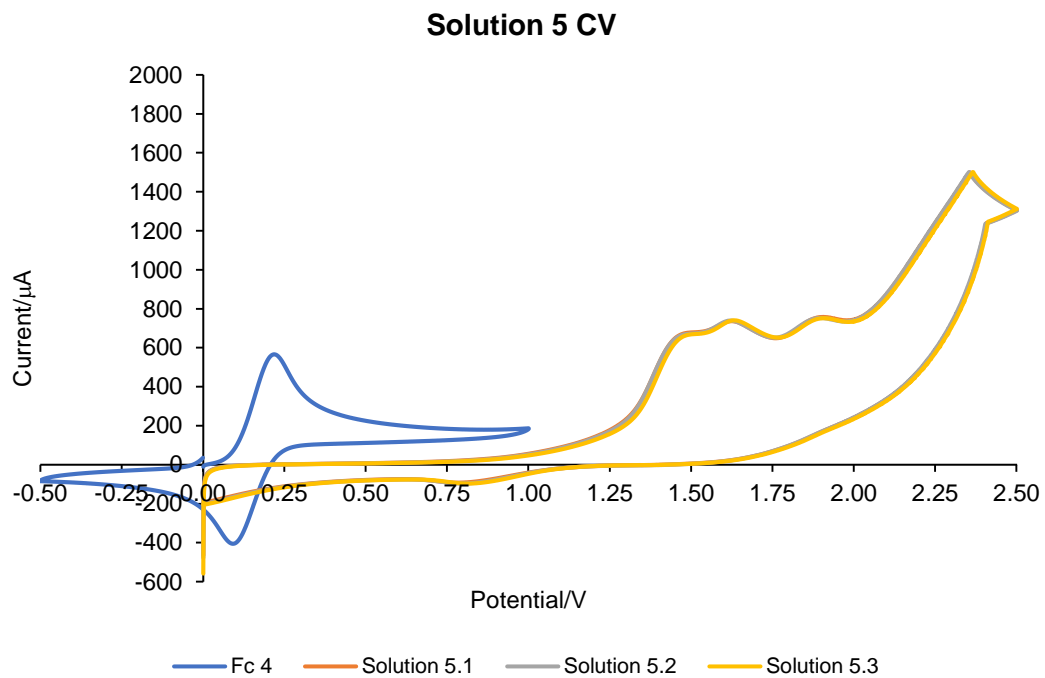
Solution 4 (including Ferrocene reference) – cut-off at 2.5 V; 10 mM Et₄NCl, 0.1 M Et₄NBF₄-MeCN



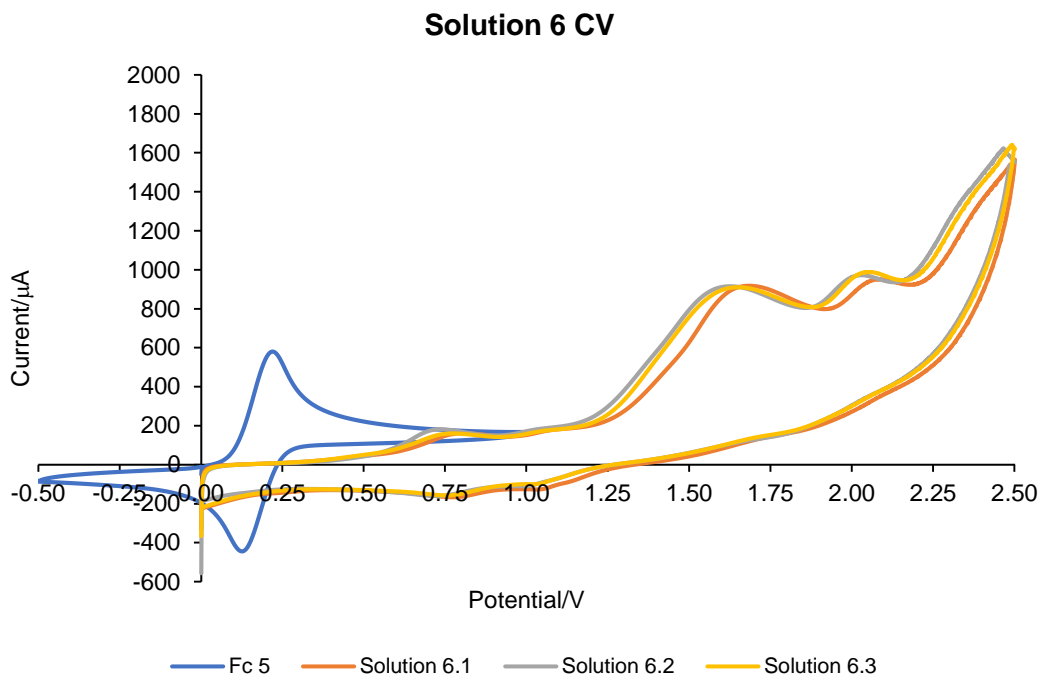
Solution 4 (including Ferrocene reference) – cut-off at 1.25 V; 10 mM Et₄Cl, 0.1 M Et₄NBF₄-MeCN



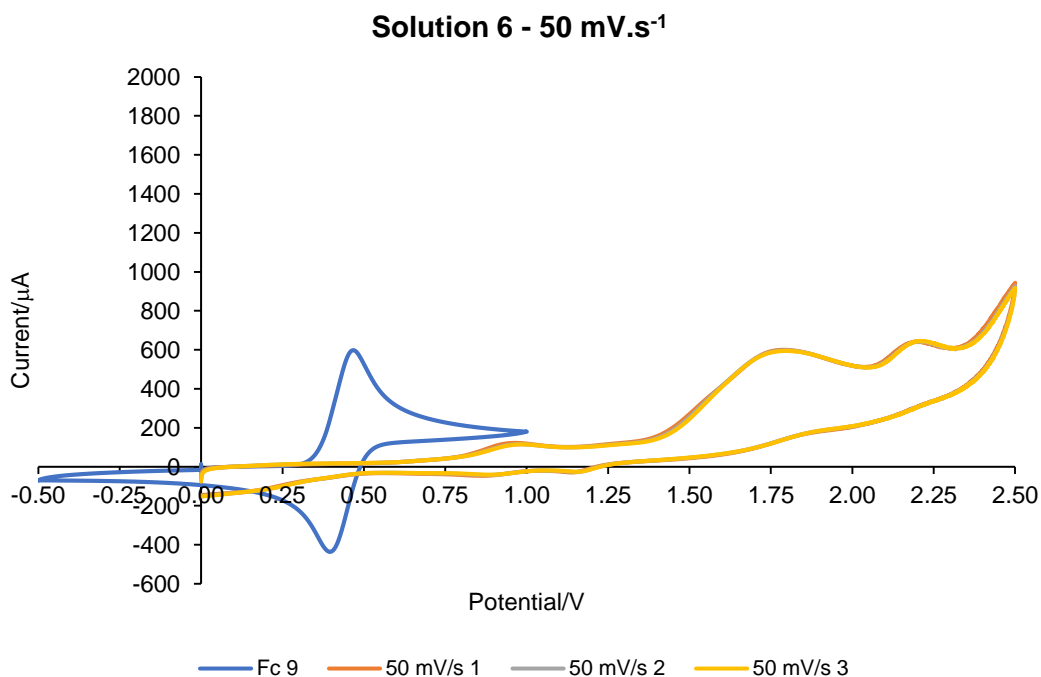
Solution 5 (including Ferrocene reference); 10 mM (*E*)-benzaldehyde oxime, 13 mM HFIP, 0.1 M Et₄NBF₄-MeCN



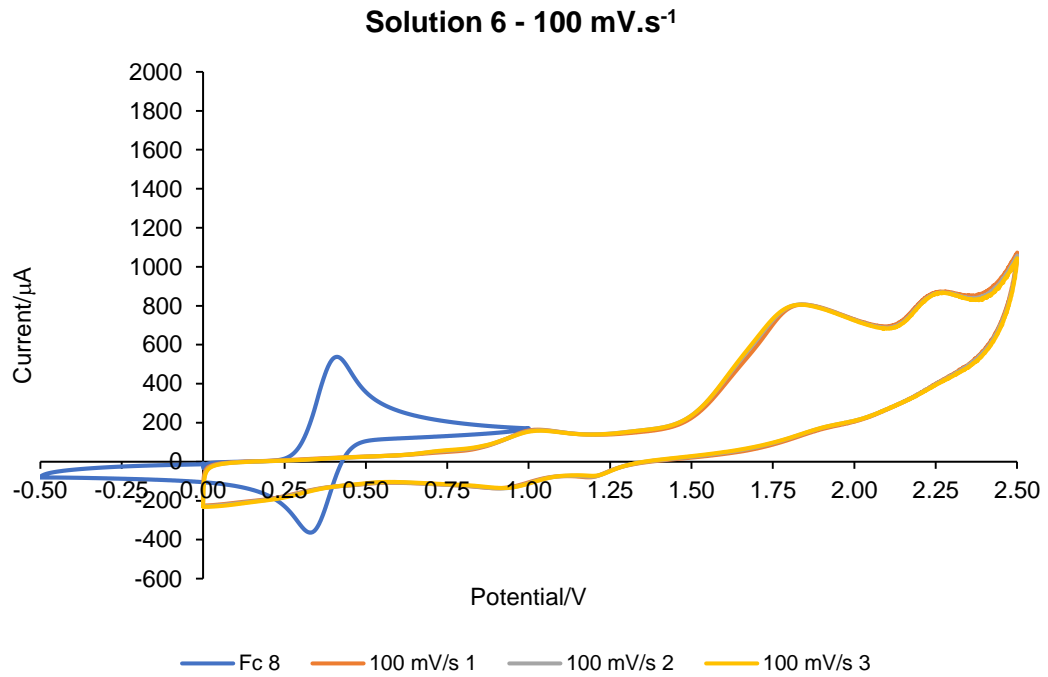
Solution 6 (including Ferrocene reference); 10 mM (*E*)-benzaldehyde oxime, 5 mM Et₄NCl, 0.1 M Et₄NBF₄- MeCN



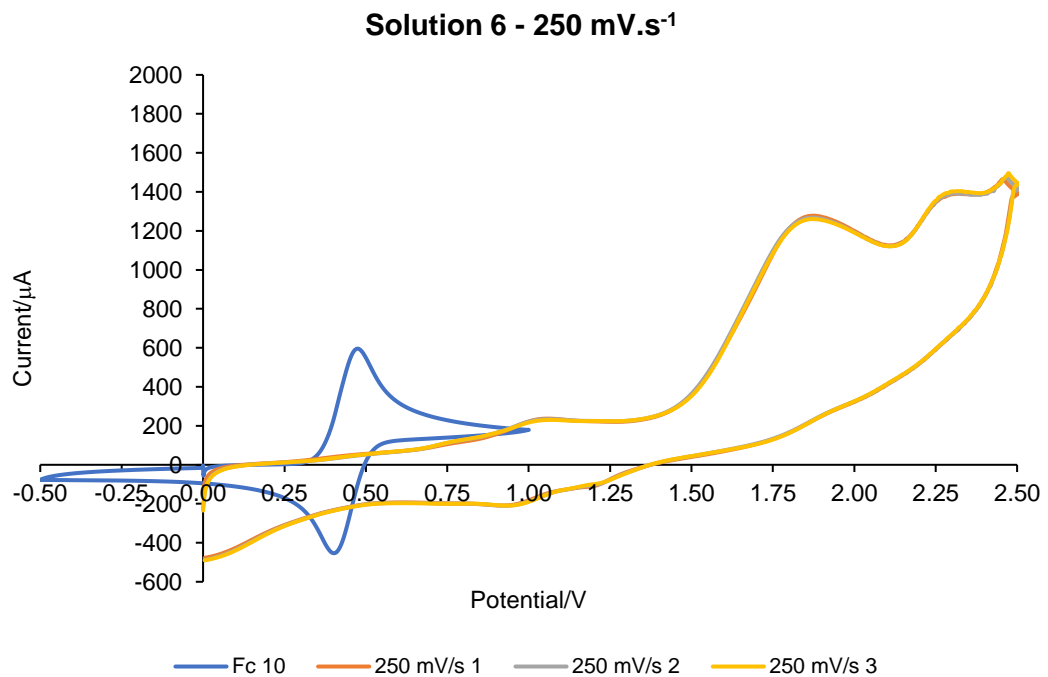
Solution 6 (including Ferrocene reference) – 50 mV.s⁻¹; 10 mM (*E*)-benzaldehyde oxime, 5 mM Et₄NCl, 0.1 M Et₄NBF₄-MeCN



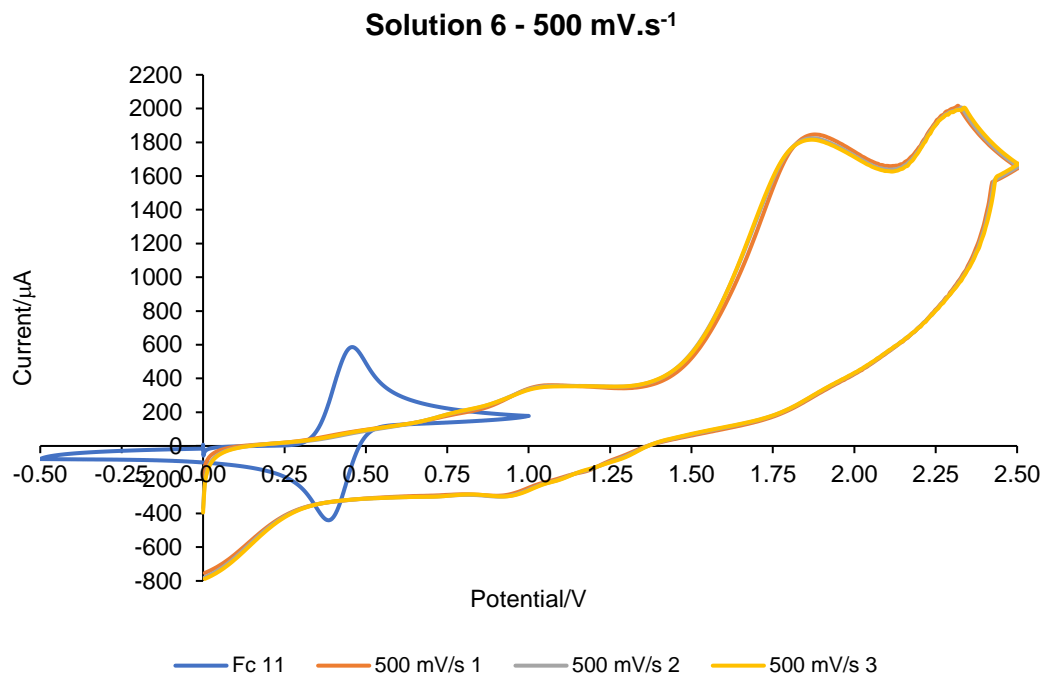
Solution 6 (including Ferrocene reference) – 100 mV.s⁻¹; 10 mM (*E*)-benzaldehyde oxime, 5 mM Et₄NCl, 0.1 M Et₄NBF₄-MeCN



Solution 6 (including Ferrocene reference) – 250 mV.s⁻¹; 10 mM (*E*)-benzaldehyde oxime, 5 mM Et₄NCl, 0.1 M Et₄NBF₄-MeCN



Solution 6 (including Ferrocene reference) – 500 mV.s⁻¹; 10 mM (*E*)-benzaldehyde oxime, 5 mM Et₄NCl, 0.1 M Et₄NBF₄-MeCN

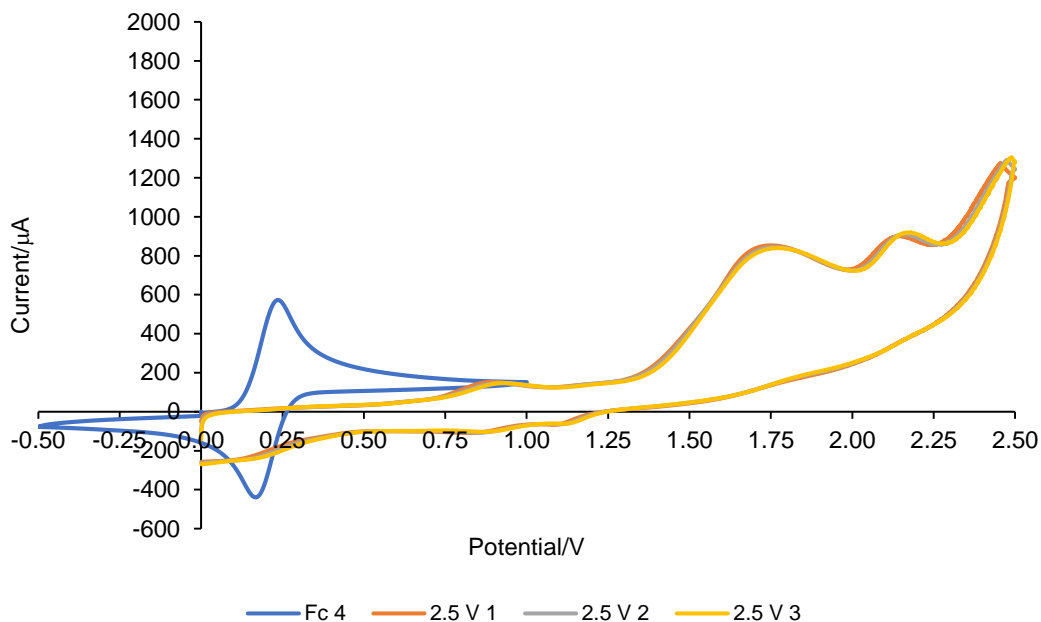


v/ mV.s ⁻¹	$\sqrt{v}/$ V ^{1/2} .s ^{-1/2}	Log(v)	Potential/V			Current/x10 ⁻³ A		
			Peak 1	Peak 2	Peak 3	Peak 1	Peak 2	Peak 3
50	0.2236	1.6990	0.970	1.786	2.210	0.117	0.597	0.642
100	0.3162	2.0000	1.036	1.833	2.271	0.162	0.806	0.869
250	0.5000	2.3979	1.044	1.879	2.314	0.233	1.270	1.400
500	0.7071	2.6990	1.059	1.874	2.324	0.355	1.830	2.000

Table 42: Scan rate data used for the analysis of the cyclic voltammetry experiments for Solution 6.

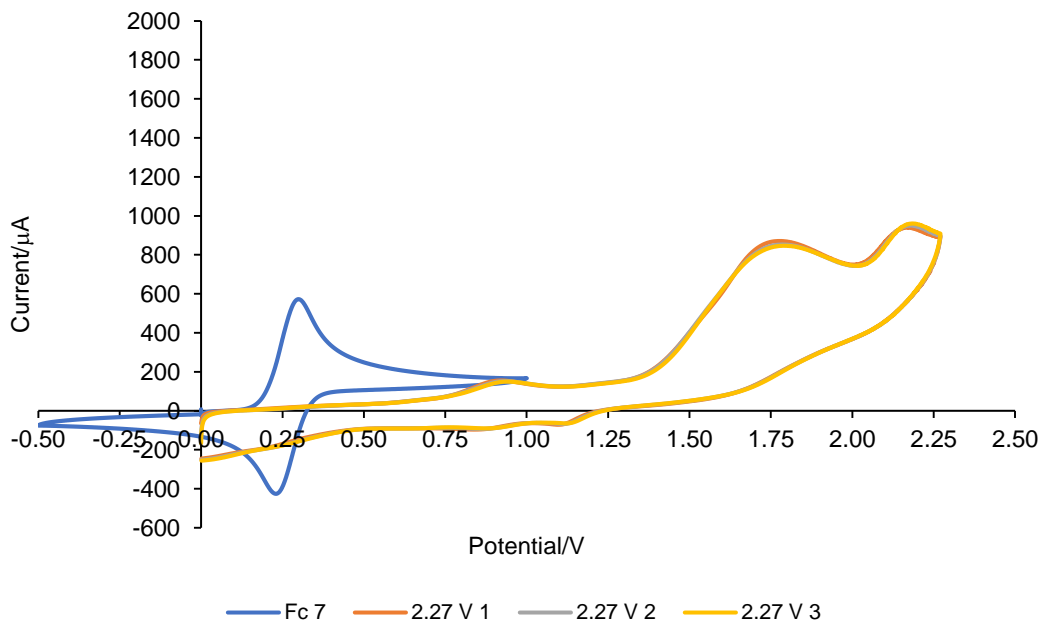
Solution 6 (including Ferrocene reference) – cut-off at 2.5 V; 10 mM (*E*)-benzaldehyde oxime, 5 mM Et₄NCl, 0.1 M Et₄NBF₄-MeCN

Solution 6 - Cut-Off at 2.5 V



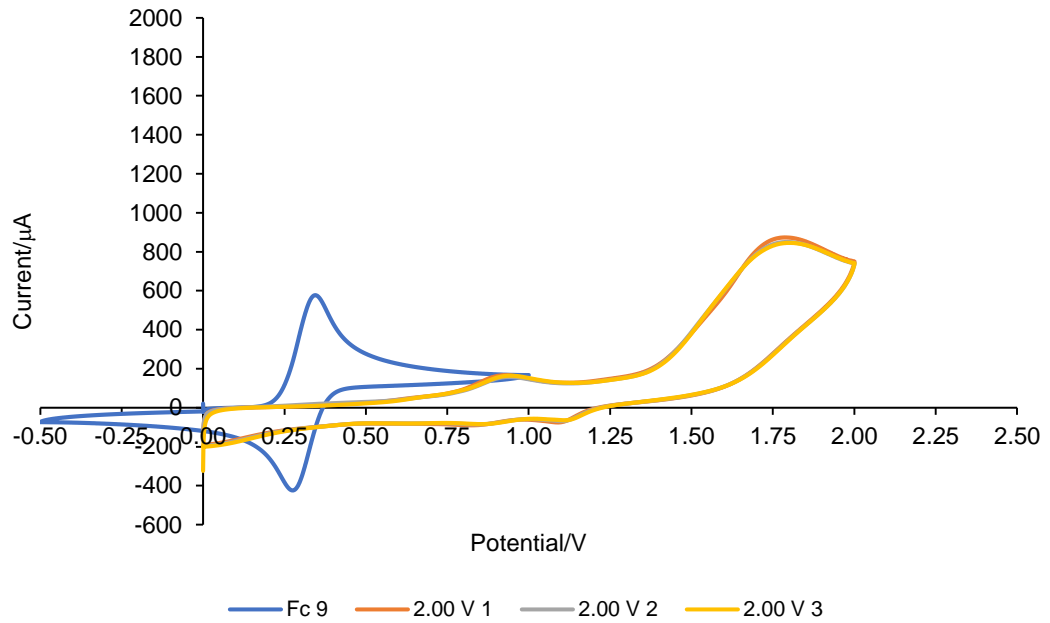
Solution 6 (including Ferrocene reference) – cut-off at 2.27 V; 10 mM (*E*)-benzaldehyde oxime, 5 mM Et₄NCl, 0.1 M Et₄NBF₄-MeCN

Solution 6 - Cut-Off at 2.27 V



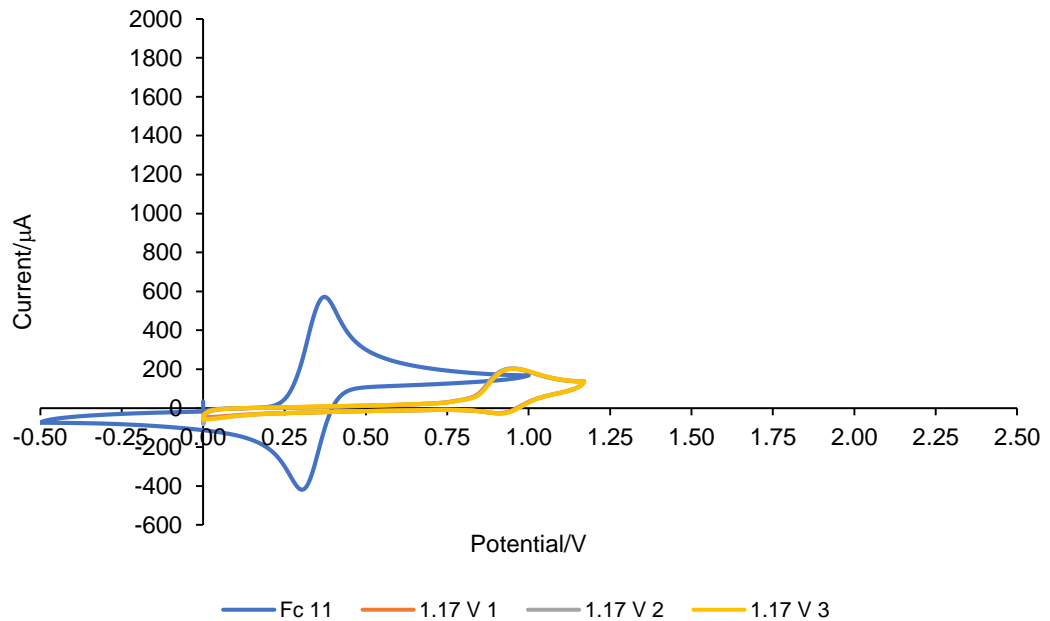
Solution 6 (including Ferrocene reference) – cut-off at 2.00 V; 10 mM (*E*)-benzaldehyde oxime, 5 mM Et₄NCl, 0.1 M Et₄NBF₄-MeCN

Solution 6 - Cut-Off at 2.00 V

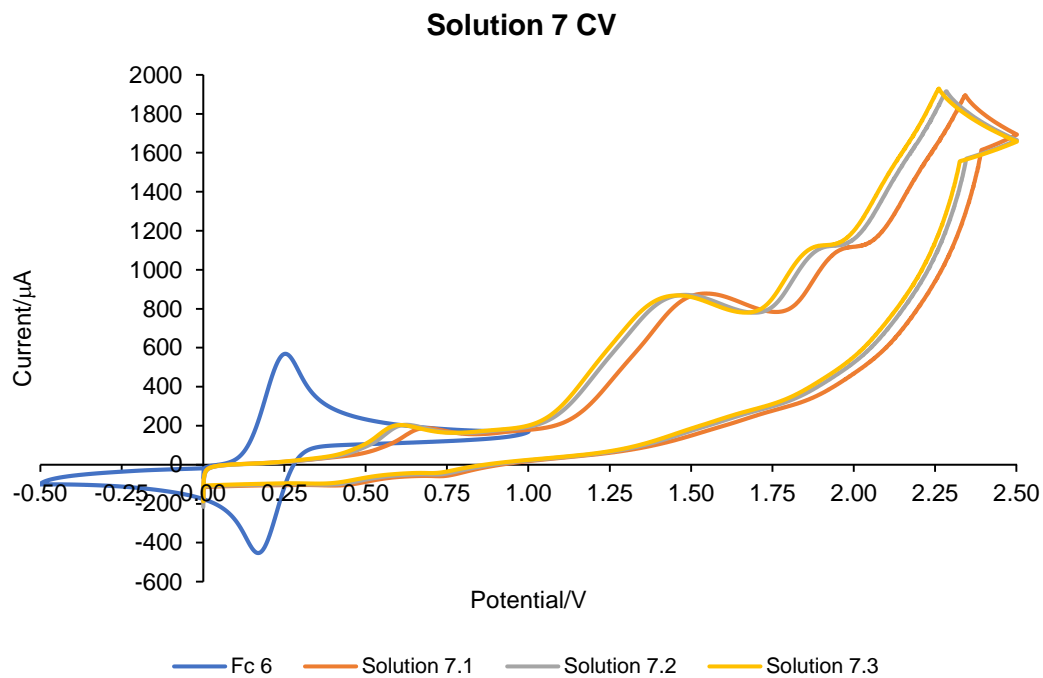


Solution 6 (including Ferrocene reference) – cut-off at 1.17 V; 10 mM (*E*)-benzaldehyde oxime, 5 mM Et₄NCl, 0.1 M Et₄NBF₄-MeCN

Solution 6 - Cut-Off at 1.17 V

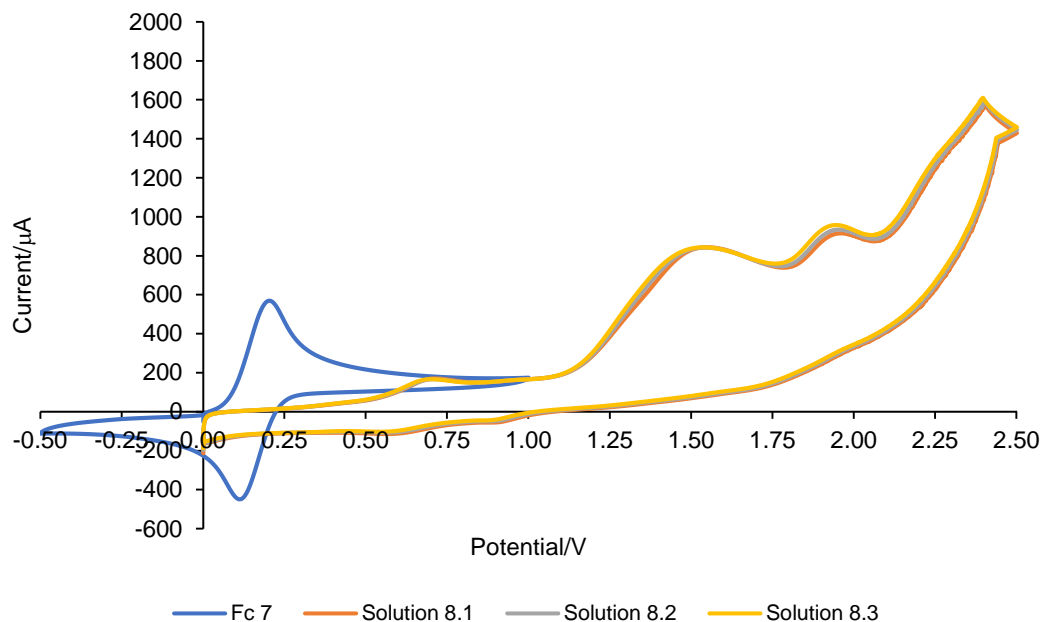


Solution 7 (including Ferrocene reference); 10 mM (*E*)-benzaldehyde oxime, 50 mM *tert*-butyl acrylate, 13 mM HFIP, 5 mM Et₄NCl, 0.1 M Et₄NBF₄-MeCN



Solution 8 (including Ferrocene reference); 10 mM (*E*)-benzaldehyde oxime, 13 mM HFIP, 5 mM Et₄NCl, 0.1 M Et₄NBF₄-MeCN

Solution 8 CV



Entry	Solution	Peak 1		Peak 2		Peak 3	
		<i>i</i> /μA	V/V	<i>i</i> /μA	V/V	<i>i</i> /μA	V/V
1	2	-	-	637	1.50	744	1.91
2	3	-	-	-	-	-	-
3	4	403	0.96	-	-	-	-
4	5	-	-	662	1.47	753	1.89
5	6	165	0.77	707	1.49	813	1.90
6	7	189	0.66	864	1.49	1083	1.90
7	8	168	0.71	840	1.52	935	1.95

Table 43: Tabulated peak currents and peak potentials from all full cyclic voltammograms, acquired at $v = 100 \text{ mV}\cdot\text{s}^{-1}$. *i* = current; *V* = potential.

7. References

1. Yan, M.; Kawamata, Y.; Baran, P. S., *Chem. Rev.*, **2017**, *117*, 13230.
2. (a) Kumar, K. A.; Govindaraju, M.; Renuka, N.; Kumar, G. V., *J. Chem. Pharm. Res.*, **2015**, *7*, 250; (b) Hu, F.; Szostak, M., *Adv. Syn. Cat.*, **2015**, *357*, 2583.
3. Welsch, M. E.; Snyder, S. A.; Stockwell, B. R., *Curr. Op. in Chem. Bio.*, **2010**, *14*, 347.
4. Kaur, K.; Kumar, V.; Sharma, A. K.; Gupta, G. K., *Eur. J. Med. Chem.*, **2014**, *77*, 121.
5. Abou-Shoer, M. I.; Shaala, L. A.; Youssef, D. T. A.; Badr, J. M.; Habib, A.-A. M., *J. Nat. Prod.*, **2008**, *71*, 1464.
6. Kalaitzis, J. A.; Leone, P. d. A.; Hooper, J. N. A.; Quinn, R. J., *Nat. Prod. Res.*, **2010**, *22*, 1257.
7. Ichiba, T.; Scheuer, P. J.; Kelly-Borges, M., *J. Org. Chem.*, **1993**, *58*, 4149.
8. (a) Bode, J. W.; Hachisu, Y.; Matsuura, T.; Suzuki, K., *Org. Lett.*, **2003**, *5*, 391; (b) Bode, J. W.; Hachisu, Y.; Matsuura, T.; Suzuki, K., *Tetrahedron Lett.*, **2003**, *44*, 3555.
9. Bode, J. W.; Uesuka, H.; Suzuki, K., *Org. Lett.*, **2003**, *5*, 395.
10. (a) Moeller, K. D., *Tetrahedron*, **2000**, *56*, 9527; (b) Sperry, J. B.; Wright, D. L., *Chem. Soc. Rev.*, **2006**, *35*, 605; (c) Yoshida, J.-i.; Kataoka, K.; Horcajada, R.; Nagaki, A., *Chem. Rev.*, **2008**, *108*, 2265; (d) Francke, R.; Little, R. D., *Chem. Soc. Rev.*, **2014**, *43*, 2492.
11. Anastas, P. T.; Warner, J. C., *Green Chemistry: Theory and Practice*. Oxford University Press: New York, 1998.
12. (a) Studer, A.; Curran, D. P., *Nat. Chem.*, **2014**, *6*, 765; (b) Saveant, J. M., *Accounts of Chemical Research*, **1980**, *13*, 323.
13. Grotheer, M.; Alkire, R.; Varjian, R.; Srinivasan, V.; Weidner, J., *Electrochem. Soc. Interface*, **2006**, *15*, 52.
14. Botte, G. G., *Electrochem. Soc. Interface*, **2014**, *23*, 49.
15. Helmholtz, H., *Annalen der Physik*, **1853**, *165*, 211.
16. (a) Ševčík, A., *Collection of Czechoslovak Chemical Communications*, **1948**, *13*, 349; (b) Randles, J. E. B., *Trans. Faraday Soc.*, **1948**, *44*, 322; (c) Randles, J. E. B., *Trans. Faraday Soc.*, **1948**, *44*, 327.
17. Fuchigami, T.; Inagi, S.; Atobe, M., *Fundamentals and Applications of Organic Electrochemistry*. In *Fundamentals and Applications of Organic Electrochemistry*, John Wiley & Sons, Ltd: Chichester, 2015.
18. Kolbe, H., *Annalen der Chemie und Pharmacie*, **1848**, *64*, 339.
19. Schäfer, H.-J., Recent contributions of Kolbe electrolysis to organic synthesis. In *Electrochemistry IV*, Steckhan, E., Ed. Springer Berlin Heidelberg: Berlin, Heidelberg, 1990; pp 91.
20. Shono, T.; Matsumura, Y.; Tsubata, K., *J. Am. Chem. Soc.*, **1981**, *103*, 1172.
21. Kuleshova, J.; Hill-Cousins, J. T.; Birkin, P. R.; Brown, R. C. D.; Pletcher, D.; Underwood, T. J., *Electrochim. Acta*, **2012**, *69*, 197.
22. Kabeshov, M. A.; Musio, B.; Murray, P. R. D.; Browne, D. L.; Ley, S. V., *Org. Lett.*, **2014**, *16*, 4618.
23. Morofuji, T.; Shimizu, A.; Yoshida, J.-i., *J. Am. Chem. Soc.*, **2014**, *136*, 4496.
24. Morofuji, T.; Shimizu, A.; Yoshida, J.-i., *J. Am. Chem. Soc.*, **2015**, *137*, 9816.
25. O'Brien, A. G.; Maruyama, A.; Inokuma, Y.; Fujita, M.; Baran, P. S.; Blackmond, D. G., *Agew. Chem. Int. Ed.*, **2014**, *53*, 11868.
26. Fujiwara, Y.; Dixon, J. A.; Rodriguez, R. A.; Baxter, R. D.; Dixon, D. D.; Collins, M. R.; Blackmond, D. G.; Baran, P. S., *J. Am. Chem. Soc.*, **2012**, *134*, 1494.

27. Jensen, K. L.; Franke, P. T.; Nielsen, L. T.; Daasbjerg, K.; Jørgensen, K. A., *Angew. Chem. Int. Ed.*, **2010**, *49*, 129.
28. Fu, N.; Li, L.; Yang, Q.; Luo, S., *Org. Lett.*, **2017**, *19*, 2122.
29. Bard, A. J., *J. Am. Chem. Soc.*, **2010**, *132*, 7559.
30. Wu, X.; Dube, M. A.; Fry, A. J., *Tetrahedron Lett.*, **2006**, *47*, 7667.
31. Zeng, C.-c.; Zhang, N.-t.; Lam, C. M.; Little, R. D., *Org. Lett.*, **2012**, *14*, 1314.
32. Li, C.; Zeng, C.-C.; Hu, L.-M.; Yang, F.-L.; Yoo, S. J.; Little, R. D., *Electrochim. Acta*, **2013**, *114*, 560.
33. Gao, W.-J.; Li, W.-C.; Zeng, C.-C.; Tian, H.-Y.; Hu, L.-M.; Little, R. D., *J. Org. Chem.*, **2014**, *79*, 9613.
34. Liang, S.; Zeng, C.-C.; Luo, X.-G.; Ren, F.-z.; Tian, H.-Y.; Sun, B.-G.; Little, R. D., *Green Chemistry*, **2016**, *18*, 2222.
35. Kang, L.-S.; Luo, M.-H.; Lam, C. M.; Hu, L.-M.; Little, R. D.; Zeng, C.-C., *Green Chemistry*, **2016**, *18*, 3767.
36. Tang, S.; Gao, X.; Lei, A., *Chemical Communications*, **2017**, *53*, 3354.
37. Catino, A. J.; Forslund, R. E.; Doyle, M. P., *J. Am. Chem. Soc.*, **2004**, *126*, 13622.
38. Yu, J.-Q.; Corey, E. J., *Org. Lett.*, **2002**, *4*, 2727.
39. Wilde, N. C.; Isomura, M.; Mendoza, A.; Baran, P. S., *J. Am. Chem. Soc.*, **2014**, *136*, 4909.
40. Horn, E. J.; Rosen, B. R.; Chen, Y.; Tang, J.; Chen, K.; Eastgate, M. D.; Baran, P. S., *Nature*, **2016**, *533*, 77.
41. (a) Buchner, E., *Berichte der deutschen chemischen Gesellschaft*, **1888**, *21*, 2637; (b) Michael, A., *J. Prakt. Chem.*, **1893**, *48*, 94.
42. Smith, L. I., *Chem. Rev.*, **1938**, *23*, 193.
43. Firestone, R. A., *J. Org. Chem.*, **1968**, *33*, 2285.
44. Huisgen, R., *J. Org. Chem.*, **1968**, *33*, 2291.
45. (a) Wheland, G. W.; Pauling, L., *J. Am. Chem. Soc.*, **1935**, *57*, 2086; (b) Pauling, L.; Wheland, G. W., *J. Chem. Phys.*, **1933**, *1*, 362.
46. Hoffmann, R.; Woodward, R. B., *J. Am. Chem. Soc.*, **1965**, *87*, 2046.
47. Siadati, S. A., *Tetrahedron Lett.*, **2015**, *56*, 4857.
48. (a) Zimmerman, H. E., *Accounts of Chemical Research*, **1971**, *4*, 272; (b) Dewar, M. J. S., *Angewandte Chemie*, **1971**, *83*, 859.
49. Geittner, J.; Huisgen, R.; Sustmann, R., *Tetrahedron Lett.*, **1977**, *18*, 881.
50. Huisgen, R.; Szeimies, G.; Möbius, L., *Chemische Berichte*, **1967**, *100*, 2494.
51. Williamson, D. G.; Cvetanovic, R. J., *J. Am. Chem. Soc.*, **1968**, *90*, 3668.
52. (a) Caramella, P.; Gandour, R. W.; Hall, J. A.; Deville, C. G.; Houk, K. N., *J. Am. Chem. Soc.*, **1977**, *99*, 385; (b) Caramella, P.; Houk, K. N., *J. Am. Chem. Soc.*, **1976**, *98*, 6397.
53. Huisgen, R., *Angew. Chem. Int. Ed.*, **1963**, *2*, 565.
54. Huisgen, R.; Bihlmaier, W.; Geittner, J.; Reissig, H.-U., *Heterocycles*, **1978**, *10*, 147.
55. Huisgen, R.; Scheer, W.; Huber, H., *J. Am. Chem. Soc.*, **1967**, *89*, 1753.
56. Padwa, A.; Smolanoff, J., *J. Am. Chem. Soc.*, **1971**, *93*, 548.
57. Takashi, I.; Takenori, K.; Hiroshi, K., *Chem. Lett.*, **1979**, *8*, 1337.
58. Wang, C.-I. J.; Ripka, W. C.; Confalone, P. N., *Tetrahedron Lett.*, **1984**, *25*, 4613.
59. (a) Liu, K.-C.; Shelton, B. R.; Howe, R. K., *J. Org. Chem.*, **1980**, *45*, 3916; (b) Gi, H.-J.; Xiang, Y.; Schinazi, R. F.; Zhao, K., *J. Org. Chem.*, **1997**, *62*, 88.
60. Lee, G. A., *Synthesis*, **1982**, *1982*, 508.
61. Ye, Y.; Zheng, Y.; Xu, G.-Y.; Liu, L.-Z., *Heteroatom Chem.*, **2003**, *14*, 254.

62. Armstrong, S. K.; Collington, E. W.; Knight, J. G.; Naylor, A.; Warren, S., *Journal of the Chemical Society, Perkin Transactions 1*, **1993**, 1433.
63. Moriya, O.; Nakamura, H.; Kageyama, T.; Urata, Y., *Tetrahedron Lett.*, **1989**, 30, 3987.
64. Mukaiyama, T.; Hoshino, T., *J. Am. Chem. Soc.*, **1960**, 82, 5339.
65. Basel, Y.; Hassner, A., *Synthesis*, **1997**, 1997, 309.
66. Knight, D. W.; Proctor, A. J.; Clough, J. M., *Synlett*, **2010**, 2010, 628.
67. Schmidt, E. Y.; Tatarinova, I. V.; Ivanova, E. V.; Zorina, N. V.; Ushakov, I. A.; Trofimov, B. A., *Org. Lett.*, **2013**, 15, 104.
68. He, Y.-T.; Li, L.-H.; Yang, Y.-F.; Wang, Y.-Q.; Luo, J.-Y.; Liu, X.-Y.; Liang, Y.-M., *Chemical Communications*, **2013**, 49, 5687.
69. Minakata, S.; Sasaki, I.; Ide, T., *Angew. Chem. Int. Ed.*, **2010**, 49, 1309.
70. (a) Minakata, S.; Morino, Y.; Ide, T.; Oderaotoshi, Y.; Komatsu, M., *Chemical Communications*, **2007**, 3279; (b) Minakata, S.; Morino, Y.; Oderaotoshi, Y.; Komatsu, M., *Org. Lett.*, **2006**, 8, 3335; (c) Minakata, S.; Morino, Y.; Oderaotoshi, Y.; Komatsu, M., *Chemical Communications*, **2006**, 3337.
71. Minakata, S.; Okumura, S.; Nagamachi, T.; Takeda, Y., *Org. Lett.*, **2011**, 13, 2966.
72. Yoshimura, A.; Middleton, K. R.; Todora, A. D.; Kastern, B. J.; Koski, S. R.; Maskaev, A. V.; Zhdankin, V. V., *Org. Lett.*, **2013**, 15, 4010.
73. Han, L.; Zhang, B.; Zhu, M.; Yan, J., *Tetrahedron Lett.*, **2014**, 55, 2308.
74. Weidner-Wells, M. A.; Fraga-Spano, S. A.; Turchi, I. J., *J. Org. Chem.*, **1998**, 63, 6319.
75. Muri, D.; Bode, J. W.; Carreira, E. M., *Org. Lett.*, **2000**, 2, 539.
76. Dubrovskiy, A. V.; Larock, R. C., *Org. Lett.*, **2010**, 12, 1180.
77. Medina, J. M.; Mackey, J. L.; Garg, N. K.; Houk, K. N., *J. Am. Chem. Soc.*, **2014**, 136, 15798.
78. Lassaletta, J.; Fernández, R.; Ros, A.; Alvarez, E.; Dietrich, H., *Synlett*, **2005**, 2005, 2899.
79. Svejstrup, T. D.; Zawodny, W.; Douglas, J. J.; Bidgeli, D.; Sheikh, N. S.; Leonori, D., *Chemical Communications*, **2016**, 52, 12302.
80. Shono, T.; Matsumura, Y.; Tsubata, K.; Kamada, T.; Kishi, K., *J. Org. Chem.*, **1989**, 54, 2249.
81. Hartmer, M. F.; Waldvogel, S. R., *Chemical Communications*, **2015**, 51, 16346.
82. Hashimoto, T.; Maruoka, K., *Chem. Rev.*, **2015**, 115, 5366.
83. Kissane, M.; Maguire, A. R., *Chem. Soc. Rev.*, **2010**, 39, 845.
84. Gothelf, K. V.; Jørgensen, K. A., *Chem. Rev.*, **1998**, 98, 863.
85. (a) Ukaji, Y.; Inomata, K., *Synlett*, **2003**, 2003, 1075; (b) Yutaka, U.; Kazunori, S.; Katsuhiko, I., *Chem. Lett.*, **1993**, 22, 1847.
86. Masamichi, T.; Yutaka, U.; Katsuhiko, I., *Chem. Lett.*, **2002**, 31, 1112.
87. Makoto, S.; Yutaka, U.; Katsuhiko, I., *Chem. Lett.*, **1996**, 25, 455.
88. Sibi, M. P.; Itoh, K.; Jasperse, C. P., *J. Am. Chem. Soc.*, **2004**, 126, 5366.
89. Suga, H.; Adachi, Y.; Fujimoto, K.; Furihata, Y.; Tsuchida, T.; Kakehi, A.; Baba, T., *J. Org. Chem.*, **2009**, 74, 1099.
90. Lian, X.; Guo, S.; Wang, G.; Lin, L.; Liu, X.; Feng, X., *J. Org. Chem.*, **2014**, 79, 7703.
91. Kawamata, Y.; Yan, M.; Liu, Z.; Bao, D. H.; Chen, J.; Starr, J. T.; Baran, P. S., *J. Am. Chem. Soc.*, **2017**, 139, 7448.
92. (a) Tye, H., *Drug Discovery Today*, **2004**, 9, 485; (b) Gooding, O. W., *Curr. Op. in Chem. Bio.*, **2004**, 8, 297; (c) Owen, M. R.; Luscombe, C.; Lai, L.-W.;

- Godbert, S.; Crookes, D. L.; Emiabata-Smith, D., *Org. Proc. Res. Dev.*, **2001**, 5, 308; (d) Lendrem, D.; Owen, M.; Godbert, S., *Org. Proc. Res. Dev.*, **2001**, 5, 324.
93. Poole, D., Title, **2017**.
94. Bonnet-Delpon, D.; Bégué, J.-P.; Crousse, B., *Synlett*, **2004**, 2004, 18.
95. (a) Reich, H. J. Bordwell pKa Table. <https://www.chem.wisc.edu/areas/reich/pkatable/> (accessed 22/01/2020); (b) Taft, R. W.; Bordwell, F. G., *Accounts of Chemical Research*, **1988**, 21, 463; (c) Olmstead, W. N.; Margolin, Z.; Bordwell, F. G., *J. Org. Chem.*, **1980**, 45, 3295; (d) Matthews, W. S.; Bares, J. E.; Bartmess, J. E.; Bordwell, F. G.; Cornforth, F. J.; Drucker, G. E.; Margolin, Z.; McCallum, R. J.; McCollum, G. J.; Vanier, N. R., *J. Am. Chem. Soc.*, **1975**, 97, 7006.
96. D. H. Ripin, D. A. E. Evans pKa Table. http://evans.rc.fas.harvard.edu/pdf/evans_pKa_table.pdf (accessed 22/01/2020).
97. Bordwell, F. G.; McCallum, R. J.; Olmstead, W. N., *J. Org. Chem.*, **1984**, 49, 1424.
98. Shao, X.; Zheng, Y.; Tian, L.; Martín-Torres, I.; Echavarren, A. M.; Wang, Y., *Org. Lett.*, **2019**, 21, 9262.
99. Zhao, G.; Liang, L.; Wen, C. H. E.; Tong, R., *Org. Lett.*, **2019**, 21, 315.
100. Hammett, L. P., *Trans. Faraday Soc.*, **1938**, 34, 156.
101. Hansch, C.; Leo, A.; Taft, R. W., *Chem. Rev.*, **1991**, 91, 165.
102. Swain, C. G.; Lupton, E. C., *J. Am. Chem. Soc.*, **1968**, 90, 4328.
103. Simmons, E. M.; Hartwig, J. F., *Angew. Chem. Int. Ed.*, **2012**, 51, 3066.
104. Roth, H. G.; Romero, N. A.; Nicewicz, D. A., *Synlett*, **2016**, 27, 714.
105. (a) Owston, N. A.; Parker, A. J.; Williams, J. M. J., *Org. Lett.*, **2007**, 9, 3599; (b) Owston, N. A.; Parker, A. J.; Williams, J. M. J., *Org. Lett.*, **2007**, 9, 73; (c) Forrester, J.; Jones, R. V. H.; Newton, L.; Preston, P. N., *Tetrahedron*, **2001**, 57, 2871; (d) Ogata, Y.; Takagi, K.; Mizuno, K., *J. Org. Chem.*, **1982**, 47, 3684.
106. Design, C. R. The Ammonite Family of Electrolysis Cells. <https://www.cambridgereactordesign.com/ammonite/ammonite.html> (accessed 22/01/2020).
107. Vapourtec Ion Electrochemical Reactor. <https://www.vapourtec.com/products/flow-reactors/ion-electrochemical-reactor-features/> (accessed 22/01/2020).
108. van Melis, C. G. W.; Penny, M. R.; Garcia, A. D.; Petti, A.; Dobbs, A. P.; Hilton, S. T.; Lam, K., *ChemElectroChem*, **2019**, 6, 4144.
109. Patil, V. V.; Gayakwad, E. M.; Shankarling, G. S., *J. Org. Chem.*, **2016**, 81, 781.
110. Kapuriya, N.; Kapuriya, K.; Dodia, N. M.; Lin, Y.-W.; Kakadiya, R.; Wu, C.-T.; Chen, C.-H.; Naliapara, Y.; Su, T.-L., *Tetrahedron Lett.*, **2008**, 49, 2886.
111. Yu, J.; Cao, X.; Lu, M., *Tetrahedron Lett.*, **2014**, 55, 5751.
112. Blackwell, M.; Dunn, P. J.; Graham, A. B.; Grigg, R.; Higginson, P.; Saba, I. S.; Thornton-Pett, M., *Tetrahedron*, **2002**, 58, 7715.
113. Hou, Y.; Lu, S.; Liu, G., *J. Org. Chem.*, **2013**, 78, 8386.
114. Yu, J.; Jin, Y.; Lu, M., *Adv. Syn. Cat.*, **2015**, 357, 1175.
115. Jiang, X.; Xu, X.; Lin, Y.; Yan, Y.; Li, P.; Bai, R.; Xie, Y., *Tetrahedron*, **2018**, 74, 5879.
116. Berger, R.; Rabbat, P. M. A.; Leighton, J. L., *J. Am. Chem. Soc.*, **2003**, 125, 9596.
117. Arunprasath, D.; Muthupandi, P.; Sekar, G., *Org. Lett.*, **2015**, 17, 5448.

118. Lutun, S.; Hasiak, B.; Couturier, D., *Syn. Commun.*, **1999**, 29, 111.
119. Wang, D.-J.; Chen, B.-Y.; Wang, Y.-Q.; Zhang, X.-W., *Eur. J. Org. Chem.*, **2018**, 2018, 1342.